OBSERVATOIRE DE GRENOBLE
LABORATOIRE DE GEOPHYSIQUE INTERNE ET TECTONOPHYSIQUE

Thèse

par

Farokh Tavakoli

le 21 Décembre 2007

pour obtenir le grade de
Docteur de l'Université Joseph Fourier
Spécialité Sciences de la Terre de l'Univers et de l'Environnement

Titre :

Déformation actuelle et cinématique des failles actives observées par GPS dans le Zagros et l'Est iranien

"Present-day deformation and kinematics of the active faults observed by GPS in the Zagros and east of Iran"

JURY

M. Denis Hatzfeld	**LGIT, Grenoble**	**Directeur de thèse**
Mme. Andrea Walpersdorf	**LGIT, Grenoble**	**Directeur de thèse**
M. Olivier Bellier	**CEREGE, Aix-en-Provence**	**Rapporteur**
M. Frédéric Masson	**EOST, Strasbourg**	**Rapporteur**
M. Jean-Mathieu Nocquet	**Géosciences Azur, Nice**	**Examinateur**
M. Peter Van Der Beck	**LGCA, Grenoble**	**Président**

Acknowledgments

I would like to thank many people who contributed to make this work possible. In 1998, when I was working at National Cartographic Center of Iran (NCC) as the responsible of the Geodesy department, Denis Hatzfeld proposed us to have a scientific cooperation on GPS measurements to study the kinematics and deformation of Iran both regionally and locally. Since that time NCC has increased its knowledge of the application of geodetic tools to crustal deformation and has installed more than 100 permanent GPS stations in Iran. Of course this cooperation benefited to both partners but without the help of Denis such a progress would have been impossible.

I would like to thank very much my supervisors Denis Hatzfeld and Andrea Walpersdorf who shared their knowledge and experience with me. Their office doors always were open for me and they made me familiar with the world of geophysics and tectonics. I learned much through their comments and corrections of my manuscript.

Andrea Walpersdorf helped me in processing data with GAMIT/GLOBK and supported me in collecting the GPS data in Iran. She always answered my strange questions patiently. Her help and support has been always much more than that to be mentioned and appreciated by my part here just in some sentences.

I would like to thank Olivier Bellier and Frederic Masson, Jean-Mathieu Nocquet and Peter Van der Beek for accepting to be a member of the jury and for their encouraging comments and helpful corrections of my thesis. I appreciate Olivier Bellier and Christine Authemayou for their help in the interpretation of the Kazerun data.

I would like to thank Erwan Pathier for running the package of the Okada model for me, and Jean-Mathieu Nocquet and Paul Tregoning to make available their computer programs for the velocity field in different reference systems, strain and rotation rates. I want to thank all LGIT colleagues and friends, especially: Nathalie Cotte, Isabelle Manighetti, Mathilde Vergnolle, Guillaume Daniel, Elizabeth Canet, Mojgan Jadidi.

I benefited of a scholar fellowship from the French Total company and without their support it would have been impossible to continue my education. I would like to

thank the managers of Total scholarship program: Mr Blumereau, Mrs Mignonac, Mr Villeleger and Mrs Ranvial.

Our GPS projects were supported by the National Cartographic Center of Iran and the French INSU-CNRS via the program Dyeti.

I like to thank all the colleagues of National Cartographic Center who contributed in the data collection: Dr Mohammad Madad and Mr Mohammad Sarpoulaki former director and technical deputy of NCC, and Dr Yahya Djamour, present director of NCC, who helped and supported me very much. Mr Emtiaz, financial and administrative deputy, Mr Masoud Javadi (unfortunately he is not among us any more) and Morteza Sedighi, former and present Director of the Geodesy Department. I will never forget Mr Sarpoulaki's help and support, he encouraged me to continue my education and asked me to use this fellowship. Dr Djamour is my first GAMIT/GLOBK instructor.

Other colleagues are also acknowledged for their help: Mr Nankali, Mrs Rahimi, Miss Mousavi, Mr Nilforoushan, Mr Anvari, Mr Sherkat Saadi, Mr Arash Safaii Asl, Mrs Mariam Falatoni, Mr Sardari, Mr Nazari, Mr Godarzi, Mr Nemati. My other colleagues, the surveyors and the drivers, were also a great help for me during the field measurements so I want to thank them one by one: M. Rahmani, Jafarzadeh, Sharif Zamani, Heidari, Golabi, Makhtomi, Marami, Ghazi, Nowroz, Pour Abdollahi, Chenari, Baba, Hatami Dana.

I would like to thank Jean Chéry, Stéphane Baize, Christian Sue, Hossein Hendi and Amir Shafii Bafti who had an important role in the field reconnaissance and site installation of our networks.

I am very thankful to my wife, Parvin and my son Kian who accompanied me and without their support and love it would be impossible to finish this thesis. I also thank my mother and my mother-in-law who always support us, as well as our brothers and sisters for their encouragements.

At the end, I am grateful to all who contributed to this work.

CONTENTS

Chapter 1 Introduction

1.1 Motivation

The subject of this thesis is the measurement by GPS of the present-day crustal deformation in selected places in Iran (the Zagros, the Kopeh Dagh and eastern Iran). Iran is an exceptional target for such a study, as it contains within its political borders the complete deformation zone of the collision of two major tectonic plates, the Arabian and the Eurasian plate. This thesis is the opportunity to document how the kinematics of the Arabia-Eurasia collision are related across the whole deformation zone, by examining if and how the Kopeh Dagh deformation at the northern border of Iran, close to the Turan platform, is driven by the constraints imposed by the northward moving Arabian plate in the south of Iran, at the southern border of the Zagros. Moreover, the Arabia-Eurasia convergence in Iran is expressed by a young continental collision, making Iran an excellent site for the studies of the geodynamics of such a tectonic event. The results could be exported to other places in the world where the complete zone of young collision is less accessible. The Arabia-Eurasia collision makes Iran a place of high seismicity (one earthquake of M=7 every 7 years, one earthquake of M=6 every 2 years). A precise velocity field covering the regions of large cities like Mashhad, Kerman and Shiraz will be used to help understanding the tectonical mechanisms driving the present-day deformation and leading to the numerous earthquakes. It will also quantify precisely the velocities of individual, selected faults. This will help constraining the seismic hazard presented by these faults, an important contribution to protect millions of inhabitants of the regions covered by our studies.

Geodetic studies for geodynamic purposes have been started in 1997 in the framework of the French-Iranian collaboration on crustal deformation and seismic hazard. Important results are already available: **i)** The convergence rate of the Arabian plate has been determined to 20-26 mm/yr oriented N7, increasing from the southwest to the southeast. **ii)** Shortening is accommodated by Zagros (8 mm/yr) and Alborz (5 mm/yr) and by the South Caspian Basin (6 mm/yr), as well as by some large strike-slip faults, in particular the NS trending faults limiting the Lut block in eastern Iran (cumulated 15 mm/yr), the Tabriz fault in NW Iran (7 mm/yr), the MRF in

northern Zagros (3-5 mm/yr), and the Mosha fault in southern Alborz (4 mm/yr). **iii)** The northeastern and eastern extremities of Iran seem to belong to Eurasia. **iv)** The Central Iran Block (the Sanandaj-Sirjan zone and part of the Great Kavir desert), the South Caspian Basin and the Lut block present low seismicity and seem to be rigid. These studies, either global and therefore large scale, or concentrating regionally on different parts of Iran, will be completed by this thesis. We will focus **1)** on the kinematics of the Zagros mountain belt as a whole, from the Zagros-Makran transition in the southeast to Iraq's border in the northwest, examining how pure shortening in SE Zagros is transferred to oblique shortening in NW Zagros, evaluating the possibility of partitioning to accommodate the oblique constraints, and presenting the Kazerun fault system which is playing a key role at the limit between the two parts of Zagros, and **2)** on the kinematics of east Iran, characterizing the present day activities at both sides of the Lut block, examining the relation between these NS trending right-lateral strike-slip faults (Nayband/Gowk and Sistan suture zone) and the EW trending left-lateral strike-slip faults to its northern extension (Dasht-e-Bayaz and Doruneh faults), and relating the Kopeh Dagh kinematics to these constraints incoming from the south.

1.2 General tectonic settings of the Arabia-Eurasia plate convergence in Iran

1.2.1 Arabia-Eurasia Convergence

One of the most widely studied areas of continental deformation is the Alpine-Himalayan belt which runs from Western Europe across the Middle East to India and China. This mountain belt results from the active convergence between Eurasia and Africa (1-2 cm/yr), Arabia (2-3 cm/yr) and India (3-4 cm/yr). Several GPS networks have recently been set up to study the deformation along the Alpine–Himalayan collision zone in Himalaya (Wang et al. 2001), in the Eastern Mediterranean and Caucasus area (Reilinger et al., 1997; McClusky et al. 2000, 2003) or in the Alps (Vigny et al., 2002; Calais et al., 2002).

Inside the Alpine-Himalayan belt, the Arabian plate moves roughly northward with respect to the Eurasian plate. NUVEL1-A (DeMets et al., 1994) predicts a relative motion of 30-35 mm/yr (Fig. 1-1) from the analysis of ocean floor magnetic anomaly reconstructions (Minster and Jordan, 1978). In this geological model the

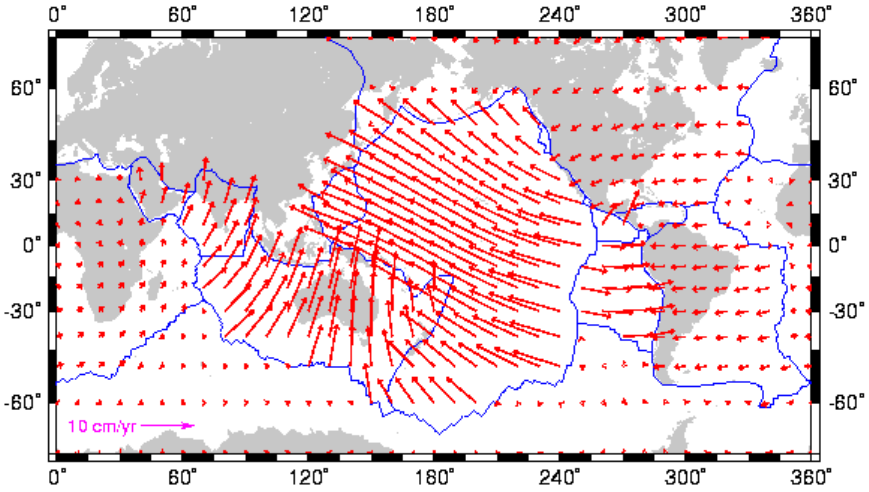

Figure 1-1. NUVEL1-A plate velocities with respect to Eurasia (DeMets et al., 1994).

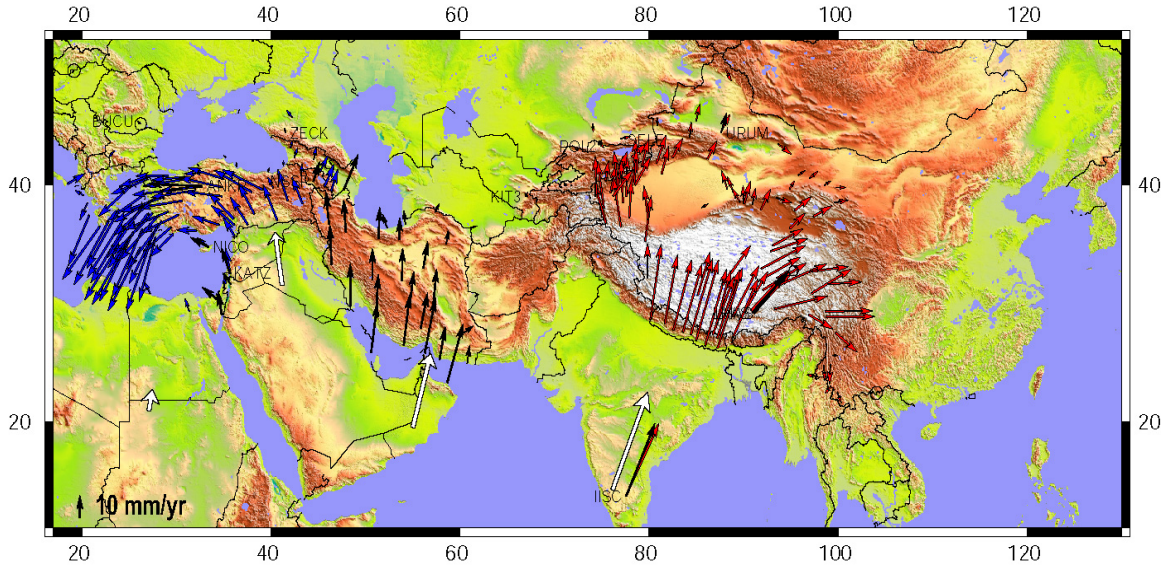

Figure 1-2. Horizontal velocity field for a major part of Alpine-Himalayan chain. The blue vectors are by McClusky et al. (2001) and the red vectors are by Wang et al. (2001). The black vectors are by Vernant et al. (2004). The white vectors are the Nuvel1-A plate velocity model by DeMets et al. (1994) (Figure from Vernant, 2003).

velocities of the plates are considered as constant over the last 3 Ma. The GPS constrained velocities (Fig. 1-2) for the northern margin of the Arabian plate are 18 ± 2 mm/yr relative to Eurasia at a longitude of 48°E (McClusky et al., 2000) and 22 ± 2 mm/yr and 26 ± 2 mm/yr at longitudes of 50.5° and 58.5°E, respectively (Vernant et al., 2004; Masson et al., 2007). The convergence rate increases eastward because the Arabia-Eurasia Euler pole lies in the northeast of Africa at ~27.4°N, 18.4°E. The

Arabian plate rotates counter clockwise relative to Eurasia with a rate of 0.4°/Myr (McClusky et al., 2003, Vernant et al., 2004a). The results of GPS observations within Iran and surrounding regions give 8.5 mm/yr lower estimate for the Arabia-Eurasia convergence rate than the NUVEL-1A plate tectonic model predicts (DeMets et al. 1990, 1994; Jestin et al., 1994). This difference may be due to systematic errors in the model or changes in plate motion rates over the last 3 Ma. McQuarrie et al. (2003) report a rate of 20 ± 4 mm/yr (38°N, 48°E) for the Arabia-Eurasia relative motion (incorporating Red Sea spreading) that also agrees well with the present-day rate determined from the Arabia-Eurasia GPS Euler vector (21±1 mm/yr).

The Arabia-Eurasia convergence is accommodated differently in eastern and western Iran. This convergence involves intracontinental collision in the west but east of 58°E, the Oman Sea subducts along the Makran Mountain belt (Byrne et al., 1992; McCall, 1997; Kopp et al., 2000). The Arabia-Eurasia convergence has produced many earthquakes (Ambraseys and Melville, 1982; Berberian and Yeats, 1999) (Fig. 1-4) inside the deforming zones of Zagros, Alborz and Kopeh Dagh and along the large strike-slip faults affecting Iran.

1.2.2 Date of initial Arabia-Eurasia Collision

Estimates for the age of the initial collision between Arabia and Eurasia vary from ~65 Ma (Berberian and King, 1981), using the end of ophiolite obduction, to ~5 Ma (Philip et al., 1989), considering the onset of coarse clastic sedimentation around parts of the Greater Caucasus. Palinspatic reconstructions (McQuarrie et al., 2003) suggest a continental collision starting in the Miocene-Pliocene time, with a continuous motion until today. Deformation and syn-tectonic sedimentation took place on the northern side of the Arabian plate in the early Miocene (~16–23 Ma) (Robertson, 2000), related to the overthrusting of allochthonous nappes originating on the Eurasian side of Neo-Tethys. Other studies in the same region put the initial collision-related deformation during the Oligocene (29-35 Ma) (Yilmaz, 1993), or middle Eocene (~40 Ma) (Hempton, 1987). A reconstruction of the Arabia-Eurasia collision is proposed by McQuarrie et al. (2003) based on sea floor magnetic anomalies across the Red Sea. According to these constrains they propose that the closure of the Neotethys ocean took place no later than 10 Ma ago (Fig. 1-3).

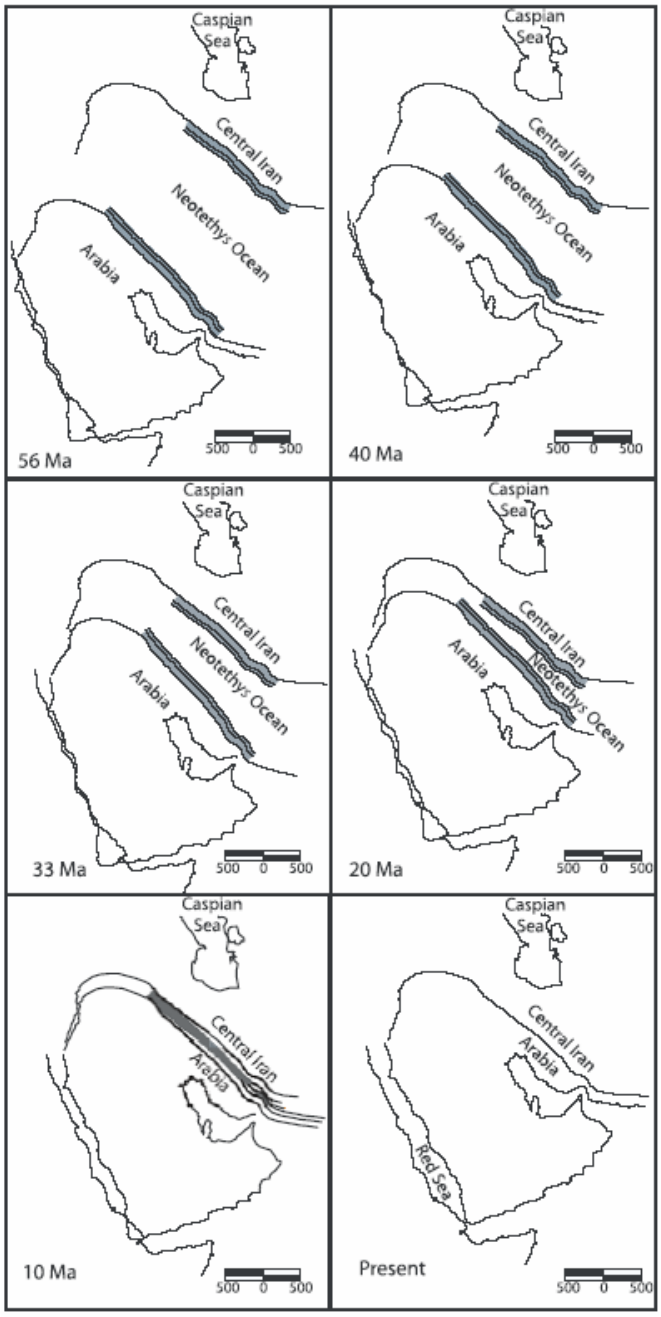

Figure 1-3. Maps showing the evolution of the Neotethys, and the relationship between opening of the Red Sea and collision of Arabia and Eurasia (McQuarrie et al., 2003).

However, 16–23 Ma is likely to be a good estimate for the age for the initial plate collision. Suturing may have been diachronous from the Arabian promontory in the north, southeastward along the Main Zagros Reverse Fault (Stoneley, 1981). Since the initial collision along the Bitlis-Zagros suture, the Arabian plate has moved ~300–500 km northward with respect to stable Eurasia, based on an extrapolation of Dewey et al.'s (1989) Africa-Eurasia motion history to include the Arabian plate (McQuarrie et al., 2003; Allen et al., 2004). Allen et al. (2004) suggest that the

deformation in the Iranian mountain belts (Zagros and Alborz) started 3-7 Ma ago and a major reorganization of the South Caspian Basin have occurred ~6 Ma ago, however the age seems to be badly constrained. Ritz et al. (2006) proposed that the reorganization has happened during the Quaternary. The onset of the deformation for Kopeh Dagh started ~5 Ma ago (Lyberis and Manby, 1999).

1.2.3 Deformation of Iran

Iran (whose dimensions are 1700 km W-E, and 1000 km N-S) is an active continental region with widely distributed deformation. This deformation is associated with large and frequent earthquakes. Iran is the country which pays the highest death toll (~5000 per year) to earthquakes. The deformation of Iran is the response to the convergence between the Arabian and Eurasian plates. The relative motion between these plates and the related overall deformation across Iran is known from GPS measurements (McClusky et al., 2000, 2003; Nilforoushan et al., 2003; Vernant et al. 2004a; Masson et al., 2007). The first GPS measurements within Iran show that the north–south shortening from Arabia to Eurasia is ~22 mm/yr at 50° longitude and ~25 mm/yr at 60° longitude (Fig. 1-4), less than the previously estimated 30–35 mm/yr from NUVEL-1A magnetic anomaly reconstructions (DeMets et al., 1994; Minster and Jordan, 1978).

The deformation in Iran involves intracontinental shortening everywhere except along the southeast margin (east of 58°E) where the Oman Sea subducts northward along the Makran belt beneath the southeast of Iran. The deforming zone of Iran is evidenced by seismicity and topography (Jackson and McKenzie, 1984; Jackson and McKenzie, 1988). Iran is surrounded by relatively rigid, aseismic blocks: Arabia to the southwest, the Turan Shield (belonging to the Eurasian plate) to the northeast and the Hellmand block (Eurasian plate) to the east (Jackson and McKenzie, 1984; Jackson et al., 1995).

The deformation is distributed on the mountain belts of Zagros, along the southwest part of Iran, of Alborz in the north, and of Kopeh Dagh in the northeast. This deformation is absorbed by shortening, thickening of the crust (mountain belts) and strike-slip motions on major faults (Fig.1-5) bounding the rigid blocks that are relatively aseismic and flat such as the Central Iran block (Great Kavir and Sanandaj-Sirjan Zone), the South Caspian basin and the Lut (Jackson and McKenzie, 1984; Jackson and McKenzie, 1988).

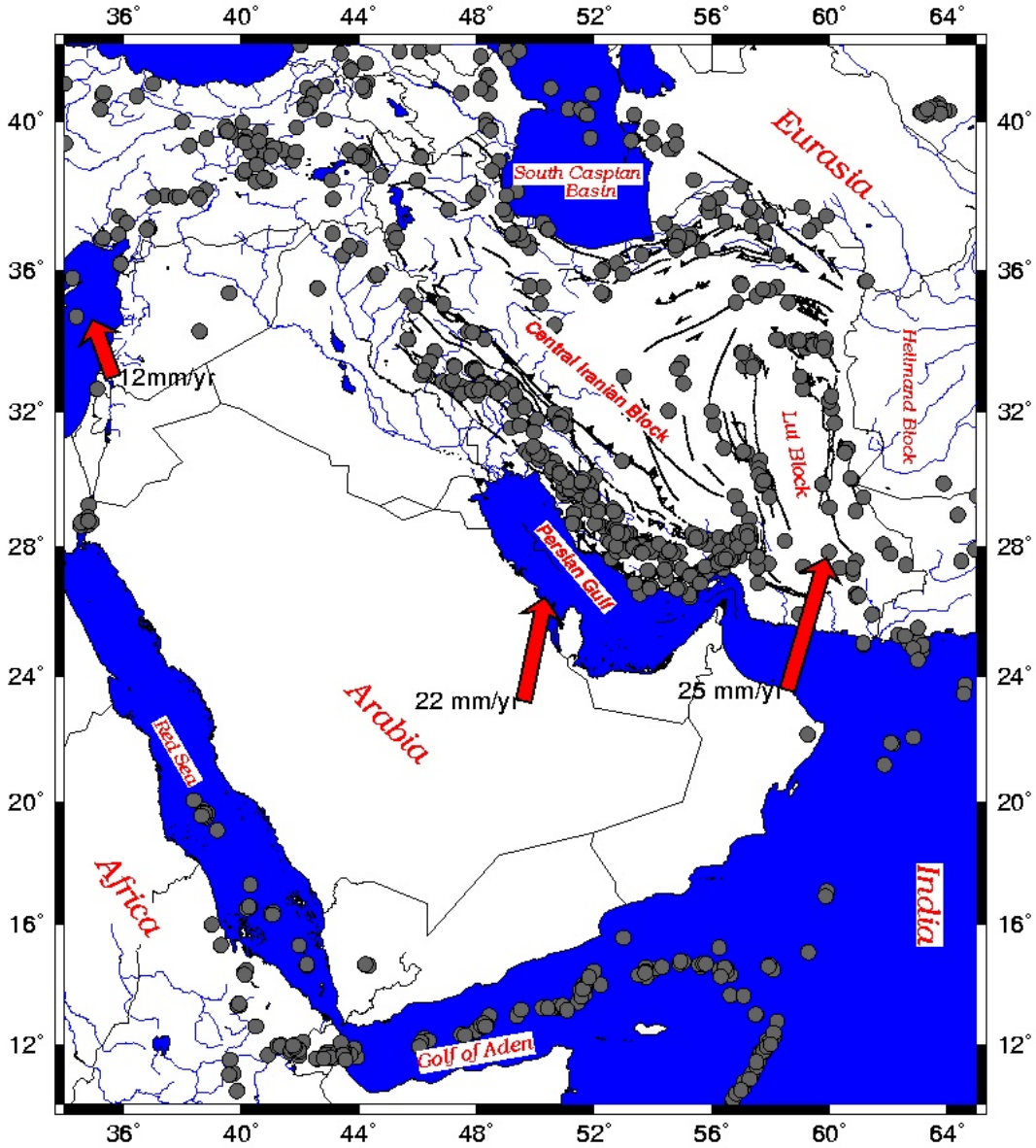

Figure 1-4. Arabian plate convergence toward Eurasia (GPS constrained). The dark grey circles are the seismicity from 1900 through 1999 (Engdahl and Villasenor, 2002). The seismicity in the Red Sea and the Golf of Aden and east of the Arabian plate defines the boundaries between the Arabian, African and Indian plates. These boundaries are very narrow. The boundary with Eurasia, however, is spread throughout Iran.

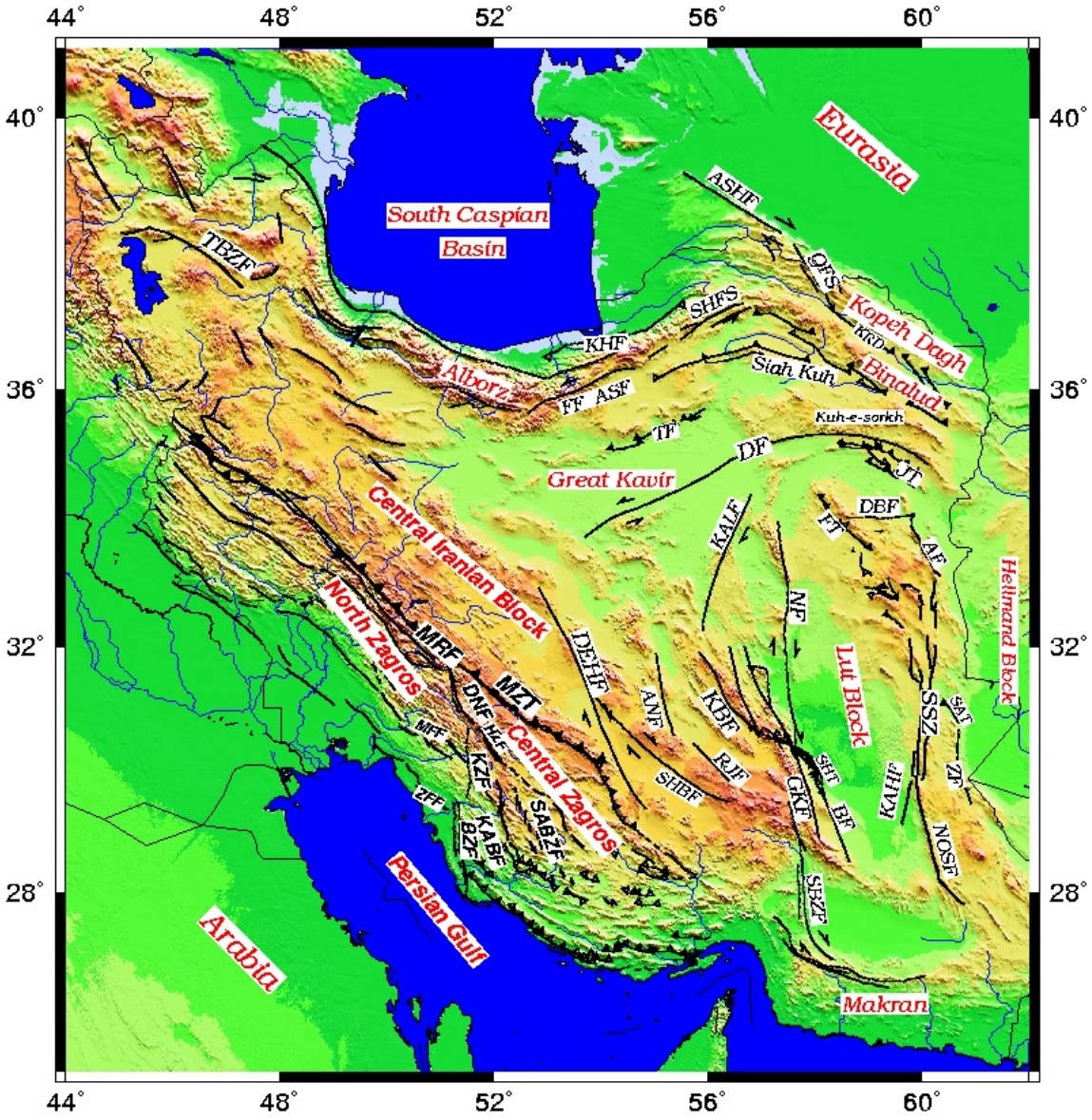

Figure 1-5. Principal faults of Iran: AF: Abiz Fault, ANF: Anar Fault, ASF: Astaneh Fault, ASHF: Ashkabad Fault, BF: Bam Fault, BZF: Borazjan Fault, DNF: Dena Fault, FT: Ferdows Thrust, DF: Doruneh Fault, DBF: Dasht-e-Bayaz Fault, DEHF: Dehshir Fault, FF: Firuzkuh Fault, GKF: Gowk Fault, HZF: High Zagros Fault, JT: Jangal Thrust, KHF: Khazar Fault, KZF: Kazerun Fault, KABF: Karehbas Fault, KAHF: Kahurak Fault KALF: Kalmard Fault, KBF: Kuhbanan Fault, LF: Lakarkuh Fault, MFF: Mountain Front Fault, MRF : Main Recent Fault, MZT: Main Zagros Thrust, NF: Nayband Fault, NOSF: Nosrat Abad Fault, QFS: Quchan Fault system, RJF: Rafsanjan Fault, SAT: Sefid Abeh Thrust, SABZF, Sabzpushan Fault, SBZF: Sabzevaran Fault, SHT: Shahdad Thrust, SHBF: Shahr Babak Fault, SHFS: Shahrud Fault System, SSZ: Sistan Suture Zone, TBZF : Tabriz fault, TF: Torud Fault ZF: Zahedan Fault, ZFF: Zagros Fore deep Fault.

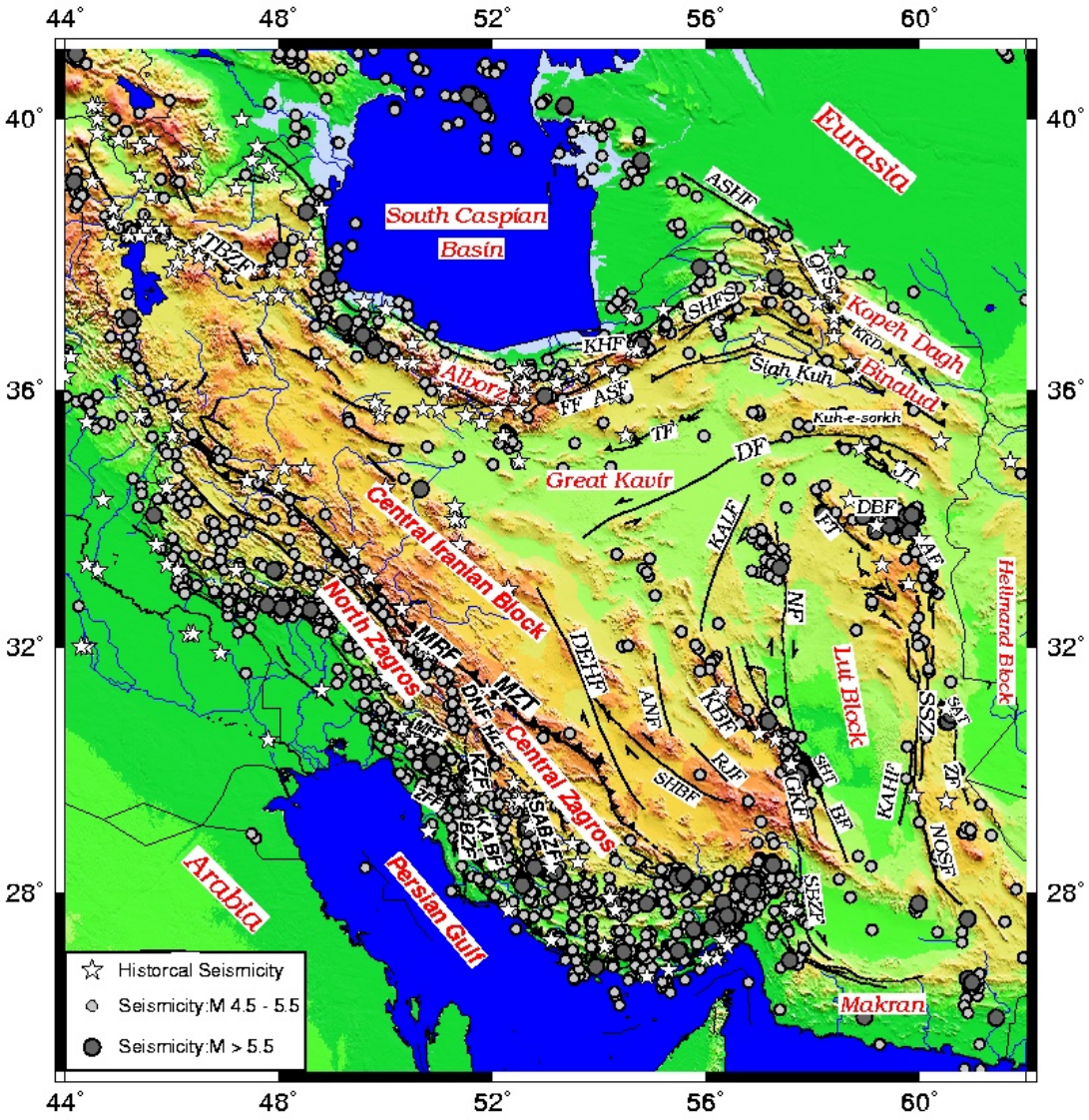

Figure 1-6. Historical and instrumental seismicity of Iran. The black points are the relocated seismicity from *Engdahl et al.* (1998). The stars are historical earthquakes collected by *Ambraseys & Melville* (1982). AF: Abiz Fault, ANF: Anar Fault, ASF: Astaneh Fault, ASHF: Ashkabad Fault, BF: Bam Fault, BZF: Borazjan Fault, DNF: Dena Fault, FT: Ferdows Thrust, DF: Doruneh Fault, DBF: Dasht-e-Bayaz Fault, DEHF: Dehshir Fault, FF: Firuzkuh Fault, GKF: Gowk Fault, HZF: High Zagros Fault, JT: Jangal Thrust, KHF: Khazar Fault, KZF: Kazerun Fault, KABF: Karehbas Fault, KAHF: Kahurak Fault KALF: Kalmard Fault, KBF: Kuhbanan Fault, LF: Lakarkuh Fault, MFF: Mountain Front Fault, MRF : Main Recent Fault, MZT: Main Zagros Thrust, NF: Nayband Fault, NOSF: Nosrat Abad Fault, QFS: Quchan Fault system, RJF: Rafsanjan Fault, SAT: Sefid Abeh Thrust, SABZF, Sabzpushan Fault, SBZF: Sabzevaran Fault, SHT: Shahdad Thrust, SHBF: Shahr Babak Fault, SHFS: Shahrud Fault System, SSZ: Sistan Suture Zone, TBZF : Tabriz fault, TF: Torud Fault ZF: Zahedan Fault, ZFF: Zagros Fore deep Fault.

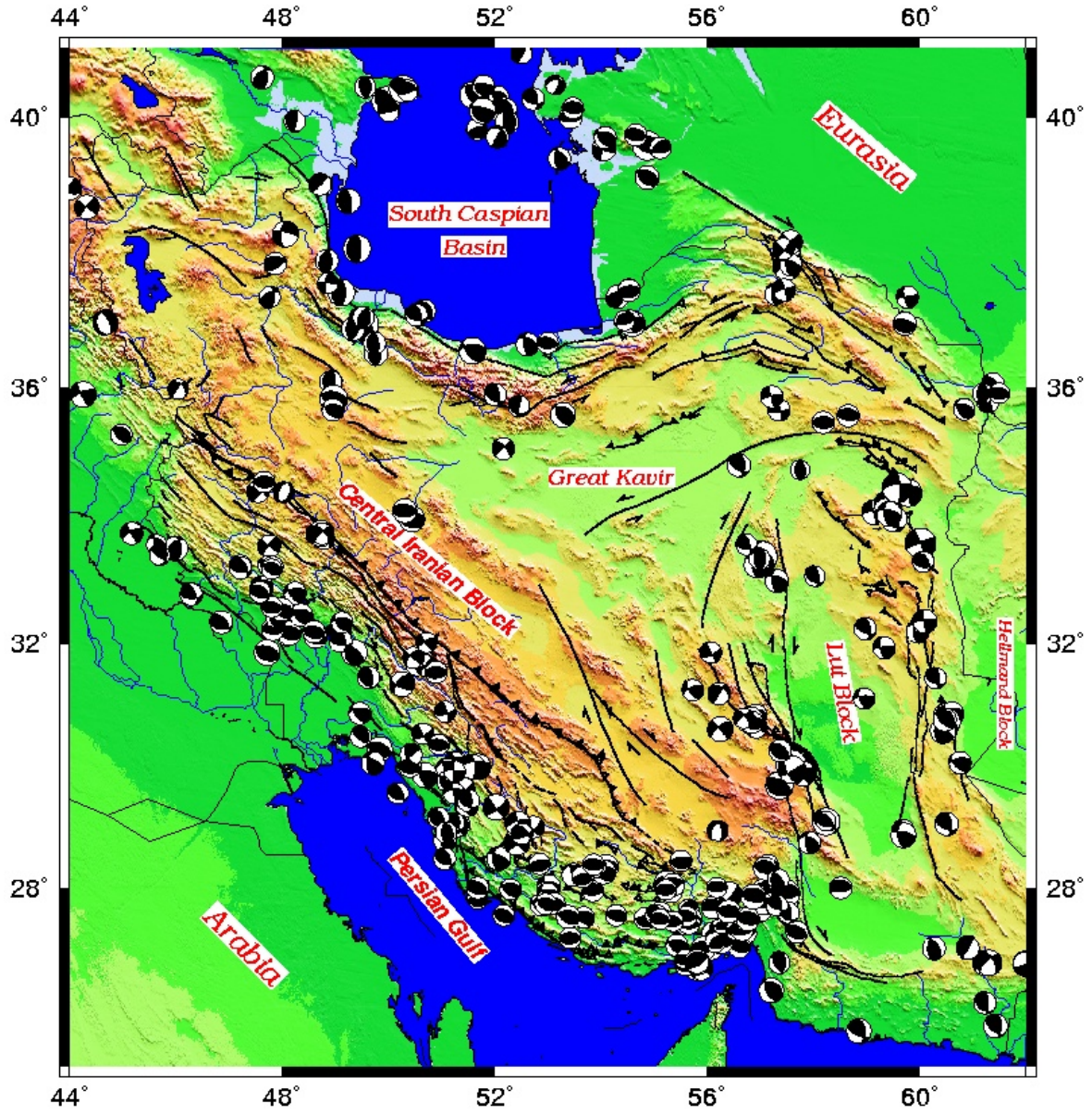

Figure 1-7. Earthquake focal mechanism of Harvard solutions from 1976-2007.

1.2.4 Seismicity of Iran

Several historical and instrumental earthquakes have been recorded in Iran (Fig. 1-6, 1-7) since the seventh century A.D. (Ambraseys and Melville, 1982; Engdahl et al. 1998; Berberian and Yeats, 1999; Berberian, 2005). Many of these earthquakes occurred within the 20th century. There have been roughly 126,000 deaths attributed to 14 earthquakes of magnitude ~7.0 (one every 7 years) and 51 earthquakes of 6.0-6.9 (one every 2 year) that occurred in Iran since 1900. During this period nine cities were devastated (one city every 10 years) (Berberian, 2005).

The earthquakes are closely related to the deforming zones described above. Earthquakes occur mostly in the Zagros, Alborz, Kopeh Dagh mountain belts, in northwest Iran and along the faults surrounding the Central Iran and Lut blocks (Jackson and McKenzie, 1984; Jackson and McKenzie, 1988). But the rate of seismic deformation is not uniform (Jackson and McKenzie, 1998; Masson et al., 2005). Alborz and Central Iran release seismically the total of the deformation whereas only a small amount (15%) is released seismically in the Zagros. Makran suffers of little seismicity along the subduction due to the underthrusting of thick layers of sediments.

1.3 Applications of geodetic techniques to the present day kinematics of Iran

Millimeteric accuracy of GPS allows geoscientists to study tectonic movements (McClusky et al. 2000; Vigny et al. 2002; Reilinger et al. 2006), postglacial uplifts (Sjöberg et al. 2000; Johansson et al. 2002), volcanic-associated deformations (Owen et al. 2000), landslides or subsidence (Motagh et al. 20007) and, in general, to recognize active deforming zones and measure their strain rates.

1.3.1 GPS capacities and applications

GPS (Global Positioning System), together with SLR (Satellite Laser Ranging), LLR (Lunar Laser Ranging) and VLBI (Very Long Baseline Interferometery), are the most precise geodetic measuring tools that up to now have been used for plate tectonics and Earth surface deformation. The advantage of GPS with respect to the other techniques is its simplicity, portability, low cost, all weather ability and precision, which results in GPS dominating the applications of geodesy in crustal deformation monitoring.

Since about 1990, applications of GPS to measure global, regional and local tectonic deformations and fault movements have been continuously increased because of its ability to measure the position and in particular the distance of points on the Earth's surface with precisions of the order of a few millimetres, on baselines of meters to thousands of kilometres. Measurements of relative positions on different dates give the changes in relative positions, which can be converted into relative

velocities or strains (Hoffman-Wellenhof, 2004; Teunissen and Kleusberg, 1996; Leick, 1995; Segal and Davis, 1997).

The nature of GPS measurements allows us to determine simultaneously vertical and horizontal positions, while previously horizontal measurements were often made by geodetic triangulation or trilateration and vertical measurements by precise levelling methods. GPS also does not require inter-visibility between measurement sites, contributing to the largely increased field of applications with respect to classical geodesy.

Velocity fields are usually estimated using GPS data from repeated occupations of the sites. Campaign type GPS is sufficient to determine displacement rates of several mm/yr, assuming constant displacement rates. However, the vertical precision is limited to about 10 mm, in particular due to setup and instrument differences between successive observations. Moreover, correlated noise (long term errors) cannot be detected by campaign type measurements limited to a few days of observations per epoch. More information and therefore a higher precision is obtained by continuous sampling of data from permanent GPS stations over a time span of a few years. Permanent stations obtain a better resolution on the vertical component and are able to resolve non linear displacements (like co- and post-seismic displacements). Permanent stations of the IGS (International GNSS Service) make their data available to complete regional networks (temporary and permanent), in particular to establish an international reference frame. IGS has installed a global network of about 400 GPS stations since 1992 (Beutler et al., 1993, Zumberg et al., 1995). This network is conceived for providing a stable reference frame for local applications, for crustal deformation studies, satellite orbit determination, Earth rotation measurements and atmospheric studies.

A local permanent GPS network has been installed in Japan by the Geographical Survey Institute (GSI) of Japan with about 1200 permanent GPS stations throughout the country (www.gsi.go.jp). The station spacing is about 20 km and the network is used for real-time surveying and research on earthquakes and volcanic eruptions. The National Cartographic Center of Iran (NCC) also has installed more than 100 permanent stations (Fig.1-8) for monitoring fault movements and earthquake research (www.ncc.org.ir). These data are included in our studies to establish a regional reference frame between different campaign measurements.

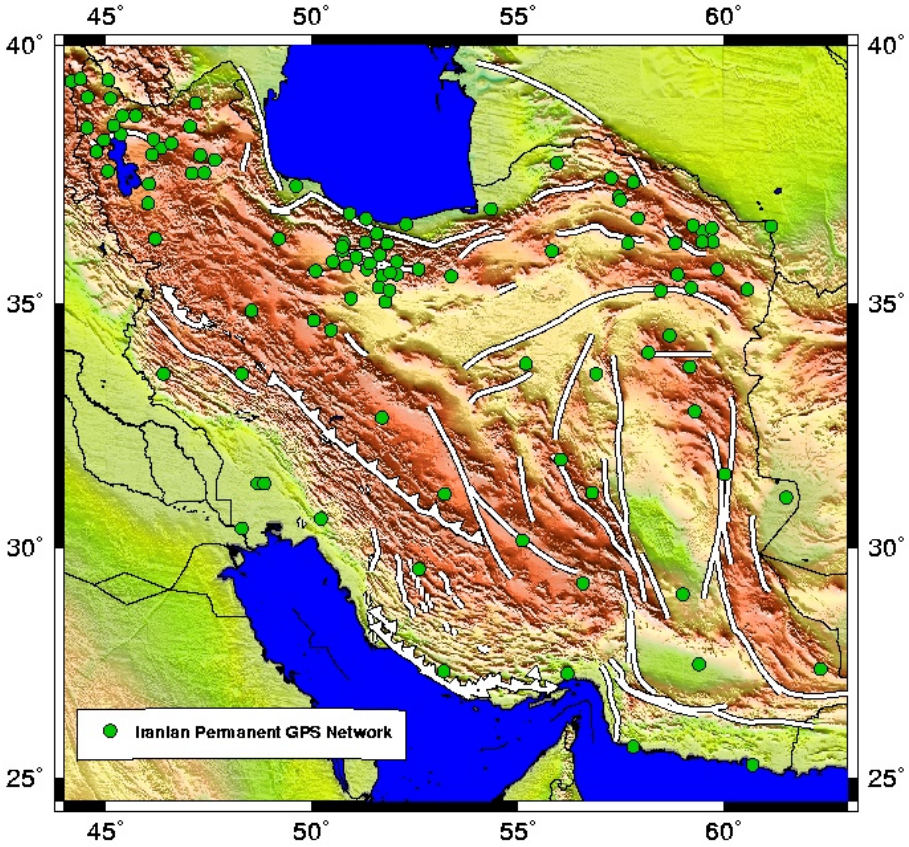

Figure 1-8. Iranian Permanent stations (www.ncc.org.ir). NCC has installed more than 100 permanent GPS stations in Iran. The priority for the site selection was to help evaluating seismic hazard for three populate cities (Tehran, Tabriz and Mashad).

It is usually assumed that the present-day velocities observed by GPS over a few years are representative of the long term velocity field. Presently, more and more quantitative information is available about the velocities of individual faults over different geological time spans, obtained for example by paleoseismology (10 000 yr), dating of geomorphological markers (100 000 yr) and geological research (1 000 000 yr). The comparison of the different time scales is an efficient method to constrain the geodynamical evolution of faults and to better appreciate the present day state for seismic hazard evaluation. Usually, the present-day slip rate determined by GPS is extrapolated back in time until the total geological offset of the fault is achieved. This permits to infer the onset time of faulting. Most often, short-tem geological (over some ka) and GPS slip rates are found to be comparable and provide a similar fault onset (Fig. 1-9, Meyer et al., 2007). Coherent values between

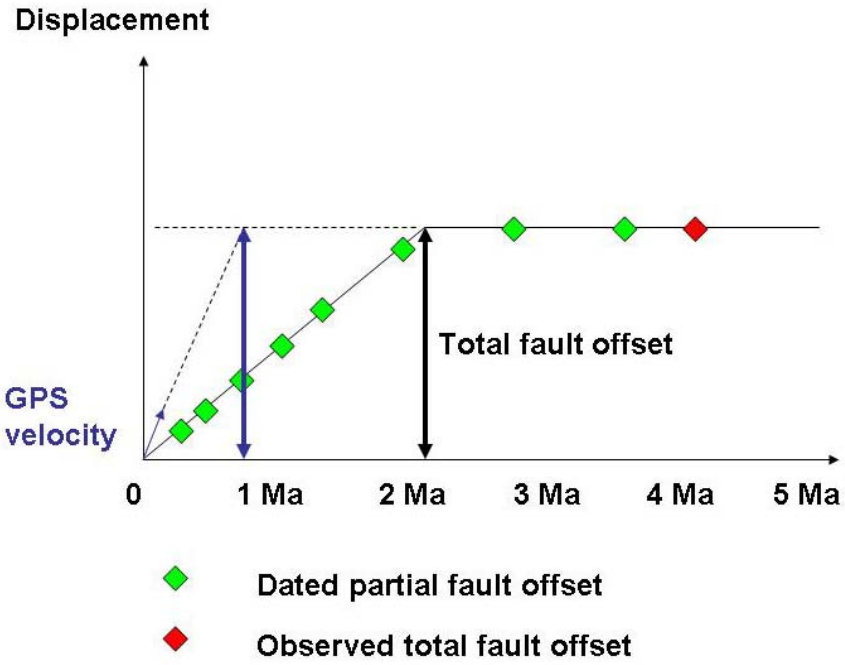

Figure 1-9. Scheme comparing GPS present day velocities and dated geomorphological offsets, combined with total geological slip inferring the fault onset age (from Meyer et al., 2007).

GPS instantaneous fault slip rates and long-term geological slip rates (over some Ma) are often limited to fault slip durations of less than 5 Ma.

Velocity fields and measurements of relative movements and rotations of stable aseismic blocks within deforming continental regions have been significantly refined by GPS (increasing number of points, increasing precision). This has greatly improved our knowledge of regional and local tectonics in and around Iran (McClusky et al., 2000, 2003; Nilforoushan et al., 2003; Vernant et al., 2004, Masson et al. 2007; Tatar et al. 2002; Walpersdorf et al. 2006). Moreover, deformation fields can be characterized by GPS measurements by comparing the obtained velocity field with the motion of a rigid block. This requires a relatively high density of GPS sites (at least 3 per block) but helps distinguishing between two major models of tectonic deformation: Rigid blocks with deformation localized on faults, or distributed deformation throughout wide areas. Cross-sections perpendicular to faults (strike-slip or thrusts) can characterize precisely the deformation field created by the locking of the fault, to constrain the degree of locking and the size of the locked zone.

Comparison of GPS estimated velocities with slip rates caused by earthquakes can show if the cumulating deformation is released in a seismic or aseismic way (Jackson et al, 1995; Masson et al. 2005).

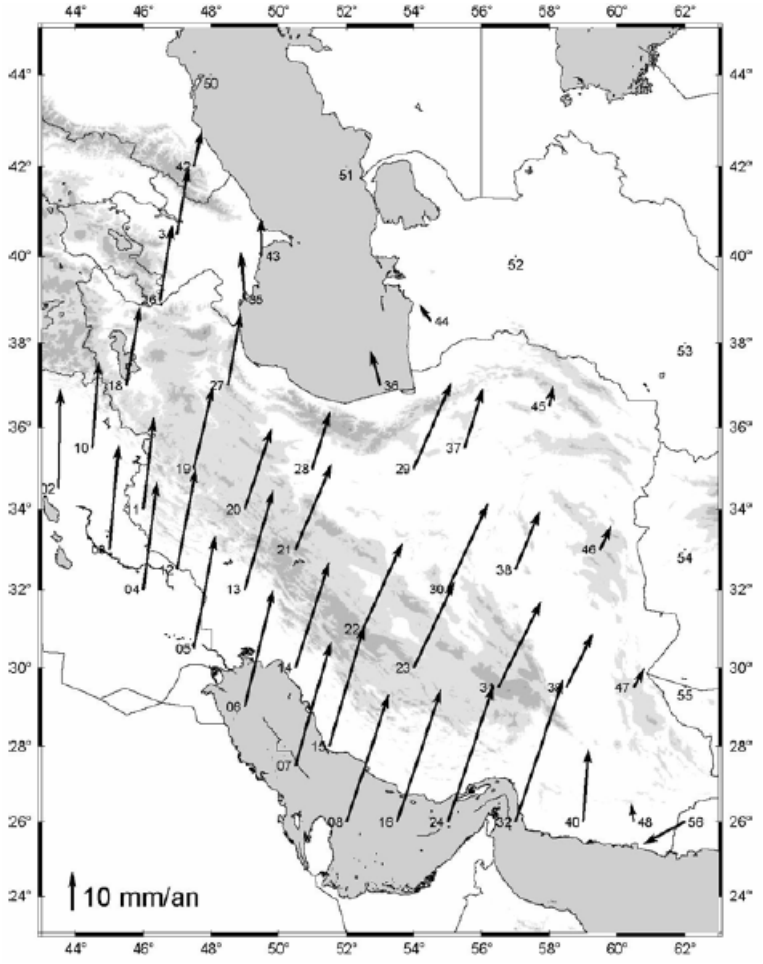

Figure 1-10. Velocity field for Iran estimated from the spatial variation in the strain rates indicated by earthquakes (from Jackson et al., 1995). Velocities are shown relative to stable Eurasia. The overall Arabia–Eurasia convergence is assumed to be close to that of NUVEL1-A (DeMets et al., 1994) and may be overestimated (Sella et al., 2002).

1.3.2 Geodetic results in Iran

The first global velocity field for Iran has been proposed by Jackson et al. (1995). This velocity field (Fig. 1-10) is relative to Eurasia and is computed from the spatial variation in the style of strain rates inferred from earthquakes, combined with the regional constraints imposed by the Arabia-Eurasia collision with velocities according to NUVEL1-A. In order to understand how the deformation is distributed and what are the present-day kinematics of the major faults in Iran we installed several GPS networks in active regions.

The GPS networks established and measured since 1997 and before this thesis have been conceived to provide on one hand a global velocity field, and on the

other hand more detailed kinematics of the deformation zones in the Central Zagros, the Zagros-Makran transition, the Alborz (Central Alborz and Tehran) and in the Tabriz region in northwest Iran.

a. Iran Global Network

A GPS network of 26 sites (Fig. 1-11) was measured in 1999, 2001 (Nilforoushan et al., 2003; Vernant et al., 2004a) and 2005 (Masson et al., 2007). This network gives an overall view of the Iran kinematics (Fig.1-12). The two first measurements in 1999 and 2001 (Nilforoushan et al., 2003; Vernant et al., 2004) show:

- At the longitude of the Strait of Hormuz, the N-S convergence rate between Arabia and Eurasia is 25±2 mm/yr, trending N12°E and at the longitude of Bahrain 22±2 mm/yr, trending N8°E, confirming the lower convergence rate with respect to the predictions of NUVEL1-A, as proposed by Sella et al. (2002). The GPS results defined the Arabia-Eurasia Euler vector of 27.9±0.5°N, 19.5±1.4°E, 0.41±0.1°/Ma (Vernant et al., 2004), close to McClusky et al. (2001 and 2003).
- The velocities relative to Eurasia of the sites located on the Hellmand block at the eastern border of Iran (YAZT and ZABO) are less than 2 mm/yr, which indicates that the Hellmand block is part of Eurasia.
- The stations KERM, HARA, ARDA, SHAH, BIJA and MIAN, covering the Central Iran block, show relative velocities of less than 2 mm/yr. This confirms the rigidity of the Central Iran block as suggested by the lack of seismicity (Jackson and McKenzie, 1984).
- Between the Central Iran block and the Arabian plate, the southeastern part of the Zagros (Central Zagros) accommodates 7±2 mm/yr of N-S shortening. The shortening rate decreases in the northwestern part of the Zagros (North Zagros), and is associated with 3±2 mm/yr of right-lateral strike-slip rate along the Main Recent Fault (MRF), much smaller than geological estimates.
- The Alborz accommodates 8±2 mm/yr of N-S shortening.
- The northern part of Alborz is located on the South Caspian basin, moving roughly northward at 6±2 mm/yr relative to Eurasia. Therefore the shortening rates of the Alborz and the South Caspian basin are consistent with Jackson et al. (2002).
- About 8±2 mm/yr of right-lateral strike-slip motion is expected northwest of Iran on the NW-SE trending Tabriz fault.

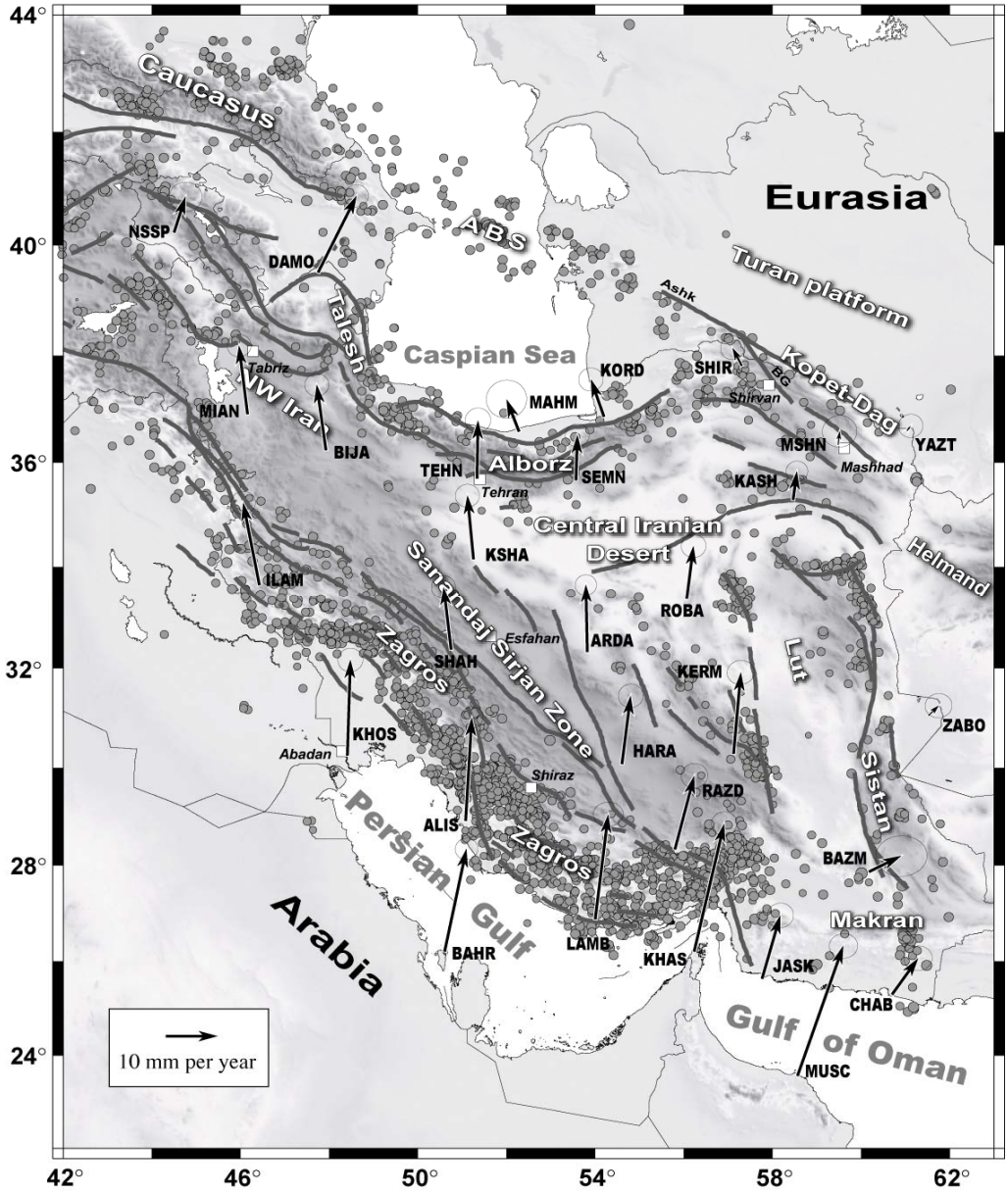

Figure 1-11. GPS horizontal velocities in a Eurasia-fixed reference frame and their 95 percent confidence interval in the Iran Global network (Masson et al., 2007).

- In the east of Iran, most deformation is concentrated in the Makran where the oceanic crust is subducting at 19.5±2 mm/yr roughly northward beneath the Makran belt. Therefore only 6.5±2 mm/yr of shortening takes place in the Kopeh Dagh.
- The shear between the Central Iran block and the Hellmand block is estimated to be 15±2 mm/yr, accommodated on the faults bounding the Lut block to the east and the west.

(Vernant et al., 2004a).

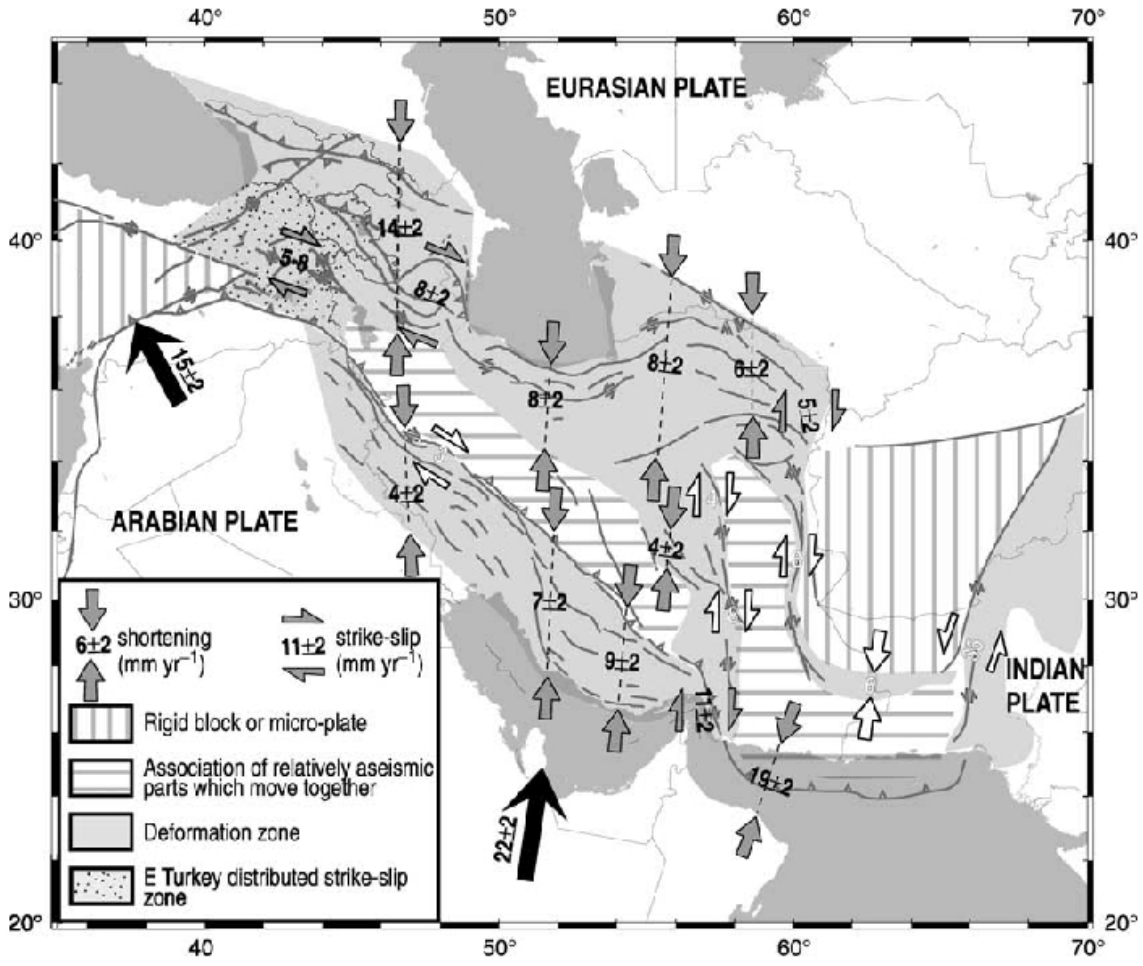

Figure 1-12. Schematic illustration of the main results of the Iran global network studied by Vernant et al. (2004). Hatching shows areas of coherent motion, grey zones are actual deformation areas (see legend). Heavy arrows in black indicate the actual motion of the Arabian plate relative to Eurasia. Grey arrows are deformation rates directly measured by GPS. Rates in Eastern Turkey are deduced by McClusky et al. (2000). White arrows are deduced rates from GPS, geological evidence and seismology. Motion along the Chaman fault and the associated deformation zone velocity is deduced from the REVEL model (Sella et al., 2002) (after Vernant et al., 2004a).

The third Iran Global measurements of 2005 (Masson et al. 2007) refined previous measurements. The improvements are significant in NE Iran. The authors estimated the present-day shortening rate across the mountain belts of NE Iran to 5±1 mm/yr. They proposed 2±1 mm/yr of N-S shortening across the Eastern Kopeh Dagh and 3±1 mm/yr of N-S shortening across the Binalud and Kuh-e-Sorkh.

b. Zagros Networks

The Zagros mountain belt (NW-SE trending) is approximately 1500 km long, 250–400 km wide, and runs from eastern Turkey to the Strait of Hormuz, where it dies out at the Makran subduction zone. This mountain range is the kinematic boundary between Iran and Arabia. The northern boundary of the Zagros is underlined by a large suture, the Main Zagros Thrust (MZT). To the west of the Kazerun fault system, the Main Recent Fault runs parallel to the MZT and accommodates the right-lateral part of the partitioned motion of the Zagros (Tchalenko and Braud, 1974; Ricou et al., 1977).

The Zagros can be divided into two main units: The North Zagros (northwest part of the belt) and the Central Zagros (southeast part of the belt) which are separated by the N-S trending right-lateral strike-slip Kazerun Fault system (Berberian, 1995; Talebian and Jackson, 2004). There are several differences between Central and North Zagros. The width of the belt is smaller in North Zagros. The MRF accommodates the strike-slip component of the partitioned motion related to the oblique plate convergence across the North Zagros. The strike-slip motion is distributed from the single MRF in North Zagros to the Kazerun fault system in Central Zagros. The decoupling Hormuz salt layer is present only in Central Zagros.

Talebian and Jackson (2002) have determined ~50 km of total right-lateral offset on the Main Recent Fault by restoration of drainage patterns, geological markers and geomorphological features, which would indicate a slip rate of 10-17 mm/yr on the MRF assuming that it has been active since 3-5 Ma. The maximum and minimum displacement rates on the fault have been inferred from these offsets by Berberian (1981, 1995), Talebian and Jackson (2002) and Authemayou et al. (2005) to be 17 and 4 mm/yr, respectively. The differences between the different results are probably due to overestimation of the offsets on the faults or underestimation of the date of initial activity of the offsets or non-constant velocity during the deformation.

Because of the salt layers present particularly in the Central Zagros, a decoupling between the superficial layers and the basement is suspected. If this is the case, the Zagros deformation as observed by GPS in the southeastern part, represents only the deformation of the sedimentary cover placed on the top of the Arabian platform.

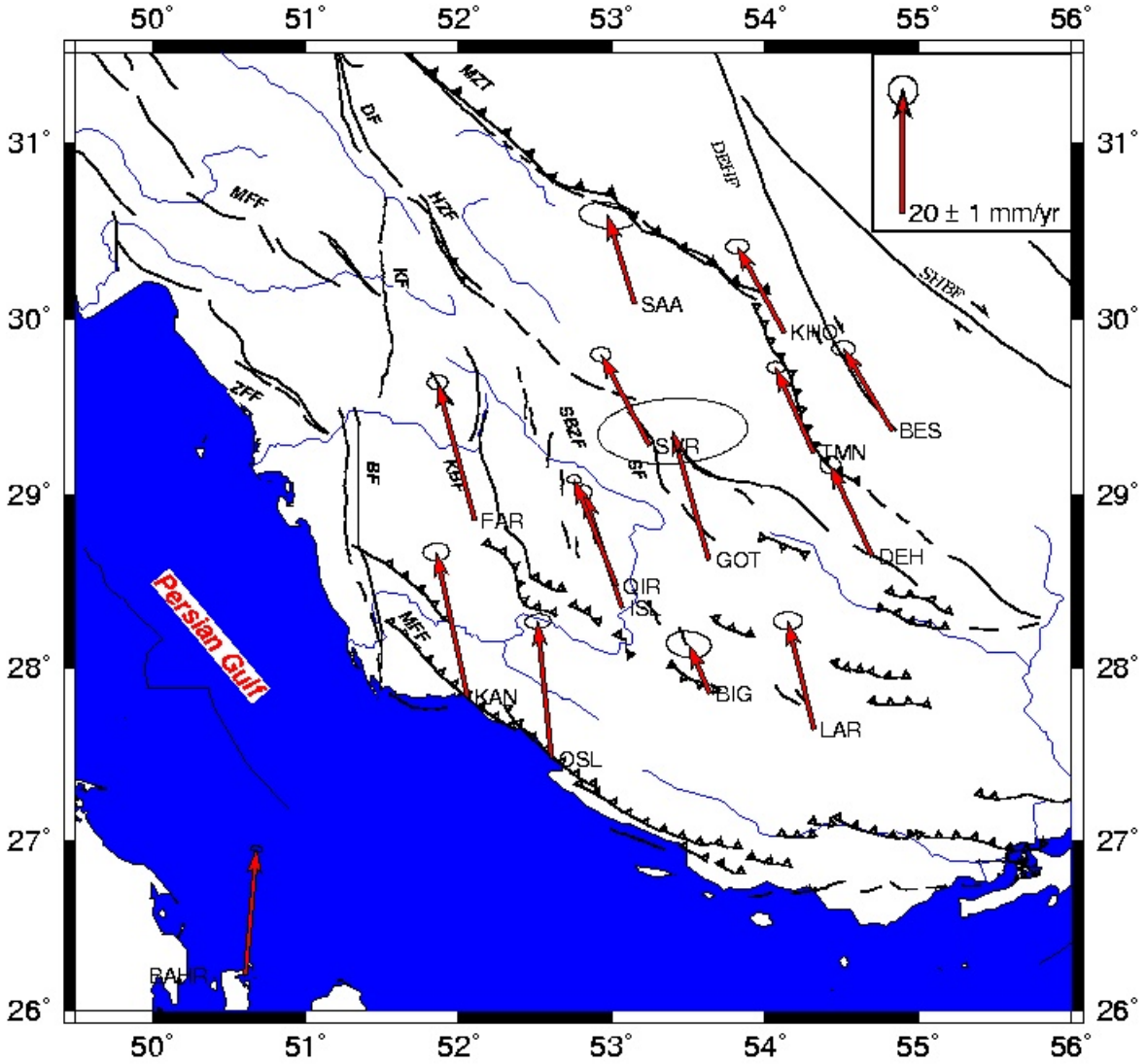

Figure 1-13. Velocity field of Central Zagros sites relative to Eurasia with 95% confidence (Tatar et al. 2002).

In 1997 and in 2000, the first GPS measurements were done on 14 geodetic sites (Fig. 1-13) across the central Zagros mountain belt (Tatar et al., 2002). The results show that about 10 mm/yr of shortening in the central Zagros is distributed across the mountain belt. This shortening corresponds to roughly 50% of the total convergence between Arabia and Eurasia and is consistent in direction. Neither the Persian Gulf nor the Main Zagros Thrust deform significantly.

c. Alborz Networks

The Alborz is a narrow (100 km) and elevated (> 5000m) mountain belt located in northern Iran that wraps around the southern side of the south Caspian basin. The range is actively deforming by range-parallel thrusts and left-lateral strike-slip faults and accommodates the differential motion between the Central Iran block in the south, and the South Caspian basin in the north. Based on a restored cross-section across the range, the total late Cenozoic shortening and left-lateral slip are estimated to be ~30 km and ~30-35 km, respectively (Allen et al. 2003). The deformation in the Alborz mountain belt has started 3-7 Ma ago (Allen et al. 2004). The thrust faults dip toward the interior of the range from both the northern and the southern sides. The major left-lateral strike-slip fault of the Alborz is the Mosha fault which is located in the southeast of the Alborz.

The Alborz region is a populated area and has experienced several destructive earthquakes. This region has a high potential of seismic risk. As Tehran, with 12 millions of inhabitants, is located in the southern domain of Alborz, to study the deformation in this area is very important. Two GPS networks have been established in the Central Alborz and Tehran areas (Vernant et al., 2004b; Djamour 2007 submitted).

c-1. Central Alborz Network:

GPS measurements of 12 geodetic sites in Central Alborz (Fig. 1-14) between 2000 and 2002 have been used to constrain the motion of the belt with respect to western Eurasia (Vernant et al. 2004b). The GPS-derived shortening rate across the range has been estimated to be 5 ± 2 mm/yr at the longitude of Tehran (which is less than the result obtained in the Iran Global network) and the overall left-lateral motion to 4 ± 2 mm/yr (Vernant et al., 2004b). One reliable site's velocity (MAHM) on the Caspian shoreline suggests that the South Caspian basin moves northwest with a velocity of 6±2 mm/yr with respect to western Eurasia.

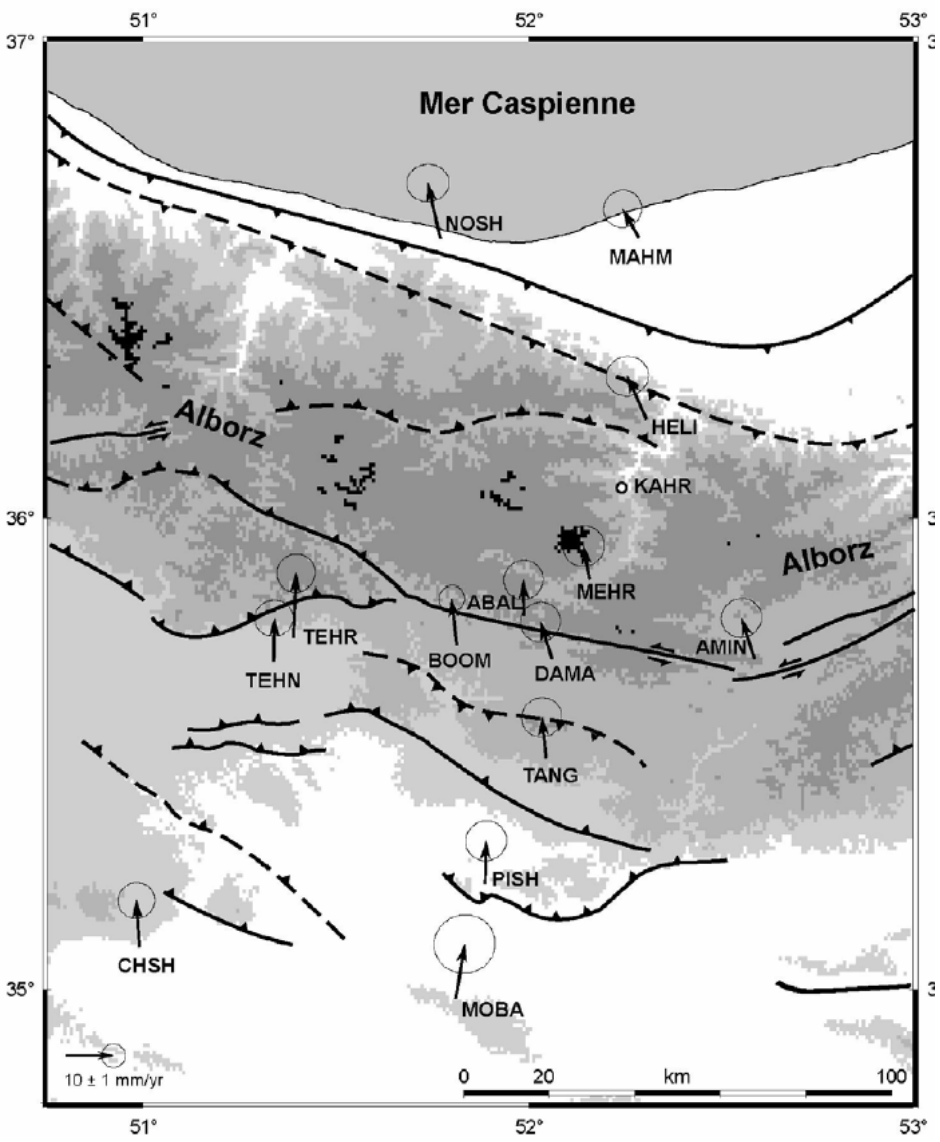

Figure 1-14. Velocity field of Central Alborz sites relative to Eurasia with 95% confidence (after Vernant et al., 2004b).

c-2. Tehran network

The region of Tehran is located in the south of Central Alborz and in the northern part of the Central Iran block. Tehran is surrounded by several faults: The Mosha and the North Tehran faults in the north and the Garmsar, Toroud, Bagh-e-Feyz, Kahrizak, Arad, South Rey and Parchin faults in the south. A GPS network of 41 almost regular spaced points (Fig. 1-15) has been installed in the Tehran region since 2000, extending from the Central Iran block in the south to the central part of Alborz in the north (Djamour et al., 2007, submitted). This network should help to see how the different faults accommodate the deformation. Most of the network sites were measured three times from 2000 to 2005.

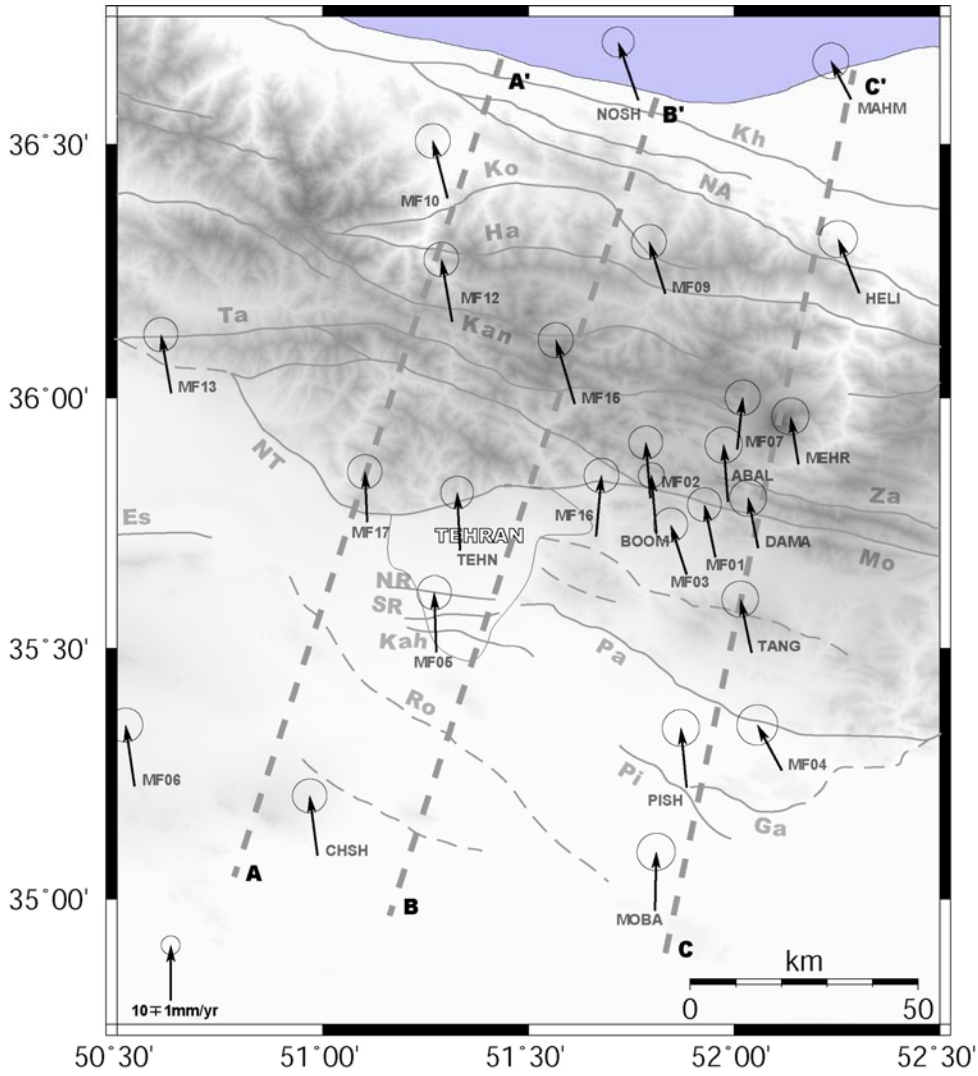

Figure 1-15. Velocity field in the Tehran network relative to Eurasia with 95% confidence interval. The dashed lines are 3 profiles. Faults are NT: North Tehran, MO: Mosha, Pa: Parchin, Ta: Taleqan, Kah: Kahrizak, Ha: Haraz, Kan: Kandovan, NA North Alborz, Kh: Khazar, Fi: Firuzkuh, Es: Eshtehard, NR: North Ray, SR: South Ray, Ko: Kojoor, Za: Zarrin Kuh (Djamour et al. 2007, submitted).

The sites in the northern part of the Central Iran block south of the Alborz mountains have a N-S velocity of ~12.5±2 mm/yr with respect to Eurasia. The velocities of MAHM and KORD at the northern edge of Alborz and situated on the South Caspian basin are ~8.8±2 mm/yr and 8.2±2 mm/yr, respectively, relative to Eurasia in direction of N21W. The estimated velocity for the South Caspian basin is therefore higher than the estimation of Vernant et al. (2004b) (6 mm/yr) and Allen et al. (2003) (5 mm/yr).

Totally GPS velocities confirm the oblique shortening across Alborz, consisting in 1.5±2 mm/yr of range-parallel left-lateral strike-slip and 4.7±2 mm/yr of SW-NE

shortening. To the north, the Khazar and North Alborz faults accommodate 3.2±2 mm/yr of shortening between the South Caspian basin and the internal zone of the central Alborz. To the south, a shortening of 1.5±2 mm/yr is suggested along the North Tehran fault zone and the southeast Garmsar, Pishva and Parchin fault system. 1.5±2 mm/yr of left-lateral motion has been observed on the Mosha fault. Ritz et al. (2003) estimated about 2mm/yr of horizontal slip rate along the eastern Mosha fault over the Holocene.

e. Northwest Iran Network

According to the results of the Iran Global network (Vernant et al., 2004a) the north component of the GPS velocities (relative to Eurasia) decreases from south to north at the longitude of Tehran (51°E). But in NW Iran this is not the case. The velocities increase again north of the Sanandaj-Sirjan zone (the Central Iran block), Indicating significant strike-slip motion on the Tabriz fault and extension in the Talesh plateau. The Tabriz fault is the main tectonical feature of NW Iran having experienced several destructive earthquakes. In order to precise its present-day activity and to better localize extension within Talesh, a GPS network of 19 points has been established in NW Iran (Fig. 1-16, Masson et al., 2006). This network has been surveyed three times in 2002, 2003 and 2004. The analysis of the measurements shows that the deformation in NW Iran is characterised by ~8 mm/yr of right-lateral movement on the Tabriz fault. Hessami et al. (2003) estimated Horizontal slip rates of 3.7-4.0 and 3.1-6.4 mm/yr for north Tabriz fault on the basis of faulted anthropic features and on offset drainages, respectively.

NNE-SSW Extension of a total of ~8 mm/yr is observed north and south of the Talesh block. This extension is observed from Armenia to the Alborz and probably results from the northward subduction of the south Caspian Basin beneath the northern Caspian and the greater Caucasus along the Apsheron sill. This questions the dominating role of the Arabian indenter driving Iranian tectonics.

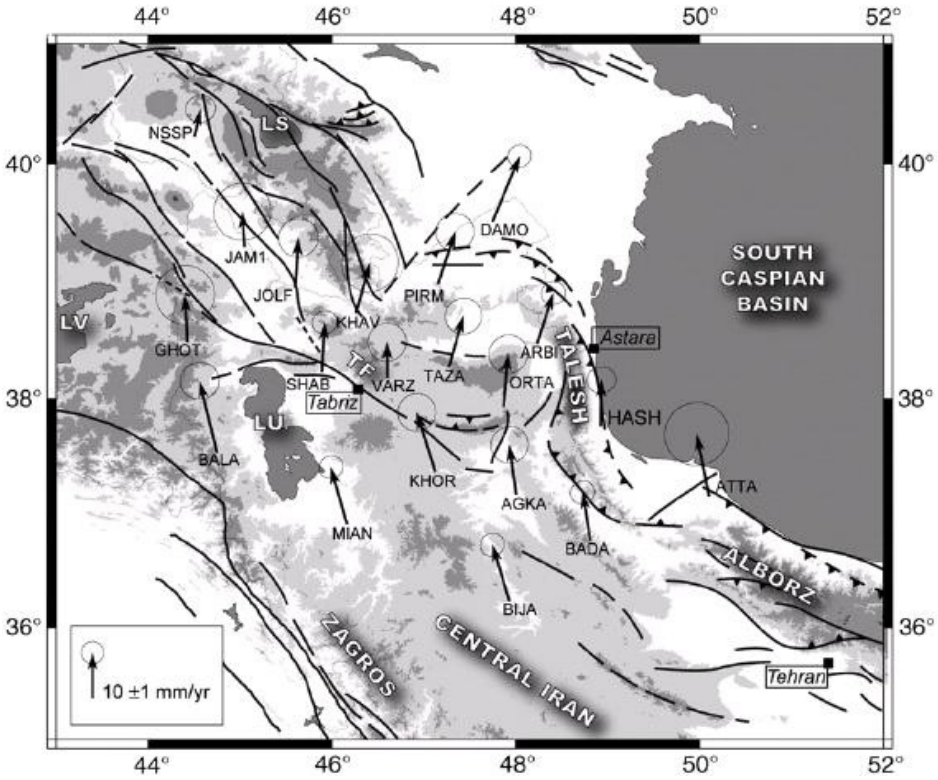

Figure 1-16. Velocity field of NW Iran with respect to Eurasia with 95% confidence interval. LU = Lake Urumieh, LV = Lake Van, LS = Lake Sevan, TF = Tabriz Fault. Shaded area indicates the Talesh block. Faults are drawn from Karakhanian et al. (2004) west of Tabriz, Jackson et al. (2002) in the Talesh and Ritz (2006) in the Alborz (from Masson et al., 2006).

f. Zagros-Makran Network

The Strait of Hormuz (Bandar-Abas) is considered as a transition between the Zagros collision and the Makran oceanic subduction. The Zagros-Makran network (Fig. 1-17) was measured in 2000 and 2002 to better understand the distribution of the deformation between the collision zone and the Makran subduction (Bayer et al., 2006). The GPS velocities show that the transfer of the deformation is mainly accommodated along the NNW–SSE-trending reverse right-lateral Zendan–Minab–Palami (ZMP) fault system at a rate estimated to be 10 ± 3 mm/yr near the faults.

Assuming that the ZMP fault system transfers the motion between the Makran and the Arabian plate, the measurements show a transpressive displacement of 15 mm/yr of dextral strike-slip and 6 mm/yr of shortening. The N–S Jiroft–Sabzevaran (JS) fault system prolongates southwards the dextral shear motion of the Nayband–Gowk (NG) fault system at an apparent rate of 3.1 ± 2.5 mm/yr (Bayer et al., 2006). Based on Geological offsets and ages the strike-slip rates associated with the

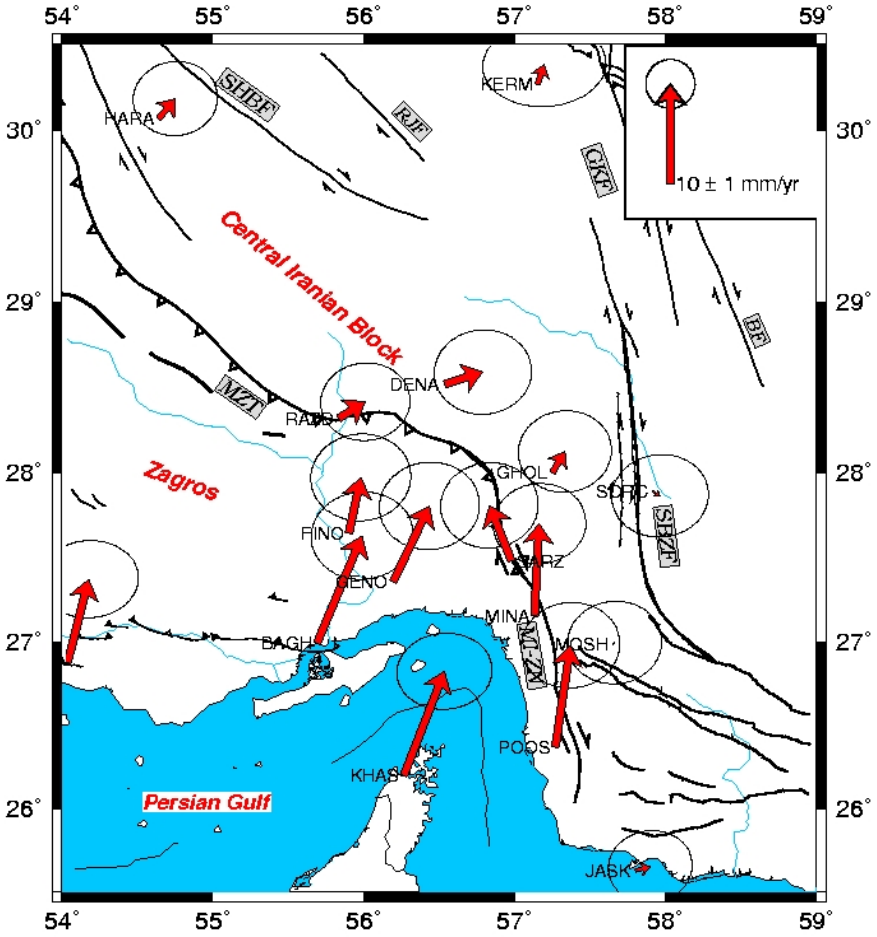

Figure 1-17. GPS horizontal velocities of Zagros-Makran Transition zone(in Central Iran fixed reference frame) and their 95 per cent confidence ellipses estimated from GPS data collected during the 2000 and 2002 campaigns. JS: Jiroft Sabzevaran fault system; BF: Bam Fault, GKF: Gowk Fault, MI-ZN Minab–Zendan fault system, MZT: Main Zagros Thrust, RJF: Rafsanjan Fault, SBZF: Sabzevaran Fault, SHBF: Shahr Babak (Bayer et al., 2006).

Minab–Zendan and the Sabzevaran–Jiroft fault systems are calculated to be 5.1 ± 1.3 or 6.6 ± 1.5, and 6.2 ± 0.7 mm yr−1, respectively (Regard et al., 2005).

1.4 Objectives

Previous studies have given a first view of the Arabia-Eurasia convergence that is accommodated by continental deformation over the Iranian territory. This convergence is 22 mm/yr at the longitude of ~51°E. The deformation is distributed over different regions of Iran and absorbed by several strike-slip and reverse faults. The deforming zones surround several blocks which are aseismic and flat and experience little deformation. These aseismic blocks are the South Caspian basin, the Central Iran block and the Lut block.

In the west of Iran, the Arabia-Eurasia convergence results in continental collision absorbed mainly in the Zagros (8 mm/yr) and the Alborz (4 mm/yr) mountain ranges and by the South Caspian Basin (8 mm/yr). In the east of Iran, the plate convergence results in the Makran subduction. This part of Iran accommodates about 19 mm/yr of shortening associated with very low seismicity. In the northeastern part, the remaining shortening is absorbed by the Kopeh Dagh, and the eastern Alborz faults.

The Central Zagros and the Zagros Makran transition zone, NW Iran and the Alborz as well as Iran on a global scale have been studied by dedicated GPS networks. Open questions on Iranian kinematics concern especially north-eastern Iran, the Kopeh Dagh and the Lut block, and the Zagros in its full extension, including North Zagros and the Kazerun fault system. So we designed and implemented several networks in these regions for the following reasons:

We want to

a) Study how the shortening and deformation are distributed in these regions;
b) Know the velocity and kinematics of the different faults and thrust belts;
c) Determine the different blocks bounded by faults and also estimate the strain and rotation rates;
d) Compare the GPS velocities with geological and tectonical estimates;
e) Model the kinematics of the regions and the fault.
f) Identify the active tectonic features / quantify the present day velocities to

- Validate/refine available tectonical models

- Provide significant present day rates to compare to long term rates from geology, paleo-seismology and tectonics for geodynamics

- Constrain seismic hazard

g) Understand deformation mechanisms:

- Zagros: Difference between Central and North Zagros deformation, partitioning in NZ, decoupling in CZ, role and present day mechanism of the Kazerun fault system at the transition between the two parts of Zagros

- NE Iran: Distribution of shear on both sides of the Lut block, transfer from NS oriented right-lateral strike-slip faults to EW oriented left-lateral strike-slip faults, identification of rotating rigid blocks, transfer of shear to Kopeh Dagh, driving mechanism of Kopeh Dagh deformation

Chapter 2 GPS Measurements

2.1 Introduction

Geodesy is the science which deals with measuring the size and shape of the Earth and its variations in time (e.g. Vanicek and Krakiwsky, 1986). Geodetic tools are used for many applications. We are interested in the use of geodetic tools for the measurement of the Earth's crustal deformation to understand the kinematics and dynamics of the Earth's crust and lithosphere. For example, the measurement of ground deformation caused by active faults is a direct way to observe and understand the different stages of the earthquake cycle (interseismic period, co-seismic and post-seismic periods from continuous measurements during an earthquake).

The application of geodetic tools to crustal deformation monitoring returns to more than a century ago when a triangulation network was established in Sumatra, Indonesia, for studying crustal deformations (Müller, 1895). In the late 1800s, several triangulation networks have been established along the California coast (Bowie, 1924, 1928; Feigl et al., 1993). Generally, the tools that were used in triangulation are confined to theodolites, tapes and levels. Since the Second World War the electronic distancemeter was added. In the late 1970s the Very Long Baseline Interferometery (VLBI), Satellite Laser Ranging (SLR) and Lunar Laser Ranging (LLR) started to be applied in large scale plate- and crustal-deformation monitoring. Beside these techniques, the geodetic Global Positioning System (GPS) revolutionized in many ways the geodetic observations applied to geodynamics and crustal deformation. Primarily, GPS started in 1978 for military navigation applications. Soon after, GPS opened an important vision of accurate positioning in civil applications. Nowadays, millimeter positioning accuracies are accessible due to improvements in the data analysis software (algorithms), hardware of GPS receivers and antennas, and the measurement techniques and strategies.

There are two ways to collect GPS data for the use in deformation studies. GPS measurements are collected either in field campaigns (survey mode), in which a network of sites is established in the study area and measured during several days depending on the required precision and the distance between the sites, or by continuous (permanent) arrays designed to continuously track ground motion over a

long period of time. Field campaigns allow the user to survey many stations with a limited number of receivers which were relative expensive until recent years. Campaign sites have relatively few constraints for their emplacements (bedrock and open view), so that the area can be monitored with high spatial resolution. On the other hand, the data are timely sparse and campaign mode observations assume measuring linear displacements. Often the time resolution is not sufficient to detect non-linear ground motion. Also small offsets due to different antenna types or differences in set up between successive measurements increase the positioning error. This leads in particular to a very poorly constrained vertical component (more than three times worse than the horizontal components). Continuous GPS overcomes these problems by providing continuous position time series without changing the antenna setup over long periods of time. These continuous observations enable us also to identify the noise characteristics in GPS measurements which have been indiscernible in campaign measurements over only a few days. Also the vertical positioning precision can reach significant values for crustal deformation studies from continuous GPS measurements.

In the following sections we are going to discuss different campaign networks which have been established in Iran and their measurement method, and then we will describe the processing strategy of the data and the analysis of the positioning results. These results will be presented as coordinate time series and linear velocities for each station. Finally, we discuss the transformation of the velocity vectors into appropriate reference frames.

2.2 GPS data collection

2.2.1 Network conception

Our objective is to determine the kinematics of the faults in the active deformation areas of the Zagros, the Kopeh Dagh and the surroundings of the Lut block. Actually, with our campaign mode measurements, we try to measure the linear interseismic motions on the faults.

According to the elastic half space models, there is little ground motion between two stations at a small distance of each side of a locked fault during the interseismic period. However, far away from the fault, the full differential motion between the two

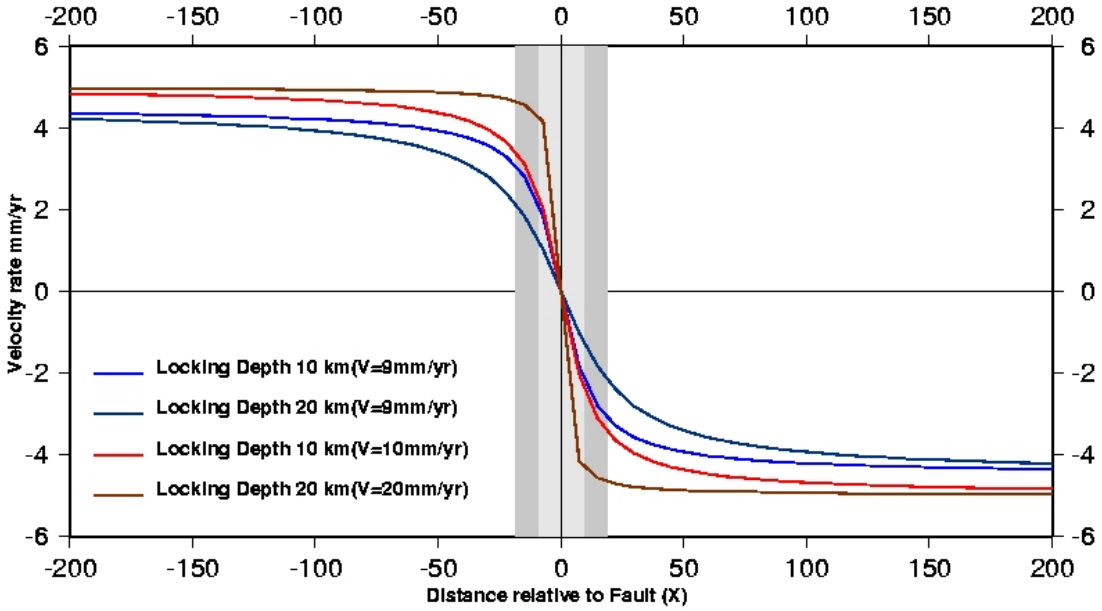

Figure 2-1. Distribution of velocities on a cross section perpendicular to a fault. Two locking depths (10 and 20 km) and two total velocities (9 and 10 mm/yr) are presented. The grey band indicates the region at distances x<d from the fault where the velocities are significantly lower than the total fault velocity

tectonical units separated by the fault can be observed. Close to the fault, the lithosphere also moves at a steady rate below the locking depth of the fault. Savage and Burford (1973) have described this phenomenon by a model presented in Fig. 2-1 according to the following equation:

$$V(x)= V_O/ л * \tan^{-1} (x/d)$$

In this model, V is the strike-slip velocity on a profile across the fault, V_O is the total far field slip rate, x is the distance from the fault trace and d is the locking depth, corresponding to the thickness of the brittle layer of the lithosphere. Considering this model, 50% of the motion of the fault are recovered at the distance of x=d from the fault trace.

The locking depths of the Iranian faults are between 10 and 20 km, according to the thickness of the brittle, seismogenic layer (Engdahl et al., 1998). So for the planning of our network we considered our station emplacements to be more than 10 km away from the faults to observe most of the total fault velocity.

In the networks covering the Zagros we tried to install one GPS site to each side of the known major active faults to measure the individual fault rates. In eastern Iran we also tried to resolve the rotation of micro blocks, which needs several GPS

sites per block. In most cases, two sites per micro block have been realized, and densifications are still foreseen.

2.2.2 Site monumentation

In order to eliminate the antenna centering errors in our measurements, we used metal forced centering benchmarks with an adaptor to install the antenna on top of the benchmark. The 150 mm long bold mark is ending in a screw and is anchored completely inside the bedrock. For the measurements, a 144 mm long adaptor is screwed on the benchmark, and the GPS antenna is screwed on the adaptor (Fig. 2-2).

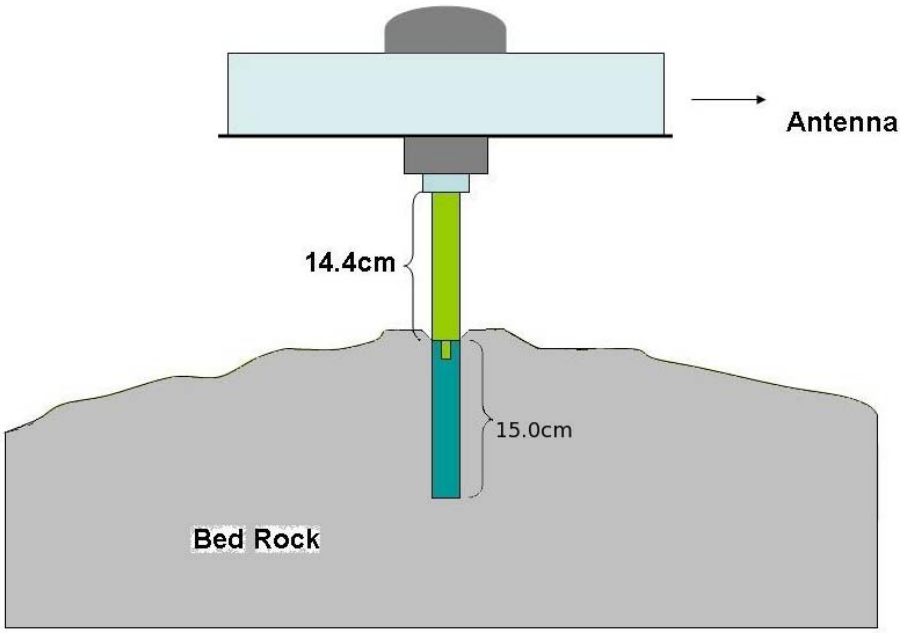

Figure 2-2. Forced centering antenna adapter used in GPS campaign measurements.

We tried to find bedrock outcrops for all of our stations to be sure that the measurements are not affected by monument instabilities or local surface movements. In places where we could not find any bedrock we constructed pillars anchored to the ground or we used the existing benchmarks of the National Cartographic Center (NCC). The pillars (Fig. 2-3) have a forced centering observation platform and are concrete structures with foundations of a volume of 1.5*1.5*1.5m,

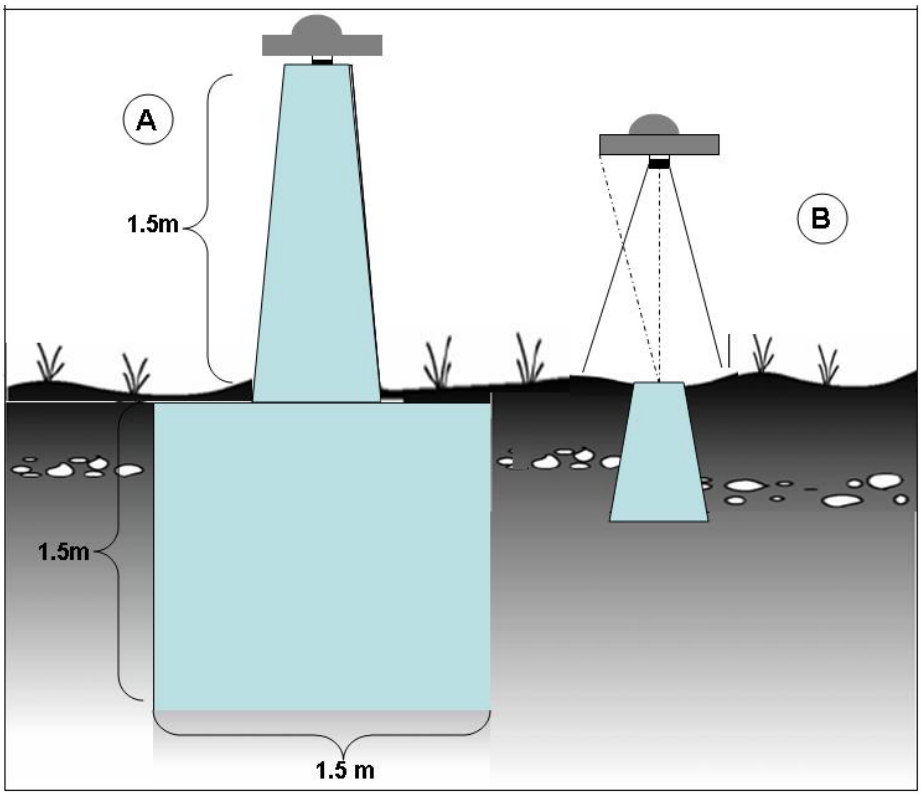

Figure 2-3. Forced centering antenna pillar and tripod set up on the benchmark used in GPS campaign measurements.

and 1.5 m height above the ground surface. These pillars have been constructed several years ago for the Iran Global network and for the Asian Pacific measurements. Therefore we can suppose that the pillars are stabilized by now and that their displacements show the tectonic motion without side effects.

For some stations with classical benchmarks (metal bold mark with point or cross on the top) or for the sites where the forced centering bench mark has been destroyed during the measurement interval but the hole in the rock is still preserved, we used tripods with optical and mechanical centering (Fig. 2-3). During the measurements we fixed the legs of the tripod with plaster.

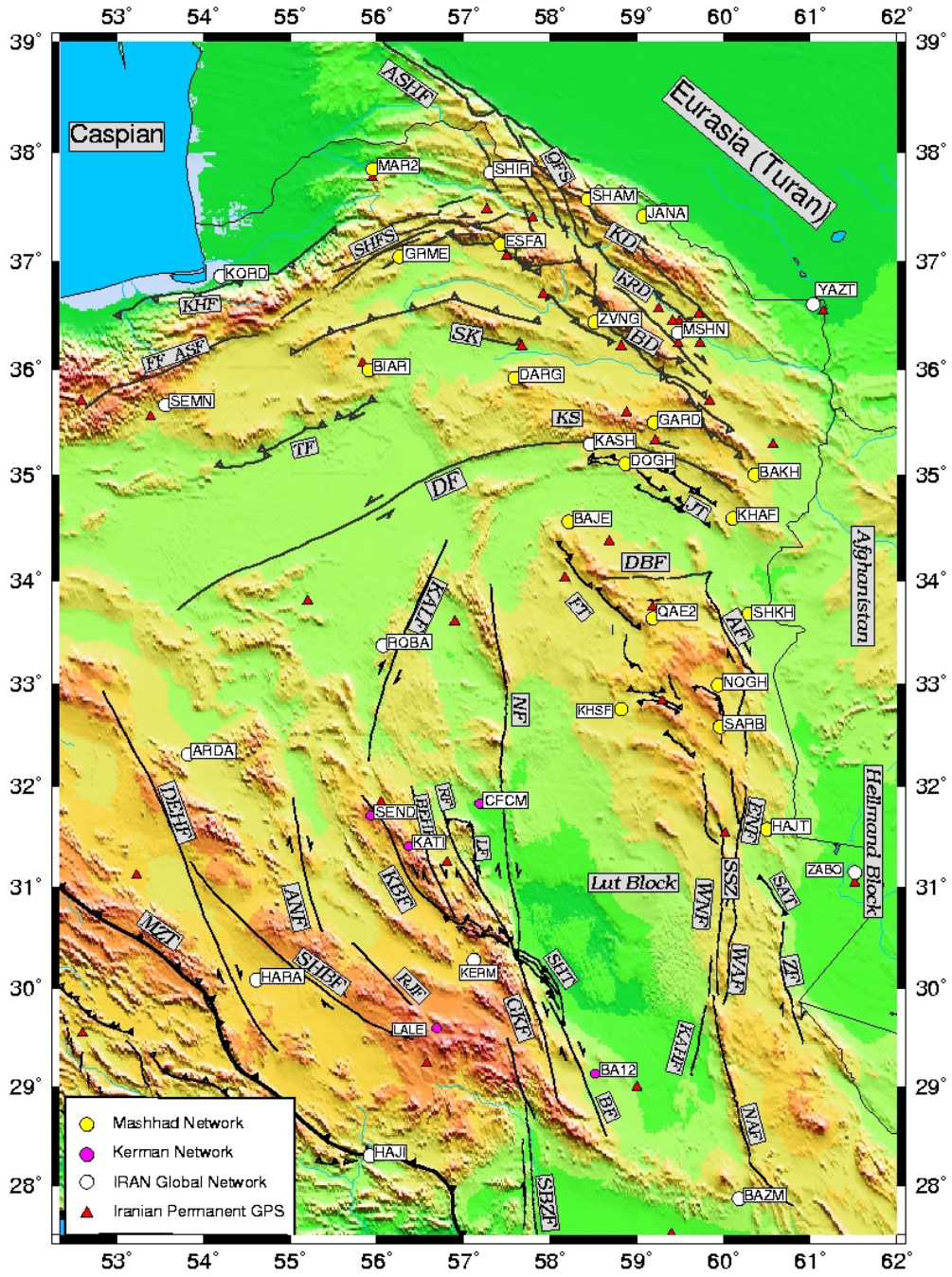

Figure 2-4. Distribution of stations of the Mashhad, Kerman and Iranian Permanent GPS networks.

2.2.3 Established Networks

2.2.3.1 Mashhad Network

A geodetic network of 12 benchmarks (Fig. 2-4) has been established in 2004 in the Khorasan province in NE Iran and some parts of the Sistan and Balochestan provinces in the east of Iran. These sites are SHAM, JANA, GRME, GARD, DARG, BAKH, MAR2, KHAF, DOGH, QAE2, BAJE and NOGH. The network was completed

with the 6 sites YAZT, KORD, SHIR, KASH, ROBA, ZABO belonging to the Iran Global network (Nilforoushan et al., 2003; Vernant et al., 2004) which have been measured several times before the Mashhad measurements. The type of monumentation for each station is indicated in Table 2-1.

Table 2-1. Type of Monumentation and name of the networks involved. Adaptor is a screw marker and BM is a classical bench mark.

Site	Pillar	Adaptor	BM	Network
SHAM		●		**Mashhad**
JANA		●		**Mashhad**
GRME		●		**Mashhad**
GARD		●		**Mashhad**
DARG		●		**Mashhad**
YAZT			●	**Iran Global**
BAKH		●		**Mashhad**
MAR2	●			**Mashhad**
SHIR			●	**Iran Global**
KORD	●			**Iran Global**
KHAF		●		**Mashhad**
DOGH		●		**Mashhad**
QAE2		●		**Mashhad**
BAJE		●		**Mashhad**
NOGH		●		**Mashhad**
KASH	●			**Iran Global**
ROBA	●			**Iran Global**
ZABO	●			**Iran Global**

The Mashhad network covers Kopeh Dagh, Binalud and the east Alborz mountains in NE Iran, the Sistan suture zone and the left-lateral Doruneh and Dasht-e-Bayaz faults. In the following we distinguish the northern part of the Mashhad network covering the Kopeh Dagh and call this part the Kopeh Dagh network.

The Mashhad network was densified by 6 stations (ESFN, BIAR, ZVNG, SHKH, HAJT, SARB) in 2005. The network was measured in 2004, 2006 and the densified stations were measured in 2005 during the Iran Global network re-measurements. As we have only one measurement epoch for the densification stations we can not yet calculate velocity estimations for them. In the first epoch measurements in 2004, each station of the network was measured at least for 48 hours between Julian days 186 and 194. In each session we used 7 GPS receivers (Trimble SSI and Ashtech ZXII with choke ring antennas). The collection of the data was done at a rate of 30 seconds. The cut off angle of the receivers was set to measure the satellites down to 10° over the horizon. We have included 6 Iranian permanent (continuous) GPS stations: AHVA, TEHN, PLOR, TABZ, MSHN and HAMD. To strengthen the reference frame and to strengthen the network with more baselines and proper orbit adjustment, we included data from 35 GPS stations of the International GNSS Service (IGS) network in our analysis data. These globally distributed stations (Fig. 2-5) are ALGO, ANKR, ARTU, BAHR, BAKO, FORT, GOLD, GRAZ, HRAO, IRKT, KERG, KOUR, LHAS, MAS1, MATE, MBAR, NICO, NKLG, NSSP, OHI2, POL2, POTS, RAMO, SANT, SELE, TIDB, TSKB, VILL, WSRT, WTZR, WUHN, YAR2, ZECK, ZIMM, and ZWEN.

In the measurement campaign of 2006 (Julian days 174 - 181) we used 7 receivers in each 48 h session, and we used the data of 23 Iranian permanent stations. The number of Iranian permanent stations strongly increased since 2004 where only 6 permanent stations have been available. We also added the data of 24 IGS stations in each session. The IGS stations are ALGO, ARTU, BAHR, GOLD, GRAZ, GUAM, HRAO, IISC, IRKT, KERG, KIT3, KOUR, MAS1, POL2, POTS, TIDB, TSKB, VILL, WSRT, WTZR, WUHN, YAR2, ZECK, and ZIMM.

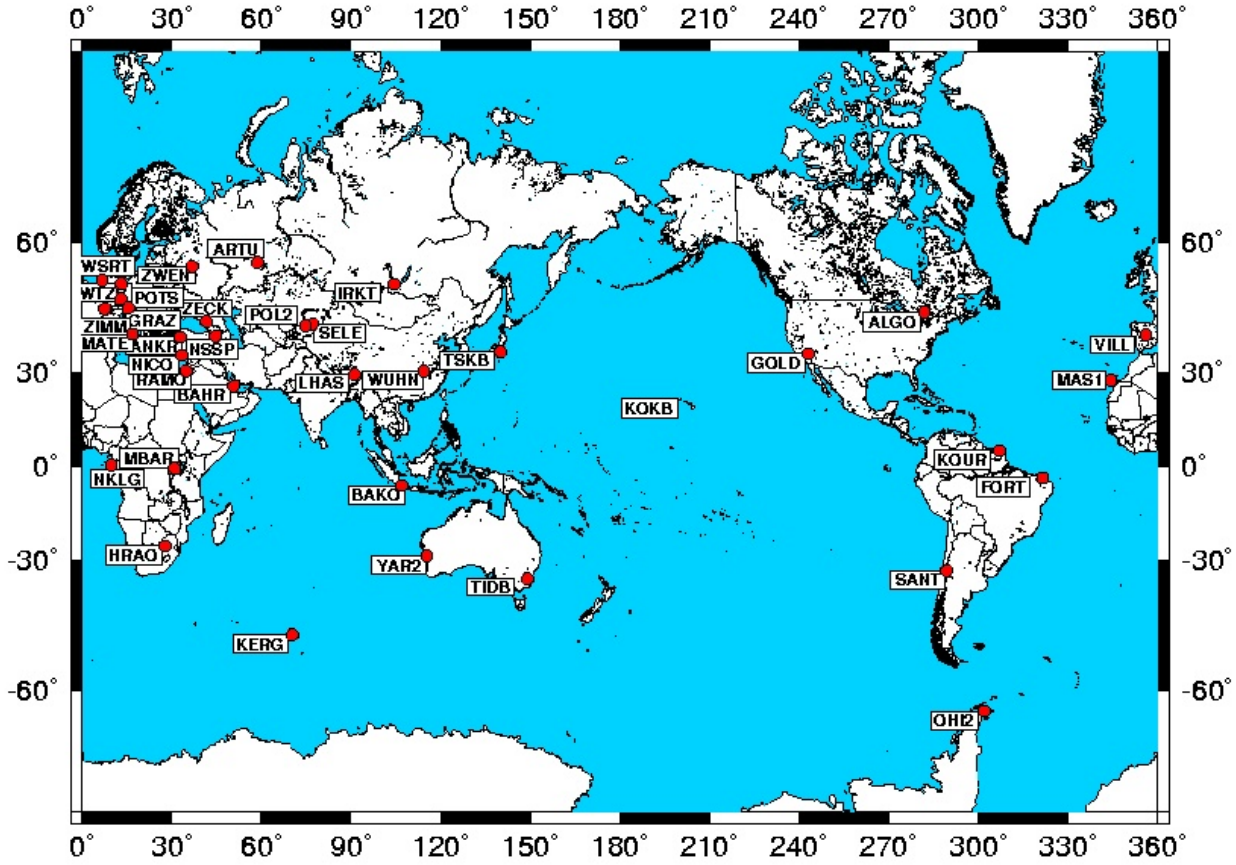

Figure 2-5. Distribution of IGS stations which have been used in the Mashhad network measurements.

2.2.3.2 Kerman Network

In 2003, before the Bam earthquake on 26th of December, we installed 5 benchmarks around the Kuhbanan, Lakarkuh, Nayband, Gowk and Bam faults (Fig. 2-4). These sites are SEND, KATI, CFCM, LALE and BA12. LALE is on the Hezar mountains and BA12 is located east of the Bam fault, on the rigid Lut block. Except CFCM, all stations were installed with forced centering bold marks far enough (≥ 10 km) from the faults to avoid contamination of the rigid block motion due to the locking of the fault. We could not find any proper bedrock around the Nayband fault so we selected a Precise Leveling Network benchmark (CFCM) which has been installed in 1996. This benchmark is a cylinder of re-enforced concrete with a diameter of 60 cm and a depth of one meter. We used a tripod for the measurements of this point.

Up to now, the network has been measured three times, in January 2004, December 2004, and February 2006. The measurement settings are like for the Mashhad network, with a 30 second measurement interval, and an elevation cut off

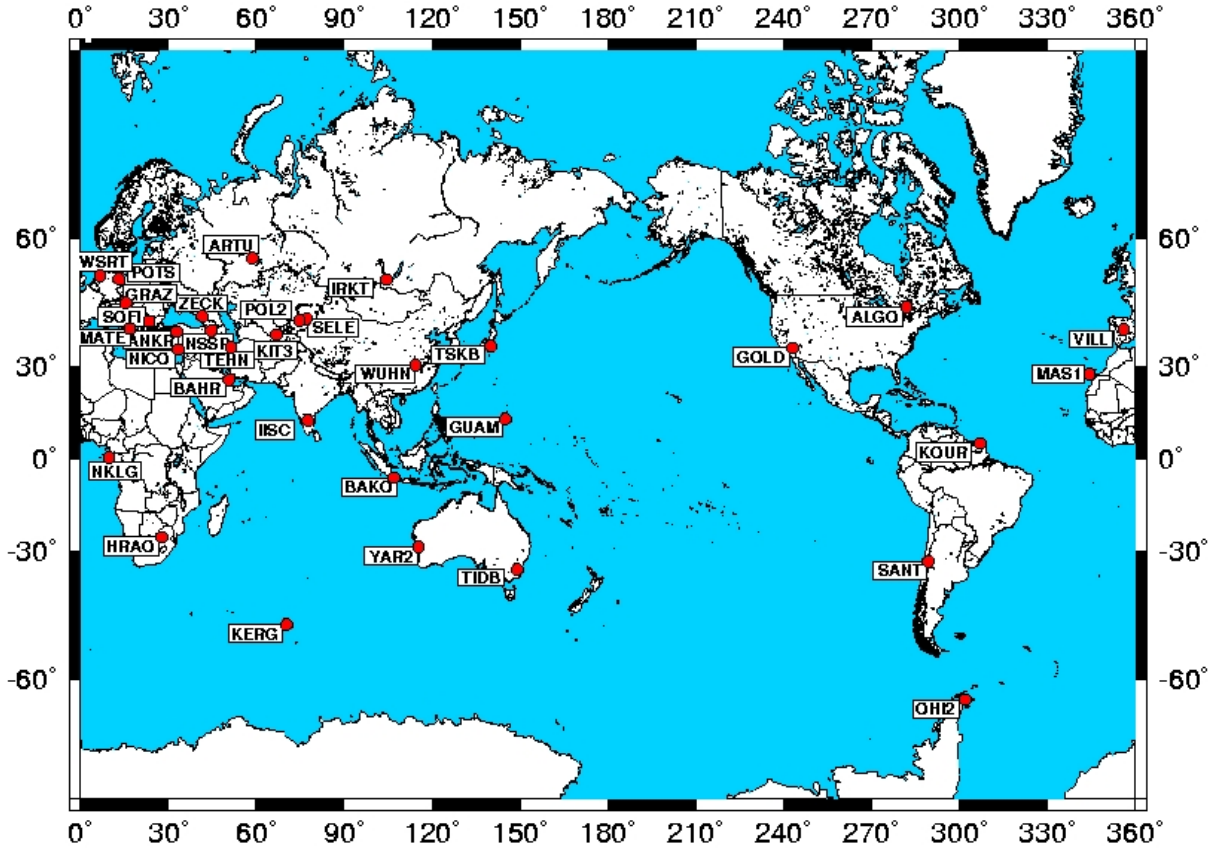

Figure 2-6. Distribution of IGS stations which have been used in the Kerman measurements.

angle of 10°. In the measurement campaigns of January and December of 2004 we have included the ROBA, KERM, HAJI and ZABO stations from the Iran Global Network, and AHVA, MSHN and TABZ from the Iranian permanent network. We have added the data of 33 IGS stations in the analysis: ALGO, ANKR, ARTU, BAHR, BAKO, GOLD, GRAZ, GUAM, HRAO, IISC, IRKT, KERG, KIT3, KOUR, MAS1, MATE, NICO, NKLG, NSSP, OHI2, POL2, POTS, SANT, SELE, SOFI, TEHN, TIDB, TSKB, VILL, WSRT, WUHN, YAR2 and ZECK (Fig. 2-6).

After the 2003 Bam earthquake, a dedicated GPS network of 25 sites was installed around the Bam and Gowk faults to measure post-seismic deformation (the Bam post-seismic network). It has been measured 5 times from January 2004 to 2006. We have used some of these stations with reliable results to add information on the western Lut block.

For the campaign in 2006 we measured the KERM and ZABO stations from the Iran Global network and included 25 Iranian permanent stations AHVA, BABS, BAFT, BIJD, BOJD, GONA, HAMD, ILLM, KADN, KALT, KRAD, KSHM, FARM, MSHN, NISH, PLOR, QAEN, QUCH, SABZ, SARK, SHRZ, TABZ, TEHN, THED,

TORQ, and 21 IGS sites BAHR, BAKO, FORT, GOLD, GRAZ, GUAM, HRAO, IISC, KERG, KIT3, KOUR, MAS1, NICO, POL2, POTS, TEHN, TIDB, TSKB, VILL, WSRT and WUHN.

The Iran Global benchmarks included in our Kerman network have well constrained velocities because they have been measured several times during the different surveys of the Iran Global network (Nilforoushan et al., 2003; Vernant et al., 2004), but also during the Mashhad (Kopeh Dagh) and Bam network measurements.

In 2006 we have densified the network in the Kerman/west Lut area with 20 sites. These stations have been measured only at one epoch. Therefore, we do not have velocity estimates for the 20 new stations.

2.2.3.3 Zagros Networks

We have measured three GPS networks in Zagros (Fig. 2-7), the Central Zagros network with 15 stations covering the southeast of Zagros, the North Zagros network with 18 stations covering the northwest of Zagros, and the Kazerun network with 11 stations covering the Kazerun fault system and its associated NNW trending strike-slip faults (Tatar et al., 2002; Walpersdorf et al., 2006; Tavakoli et al., 2007). The Kazerun network is located between the Central and North Zagros networks. For all measurements, Trimble SSI and Ashtech ZXII receivers have been employed with choke-ring antennas for multi-path protection. Elevation cut off was chosen at 15° except for the last North Zagros measurement in 2005. The measurement interval was always 30 sec. Each station was measured at least for 48 hours in each campaign, except for the first Central Zagros measurements. For each campaign, 6-8 rowing receivers were available and occupied the sites in 2-3 successive sessions. Generally, 2-3 sites were measured continuously (mostly the Iran Global sites included in the campaign) to establish the tie between each session. Data from three to eleven Iranian permanent stations (AHVA, AHVZ, CHSM, HAMD, ILLM, KRAD, MSHN, PLOR, SALF, TABZ and TEHN) were used in the campaign analyses as soon as they were available.

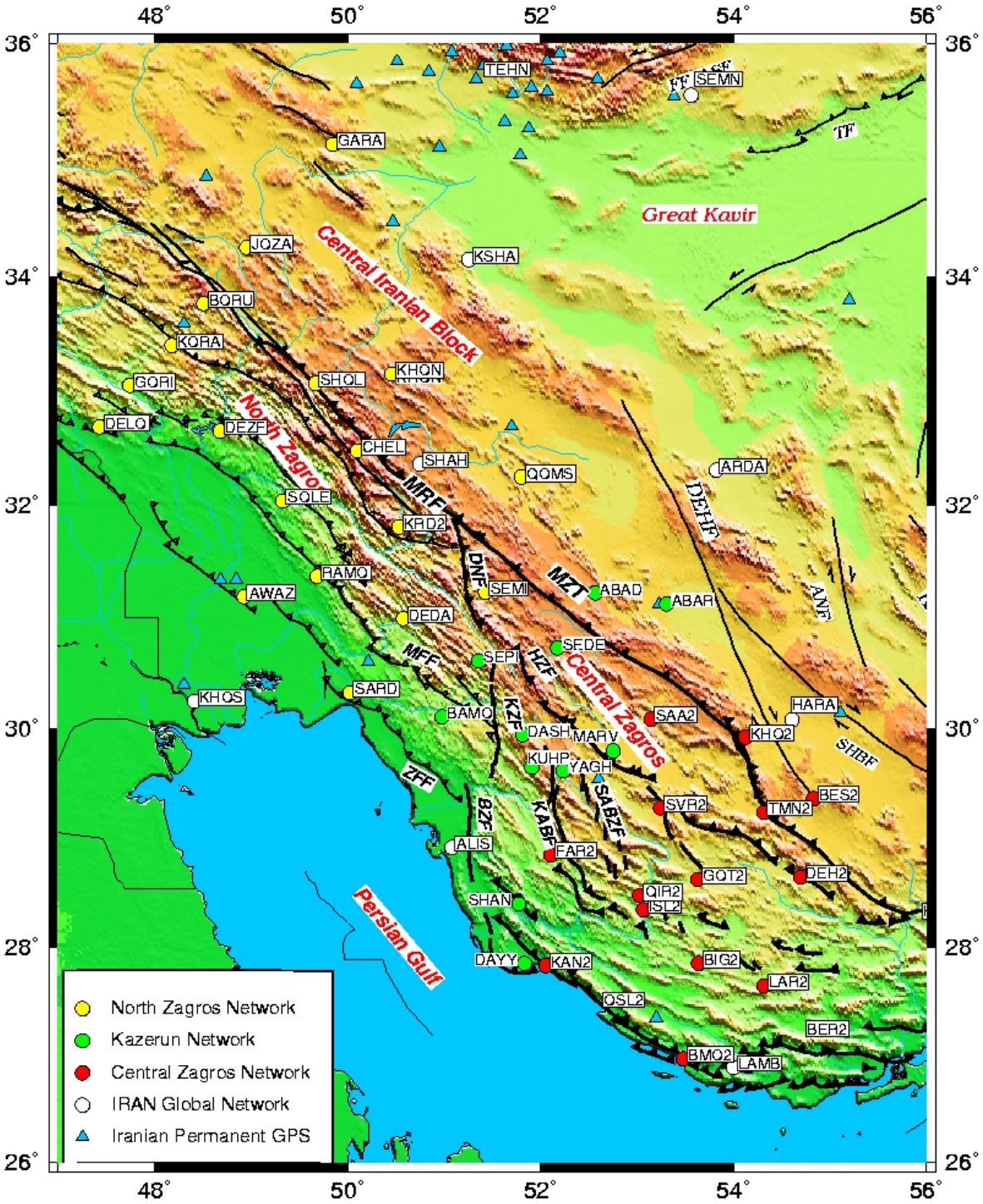

Figure 2-7. Distribution of GPS sites in the North Zagros, Central Zagros and Kazerun and Iranian Permanent networks.

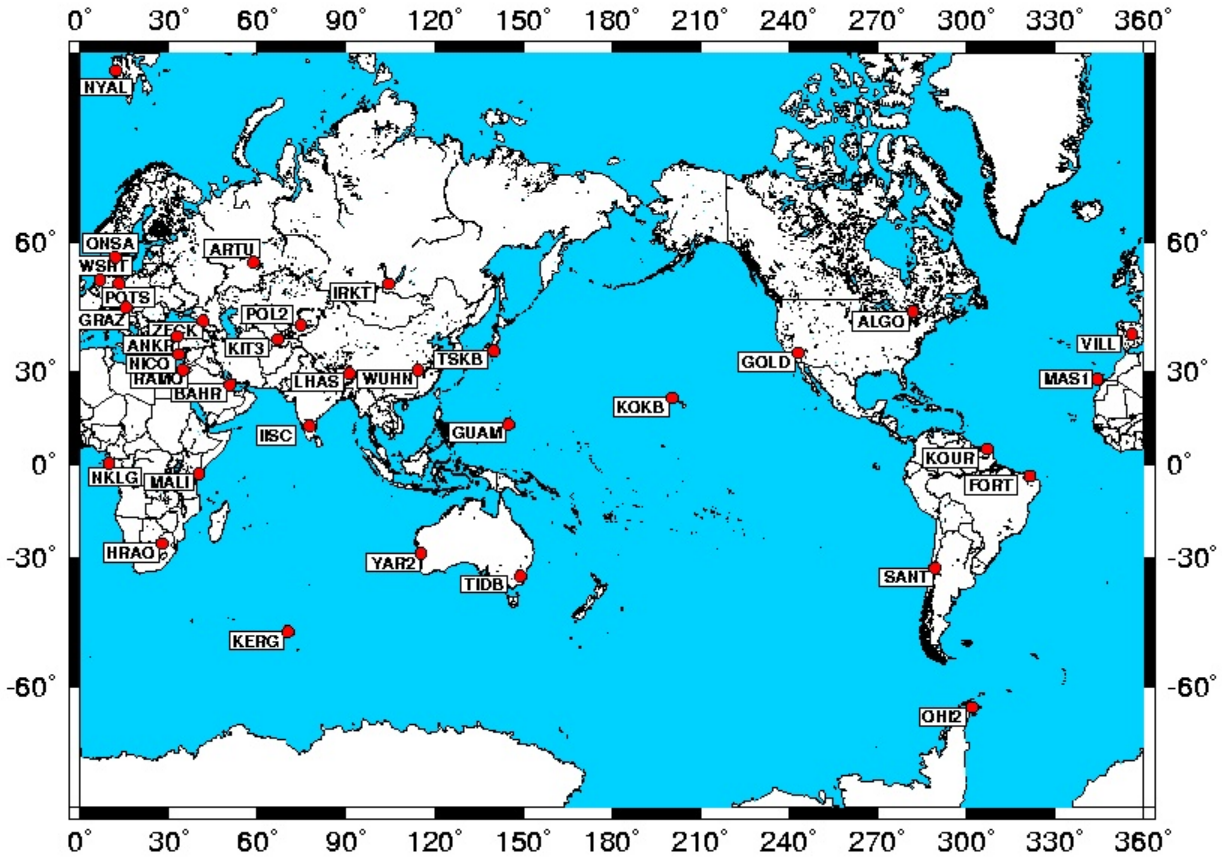

Figure 2-8. Map of the IGS stations which have been used in the Zagros networks.

The Central Zagros network is the first GPS network measured for geodynamic purposes by NCC. The measurement campaigns took place in 1997, 2000 and 2003. The 15 stations of the network (BES2, BIG2, BER2, BMO2, BMG2, DEH2, FAR2, GOT2, ISL2, KHO2, KAN2, LAR2, OSL2, QIR2, SAA2, SVR2, TMN2) are monumented by classical benchmarks (simple bold marks to be measured with tripods and optical antenna centering). During the 2003 measurements, the Iran Global stations ALIS, ARDA and LAMB have been included in the Central Zagros network.

The North Zagros network has been installed and measured in 2001, and re-measured in 2003 and 2005. The 18 stations of North Zagros are: AWAZ, BORU, BAMO, BORU, DEDA, DELO, DEZF, HAFT, GHAR, GORI, JOZA, KHON, KORA, QOMS, SARD, SEMI, SEPI, SHOL, SOLE. The KHOS (pillar) and KSHA (benchmark) sites from the Iran Global network have been included in the measurements of each campaign. The antennas were set up by forced centering except for the KSHA with a setup by tripod with legs fixed plaster.

The 11 Kazerun sites installed in 2002 and measured in 2002 and 2004 are: ABAR, ABAD, BAMO, DASH, DAYY, KUHP, MARV, SHAN, SEDE, SEPI and YAGH. This network is equipped with forced centering benchmarks. During each campaign, the Iran Global sites ALIS and ARDA were included. In order to tie the Kazerun network also to the North Zagros and Central Zagros networks, we also included the sites DEDA and SEMI from North Zagros and FAR2 and SVR2 from the Central Zagros network.

We have also included the data of the following 30 globally distributed IGS stations (Fig. 2-8) in our data processing: ALGO, ANKR, ARTU, BAHR, FORT, GOLD, GRAZ, GUAM, HRAO, IISC, IRKT, KERG, KOKB, LHAS, MALI, MAS1, NICO, NKLG, POL2, POTS, RAMO, SANT, TIDB, TSKB, VILL, WSRT, WUHN, YAR2, ZECK and ZWEN, to tie our local networks to the ITRF reference frame.

2.2.4 Measurement method

The local time of Iran has +3.5 hours difference with respect to GMT time so our measurements start at 3:30 am in the morning to be consistent with the measurement pattern of permanent GPS stations (in particular IGS stations) and also with other data like the satellite orbits and the navigation files. Each session started in the morning at 3h30m00s (00h00m00s GMT time) and finished at 3h29m30s (23h59m30s GMT time). Each station was measured at least 48 hours with a 30 second interval. In order to optimally correct the antenna phase center variations, all antennas were oriented to the north.

The analysis of GPS data in 24 h sessions is the commonly used strategy for high precision positioning (1 mm), because several sources of noise could average out over this time span (diurnal tropospheric effects, ionospheric effects, tidal effects, orbit geometry, multi-path, …). Long measurements also improve the precision of the orbit adjustments.

We have selected a minimum of 48 hours of measurements because then we can compare two independent solutions over 24 h sessions to evaluate the repeatability of the raw measurement.

We have used carrier phase measurements on both the L1 and the L2 frequencies because the baselines in our regional networks and in particular with the IGS stations used for reference frame stabilization are long (generally hundreds to thousands of km). Therefore we need to correct for significant differential ionospheric

delay between the two stations at the end of the baselines. To correct the effect of the ionosphere the ionosphere-free linear combination of the two carrier phase measurements L1 and L2 is used in the data inversion.

2.2.5 International Terrestrial Reference Frame (ITRF)

Observing crustal deformation for the purpose of studying crustal deformation needs a global reference frame to compare and combine measurements in different locations, at different times and with different techniques. For this purpose a terrestrial reference frame which rotates with the Earth's surface is most useful. The best global reference frame currently chosen for all modern geodetic techniques is the International Terrestrial Reference Frame (ITRF). ITRF is maintained by the International Earth Rotation Service (IERS) which monitors the Earth Orientation Parameters (EOP) for the scientific community through a global network of observing stations since 1988 (Boucher et al., 1999; Altamimi et al., 2002). This is done through space geodesy techniques such as Very Long Baseline Interferometery (VLBI), Lunar Laser Ranging (LLR), Satellite Laser Ranging (SLR), Doppler Orbitography and Radiopositioning Integrated by Satellite (DORIS) and GPS observations. The stability of the reference frame requires the estimation of station velocities accounting for some geophysical effects such as plate tectonic movements. The International Terrestrial Reference System (ITRS) which is realized by the ITRF is defined by its origin, scale, axes orientation and rotation rate. The orientation of the Cartesian axes is such that the z-axis coincides with the mean pole of rotation for the period 1900-1905, and the x- and z-axes are in the plane of the Greenwich meridian. By convention, the rotation rate has a no-net-rotation condition for the horizontal motions with respect to the lithosphere. This condition is met by aligning the coordinate axes to the NNR-NUVEL-1A model (DeMets et al., 1994).

The latest version of the ITRF is ITRF2005 (Altamimi et al., 2007) in which the positions of the observing stations are now considered to be accurate to the centimeter level. The ITRF solutions reflect the actual quality of space geodesy solutions, being free from any external constraints. It includes primary core stations observed by VLBI, LLR, SLR, GPS, and DORIS (usually used in previous ITRF versions) as well as regional permanent GPS networks for its densification. To

ensure its time stability, the ITRF2000 and ITRF2005 have been implemented by a selection of high quality geodetic sites (Altamimi et al., 2002, 2007).

GPS stations from the IGS network having a well constrained solution in the present version of the ITRF are included in all our campaign analyses. This allows a precise representation of our regional velocity fields in the international reference frame by constraining the IGS site velocities to their ITRF solution.

2.3 Data processing method

To get the high accuracy positions and velocity fields required for crustal deformation studies, the collected GPS data should be analyzed using scientific software to reduce or eliminate various types of errors. Several scientific software packages are available for precise GPS data processing, like Bernese (developed by AIUB), GIPSY (developed by JPL) and GAMIT (developed by MIT). These softwares are more or less user friendly and in some it is possible to have access to the code and modify it with respect to particular needs. These software packages are used for the data analysis of local, regional and global geodetic networks on scales of up to thousands of kilometers. Some programs are able to deal with different types of measurements (GPS, VLBI, and SLR).

2.3.1. Processing the daily GPS data with GAMIT

We have used the GAMIT/GLOBK package (version 10.21, King and Bock, 2004) for our GPS data processing. GAMIT is designed for estimating station coordinates for each measurement session (e.g. 24 h sessions) by a least square inversion. GLOBK is a Kalman filter to combine individual positioning solutions into global campaign solutions, time series and velocity fields. The software is designed to run under any UNIX/LINUX operating system. It is associated with several shell scripts which control automatic processing.

Many settings and files should be prepared to process daily GPS data. The initial files which are needed for processing with the GAMIT software are:

- Table of satellite types (due to renumbering of the satellites)
- Ephemeredes of Sun and Moon needed for tidal forces on satellites and solid Earth tides
- Nutation tables that give the position of the Earth’s body axis in space

- Leap second table that allows conversion from GPS time to UTC
- Polar motion and UT1 tables needed to describe the Earth's rotation variations
- Ocean tide loading grids
- Antenna phase center correction tables
- GPS receiver and setup information (antenna and receiver type, antenna height)
- A priori coordinates and velocities (if available) for sites
- Initial orbit information for satellites
- Atmospheric loading (optional).

For processing the daily GPS data by GAMIT we have followed the processing strategy of Feigl et al. (1993) and Dong et al. (1998): Double-differenced, ionosphere-free linear combinations of the L1 and L2 phase observations were used to generate weighted least squares solutions for each day. An automatic cleaning algorithm was applied to postfit residuals to repair cycle slips and to detect problematic data, and the data were cleaned for the final solution. Estimated parameters for each daily solution include the 3-dimensional loosely constrained Cartesian coordinates for each site, orbital elements for each satellite, Earth orientation parameters (pole position and motion and UT1 rate), and integer phase ambiguities. We computed the tropospheric zenith delay at each station every 2 hours and one horizontal gradient per daily session. After the computation we control different elements of the solution to be sure that the phase ambiguities have been solved properly and the postfit residuals have a reasonable value. The checked solutions represent the quasi-observations input to GLOBK.

2.3.2 Combination of Quasi-observations with GLOBK

Loosely constrained daily solutions from the GAMIT processing are the quasi-observations which were input to the GLOBK Kalman filter (Herring, 2004). The output is precise station positions and linear velocities relative to a given reference frame. For stabilizing the ITRF2000 (Altamimi et al. 2002) reference frame we have used globally distributed IGS stations listed in 2.2.2.

To get the final positions and velocities of the stations, the Kalman filter is applied in four steps:

1) In a first run we used the quasi-observation of each campaign to get the mean position for each local station (a global campaign solution). This reduces short term scattering observed between the individual daily solutions. It also reduces the run

time for subsequent combinations for velocity estimations. We have produced global campaign solutions of the Iran Global network (processed and provided by Vernant et al. 2004; Masson et al., 2007), and the Central and North Zagros, Kazerun, Mashhad and Kerman networks, and the Bam post-seismic network. These later six networks have been analyzed in this thesis.

2) In the second step we prepare 10 years (from 1997 to 2007) of continuous global quasi-observations in form of daily solutions in the IGS3 network (a sub-network of the global IGS network) performed and provided by the Scripps Orbital and Permanent Array Center (SOPAC) at University of California (Bock et al., 1997). Before combining the global SOPAC observations with our campaign solutions we have computed mean positions for each month of SOPAC quasi-observations producing global monthly solutions. This reduces again the short term scatter in the global solutions and serves as new, compact quasi-observation for the subsequent velocity estimations.

3) In this step all global campaign solutions are combined with the monthly IGS3 solutions and a linear velocity is estimated for each station. During the Kalman filtering, some of the SOPAC quasi-observations have not been used because their data are not compatible with our data and their X^2 (Chi-square) values are too high.

4) Finally, we used the forward X^2 obtained in the previous run as the weight of each quasi-observation. This down weighted those quasi-observations which are difficult to combine with previous solutions. In particular, in this step the problematic SOPAC data are completely down weighted and have therefore no influence on the final solution.

After combining all of the available quasi-observations in a single solution with unconstrained positions and velocities, this solution is transferred into a global reference frame. To stabilize our solution in the ITRF2000 reference frame a particular set of 24 stations (Fig. 2-9) were used (IGS stations distributed all over the globe with a good solution in ITRF2000). Then, differences between positions and velocities of these stations from our unconstrained solution and the ITRF2000 a priori values are minimized by applying a 7-parameter Helmert transformation to the network (translation, rotation, scale). This process is done iteratively with rejecting stabilization stations with high residuals.

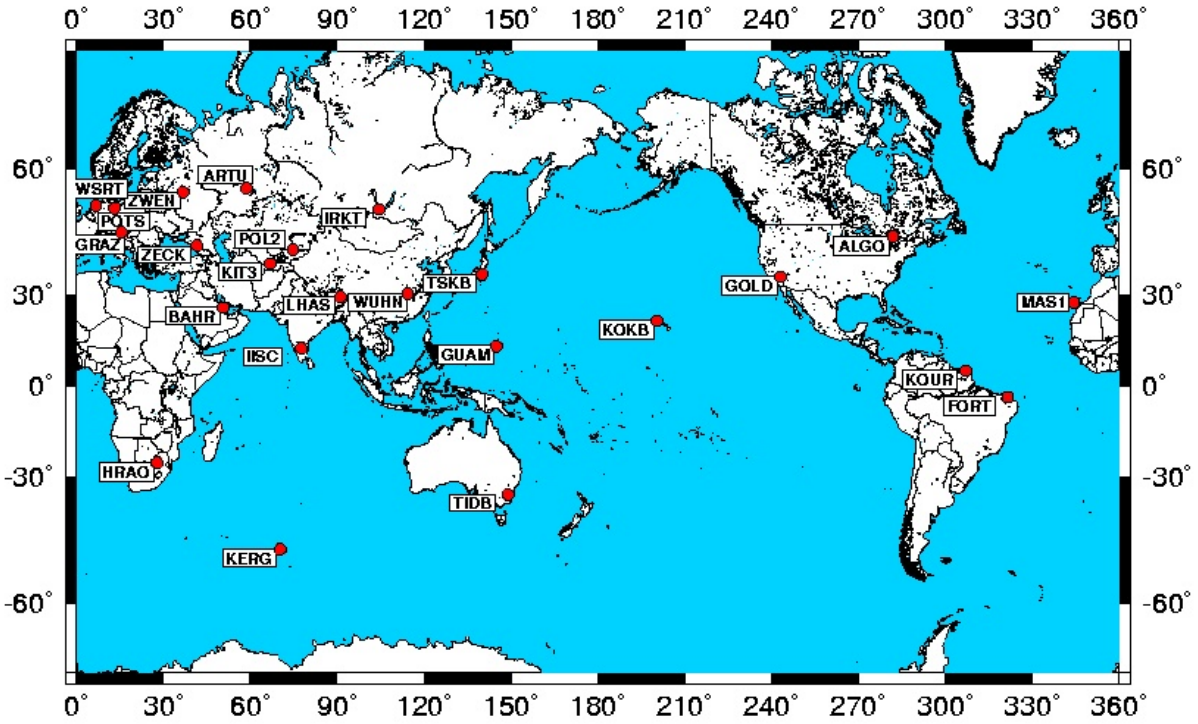

Figure 2-9. Distribution of the stations which have been used for the stabilization of the solutions in ITRF2000.

The postfit root-mean-square (RMS) of the final reference stabilization is 0.65 mm in position and 0.95 mm/yr in velocity. All of the 24 stations are retained in the stabilization. This processing with a Kalman filter allowed us to combine successfully regional and global geodetic data, to perform simultaneous, coherent adjustments and to establish a precise reference frame.

2.3.3 Computation of the velocities with respect to rigid plates

We constrained the Eurasian plate with a selection of GPS velocities from 16 IGS sites distributed across the Eurasian plate (BOR1, BRUS, GRAZ, HERS, JOZE, KIT3, KOSG, METS, NYAL, ONSA, POL2, POTS, TROM, WTZR, ZIMM, ZWEN). This selection of Eurasian sites is similar to the one used by Vernant et al. (2004). These stations data are included in the daily GAMIT solutions and some of them have already been used for the ITRF reference frame stabilization. These IGS sites also benefit from redundancy by their inclusion in different independent solutions (e.g. in campaign networks and permanent networks). The Eurasia Euler pole we obtain from our calculation is located at latitude 57.161±1.054°N, longitude

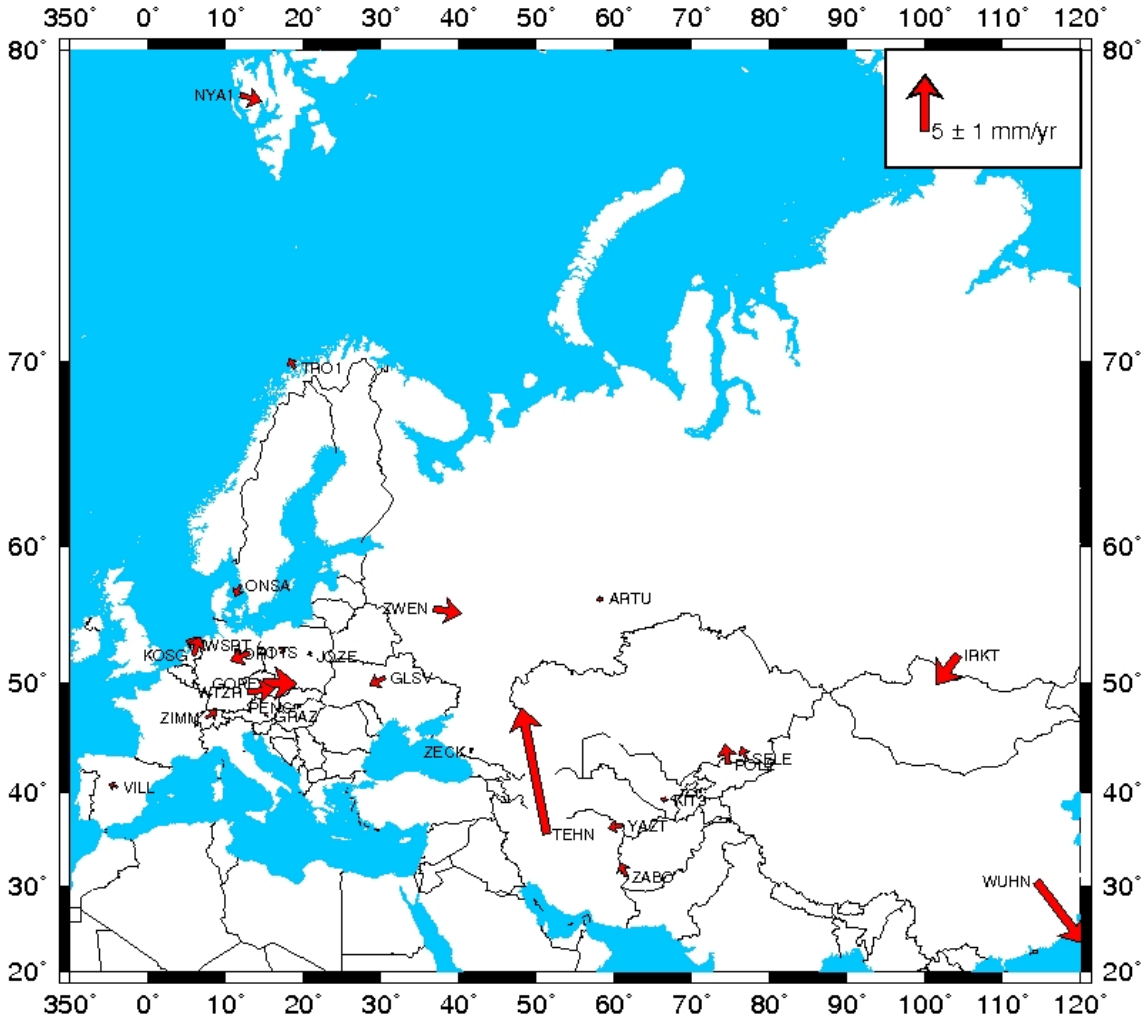

Figure 2-10. Velocity residuals of some European and Asian stations with respect to Eurasia. The velocities of the YAZT and the ZABO station in the east of Iran are less than 2 mm/yr which shows these stations are on the rigid Eurasian plate.

-100.320±1.298°W, with a rotation rate of 0.282±0.003°/Myr which is close to Vernant et al. (2004) and McClusky et al. (2001). The velocity residuals of the Eurasian sites are shown in the Figure 2-10. However, the majority of the stations considered by Vernant et al. (2004) for computation of the Eurasian Euler pole are located in western Europe and only few stations in eastern Eurasia have been used. Therefore we performed another test using more eastern sites (VILL, IRKT, SELE, POL2, KIT3, ARTU, ZWEN, JOZE, TROM, BOR1 GRAZ, POTS, WTZR, ONSA, NYAL, ZIMM, KOSG, HERS). The resulting Euler pole is situated at 58.510±0.932°N, -107.087±1.147°W with a rotation rate of 0.252±0.003°/Myr (Fig. 2-11a). After the

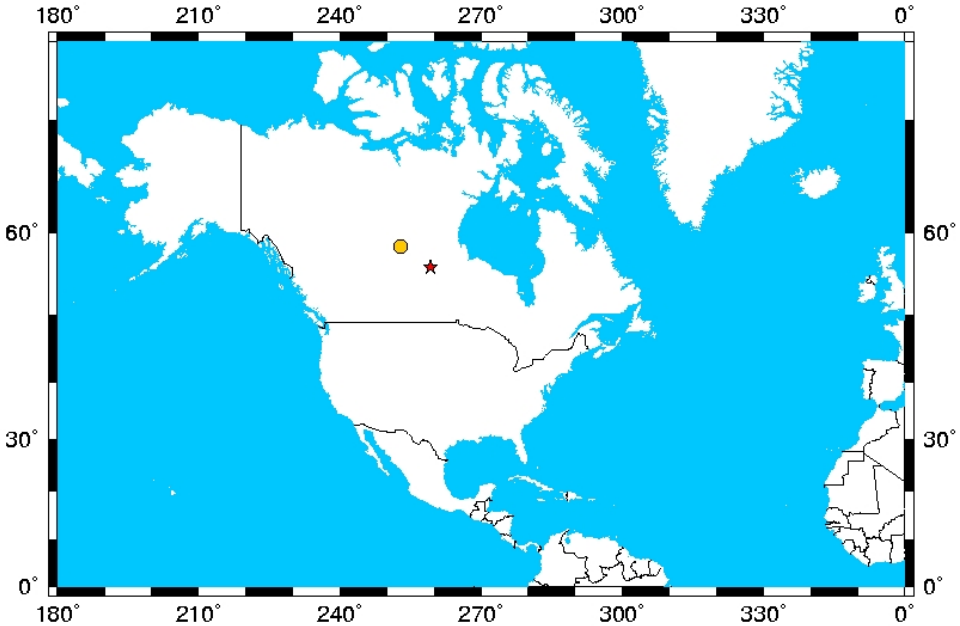

Figure 2-11a. Location of the Euler rotaion pole of the Eurasia respect to ITRF. The Red star is the our determined pole and the yellow circle is determined by Vernant et al. (2004).

Figure 2-11b. Velocity residuals of some European and Asian stations respect to Eurasia. These residuals are calculated with the second strategy which shows lower residuals. In this strategy more Asian and European sites have been used to constrain the Eurasian plate motion.

conversion of the velocities to the Eurasian plate reference frame by the latter Euler pole the velocity residuals with respect to stable Eurasia are shown in Figure 2-11b. The residuals for Asian and European sites are 0-0.5 mm/yr smaller than for the calculation with the sites that have been used by Vernant et al. (2004). With this latest Euler pole the new velocity field is rotated slightly to the east with respect to the former solution.

For a better evaluation of the Zagros deformation we considered the Central Iran block as a reference frame, as proposed by Walpersdorf et al. (2007). The velocity residuals of the sites on the Central Iran block (Sanandaj-Sirjan zone), MIAN, BIJA, SHAH, ARDA and HARA, are less than 1 mm/yr which indicates these sites are situated on the same stable block. We have estimated the Euler pole of the Central Iran block characterized by the motion of these sites, with respect to ITRF2000. The pole is located at latitude 54.868±3.313°N, longitude 47.511±11.085°W and has a rotation rate of 0.315±0.015°/Myr which is relatively coherent with the Vernant et al. (2004).

The root mean square (rms) departure of the velocities of the 5 Central Iran block sites after transformation was 0.18 mm/yr. The velocity residuals of several sites in the Central Zagros are less than 2 mm/yr which shows that these stations have a motion coherent with the stable Central Iran block.

Table 2-2. Euler vector for Central Iranian Block (CIB) and Eurasia (EU). Counterclock-wise rotation is positive.

Plates	Lat.	Long.	Rotation Rate (°/Myr)	References
CIB-EU	15.289± 6.081	-1.049±10.482	0.161±0.027	Our study
CIB-EU	23.15 ±13.2	0.98± 1.2	0.189±0.1	Vernant et al. (2004)
CIB-EU	27.5	65.8	0.56	Jackson&McKenzie (1984)

2.4 Evaluation of the results

2.4.1 Repeatabilities

The evaluation of the quality of the results is done in different ways. Generally quality of the least square adjustments (Vanicek and Krakiwsky, 1986) is controlled by the a posteriori variance factor σ_0:

$$\sigma_0 = (V^T PV) / df = X^2 / df$$

where V is the adjusted residual vector, P is the inverse of the observation covariance matrix, df is the degree of freedom or redundancy number, and X^2 is the sum of the square residuals. Consistency between the computational model and the observations can be controlled by comparing the observation residuals and the a priori observation errors. The test of X^2 allows us to reject the solutions with high systematic errors.

For the least square inversions in GAMIT, an a posteriori variance factor of 0.25 is advised (King and Bock, 2002). In our analysis, the majority of our daily solutions were determined with an a posteriori variance factor (postfit nrms) of 0.175. The quality of the positions or the baseline components can also be studied by daily repeatability which expresses the short-term correlation between data (Larson and Agnew, 1991). This short-term precision can be defined by the weighted root mean square residuals (WRMS).

$$wrms = \sqrt{\frac{\frac{n}{n-1}\sum_{i=1}^{n}\frac{(x_i - \bar{x})^2}{\sigma_i^2}}{\sum_{i=1}^{n}\frac{1}{\sigma_i^2}}}$$

where n is the number of measurements, x_i is the estimated value of one observable, $\bar{x}$ is the mean value of x_i and the σ_i is the error associated with x_i.

The WRMS is analyzed for each north, east and vertical component of the measured baselines or station positions. One possibility to evaluate the precision of our measurements is calculating baseline repeatabilities. The baseline repeatability between individual daily GAMIT solutions (which expresses the short term correlation between data) displays values of about 1-3 mm/yr for horizontal baseline components, yielding an average of 2 mm/yr as estimation of the horizontal measurement uncertainties. This estimate is conservative because the individual unconstrained solutions have been compared without transforming them into a common reference frame. However, these values can not be directly used to estimate the long term error of the measurements. The mean repeatabilities of the different campaigns are listed in Table 2-3 and some of them are illustrated in the Figure 2-12.

Table 2-3. Mean repeatability on the north, east and vertical baseline components of the campaigns of North Zagros, Central Zagros, Kazerun, Mashhad and Kerman.

Campaign	Epoch	North	East	Vertical
Central Zagros	1997	2.8	3.0	7.4
Central Zagros	2000	1.7	2.0	5.2
North Zagros	2001	1.1	1.7	4.7
Kazerun	2002	2.0	3.0	6.0
North Zagros	2003	0.7	1.5	3.2
Central Zagros	2003	0.9	1.3	2.8
Kazerun	2004	1.8	2.2	6.2
Mashhad	2004	2.8	3.0	6.2
Kerman	2004.1	2.1	2.4	6.4
Kerman	2004.2	1.2	1.2	4.5
North Zagros	2005	1.8	2.2	6.2
Mashhad	2006	2.0	2.0	5.0
Kerman	2006	1.6	2.3	5.7

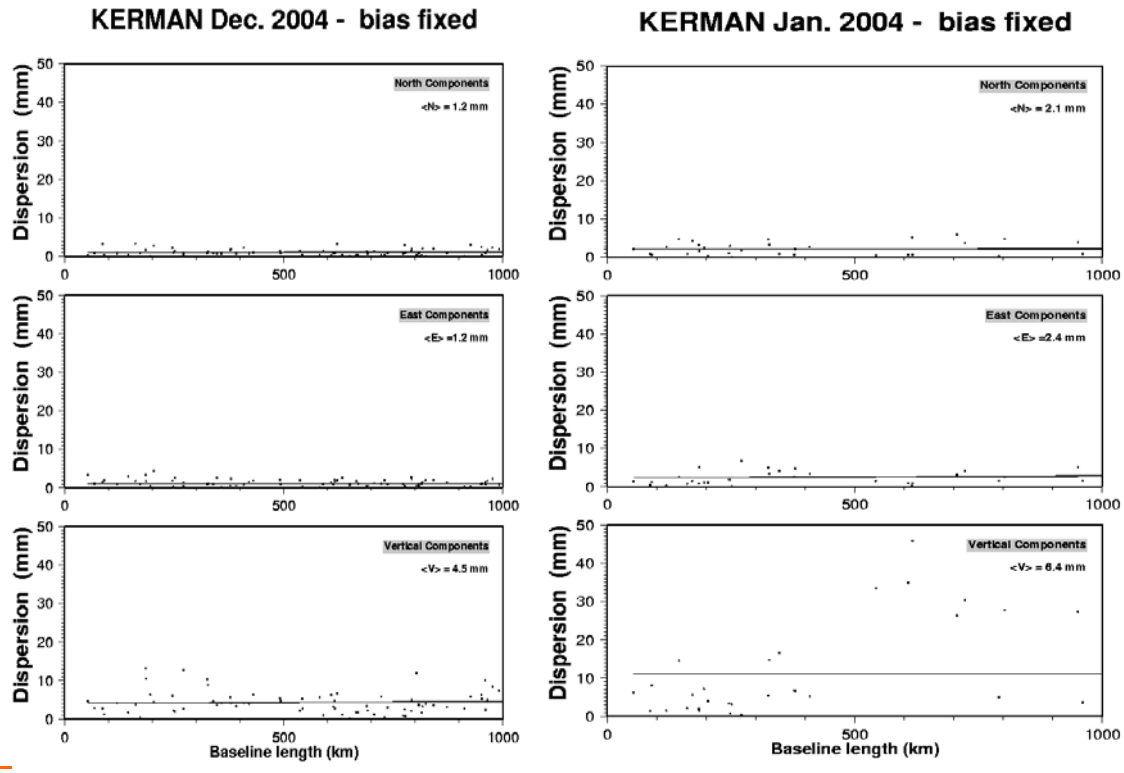

Figure 2-12. GAMIT baseline repeatabilities of some networks.

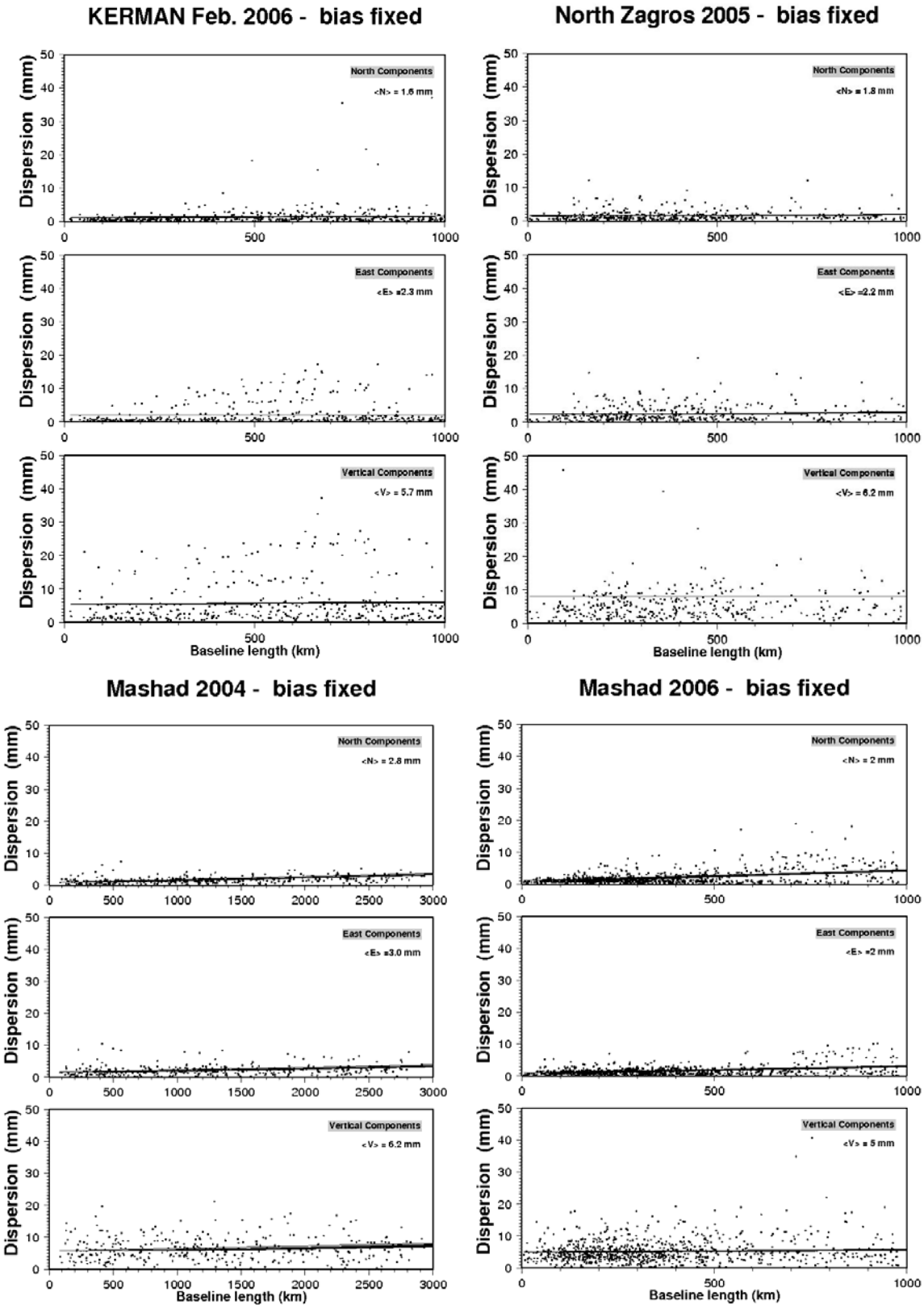

Figure 2-12. Continued .

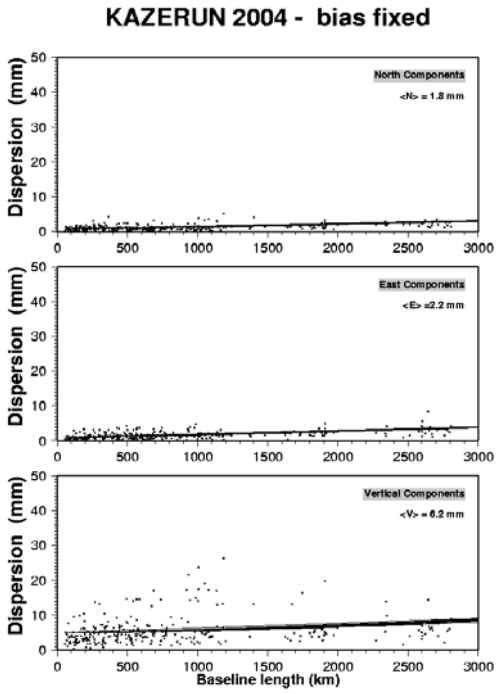

Figure 2-12. Continued .

2.4.2 Time series

Another way to evaluate the quality of the GPS measurements is to show the variability in time of the north, east and vertical component of the station positions (time series). In coordinate time series we can identify measurement or analysis outliers and we can fix the problem by correcting errors in the input data, improved modeling or calculation, or by eliminating bad individual measurements. In long time series an evaluation of the long-term error can be considered (Larson and Agnew, 1991). To estimate the long-term precision of the positioning (wrms as expressed below), measurements spanning several years for each stations should be used.

$$wrms = \sqrt{\frac{\frac{n}{n-2}\sum_{i=1}^{n}\frac{(x_i-(a+bt_i))^2}{\sigma_i^2}}{\sum_{i=1}^{n}\frac{1}{\sigma_i^2}}}$$

where a and b are the intercept and slope of the best fitting linear trend and t_i is the time of the i-th measurement (Larson and Agnew, 1991). These values are statistical values and could be evaluated with at least three measurement epochs. To evaluate significant values, it is necessary to have much more than 3 measurements over longer times.

Table 2-4. List of averaged normalized and weighted root mean squares and associated velocity uncertainties of different networks.

Network	NRMS	WRMS (mm)	Vel. uncertainty
North Zagros	2.13±1.45	1.83±1.4	1.03±0.16mm/yr
Kazerun	2.56±1.50	2.29±1.51	1.24±0.22mm/yr
Central Zagros	3.28±2.25	3.35±2.46	1.09±0.09mm/yr
Mashhad	2.46± 0.99	2.25±0.87	1.5±0.52mm/yr
Kerman	2.50±0.93	2.78±1.16	1.34±0.35mm/yr

We have plotted timeseries of the campaign stations with three or more measurements covering at least a two year time interval, with their associated long-term precision in Figure 2-13. The averaged nrms, wrms and velocity uncertainty of different networks are listed in Table 2-4. The velocity uncertainties are the average of the formal uncertainties of the linear velocity evaluated by the Kalman filter, over the north and the east components.

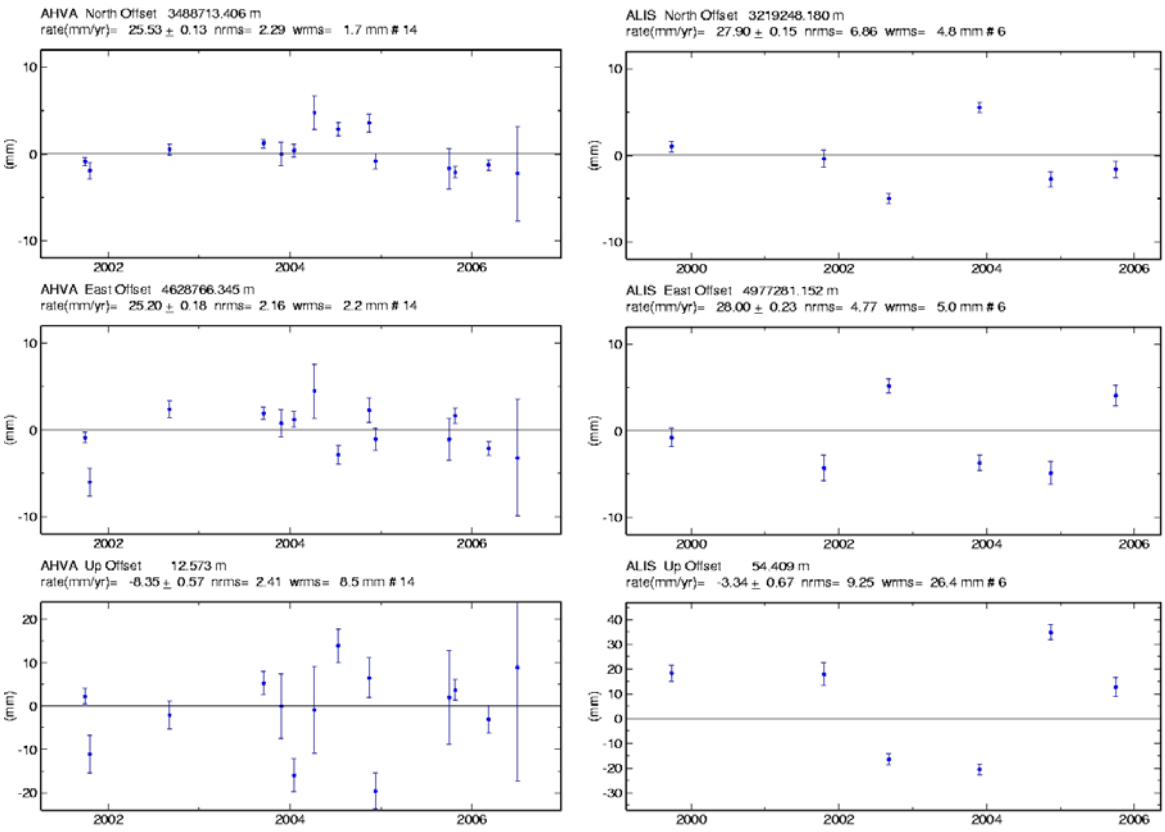

Figure 2-13. Time series plot for some stations of North Zagros, Kazerun, Mashhad and Kerman networks

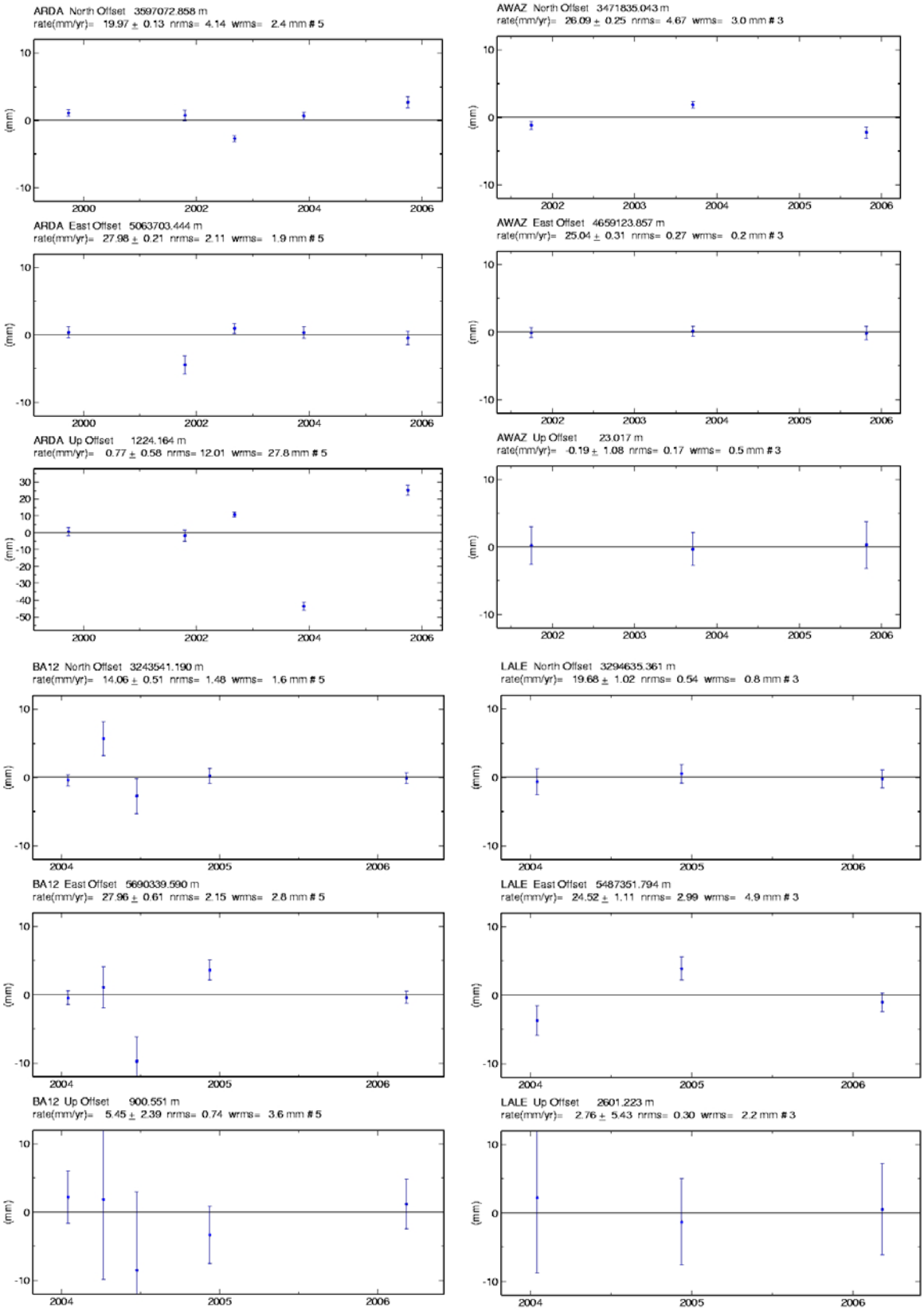

Figure 2-13. Continued.

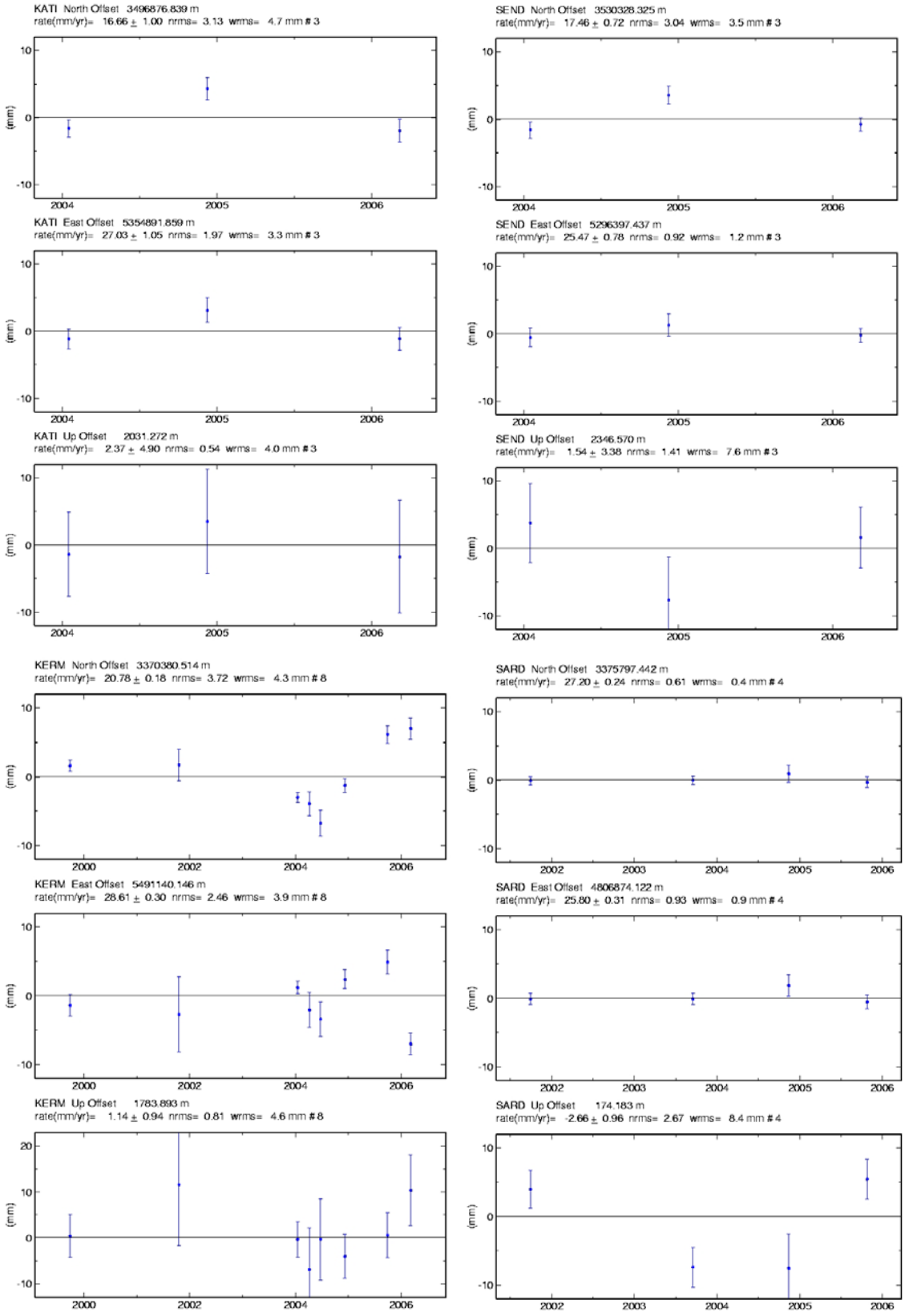

Figure 2-13. Continued.

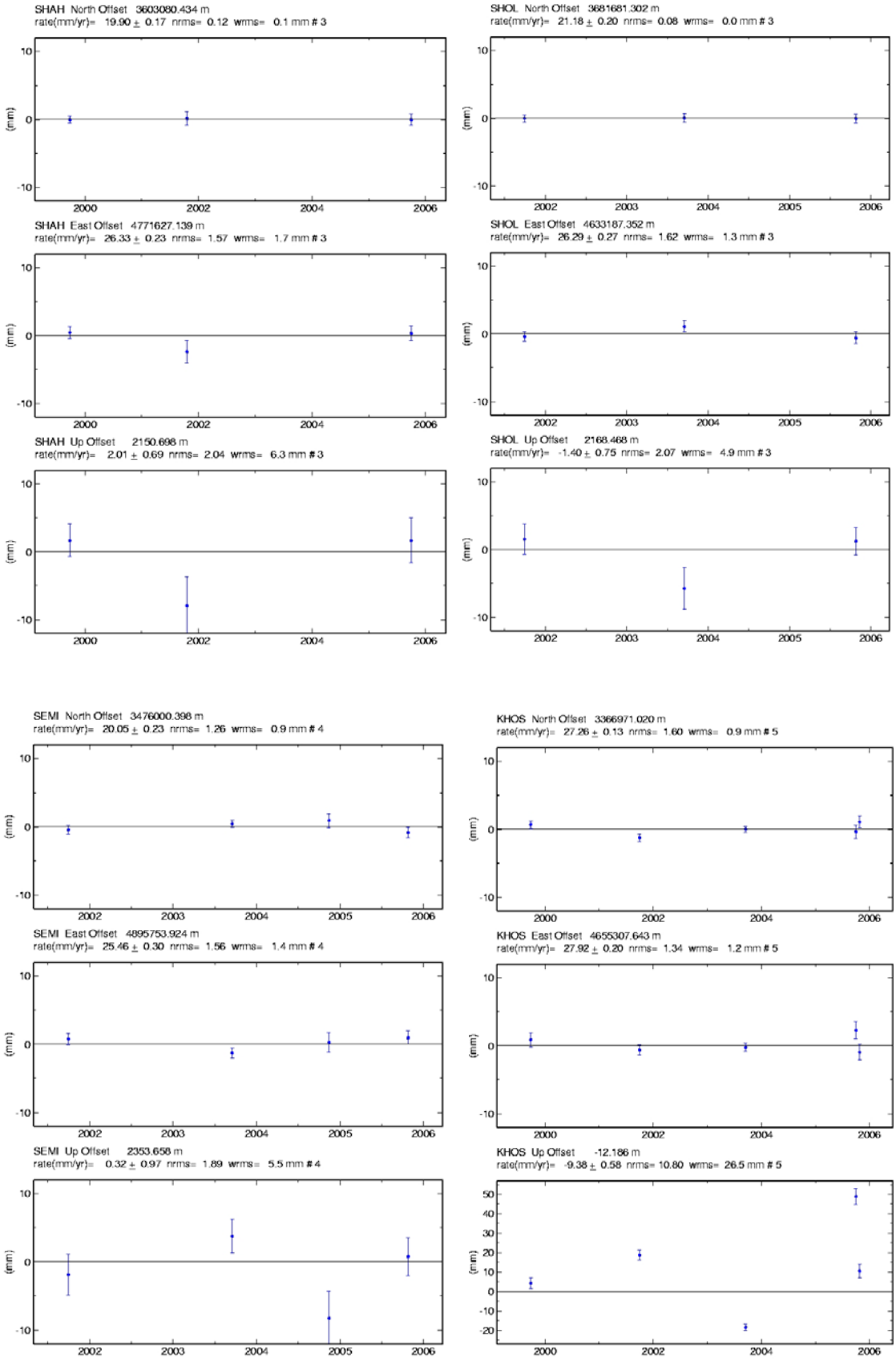

Figure 2-13. Continued.

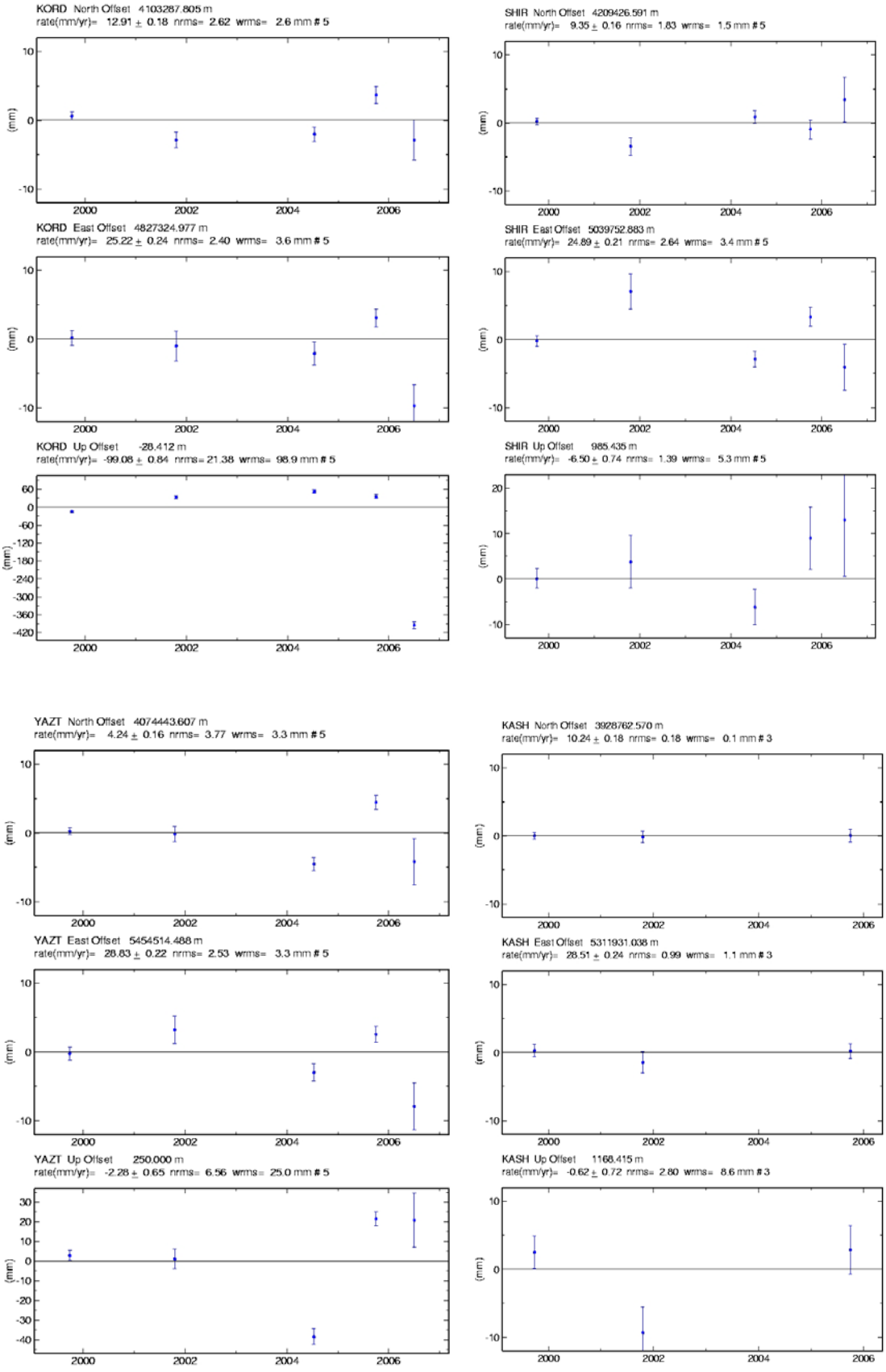

Figure 2-13. Continued.

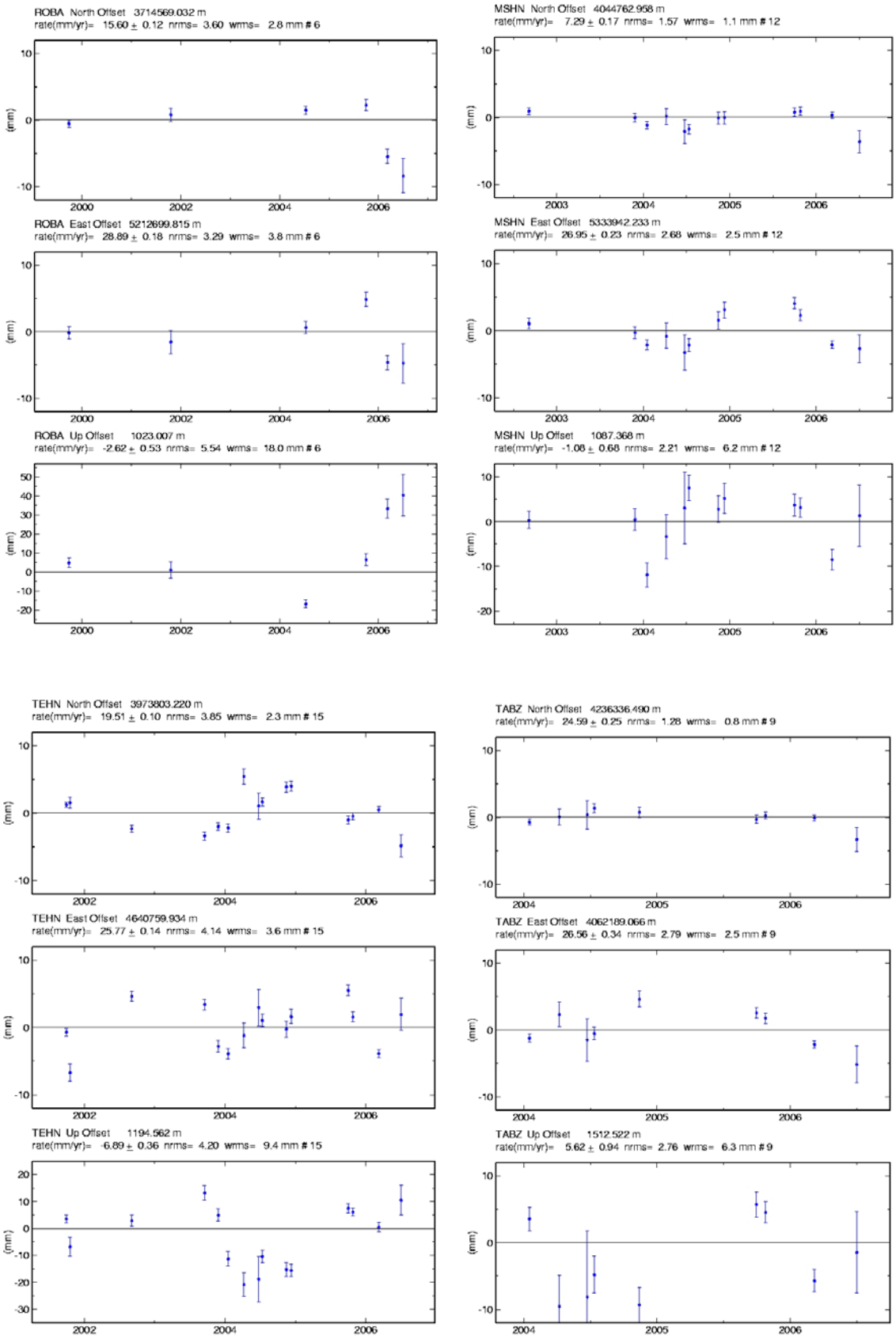

Figure 2-13. Continued.

2.5 Conclusion

We have combined 10 years of GPS measurements of Zagros (North Zagros, Kazerun and Central Zagros), Kopeh Dagh and the Lut region since 1997. Each campaign has been computed in 24 h sessions by GAMIT. The daily, loosely constrained solutions obtained by GAMIT were then combined by GLOBK to estimate linear station velocities. In this step the local measurements were combined and adjusted with other regional and global quasi-observations. The velocity field has been transformed into the ITRF2000 reference frame by constraining 24 globally distributed well known IGS stations to their ITRF values. These stations realize the ITRF2000 reference frame with residuals of 0.65 mm on positions and 0.95 mm/yr on velocities. For North Zagros, Central Zagros and the Kerman network we have acquired 3 measurement epochs covering a time interval of more than 4 and 3 (for Kerman) years. The associated uncertainties of these measurements are less than 1.5 mm/yr. However, for the Mashhad and Kazerun networks with only 2 measurement epochs covering 2 years, the associated precision is about 2 mm/yr. We have evaluated our processing and our results by the a posteriori variance factor, and short-term and long-term weighted RMS. The a posteriori variance factor (postfit nrms) of individual daily solutions is about 0.175. The repeatabilities of daily GAMIT solutions for horizontal components are about 2 mm/yr which shows the short-term errors. Unfortunately, the short term repeatabilities do not contain any information on systematic errors like antenna phase center offsets, antenna set up errors or local site instabilities.

The representation of the velocity field relative to the Eurasian plate and the Central Iran block is related to the estimation of the corresponding Euler pole in the ITRF reference frame. The Euler pole of the Eurasian plate with respect to ITRF2000 is estimated from our data as 57.876±0.911°N, 104.309±1.099°W, and 0.254±0.003°/Myr. For the Central Iran block we obtain 54.868±3.313°N, 47.511±11.085°W and 0.315±0.015°/Myr. These poles have been realized using the sites considered by Vernant et al. (2004). Our results are relatively coherent with results of Vernant et al. (2004). The coherence of rigid plate/block rotation between our solution and published reference solutions, as well as the estimates of the

measurement precision from baseline repeatabilities and coordinate variabilities are an indicator for the overall good quality of our data analysis.

Chapter 3 Kinematics of the Kopeh Dagh Region

3.1 Introduction and tectonic settings

The Kopeh Dagh fold and thrust belt extends from the Caspian Sea to the Afghanistan border and separates the stable flat Turkmenistan (the Turan shield), belonging to Eurasia, from Central Iran. The Kopeh Dagh is a linear mountain belt, 700 km long, and much broader in the west than in the east. The maximum altitude is 3000 m in the southeast (2000 m higher than the Turkmen foreland to the north). The mountain belt (Fig. 3-1) is constituted of several NW-SE trending ranges, the Kopeh Dagh range being the northern most, followed by the Binalud (south of Mashhad city), Kuh-e-Sorkh (north of Kashmar) and Siah-Kuh (north of Sabzevar). The Kopeh Dagh range is structurally and tectonically divided into three parts, the western, central and eastern parts which will be characterized below. In Figure 3-1 we see the location of the faults, the earthquake epicenters ($M_w \geq 4.5$) (Engdahl et al., 1999), the CMT solutions from the Harvard catalogue from 1976 to 2007 and the first motion solutions from McKenzie (1972), Jackson and Fitch (1979) and Jackson and McKenzie (1984) (Table 3-1). The seismicity shows that the range is tectonically active. The focal mechanisms show strike-slip motion in the central part with NE-SW trending shortening P-axes and thrust motion in the western and eastern part and along the Iran-Afghanistan border.

Hollingsworth et al. (2006) propose a model for NE Iran's tectonics (Fig. 3-2) accommodating NS shortening by thrusting in the eastern part of the range, by NS shortening and EW extension in the central part through the anticlockwise rotation of a series of blocks bounded by the Quchan fault zone, and by expelling the west Kopeh Dagh to the west.

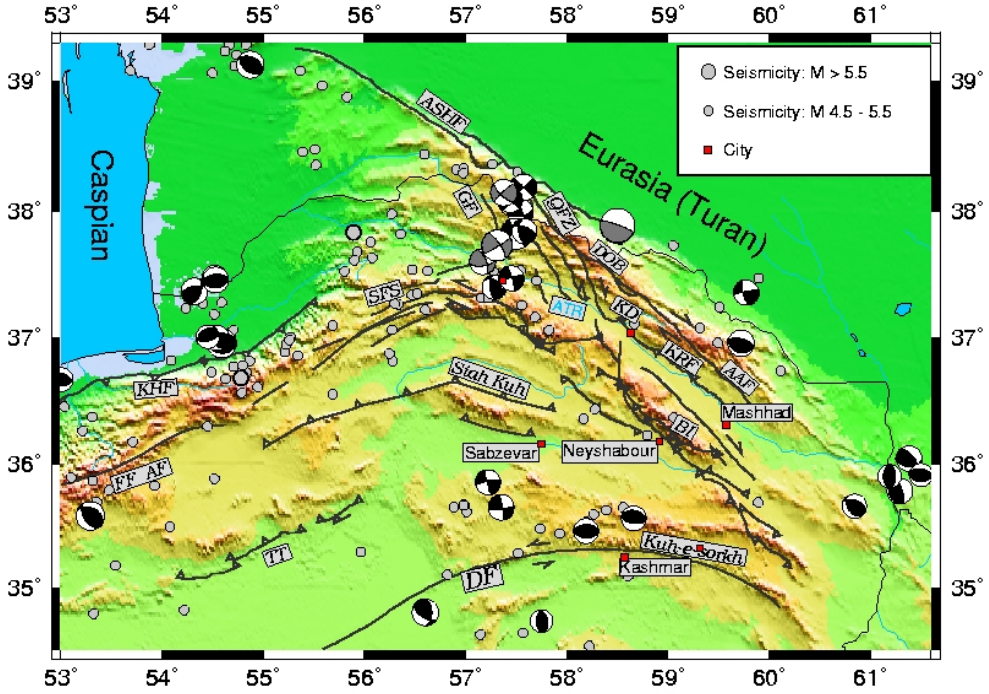

Figure 3-1. Summary seismotectonic map of NE Iran. Grey circles are locations of earthquake epicentres (Mw ≥ 4.5) during the period 1964–1998 (Engdahl et al., 1998). Black fault-plane solutions are CMT from the Harvard catalogue during the period 1976-2007. Grey fault-plane solutions are first motion solutions from McKenzie (1972), Jackson & Fitch (1979) and Jackson& McKenzie (1984). KD is Kopeh Dagh and BI is Binalud. Active faults of the region are: AAF: Alah-o-Akbar Fault, AF: Astaneh Fault, ASHF: Ashkabad Fault, DF: Doruneh Fault, DOB: Dorbadam, FF: Firuzkuh Fault, GF: Gholaman Fault, KRF: Kashafrud Fault, KHF: Khazar Fault, QFZ: Quchan Fault Zone, SFS: Shahrud Fault System, TT: Torud Thrust (Berberian 1976; Hollingsworth et al., 2006). ATR is the Atrak River (Valley).

3.1.1 The western part of Kopeh Dagh

The part of Kopeh Dagh located west of 57° comprises the Ashkabad fault (Fig. 3-1) which is associated with thrusting and right-lateral strike-slip motion. Berberian and Yeats (2001) and Trifonov (1978) use the term ”Main Kopeh Dagh fault” for the Ashkabad fault. The Ashkabad fault is not a continuous fault but is constituted of several segments and stopovers. Toward their ends, these segments splay into (or end at) thrust faults, which die out with distance from the strike-slip fault segment (Berberian and Yeats, 2001). At the southern termination of the Ashkabad fault, near the city of Ashkabad, a large destructive earthquake (M=7.2) occurred in1948 (Fig. 3-1, Table 3-1), killing more than 10,000 people in Turkmenistan, more than 350 people in the Dareh Gaz region (Iran) alone, and destroying more than 30 villages in

Table 3-1. The most significant earthquakes in the Kopeh Dagh and Binalud for the last 800 years (Ambraseys & Melville, 1982; McKenzie 1972; Jackson et al. 2002). The magnitude for the instrumental records is Mw.

Lat.	Long.	Mag.	Depth	Strike	Dip	Rake	Date
36.4	58.7	7.6					1209
36.05	58.8	7.1					1270
36.20	58.8	7.6					1389
36.25	58.75	7.6					1405
38.0	57.2	6.5					1810
37.36	58.39	7.2					1871.12.23
37.36	58.39	7.0					1872.01.06
37.88	58.50	7.2	-	290	85	90	1948.10.05
37.660	57.268	5.4	13	338	67	150	1997.02.04
37.728	57.310	6.4	8	326	75	173	1997.02.04
38.140	57.376	5.6	4	133	69	171	2000.08.22

Iran. This was the strongest earthquake to strike this region since at least AD 1455 (Tchalenko, 1975; Lyberis and Manby, 1999; Berberian & Yeats, 2001; Hollingsworth et al., 2006). The focal mechanism is a low angle thrust parallel to the range. Berberian and Yeats (2001) proposed a 'maximum recurrence interval' of about 2000 years for earthquakes in this region.

Trifonov (1978) reported active displacement along the Ashkabad fault over distances of more than 500 km. He estimated right-lateral Holocene-Pleistocene (0.01 - 1.5 Ma ago) displacement of 55-60 m along the Ashkabad fault. He also estimated the average right-lateral displacement rate of 3-8 mm/yr for the Ashkabad fault by measurements of sheared qanats Trifonov (1971). Lyberis and Manby (1999) found a total strike-slip offset of ~35 km on the Ashkabad fault, by resolving their estimate of ~75 km of total N-S shortening onto the Ashkabad with strike-slip parallel to the fault and thrust perpendicular to it.

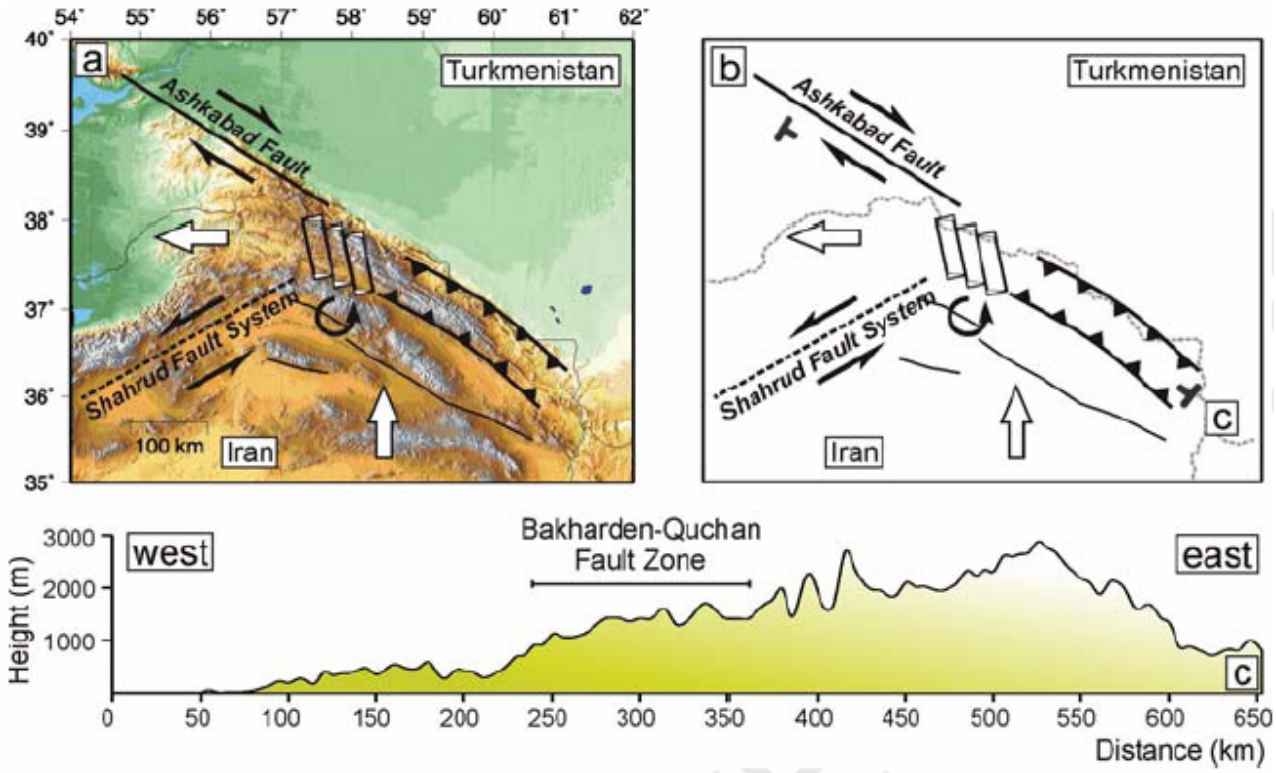

Figure 3-2. a) Topographic map of NE Iran, with a schematic tectonic summary. West of 59°, N–S Iran–Eurasia convergence is accommodated mainly by strike-slip motion on the Ashkabad and Shahrud fault systems. The Bakharden–Quchan fault zone (QFZ in Fig. 3-1) accommodates N–S shortening and E–W extension by rotating anticlockwise as a series of blocks. Thus, the west Kopeh Dagh is being expelled to the west. (b) Simplified view of the tectonics of NE Iran. The location of a topographic profile NW–SE across the Kopeh Dagh is shown. (c) NW–SE topographic profile extracted from SRTM digital topography across the entire Kopeh Dagh range. The highest relief is east of the Bakharden–Quchan fault zone, where shortening occurs only by thrust faulting. To the west of the zone, the relief dies away as strike-slip faulting plays a more important role in accommodating N–S shortening (after Hollingsworth et al., 2006).

Two GPS measurement campaigns of the Iran Global network (1999, 2001) give first velocity estimates for some GPS stations in NE Iran (KASH, YAZT and SHIR). Vernant et al. (2004a) evaluated ~7 mm/yr of N-S shortening between KASH and SHIR, in the northeast part of Kopeh Dagh. They estimated the Ashkabad fault slip to be ~3.5 mm/yr, and the shortening across the range to be ~6 mm/yr. Masson et al. (2007) have estimated 3±1 mm/yr of strike-slip between SHIR (located west of the Quchan fault zone) and YAZT (on the Turan shield) based on three Iran Global measurement campaigns (1999, 2001 and 2005). This value has been considered as the strike-slip rate accommodated by the Ashkabad fault.

3.1.2 The central part of Kopeh Dagh

The tectonic features of the central part (57°-58.5°E) are different from the western part of the Kopeh Dagh. Here the Ashkabad fault meets a zone of NNW-SSE trending right-lateral strike-slip faults (Fig. 3-1) (Ambraseys & Melville, 1982; Tchalenko, 1975; Hollingsworth et al., 2006). These faults are called the Bakhaderan-Quchan fault zone or Quchan fault zone (QFZ) (Hollingsworth et al., 2006). The QFZ is constituted of several parallel strike-slip faults (the major ones are the Quchan, Baghan faults) which, based on the Shabanian et al. (2007) fault map (3-3a), continue to the south into the Alborz-Binalud range, but based on the Hollingsworth et al. (2006) fault map terminate at the Atrak river valley which forms the southern margin of the Kopeh Dagh range (Fig. 3-3b). The southern terminations of these faults turn to the east and behave as thrust faults. In contrast to Hollingsworth et al. (2006) there is no Bajgiran fault present on the Shabanian et al. (2006) fault map and instead of the Bajgiran fault the Dorbadam fault has been introduced.

The Quchan fault with a length of approximately 100 km is located north of Quchan city. The fault cuts obliquely the topography and the structure of the Kopeh Dagh and offsets them by right-lateral strike-slip. To the north, it turns obliquely into the Ashkabad fault and its southern termination ends in the Atrak river valley (Fig. 3-1) where it turns to the east as a thrust, without any right-lateral strike-slip motion found in this part (Hollingsworth et al., 2006). The Baghan fault located west of the Quchan fault is approximately 70 km long. The northern part of this fault is situated at the political border between Iran and Turkmenistan and does not cross the Ashkabad fault. The southern termination is similar to the southern part of the Quchan fault. It seems that some segments of the Quchan fault zone pass the Atrak valley, continue across the Alborz-Binalud mountain and connect to the Binalud thrust (Shabanian et al., 2007).

Hollingsworth et al. (2006) have measured ~10km, ~15km and ~15km of total right-lateral offset on the Baghan, the Quchan and the Bajgiran faults (Fig. 3.3b), respectively. Several NW-SE right-lateral faults are in the Gholaman region. Offsets on individual faults are relatively small, despite their length, but the overall distributed shear in the region is about 2 km. There are other faults in the Quchan fault zone like

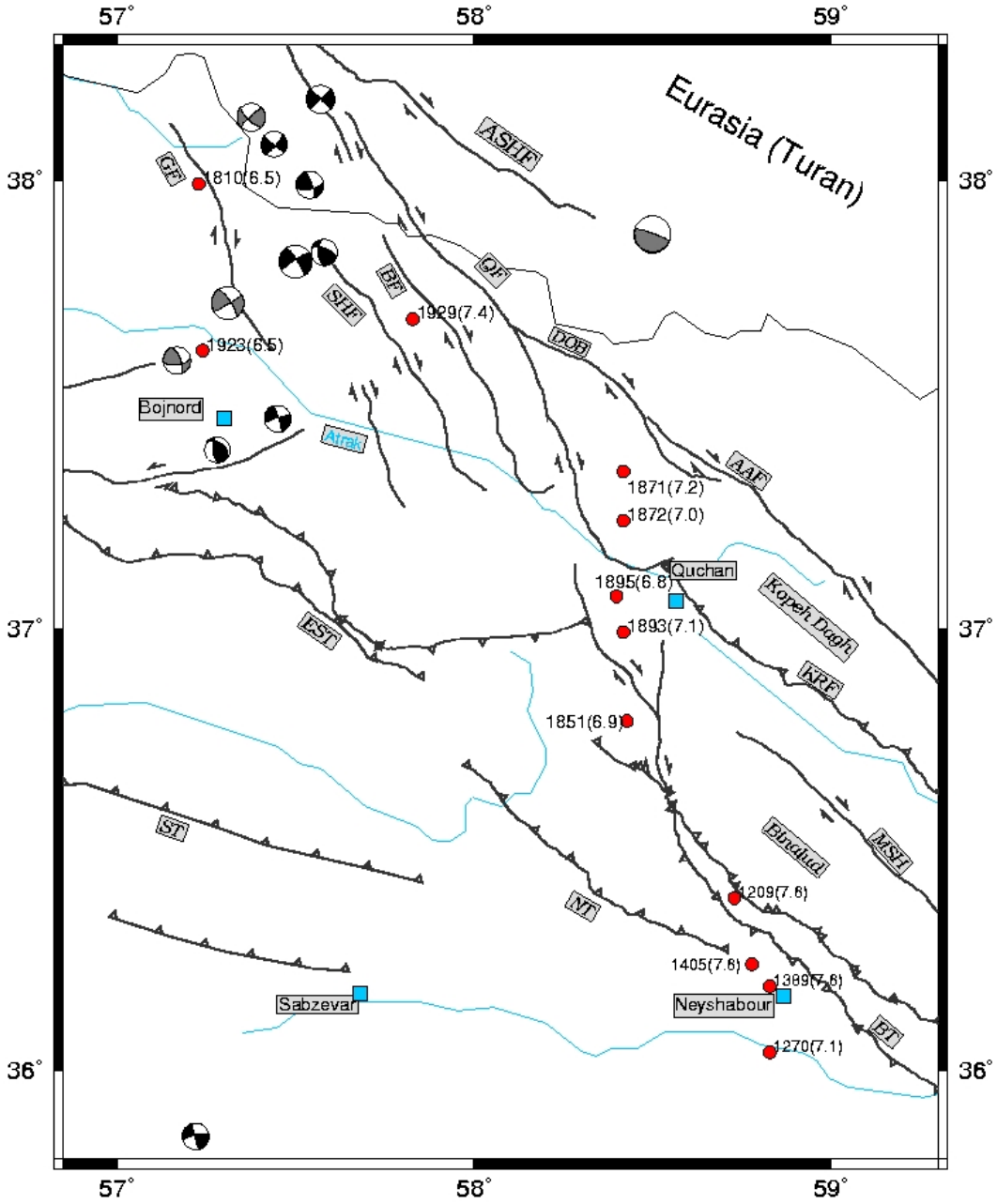

Figure 3-3a. Summary seismotectonic map of the Quchan Fault Zone. The faults are by Shabanian et al. (2007). Grey circles are locations of earthquake epicentres (Mw ≥ 4.5) during the period 1964–1998 (Engdahl et al., 1998). Blue squares are the populated cities of the region. Black fault-plane solutions are CMT from the Harvard catalogue during the period 1976-2007. Grey fault-plane solutions are first motion solutions from McKenzie (1972), Jackson & Fitch (1979) and Jackson & McKenzie (1984). Red circles show earthquake epicentres from historic records, during the period 400 BC to 1962 AD (Ambraseys & Melville 1982). AAF: Allah-o-Akbar Fault, ASHF: Ashkabad Fault, BF: Baghan Fault, BT: Binalud Thrust, DOB: Dorbadam Fault, EST: Esferaien Thrust, GF: Gholaman Fault, KRF: Kashafrud Fault, MSH: Mashad Fault, NT: Neyshabur Thrust, QF: Quchan Fault , ST: Sabzevar Thrust, SHF: Shirvan Fault, (Hollingsworth et al., 2006; Berberian and Yeats, 1999).

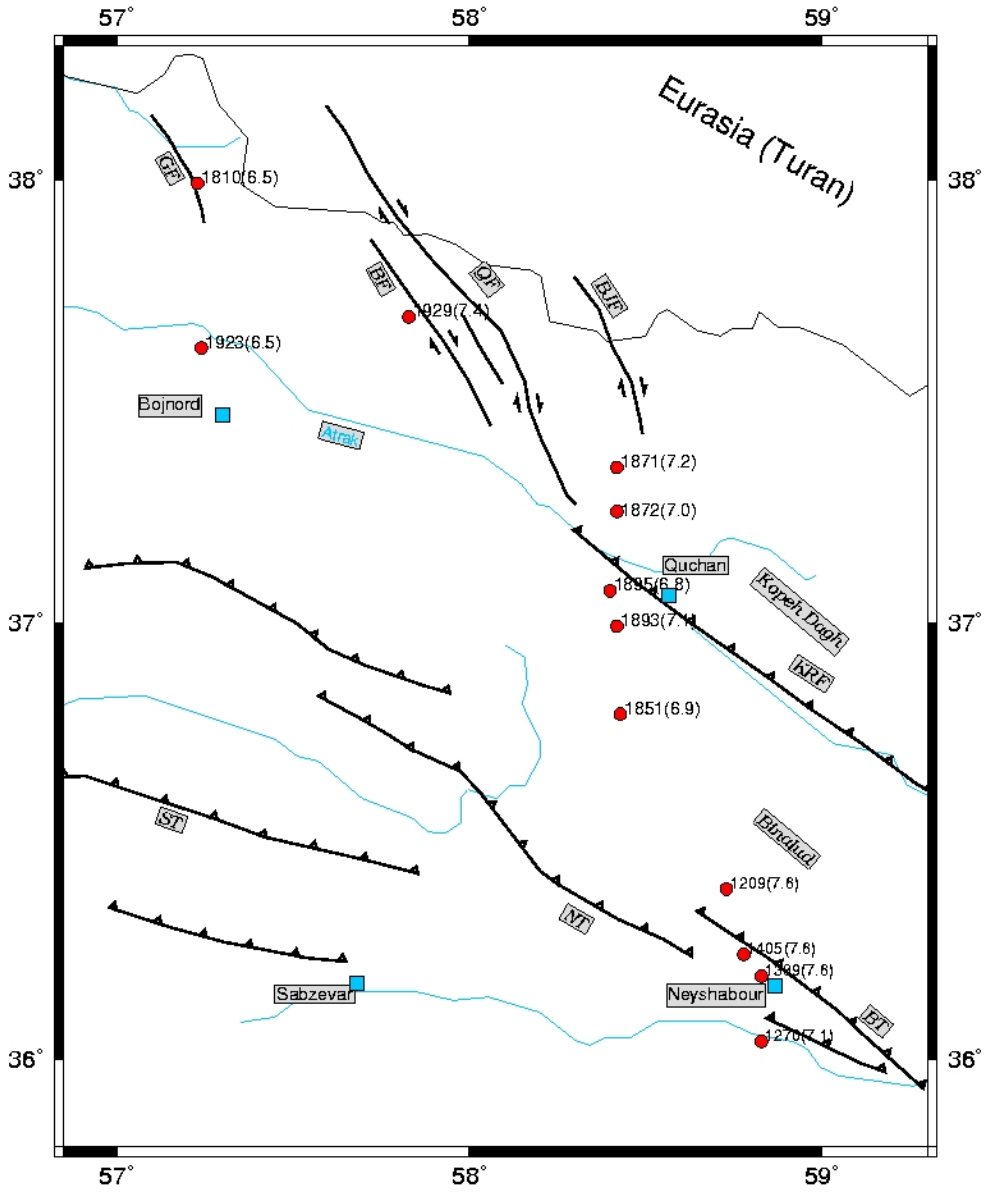

Figure 3-3b. Summary seismotectonic map of the Quchan Fault Zone. The faults are by Hollingsworth et al. (2007). Red circles show earthquake epicentres from historic records, during the period 400 BC to 1962 AD (Ambraseys & Melville 1982). Blue squares are the populated cities of the region. BF: Baghan Fault, BJF: Bajgiran Fault, BT: Binalud Thrust, GF: Gholaman Fault, KRF: Kashafrud Fault, NT: Neyshabur Thrust, QF: Quchan Fault , ST: Sabzevar Thrust (Hollingsworth et al., 2006; Berberian and Yeats, 1999).

Shirvan fault which is shorter than the Baghan and the Quchan faults and shows a smaller offset (~8 km) but which seems to be active as well (Hollingsworth et al., 2006).

Further, Hollingsworth et al. (2006) estimated an along-strike extension of 30 km across the Quchan fault zone by modelling rigid block (domino-style) rotation and

an across-strike shortening of ~50 km, corresponding to the ~60 km N-S total shortening. The total extension is accommodated by right-lateral strike-slip motion on the Ashkabad fault. Masson et al. (2007) have evaluated 2±1 mm/yr of strike-slip rate for the Quchan fault zone between stations SHIR, YAZT and MSHN (Mashhad permanent GPS site).

Based on satellite images and In situ produced ^{36}Cl aging studies, Shabanian et al. (2007) have estimated 1 km of right-lateral horizontal offset on the Baghan fault which has been observed on alluvial fans and has cumulated during the last 330 ka, suggesting a slip rate of 2.9 mm/yr. A slip rate of 3.7 mm/yr has been estimated on the Quchan fault based on 330 m of offset on the alluvial fans which has occurred in the last 90 ka (Shabanian et al., 2007). They have estimated 11 and 14 km of total offset on the Baghan and Quchan fault, respectively, which have started roughly 3.5-4.0 Ma ago.

In the last 150 years, several destructive earthquakes occurred in the central part of Kopeh Dagh (Fig. 3-3a, Table 3-1). This region is a populated area with the cities of Quchan, Bojnord and Shirvan. Five large destructive earthquakes (1851, 1871, 1872, 1893 and 1895) have been recorded on the Quchan fault zone, of magnitudes ranging between 6.8 and 7.2 (Ambraseys & Melville, 1982, Tchalenko, 1975, Hollingsworth et al., 2006). These earthquakes caused some destruction in the Quchan region. In May 1929, a large earthquake of magnitude 7.0 occurred on the Baghan fault and damaged the north and the east of the city of Shirvan. It produced more than 50 km co-seismic ground ruptures and killed 3,500 people. On July 13, 1929, a large aftershock was recorded in the town of Faro which is located south east of the Baghan fault, within the Atrak valley. The February 4, 1997, a $M_{w=}$6.4 earthquake occurred near Bojnord (Jackson et al., 2002). The aftershock distribution, as well as geomorphological and geological evidence, shows a right-lateral mechanism similar to the other faults of the Quchan fault zone (Hollingsworth et al., 2006). The August 22, 2000, M_w=5.4 earthquake was recorded in the town of Gholaman which lies in a valley near the Iran-Turkmenistan border, ~50 km north of Bojnord (Jackson et al., 2002, Hollingsworth et al., 2006). In this valley an earthquake (M=~6.5) occurred in 1810 (Ambraseys & Melville, 1982). The teleseismic location of this earthquake does not fall on a particular fault but both earthquakes showed right-lateral strike-slip mechanisms.

3.1.3 The eastern part of Kopeh Dagh

The tectonical feature of the eastern part of Kopeh Dagh (Figs. 3-1, 3-3a) is again different from the central and the western part. The eastern part extends from longitude ~59° to the border of Afghanistan. In the eastern part, there is little evidence for strike-slip faulting along the mountain range or oblique to the range, but a recent earthquake shows a strike-slip focal mechanism related to an unknown fault inside Turkmenistan. The main tectonical feature is shortening accommodated by thrusting along the northern and southern edges of the range (Hollingsworth et al., 2006). In the south of eastern Kopeh Dagh is situated the Kashafrud reverse fault. This NW-SE trending fault is 120 km long and located north of Mashhad city. Several large earthquakes have been recorded on this fault (1598, 1673: M_s=6.6, 1687: M_s=5.5-5.8, 1883) (Ambraseys & Melville, 1982; Berberian 1979, 1981). Masson et al. (2007) estimated a shortening rate across the whole Kopeh Dagh mountain belt (Kopet Dagh and Binalud), by the differential velocities of KASH (Kashmar) and YAZT (close to Sarakhs city situated on Turan shield), to 5±1 mm/yr N-S shortening. They also estimated 2±1 mm/yr of N-S shortening across the eastern part of the Kopeh Dagh range only (excluding Binalud) between MSHN and YAZT. The shortening is oblique to the mountain range and can be split into 1±1 mm/yr of range-perpendicular shortening and 1±1 mm/yr of range-parallel strike-slip.

3.1.4 The Binalud mountain range

Besides the Kopeh Dagh mountain range (Fig. 3-1), the other important tectonical feature of north-east Iran is the Binalud mountain range, which is structurally and geologically the eastward continuation of the Alborz (Alavi, 1992). In contrast to the rocks of the Kopeh Dagh which are distinct from those of Central Iran and belong to the Turan platform (Stöcklin 1974; Alavi 1996), the Alborz-Binalud range forms the north-eastern limit to Central Iran. The boundary between Alborz-Binalud and the Kopeh Dagh runs along the Atrak valley (Figs. 3-1, 3-3a) and represents the northeastern suture between Iran and Eurasia (Alavi 1992, 1996). The tectonic history of the Alborz-Binalud range is older and more complicated than that of the Kopeh Dagh. The most recent phase of uplift began in the Late Cretaceous-Palaeocene (60 Ma ago, Stöcklin 1974). During this time the Kopeh Dagh was not yet formed (Berberian 1976; Berberian & King 1981).

The Binalud mountain range is situated in the south-west of Mashhad and north-east of Neyshabur, two populated cities of the region. Several active reverse faults (Figs. 3-1, 3-3a) follow the Binalud mountain trend in the north and the south of the range. The two most important faults are two reverse faults associated with historical earthquakes in the south-west of Binalud, the Neyshabur and Binalud reverse faults. The Binalud thrust that trends NW-SE for 92 km experienced destructive earthquakes in 1209 (M_s=7.3) and 1389 (M_s=7.3). The Neyshabur fault is 50 km long and is located 15 km east of Neyshabur city. Historical destructive earthquakes occurred on this fault in 1270 (M_s=7.1) and 1405 (M_s =7.4) (Ambraseys & Melville, 1982; Berberian, 1995; Berberian and Yeats, 1999; Berberian et al., 2000). Berberian et al. (2000) propose a 500 years interval of earthquake recurrence for the Neyshabur region.

Former GPS results indicate a present-day shortening rate of 3±1 mm/yr cumulated over the Binalud and the Kuh-e-Sorkh mountain belt south of Binalud (Masson et al., 2007). Assuming a constant deformation rate, the onset of deformation would be estimated to a minimum of ~10 Ma ago, using the total shortening of 30 km which is proposed by Allen et al. (2003a) for the Alborz-Binalud.

3.2 GPS Measurements and Analysis

A geodetic network of 10 benchmarks has been established in 2004 in the Khorasan province (Fig. 3-4) covering the Kopeh Dagh and north-east Iran (SHAM, JANA, GRME, GARD, DARG, BAKH, MAR2, KHAF, DOGH and BAJE). The network was densified with 3 more stations in 2005 (BIAR, ESFN and ZVNG). All sites are installed on bedrock with forced antenna centering (Fig 3- 5) except MAR2 which is a pillar installed in 1996 for the Asia Pacific measurements. The network has been measured in 2004 and 2006, including several sites (YAZT, SHIR, KORD, SEMN, KASH) of the Iran Global network (Nilforoushan et al., 2003; Vernant et al., 2004; Masson et al., 2007). The campaign data were completed by 6 and 23 Iranian permanent GPS stations in 2004 and 2006, respectively. The daily mean repeatabilities, for the north, east and vertical baseline components in 2004 and 2006 are respectively 2.8 mm, 3.0 mm, 6.2mm, and 2.1mm, 1.8mm, 5.3mm. These repeatabilities represent the short term errors of the GPS measurement and result in an estimate of the horizontal velocity uncertainties of 2 mm/yr. To establish the

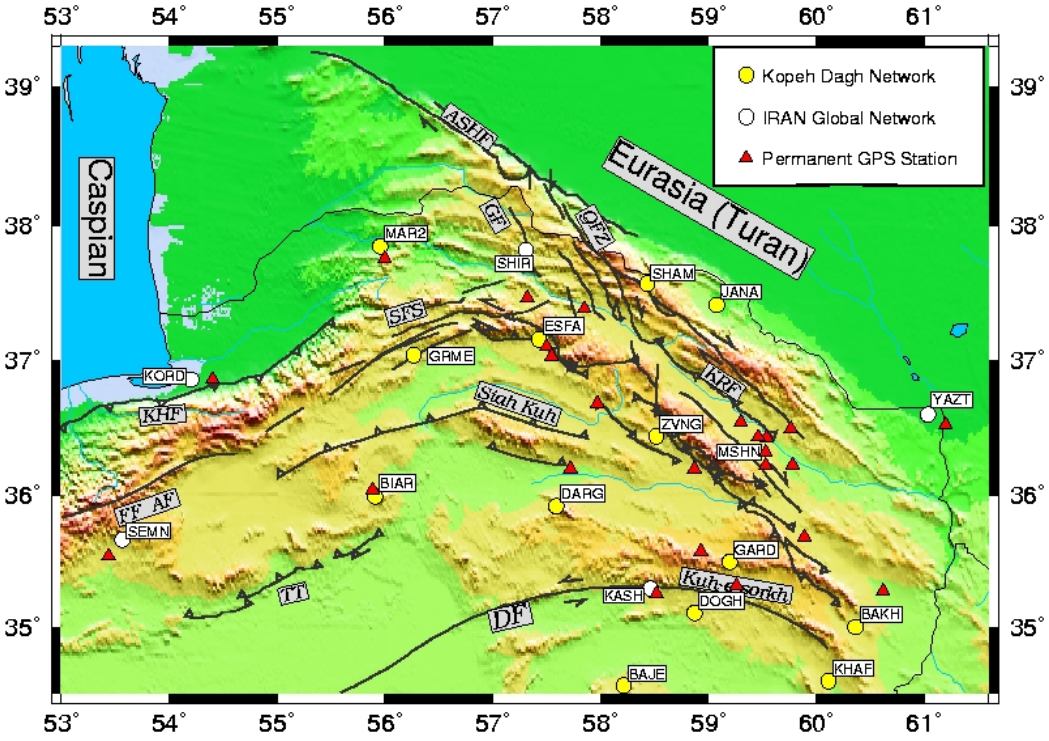

Figure 3- 4. Distribution of GPS stations in Kopeh Dagh Area. The name of the faults are like figure 3-1.

Figure 3-5. Example for a GPS station of the Kopeh Dagh network (site JANA) with forced antenna centring on bed rock.

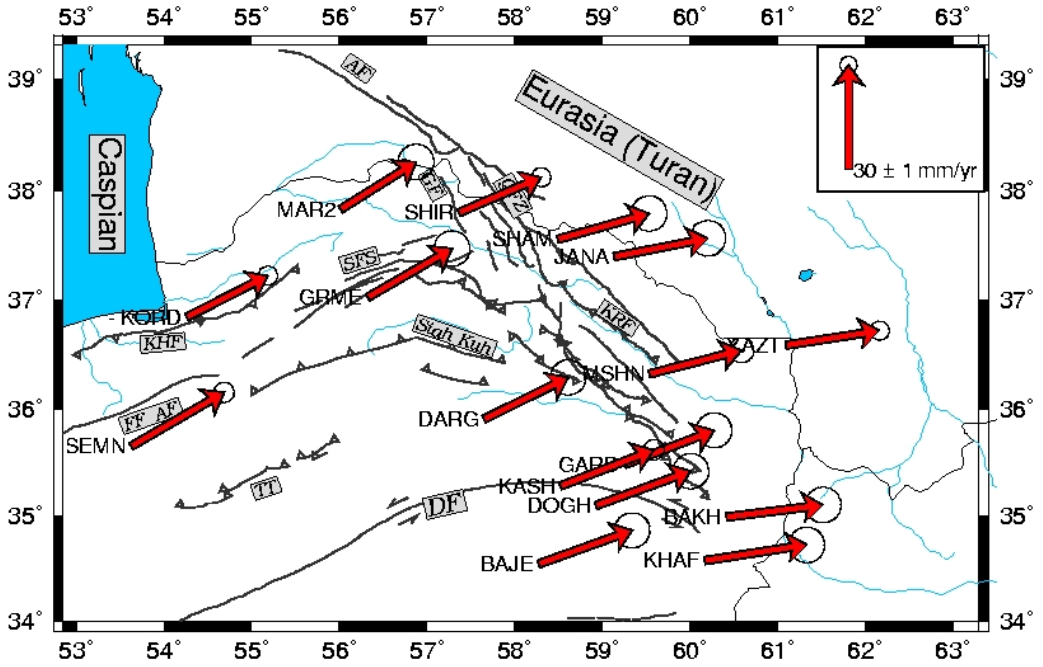

Figure 3-6. Kopeh Dagh velocities relative to the ITRF2000 reference frame. The scale vector corresponds to 30 mm/yr. The error ellipses indicate formal errors within a 95 per cent confidence interval. The name of the faults are like figure 3-1.

velocity field in the Kopeh Dagh network, we combined our local measurements with data from surrounding regional measurement campaigns (Iran Global 1999, 2001, Nilforoushan et al., 2003; Vernant et al., 2004; Central Zagros 1997, 2000, 2003, North Zagros 2001, 2003, Tatar et al., 2002; Walpersdorf et al., 2006, Kerman 2004 (January and December), Kerman 2006, Iran Global 2005, Masson et al., 2007), and quasi-observations (h-files) of a global IGS network from SOPAC from 1997 to 2006. Details about the processing of the data are given in chapter 2.

3.3 Kopeh Dagh velocity field

The velocity field of northeastern Iran has been calculated relative to ITRF2000 (Table 3-2, Fig 3-6) and Eurasia (Table 3-2, Fig. 3-7). The station YAZT, northeast of the Kopeh Dagh, is located on the Turan shield which is part of the Eurasian plate (Vernant et al., 2003). YAZT has a residual velocity of less than 1±2 mm/yr in our realization of the Eurasian reference system (Table 3-2). To facilitate the visualization of differential velocities in the Kopeh Dagh we present also the velocities with respect to YAZT (Fig 3-8, Table 3-2). We consider this velocity field as

Table 3-2. Kopeh Dagh Velocity field list in ITRF2000, EURASIA and YAZT refrence frame. Ve and Vn are east and north velocities components, σe and σn are the uncertainties on the east and north velocity components (one sigma).

SITE	Long.	Lat.	ITRF2000		EURASIA		YAZT		Uncertainty	
	(°E)	(°N)	Ve	Vn	Ve	Vn	Ve	Vn	σe	σn
BAKH	60.360	35.002	22.20	-2.40	-1.85	-1.00	-1.27	-0.76	1.89	1.89
BAJE	58.215	34.558	21.92	3.83	-2.77	4.81	-2.26	5.58	1.82	1.80
DARG	57.589	35.915	19.39	6.06	-5.16	7.04	-4.72	7.96	1.81	1.84
DOGH	58.869	35.108	21.92	3.83	-2.10	5.05	-1.58	5.66	1.90	1.94
GARD	59.197	35.495	20.73	4.00	-3.87	5.23	-3.35	5.76	1.76	1.78
GRME	56.264	37.042	19.52	7.88	-5.06	8.31	-4.73	9.56	2.02	2.09
JANA	59.076	37.413	21.90	-0.52	-2.77	0.48	-2.35	1.04	2.23	2.15
KASH	58.464	35.293	22.78	4.15	-0.82	4.86	-0.32	5.57	0.86	0.85
KHAF	60.110	34.589	23.78	-1.30	-0.36	0.02	0.22	0.32	1.98	2.00
KORD	54.199	36.860	19.50	5.50	-3.53	5.59	-3.29	7.34	0.84	0.83
MAR2	55.956	37.845	17.10	7.48	-7.44	8.07	-7.18	9.39	1.96	2.02
MSHN	59.480	36.335	21.99	0.66	-1.70	1.83	-1.21	2.29	1.08	1.07
NOGH	59.937	32.988	23.95	3.79	-0.84	5.02	-0.23	5.36	2.01	1.95
SEMN	53.564	35.662	23.04	9.02	-0.55	8.67	-0.28	10.58	0.86	0.85
SHAM	58.431	37.570	21.40	1.62	-3.09	2.71	-2.70	3.43	1.78	1.82
SHIR	57.308	37.814	19.48	3.88	-3.84	3.90	-3.51	4.89	1.78	1.82
YAZT	61.034	36.601	22.60	-1.93	-0.53	-0.07	0.00	0.00	0.84	0.83

being close to the Eurasian reference frame. Therefore, our analysis is based on differential velocities with respect to the YAZT site.

3.3.1 Eastern part of Kopeh Dagh

In the eastern part of the Kopeh Dagh belt, the present-day N-S shortening rate cumulated over the Kopeh Dagh and Binalud mountain ranges is evaluated to 6±2 mm/yr by the differential velocities of KASH (Kashmar) and GARD (north of Torbat Heydarieh) relative to the Turan shield (YAZT). Comparing the velocities of MSHN and GARD we can see that the NS shortening across the Binalud and Neyshabur thrusts (south of Binalud mountains) and part of the Kuh-e-Sorkh mountain is about 3.5±2 mm/yr (3 mm/yr shortening perpendicular to the mountain range). The remaining N-S shortening across the Kopeh Dagh range in its eastern part is about 2.5±2 mm/yr. As the Kopeh Dagh range is oriented 120º N, we can also evaluate the range perpendicular shortening and range parallel strike-slip components. Considering MSHN, JANA and YAZT, we have found 2±2 mm/yr of shortening perpendicular to the mountain range and 1±2 mm/yr of right-lateral strike-slip motion along strike in the eastern part of Kopeh Dagh

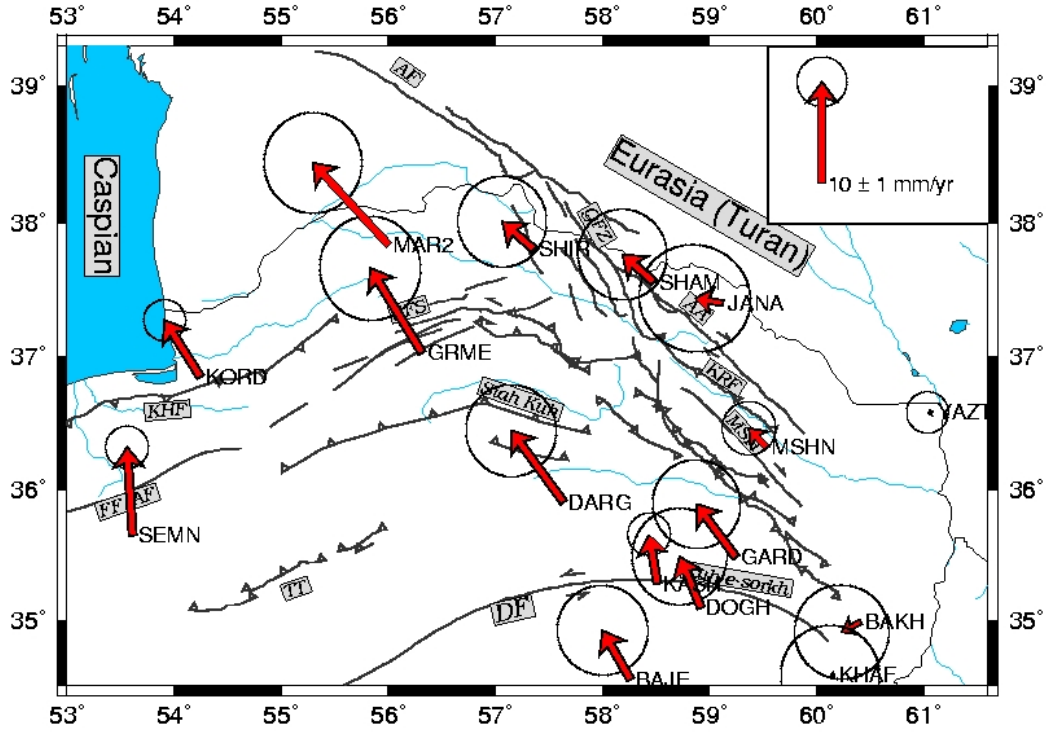

Figure 3-7. Kopeh Dagh Velocities relative to the Eurasian reference frame. The scale vector corresponds to 10 mm/yr. The error ellipses indicate formal errors within a 95 per cent confidence interval. The name of faults are like figure 3-1.

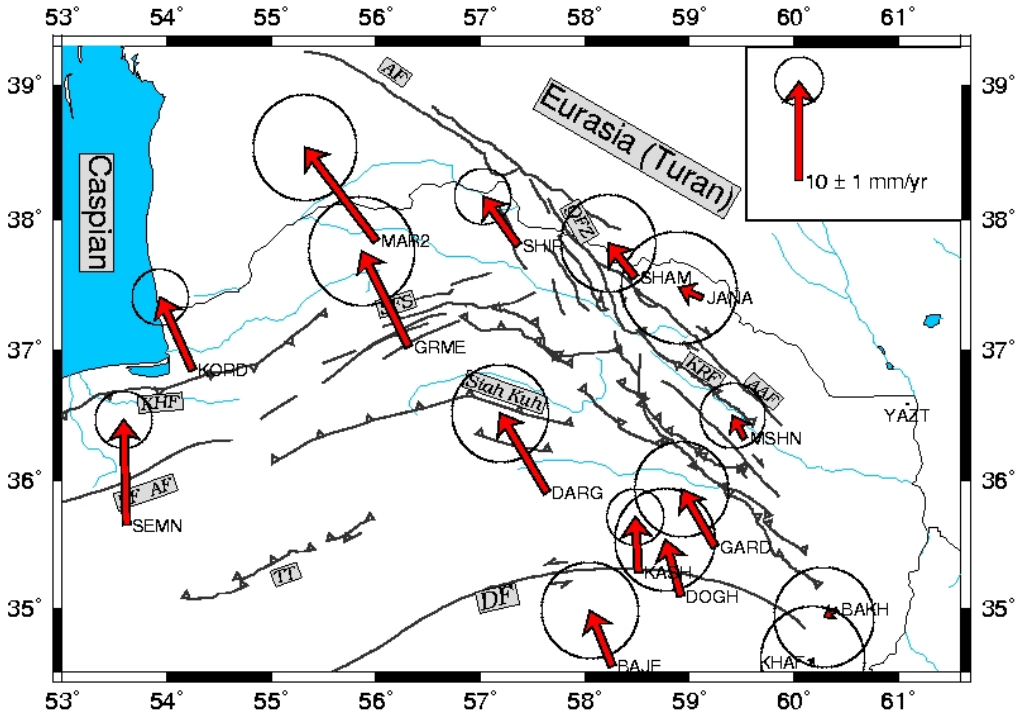

Figure 3-8. Kopeh Dagh velocities relative to YAZT site. The scale vector corresponds to 10 mm/yr. The error ellipses indicate formal errors within a 95 per cent confidence interval. The fault names are indicated in the Figure (3-1).

Hollingsworth et al. (2006) evaluated a minimum of 60 km of N-S shortening for the central Kopeh Dagh from the offsets of the faults of the Quchan fault system and their block rotation model. If these 60 km apply to eastern Kopeh Dagh and considering the N-S shortening rate across the Kopeh Dagh range of 2.5 mm/yr from our GPS measurements is constant, the onset of the Kopeh Dagh shortening is estimated at 24 Ma. This is clearly older than the estimate of Hollingsworth et al. (2006) who did not dispose of the MSHN and GARD velocities and attributed a KASH-YAZT differential velocity of 7 mm/yr (Vernant et al., 2004) to 70 km of N-S shortening on either the Kopeh Dagh only (yielding an onset at 10 Ma) or cumulated on Kopeh Dagh and Binalud (yielding 14 Ma for the Kopeh Dagh shortening onset).

3.3.2 The Quchan fault zone

The Quchan fault zone is a NNW-SSE trending fault zone composed of several parallel right-lateral strike-slip faults, the Shirvan, Baghan, Quchan and Dorbadam faults from west to east (Figs. 3-3a and 3-9). To evaluate the present-day displacement rate of the Quchan fault system, we have used the differential velocity between the stations MAR2, and SHIR on the west side of the Gholaman and Quchan fault zones and JANA and SHAM on the eastern side. On the Quchan fault zone including the Gholaman fault we have measured 5±2 mm/yr of cumulative right-lateral strike-slip motion. Hollingsworth et al. (2006) proposed 10km, 15km and 15km of total offset for the Baghan, Quchan and Bajgiran faults, respectively (totally 40 km cumulative offset). To estimate present-day rates from their total geological offsets, Hollingsworth et al. (2006) needed to infer the onset time of the QFZ deformation. For that, they postulated that the QFZ onset is simultaneous with the east Kopeh Dagh deformation onset. The authors presume that total NS shortening of 70 km in the eastern Kopeh Dagh range is accommodated in the Kopeh Dagh belt only (and not in Binalud) – which we know now is incorrect, and at a rate of 7mm/yr (Vernant et al., 2004) – which is also incorrect. They infer an onset time of 10 Ma, and deduce therefore the individual velocities on the QFZ faults to be ~1mm/yr, ~1.5mm/yr, ~1.5mm/yr on Baghan, Quchan and Bajgiran (Dorbadam) faults, respectively. At the end, this is consistent with our more precise GPS measured results. Considering our GPS velocities of 5±2 mm/yr of strike-slip across the Quchan fault system, and assuming it is constant in time, the onset of deformation on the Baghan, Quchan and

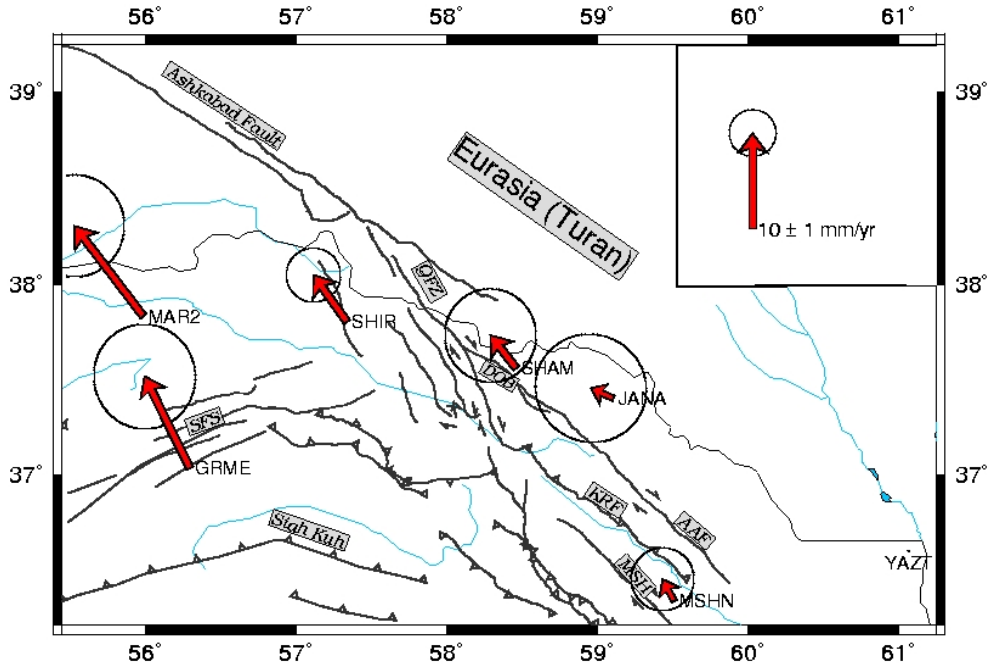

Figure 3-9. Velocity field of Quchan Fault Zone relative to YAZT located on the Eurasia plate. The scale vector corresponds to 10 mm/yr. The error ellipses indicate formal errors within a 95 per cent confidence interval.

Bajgiran (Dorbadam) faults have occurred about 10 Ma ago, probably much later than the Kopeh Dagh deformation onset at 24 Ma.

Shabanian et al. (2007) propose 2.9 mm/yr and 3.7 mm/yr (total cumulative velocity of 6.6 mm/yr) of strike-slip rate for Baghan and Quchan faults, respectively. It seems that their short-term geological estimation is comparable with present-day GPS velocities.

3.3.3 West Kopeh Dagh and Ashkabad fault

North of Kopeh Dagh at the longitude of the MAR2 and SHIR stations, we do not have any station on the Turan shield in Turkmenistan. But considering the velocity difference between YAZT on the Turan shield and SHIR south of the Ashkabad fault, we estimate 3±2 mm/yr of N-S shortening or 2.5±2 mm/yr of fault perpendicular shortening across the Ashkabad fault. The fault parallel strike-slip velocity is estimated to 5±2 mm/yr. Lyberis and Manby (1999) proposed ~ 35 km strike-slip offset along the west of the range starting ~5 Ma ago. This implies that the average geological strike-slip rate of the Ashkabad fault is ~7 mm/yr, consistent with the GPS rate of 3-7 mm/yr, suggesting that it could have been constant over the 5 Ma of fault activity. The MAR2 station, located 120km west of SHIR, has a different

velocity of 3±2 mm/yr. The MAR2 velocity is evaluated by only 2 measurements over 2 years and could contain a systematic error which cannot be detected by only 2 measurement campaigns, so the velocity uncertainty could be underestimated. SHIR has been measured at least 5 times from 1999 to 2006. We have not identified any tectonical structure between these two stations, so the differential velocity of 3±2mm/yr could be absorbed by distributed deformation between MAR2 and SHIR. Moreover, the MAR2 station also evaluates a slightly higher strike-slip rate across the Ashkabad fault (8±2 mm/yr), but closer to geological estimations (~7 mm/yr, Lyberis and Manby, 1999) than the strike-slip rate of 5±2 mm/yr evaluated by the SHIR station.

Both the SHIR and the MAR2 velocities to the west of the Quchan fault zone result in an along-strike extension on the Kopeh Dagh mountain range and westward expelling of the western Kopeh Dagh with respect to YAZT on the Turan shield. This expulsion is evaluated between 5±2 mm/yr (SHIR) and 8±2 mm/yr (MAR2) and accommodated by the Ashkabad fault between the Turan shield and the western part of Kopeh Dagh. On the Ashkabad fault, Hollingsworth et al. (2006) estimated 30 km of along-strike extension. With GPS rates of 5-8 mm/yr it would take 4-6 Ma to achieve this extension. This is coherent with the results of Lyberis and Manby (1999) who have evaluated 35 km of along strike offset and who suggest that the onset of the deformation in the western Kopeh Dagh started 5 Ma ago.

3.3.4 Summary of the Kopeh Dagh deformation onset

Different researchers have given different timing for the first collision between the Arabia and Eurasia plates: Berberian and King (1981, ~65 Ma), Philip et al. (1989, ~5 Ma), Yilmaz (1993, ~35 Ma), Hempton (1987, ~40 Ma), Robertson (2000, ~16-23 Ma), McQuarrie (2003, before 10Ma). The 16-23 Ma is likely to be a reasonable range for initial plate collision. This date is estimated from the deformation and syn-tectonic sedimentation which took place on the northern side of the Arabian plate. Suturing may have been diachronous from the Arabian promontory in the north, southeast along the Zagros (Allen et al., 2004). Based on an extrapolation, Dewey et al. (1989) estimate ~300-500 km northward motion of the Arabian plate with respect to the stable Eurasia since initial collision along the Bitlis-Zagros suture.

Wells (1989), Quennel (1984), Westaway (1994) and Axen et al. (2001) propose that the way the plate convergence might have occurred in different regions depends on the long-term evolution of continental collisions. Therefore it is relevant to remember that the Arabia-Eurasia collision underwent reorganization at 5 Ma (Allen et al. 2004). This is the time when deformation started or intensified 3-7 Ma ago in many of the currently active regions, such as the East and North Anatolian faults, the South Caspian Basin, the Kopeh Dagh, the Zagros and the Alborz.

In Table 3-3 we resume the GPS and geologically estimated ages of deformation for different parts of the Kopeh Dagh. The GPS velocities and total geological offsets provided by different authors result in successive onsets of the deformation along the Kopeh Dagh. Postulating that the GPS velocities have been constant during geological times, we obtain a deformation onset at up to 24 Ma in the eastern part of the range, at 8 Ma for the central part and at 5 Ma for the western part. This clearly indicates that the deformation in the central and the eastern part of Kopeh Dagh is older than the deformation in other Iranian mountain belts (Zagros, Alborz at 3-7 Ma) but still consistent with other geological constraints, e.g. with Berberian and King (1981), evaluating the deformation onset in the Kopeh Dagh loosely at post 30 Ma.

Shabanian et al. (2007) have estimated 11 and 14 km of total offset on the Baghan and Quchan fault, respectively, which have started roughly 3.5-4.0 Ma ago. With considering the total offset of 25 km on Quchan fault zone estimated by Shabanian et al. (2007) and a GPS velocity of 5 mm/yr we estimate the age of Quchan faulting to 5 Ma. Considering the total offset of 40 km estimated by Hollingsworth et al. (2006) we estimate an age of 8 Ma for the faulting of the Quchan fault zone. The slip onset of the Quchan fault zone can therefore be evaluated to 5-8 Ma reflecting the uncertainty of the total geological fault offset.

Lyberis and Manby (1999) have estimated ~75 km NS shortening across the western part of the Kopeh Dagh according to the construction of geological balanced sections. The projection of this NS shortening on the Ashkabad fault oriented $N120^0$ yields a total dextral strike-slip displacement of 35 km, which is coherent with an onset of deformation 5 Ma ago and a present-day strike-slip rate of 5-8 mm/yr. However, if the 75 km of NS shortening started 5 Ma ago, the average NS shortening rate is evaluated to be 15 mm/yr, in contrast to the 4-9 mm/yr observed across western Kopeh Dagh (north velocities of MAR2 and SHIR with respect to Eurasia or

Table 3-3. Comparison of GPS and geologically determined ages, for onset of deformation in different parts of the Kopeh Dagh. KD: Kopeh Dagh, FZ: Fault Zone, SS: Strike-slip.

Kopeh Dagh Segments	Geologic Offsets	GPS velocities	GPS Age	Geologic Age
Eastern KD	60 km NS shortening	2.5 mm/yr	24 Ma	< 30 Ma (Berberian & King, 1981)
Quchan FZ (HW)	40 km right-lateral SS	5mm/yr	8 Ma	< 30 Ma (Berberian & King, 1981)
Quchan FZ (SH)	25 km right-lateral SS	5mm/yr	5 Ma	
Ashkabad fault	35 km right-lateral SS	5-8 mm/yr	4-7Ma	5 Ma (Lyberis & Manby, 1999)
	75 km NS shortening	4-9 mm/yr	8-19 Ma	5 Ma (Lyberis & Manby, 1999)

YAZT, (Table 3-2). This means either that a part of the 75 km of NS shortening must be localized outside of the Kopeh Dagh range, or that the shortening rate has changed during the last 5 Myr. The topography between the Shahrud fault system and the Ashkabad fault is formed by N-S shortening (Hollingsworth et al., 2006) which supports the hypothesis that presently a part of the NS shortening is absorbed outside of the Kopeh Dagh range (but north of the Shahrud fault).

As much as 16 mm/yr of NS shear with respect to the Hellmand block (part of Eurasia) have been measured, however, for the Central Iran block (Vernant et al., 2004). This shear is accommodated on NS right-lateral strike-slip faults bounding the Lut block to the east and the west. The resulting NS shortening north of the Lut block decreases from west to east, and a part is absorbed by different EW oriented faults before reaching the Kopeh Dagh belt. Therefore, only ~7 mm/yr of NS shortening is left north of the Doruneh fault at longitude of ~57° (the longitude of western Kopeh Dagh), even south of the Shahrud fault. The shortening rate of 15 mm/yr proposed by Lyberis and Manby (1999) for western Kopeh Dagh is therefore not coherent with present-day kinematics.

3.3.5 The Alborz-Binalud deformation

The Binalud is, tectonically and geologically, the eastern continuation of the Alborz mountain belt. Allen et al. (2003a) estimated 30 km of NS shortening across the Alborz-Binalud range. Our GPS measurements (Fig. 3-8) evaluate a NS

shortening rate of 3.5±2 mm/yr across the Binalud, comparing the velocities of GARD and KASH with MSHN. If this shortening rate was constant in the past, it takes about 9 Ma to achieve this shortening. The Binalud is oriented N120° so the shortening perpendicular to the range and along-range strike-slip are estimated to be 3 mm/yr and 2 mm/yr, respectively.

The comparison of the velocities at MAR2 and GRME on both sides of the 60° N trending Shahrud fault (east Alborz mountain range) shows 2.5±2 mm/yr of EW left-lateral strike-slip. Also, comparing the velocities of SEMN and KORD further west at longitude ~54°, we observe 3.5 ±2 mm/yr of shortening and 3.5 ±2mm/yr of left-lateral strike-slip motion. Even further west in central Alborz, Vernant et al. (2004) proposed 5 mm/yr of shortening and Djamour et al. (2007 submitted) proposed 1.5 mm/yr of strike-slip on the Mosha fault and 5 mm/yr of shortening for the range. Considering these results (Table 3-4), the shortening rate decreases from central to eastern Alborz (5 mm/yr at longitude 52°, 3.5±2 mm/yr at the longitude of ~54° and 1±2 mm/yr at the longitude of ~56°). In the Binalud (longitude ~59°) the shortening increases again to 3.5 ±2 mm/yr. The left-lateral strike-slip rate in the central Alborz (~52°) is slightly lower than in the eastern Alborz (~54°). This left-lateral rate is accommodated on the Firuzkuh and Astaneh faults in the south of the Alborz mountain range. In the Binalud segment we observe only 1±2 mm/yr of right-lateral strike-slip rate. Our results suggest that the tectonic feature of the eastern Alborz and Alborz-Binalud deformation is different than the central Alborz. We believe that the total deformation decreases from central Alborz to Binalud, to be zero at the limit of the Hellmand block corresponding to the incoming velocities from south. Strike-slip activity in the Alborz-Binalud range is related to NS shortening projected on the trend of the mountain belt: faults oriented between 0 and 90°N have a left-lateral component, faults oriented between 90 and 180°N have a right-lateral component. The trend of the eastern Alborz faults is ~60°N and they move left-laterally. Binalud is oriented 120°N, with right-lateral strike-slip motion. A zone of zero strike-slip is situated between the segments with left and right-lateral motions at about 57° E, at the eastern termination of the Shahrud fault system.

South of eastern Alborz and Binalud, on the Siah-Kuh and Kuh-e-Sorkh mountain ranges (between the DARG and GRME and the GARD, DARG, KASH and DOGH stations, respectively) no significant deformation has been found at the level of 1

Table 3-4. Comparison of deformation in the different parts of Alborz-Binalud. LL and RL for left-lateral and right-lateral strike-slip motion.

Location	Central Alborz	East Alborz	Shahrud FS	Binalud
Longitude	~52°	~54°	~56°	~59°
Reference	Vernant/Djamour	SEMN/KORD	MAR2/GRME	GARD/KASH/MSHN
Mountain trend	100°N	60°N	60°N	120°N
NS (shortening)	5±2mm/yr	3.5±2mm/yr	1±2mm/yr	3.5±2mm/yr
Strike-slip	1.5-4mm/yr LL	3.5±2mm/yr LL	2.5±2mm/yr LL	2±2mm/yr RL

mm/yr, consistent with Fattahi et al. (2006) who infer from geological observations only 1 mm/yr of shortening across the Siah-Kuh range.

3.3.6 Interpretation of the velocity components on transects

To estimate the shortening and the strike-slip components of different faults, we have projected the north and east velocity components measured in the Kopeh Dagh network on two E-W transects TR-A and TR-B, located at latitude ~37.2°N and ~35.7°N, respectively (Figs. 3-10, 3-11a and 3-11b). On TR-A, the NS velocity component decreases from west to east. The maximum shear between the sites MAR2 and YAZT is about 9±2 mm/yr. This motion is accommodated in the region mainly around the Quchan fault zone (5±2 mm/yr), in eastern Kopeh Dagh (1.5±2 mm/yr) and some part by distributed deformation. The Euler pole of the Kopeh Dagh region is located in Turkmenistan so it is normal that the velocities increase from east to west.

The E-W velocity component on TR-A has a significant value of 4.5 mm/yr in average over sites KORD, MAR2, GRME and SHIR to the west of the Quchan Fault Zone and an average value of 0.5 mm/yr over sites SHAM, JANA, MSHN and YAZT to the east of this zone. This 4.5 mm/yr of elongation across the QFZ shows that the Kopeh Dagh expels westward the South Caspian Basin. This extension is created by anti-clockwise rotation around a vertical axis of the right-lateral Baghan, Quchan and Bajgiran faults of the QFZ (Hollingsworth et al., 2006) and accommodated by strike-slip on the Ashkabad fault in the north and the Shahrud fault system in the south of

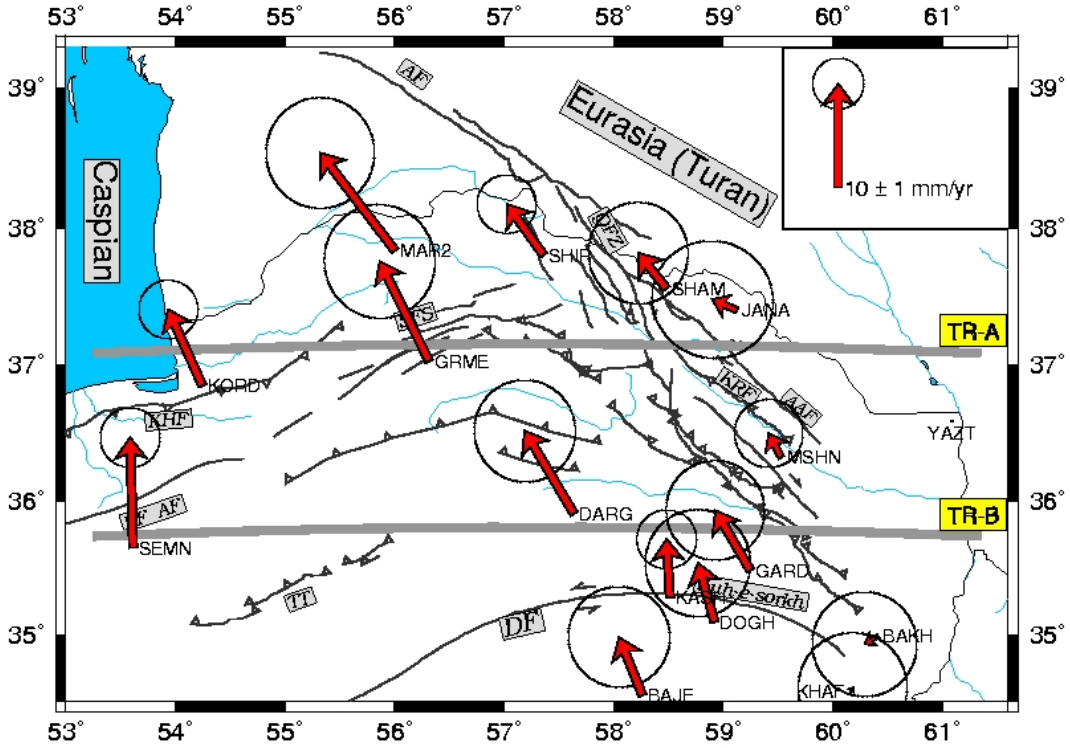

Figure 3-10. Kopeh Dagh velocity field with respect to YAZT and situation of two EW transects TR-A and TR-B presented in Fig. 3-11a and b.

the South Caspian block. Across the Shahrud fault system we observe a differential EW velocity of 2.5 mm/yr between MAR2 and GRME. Although the MAR2 velocity is suspected to be still too high after only two measurement campaigns over 2 years, the sense of the motion is coherent with left-lateral strike-slip as expected on the Shahrud fault. Moreover, KORD, MAR2 and SHIR are all situated on the rigid South Caspian block, but we observe a 2.5 mm/yr higher velocity on MAR2 than on the two other sites. We believe that this difference is related to the measurement uncertainty of the MAR2 velocity and that a re-measurement of this site will yield a lower site velocity, closer to the values of KORD and SHIR.

As the Kopeh Dagh region is limited to the stable and rigid Turan shield to the east and the north, the incoming NS shortening induces a westerly motion of the region facilitated by the subduction of the South Caspian block underneath the Talesh to the west and leading to the expulsion of the South Caspian block to the west. The incoming NS shortening is also partially accommodated by transpression along the Ashkabad fault and subduction of the South Caspian basin beneath the Apsheron Sill in the north-west. The sinking of the South Caspian lithosphere and the Kura basin indicates the closure of the South Caspian basin.

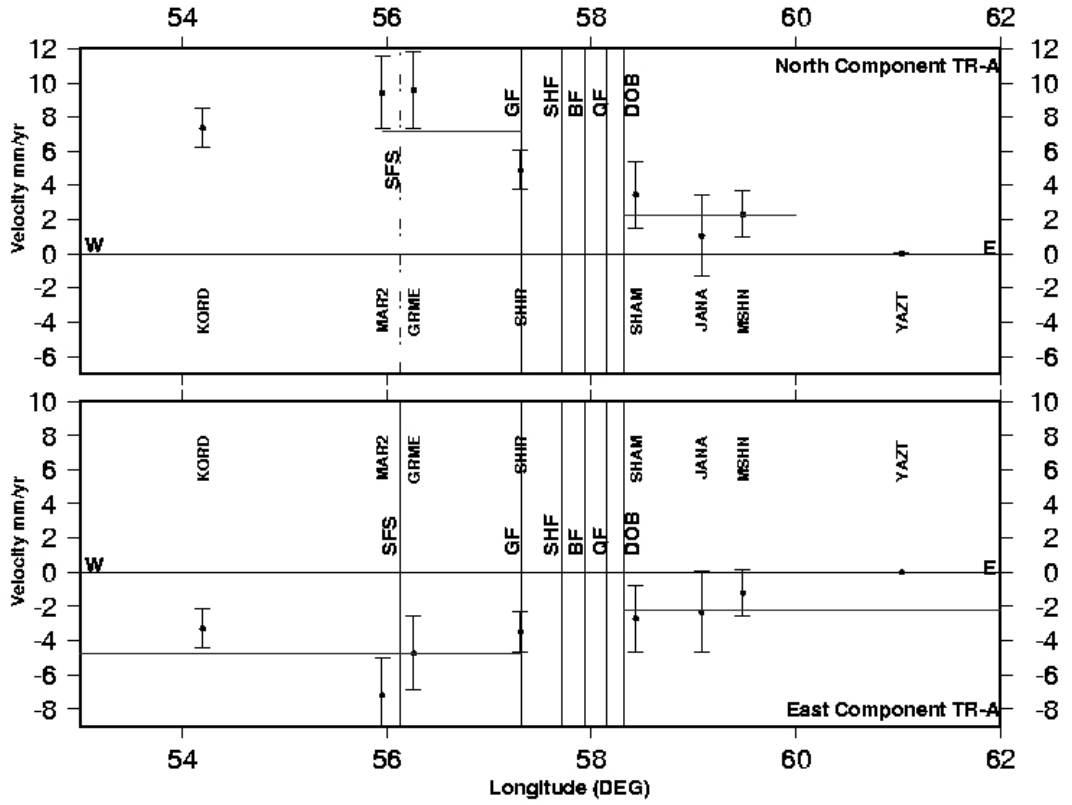

11 a.

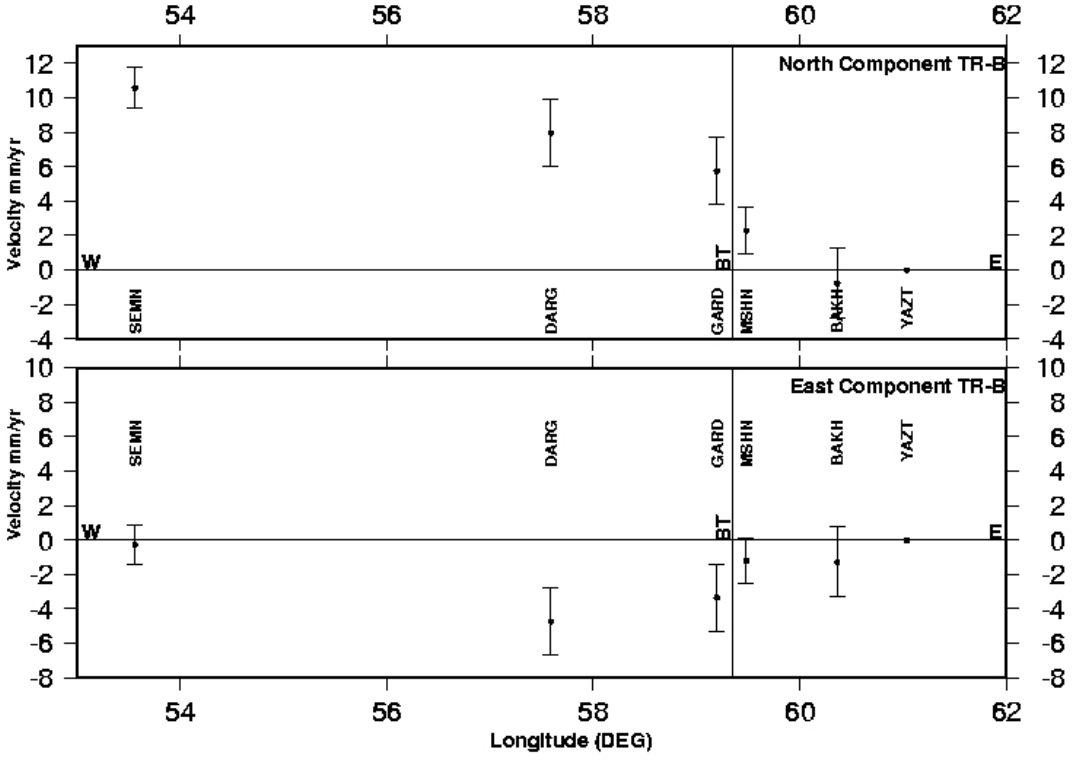

11b

Figure 3-11. North and east station velocity components (mm/yr) with respect to the site longitudes (DEG) projected on two EW transects, TR-A (11 a) and TR-B (11 b). The transects TR-A and TR-B pass at the latitudes 37.2° and 35.7°, respectively (for situation see Fig 3- 10).

On the transect TR-B (Fig. 3-11b), the N-S velocity components show the same behavior as on transect TR-A, diminishing from west to east. The maximum shear between SEMN and YAZT on the Turan shield is 10 mm/yr and therefore higher than on TR-A (6 mm/yr). The differential shear between transects TR-A and TR-B is accommodated by the khazar, Firuzkuh and Shahrud fault systems. A 2-3 mm/yr difference on the west velocity components is found between sites DARG and GARD in the south and MSHN, BAKH and YAZT in the north of Binalud which can be related to right-lateral motion across the Binalud range.

3.4 A kinematic model

A regional deformation field has been computed from GPS measurements (Fig. 3-10) covering the Kopeh Dagh, eastern Alborz and Binalud mountain belts. At the scale of north-east Iran, the NS shortening increases from east to west, with shortening rates of 6±2 mm/yr, 7±2 mm/yr and 8±2 mm/yr, at longitudes ~59°, ~57° and ~55.5°, respectively (Fig. 3-12a, 3-12b and Fig3c). Toward the Afghanistan border (east of 60°), the deformation fades out completely. These increasing velocities are related to 16 mm/yr NS shear between Central Iran and the Hellmand block (Vernant et al., 2004), accommodated on the east and west borders of the Lut block. This regional shear is spread over ~400 km and creates a Kopeh Dagh deformation which varies with longitude. One of the effects is an average and rather homogeneous clockwise rotation of the whole Kopeh Dagh range with between 0.7±0.2°/Ma and 1.2±0.8°/Ma, with respect to an Euler pole situated in Turkmenistan (39.1°±0.7° N, 60.5°±0.8°E) or with respect to the nearest point in stable Eurasia (YAZT), respectively.

In the eastern part of the network, the Kopeh Dagh deformation is characterized by 2±2 mm/yr of across-strike shortening and 1±2 mm/yr of along-strike dextral strike-slip motion. South of the eastern part of Kopeh Dagh, the Binalud range absorbs 3.5 mm/yr of the NS shortening and the strike-slip motion is about 2 mm/yr along the range. This is different from the western part of the Kopeh Dagh range where most of the shortening is absorbed both by right-lateral strike-slip motion along the Ashkabad Fault and left-lateral strike-slip motion on the Shahrud Fault. In

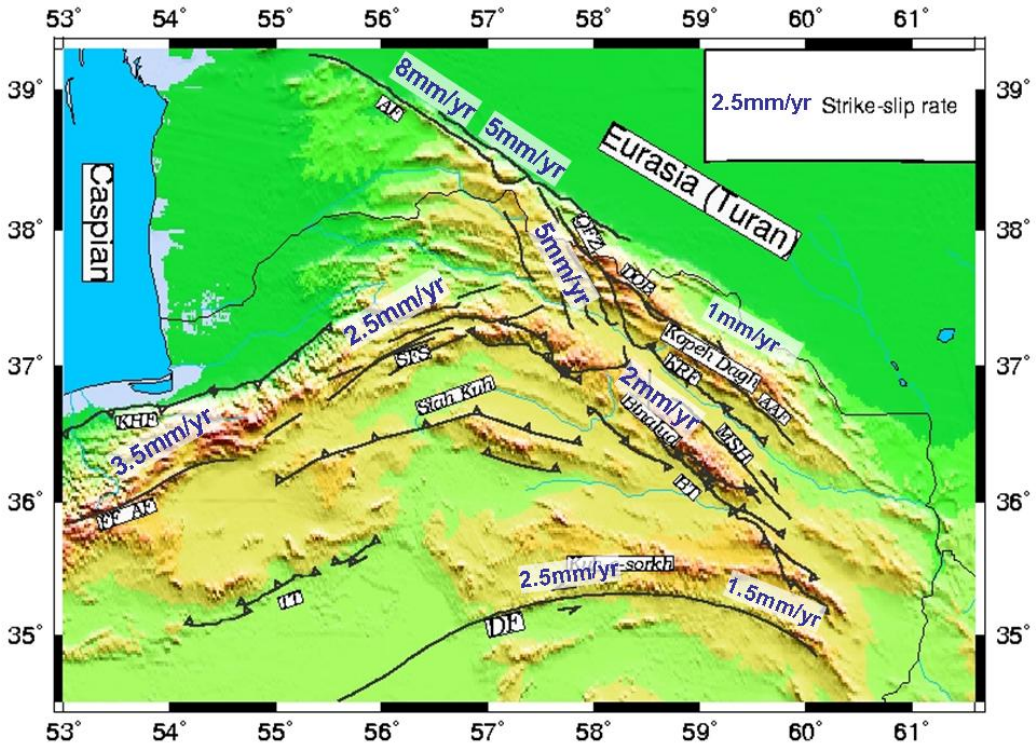

Figure 3-12a. Summary of strike-slip rates in the Kopeh Dagh region.

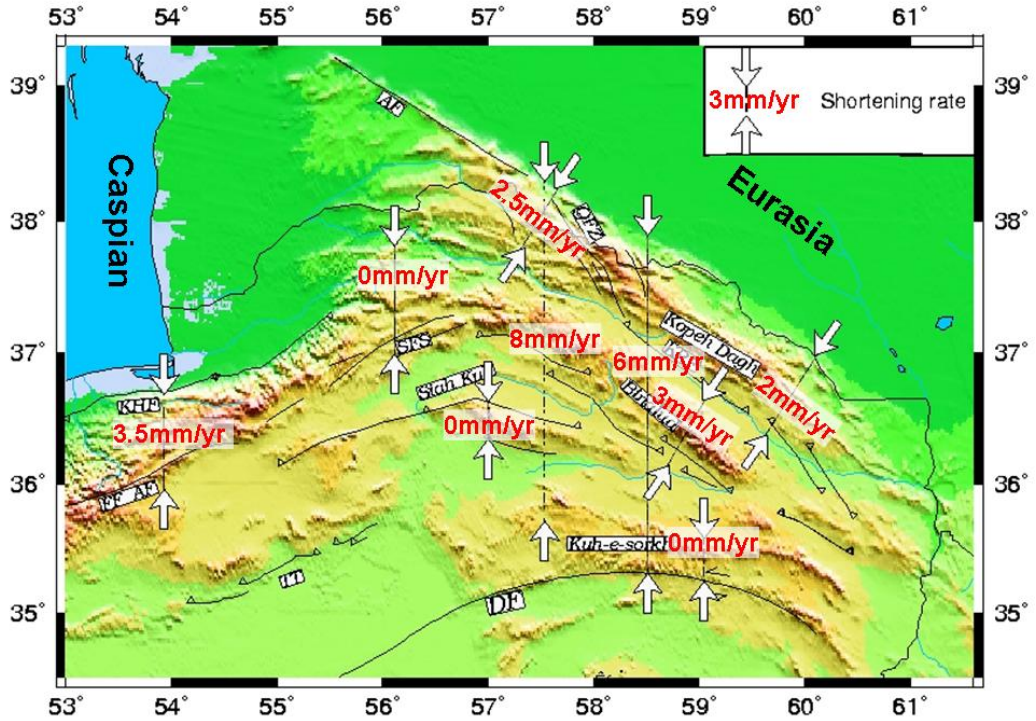

Figure 3-12b. Summary of the shortening rates in the Kopeh Dagh region.

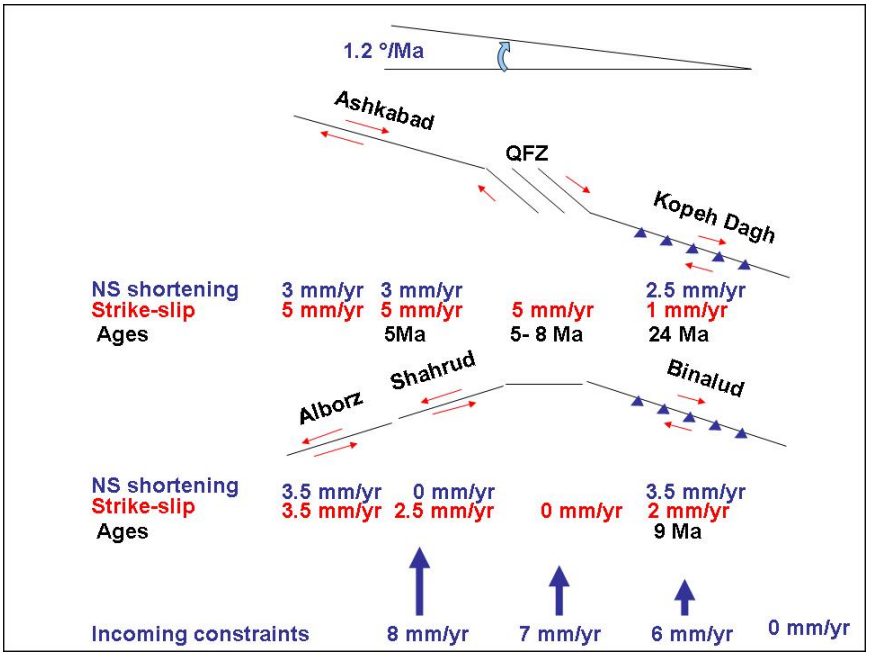

Figure 3-12C. Schematic presentation of the shortening and strike-slip rates and the ages of the faulting inferred by GPS constant velocity and geological total offset in the Kopeh Dagh region. The red values indicate strike-slip rates, the blue values are shortening rates and black values are the age of the faulting.

the central part of Kopeh Dagh, the incoming N-S shortening rate of 7±2 mm/yr is accommodated in the Quchan fault zone by anticlockwise rotation of blocks which creates 5±2 mm/yr of EW extension across the fault zone (Hollingsworth et al. 2006). Note that the incoming shortening is not absorbed in the Alborz-Binalud range, before reaching the QFZ. Our GPS measurements show a total of 5±2 mm/yr right-lateral strike-slip on the Quchan fault zone and 5±2 mm/yr right-lateral strike-slip on the Ashkabad fault to accommodate this extension.

In the western part of Kopeh Dagh, at the longitude of ~56°, the total shortening rate is about 8±2 mm/yr which is accommodated partly on the Ashkabad and Shahrud faults by right-lateral and left-lateral strike-slip, respectively, and partly by shortening on the Ashkabad fault and on other thrust faults like Khazar fault, because the Topography of the North of Shahrud Fault system is a good evidence. If the block limited by the Ashkabad and Shahrud faults (the eastern extension of the South Caspian Basin block), is rigid and the two faults are the only active tectonic features in the region, we can calculate a theoretical value for the westward expulsion of the south Caspian block corresponding to the observed total 8 mm/yr of NS shortening. The EW motion is constrained only by the orientation of the Ashkabad

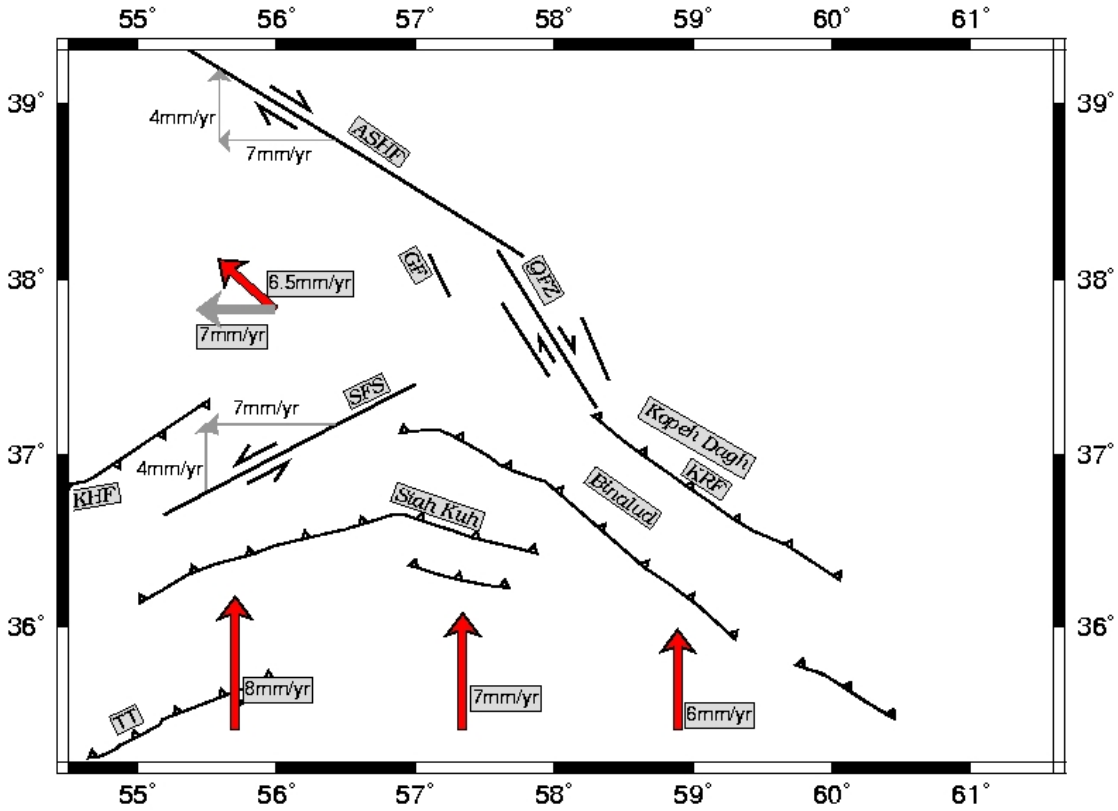

Figure 3-13. Simple kinematics model of the westward expulsion of the South Caspian Basin block along the Ashkabad and Shahrud faults.

fault and the Shahrud fault. We present a rough calculation with a simplified fault scheme (Fig. 3-13). The Ashkabad and Shahrud faults are symmetric to the EW axis, Ashkabad oriented 300°N and Shahrud 240°N. The 8 mm/yr of shortening are split equally over both faults. On each fault, 4 mm/yr of NS shortening should produce ~ 7 mm/yr of EW motion of the South Caspian block. The difference in orientation makes the strike-slip right-lateral along the Ashkabad fault and left-lateral along the Shahrud fault. This theoretical westward expulsion rate (grey vector on Fig. 3-13) is comparable with the observed GPS velocities on the South Caspian block of 6.5±2 mm/yr (red vector on Fig. 3-13). The difference with the simple model could be due to the fact that no significant shortening is observed so far on the Shahrud fault. Other reasons could be internal deformation experienced by a not completely rigid block, with the Khazar thrust fault northwest of the Shahrud fault system being a candidate. Re-measurements of the existing stations (in particular MAR2 with only 2 measurements by now) and densification of the network on the South Caspian block could help better constraining the mechanism of the SCB westward expulsion.

Our kinematics model is generally compatible with Hollingsworth et al. (2006). We provide precise present-day rates and orientations of the active tectonic mechanisms. These rates help to characterize the role of the different faults involved in the present-day deformation. If we extrapolate these short-term rates over geological time spans, they give some constraints on the age of the different parts of Kopeh Dagh and on the long term stability of the deformation rates.

3.5 South Caspian Basin Deformation

Our GPS measurements in NE Iran add some new information on the present-day kinematics of the South Caspian Basin, covered by the NW part of our network. The only significant part “on-land” allowing a measure of its displacement by GPS is located east of the South Caspian Sea.

3.5.1 Tectonic settings and seismicity

The South Caspian Basin is aseismic, with low height (much of it is 500–1000 m below sea level), and a surface of 350x450 square km (Fig. 3-14). It is surrounded by several seismic belts on all sides. The lack of earthquake records within the basin shows that the basin is probably rigid (Fig. 3-15). The basin is bounded by the Apsheron sill to the north, the Talesh, Alborz and Kopeh Dagh mountains, to the west, the south and the east, respectively, with the western Kopeh Dagh and the eastern Alborz measured by our study.

The Apsheron (Apsheron-Balkhan) sill is a prominent bathymetric feature separating the deep South Caspian basin from the shallower northern Caspian basin. This sill connects the Greater Caucasus and the Kopeh Dagh range. The depth of recorded earthquakes for the Kopeh Dagh, Talesh and Alborz forming the east, south and west boundary of basin is less than 30 km (Table 3-5) but in the northern part of the Caspian along the Apsheron sill, the depth of the earthquakes extends at least as deep as 75 km. Focal mechanisms of the earthquakes (Mw > 6) indicate normal faulting parallel to the strike of the sill. Depth and focal mechanisms support the northward subduction of the South Caspian Basin under the northern Caspian Basin (which is part of the Eurasian plate) (Jackson et al. 2002; Masson et al. 2007).

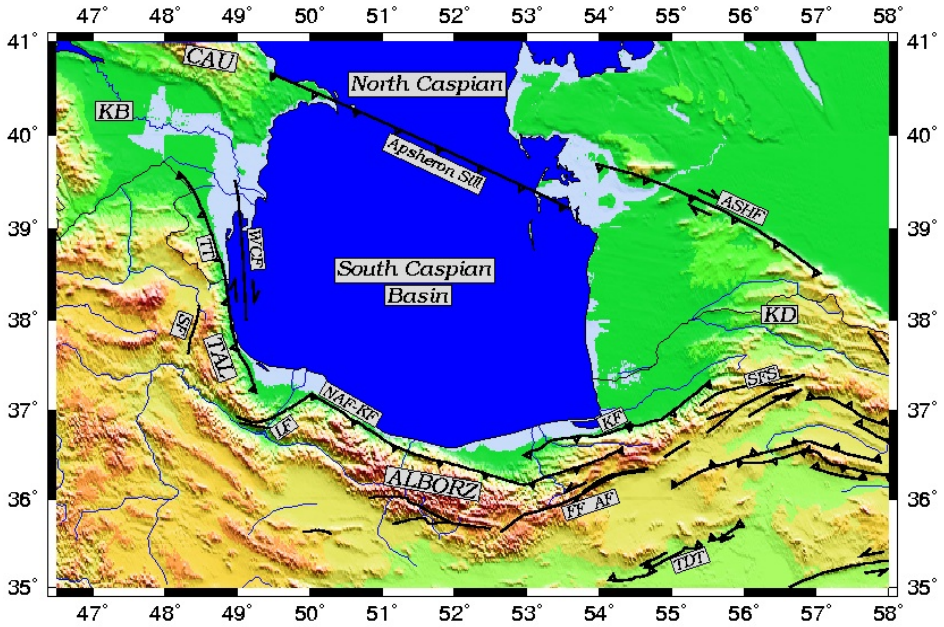

Figure 3-14. Tectonics of the South Caspian Basin region. KB: Kura Basin, CAU: Caucasus, KD: Kopeh Dagh, TAL: Talesh, ASHF: Ashkabad Fault, SFS: Shahrud Fault System, KF: Khazar Fault, FF: Firuzkuh Fault, AF: Astaneh Fault, NAF: North Alborz Fault, LF: Lahijan Fault, SF Sangavar Fault, TT: Talesh Thrust, TDT: Torud Thrust, WCF: West Caspian Fault.

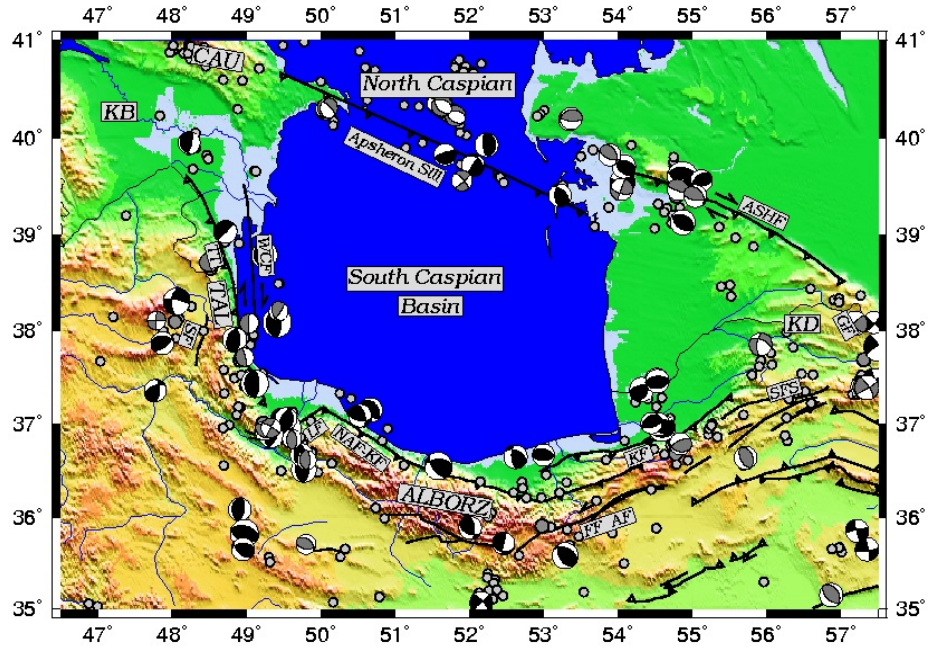

Figure 3-15. Seismicity of the South Caspian Basin region. Grey fault planes are events which are constrained by waveform modelling (Table 3-5; Jackson et al. 2002). Black fault planes are all Harvard CMT solutions (1976-2007). White and grey circles are instrumental seismicity (1964-1998) (white: mb 4.5-5.5, grey: mb > 5.5) (Engdahl et al., 1998). KB: Kura Basin, CAU: Caucasus, KD: Kopeh Dagh, TAL: Talesh, ASHF: Ashkabad Fault, SFS: Shahrud Fault System, KF: Khazar Fault, FF: Firuzkuh Fault, AF: Astaneh Fault, NAF: North Alborz Fault, LF: Lahijan Fault, SF Sangavar Fault, TT: Talesh Thrust, TDT: Torud Thrust, WCF: West Caspian Fault.

Table 3-5. Earthquake source parameters, determined by body wave modelling. Epicentres are from Engdahl et al. (1998) and their updated catalogue. Mw is the moment-magnitude, calculated from the formula: Mw=(log10M0x16.1)/1.5, where M0 is the moment in Nm. The strike, dip and rake of the two nodal planes are s1, d1, r1 and s2, d2 r2. sv is the slip vector azimuth of the earthquakes. The centroid depth in km is z. The penultimate column refers to the work where the inversion is published: P is Priestley et al. (1994), B is Baker (1993), J is Jackson (2002), C is Campos et al. (1994). After Jackson (2002).

Date	Time	Lat.	Long.	Mw	s1	d1	r1	s2	d2	r2	sv	z	R
1962 9 1	1920	35.70	49.80	6.98	311	42	113	100	52	70	41	10	P
1969 1 3	0316	37.11	57.81	5.45	304	40	84	132	49	95	34	7	P
1970 7 30	0052	37.85	55.92	6.35	293	56	-150	185	65	-37	23	11	P
1971 2 14	1627	36.64	55.72	5.67	336	39	93	152	51	87	66	11	P
1972 12 1	1139	35.45	57.92	5.38	156	65	-176	64	87	-25		8	P
1978 11 4	1522	37.71	48.97	6.12	141	12	65	346	79	95	76	21	P
1979 12 9	0912	35.15	56.87	5.55	325	36	99	133	54	83		9	B
1980 5 4	1835	38.07	49.04	6.34	27	6	-63	181	84	-93	91	15	P
1981 8 4	1835	38.20	49.43	5.52	154	35	32	36	72	120	126	20	P
1983 7 22	0241	36.93	49.24	5.45	120	35	83	308	55	94	30	10	P
1984 2 22	0544	39.47	54.05	5.74	106	60	174	199	84	30	289	27	P
1985 10 29	1423	36.79	54.84	6.16	106	30	126	246	65	71	336	13	P
1986 3 6	0005	40.38	51.62	6.38	50	5	-158	299	88	-85		31	P
1987 9 7	1132	39.47	54.81	5.51	305	10	103	111	80	87	31	30	P
1989 9 16	0205	40.35	51.57	6.49	80	26	-135	308	71	-70		31	P
1989 9 17	0053	40.23	51.81	6.16	127	44	-66	277	49	-111		35	P
1990 6 20	2100	36.96	49.33	7.30	301	82	5	210	85	171	120	12	C
1990 6 21	0902	36.61	49.81	5.59	170	28	81	1	62	95		10	A
1991 11 28	1720	36.84	49.61	5.66	185	44	101	350	47	80		8	A
1993 8 31	0655	41.87	49.47	5.13	221	37	37	100	69	121		76	A
1994 7 1	1012	40.19	53.35	5.58	259	24	78	92	67	95		42	A
1994 7 1	1950	40.20	53.37	5.11	251	20	69	94	71	97		41	A
1995 10 29	0627	39.56	51.90	5.32	49	77	-166	316	76	-13		61	A
1997 2 4	0953	37.39	57.33	5.40	338	67	150	80	63	26	350	13	A
1997 2 4	1037	37.39	57.35	6.44	326	75	173	58	83	15	328	8	A
1997 2 28	1257	38.10	47.79	6.00	183	81	-1	273	89	-171		9	A
1997 5 7	1616	40.33	51.63	5.20	287	40	-115	138	53	-69		50	A
1998 7 9	1419	38.71	48.50	5.69	72	8	0	342	90	98	72	27	A
2000 8 22	1655	38.07	57.19	5.59	133	69	171	227	81	-150	317	4	A
2000 11 25	1809	40.29	50.06	6.18	317	76	-80	101	17	-124		40	A
2000 11 25	1810	40.31	50.09	6.08	313	70	-115	187	32	-41		33	A
2000 12 06	1711	39.40	55.04	6.86	322	36	127	100	62	67	10	31	A
2001 6 10	0152	39.83	53.89	5.31	335	40	125	112	58	64	22	31	A

To the east, the South Caspian Basin is bounded by the right-lateral Ashkabad fault in the Kopeh Dagh and the left-lateral Shahrud fault system at the eastern continuation of Alborz, expelling the South Caspian Basin in NW direction. In addition to the right-lateral strike-slip along the Ashkabad fault, the Kopeh Dagh is also overthrusting the Turan shield. The earthquakes located in the western Kopeh Dagh involve mostly reverse faulting parallel to the NW regional strike, near the Ashkabad

fault, from longitude 53° to 55° (Tchalenko 1975; Berberian 1981; Hollingsworth et al. 2006).

In the south, the Caspian Basin is bounded by the Alborz Mountains. This east-west range extends from longitude ~49° to ~56°. The depths of the well constrained earthquakes in the Alborz are generally less than 15 km. Most of the focal mechanisms in this belt show either reverse faulting or left-lateral strike-slip activity.

The NS trending Talesh Mountains form the western boundary of the South Caspian Basin. The range is the westward continuation of the Alborz but it is narrower. The earthquake mechanisms in the Talesh and along the south-west Caspian shore show shallow thrusting. This suggests that the continental crust of NW Iran is overthrusting the oceanic crust of the South Caspian Basin (Priestley et al., 1994; Jackson et al., 2002; Allen et al., 2003). Part of the Arabia-Eurasia convergence is absorbed along the West Caspian fault (WCF, Fig. 3-14 and 3-15) extending from the Kura Basin down to the SW corner of the South Caspian Basin and allowing the Talesh to move northward with respect to the South Caspian Basin (Karakhanian et al. 1997; Nadirov et al. 1997; Allen et al. 2003). However, its activity is not reflected by the focal mechanisms in vicinity of the WCF which are exclusively EW oriented thrust mechanisms.

3.5.2 Present-day tectonics model of the South Caspian Basin

Jackson et al. (2002) suggested a model for the active tectonics of the South Caspian Basin (Figure 3-16). They believe that left-lateral motion on eastern Alborz and right-lateral displacement on Ashkabad fault expels the South Caspian Basin northwestward relative to Eurasia. They suggest that the basin is underthrusting beneath the Alborz, Talesh and the northern Caspian sea. They estimate very roughly a South Caspian NW velocity of 7-10 mm/yr relative to Eurasia and SW 13-17 mm/yr relative to Iran.

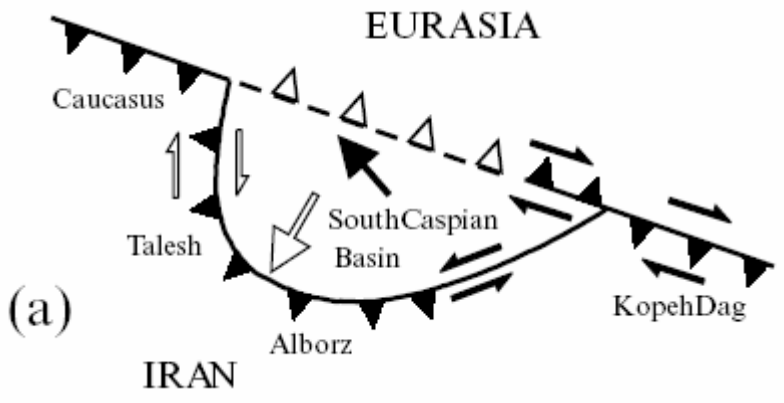

Figure 3-16. The tectonics model of South Caspian Basin, showing S to SW underthrusting in the Kopeh Dagh, Alborz, Talesh and eastern Greater Caucasus and north-dipping underthrusting in the central Caspian. Note the left-lateral strike-slip component in the eastern Alborz, and right-lateral component in the Kopeh Dagh. The white arrow shows the approximate direction of the South Caspian Basin relative to Iran, and the black arrow shows its motion relative to Eurasia (after Jackson et al., 2002).

3.5.3 GPS evaluations of the South Caspian Basin kinematics

Previous work shows that the Alborz accommodates part of the Arabia-Eurasia convergence. The remaining part must be absorbed by the independent motion of the South Caspian Basin (SCB) with respect to central Iran and Eurasia. The shortening rate across the Central Alborz is about 5 mm/yr and the South Caspian basin moves northwest at a rate of 6±2 mm/yr with respect to western Eurasia (Vernant et al. 2004b; Djamour 2004).

To assess the South Caspian Basin deformation, we collected all GPS measurements surrounding the basin within Iran (Fig. 3-17a, Table 3-6) (Masson et al. 2007; Vernant et al., 2004a; Nilforoushan et al., 2003; Vernant et al., 2004b, and our study). The stations which can be considered as located on the South Caspian Basin are: SHIR, MAR2, KORD, MAHM and NOSH. According to private communication from Jean Chéry and Frédéric Masson, the sites ATTA and HASH are at the limit between the South Caspian block and Central Iran, and it is not clear whether they are located on the South Caspian Basin or not. Our study permits a re-evaluation of the SCB kinematics through refined velocity estimates for KORD, SHIR and by a new velocity at site MAR2, all three being situated clearly on the rigid SCB block.

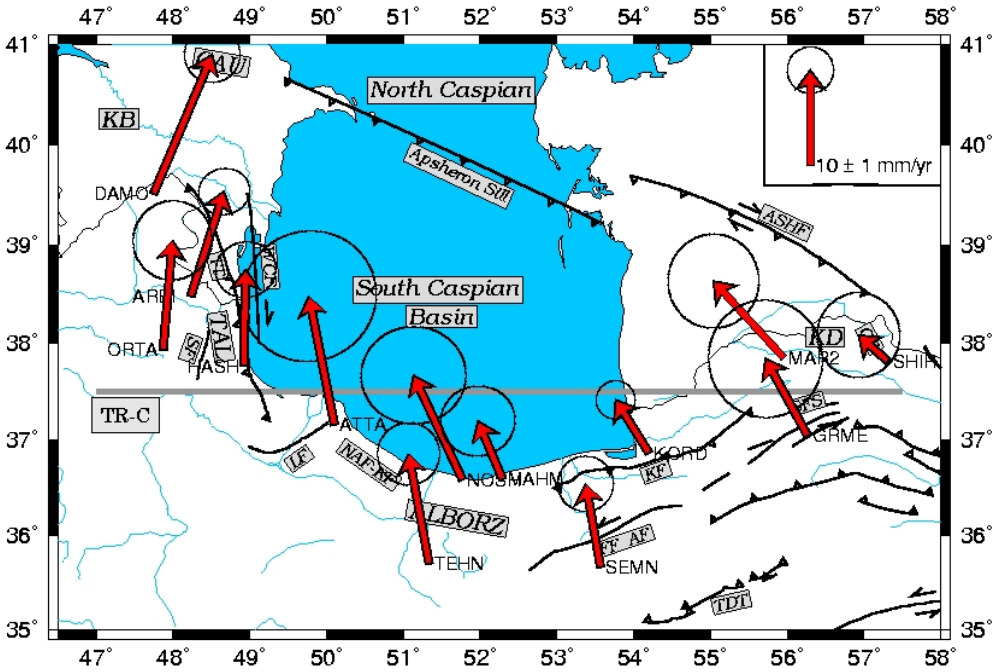

Figure 3-17a. South Caspian Basin region velocity field relative to Eurasia. The scale vector corresponds to 10 mm/yr. The error ellipses indicate formal errors within a 95 per cent confidence interval. KB: Kura Basin, CAU: Caucasus, KD: Kopeh Dagh, TAL: Talesh, ASHF: Ashkabad Fault, SFS: Shahrud Fault System, KF: Khazar Fault, FF: Firuzkuh Fault, AF: Astaneh Fault, NAF: North Alborz Fault, LF: Lahijan Fault, SF Sangavar Fault, TT: Talesh Thrust, TDT: Torud Thrust, WCF: West Caspian Fault. TR-C is the EW transects , the velocity components projected on this transect.

Table 3-6. Velocities of stations around the South Caspian Basin relative to Eurasia (Vernant et al., 2004; Masson et al., 2007 ; this study). AZ is the azimuth of the velocities with uncertainty of ±3°.

	Long.	Lat.	Velocities		Uncertainty		AZ
SITE	(°E)	(°N)	Ve	Vn	σe	σn	DEG
ARBI	48.231	38.477	3.50	11.00	1.10	1.00	18°
ATTA	50.102	37.156	-2.70	13.50	2.90	2.80	349°
DAMO	47.744	39.513	6.20	14.62	1.20	1.19	23°
HASH	48.922	37.764	0.20	10.10	1.30	1.20	1°
KORD	54.199	36.860	-3.53	5.0	1.13	1.12	324°
MAHM	52.290	36.590	-2.60	6.10	1.60	1.50	337°
MAR2	55.956	37.845	-7.44	8.07	2.09	2.09	317°
NOSH	51.768	36.586	-5.50	10.63	2.22	2.07	333°
TEHN	51.334	35.697	-2.00	11.08	1.33	1.32	350 °
SHIR	57.308	37.814	-3.09	2.71	1.13	1.12	359°

According to the velocity of SHIR and KORD, in the east, the basin moves toward the NW with a velocity of 6.5±2 mm/yr relative to Eurasia, which is consistent with the result of Jackson et al. (2002) and previous GPS results. The orientation of the velocity vectors are N359°±3° for SHIR, N317°±3° for MAR2, N324°±3° for KORD, N337°±3° for MAHM and N333°±4° for NOSH showing that the basin rotates clockwise. This rotation is also consistent with the velocities of the western stations ATTA and HASH, although it is not sure they are situated on the rigid part of the plate.

We can test the hypothesis of rigid rotation by evaluating theoretical velocities with respect to a rotation pole for the SCB (3-17b) which should fit especially the observed velocities of SHIR and KORD which are the most reliable to characterize the SCB. A rotation pole located in Turkmenistan (Lat. 39.8°E, Long. 59.8°N, rot. rate 0.7°/Ma) corresponds to the 6.5 mm/yr northwestward velocities observed. It also yields increasing velocities from east to west. The site velocities of NOSH, KORD, SHIR and MAHM are also coherent with this rotation pole, indicating these sites could belong to the SCB. The high residuals of MAR2 could be due to existence of the systematic error in the observed velocity. The differences with other Stations are due to realization of different Eurasia reference plate in our and Vernant et al; (2004B), Masson et al. (2007) solution.

The big residuals on the DAMO, ORTA, ARBI, TEHN, SEMN and GRME indicates that these stations are on different blocks for ATTA still needs more measurements to fix precise velocity.

Information on the kinematics along the southern and western border of the SCB are completed from previous studies (Djamour, 2004, Vernant et al., 2004b, Masson et al., 2006, 2007). West of the South Caspian Basin, between HASH, ARBI and ORTA, we measure 4 mm/yr of shortening perpendicular to Talesh which behaves as a thrust these shortening is observed between stations ORTA, HASH, ARBI, ATTA and NOSH.

The DAMO velocity indicates the presence of a NS extension around the Talesh block, of 4 mm/yr north and 4 mm/yr south of the Talesh block as estimated by Masson et al. (2006) in a densified network in NW Iran. This phenomenon is attributed to back arc extension related to the northward subduction of the SCB and the Kura Basin beneath the Apsheron-Balkhan sill and the Greater Caucasus, respectively.

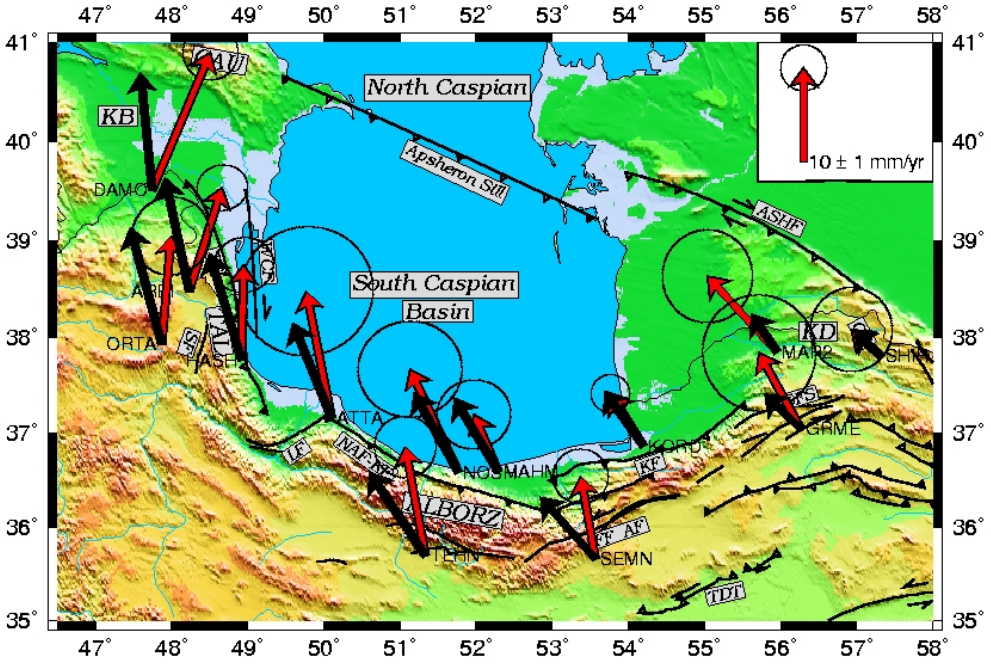

Figure 3-17b. Comparison between observed and theoretical velocity field for the South Caspian basin. The black vectors are theoretical velocity and red ones are observed.

The velocity of ATTA is even larger than the velocity of the TEHN station (south of Alborz on the Central Iran block). This indicates that there is no shortening across the limit between the CIB and the SCB at the location of ATTA. The ATTA velocity would indeed be compatible with the Central Iran block, following Masson et al., (2006), who postulate that the west Alborz (longitude of ATTA) is the transition zone between the zone of NS shortening in central Alborz and the zone of NS extension west of the Talesh.

According to our model (Fig. 3-19) the westward component of the South Caspian Basin motion is accommodated by 5±2 mm/yr of shortening across the Talesh and the northward motion of 5±2mm/yr by underthrusting beneath the northern Caspian plate along the Apsheron sill. Considering the velocity uncertainties, our result is consistent with the 6 mm/yr proposed by Vernant et al. (2004b).

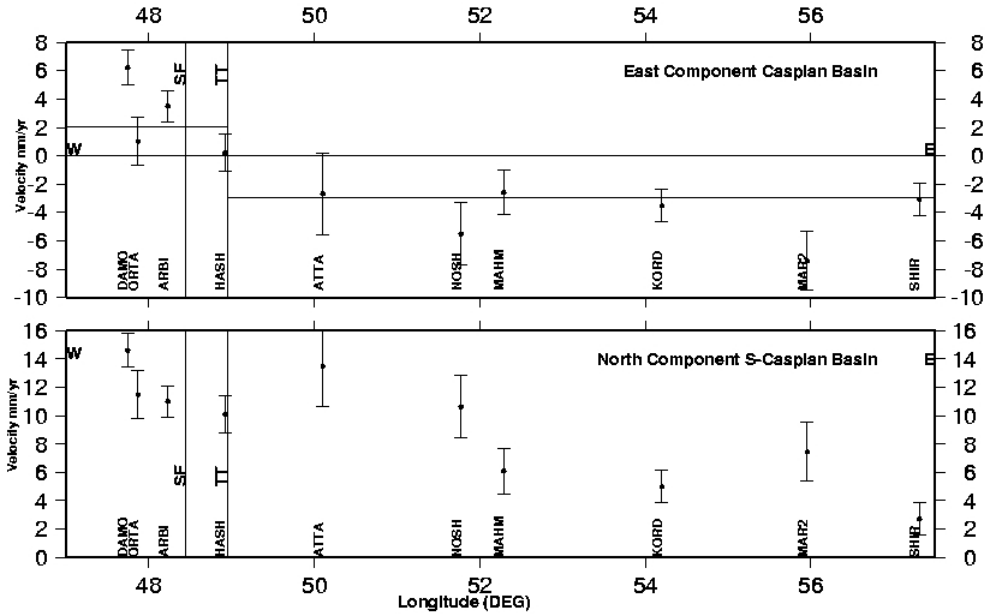

Figure 3-18. East and North components of the site velocities (mm/yr) with respect to the site longitude (DEG) projected on the transect TR-C (Fig. 3-16).

To confirm the results presented above we project the site velocities on an EW transect passing at 37.5°N (Fig. 3-17a). In the east component we can see 5 mm/yr of shortening in the Talesh Thrust. Here we assumed that ATTA is located on the SCB. The North component increased from east to west. On the north component the velocities of the stations SHIR, KORD, MAHM, NOSH and the site ATTA which are supposed to be on the SCB increase from east to west because the Euler pole of the SCB is located in the east of the network (Turkmenistan). Moreover, we believe it is too soon to decide that the ATTA station is situated on the Central Iran block because it has been measured only twice in one year. With the next measurement the precision of ATTA will be better and we will probably be able to distinguish more clearly if this station is on the SCB or on the CIB.

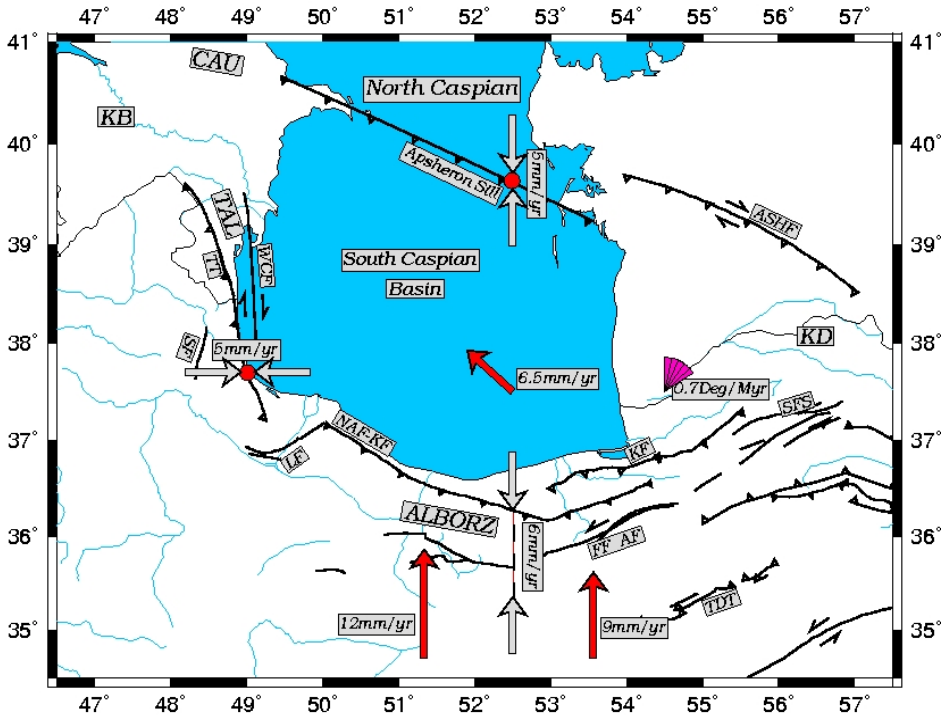

Figure 3-19. Kinematics model of the South Caspian Basin. The shortening rate decreases from west to east. The observed GPS NW velocity rate of 6.5±2mm/yr of the South Caspian Basin is absorbed by the underthrusting beneath Talesh (5mm/yr) in the west and the subduction under the northern Caspian (5mm/yr). The rotation pole of South Caspian Basin is located in Turkmenistan with rate of about ~0.7deg/Myr.

3.6 Strain and rotation rate distribution in the Kopeh Dagh

We have computed the horizontal velocity gradient in Delaunay triangles which cover Kopeh Dagh and the north Lut region. The result is a tensor which can be divided into a symmetric and an anti-symmetric part. Its symmetric part is the strain rate and the anti-symmetric part is the rotation rate (Vaniček and Krakiwsky, 1986; Cross et al., 1987). We construct the triangles between the 9 GPS sites of our network covering NE Iran, from the Kopeh Dagh to the Lut Block, at the latitude of Kerman and Zabol (Fig. 3-20). We have included only stations which have been measured three times and more. Our Delaunay triangles are similar to Masson et al. (2007) except for TR2 (A, B, C), where we have included MSHN, a NCC permanent GPS station collecting data since 2003.

3.6.1 Strain rate

Because of the sparseness of sites with 3 and more measurements, our triangles are not homogeneous in size. This makes it more difficult to compare strain

rates. Necessarily the strain rates are smaller in large triangles than in small triangles for the same velocity differences between the corner points. We excluded sites with only two measurements over a time span of two years because the strain evaluation is not yet significant, the uncertainties being greater than the absolute strain rate values. All presented triangles cross active faults and are therefore not representative for single block rigidity or rotation, but for fault activity and mechanisms.

The main result of the strain rate tensor computation (Table 3-7, Fig. 3-20) is the homogeneity of the orientation of the principal axis of the strain rates. In all triangles except TR7, the azimuth of the compressional axis is trending ~30°, which is almost perpendicular to the Kopeh Dagh mountain range. Also the orientations of the compressional axes are slightly clockwise rotated with respect to the regional direction of shortening from the Arabia-Eurasia collision. This reflects the regional NS shear between Central Iran and the Hellmand block creating increasing northward velocity components from east to west. This is one of the major kinematic features of the Kopeh Dagh region.

The major difference of our strain rate distribution compared to Masson et al. (2007) is the split of the northeastern-most triangle into three by adding the MSHN station. Here the regional deformation pattern is more detailed, giving clear evidence for an extensional component representing the westward expulsion of the SCB in the two western triangles, and a prevailing compressional mechanism in the eastern triangle.

The maximum and minimum observed values are -30.7 nanostrain/yr and -3.2 nanostrain/yr for the triangles TR3 and TR1, respectively. The uncertainties of the rates vary between 2.4 and 8.6 nanostrain/yr. Only in triangles TR2A and TR2B the uncertainties reach 19.4 nanostrain/yr due to the less well constrained MSHN velocity. The measurement time span of MSHN (starting in 2003) is not as long as the coverage by the Iran Global network (1999).

In triangles TR1, TR4 and TR5 we can see significant differences in the amplitude of strain rate compared to Masson et al. (2007), however, without changing the style of deformation. These differences occur because our estimated velocities are different by 1-2 mm/yr from the results of Masson et al. (2007), due to additional measurement epochs on Iran Global sites during the Mashhad network measurement

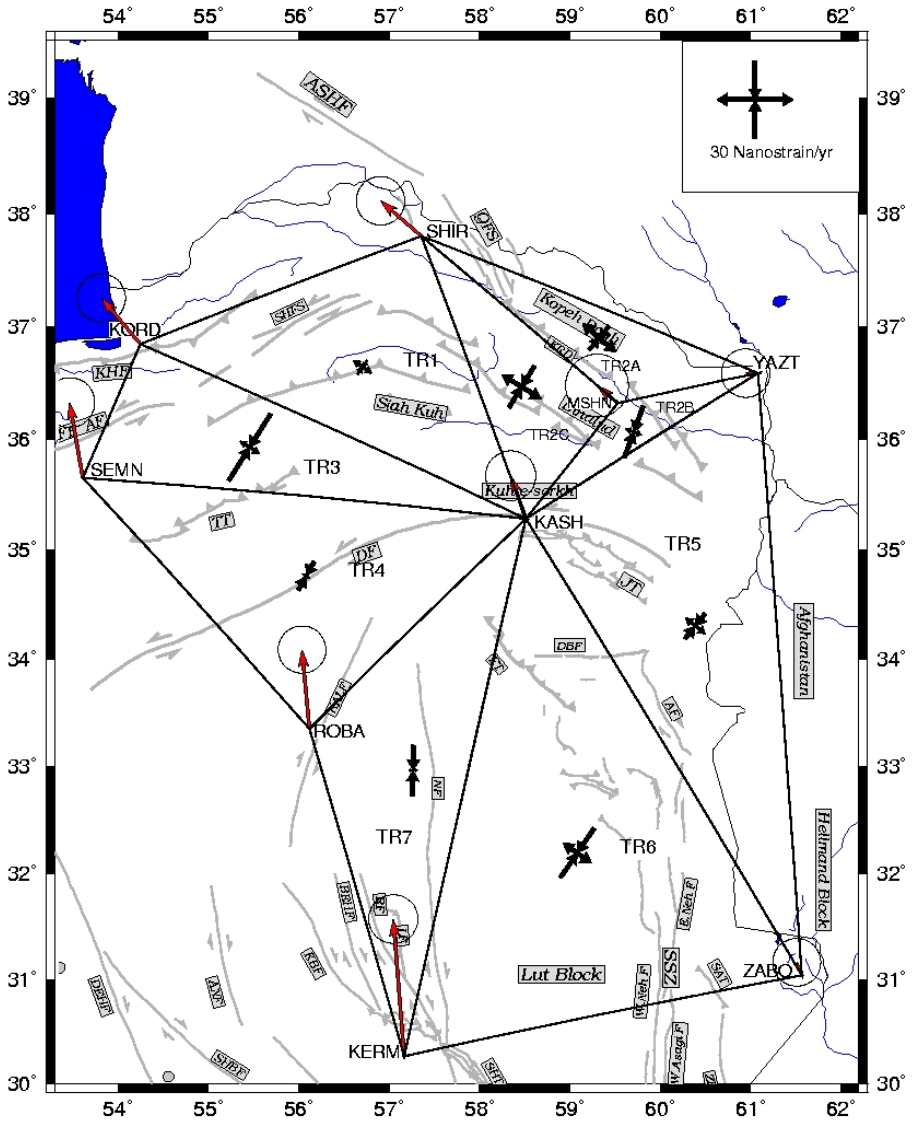

Figure 3- 20. Strain Rate distribution in North East Iran. Numerical values are indicated in Table 3-7.

campaigns. For example, SHIR has an increased velocity closer to the KORD velocity, decreasing the shortening in the SHIR-KORD-KASH triangle. These more similar velocities are more consistent with the existence of a rigid SCB block.

A major difference to Masson's results is the densification of triangles in the Kopeh Dagh by including the MSHN site in the deformation calculation (triangles 2A, 2B and 2C). In triangles TR2A and TR2C the extensional component is higher than the compressional component, which is related to strike-slip and rotation about a vertical axis on the Quchan fault zone between YAZT and SHIR, leading to the northwestward expulsion of the South Caspian Block. In TR2B the compressive

Table 3-7. Strain rates of NE Iran and their uncertainties for 7 Delaunay triangles in nanostrain/yr.

Triangle No	Extensional Component	Compressional Component	Azimuth
TR1	8.7±2.9	-6.8±4.6	34.7°
TR2A	17.3±5.2	-12.3±14.3	40.1°
TR2B	6.8±19.4	-21.4±15.3	20.2°
TR2C	18.1±6.14	-19.2±8.6	31.4°
TR3	9.0±3.5	-30.7±7.6	32.3°
TR4	3.4± 3.03	-12.9±4.1	28.9°
TR5	9.9±3.1	-12.9±3.6	38.9°
TR6	13.5± 2.5	-23.5±2.4	34.6°
TR7	-3.2±5.9	-19.6±2.4	1.1°

component is dominating, due to the prevailing shortening in the eastern Kopeh Dagh and Binalud.

The strain pattern for triangle TR5 is coherent with NS shear across the Sistan fault zone. In triangle TR6 we also see a strain tensor with strike-slip mechanism which is related to ~14 mm/yr of right-lateral NS shear across the Lut block (the total shear between Central Iran and the Hellmand block). In TR7 the strain rate tensor is dominated by a NS oriented compressive component and is coherent with the North oriented regional strain. The major result of the strain analysis of the Kopeh Dagh and northern Lut velocity field is that the NS shear between Central Iran and the Hellmand block across the Lut block is a prevailing feature in most of the area, reflected by shortening axes rotated slightly clockwise with respect to the regional shortening direction imposed by the Arabia-Eurasia collision. With densifying the network and increasing the precision of the velocities the strain field presents more significant details than the one presented by Masson et al. (2007).

3.6.2 Rotation Rate

3.6.2.1. Rotation in Delaunay Triangles

We computed rotation rates (Fig. 3-21, Table 3-8) for the same selected triangles than in the strain rate estimation. The maximum rate is about 0.9±0.2°/Myr (TR6) and the minimum is 0.0±0.4°/Myr (TR7) the average uncertainty is about 0.5°/Myr. The highest rotation corresponds to TR6 which is associated to shear

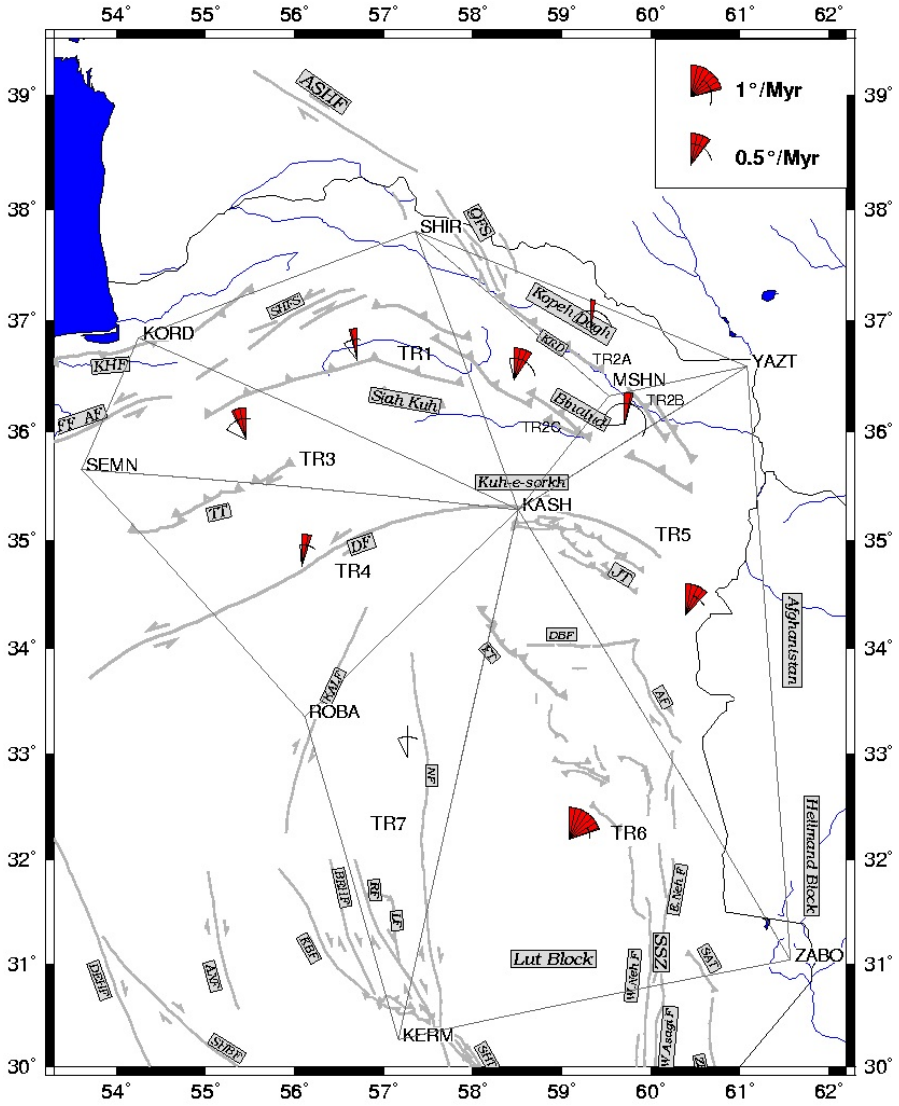

Figure 3- 21. Rotation rates in NE Iran in Delaunay triangles between stations with more than three.

Table 3-8. Rotation rates in Delaunay triangles in NE Iran

Triangle No:	Rotation rate DEG/Myr	Uncertainty DEG/Myr
TR1	-0.2	± 0.3
TR2A	0.1	± 0.9
TR2B	0.2	± 1.4
TR2C	0.4	± 0.6
TR3	-0.3	± 0.5
TR4	0.2	± 0.3
TR5	0.6	± 0.3
TR6	0.9	± 0.2
TR7	0.0	± 0.4

between the western Lut and the Hellmand block. Generally the uncertainties of the rotation rates are higher than the rotation rates themselves except for TR5 and TR6. In TR2A, TR2B, TR2C, TR4, TR5, TR6, TR7, the rotations are clockwise corresponding to right-lateral shear, but in TR1 and TR3 the rotations are anticlockwise which suggest they are related to the left-lateral motion of Shahrud, Astaneh and Firuzkuh fault systems.

3.6.2.2 Rotation on EW transect

We have calculated the rotation of the sites with respect to the YAZT station (Fig. 3-22). We used the site velocity divided by the distance to the fixed site to evaluate a rotation rate for each site. YAZT has been chosen as reference because it is situated on the stable Eurasian plate, but close to the limit with Kopeh Dagh. The rotation rate is presented with respect to the distance to the fixed site in Figure 3-22.

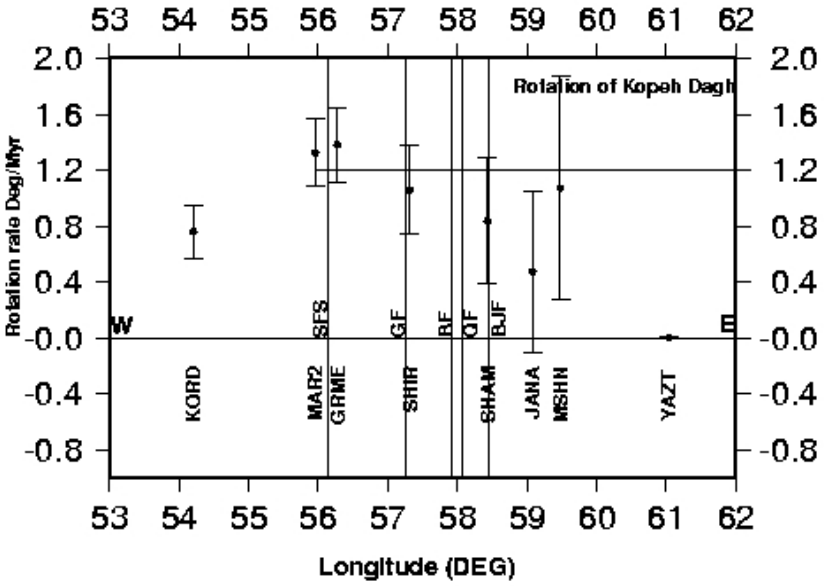

Figure 3-21. Rotation rate of the Kopeh Dagh with respect to YAZT which is located on the Eurasian plate. BF: Baghan fault, BJF: Bajgiran fault, GF: Gholaman fault, SFS: Shahrud Fault system.

We obtain an average rotation of 1.3°/Ma across the Kopeh Dagh with respect to a point (YAZT) situated on the Eurasian plate. The coherence of the rotation rates between MSHN and KORD reflects the homogeneity of the regional shear field which is the major kinematic constraint in the Kopeh Dagh region, as shown also by the strain field. In contrast, the rotation rates in Delaunay triangles are not directly comparable with the regional rotation, because these rotation rates between three

close-by stations are dominated by the strike-slip activity of the faults these triangles are covering.

3.7 Future earthquake potential

Precise surface deformation measurements, as provided by GPS, have an important contribution to seismic hazard assessment. Our measurements can indeed constrain the direction and the magnitude of charging a seismogenic fault. This is important to know how a future earthquake will behave (which mechanism it will have), and which is the minimum magnitude of the next earthquake. This information can tell us whether a future earthquake will damage our structures and cities or not. To answer these questions, it is necessary to know the relation of the surface deformation related to an active fault and the magnitude of the earthquake. In this regard Wells and Coppersmith (1994) have developed empirical relationships between the earthquake magnitude and the rupture length, rupture width, rupture area and surface displacements. Their models are based on information collected on recent and historical earthquakes. They studied the earthquake magnitude correlation with the amount of displacement along the causative faults. By applying ordinary least square regression analyses, they found relations between earthquakes and maximum and average fault displacement:

M = 6.69+0.74*Log(MD) (Fig. 3-22)

M = 6.93+0.82*Log(AD) (Fig. 3-23)

In these relations M is the magnitude and MD and AD are the maximum and average displacements, respectively.

Based on the earthquake recurrence interval (if available), the date and the magnitude of the previous earthquakes and GPS displacement rates, we can predict empirically the magnitude of the next earthquake. This is crucial information to assess the potential damage which will be caused by earthquakes close to large cities or in populated areas.

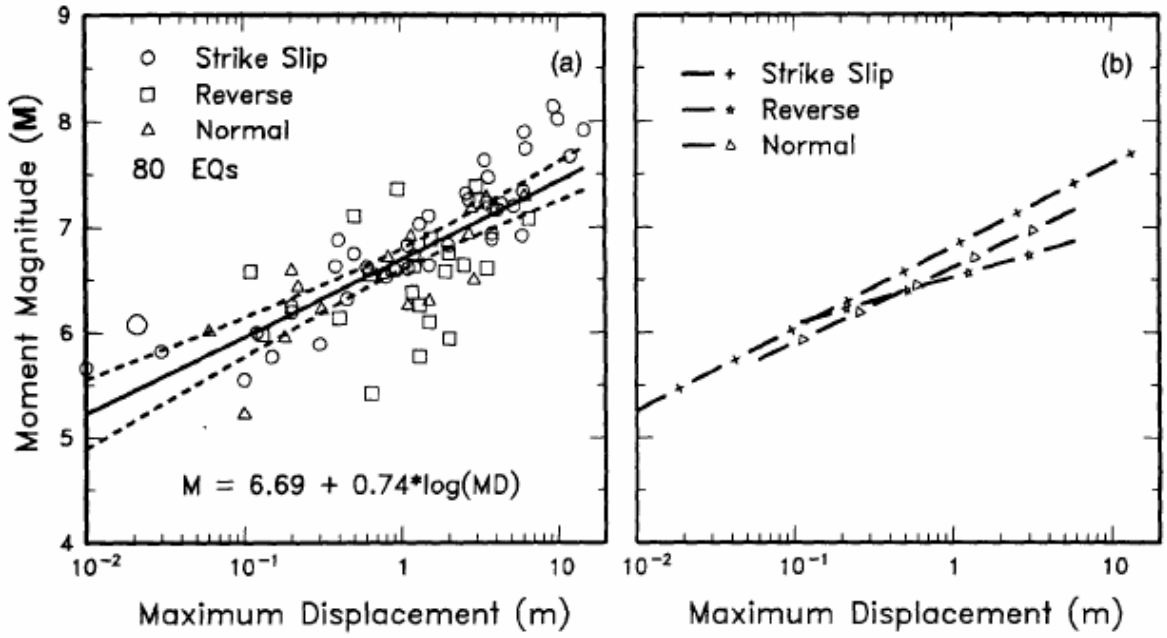

Figure 3-22. (a) Regression of maximum surface displacement on magnitude (M). Regression line shown for all-slip-type relationship. Short dashed line indicates 95% confidence interval. (b) Regression lines for strike-slip, reverse, and normal-slip relationships.

Among the largest earthquakes which occurred in the Kopeh Dagh during the last 150 years, five occurred around the town of Quchan in the Atrak river valley (1851, 1871, 1872, 1893, and 1895, magnitudes of ~7). Since 1895, no other large earthquake occurred in this area. Considering the GPS constrained displacement rate of 5 mm/yr across the Quchan fault zone, the cumulative offset of the fault zone is today (after 111 years of loading) 55.5 cm. Using the empirical relationship between average displacement and moment magnitude (Wells and Coppersmith, 1994), this cumulative offset corresponds to an earthquake of magnitude ~6.7. As the Quchan region is highly populated, an earthquake of magnitude 6.7 will cause large damage and destroy many villages. However, the cumulative offset is probably distributed over several faults. More time is needed to cumulate a comparable offset on an individual fault.

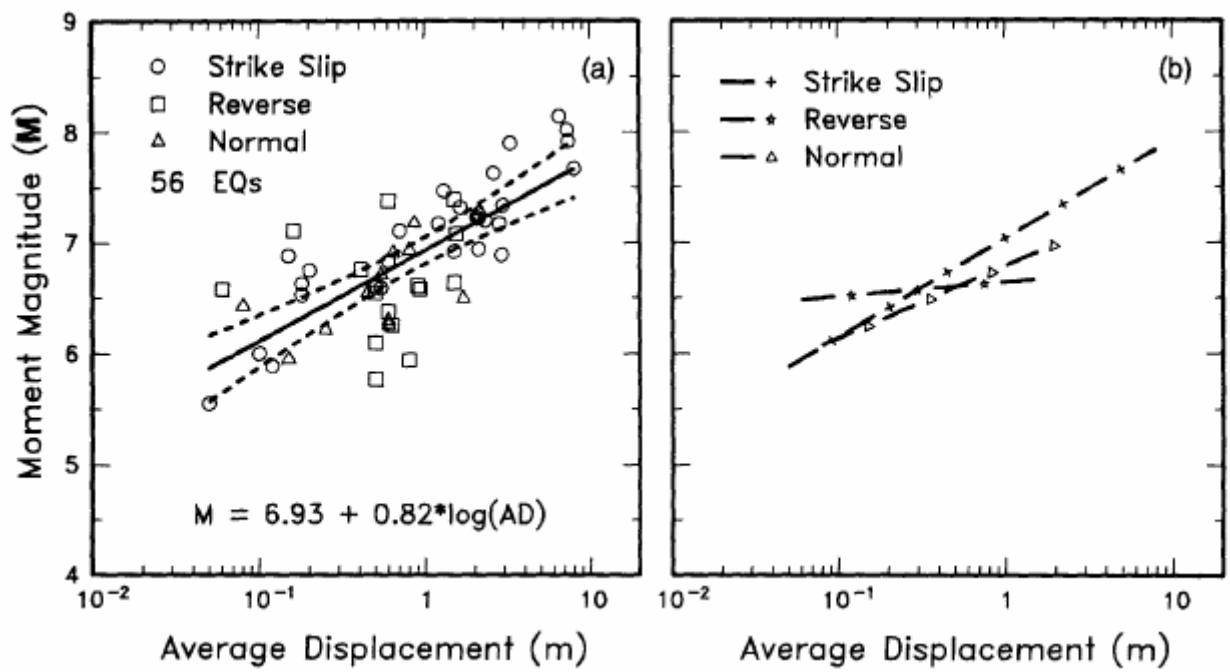

Figure 3-23. (a) Regression of average surface displacement on magnitude (M). Regression line shown for all-slip-type relationship. Short dashed line indicates 95% confidence interval. (b) Regression lines for strike-slip, reverse, and normal slip relationships. Line lengths show the range of data for each relationship (Wells & Coppersmith 1994).

Berberian and Yeats (2001) proposed a maximum recurrence interval of about 2000 years for earthquakes in the region of Ashkabad city close to the Ashkabad fault, based on an archaeological study of earthquakes. Our GPS measurements show 2.5 mm/yr of shortening and 5 mm/yr of strike-slip on the Ashkabad fault. With this shortening rate and the recurrence interval of 2000 years, we can estimate the average displacement during the earthquake to ~5 m for each event, corresponding to a magnitude 7.5 (according to the empirical relation of Wells and Coppersmith, 1994). The last large earthquake recorded on the Ashkabad fault was in 1948 (M=7.2). There is no information about the displacements caused by this earthquake. Considering the recurrence interval of 2000 years the next earthquake will occur around the year 4000 with a magnitude of 7.5.

The Alborz-Binalud region is characterized by active reverse faults that follow the structure of the Binalud. The oldest recorded seismic event in the Alborz-Binalud mountain range dates from the seventh century A.D. It is followed 500 years later by at least four historical earthquakes with M>7 during less than 200 years (1209-1405), near the city of Neyshabur (Ambraseys and Melville, 1982; Berberian and Yeats,

1999). Considering a recurrence time interval of 500 year and 3.5±2 mm/yr of shortening, the average displacement is ~1.7 m for each event. This corresponds to a magnitude ~7.2. Since the 1405 event the Binalud did not experience any major earthquake. We could therefore expect an earthquake with an average displacement of ~2.1m and a magnitude larger than ~7.2 in this century.

3.8 Conclusions

In the western part of Kopeh Dagh, the Ashkabad fault is the major tectonical feature with thrusting and right-lateral strike-slip motion. In this area, the GPS velocity is estimated to be 5±2 mm/yr to 8±2 mm/yr along strike-slip motion and 2±2 mm/yr of shortening perpendicular to the range. Considering the total geological offset of 35 km (Lyberis & Manby, 1999) and constant slip rates corresponding to the present-day GPS rates, the onset of deformation is estimated to about 7 Ma ago which is consistent with Lyberis & Manby (1999).

In the central part of Kopeh Dagh, on the Quchan Fault Zone, we have several parallel NNW-SSE strike-slip faults. We have estimated 5±2 mm/yr of cumulative right-lateral slip rate on the Quchan fault zone. The strike-slip motion on these faults is related to an anti-clockwise rotation of the blocks limited by the faults (domino model). This block rotation produces along strike-slip elongation of about 5±2 mm/yr between eastern Kopeh Dagh and the South Caspian Basin, which accommodated by right-lateral slip (5-8 mm/yr) on the Ashkabad fault and by left-lateral slip (2.5±2 mm/yr) on the Shahrud fault system. Such an elongation is consistent with the westward expulsion of the South Caspian Basin as proposed by Jackson et al. (2002) and Hollingsworth et al. (2006).

Knowing the geological offsets cumulated on the three faults of the QFZ to about 40 km (Hollingsworth et al., 2006) and 25 km (Shabanian et al., 2007)and supposing constant fault velocities in the past corresponding to our GPS rates, we estimate that the deformation on the strike-slip faults of central Kopeh Dagh started about 5-8 Ma ago. The GPS network is not dense enough in the Quchan fault zone to evaluate the rotation rate of the blocks which are bounded by the right-lateral faults.

For the eastern part of Kopeh Dagh we estimated 2.5 mm/yr NS shortening which can be split up into 2±2 mm/yr of shortening perpendicular to the range and 1±2 mm/yr along strike motion. Supposing a total geological NS shortening of 60 km, the beginning of deformation at a constant GPS rate is 24 Ma ago.

A second continuous mountain belt in NE Iran has been analyzed by our GPS measurements, the Alborz-Binalud belt. We distinguish three segments, the eastern Alborz, the Shahrud fault system and the Binalud range. Our GPS measurements show shortening of 3.5 mm/yr in eastern Alborz and across Binalud, with lower, not significant rates along the central Shahrud segment. Left-lateral strike-slip decreases from 3.5 mm/yr to zero from eastern Alborz to the eastern extension of the Shahrud fault system. Even further east, across the Binalud, the strike-slip motion becomes right-lateral with a rate of 2 mm/yr. South of the Alborz-Binalud belt, the Siah-Kuh and Kuh-e-Sorkh ranges do not show significant deformation.

A remarkable feature is the relatively high present-day NS shortening rate across Binalud, which is with 3.5 mm/yr slightly higher than the shortening across the eastern part of Kopeh Dagh at the same longitude (2.5 mm/yr). If the total geological shortening of 30 km proposed by Allen et al. (2003) for the Alborz applies to Binalud, this amount could be achieved in 9 Ma, while the east Kopeh Dagh shortening of 60 km needs 24 Ma to be accomplished with present-day rates. This is in contrast to the presumed ages of the two mountain belts, loosely indicated as post 30 Ma for Kopeh Dagh (Berberian and King, 1981) and ~60 Ma for Binalud (Stöcklin, 1974). We observe an inconsistency between the average long term shortening rate of the Binalud belt (30 km in 60 Ma corresponding to 0.5 mm/yr) and the present-day rate (3.5 mm/yr). This fact and the indications of a global reorganization of the tectonic regimes about 5 Ma ago on many of the presently active fault zones suggests that deformation rates vary probably over time spans of more than 5 Ma. In particular, the Binalud deformation (and eventually also the eastern Kopeh Dagh) has been most probably achieved in different kinematical steps and under different tectonical regimes.

The lack of seismicity inside the South Caspian Basin suggests that the basin is rigid and that its eastern limits extend on land to the Ashkabad fault in the NE and the Shahrud fault system in the SE. Some of our GPS stations of the Mashhad network situated in this zone could therefore be used to constrain a rigid block model

for the SCB kinematics. We confirm the results of Vernant et al. (2004b) showing that the South Caspian Basin is moving NW with respect to Eurasia with a velocity of about 6 mm/yr. Our model is also consistent with 5 mm/yr of EW shortening across the Talesh thrust at the western limit of the SCB (Masson et al., 2006). However, 3 out of 7 stations situated along the Caspian Sea shore have residuals of more than 3 mm/yr with respect to our model. This could be due to the uncertainty of their location on the rigid SCB block, to still badly determined velocities or to differences in the reference system of the individual solutions (south and west Caspian velocities are from Vernant et al., 2004b and Masson et al., 2006). A better constraint on the SCB motion could mainly be achieved by adding GPS stations in the eastern (and the only emerging) part of the basin. However, the lack of GPS stations located clearly inside the southern and western part of the basin (and not in the deformation zones) prohibits any clear evidence for the rigidity of the basin and therefore for the validation of the rigid block assumption.

The strain and rotation rate analysis in Delaunay triangles shows prevailing thrust and strike-slip mechanisms. The major axes of the strain rate tensors are oriented ~30°N, perpendicular to the mountain ranges but rotated clockwise with respect to the regional shortening direction from the Arabia-Eurasia collision. This suggests that the present-day driving mechanism of the Kopeh Dagh deformation is the NS shortening which is modulated by the 15 mm/yr EW shear between the Hellmand block and Central Iran and distributed over 400 km between the east and west borders of the Lut block. This is coherent with a homogeneous rotation rate of 1.2°/Ma across the Kopeh Dagh range with respect to the nearest point on the Eurasian plate. The inclusion of the Mashhad permanent station in the strain analysis provides a detailed view of the local deformation pattern and gives evidence for an extensional component coherent with the strike-slip deformation across the Quchan Fault Zone.

From historical earthquake catalogs, characteristic magnitudes and present-day fault slip rates we could infer repeat times and minimum magnitudes of future earthquakes on different faults in NE Iran. In the Quchan Fault Zone, in the worst case an earthquake of magnitude 6.7 could happen today, in a more realistic case, some 100 years are still needed to cumulate enough displacement on a single fault to release an earthquake of this magnitude. As the average magnitudes in the QFZ are higher than 6.7 (about 7.0), it is possible that the seismic cycle is not yet

revolved. On the Ashkabad fault, large earthquakes (typical magnitude 7.5) with long recurrence interval (2000 years) are expected. As the last earthquake happened in 1948 (M=7.2), no large earthquake is expected in the near future. On the Binalud, a recurrence time of ~500 years for magnitude 7.2 earthquakes is estimated. The last earthquake taking place in 1405, the seismic cycle should be achieved and the next earthquake of M=7.2 is overdue. This event risks will be a disaster for the highly populated cities of Neyshabour and Mashhad.

Chapter 4: Kinematics of Lut

4.1 Introduction and tectonic settings

The Dasht-e-Lut (Fig. 4-1) is one of the largest deserts in Iran, 480 kilometers long and 320 kilometers wide, and also one of the driest and hottest regions of the world. During the spring wet season, water briefly flows down from the Kerman mountains, but it soon dries up, leaving behind only rocks, sand and salt. The other large desert of Iran is the Dasht-e-Kavir (Great Kavir). The Lut desert (Lut block) is an aseismic rigid block (Berberian, 1976; Vernant et al., 2004; Walker and Jackson, 2004). Two narrow NS trending mountain ranges limit the Lut block to the east and the west. Along each of these mountain ranges runs a right-lateral strike-slip fault system. In the western part is the Gowk-Nayband fault system and in the east is the Sistan suture zone with the Neh-Abiz-Zahedan fault systems. Shear motion on these N-S right-lateral fault systems is also evidenced by the activity of two EW-trending left-lateral strike-slip faults located north of the Lut block: The Doruneh and the Dasht-e-Bayaz faults which must rotate clockwise to absorb the N-S shear on the Nayband and Sistan fault systems (Jackson and McKenzie, 1984; Walker and Jackson, 2004). While the orientation and the slip mechanism of the Dasht-e-Bayaz fault are similar to the Doruneh fault, it has been the location of more historical destructive earthquakes (Jackson and McKenzie, 1984; Berberian and Yeats, 1999; Walker and Jackson, 2004).

The large scale tectonic constraints are imposed on the Lut block by the Arabia-Eurasia collision. Arabia moves northward relative to Eurasia with velocities increasing from west to east, of about 18, 22 and 25 mm/yr at the longitudes of 48 °, 52° and 56° (Nilforoushan et al., 2003; Vernant et al., 2004; Masson et al., 2007). Between 48^0E and 56^0E this convergence is completely accommodated inside the Iranian territory by shortening across the Zagros and Alborz mountain ranges, some large strike-slip faults and residual motion of the South Caspian Sea. East of 56°, the convergence is absorbed by the Makran subduction, the Kopeh Dagh and Alborz-Binalud ranges. In contrast to Iran, the neighboring countries that surround Iran to the east and northeast, like Pakistan, Afghanistan and Turkmenistan, are only slightly deformed, because they are located on the stable Eurasian plate (Vernant et al., 2004; Walker and Jackson, 2004; Hollingsworth et al., 2006). In east Iran, this results

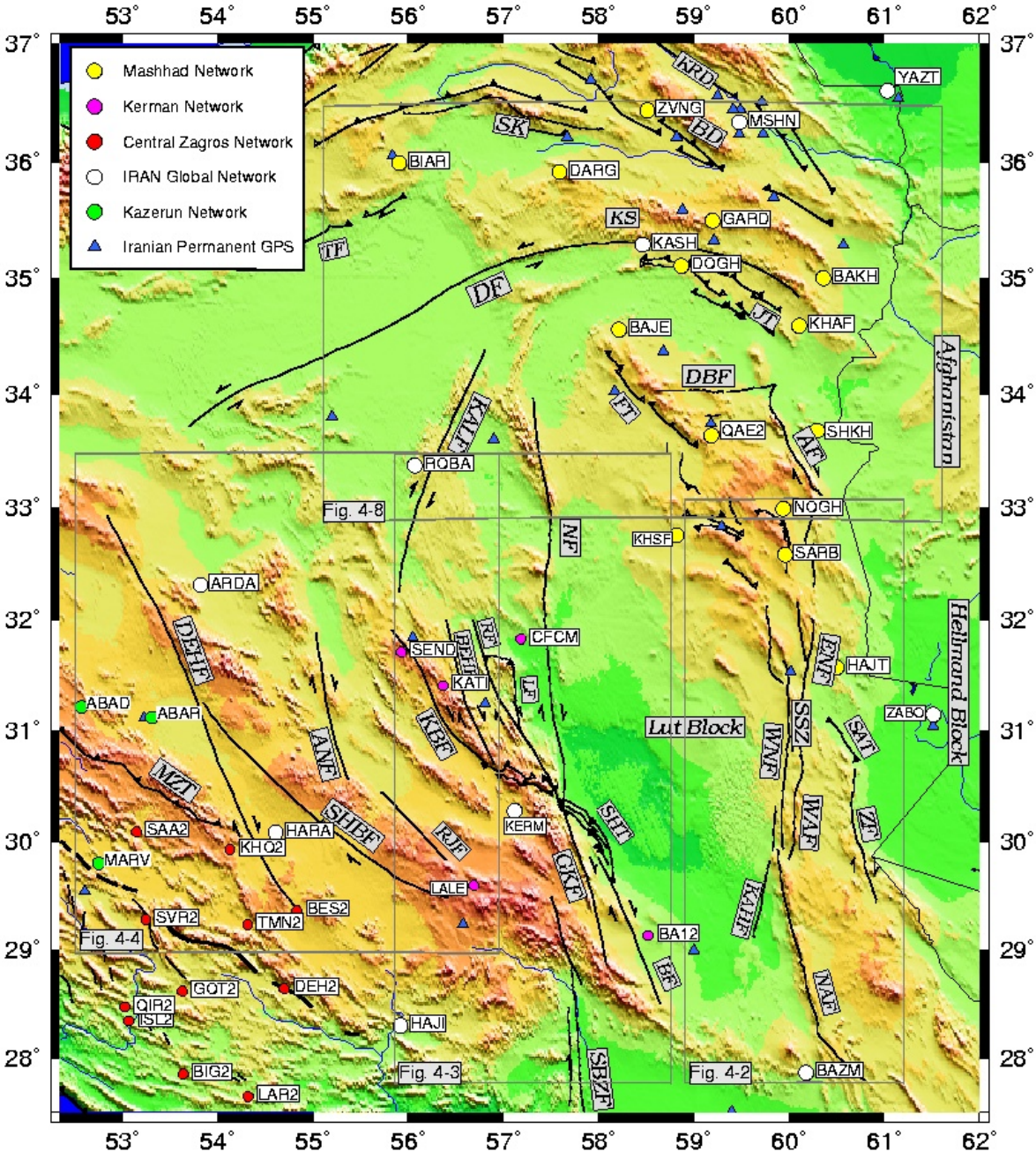

Figure 4-1. Tectonics of the Lut region east of Iran. The colored circle shows the distribution of different GPS networks. AF: Abiz Fault, ANF: Anar Fault, BF: Bam Fault, BEHF: Behabad Fault, FT: Ferdows Thrust, DF: Doruneh Fault, DBF: Dasht-e-Bayaz Fault, DEHF: Dehshir Fault, GKF: Gowk Fault, JT: Jangal Thrust, KAHF: Kahurak, Fault, KALF: Kalmard Fault KBF: Kuhbanan Fault, LF: Lakarkuh Fault, MZT: Main Zagros Thrust, NAF: Nosrat Abad Fault, NF: Nayband Fault RF: Ravar Fault, RJF: Rafsanjan Fault, SBZF: Sabzevaran Fault, SHF: Shahdad Fault, SHBF: Shahr Babak Fault, SSZ: Sistan suture zone, TF: Torud Fault, WAF: West Asagie Fault, WNF: West Neh Fault, ZF: Zahedan Fault.

in a zone of strong right-lateral shear between Central Iran and Afghanistan. The Iran Global GPS measurements (Vernant et al., 2004) have evaluated this shear to be approximately 15 mm/yr. The Lut block being rigid and non deformable (Berberian, 1976, Walker and Jackson, 2004), these 15 mm/yr of right-lateral shear should be accommodated by displacement on the NS trending strike-slip faults bounding the Lut block to the east and to the west and associated to the activity of the EW trending left-lateral strike-slip faults located north of the Lut block.

We will discuss the different active faults bounding the Lut block and their role in the tectonics of the region. We will present the seismic activity of these faults and their geological (long term) displacement rates. Then, we will show their present day activity obtained by measurements of a GPS network dedicated to constrain the kinematics of the Lut block boundaries. These present-day fault slip rates will be compared to the geological (long term) velocities, when available.

4.2 Tectonic features of the Lut block

4.2.1 NS trending right-lateral faults

4.2.1.1 The Sistan suture zone to the east of Lut

The eastern margin of the Dasht-e-Lut (Lut Block) is bounded by the N-S trending Sistan mountain belt (Berberian et al., 1999). Igneous rocks in the Sistan suture zone are correlated with several important tectonic events. During the Late Cretaceous (~89 to 55 Ma ago), Tertiary rocks of the Sistan suture zone separated two blocks: The Dasht-e-Lut belonging to the Iranian Plateau and the Dasht-e-Margo (desert of death) on the Hellmand block (Camp and Griffis, 1982). The Sistan suture zone is composed of two accretionary prisms (The Neh and Ratuk complexes) separated by sediments and volcanism of the Sefidabeh fore arc basin. A series of N-S trending active right-lateral and thrust faults are stretched along the Sistan mountains ranges. They are shown in Fig. 4-2 together with the seismicity of the region.

a) The Neh Fault system

The N-S trending Neh fault system (Berberian, 1976) consists of a western and an eastern segment. The West- and East-Neh faults are running parallel, 10 to 20 km apart, and are both ~200 km long. The Neh faults end up in the south at

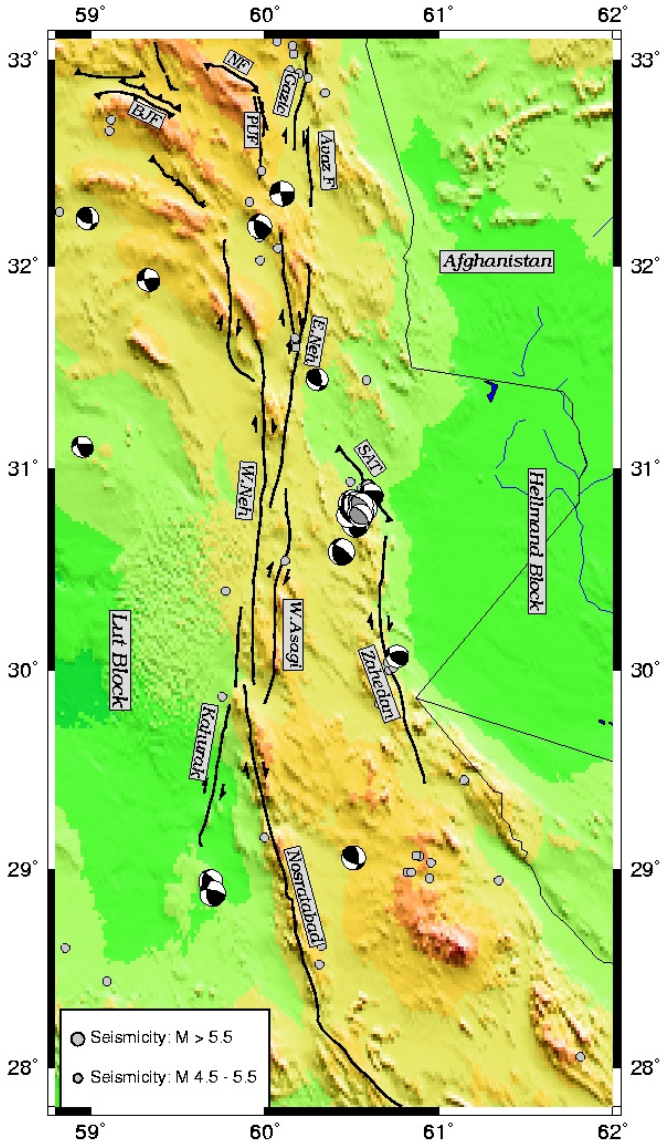

Figure 4-2. Active strike-slip and thrust faults of the Sistan suture zone east of Iran. Earthquake epicentres (M>4.5) are from Engdahl et al. (1998) as well as earthquake fault plane solutions. Grey solutions are solutions modelled by body waveforms (Berberian et al. 2000). Black spheres are Harvard CMT solutions from 1976-2007. BJF: Birjand Fault, NF: Nauzad Fault, PUF: Purang Fault.

Nosratabad city and connect to the Kahurak and Nosratabad faults. To the north, the Neh faults connect to a zone of NW-SE trending strike-slip and thrusts faults, namely the Birjand, Purang, Gazik and Avaz fault system. In particular, the East Neh fault continuation to the north is the Abiz fault which experienced a Mw=7.2 earthquake in 1997.

The East Neh fault includes two segments, both ~100 km long. The southern segment is called the West Asagie fault. In 1928, an earthquake (Mb=5.2) occurred

in Nehbandan city located between the east and the west Neh fault. The earthquake destroyed and damaged many houses. It might have originated on the East Neh fault (Berberian, 1976). Walker and Jackson (2004) propose 50-65km of total offset on the East Neh fault based on the satellite image observations of geomorphological markers in the Neh complex as well as the previously published work of Tirrul et al. (1983) .On the West Neh fault, Walker and Jackson (2004) have observed ~10 km of total offset.

b) The Zahedan Fault

The ~200 km long right-lateral strike-slip Zahedan fault is the easternmost active fault at the eastern limit of the Lut block (Berberian, 1976). Its northern termination ends at the Palang Kuh Mountain, in the Sefidabeh blind thrust, which experienced a series of earthquakes (Mw ~6) in 1994. According to the offset of similar beds of Paleocene Eocene age, Freund (1970) proposes 13 km of dextral displacement along the fault. Walker et al. (2004) observed 13 km, or possibly up to 20 km, of strike-slip motion during a Late Cretaceous to Eocene sequence with mudstones and phyllite (rocks that develops from slate) in the mountains located immediately north of Zahedan city. This fault accommodates some shortening in its northern part evidenced by the formation of thrusts. One of these thrusts is the Sefidabeh blind thrust which ruptured during a sequence of earthquakes in 1994.

Walker and Jackson (2004) suggest 70-95 km of total offset on the eastern limit of the Lut block by cumulating the observed offsets of 13-20 km on the Zahedan fault, 50-65 km on the East Neh and ~10 km on the West Neh fault.

c) The Abiz fault

The Abiz fault is the northernmost fault of the Sistan suture zone. This NNW-SSE trending right-lateral strike-slip fault is more than 120 km long and is connected to the EW left-lateral Dasht-e-Bayaz fault to the north, and to the NS right-lateral Gazik fault to the south. Several large magnitude earthquakes (Mw 6.0-7.2) occurred on this fault (Table 4-1 and 4-5). In 1997, the Zirkuh earthquake (Mw=7.2) ruptured ~125 km of the Abiz fault. This is the longest rupture among all documented Iranian earthquakes (Berberian et al. 1999). The average coseismic surface displacement of the Zirkuh earthquake was approximately 2 m.

Table 4-1. The earthquake sequence in NE Sistan, 1936-1997 (after Berberian et al. 1999).

Date	Lat.	Long.	Ms	Mw	Mechanism	Fault
1936 June30	33.61	59. 96	6.0		N-S right-lateral	Abiz (middle)
1968 Aug 31	34.02	59. 03	7.4	7.1	E-W left-lateral	Dasht-e-Bayaz (west)
1968 Sept 11	34.03	59. 54	5.4	5.6	(E-W left-lateral)	? (Dasht-e-Bayaz)
1976 Nov 7	33.86	59. 23	6.5	6.0	(E-W left-lateral)	? (Avash)
1979 Jan 16	33.96	59. 53	6.7	6.5	(reverse/N-S right-lateral)	? (Boznabad or Parak)
1979 Nov14	33.90	59. 83	6.6	6.6	N-S right-lateral	Abiz (north)
1979 Nov 27	34.05	59. 63	7.1	7.1	E-W left-lateral	Dasht-e-Bayaz (east)
1979 Dec 7	34.03	59. 80	6.1	5.9	N-S right-lateral	Abiz (north)
1997 May10	33.86	59. 83	7.3	7.2	N-S right-lateral	Abiz
1997 June16	33.00	59. 00	5.0	5.0	reverse ?	
1997 June 20	32.33	59. 96	5.4	5.4	(N-S right-lateral)	? (Purang)
1997 June 25	33.94	59. 48	5.8	5.7	(N-S right-lateral)	? (Boznabad or Parak)

This earthquake destroyed 147 villages and killed 35,000 people. The same region also experienced earthquakes in 1936 and 1979 which ruptured parts of the fault. The northern part of the Abiz fault is linked to a system of E-W trending left-lateral strike-slip faults (Dasht-e-Bayaz) which have experienced destructive earthquakes in the last 35 years (Ambraseys and Tchalenko, 1969, Haghipour and Amidi, 1980, Berberian, 1999) and which will be discussed later.

4.2.1.2 The Western Lut faults

To the west, the Lut block is limited by N-S trending narrow mountain belts which separate the Lut depression from central Iran. Extending along these mountain ranges are the Nayband fault system in the north and the Gowk fault in the south. To the west, several associated faults (Anar, Dehshir) accommodate the remaining shear between the Lut block and the Central Iranian plateau.

a) The Nayband fault

The Nayband fault represents the western limit of the Lut block and is ~250 km long (Fig. 4-3). This fault strikes almost N-S (N175°) and its name is taken from a village that lies near the center of the fault. Geomorphological marker offsets show that this fault is a right-lateral strike-slip fault (Wellman, 1965; Walker and Jackson, 2002). To the north, this fault is connected to the NNW trending Tabas thrust fault

system. Toward the south, the Nayband fault is connected to the Gowk fault and the Shahdad thrust, situated southeast of Kerman. To the west of the Nayband fault, associated faults (Kuhbanan, Lakarkuh, Ravar, and Behabad) run parallel and are connected to the Nayband fault north of Kerman. Since 1900, no important earthquake has been recorded on the Nayband fault. However, the Tabas thrust at its northern end and the Shahdad thrust at its southern end experienced destructive earthquakes (Berberian, 1976, Berberian and Yeats, 1999). The slip rate on the Nayband fault has been proposed to be ~1.5 mm/yr, on the basis of the 3.2 km offset of quaternary basalts which have been cut by the fault and which could have been achieved in 2.08±0.07 Ma (Walker and Jackson, 2002).

b) The Kuhbanan Fault

The Kuhbanan fault (L>200 km) is a major active fault (Berberian 1976; Berberian et al. 1979; Berberian, 2005) striking NW-SE in the vicinity of the provincial capital city of Kerman. The Kerman plane is bounded to the northeast and to the southwest by two subparallel active right-lateral strike-slip faults, the Kuhbanan and the Rafsanjan faults (Fig. 4-3). Unlike the Kuhbanan fault, which has a limited recorded seismic history since 1875. In 1923 a destructive earthquake occurred in Southeast of the Rafsanjan Fault (Ambraseys and Melville, 1982) but the causative fault of the earthquake is not known (Walker et al., 2006). The Kuhbanan strike-slip fault lies on the boundary between the Kuhbanan fold-thrust mountains (underlain by the Lower Cambrian Ravar/Dezu/Hormuz evaporate complex decollement layer with numerous piercing salt plugs) in the northeast (elevation ~3,000 m) and the Kerman-Zarand plane in the southwest (elevation ~1,500 m). For much of its length, the Kuhbanan strike-slip fault consists of a series of right-lateral strike-slip segments that step to the right. The southern part of the Kuhbanan strike-slip fault, where the trace of the fault gradually disappears, is bounded by cross-reverse faults and folds which are well developed at almost right angles due to shortening along the cross-faults. Based on preliminary morphotectonic studies, the Kuhbanan right-lateral strike-slip fault can be divided into four segments (Zarand, Kuhbanan, Rizu and Behabad). A

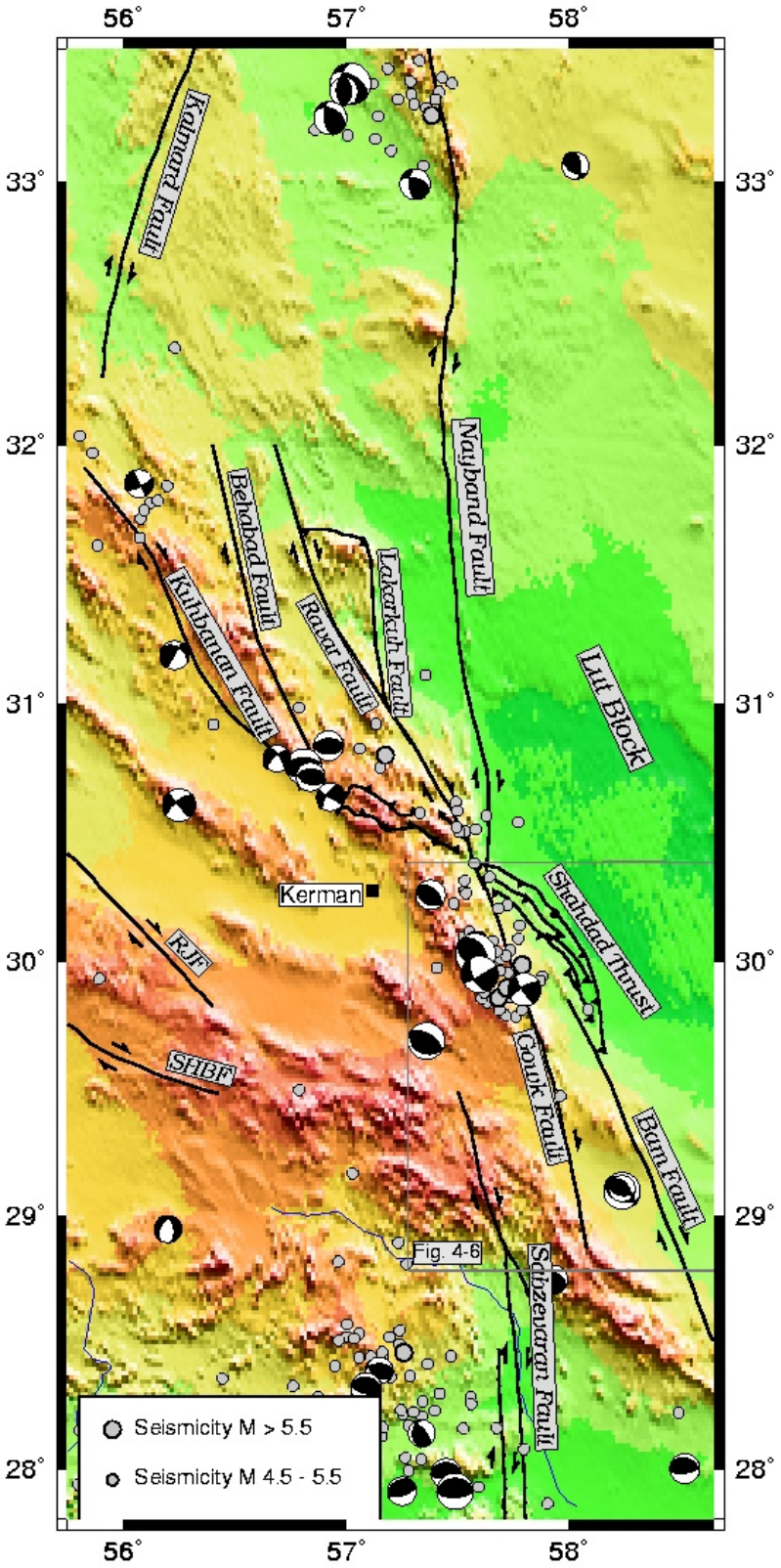

Figure 4-3. Seismotectonic map of the western Lut. Epicenter of the earthquakes M>4.5 are from Engdahl et al. (1998). Black spheres are Harvard CMT solutions (1976-2007). RJF: Rafsanjan Fault, SHBF: Shahr Babak Fault.

total right-lateral offset of approximately 200 meters and a vertical motion of four meters are visible in the area located 9 km south of the Kuhbanan town. A minimum of 5 km right-lateral displacement of the Lower Cambrian Desu Series, the Cambrian Lalun Sandstone, and of the Upper Jurassic Bidu Formation keybeds is visible in the area NW of Kerman (NNW of Chatrud, in the Tigur-Khunik area: Berberian 1976; Berberian et al. 1979; Berberian, 2005).

The area between the south-eastern segment of the Kuhbanan and the north-western segment of the Gowk strike-slip fault systems (east and northeast of Kerman), where both faults show a step to the left, is composed of several active approximately E-W to WNW-ESE trending cross-thrust faults (Berberian, 2005). These cross-thrusts were associated with a cluster of five recorded medium-magnitude earthquakes in 1854 (Ms=5.8), 1864 (Ms=6.), 1897 (Ms=5.7), 6 August 1984 (M=5.3; with an E-W thrust focal mechanism and a centroid depth of 11 km) and 22 February 2005 (Mw=6.4) with a thrust focal mechanism. Reverse focal mechanisms of the 1984 and the 2005 earthquakes along cross-thrust faults contrast with the strike-slip focal mechanisms of the other earthquakes in this zone (Berberian, 1976; Berberian, 1995b; Berberian, 2005; Talebian et al. 2006). The full

Table 4-2. Historical and instrumental earthquakes occurred around the Kuhbanan and its associated faults.

Event	Ms	Location	Fault
1854 November	~5.8	Hurjand (30km NE Kerman)	Cross Thrust?
1864 January 17	~6.0	Chatrud (40km NW Kerman)	Cross Thrust?
1875 May	~ 6.0	120km NW Kerman	Strike-slip Kuhbanan?
1897 May 22	~ 5.5	Kuhbanan town	Strike-slip Kuhbanan
1897 May 27	~5.5	25km NW Kerman	Cross Thrust?
1911 April 18	~ 6.4	Ravar (110km N-Kerman)	Cross Thrust Lakarkuh
1933 November 28	~ 6.2	Behabad town	Strike-slip Kuhbanan
1953 January 15	~5.5	80 km N-Kerman	?
1977 December 19	~ 5.8	Zarand (70km NW Kerman)	Strike-slip Kuhbanan
1978 May 22	~5.3	Behabad town	Strike-slip Kuhbanan
1984 August 6	~5.3	35km N-Kerman	Cross Thrust?
2005 February 22	Mw=6.5	Zarand (60km NW Kerman)	Cross Thrust?

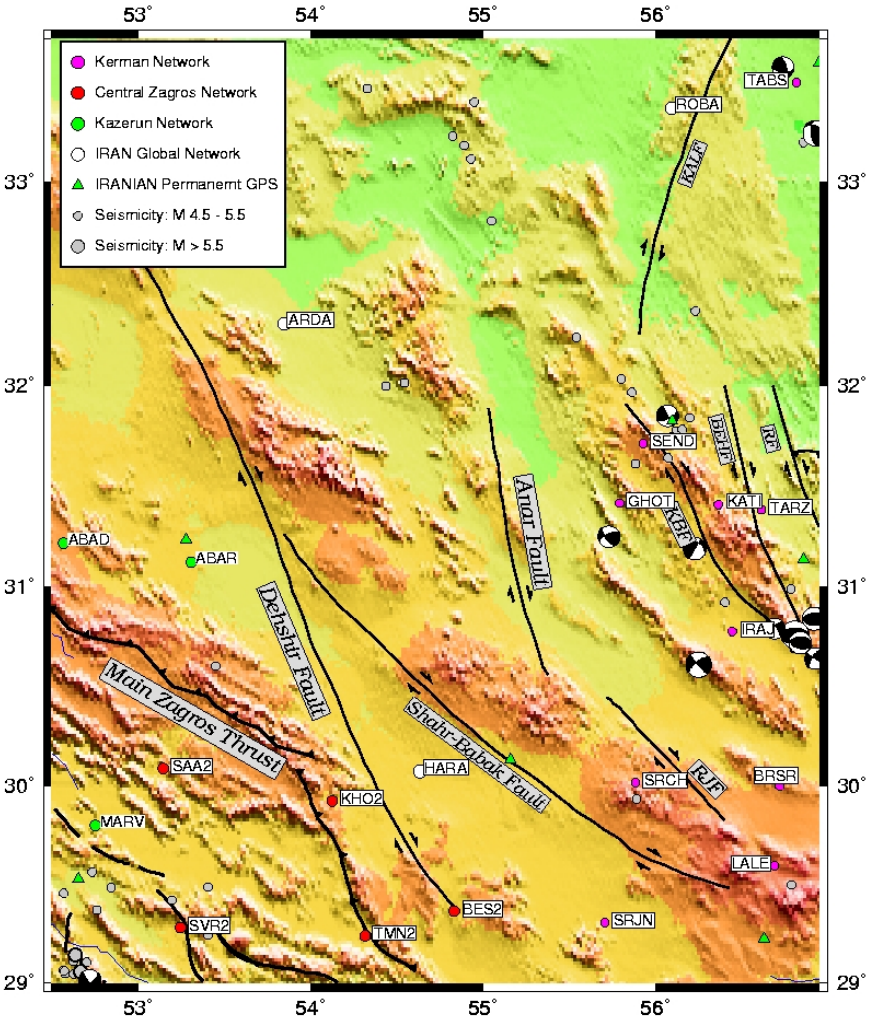

Figure 4-4. Topography, fault and distribution of the GPS stations map of the Dehshir region in the Central Iran block. Epicenters of earthquakes M>4.5 are from Engdahl et al. (1998). Black spheres are Harvard CMT solutions during 1976-2007. BEHF: Behabad Fault, KALF: Kalmard Fault, KBF: Kuhbanan Fault, RF: Ravar Fault, RJF: Rafsanjan Fault.

record of pre-instrumental and instrumental seismicity (1854 to 2006) on the Kuhbanan fault region is listed in Table 4-2.

c) The Anar Fault

The Anar fault (Fig. 4-4, 4-5) is located just west of the Anar town on the Central Iran block with a NNW-SSE trend and a length of ~200 km. It dies out in the mountains of Kuh-e-mozahem in the south, and in an isolated zone of folding in the north. On this right-lateral fault no historical earthquakes have been recorded (Berberian, 1976; Ambraseys and Melville, 1982; Walker and Jackson, 2002). The fault displaces sand stone units of a lower Cretaceous shale sequence exposed in the Kuh-e-Bafg mountain range, apparently right-laterally by up to ~20 km (Nabavi,

1970). Walker and Jackson (2004) have reported a minimum of 5 km of right-lateral displacement of bedrocks on the Anar fault in the Kuh-e-Kharanaq mountain range strands from satellite image observations.

d) The Dehshir Fault

The Dehshir fault (Fig. 4-4) is a right-lateral strike-slip fault ~400 km long with a NNW-SSE trend. This fault starts in the northwest close to the town of Naiin and ends to the southeast near Sirjan. It is a old fault with a lack of recorded seismicity (Berberian, 1976; Ambraseys and Melville, 1982; Walker and Jackson, 2004; Meyer et al., 2006). Amidi (1975) proposes that this fault might have displaced right-laterally the upper Cretaceous deposits of about 50 km. Meyer et al. (2006) estimated 65±15 km of total offset which has been accumulated over the last 25-40 Ma. Therefore, they estimate a right-lateral slip rate of 2 mm/yr for the Dehshir fault. Vernant et al. (2004) proposed that the Central Iran block, crossed by the Dehshir fault, is rigid experiencing only little internal deformation (≤ 2mm/yr). Vernant et al. (2004) did not resolve any velocity for the Dehshir fault as the uncertainties of their GPS measurements is of the same order as the presumed Dehshir velocity of 2 mm/yr. However, their work suggests that the present day velocity of the Dehshir fault does not exceed the 2 mm/yr. Because the Anar and Dehshir faults are probably as much active as the Nayband and the Gowk faults with geological velocities of about 2 mm/yr, they might be able to produce similar earthquakes as on the faults located further east.

e) The Gowk fault

The Gowk fault (Fig. 4-5) is an almost NNW-SSE (N155°) trending right-lateral strike-slip fault with a length of ~170 km. This fault is connected to the Nayband and Kuhbanan fault in the north and the Jebal Barez mountains in the south (Berberian, 1976; Walker and Jackson, 2002; Berberian, 2005). The Gowk fault has experienced five earthquakes of Mw=5.4 to 7.1 in the last 25 years (Table 4-3). In 1981, an earthquake of Mw=6.6 produced 15 km of right-lateral ruptures in the south of Golbaf town with surface displacements of up to 3 cm. In July 1981, another earthquake occurred in the region of the Sirch village located south-east of Kerman and produced a rupture 65 km long and with a maximum surface displacement of 50 cm.

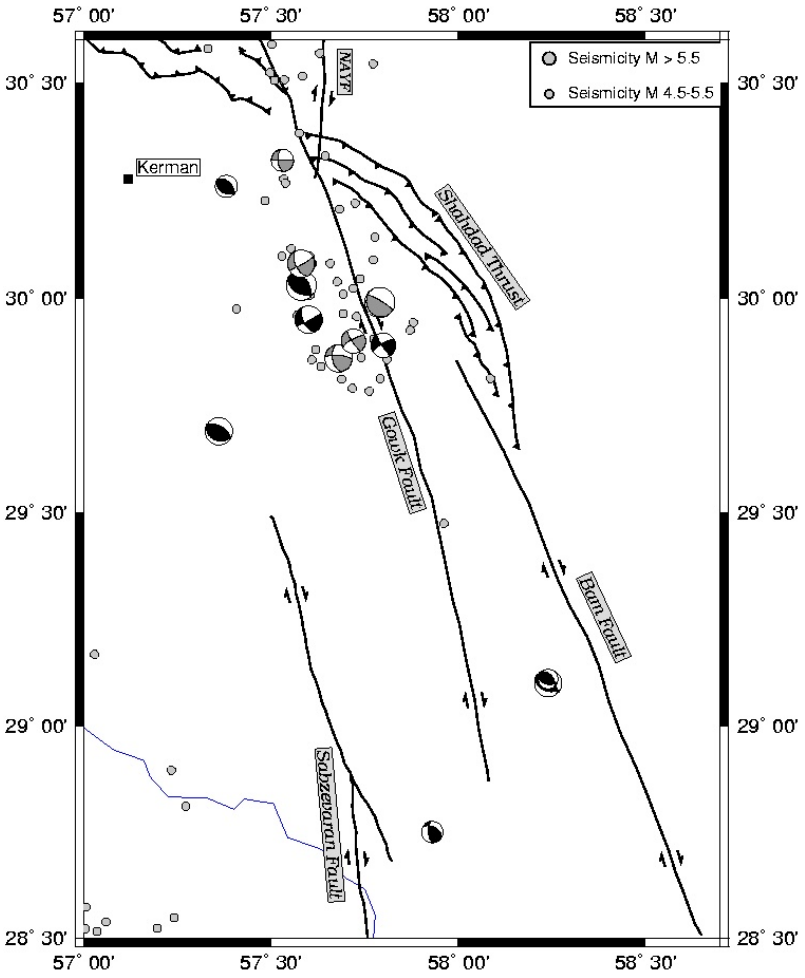

Figure 4-5. Seismotectonic map of the Gowk region. Earthquake epicenters M>4.5 are from Engdahl et al. (1998). Black spheres are Harvard CMT solutions from 1976-2007. Grey spheres are CMT solutions from Berberian et al. (2001). NAYF: Nayband Fault.

In 1998 occurred an earthquake of Mw=6.6 close to the village of Fandoqa. This earthquake ruptured 23 km of the Gowk fault with an average right-lateral slip of ~1.3 m reaching up to 3 m in some places (Berberian et al. 2001; Walker and Jackson, 2002). Walker and Jackson (2002) suggest 12 km of total offset for the Gowk fault with most of it being produced over the last 5 Ma. Therefore, they estimate a slip rate of 1.5 - 2.4 mm/yr on the Gowk fault.

f) The Bam Fault

The NW-SE trending Bam fault system (Figs. 4-5, 4-6) with a total length of 110 km is located in the western part of the Lut block, east of the Gowk fault (Berberian, 2005). This right-lateral strike-slip fault starts at ~29.5°N in the north and ends at the

Table 4-3. Source parameters of the Gowk-valley main earthquakes. Epicentres are from Engdahl et al. (1998). Magnitudes (mb and Ms) are from the USGS. Seismic moment (M0) is in units of 10E18Nm, and sv is the slip vector azimuth, assuming that the west-dipping nodal plane is the fault plane. The last column is the reference: B is computed by body wave modelling, B& and B2 are the first and second event, H is Harvard solution.

Date	Lat.	Long.	Depth	mb	Ms	Mw	M0	Strike	Dip	Rake	sv	R
1981.06.11	29.86	57.68	20	6 .1	6.7	6.58m	4.18	169	52	156	184	B1
(Golbaf)			12				5.30	182	88	198	182	B2
1981.07.28	29.99	57.79	18	5.7	7.1	6.98	36.69	177	69	184	176	B
(Sirch)			15			7.24	90.10	150	13	119	210	H
1989.11.20	29.90	57.72	10	5.6	5.5	5.83	0.70	145	69	188	142	B
(S. Golbaf)			15			5.88	0.82	148	81	165	150)	H
1998.03.14	30.08	57.58	5	5.9	6.9	6.57	9.09	156	54	195	147	B
(Fandoqa)			15			6.58	9.43	154	57	186	151	H
1998.11.18	30.32	57.53	15	4.9	5.1	5.34	0.13	174	55	173	178	H
(C. Farsakh)												

Jebal Barez Mountain in the south (~28.5°N). This fault has several segments. The Bam-Baravat segment lies approximately 5 km to the east of the centre of Bam city, and 45 km east of the southern end of the Gowk fault system. This segment with a scarp ~25 m high passes between the Bam and Baravat cities. The scarp is clearly visible on aerial photos and satellite images because of right-lateral offset of streams and Qanats (Talebian et al., 2004; Berberian, 2005). Before the 26 December 2003, no earthquake has been recorded near Bam (Ambraseys and Melville, 1982; Berberian and Yeats, 1999; Talebian et al., 2004; Berberian, 2005). The Bam Citadel (Arg-e-Bam) has been reconstructed several times but at last in 1751. The Bam 26 December 2003 earthquake (M_W=6.5) destroyed the Bam city and the surrounding villages and killed about 30,000 people. The focal mechanism from Harvard CMT and Talebian et al. (2004) suggest that the earthquake involved predominantly strike-slip motion (strike=357°, dip=88° and rake=-166°). The analysis of the data shows that the main surface rupture of the earthquake did not occur on the Bam-Baravat segment of the Bam fault, but on a vertical N-S trending fault which had not previously been identified, located 4 km to the west of the Bam-Baravat segment, immediately south of the city of Bam. The larger slip on the fault occurred over a region of 12 km by 8 km with a peak slip of 2.5 m at a depth of ~5 km. Only a small amount of the slip reached the surface. The second part of the shock shows thrust

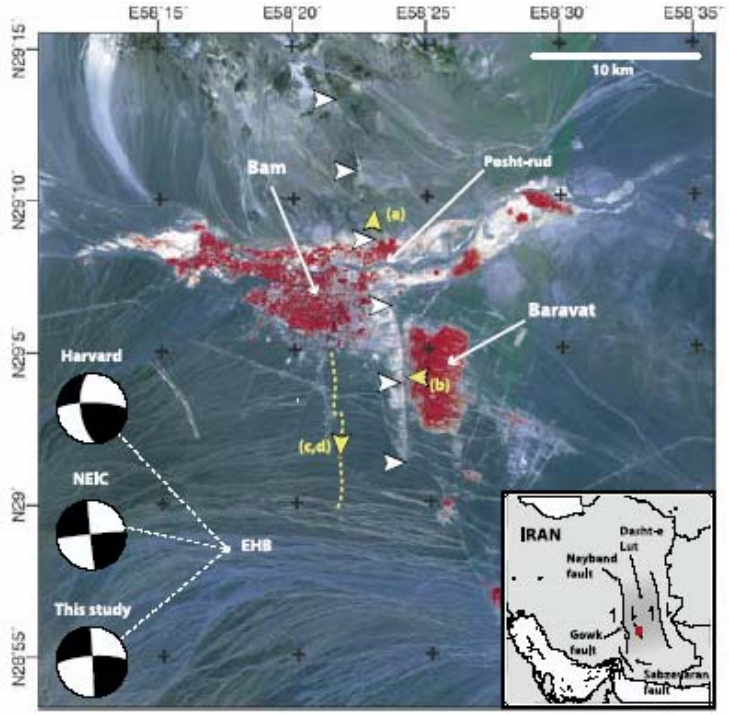

Figure 4-6. ASTER false colour image of the epicentral Bam region. Red colours indicate the presence of vegetation in the cities of Bam and Baravat. Focal mechanisms are from Harvard, NEIC and Talebian et al. (2004); the EHB epicentre is provided by E. R. Engdahl (unpublished data, 2004). White arrowheads are locations of the previously-identified Bam fault; the yellow dashed line is the surface trace of the newly-revealed blind strike-slip fault responsible for this earthquake (after Talebian et al., 2004).

motion beneath the previously mapped Bam fault, located 5 km to the east of the main rupture. The total rupture length estimated by Wang et al. (2004) is about 24 km. Detailed works on the Bam earthquake can be found in e.g. Talebian et al. (2004), Funning et al. (2005), Fielding et al. (2005), Berberian (2005) and Motagh et al. (2006).

4.2.2 East-west left-lateral faults

4.2.2.1 The Doruneh Fault

a) Tectonics

The Doruneh fault (Fig. 4-7) extends for about 700 km from the eastern border of Iran to the central Dasht-e-kavir (Great Kavir Desert). It was named by Wellman (1966) after the small village of Doruneh at longitude 57°E. The Doruneh fault is a left-lateral strike-slip fault trending east-west and located north of the Lut block. After the Main Zagros Thrust, the Doruneh fault is the longest fault of Iran. It plays an

important role in the regional tectonics. The eastern part of the Doruneh fault is bending to the south. The western part trends WSW and crosses the Dasht-e-Kavir and ends near the Naiin city of the Yazd province. This western part is generally called the Great Kavir fault and little topography is associated with this part of the fault. Two big cities, Kashmar and Torbat-e-Heydarieh, are located near the fault trace at a longitude of about 58.5°E and 59.5°E, respectively. Jackson and McKenzie (1984) propose that the N-S right-lateral shear produced by the strike-slip motion of the faults located both on the west and on the east sides of the Lut block is reflected by the evolution of the Doruneh fault. The fault must rotate clockwise around a vertical axis located at the border with Afghanistan in order to accommodate the N-S shear. Walker and Jackson (2004) observed a shortening component across the eastern part of the fault parallel to the Jangle thrust. Fattahi et al. (2006) estimated 2.5 mm/yr of left-lateral slip-rate on the Doruneh fault, based on the dating of the uppermost deposition on a section of the Doruneh fault at longitude ~58° to 10-12 ka, by an Infrared Stimulated Luminescence (IRSL) technique.

b) Seismicity on the Doruneh fault

On the Doruneh fault, only moderate historical and recent earthquakes have been recorded (Fig. 4-7). In Table 4-4, a summary of the recent earthquakes is presented.

The historical seismicity is registered since 1336 AD, when an earthquake occurred in the Khaf city and destroyed many villages between Khaf and Torbat-e-Heydarieh. This earthquake has ruptured the Jangal thrust fault south of the south-eastern end of Doruneh (Ambraseys and Melville, 1982; Jackson and McKenzie, 1984, Fattahi et al., 2006). In 1619, another earthquake occurred close to the Doruneh fault and destroyed the Doghabad village south of Torbat-e-Heydarieh, killing ~800 people. There is not enough information available to infer the intensity of the earthquake (Ambraseys and Melville, 1982; Jackson and McKenzie, 1984; Fattahi et al., 2006). In 1903, an earthquake occurred in the village of Turshiz (renamed to Kashmar) and damaged a wide area in the east, west and south of Kashmar, killing ~350 people. The damaged area is located south of the Doruneh fault. There are no damaged places north of the Doruneh fault (Ambraseys and Moeinfar , 1975; Ambraseys and Melville, 1982; Fattahi et al., 2006). In 1923, the last

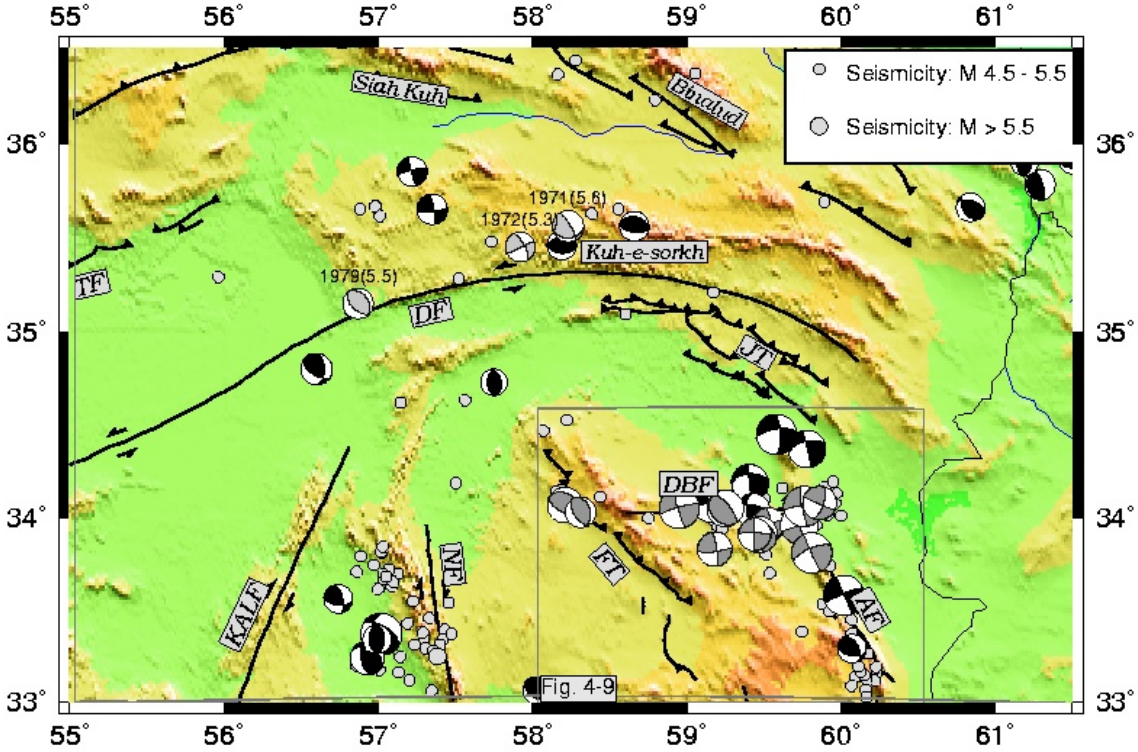

Figure 4-7. Seismotectonic map of the Doruneh fault. The grey CMT are from Fattahi et al. (2006) and Walker and Jackson (2004). AF: Abiz Fault, DBF: Dasht-e-Bayaz Fault, DF: Doruneh Fault, FT: Ferdows Thrust, JT: Jangal Thrust, KALF: Kalmard Fault, NF: Nayband Fault, TF: Torud Fault.

Table 4-4. Epicentre and source parameters of earthquakes in the Doruneh region. Events 1 to 3 are from Baker (1993), and are also listed in Jackson (2001). Events 4 and 5 are from the Harvard CMT catalogue. Depths reported for the CMT events are not necessarily reliable (e.g. Jackson 2001).

Event	Date	Time (GMT)	Lat.	Long.	Depth	*Mw*	Strike	Dip	Rake
1	1971.05.26	02:41:35	35.56	58.23	13	5.6	89	26	32
2	1972.12.01	11:39:35	35.45	57.92	8	5.3	65	87	25
3	1979.12.09	09:12:35	35.15	56.87	9	5.5	325	36	99
4	1996.02.25	17:42:04	35.65	57.07	33	5.4	82	77	10
5	2000.02.02	22:58:01	35.29	58.22	26	5.3	83	43	79

destructive earthquake in Doruneh destroyed and damaged ~20 villages and killed ~770 people. The damaged area had a radius of ~5 km. An intensity of Ms=5 has been estimated for this earthquake (Ambraseys and Moeinfar, 1977; Ambraseys and Melville, 1982; Fattahi et al., 2006).

4.2.2.2 The Dasht-e-Bayaz fault

a) Tectonics

The Dasht-e-Bayaz fault (Fig. 4-8) is an E-W trending left-lateral fault system located to the north of the Lut block at latitude 34°N. The westernmost segment is ~70 km long and starts from the NW-SE trending Ferdows reverse fault. It is separated from the eastern segment by the N-S trending right-lateral Mahyar fault. The eastern segment is ~50 km long and is connected to the east to the N-S trending right-lateral Abiz fault (Berberian and Yeats, 1999). Berberian and Yeats (1999) estimated a minimum of 2.5 mm/yr of left-lateral displacement on the Dasht-e-Bayaz fault based on the qanats (underground water channel as old as 4000 years) offset. Based on this slip rate and the left-lateral slip (250 cm) released during the 1968 earthquake (Tchalenko and Berberian, 1975), the return period could be of about 1000 years. Walker et al. (2004) have estimated 4-5 km total cumulative offset on the fault system which is small compared to the total amount of Late Tertiary deformation expected in this part of Iran. This may indicate that the Dasht-e-Bayaz fault is relatively young. The Dasht-e-Bayaz fault is parallel to the Doruneh fault and presents a similar mechanism. It will therefore probably rotate about a vertical axis like the Doruneh fault to accommodate the regional NS right-lateral shear (Jackson and McKenzie, 1984; Walker and Jackson, 2004).

b) Seismicity of Dasht-e-Bayaz fault:

The Dasht-e-Bayaz fault has recorded several large historical and instrumental earthquakes larger than magnitude 7 (Tables 4-5 and 4-6, Fig. 4-8). These earthquakes have been studied in detail (Ambraseys and Tchalenko, 1969; Ambraseys and Melville, 1982; Jackson and McKenzie, 1984; Berberian and Yeats, 1999; Walker and Jackson, 2004).

In 1968, the western segment of the Dasht-e-Bayaz fault produced an earthquake of Mw=7.1 which created a 80 km long surface rupture with a maximum of 4.5 m of left-

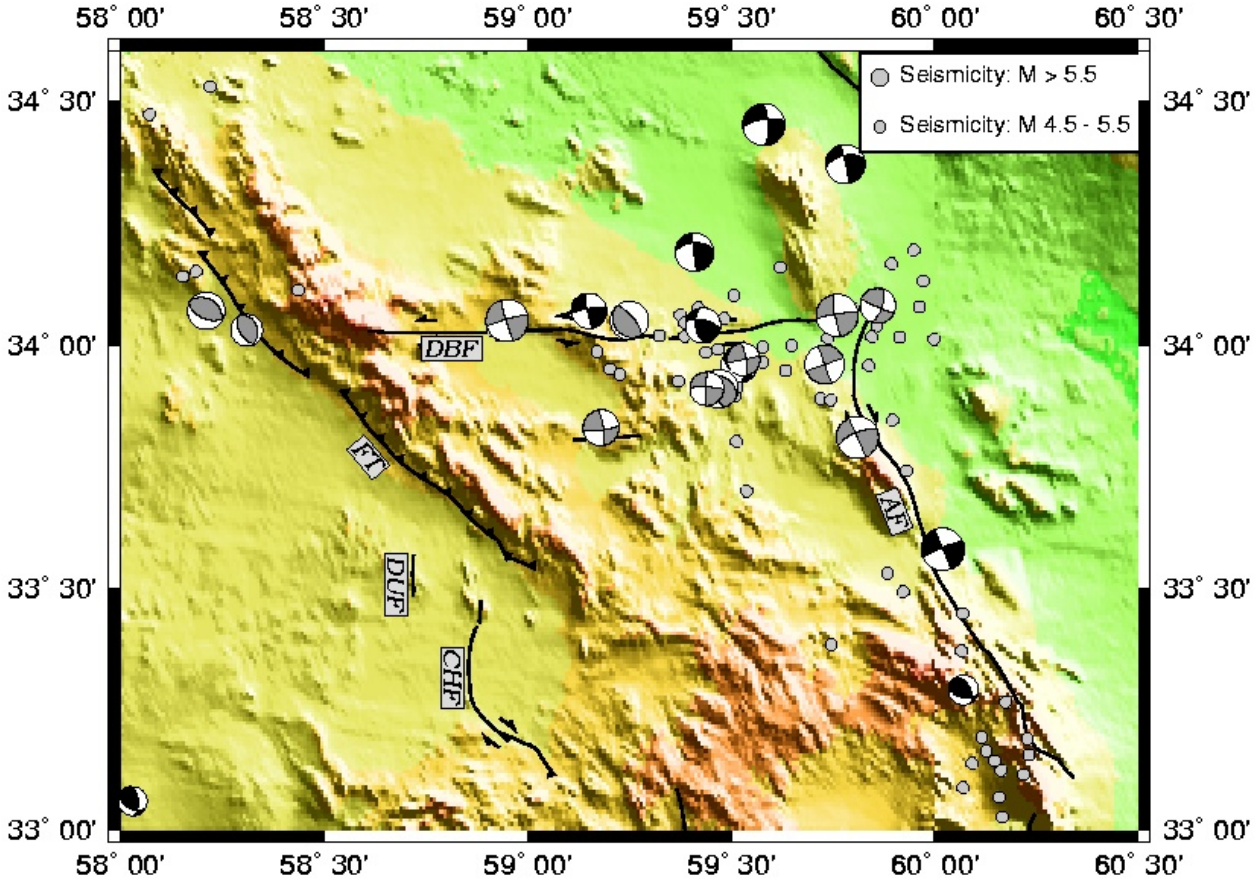

Figure 4-8. Seismotectonics of the Dasht-e Bayaz fault. The earthquake epicenters M>4.5 are from Engdahl et al.(1998) The grey CMT is from Walker et al. (2004) and black spheres are Harvard CMT solutions from 1976-2007. DBF: Dasht-e-Bayaz Fault, AF: Abiz Fault, DUF: Dustabad Fault, CHF: Chahak Fault, FT: Ferdows Thrust.

lateral offset and 2.5 m of vertical uplift. This earthquake killed between 7,000 and 12,000 people and destroyed many villages (Ambraseys and Tchalenko, 1969; Berberian and Yeats, 1999). In November 1979, an earthquake of Mw=7.1 occurred on the eastern segment of the fault and ruptured about 60 km of the fault. As the region is not so populated only a few people were killed. A total left-lateral displacement of 1-4 m and vertical uplift of 2.5m were reported by Haghipour and Amidi (1980).

Table 4-5. Historical earthquakes in the Dasht-e-Bayaz region. Details are taken from: (1) Ambraseys & Melville (1982), (2) Berberian & Yeats (1999), (3) Berberian & Yeats (2001), (4) Berberian *et al.* (1999) and (5) Ambraseys & Tchalenko (1969).

Date	Time	Location	Mag.	Ref.	Fault
AD856 December	?	Widespread damage	?	5	Several?
AD1066 May	?	Qaen	?	2, 3	?
1238	?	Gonabad	?	2, 3	Gonabad/Bidokht?
1549 February 15	?	E. Qaen/Birjand	*ca* 6.7	1, 4	N. Birjand?
1675 Winter	?	Gonabad	?	2, 3	Gonabad/Bidokht?
1847	?	Qaen	?	4	?
1923 November 29	?	S.E. of Qaen	5.6	4	?
1936 June 30	?	Abiz	6	4	Abiz
1941 February 16	Late evening	Muhammadabad	?	1	Chahak
1947 September 23	Morning	Dustabad	?	1	Dustabad
1962 April 1	Dawn	Musaviyeh	?	1	Chahak?

Table 4-6. Instrumentally recorded earthquakes for the Dasht-e-Bayaz region that have been modelled using body waves. 'm' in the *Mw* column signifies a multiple event. The fault-plane solutions are shown on Fig. 4-9. Epicentres are from Engdahl *et al.* (1998). References are: (1) Baker (1993), (2) Berberian *et al.* (1999), (3) Walker *et al.* (2003), (4) Jackson (2001), (5) Walker et al. (2004) (from Walker et al., 2004).

Date	Time	Lat.	Long.	Depth	*Mw*	Strike	Dip	Rake	Ref.	Fault
1968 August 31	10:47	34.05	58.95	17	7.10	254	84	5	5	W. D-e-Bayaz
1968 August 31	10:47	34.05	*ca* 59.25	10	6.44	320	70	90	5	W. D-e-Bayaz
1968 September 1	07:27	34.07	58.21	9	6.25	115	54	85	3	Ferdows
1968 September 4	23:24	34.03	58.31	9	5.48	148	56	81	3	Ferdows
1968 September 11	19:17	33.97	59.53	6	5.6	78	90	16	1	D-e-Bayaz
1976 November 7	04:00	33.83	59.18	8	6.03m	84	79	12	1,4	Qaen
1979 January 16	09:50	33.91	59.47	11	6.48m	162	66	115	1, 4	Qaen
1979 November 14	02:21	33.96	59.73	10	6.5 m	160	89	−177	1, 4	Abiz
1979 November 27	17:10	34.06	59.76	8	7.1	261	82	8	5	E. D-e-Bayaz
1979 December 7	09:23	34.08	59.86	10	5.9	113	84	21	1	Abiz
1997 May 10	07:57	33.81	59.81	13	7.12	156	89	−160	2	Abiz
1997 June 25	19:38	33.91	59.44	8	5.7	181	87	170	2	Boznabad

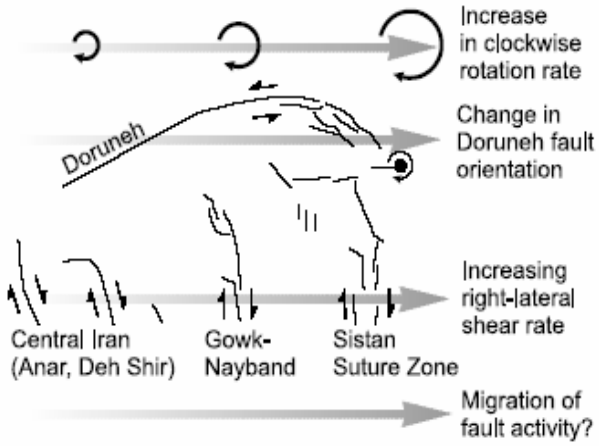

Figure 4-9 Cartoon showing the influence of an uneven distribution of N–S right-lateral shear on the fault systems of central Iran (Anar and Dehshir), the Gowk-Nayband fault system, and the active faults of the Sistan suture zone. From west to east, an increase in the cumulative N–S right-lateral shear is seen. This increase is reflected in the orientation of the Doruneh fault, as it rotates clockwise to accommodate the right-lateral shear. More rotation is required in the east than in the west. The concentration of the present-day activity on the active fault systems along the eastern margin of Iran may reflect a gradual eastward migration of activity away from central Iran over the last 5 to 10 Ma (Walker and Jackson, 2004).

4.3 Tectonical model

Walker and Jackson (2004) propose a model for the tectonics of the Lut region (Figs. 4-9 and Fig. 4-10). In their model, the N-S right-lateral shear between Central Iran and the Hellmand block is accommodated on the faults of Dehshir, Anar, and Nayband-Gowk to the west of the Lut block, and on the Sistan fault system to the east of the Lut block. They believe that the total north-south right-lateral shear expected between central Iran and the Hellmand block is about 75-105 km, with 10 km, 15 km and 70 km of total displacement on the Dehshir and Anar, Gowk-Nayband and Sistan fault system, respectively. They suggest that this shear occurred over the last 3 to 7 Ma, which evaluates average fault slip rates of 1–3 mm/yr, 2-5 mm/yr and 10-23 mm/yr, respectively. GPS measurements estimate ~15 mm/yr of right-lateral shear cumulated across the Lut block (Gowk-Nayband and Sistan fault system, Vernant et al., 2004).

At the time of its onset, the Doruneh fault was oriented EW, but in order to absorb the ~70 km NS shear across the Sistan suture zone, it rotated clockwise of about 20°. This ~20° is the angle between the Doruneh and Dasht-e-Bayaz trace

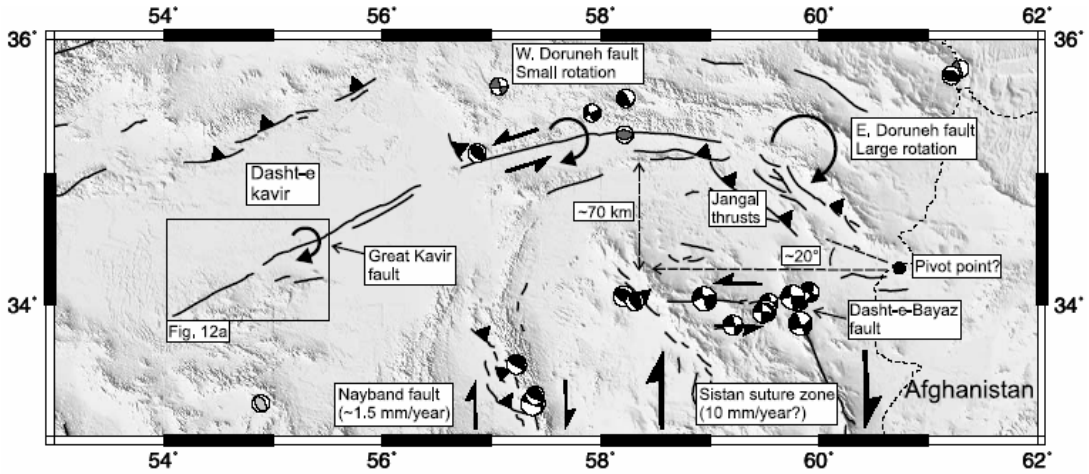

Figure 4-10. Topography and fault map the Lut region and the velocity rate of the faults in both side of the Lut block and the rotation of the the Doruneh and Dasht-e-Bayaz faults. These left-lateral faults accommodate N–S right-lateral shear by clockwise rotation about vertical axes, possibly pivoting at a point close to the Afghan border (marked as a black circle). The prominent curvature of the Doruneh fault could be due to the larger finite rotations in the eastern part of the fault, probably caused by a large proportion of the right-lateral shear being taken up across faults in the Sistan suture zone. Fault plane solutions of shallow (<35 km) earthquakes are shown. Black balloons are body-wave modelled solutions (Jackson, 2001; Walker 2003; and Walker et al. 2003, 2004); dark grey are Harvard CMT solutions, and light grey represents first-motion polarity solutions (McKenzie, 1972). After Walker and Jackson (2004).

rotating around a point fixed at the Afghan border. After moving outside the zone of maximum shear (EW), the rotation of the Doruneh fault is transferred to the EW oriented Dasht-e-Bayaz fault. The Doruneh fault accommodates now the NS shear by shortening in the Jangal thrust south of its eastern termination, while the Dasht-e-Bayaz fault seems to rotate with a rate of 6° per Ma (Walker and Jackson, 2004; Walker et al. 2004). Walker et al. (2004) presented a schematic model showing how N–S right-lateral shear can be accommodated by the clockwise rotation about vertical axes of blocks with left-lateral strike-slip faults at their edges. This model does not account for internal deformation within the fault-bounded blocks, but is a useful approach for determining the fault displacements caused by N–S right-lateral shear. With this model the authors estimated ~2.5° clockwise rotation on the Dasht-e-Bayaz fault assuming ~4 km total left-lateral offset on the fault, 100 km for the width of the fault bounded block and ~8 km N-S right-lateral shear (Fig. 4-11).

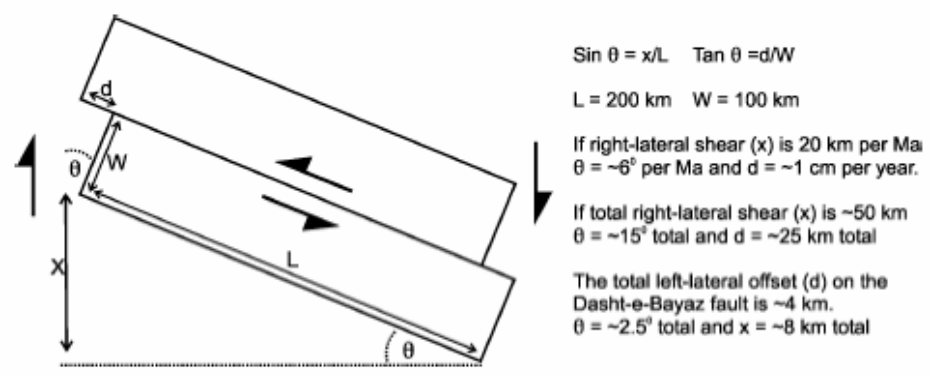

Figure 4-11. Cartoon showing how N–S right-lateral shear can be accommodated by the clockwise rotation about vertical axes of blocks with left-lateral strike-slip faults at their edges. This model does not account for internal deformation within the fault-bounded blocks, but is a useful approach for determining the fault displacements caused by N–S right-lateral shear. The total left-lateral offset (d) on these faults depends not only on the amount of N–S right-lateral shear (x) but also on the length (L) and width (W) of the blocks. The clockwise rotation (*θ*) can be expressed in terms of these dimensions. The values of 200 km and 100 km for L and W, has been used. Although the calculated values of d and *θ* are not precise, as we have assumed values of L and W, they provide an estimate that can be compared to observed values of d and *θ* (Walker et al., 2004).

The 50 km and 20 km of right-lateral slip on the Dehshir and Anar faults correspond to a ~25° and ~11° anticlockwise rotation respectively between the faults in central Iran and the Nayband fault .These large offsets cumulated over the Dehshir and Anar faults as mentioned above suggest some contribution predating present-day tectonics (3-7 Ma) (Walker and Jackson, 2004).

4.4 GPS Measurements

In order to measure the displacement and the deformation rate of the western Lut faults, we installed end of 2003 5 benchmarks around the Kuhbanan, Lakarkuh, Nayband, Gowk and Bam faults (Fig. 4-1). These benchmarks are SEND, KATI, CFCM, LALE and BA12. LALE is on the Hezar mountains and BA12 is located east of the Bam fault, on the rigid Lut block. Except CFCM, all stations were installed with forced centering bold mark far enough (≥ 10 km) from the faults to avoid contamination of the rigid block motion due to the locking of the fault. We could not find any bedrock around the Nayband fault so we selected a Precise Leveling Network benchmark (CFCM) which has been installed in 1996. This benchmark is a

cylinder of re-enforced concrete with a diameter of 60 cm and a depth of one meter. We used a tripod for the measurements of this point.

Up to now, the network has been measured three times, in January 2004, December 2004, and February 2006. We also included ROBA, KERM, and ZABO stations from the Iran Global Network in our measurements. These benchmarks have been measured several times during the surveys of the Iran Global (Nilforoushan et al., 2003; Vernant et al., 2004; Masson et al., 2005), Mashhad (Kopeh Dagh) and Bam networks.

After the 2003 Bam earthquake, a GPS network of 25 sites was installed around the Bam and Gowk faults to measure post-seismic deformation. It has been measured 5 times. To estimate the deformation of the western Lut we used some of the Bam network measurements.

In the eastern part of the Lut we have used the southern points of the Mashhad network which has been installed in 2004 and remeasured in July 2006. The southern Mashad network benchmarks are GARD, BAKH, KHAF, DOGH, BAJE, QAE2, and NOGH.

We combined our local observations with data from other regional campaigns, in particular the surrounding Iran Global network which has been measured in 1999, 2001 and 2005 (Nilforoushan et al.,2003; Vernant et al., 2004; Masson et al., 2007), the Central Zagros network measured in 1997, 2000, 2003 (Tatar et al. 2002; Walpersdorf et al. 2006), the Kazerun network measured in 2002, 2004 (Tavakoli et al., 2007) and the Mashhad network measured in 2004, 2006 (Tavakoli et al., 2006). Details on the processing are given in Chapter 2.

4.5 Velocity field

We determined the site velocities of the Lut region in the ITRF (Fig. 4-12, Table 4-7) and Eurasia (Fig. 4-13, Table 4-7) reference frame (for details see chapter 2). As the velocity of ZABO which is located on the Hellmand block is less than 2 mm/yr relative to Eurasia it suggests that the Hellmand block is part of the Eurasian plate. Therefore, we also computed the velocities relative to ZABO as an alternative realization of the Eurasian reference frame (Fig. 4-14, Table 4-7).

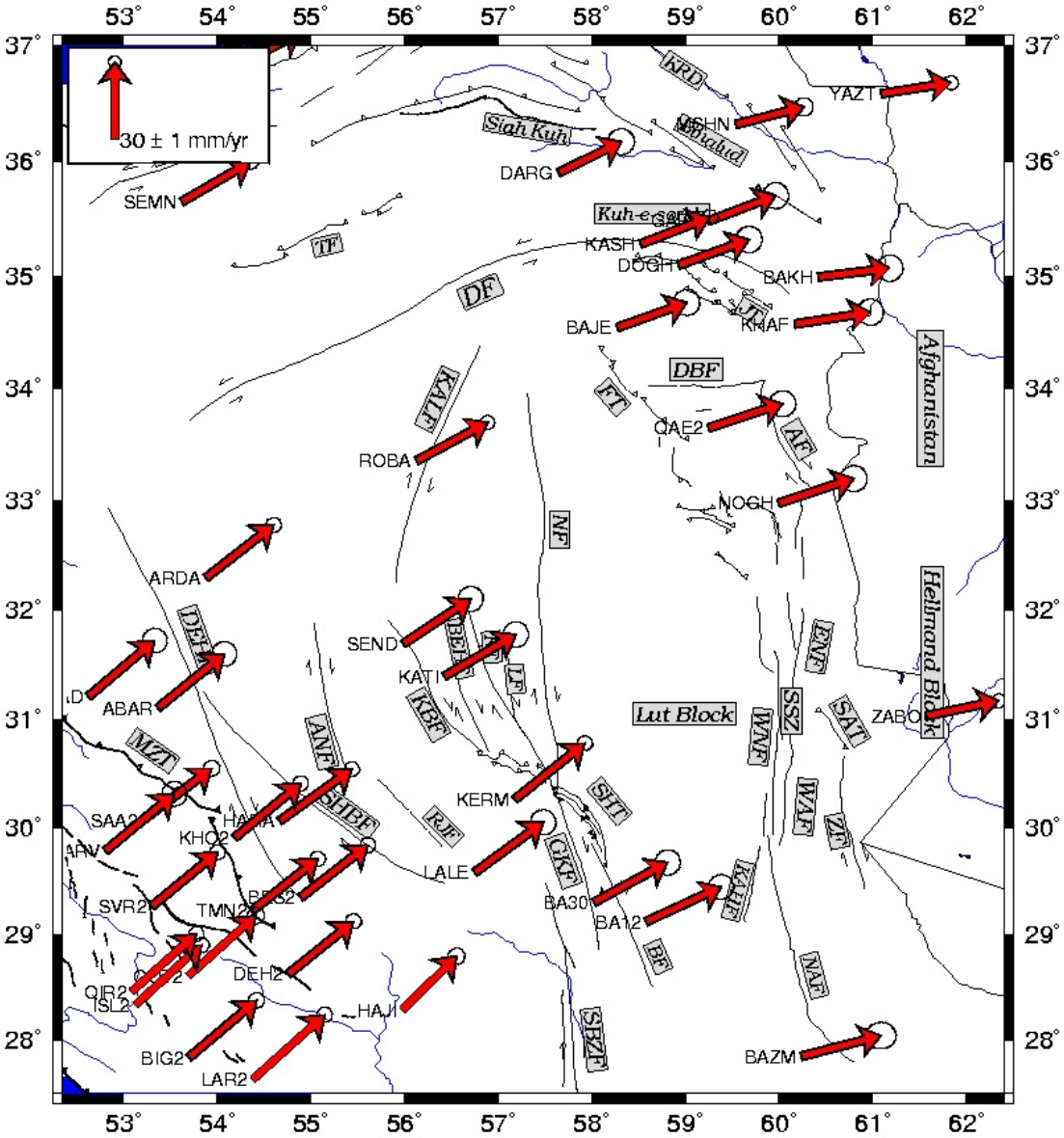

Figure 4-12. Station velocities in the Lut region relative to the ITRF2000 reference system. The error ellipses indicate formal errors within a 95% confidence interval. AF: Abiz Fault, ANF: Anar Fault, BF: Bam Fault, BEHF: Behabad Fault, FT: Ferdows Thrust, DF: Doruneh Fault, DBF: Dasht-e-Bayaz Fault, DEHF: Dehshir Fault, GKF: Gowk Fault, JT: Jangal Thrust, KAHF: Kahurak, Fault, KALF: Kalmard Fault KBF: Kuhbanan Fault, LF: Lakarkuh Fault, MZT: Main Zagros Thrust, NAF: Nosrat Abad Fault, NF: Nayband Fault RF: Ravar Fault, RJF: Rafsanjan Fault, SBZF: Sabzevaran Fault, SHF: Shahdad Fault, SHBF: Shahr Babak Fault, SSZ: Sistan suture zone, TF: Torud Fault, WAF: West Asagie Fault, WNF: West Neh Fault, ZF: Zahedan Fault.

Table 4-7. Velocity (mm/yr) of the Lut stations relative to the ITRF2000, Eurasia reference frames and ZABO station. Ve and Vn are east and north velocity components. δe and δn are east and west velocity uncertainties in mm/yr.

SITE	LONG.	LAT.	ITRF2000		Eurasia		ZABO		Uncertainty	
NAME	Deg	Deg	Ve	Vn	Ve	Vn	Ve	Vn	δe	δn
ZABO	61.517	31.049	27.74	5.87	0.23	1.42	0.00	0.00	0.83	0.82
YAZT	61.034	36.601	26.79	4.14	-0.53	-0.07	-0.91	-1.36	0.84	0.83
BAKH	60.360	35.002	27.54	3.44	-1.85	-1.00	-2.18	-2.12	1.89	1.89
BAZM	60.180	27.865	30.56	7.95	3.55	3.33	3.24	2.24	2.11	1.61
KHAF	60.110	34.589	29.10	4.54	-0.36	0.02	-0.69	-1.05	1.98	2.00
NOGH	59.937	32.988	28.90	9.48	-0.84	5.02	-1.13	4.00	2.01	1.95
MSHN	59.480	36.335	26.23	6.75	-1.70	1.83	-2.12	0.92	1.08	1.07
GARD	59.197	35.495	25.51	9.72	-3.87	5.23	-4.26	4.40	1.76	1.78
QAE2	59.188	33.663	28.52	9.34	-1.09	4.77	-1.42	3.93	1.87	1.89
JANA	59.076	37.413	26.70	5.24	-2.77	0.48	-3.26	-0.32	2.23	2.15
DOGH	58.869	35.108	27.09	9.86	-2.10	5.05	-2.49	4.30	1.90	1.94
BA12	58.523	29.137	28.84	13.39	0.16	8.19	-0.17	7.52	1.49	1.46
KASH	58.464	35.293	26.65	10.36	-0.82	4.86	-1.23	4.21	0.86	0.85
SHAM	58.431	37.570	26.12	7.39	-3.09	2.71	-3.61	2.07	1.78	1.82
BAJE	58.215	34.558	26.69	9.62	-2.77	4.81	-3.16	4.21	1.82	1.80
BA30	57.967	29.316	28.31	15.42	-0.62	9.84	-0.96	9.31	1.63	1.61
DARG	57.589	35.915	24.09	11.97	-5.16	7.04	-5.63	6.60	1.81	1.84
SHIR	57.308	37.814	23.40	10.10	-3.84	3.90	-4.42	3.53	0.84	0.84
KERM	57.119	30.277	26.99	21.68	-0.39	15.76	-0.75	15.43	0.87	0.84
LALE	56.690	29.596	26.43	19.35	-2.14	13.35	-2.52	13.13	1.76	1.71
KATI	56.365	31.413	27.63	16.15	-0.57	10.52	-0.96	10.38	1.70	1.69
GRME	56.264	37.042	24.05	13.93	-5.06	8.31	-5.64	8.20	2.02	2.09
ROBA	56.070	33.369	27.42	14.84	0.02	9.23	-0.42	9.17	0.82	0.81
MAR2	55.956	37.845	21.52	13.49	-7.44	8.07	-8.09	8.02	1.96	2.02
SEND	55.929	31.713	26.00	17.25	-1.98	11.27	-2.39	11.24	1.56	1.55
HAJI	55.918	28.302	20.88	20.81	-5.26	15.06	-5.69	15.04	1.04	0.98
BES2	54.832	29.363	25.84	20.21	-0.09	14.05	-0.54	14.29	0.97	0.93
DEH2	54.700	28.645	25.07	20.25	-0.63	13.89	-1.09	14.15	0.97	0.93
HARA	54.608	30.079	27.79	19.90	0.54	13.56	0.08	13.86	0.86	0.85
LAR2	54.320	27.644	27.72	24.94	2.22	18.42	1.72	18.78	1.00	0.96
TMN2	54.316	29.239	25.23	20.01	-0.64	13.55	-1.11	13.92	0.95	0.92
KORD	54.199	36.860	23.20	11.86	-3.53	5.59	-4.20	5.97	0.84	0.83
KHO2	54.126	29.923	25.50	20.92	-0.59	14.58	-1.07	14.98	0.95	0.92
ARDA	53.822	32.313	26.00	20.33	-1.18	13.78	-1.69	14.26	0.86	0.84
BIG2	53.637	27.852	26.12	22.05	1.35	16.10	0.83	16.62	1.02	1.00
GOT2	53.631	28.624	26.13	23.30	0.19	15.93	-0.32	16.45	1.07	1.04
SEMN	53.564	35.662	26.53	15.44	-0.55	8.67	-1.18	9.22	0.86	0.85
ABAR	53.308	31.123	25.60	20.81	-1.35	13.89	-1.87	14.50	1.46	1.43
SVR2	53.244	29.281	25.36	20.88	-0.28	14.21	-0.80	14.84	0.98	0.94
SAA2	53.146	30.087	26.60	19.89	0.98	12.93	0.46	13.57	1.05	0.98
ISL2	53.066	28.347	25.58	23.29	-0.20	16.36	-0.73	17.02	0.94	0.90
QIR2	53.029	28.477	24.93	22.29	-1.17	15.60	-1.71	16.27	0.90	0.87
MARV	52.752	29.798	26.36	21.97	-0.54	14.93	-1.08	15.66	1.49	1.46
ABAD	52.568	31.228	25.48	21.57	-1.41	14.44	-1.95	15.23	1.44	1.42

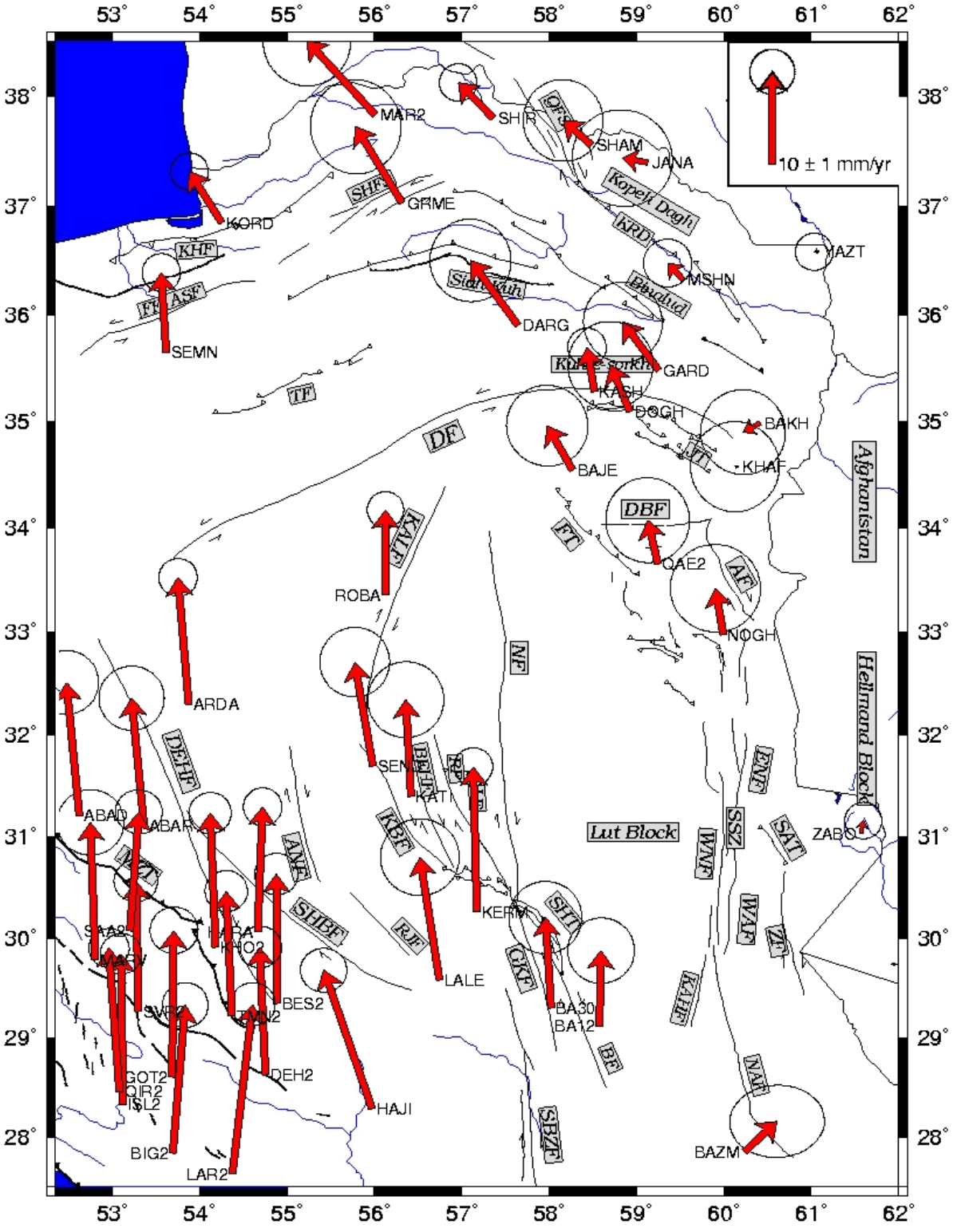

Figure4-13. Velocities of Lut benchmarks relative to Eurasia. The error ellipses indicate formal errors within a 95 per cent confidence interval. The grey lines are the transect TR-AA' and TR-BB'. Fault name abbreviations as in Fig. 4-12.

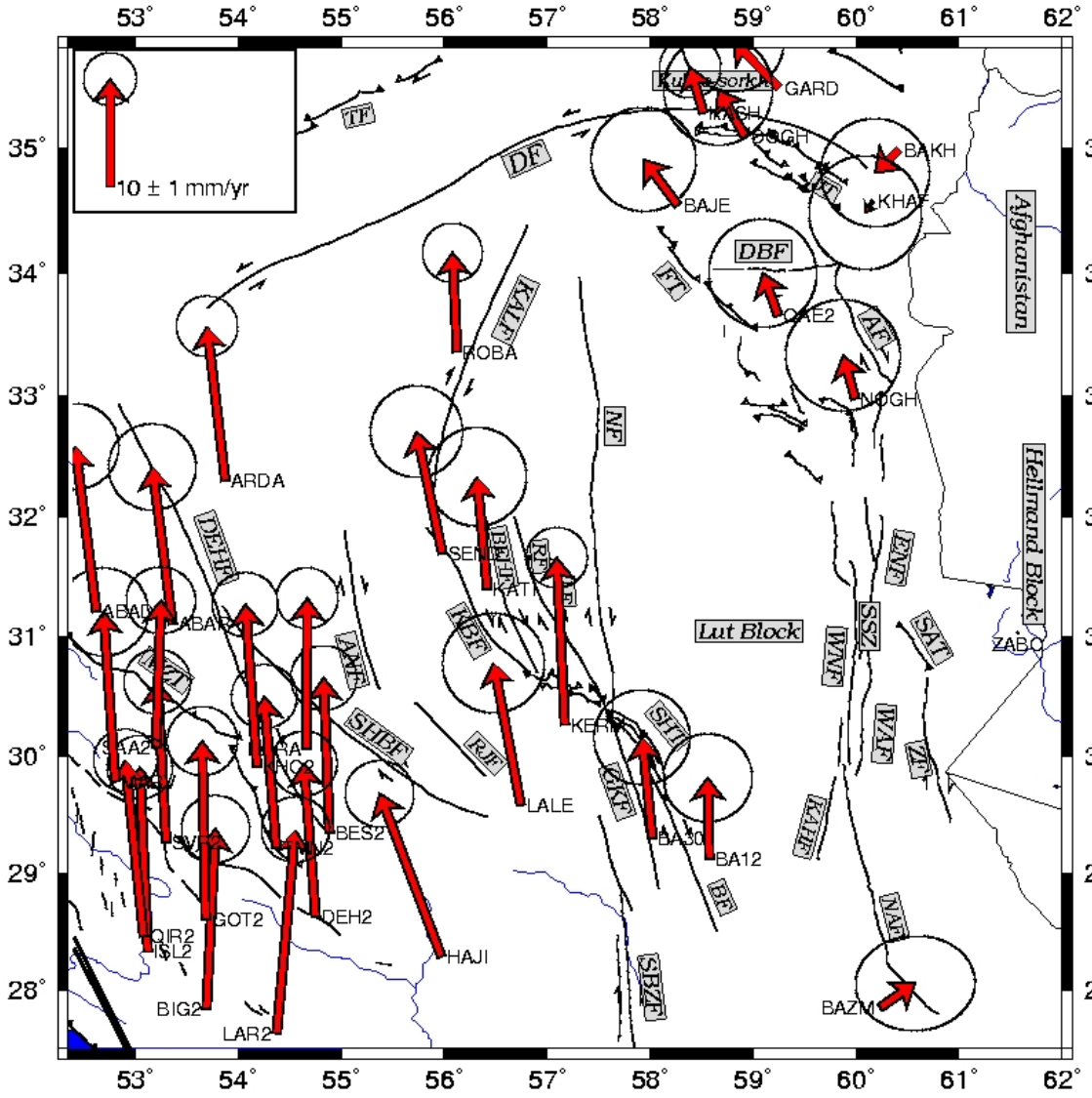

Figure 4-14. Velocities of Lut benchmarks relative to ZABO. ZABO is located on the Hellmand block which is part of Eurasia. The error ellipses indicate formal errors within a 95% confidence interval. Fault name abbreviations as in Fig. 4-12.

Doruneh fault velocities

As described above, the Doruneh fault is a large left-lateral strike-slip fault. Our GPS measurements (Fig. 4-15) enable us to evaluate the present-day strike-slip velocity in several places along the Doruneh fault. At ~58°E we use the difference between the BAJE and DARG which gives a left-lateral strike-slip motion of about 2.5 ± 2.0 mm/yr. Further east, at ~58.5°E, the comparison between GARD and BAJE yields 1.5 ± 2.0 mm/yr of left-lateral strike-slip motion. We observe 1 and 1.5 mm/yr strike-slip between DOGH-GARD and KASH-GARD at ~59°E. Comparing KHAF and GARD velocities at ~59.6°E a slip rate of 1 ± 2 mm/yr can be evaluated. The measurements of DOGH, BAKH and KHAF in 2006 were affected by an offset phase

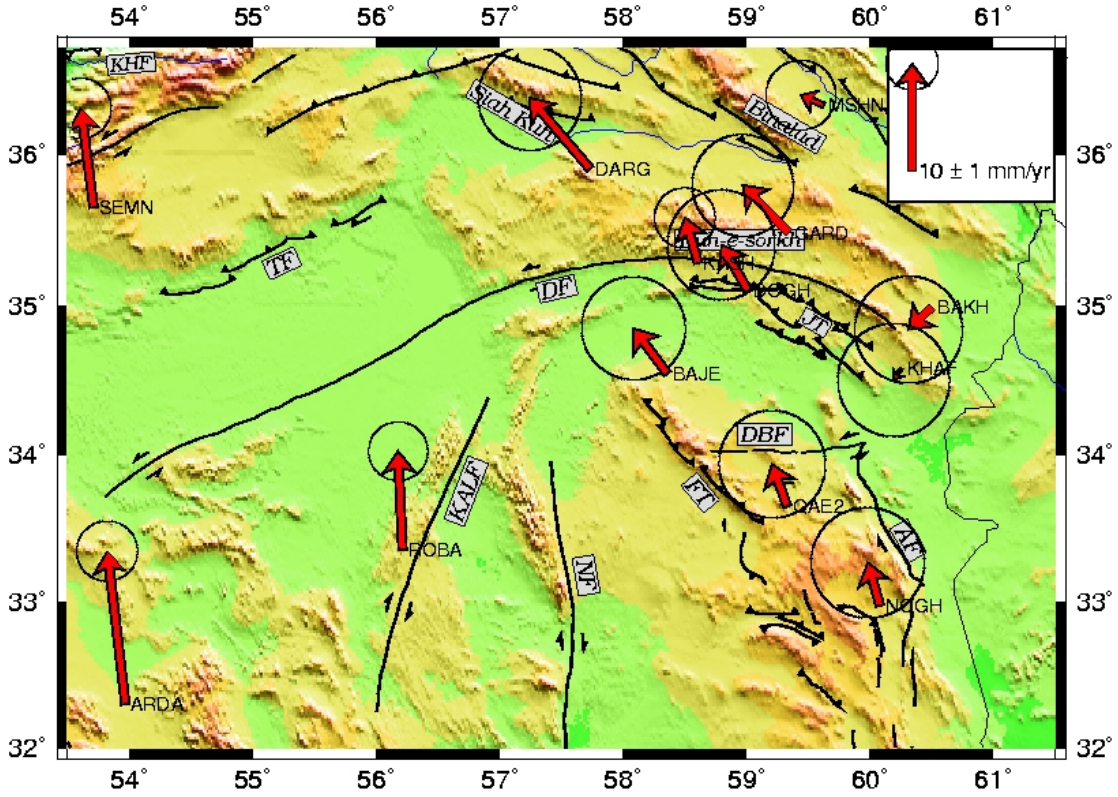

Figure 4-15. Velocities around the Doruneh and Dasht-e-Bayaz faults relative to ZABO. ZABO is located on the Hellmand block which is part of Eurasia. The error ellipses indicate formal errors within a 95 per cent confidence interval. AF: Abiz Fault, FT: Ferdows Thrust, DF: Doruneh Fault, DBF: Dasht-e-Bayaz Fault, JT: Jangal Thrust, Fault, KALF: Kalmard Fault, LF: Lakarkuh Fault, NF: Nayband Fault, TF: Torud Fault.

center of the antenna used at all three sites. While the calibration of the antenna is ongoing, we corrected the phase center offset using the assumption that the DOGH velocity should be similar to that at station BAJE. This certainly decreases the precision of these three measurements with respect to the rest of the network, but allows us to start a preliminary interpretation of the data until the results of the antenna calibration are available. At the eastern termination of the Doruneh fault, between KHAF and BAKH (~60.2°E), we observe 1 ± 2 mm/yr of transpressive displacement (strike-slip and shortening).

Therefore, the velocity on the Doruneh fault decreases from its central part (long~58°, 2.5±2 mm/yr) to its eastern termination (long ~60.2°, 1±2mm/yr). This means that our measurements provide the first evidence for a spatial strike-slip velocity variation along the Doruneh fault. Some shortening also occurs towards the eastern end of the fault. A significant shortening is evaluated, however, between

QAE2 and KHAF, south of the eastern end of the Doruneh fault (5 ± 2 mm/yr of shortening). It seems that this shortening can be attributed to the Jangal thrust located south of the Doruneh fault.

In the western part of the Doruneh fault, we do not have enough stations to evaluate precisely the velocity but we can use SEMN, ARDA and ROBA which are more than 350 km apart for a rough estimate (Fig. 4-15). Between ARDA and SEMN, we measure 5±2 mm/yr of shortening and 0.5±2 mm/yr of right-lateral motion. With SEMN and ROBA we measure only about 1± 2 mm/yr left-lateral displacement and no shortening. The baselines between ARDA and SEMN and ROBA and SEMN are about 350 km long and cross not only the Doruneh fault, but also the Torud thrust fault. The ROBA-SEMN baseline shows that the Torud thrust fault is not very active today. Therefore, the 5 mm/yr of shortening on the ARDA-SEMN baseline could be absorbed by distributed deformation in a zone around ARDA. The right-lateral motion measured on these baselines is not significant. Our GPS measurements show first details about the Doruneh slip rate, in particular in the eastern part of the fault where we found evidence for slip rate variations along the fault. However, these results are at the limit of resolution, due to still limited precision of the GPS velocities and the sparse network along the fault. A dedicated network around the Doruneh fault would permit to characterize the slip and the slip variations on the Doruneh fault more precisely.

Dasht-e-Bayaz velocities

The EW trending Dasht-e-Bayaz fault runs parallel to the Doruneh fault, about 100 km further south. It presents a left-lateral strike-slip activity, as attested by recent earthquake mechanisms. This fault has the same orientation and mechanism as the Doruneh fault but is shorter (120 km). To evaluate the motion on this fault, we used the differential velocities between QAE2, BAJE and KHAF yielding a left-lateral slip rate of 1.5 ± 2 mm/yr. This result is still coherent with Berberian and Yeats (1999) who found that the Dasht-e-Bayaz fault may experience a slip rate greater than 2.5 mm/yr (based on qanats offset).

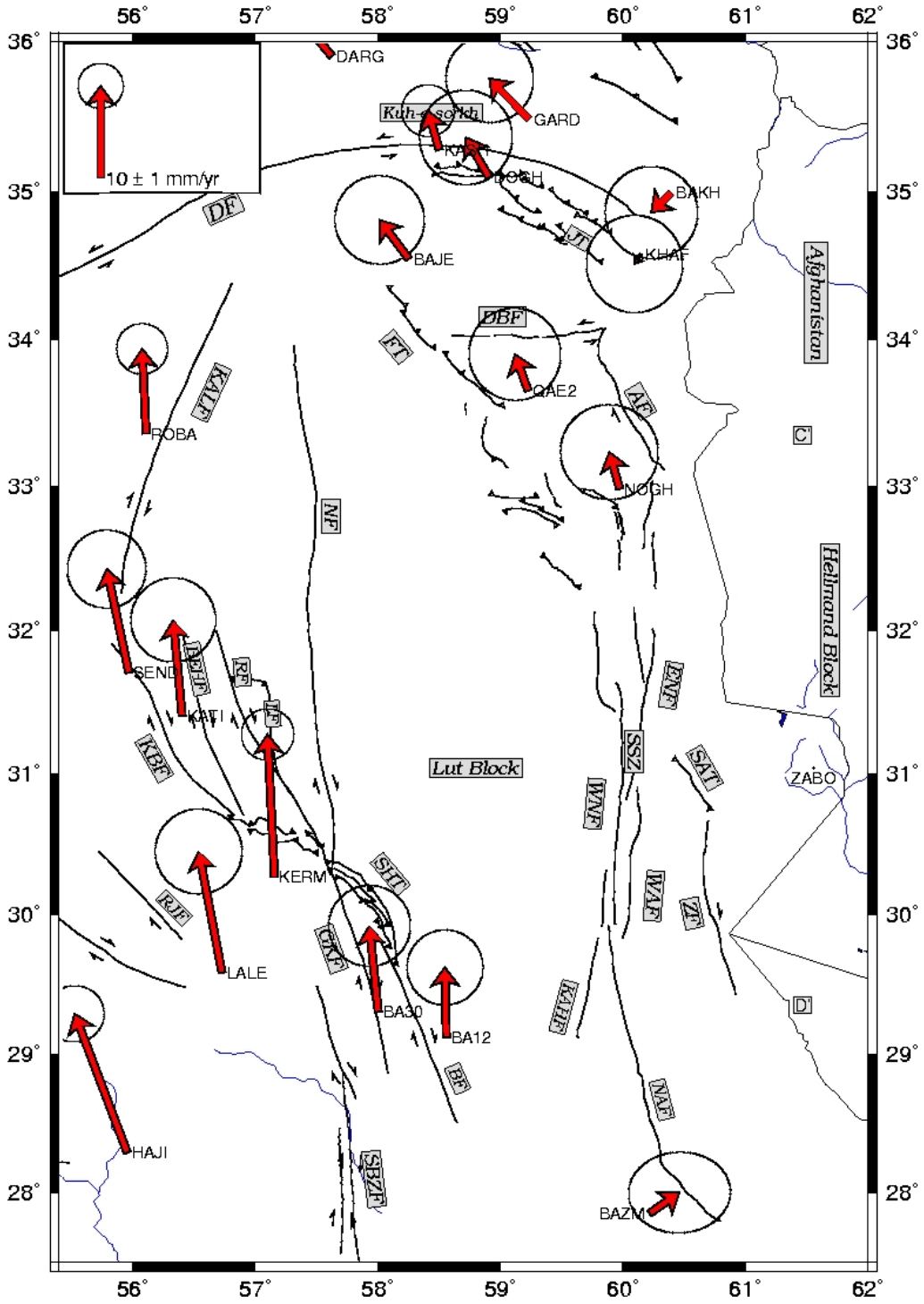

Figure 4-16 . Velocities of Lut benchmarks relative to ZABO. ZABO is located on the Hellmand block which is part of Eurasia. The error ellipses indicate formal errors within a 95% confidence interval. Fault name abbreviations as in Fig. 4-13.

Sistan fault zone velocities

Individual fault velocities can also be established for some faults of the Sistan fault system located at the eastern limit of the Lut block (4-16). Considering the differential velocities between NOGH and ZABO, we evaluate 4 ± 2 mm/yr of dextral strike-slip concentrated on the Abiz and East Neh faults. The differential velocity between NOGH and KHAF yields 5 ± 2mm/yr of shortening accommodated on the southern part of the Jangal thrust and distributed north of the Dasht-e-Bayaz fault. Comparing BA12 and ZABO we estimate a total right-lateral displacement of 7.5 ± 2 mm/yr across this southern part of the Sistan fault system. WITH BA12 and NOGH we estimate 3.5 mm/yr for Ferdows Thrust.

West Lut velocities

To the west of the Lut, we estimate the present-day velocities for the NS trending right-lateral strike-slip Kuhbanan, Nayband, Gowk and Bam fault systems (Fig. 4-17).

Gowk and Bam faults:

Considering KERM and BA12, we obtain 8 ± 2 mm/yr of strike-slip motion and 1 ± 2 mm/yr of extension. As BA12 is situated east of the Bam fault, this cumulative velocity can be attributed to the two faults (Gowk and Bam) situated between KERM and BA12. The stations LALE and BA12 span the same faults, eventually including the northern extension of the Sabzevaran fault. The velocity differences between LALE and BA12 evaluate 6 ± 2 mm/yr of right-lateral velocity cumulated over the Sabzevaran, Gowk and Bam faults. The difference between the two results is at the limit of the measurement uncertainties. However, LALE and KERM are supposed to be situated on the same rigid block, in particular, there is no tectonical evidence for extension between LALE and KERM. The regional strain field is ~NS shortening imposed by the Arabia-Eurasia collision. Therefore, there is no reason for measuring a higher strike-slip velocity on a more northerly cross section of the Gowk and Bam faults than in the south. While LALE is a bedrock forced centering site and measured 3 times in almost 3 years, KERM is a pillar on bedrock in the city of Kerman and measured at least 6 times since 1999. To explain the velocity difference between LALE and KERM, we suggest that the KERM measurements have been affected by

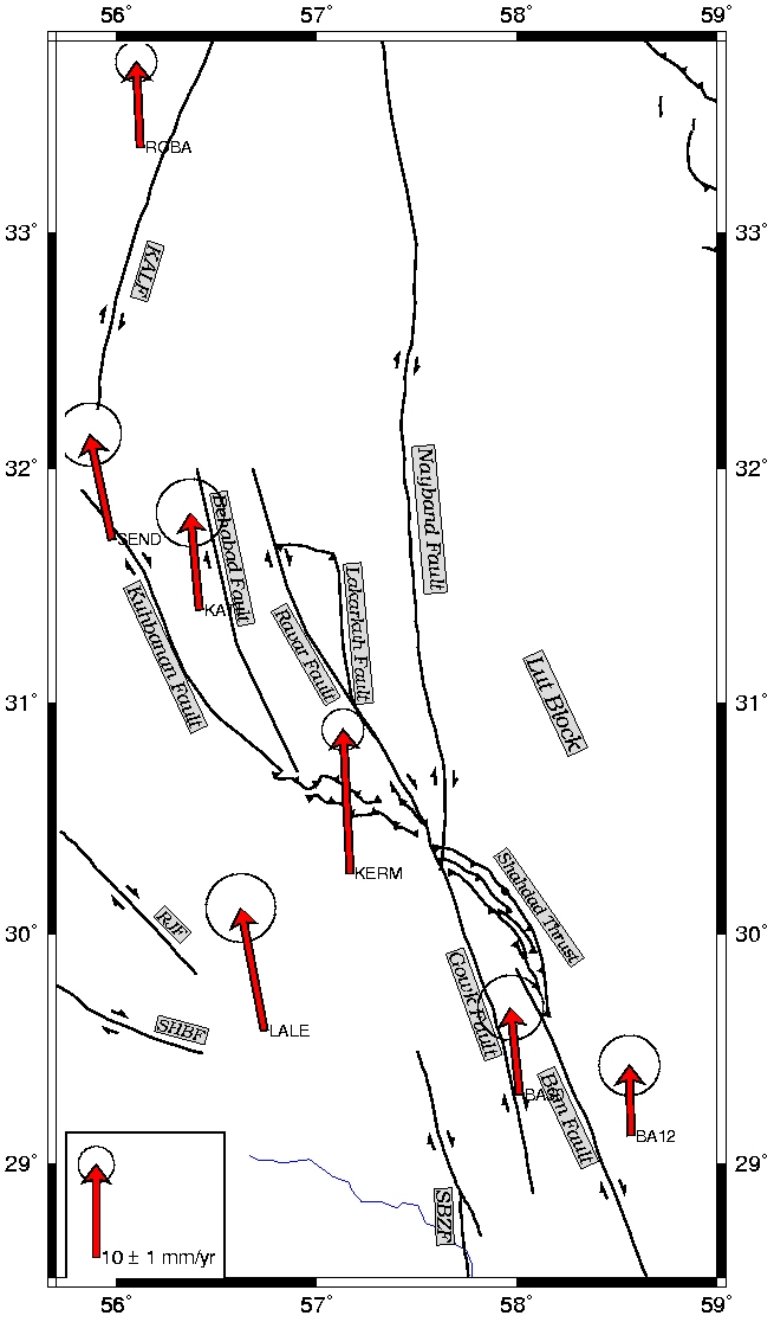

Figure 4-17. Velocity field west of Lut relative to ZABO. ZABO is located on Hellmand block which is part of Eurasia. The error ellipses indicate formal errors within a 95% confidence interval. SBZF: Sabzevaran Fault, SHBF: Shahr Babak Fault, RJF: Rafsanjan Fault.

local factors such as rapid underground water table variations. Therefore we prefer considering the result of LALE to characterize the tectonical unit west of the Gowk fault. As BA12 was measured shortly after the Bam 2003 earthquake, post-seismic motion may affect the BA12 velocity measurements. According to the location of the earthquake and its mechanism, the BA12 velocity could be under-estimated if it

suffered any post-seismic motion. This implies a possibility that the cumulated Gowk-Bam fault velocities mentioned above are over-estimated.

We included in our analysis one of the most stable stations of the Bam post-seismic network, the site BA30, situated west of the Bam fault and east of the Gowk fault. Using BA30, BA12 and LALE, we can evaluate a distinct displacement rate of 2 mm/yr for the Bam fault and 4 mm/yr of cumulative strike-slip rate for the Sabzevaran and Gowk faults.

The Kuhbanan fault is monitored by SEND, KATI, and KERM. Comparing SEND and KATI close to the fault, we obtain 1.5 ± 2 mm/yr of right-lateral strike-slip and a smaller reverse component (~1 mm/yr) in the northern part of the fault. Differential velocities between KATI and KERM at ~150 km to the south show a total of 5.5 ± 2 mm/yr transpressive right-lateral motion on the southern part of the Kuhbanan fault. However, since KERM seems to be affected by local phenomena, we prefer considering LALE instead of KERM, although LALE is still further away from the Kuhbanan fault (~200 km to the south). With respect to this station we obtain with KATI only 3 ± 2 mm/yr of transpressive right-lateral strike-slip motion on the south Kuhbanan fault.

While measurements on intermediate stations differencing between the different fault motions in the Nayband fault system still need to be acquired, the velocity of KATI can be compared with site velocities on the Lut block and used to quantify the cumulated fault slip rates of the Nayband fault system faults east of KATI. Toward the northeast, the next sites are QAE2 and BAJE. The differential velocities evaluate about 7±2 mm/yr of total right-lateral strike-slip cumulated over the Behabad, Ravar, Lakarkuh and Nayband faults, including also the Ferdows thrust faults in the north of the Lut block. Toward the southeast, the next station on the Lut block is the BA12 station east of Bam. Between KATI and BA12, we estimate 3±2 mm/yr of cumulative right-lateral motions on Nayband, Lakarkuh, Behabad and Ravar faults between which stations KATI and BA12. Using the differential velocity between ROBA and BA12 (Figs. 4-16 and 4-17), we estimate 1.5±2 mm/yr of cumulative motion on the Kalmard fault and the Nayband fault at a latitude where the western splays of the Nayband fault have already faded out.

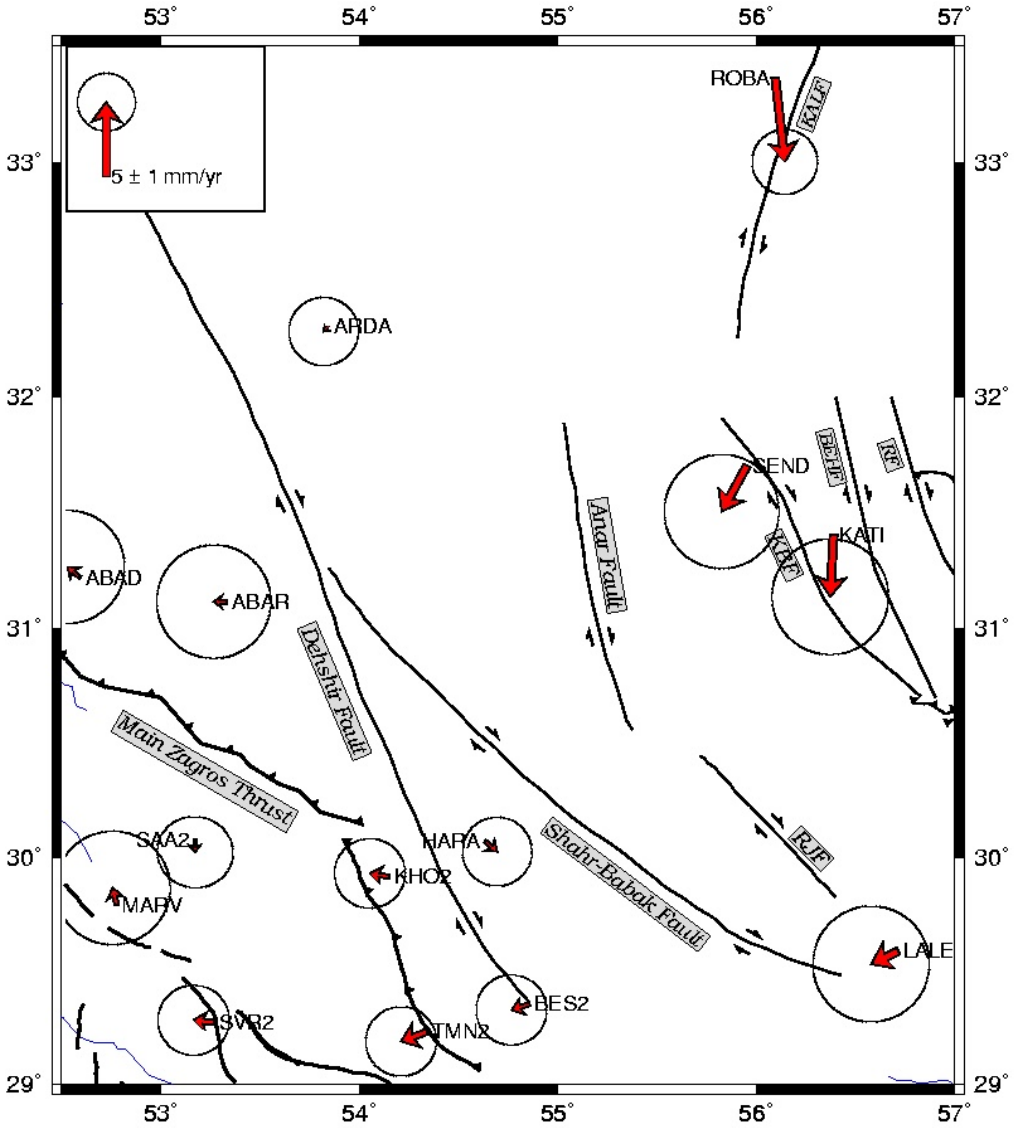

Figure 4-18. Velocities around the Dehsir and Anar faults relative to the Central Iran block (CIB). The error ellipses indicate formal errors within a 95% confidence interval. BEHF: Behabad Fault, KALF: Kalmard Fault, RF: Ravar Fault, RJF: Rafsanjan Fault.

Dehshir and Anar fault velocities

In order to get a better estimate of the displacement rates on the Dehshir and Anar faults, we transformed the velocities into the Central Iran block reference frame (Fig. 4-18, Table 4-8). By comparison of the HARA and KHO2 north velocity components, we estimate a minimum of 1.5±2 mm/yr of right-lateral motion on the southern segment of the Dehshir fault. The differential velocities between ARDA, ABAD and ABAR show again 1±2 mm/yr on the northern segments of this fault. Our GPS stations LALE and HARA around the Shahr Babak fault show that this fault is probably not active.

Table 4-8. Velocities (mm/yr) for stations around the Dehshir, Anar and Shahr Babak faults relative to CIB. Ve and Vn are east and north velocity components. δe and δn are east and north uncertainties of velocity components, respectively, in mm/yr.

SITE	LONG.	LAT.	Ve	Vn	δe	δn
KERM	57.119	30.277	-0.51	1.32	1.19	1.16
LALE	56.690	29.596	-1.81	-0.88	2.01	2.00
KATI	56.365	31.413	-0.23	-4.16	2.01	2.00
ROBA	56.070	33.369	0.65	-5.66	1.13	1.12
MAR2	55.956	37.845	-4.82	-6.78	2.09	2.09
SEND	55.929	31.713	-1.71	-3.10	1.98	1.97
HAJI	55.918	28.302	-6.53	0.32	1.36	1.30
BES2	54.832	29.363	-1.21	-0.42	1.22	1.21
DEH2	54.700	28.645	-2.08	-0.37	1.22	1.21
HARA	54.608	30.079	0.82	-0.71	1.20	1.19
LAR2	54.320	27.644	0.47	4.32	1.24	1.22
TMN2	54.316	29.239	-1.74	-0.65	1.22	1.20
KHO2	54.126	29.923	-1.31	0.22	1.22	1.20
ARDA	53.822	32.313	-0.36	-0.38	1.20	1.18
BIG2	53.637	27.852	-0.97	1.38	1.27	1.25
GOT2	53.631	28.624	-0.83	2.61	1.36	1.31
ABAR	53.308	31.123	-0.89	0.01	1.97	1.96
SVR2	53.244	29.281	-1.39	0.14	1.23	1.21
SAA2	53.146	30.087	0.01	-0.87	1.31	1.23
ISL2	53.066	28.347	-1.31	2.58	1.21	1.20
QIR2	53.029	28.477	-1.92	1.57	1.20	1.19
MARV	52.752	29.798	-0.27	1.15	1.98	1.96
ABAD	52.568	31.228	-0.83	0.72	1.96	1.95

The stations surrounding the Anar fault (SEND-ARDA and ABAR) are about 350 km apart from each other. With these stations we evaluate 3-4 mm/yr of right-lateral motion, but it seems that part of this rate could be distributed deformation in the region between the stations.

4.6 Velocity projection on transects

To study in detail the displacement rates in the Lut region we plotted two series of EW and NS transects (Figs. 4-19 and 4-20).

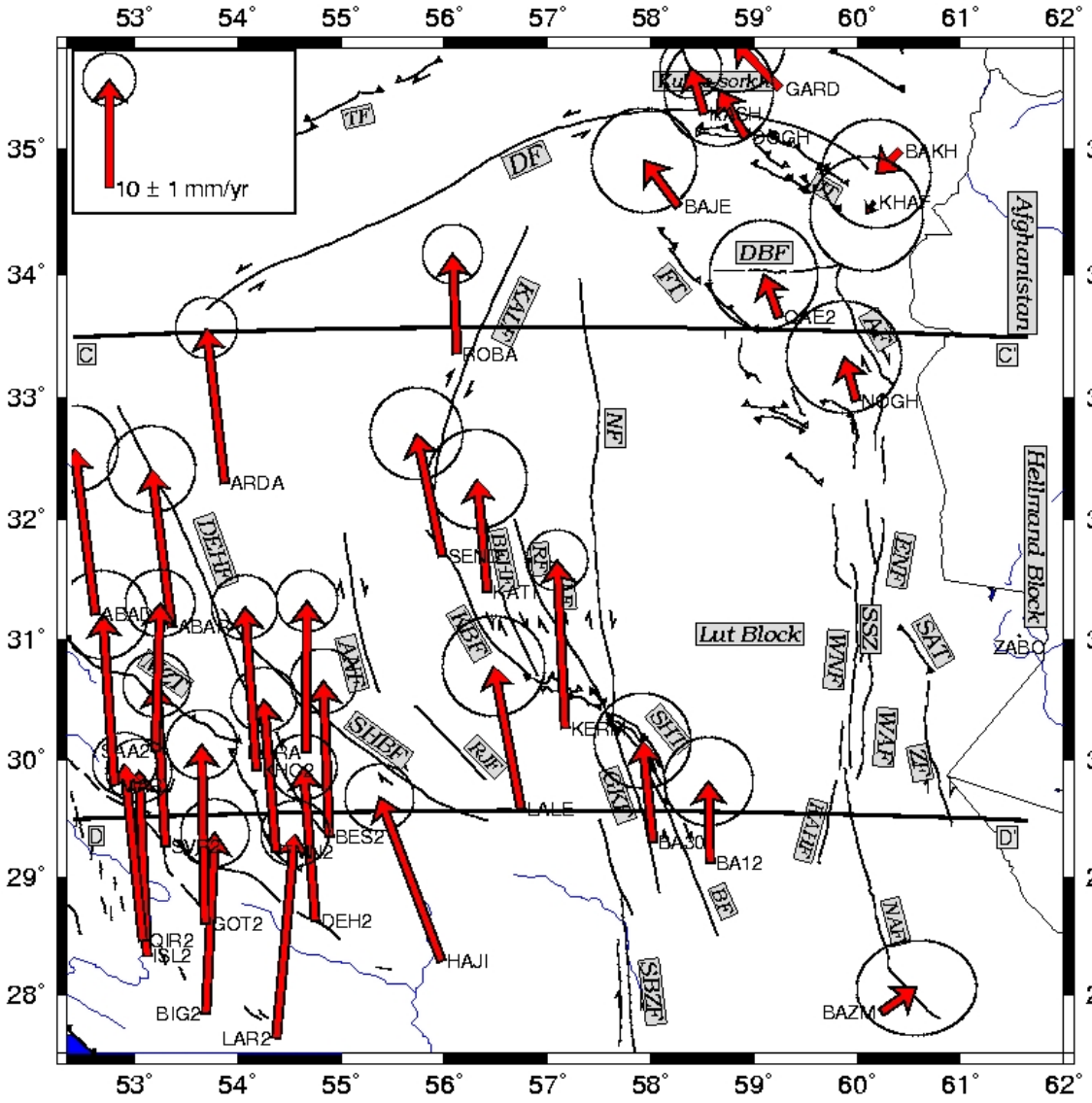

Fig. 4-19. Velocities of Lut benchmarks relative to ZABO. ZABO is located on the Hellmand block which is part of Eurasia. The error ellipses indicate formal errors within a 95% confidence interval. Fault name abbreviations as in Fig. 4-13. The locations of EW transects TR-CC' and TR-DD' are indicated.

a) East-West transects:

The two EW transects (Fig. 4-19) are situated at the latitudes 33.5°N (TR-CC') and 29.5°N (TR-DD') with a length of about 350 km. We present the north and east velocity components of the sites located close to these transects with respect to longitude (Fig. 4-20 and 4-21).

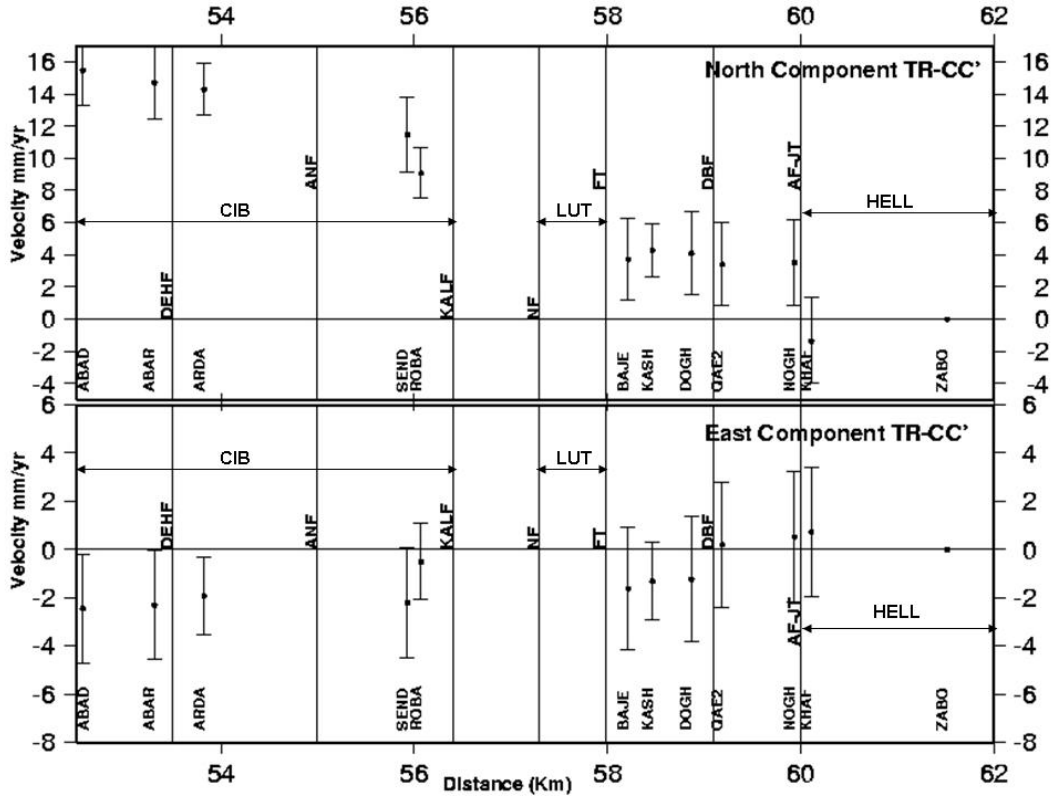

Figure 4-20. North and east motion (mm/yr) as function of the longitude (DEG) along the transect TR-CC'. The transect TR-CC' is EW oriented and passes at 33.5°N (Fig. 4-15). CIB: Central Iran Block; HELL: Hellmand Block and LUT: Lut block.

On the transect TR-CC' (Fig. 4-20), the north velocity decreases of about 15±2 mm/yr from west (52.5°E) to east (61.5°E), while the east velocities vary only slightly from -2 to 1 mm/yr from west to east, before fading out on the Hellmand block. The western sites ARDA, ABAD, ABAR, SEND and ROBA are on the Central Iran Block (Sanandaj-Sirjan Zone) which is roughly rigid (within ±2 mm/yr, Vernant et al., 2004; Masson et al., 2007; Walpersdorf et al., 2007). There is no notable change in velocities across the Dehshir fault (a comparison of ABAR and ABAD with ARDA gives not more than 1±2 mm/yr of NS right-lateral strike-slip rate on the northern part of the fault. However, considering the difference between ARDA on one hand, and ROBA and SEND on the other hand, we estimate 4.5±2 mm/yr of differential NS motion. The differential motion is slightly higher with respect to ROBA than with respect to SEND, although there is no fault localized between ARDA and ROBA, but the Anar fault between ARDA and SEND (which is fading out rapidly toward the north). We therefore suggest that this motion is related to a significant amount of distributed deformation between the stations in the east of the CIB.

To the east, the CIB is delimited by the Kalmard and Nayband faults before reaching the Lut block. The first stations on this transect situated on the Lut block are also east of the Ferdows thrust cutting through the NE part of the Lut block. The NS velocities at BAJE, KASH, DOGH, QAE2 and NOGH are almost the same and evaluate a total NS displacement rate of 6±2 mm/yr with respect to SEND and ROBA. This displacement rate is cumulated over the Kalmard and Nayband faults and the Ferdows thrust. The EW velocities show no significant change across the limit between the CIB and the Lut block, when regarding the western Lut sites BAJE, KASH and DOGH. An increase of east velocity can be noted, however, between these stations and QAE2 and NOGH, situated south of the Dasht-e-Bayaz fault. This differential velocity of 2 mm/yr is coherent with left-lateral strike-slip motion on the EW oriented Dasht-e-Bayaz fault. The absence of NS velocity changes across this fault shows that the fault motion is purely strike-slip without any shortening component.

We find 4±2 mm/yr of differential NS motion across the Abiz fault and the Jangal thrust by comparing the velocities of QAE2 and NOGH with KHAF and ZABO on the Hellmand block. This motion is coherent with right-lateral displacement on the NS oriented Abiz fault and with active shortening on the WNW-ESE oriented Jangal thrust. There is no related EW motion between QAE2, NOGH and KHAF, but KHAF shows a slight (1 mm/yr) residual motion with respect to ZABO although there is no tectonic feature anymore between KHAF and the Hellmand block. If this residual motion is not due to measurement uncertainties, it could be an indication for distributed deformation at the western limit of the Hellmand block.

On the transect TR-DD' situated south of TR-CC' (Fig. 4-19), the north velocity (Fig. 4-20) shows a total shear of 14±2 mm/yr between the Central Iran block and the Hellmand block. The EW component shows an east-west increase of up to 3±2 mm/yr of the westward motion. On the Central Iran block, the NS and EW velocities do not vary more than 2 mm/yr between SAA2, KHO2, TMN2, BES2, SEND and LALE which confirms the rigidity of the Central Iran block at this level. Two exceptions are KERM where we have some doubts about the quality of the measurement site, and HARA, with about 2 mm/yr of residual eastward velocity with respect to CIB sites. This east velocity would yield a slight right-lateral displacement on the Dehshir fault comparing HARA with BES2, TMN2, and KHO2, but a slight left-lateral motion on the Shahr Babak fault comparing HARA with LALE, SEND and

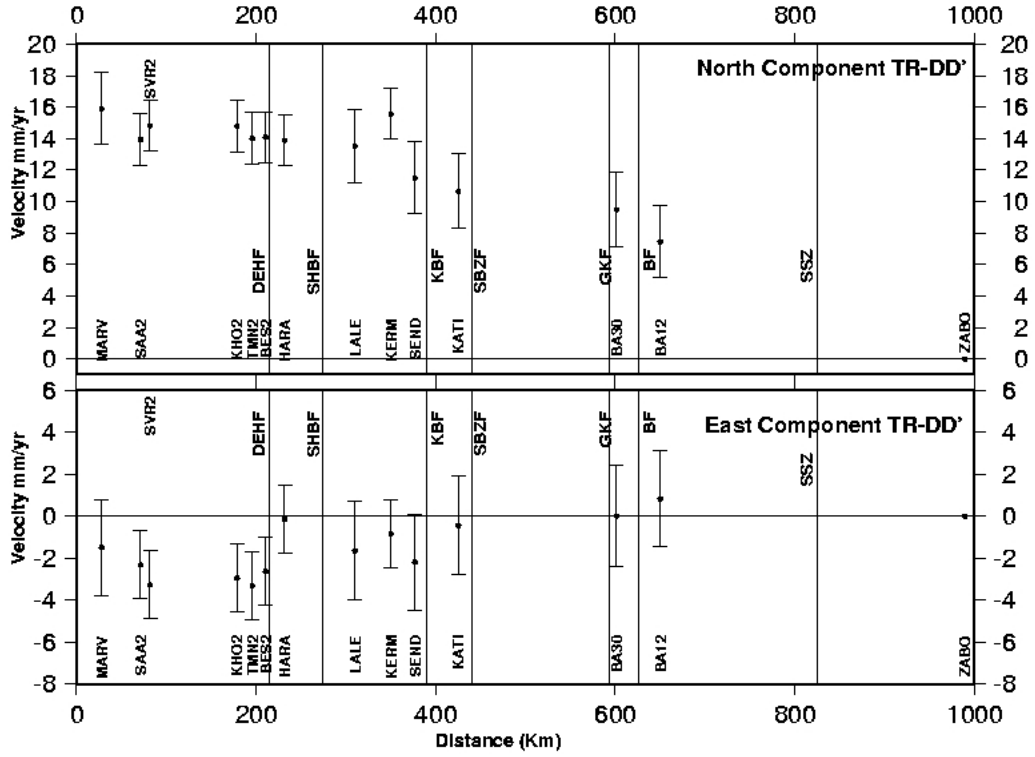

Figure 4-21. North and east motion (mm/yr) projected on transect TR-DD'. The transect TR-DD' is EW oriented and passes at the latitude 29.5°N (Fig. 4-19. The faults are represented with respect to the longitude of their intersection with the transect, but for more clarity, the stations are localized with respect to their relative position to the fault, not with respect to their longitude.

KERM. This is in contradiction with the Shahr Babak fault slip mechanism which is right-lateral. The north component of HARA is more consistent and yields no motion with respect to CIB, and a slight northward motion with respect to SEND and LALE, which could be accommodated by right-lateral motion on the Shahr Babak fault or by the distributed deformation already evidenced in this region.

We estimate 1±2 to 5.5±2 mm/yr of NS displacement and up to 1.5 mm/yr of EW displacement across the Kuhbanan fault comparing SEND, LALE and KERM with KATI. This corresponds to right-lateral motion in the north and an increasingly transpressive motion in the south of the Kuhbanan fault. Due to the obliqueness of the faults, KERM, LALE and SEND are in fact all situated to the west of KB, but at different latitudes. For this reason we have reorganized the distribution of sites on the transect and present them in Fig. 4.21 according to their relative location with respect to the faults (east or west of the faults). When respecting this geometry, comparing

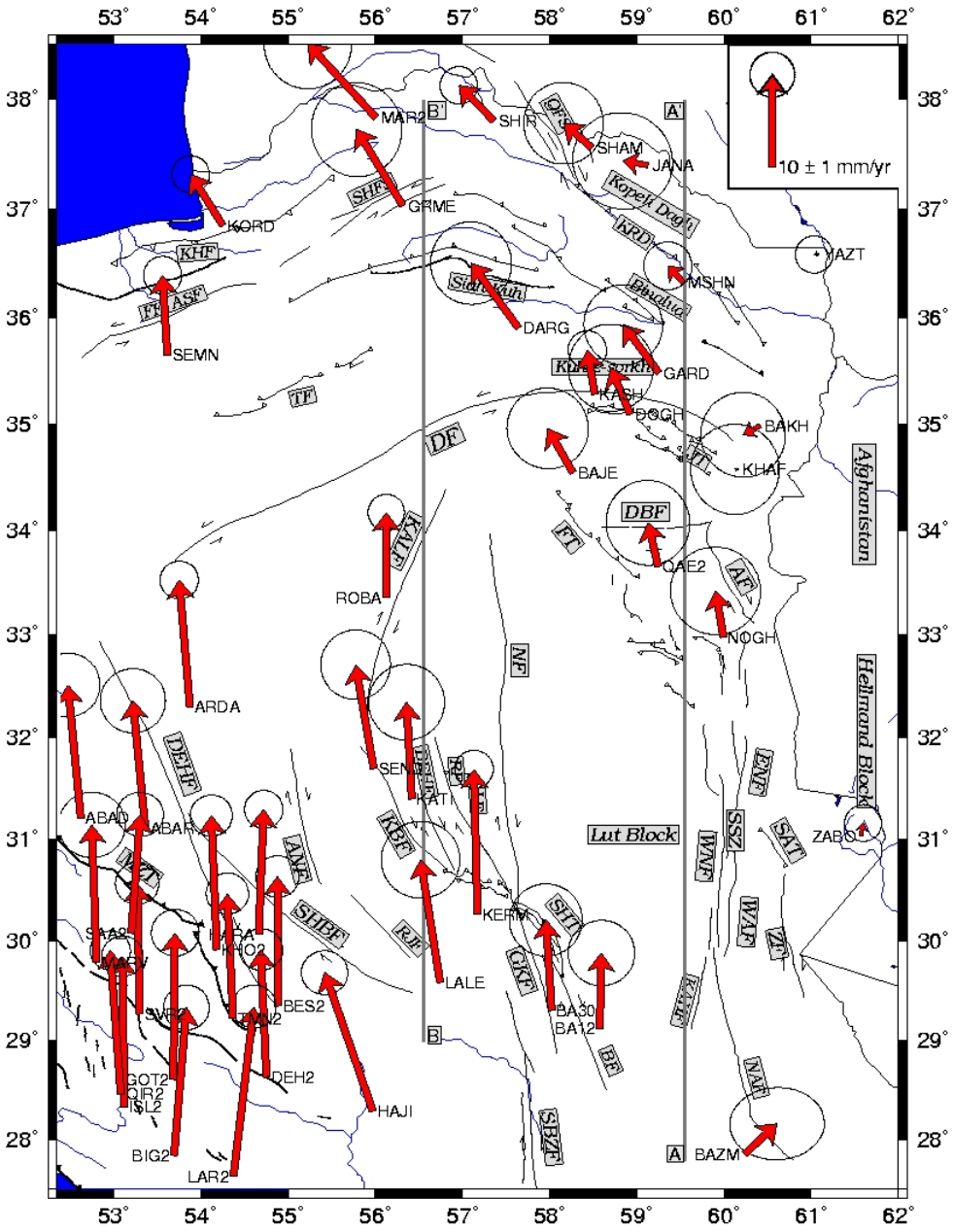

Figure 4-22. Velocities of Lut benchmarks relative to ZABO. ZABO is located on the Hellmand block which is part of Eurasia. The error ellipses indicate formal errors within a 95% confidence interval. Fault name abbreviations as in Fig. 4-13. The locations of NS transects TR-AA' (Fig. 4-23) and TR-BB' (Fig. 4-24) are indicated.

KERM, LALE and KATI, we observe 4±2 mm/yr of right-lateral transpressive motion. The comparison of SEND, LALE and KERM with BA30 yields 4±2 mm/yr of cumulative displacement rate for the Gowk and Sabzevaran faults. Further east, we have only one station per block (BA30 for the block between Gowk and Bam fault, BA12 for the Lut block and ZABO for the Hellmand block). The representation of these site velocities on the EW transect shows their consistency with respect to the

other measurements, but does not help increasing the precision of fault slip measurements as no velocities can be averaged. So, the Bam fault and Sistan Suture zone slip rates are evaluated by single stations to the values of 2±2 mm/yr NS slip for the Bam fault and about 7.5±2 mm/yr of NS slip across the Sistan suture zone, as indicated earlier.

On both EW transects CC' and DD' we see a lack of eastward displacement with respect to the ZABO station on the Hellmand block. The relative velocities have even a westward component on transect DD'. This gives evidence for the fact that the accommodation of the Arabia-Eurasia collision in central Iran is not related to an eastward expulsion of the CIB.

b) North-South transects:

We selected two NS trending transects: TR-AA' and TR-BB' located at 59.5°E and 56.5°E (Fig. 4-22). We present the north and east component of the site velocities along these two transects (Fig. 4-23 and Fig. 4-24).

On transect AA' very little variation is observed on both the NS and EW velocities, due to fading velocities in proximity of the stable Hellmand block. However, the variations are higher on the NS component than on the EW component. On the NS component, we can see motions due to shortening across EW oriented thrust faults and lateral motion across NS oriented strike-slip faults. These mechanisms seem to prevail at this longitude over strike-slip motion on east-west trending faults like the Doruneh and the Dasht-e-Bayaz faults.

On the transect TR-BB' further to the west, we observe a total NS shortening of ~8 mm/yr. Linear fits between the stations north and south of the Doruneh fault show that, at this longitude, most of the shortening is absorbed south of the Doruneh fault (5.7 mm/yr), while further north, the east component shows a cumulative far-field left-lateral motion of 3.8 mm/yr on the EW trending Doruneh and Dasht-e-Bayaz faults, averaging the velocities to the north and to the south of these faults. This is coherent with our observations on the stations close to the faults which evaluated the Doruneh slip rate to 2.5 mm/yr and the Dasht-e-Bayaz slip rate to 1.5 mm/yr

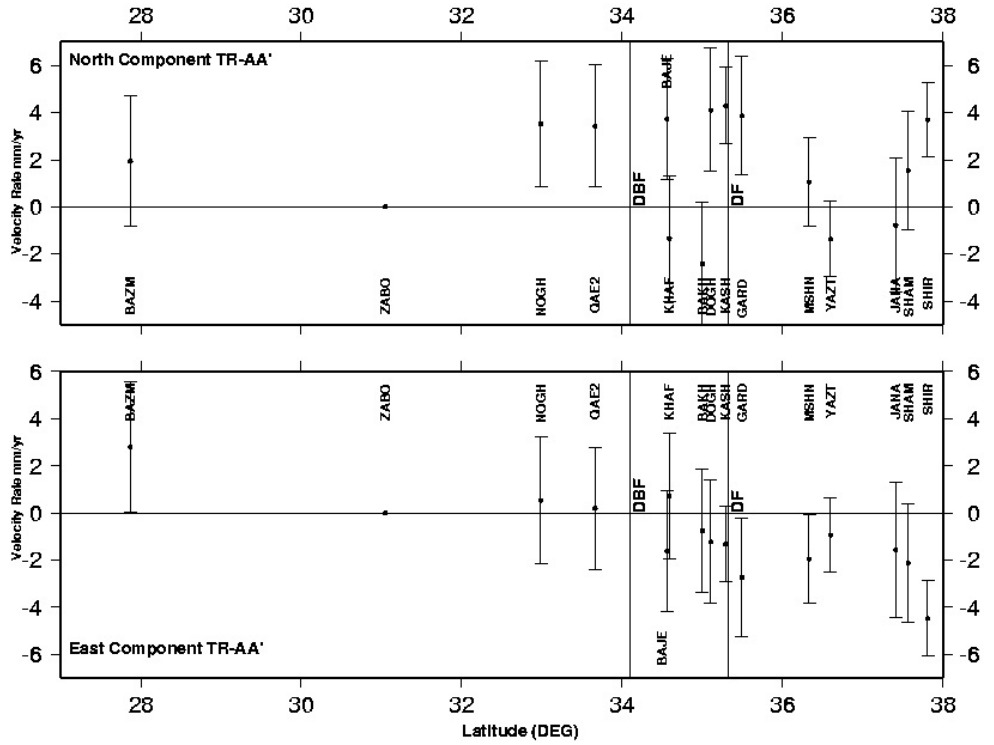

Figure 4-23. North and east velocities (mm/yr) function of the longitude (DEG) projected on transect TR-AA'. The transect TR-AA' is NS oriented and passes at longitude 59.5°E (Fig. 4-22).

.

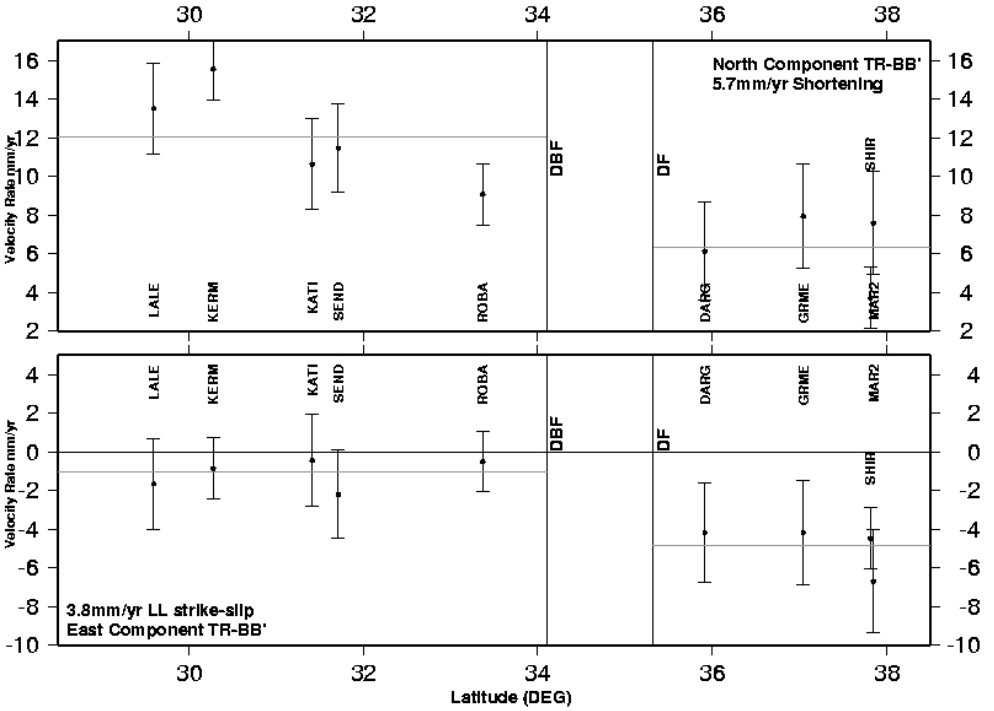

Figure 4-24. North and east velocities (mm/yr) function of the longitude (DEG) projected on transect TR-BB'. The transect TR-BB' is NS trending at the longitude 56.5°E (Fig. 4-22).

4.7 Discussion

As mentioned before, the Lut block is bounded to the north by the Doruneh and Dasht-e-Bayaz left-lateral strike-slip faults and to the east and the west by two NS trending right-lateral strike-slip fault zones. To the east, the Sistan suture zone separates the Lut block and the Hellmand block and to the west a series of N and NNW striking faults (Gowk, Bam, Nayband and Kuhbanan) separates the Lut block from the Central Iran block.

In order to estimate the kinematics of the Lut block, we measured a regional GPS network. The analysis of the GPS data shows that part of the Arabia-Eurasia plate convergence is accommodated in the Lut region by shear along the major NS and NNW trending faults at its eastern and western boundaries. In a Eurasia fixed reference frame, the direction of the residual velocities across the Lut block is predominantly trending NS and decreases of about 14±2 mm/yr from west to east. This is consistent with the result of Vernant et al. (2004). In the following section, we examine in greater details the kinematics of each fault and its role in the accommodation of shear between the Central Iran block and the Hellmand block.

4.7.1. The Dehshir and Anar faults

Only a few historical and instrumental earthquakes (Ambraseys and Melville, 1982; Jackson and McKenzie, 1984) have been located in the Central Iran block. Vernant et al. (2004) reported velocity residuals within the block smaller than 2 mm/yr for the stations ARDA, BIJA, MIAN, HARA and SHAH located in the Sanandaj-Sirjan zone. This suggests that this block is rigid. However, with the Dehshir, Anar and Shahr Babak faults some major faults are crossing this rigid block. Walker and Jackson (2004) propose that these faults are active and accommodate part of the shortening related to the Arabia-Eurasia plate convergence. They suggest that the Dehshir fault is an old structure as old as ~12 Ma and has little to do with the accommodation of the shear between Central Iran and eastern Lut (Hellmand block) as, according to their studies, much of the deformation in the Lut region is concentrated on the Sistan suture zone further east. Meyer et al. (2005) propose that the Dehshir fault is active with a slip rate of 2 mm/yr and a total displacement of 65±15 km which probably started between 25 and 40 Ma ago, and is much older than

the suggestion of Walker and Jackson (2004). On the Anar fault, Walker and Jackson (2004) propose a ~25 km total offset from offsets of geological markers in the southern part of the fault, and Meyer et al. (2007) 10 km offsets of geological markers cumulated over several fault splays in the northern part of the faults. Meyer et al. (2007) also propose Holocene ages for geomorphological marker offsets and obtain recent fault velocities (over 12 ka) of 0.5 to 0.75 mm/yr on the Anar fault.

Our GPS network is not designed to study the kinematics of the Central Iran faults but with the help of different Central Zagros, Kazerun, Iran Global and Kerman regional networks we try to estimate the present-day deformation accommodated by the Dehshir and Anar faults. The sites around the Dehshir and Anar faults suggest that these faults move right-laterally with a velocity of 1±2 mm/yr and 2±2 mm/yr, respectively. For the determination of the Anar motion, we used the velocity at SEND and HARA which are about 350 km apart and span both the Shahr Babak and the Anar faults with similar orientations and the same right-lateral strike-slip mechanism. Therefore it is difficult to say that all of the 2 mm/yr motion is absorbed only by the Anar fault. However, on another 350 km EW baseline passing just north of the northern termination of the Anar fault (the ARDA-ROBA baseline) we observe 5 mm/yr of right-lateral NS shear without crossing any tectonical structure. This provides evidence for high present-day tectonic activity with the same mechanism and in a zone close to the Anar fault. The Anar fault could be connected to the Rafsanjan fault in the south which itself could be related to the Sabzevaran fault further south. Bayer et al. (2006) estimate motion of 3±2.5mm/yr for the Sabzevaran fault.. There is some evidence that the Rafsanjan fault transfers the tectonic strain from the Sabzevaran fault to the Anar fault. As the Anar fault does not connect to any fault in the north, it accommodates the motion by an anticlockwise rotation as Walker and Jackson (2004) proposed. If we postulate that the 2 mm/yr displacement rate on the Anar fault is the upper limit of the fault velocity and stable for the duration of the total geological displacement, then the 20 km total offset on the Anar fault could have been achieved during a minimum of 10 Ma. The present-day orientation of the Anar fault with 350° N could have been reached from an initial NS orientation according to the direction of regional shear between the CIB and the Hellmand block by a rotation with a maximum velocity of 1°/Ma. However, the comparison with the long term slip rates proposed by Meyer et al. (2007) (0.5 – 0.75 mm/yr) suggest that the present-day velocity on the Anar fault is probably lower than 2 mm/yr.

For the Dehshir fault we can consider 65 km of total displacement (Meyer et al., 2005), and infer the onset of the deformation 65 Ma ago supposing the present-day GPS velocity of 1 mm/yr is representative for the past deformation. This is older than the 25 – 40 Ma proposed by Meyer et al. (2005) because our observed slip rates are 50 % lower. If the Dehshir velocity was always as small as 1 mm/yr it must have accommodated motion before the collision between Arabia and Eurasia (16-23 Ma proposed by Robertson et al., 2000). The more probable explanation is that the slip velocity has decreased since the onset of fault slip. With 1 mm/yr of slip rate, the Dehshir fault has not a significant role in the present-day accommodation of the Arabian-Eurasian convergence. The slip rate on the Dehshir fault is relatively small and traces of the last earthquakes are difficult to find. This indicates a long recurrence interval of earthquakes on the fault. Meyer et al. (2006) indicate one place along the Dehshir fault where a ~5 m offset is observed that is eventually created by a single event. If such a huge event is the characteristic earthquake for the Dehshir fault, a recurrence time of several thousand years is needed to cumulate several meters of fault displacement with the present-day rates.

4.7.2 The Gowk and Bam faults

Based on our GPS measurements, we found 6±2 mm/yr of right-lateral shear between Lut and Central Iran. This shear is accommodated on the Sabzevaran and Gowk faults with a total cumulative slip rate estimated to be 4±2 mm/yr and a motion of 2±2 mm/yr on the Bam fault. As the sites around the Bam fault were installed and measured just a few days after the 2003 earthquake (Mw=6.5), they may partially record post-seismic deformation. An offset of the first measurement epoch with respect to the linear evolution between the following positioning measurements has been observed at the BA12 site. For this site, a component of post-seismic displacement would lead to an under-estimation of the northward site velocity and an over-estimation of the Bam fault rate with respect to sites to the west of the right-lateral fault. How ever with linear velocity over 5 measurements is now close to inter seismic rate. The co-seismic slip of the 2003 Bam earthquake is estimated to a maximum of ~2 m in 5 km depth (Funning et al., 2005). With a slip rate of 2 mm/yr the recurrence time of such an event is 1000 years that are needed to cumulate this amount of fault displacement.

The Gowk fault has experienced several earthquakes (Mw=5.4-7.1) in the last 25 years. Walker and Jackson (2002) proposed ~12 km of total offset for the Gowk fault during the last ~5-7 Ma which indicates ~1.5-2.4 mm/yr of displacement rate. We don't have an individual slip rate of the Gowk fault. However, to attribute the part of the 4 mm/yr of right-lateral slip measured over both the Sabzevaran and the Gowk faults to each of the faults, we could use the Anar fault slip rate of 2mm/yr which is thought to be transferred onto the Anar fault from the Sabzevaran fault and postulate the Sabzevaran velocity is also 2 mm/yr. Then the Gowk fault moves with the remaining rate of 2 mm/yr, consistent with the results of Walker and Jackson (2002). We infer that the Gowk deformation started about 6 Ma ago.

The Bam fault connects with the Gowk fault to the Nayband fault system in the north. The cumulative slip rate of 4 mm/yr is then transferred to the north and absorbed by right-lateral strike-slip and thrust faults.

4.7.3. The Kuhbanan, Nayband and Kalmard faults

The Bam and Gowk faults are connected to the Nayband fault system, consisting in the Kuhbanan, Behabad, Ravar, Lakarkuh and Nayband faults, to the north. These faults accommodate a part of the total Bam and Gowk slip rate of 4 mm/yr. Our GPS network is not yet dense enough to evaluate the individual slip rate of all of the segments but we can estimate some cumulative displacement rates.

The Kuhbanan fault activity decreases from 5±2 mm/yr of transpressive motion in its southern part to 1±2 mm/yr of right-lateral strike-slip motion in its northern part. The shear between ROBA, west of the Lut block and the Nayband fault system, and BAJE, NOGH and QAE2 on the eastern part of Lut is about 5.5±2mm/yr. Between ROBA and the eastern Lut stations pass the Kalmard fault, the Nayband fault and thrust faults, in particular the Ferdows thrust. If we compare the velocity of BA12 located on the rigid Lut block with ROBA, separated only by the Nayband and Kalmard faults but 400 km apart, we find 2±2 mm/yr of total slip rate cumulated over both faults. But as the Kalmard fault is located in the area which has no seismicity (Ambraseys and Melville, 1982; Engdahl et al., 1998) and we do not have any information on a geological offset of the Kalmard fault, we believe that this 2±2 mm/yr motion is related only to the Nayband fault.

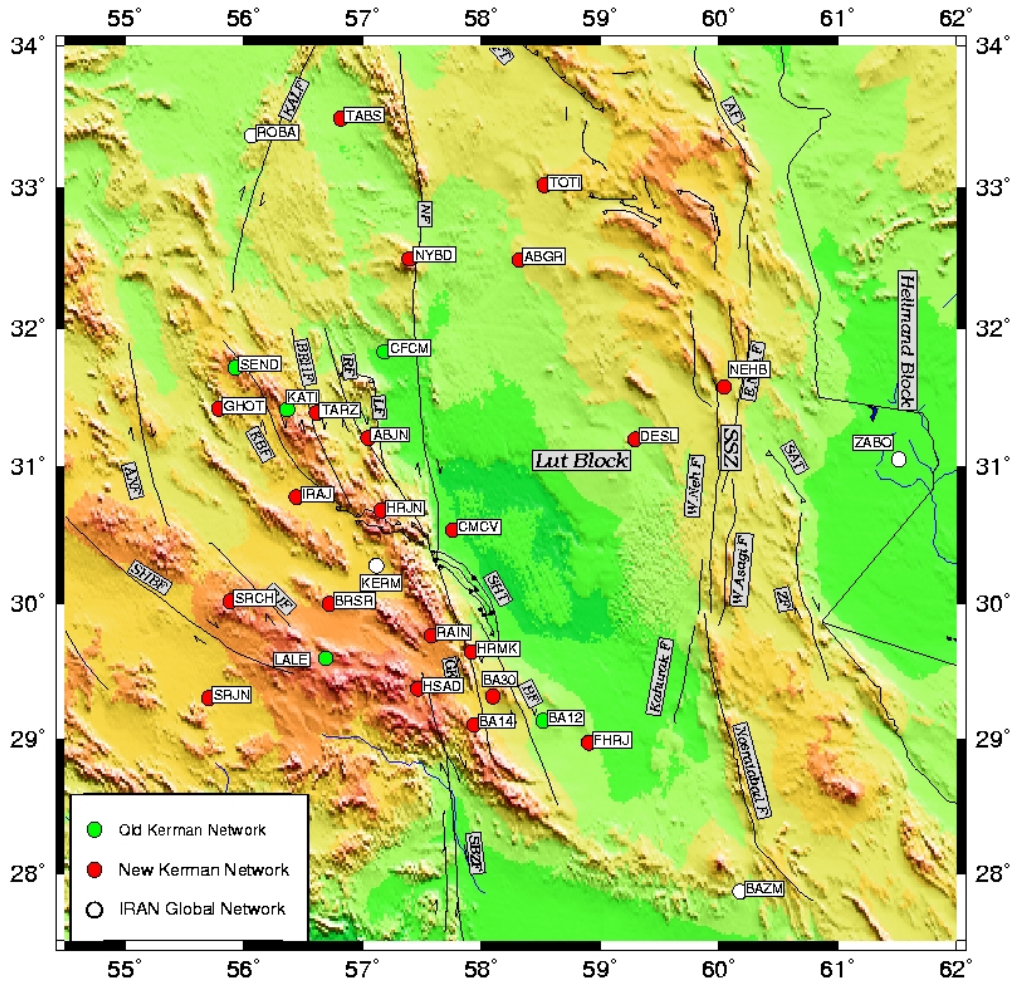

Figure 4-24. Distribution of new and old Kerman network GPS sites.

Differential motion of KATI with respect to the Lut block (represented by BA12, still 250 km apart) shows 3 mm/yr of cumulative strike-slip motion on the Behabad, Ravar, Lakarkuh and Nayband faults. As we have identified before 2±2 mm/yr of slip rate on the Nayband fault only, we estimate the cumulative slip rate of Behabad, Ravar and Lakarkuh to be about 1±2 mm/yr. All these faults experienced earthquakes (Berberian, 2005). Our densified GPS network (Fig. 4-24) installed in 2006 will help to estimate the kinematics of each individual fault.

4.7.4. The Sistan suture zone

The Sistan suture zone is the easternmost active tectonical feature of Iran. With a length of 550 km it has an important role in the shear accommodation between the Central Iran and the Hellmand blocks (Walker and Jackson 2004). We find 7.5±2 mm/yr of right-lateral strike-slip motion on the Sistan suture zone comparing BA12 and ZABO. This shear is accommodated along the Kahurak, West

Asagie and Zahedan faults. Lacking intermediate stations, we could not resolve the slip rate of each individual fault. Walker and Jackson (2004) proposed 70 km and possibly up to 95 km of bedrock offset across the three faults of the Sistan suture zone which occurred since ~5-7Ma. If the GPS estimated present-day rate has been constant, this total cumulative offset (70-95km) has been achieved in 9-13 Ma, ante-dating the onset of the Sistan suture zone.

The present-day deformation along the Sistan suture zone is transferred to the north by strike-slip faults. In the northern part we use QAE2 and NOGH to evaluate 4 mm/yr of slip rate for both the Abiz and Gazik faults. The remaining motion (4mm/yr estimated between BA12 and NOGH) is distributed on the eastern faults of the Sistan suture zone (mainly NW-SE trending thrust faults).

The destructive 1997, May 10, Qaen earthquake (Mw=7.2) ruptured 125 km of the Abiz fault and produced 2 m of right-lateral average displacement. With 4 mm/yr for the present-day slip rate, it takes about 500 to 600 years to build up an earthquake of such a magnitude.

If we assume a total offset of 50-65 km for the East Neh, of 10 km for the West Neh, and of 13-20 km for the Zahedan faults during the last 5 to 7 Ma (Walker and Jackson, 2004), then we infer a slip rate of 8-11mm/yr for the East Neh, 1.5 mm/yr for the West Neh and 2-3 mm/yr for the Zahedan faults and the total offset of the Sistan suture zone will be 11.5 – 15.5 mm/yr. This is almost twice as much as the present-day rate of 7.5 mm/yr measured by GPS and indicates that either the fault velocities are not constant but have decreased until now, or that the total fault offsets have been created over a clearly longer time span than 5-7 Ma.

An evaluation of fault slip rates over intermediate time scales (~12 ka) is provided by Meyer et al. (2007) for the East Neh, West Neh and Asagie faults. From offsets of geomorphological markers dated with the help of a coherent morphoclimatic scenario, the authors determine ~1.75-2.5 mm/yr, ~1-5 mm/yr and ~1-2.5 mm/yr for the East and West Neh and the Asagie faults, respectively. The cumulative velocities of East and West Neh at about 30.5°N yield ~2.75-7.5 mm/yr and could reach alone the 7.5 mm/yr of strike-slip measured by GPS across the total Sistan suture zone that includes also the Zahedan fault. Further south, the cumulative slip of the West Neh and the Asagie fault yield 2 – 7.5 mm/yr. This evaluates the Zahedan fault velocity to 0 – 5.5 mm/yr to complete to the present day rate of 7.5 mm/yr. These (intermediate) long term fault velocities are more consistent

with GPS rates than the very long term velocities inferred by total geological offsets dated to an inception of deformation 5-7 Ma ago. This indicates that present-day slip rates have probably been stable over some tenths of thousand years. Over geological time scales, the slip rates must either have decreased from initially higher values to achieve the total deformation in the suggested 5-7 Ma, or the deformation started earlier than that. Constant present day velocities evaluate at least 10 Ma. This seems to be coherent with another deformation zone in eastern Iran, in the Kopeh Dagh, which is dated to 10 Ma by Hollingsworth et al. (2006), and to older onsets from our GPS measurements and by Berberian and King (1981), in particular in the eastern part of Kopeh Dagh (see chapter 3).

4.7.5 The Doruneh and Dasht-e-Bayaz faults

The N-S right-lateral faults around the Lut block die out around ~34°N where the remaining shear is absorbed by the EW trending left-lateral strike-slip faults of Doruneh and Dasht-e-Bayaz bounding the Lut to the north.

Comparing NOGH and QAE2 in the southern part of Dasht-e-Bayaz fault to BAJE, DOGH and KASH, we find 1.5±2 mm/yr for the present-day slip rate on the Dasht-e-Bayaz fault which is 1 mm/yr less than the rate proposed by Berberian & Yeats (1999) and Walker and Jackson (2004). We also estimate 3.5±2 mm/yr of shortening perpendicular to the Jangal thrust. We could not find a significant shortening rate on the Dasht-e-Bayaz fault, confirming its pure strike-slip character. Walker and Jackson (2004) estimated 4-5 km of total left-lateral offset on this fault so with a 1.5mm/yr slip rate we evaluate the onset on the Dasht-e-Bayaz fault to be 2.5-3.5 Ma old. This is young compared to other faults in the region.

During the 1968 August 31 Dasht-e-Bayaz earthquake (Mw=7.1), a left-lateral displacement of 2.5 m was observed (Tchalenko & Berberian, 1975). If this is the size of a characteristic earthquake on the Dasht-e-Bayaz fault and with their suggested displacement rate of 2.5 mm/yr, Berberian & Yeats (1999) proposed 1000 years for the recurrence time between earthquakes. With our lower fault velocity, we propose rather ~1600 years for recurrence between each event.

The displacement rate on different segments of the Doruneh fault varies. We have observed 2.5±2 mm/yr of left-lateral slip rate at the longitude of ~58°E, 1.5±2 mm/yr at the longitude of ~59°E and 1±2 mm/yr at the longitude of ~60.5°E. We do

not know exactly the velocity of the western part of the Doruneh fault where it is commonly called the Great Kavir fault, but the large scale network around this part of the fault gives no evidence for any increase in slip rate to the west. It will probably decrease from ~58°E also to the west as it decreases to the east.

Walker and Jackson (2004) propose that the Doruneh and Dasht-e-Bayaz faults accommodate the regional NS shear by clockwise rotation. The two faults have a common rotation pole close to the Afghanistan border at a latitude of 34.3°N. They also estimate that since ~5-7 Ma a total clockwise rotation of ~20° (3-4°/Ma) has affected the Doruneh fault. Now the rotation of the eastern part of Doruneh has been transmitted to the young Dasht-e-Bayaz fault, and some of the Sistan shear is accommodated by shortening across the Jangal thrust, parallel and just south of the eastern extension of the Doruneh fault. The authors further propose that the clockwise rotation increases with increasing shear from west to east.

We tried to characterize the rotation in the Doruneh and Dasht-e-Bayaz region by estimating a regional Euler pole and the rotation rate of the zone. We also tried to determine the different micro-blocks in this region that present an independent and coherent motion with respect to Eurasia. This required several tests. First we used the stations located north of the Doruneh fault (stations BAKH, GARD and DARG) and we find that the best Euler pole for these three stations is at 37.5±0.5°N and 61.7±0.5°E, with a rotation rate of 1.2±0.7°/Ma. We also find an Euler pole for the stations located south of Doruneh (KHAF, DOGH, KASH, BAJE) at 36±0.5°N and 61±0.5°E with a rotation rate of 1.2±0.8°/Ma. These two Euler poles are situated close to each other and the rotation rates are the same. While formally the two Euler poles seem to be coherent, looking at the residuals show that they describe well distinct motions. In Figure 4-25a the GARD and DARG, observed velocities fit the best the theoretical vectors according to the rigid block rotation with respect to the first Euler pole. This indicates these stations are on the same block. Fig. 4-25b shows that the stations DOGH, KASH and BAJE are located on another block, because the second Euler pole describes correctly their velocities, but not the velocities of the stations mentioned above. The two identical rotation rates for the blocks north and south of the Doruneh fault indicates that the same 1.2°/Ma of rotation rate applies also to the Doruneh fault, with respect to a pole which is also situated at the Afghanistan border (61°E).The GPS velocity of the BAKH and KHAF do not fit theoretical velocities of neither of these blocks, suggesting that these

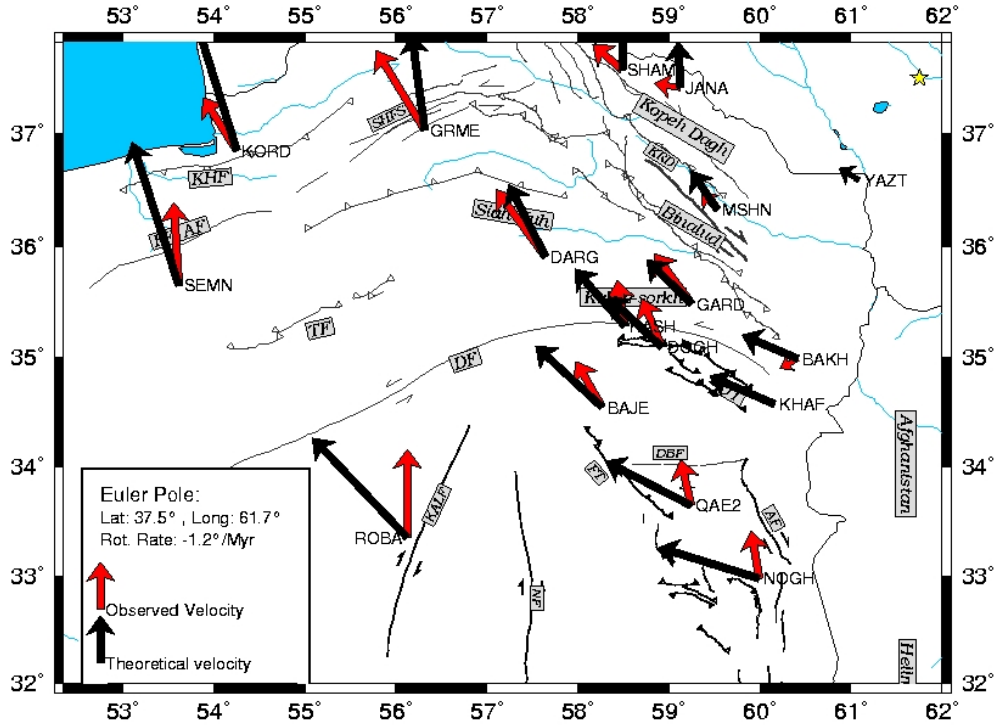

Figure 4-25a. Observed and theoretical velocities assuming an Euler rotation pole indicated by the yellow star. In the north of the Doruneh fault, the observed velocities in DARG, MSHN, YAZT and GARD fit the theoretical velocity which suggests they are on the same block.

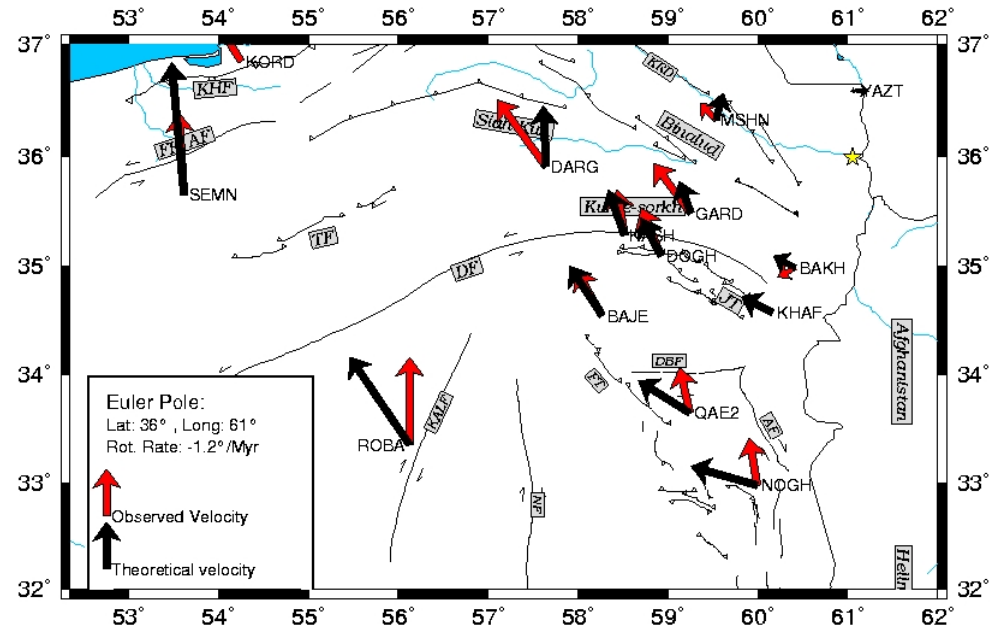

Figure 4-25b. Observed and theoretical velocities assuming an Euler rotation pole indicated by the yellow star. South of the Doruneh fault, the observed velocity of KASH, DOGH and BAJE fit the theoretical velocities which suggests these stations are located on the same block.

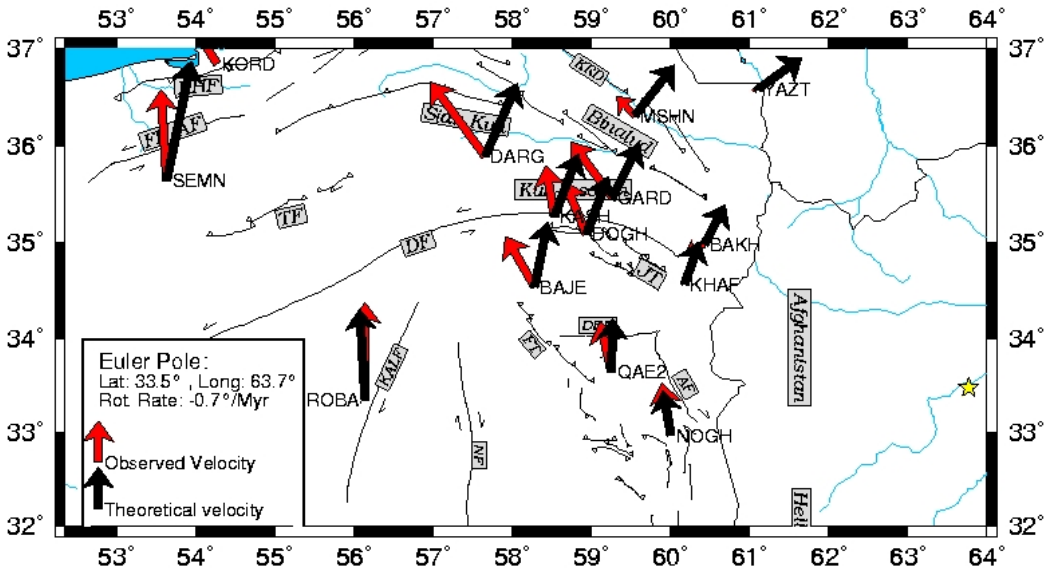

Figure 4-25c. Observed and theoretical velocities assuming an Euler pole indicated by the yellow star. South of the Dasht-e-Bayaz fault the observed velocities at NOGH and QAE2 best fit the theoretical velocities which suggest these stations are on the same block.

stations might be located in a deformation zone (probably on the border of the Hellmand block).

We estimate the rotation rate for the Dasht-e-Bayaz fault to be ~0.7°/Ma around a pole located at 33.5°N and 63.7°E by comparing QAE2 and NOGH (Fig. 4-25c). The Dasht-e-Bayaz and Doruneh faults do not rotate around a single pole and the Dasht-e-Bayaz rotation rate is clearly lower than that of the Doruneh fault. However, with only two stations this block motion is only weakly constrained.

We needed three different Euler rotation poles to describe the motion of stations in the three regions of North Doruneh, South Doruneh and Dasht-e-Bayaz (although the poles of North and South Doruneh are very similar). This suggests that we have three distinct blocks for the regions north and south of Doruneh and for the south of Dasht-e-Bayaz (Fig. 4-26).

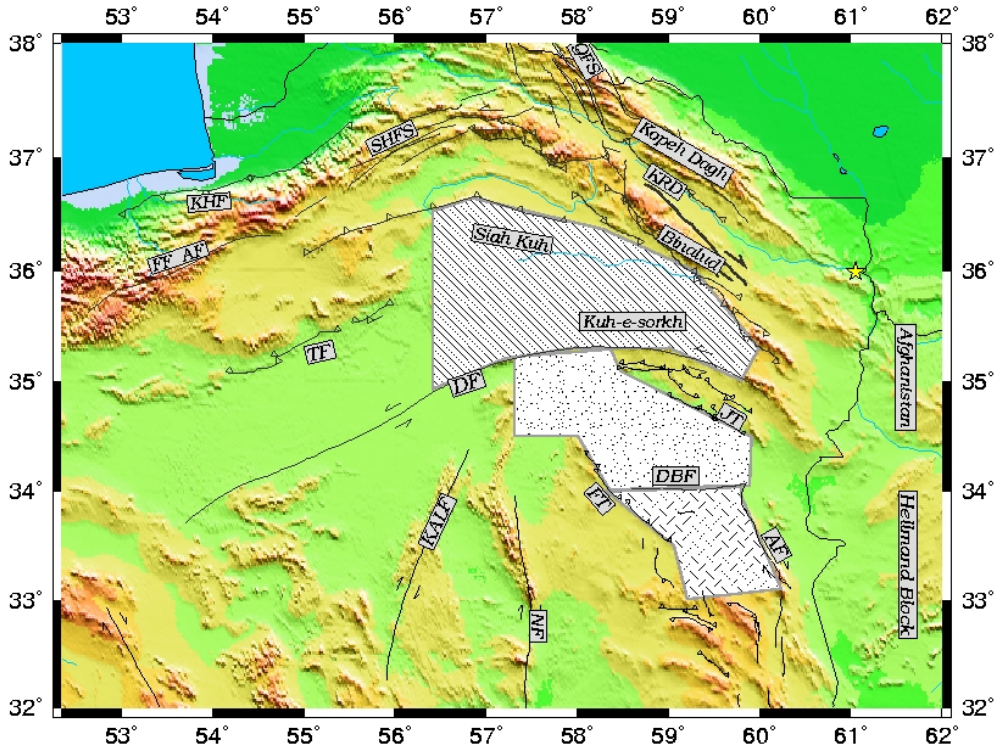

Figure 4-26. Tectonical map of the Doruneh region. The shaded areas are three blocks inferred from the different Euler poles.

4.8 Summary and simplified kinematic model of the Lut region

Our new measurements result in a new kinematical model (Fig. 4-27). A total shear of 14 mm/yr between the Central Iranian and the Hellmand blocks is accommodated by several faults located on both the east and the west of Lut. The velocity of the Central Iran, the Lut and the Hellmand blocks relative to Eurasia are about 15 mm/yr, 8.5 mm/yr and 1 mm/yr respectively. There is no significant westward motion south of ~34°N.

East of the Lut, the Sistan suture zone absorbs 7.5 mm/yr of the total shear which is accommodated by different NS right-lateral faults. West of the Lut block, the Bam fault accommodates 2±2 mm/yr of the N-S motion. The cumulative slip rate on the Sabzevaran and Gowk faults is about 4±2mm/yr. The Anar fault motion of 2±2 mm/yr is connected to the Sabzevaran fault Walker (2006) and therefore the motion on Sabzevaran and Gowk fault is probably 2mm/yr each. The Dehshir fault accommodates a slip rate of 1±2 mm/yr inside the Central Iran block. Our GPS results show that the Dehshir fault has no major role in the accommodation

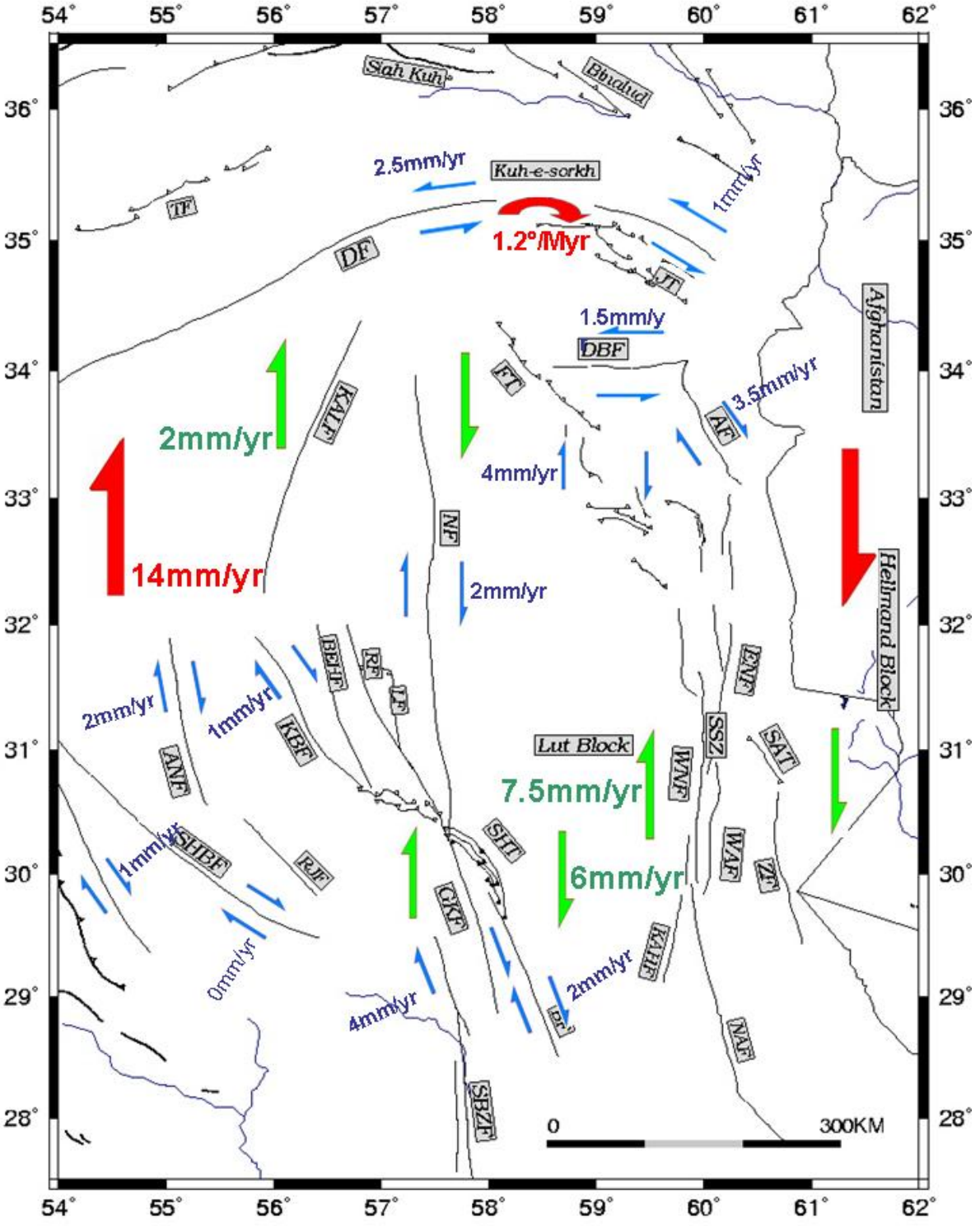

Figure 4-27. Kinematic model of the Lut region from GPS measurements. A total shear of 14±2 mm/yr is observed between the Central Iran block and the Hellmand block. About 7.5±2 mm/yr of shear is accommodated east of Lut and the remaining 6 mm/yr is accommodated west of Lut. The blue vectors show the lateral motion on each fault.

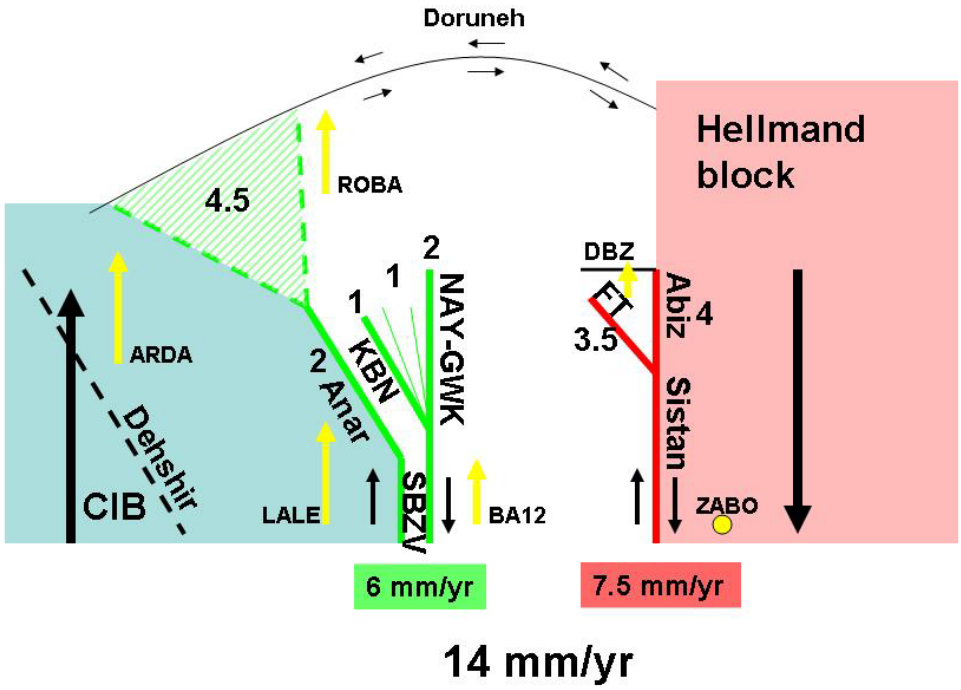

Figure 4-28. Cartoon showing the distribution of shear (14 mm/yr) between the Central Iran block in the west and the Hellmand block in the east. The maximum shear accommodation is concentrated in the Sistan suture zone. Yellow arrows are velocity field respect to ZaboThe Doruneh fault absorbs the N-S motion of the faults by a clockwise rotation along its vertical axis. DBZ: Dasht-e-Bayaz Fault, KBN: Kuhbanan Fault, NAY-GWK: Nayband-Gowk Faults, CIB: Central Iran Block.

of the shear between the Central Iran and Hellmand blocks. There is no tectonical feature transferring the Anar and Dehshir fault motions to the north. These faults are supposed to accommodate their motion by an anticlockwise rotation (Walker and Jackson, 2004).

West of the Kuhbanan fault, we estimated 4.5±2 mm/yr of differential motion between SEND and ARDA. As there is no fault between these stations we think that the deformation of 4.5±2 mm/yr is distributed over the region.

We could not evaluate the kinematics of the Nayband fault directly, only a cumulated slip rate of 2±2 mm/yr over the Nayband and Kalmard faults. However, as the Kalmard fault is in an aseismic region, we believe that the Kalmard fault is not active and that the Nayband fault moves at a rate of 2±2 mm/yr. The cumulated motion on the, Gowk and Bam faults of 4 mm/yr is probably transferred to the Nayband fault system to 100%. We evaluated to 1±2mm/yr the motion on the Kuhbanan fault which is not significant but as this fault has experienced several

earthquakes, it has potential for future earthquakes. The cumulative slip rate on the Behabad, Ravar and Lakarkuh faults is about 1 mm/yr. The remaining 2 mm/yr are localized on the Nayband fault.

To the northeast of Lut, the western NW-SE Ferdows thrust faults accommodate 4 mm/yr of shortening between BA12 and QAE2/BAJE. The NS oriented Abiz/Gazik faults to the east slip with 3.5 mm/yr right-laterally as evaluated from QAE2/BAJE with respect to ZABO.

The east-west left-lateral Dasht-e-Bayaz fault is a young structure moving at 1.5±2 mm/yr (slightly slower than the 2.5 mm/yr proposed by Berberian and Yeats, 1999) and started about 3 Ma ago.

We evaluated 2.5±2mm/yr, 1.5±2mm/yr and 1±2mm/yr of slip rate for the Doruneh fault at the longitudes ~58°E, ~59°E, ~60.5°E, respectively, which shows a decreasing slip rate from west (~58°) to east. The Doruneh fault rotates at a rate of 1.2°/Ma around a pole at 36°N and 61°E and the Dasht-e-Bayaz fault rotates at 0.7°/Ma around a pole located at 33.5°N and 63°E. The Doruneh rotation rate is also found in the Kopeh Dagh region (see chapter 3) and seems to be the major tectonic feature of eastern Iran, imposed by dominating NS shear across the Lut block.

We have simplified the distribution of shear between the Central Iran block and the Hellmand block in the cartoon shown in Fig. 4-28. The Anar, Kuhbanan and Nayband-Gowk faults and the Sistan suture zone accommodate the NS shear between Central Iran and the Hellmand block. The Doruneh fault accommodates only 1 mm/yr of left-lateral motion and plays therefore no important role in the accommodation of shear between the CIB and Eurasia.

Chapter 5: Kinematics of Zagros

5.1 Introduction and Tectonics Settings

The Zagros mountain fold-and-thrust belt results from the Neo-Tethys ocean closure. This belt is now the region of intracontinental collision between the Arabian shield and central Iran and accommodates part of the Arabia-Eurasia collision by its present-day deformation.

The Zagros mountain belt is ~1200 km long, trends NW-SE between eastern Turkey where it connects to the North and East Anatolian faults and the Strait of Hormuz where is connects to the Makran subduction. Its width varies from ~200 km to the west to ~350 km to the east. The highest elevation is more than 4.500 m. The Zagros belt lies on the former Arabian passive margin that is covered by up to 10 km of Infracambrian to Miocene sediments (e.g. Haynes & McQuillan 1974; Stocklin 1974; Stoneley 1981). These sediments contain several layers of evaporite at different depths that decouple the surface deformation from the basement (Berberian 1981, 1995; Berberian & King 1981). During the Mesozoic, the Zagros underwent a major episode of convergence, mostly accommodated by subduction along the Main Zagros Thrust (MZT) (Stocklin 1974; Stoneley 1981). After the closure of the oceanic basins, a second episode of deformation during the Neogene led to the folding that affected the Simple Folded Belt located between the MZT and the Persian Gulf (Falcon, 1974).

The Zagros belt is divided in two or more lateral structural units (Fig. 5-1), the High Zagros Belt and the Simple Folded Belt (Stocklin, 1968; Berberian, 1995; Talebian and Jackson, 2004). The High Zagros Belt is a narrow thrust belt up to 80 km wide, with a NW-SE trend. This belt is the highest part of the Zagros and the elevation reaches 4500 m. The High Zagros belt is bounded to the NE by the Main Zagros Thrust (MZT, also called Main Zagros Reverse Fault, MZRF) and to the SW by the High Zagros Fault (HZF).

According to its tectonical characteristics, we have divided the Zagros into three areas, the North Zagros**,** the Central Zagros, and the region of the Kazerun Fault system separating North and Central Zagros**.** In the North Zagros the deformation is partitioned between shortening on reverse faults and right-lateral strike-slip motion on the Main Recent Fault (MRF). The orientation of the exposed

fold trends on this segment is about ~45°. In Central Zagros, the fold trends turn to E-W. The deformation is not partitioned and accommodated mainly in the south along the Persian Gulf. The particularity of Central Zagros is that it is underlain by the Hormuz salt layer which decouples the superficial layers from the basement. Therefore, the GPS determined velocities might represent only the deformation of the sedimentary cover (Talebian and Jackson, 2004; Authemayou et al., 2005 and 2006; Walpersdorf et al. 2006). The NS trending Kazerun fault system is situated in the transition zone between the region of pure shortening in the SE (the Central Zagros) and the region of oblique shortening in the NW (the North Zagros) with partitioning of the deformation into shortening and strike-slip on different faults. The earthquake focal mechanisms on the Kazerun Fault system indicate right-lateral strike-slip motion.

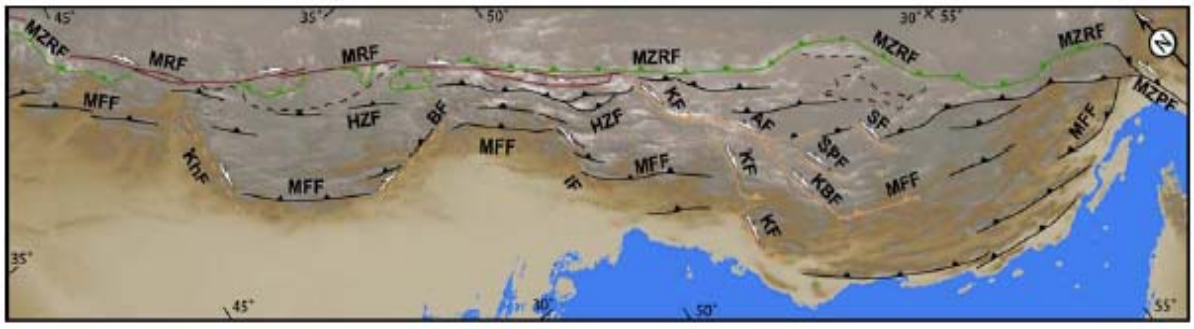

Figure 5-1. Map showing the principal faults of Zagros. AF: Ardakan Fault, BF: Balarud Fault, HZF: High Zagros Fault, IF: Izeh Fault, KBF: Kareh-Bas Fault, KF: Kazerun Fault, KhF: Khanaqin Fault, MFF: Main Frontal Fault, MRF: Main Recent Fault, MZPF: Minab-Zendan-Palami Fault, MZRF: Main Zagros Reverse Fault (=MZT: Main Zagros Thrust), SAF: Sarvestan Fault, SPF: Sabz Pushan Fault (Authemayou, 2006).

5.1.1 The Main Zagros Thrust

The Zagros mountain belt approximately follows an important geological boundary called the 'Zagros suture', the 'Main Zagros Thrust (MZT)' or the 'Main Zagros Reverse Fault (MZRF)' by various authors (e.g. Stöcklin 1974; Falcon 1974; Berberian, 1995). This boundary approximately separates the rocks of the Arabian continental margin to the SW from metamorphic and volcanic rocks of Central Iran to the NE (e.g. Berberian & King 1981). This geological boundary is also an important seismotectonic feature today, marking an abrupt cut-off between the intense seismicity of the Zagros and the almost aseismic Central Iran block along the

Sanandaj-Sirjan zone. This thrust starts in North Zagros at the longitude ~49°E and dies out at the longitude ~57°E when reaching the Makran subduction zone.

5.1.2 Main Recent Fault

The Main Recent Fault (MRF) was first identified from offset drainage features by Wellman (1966), and was then later described in more detail and named by Tchalenko & Braud (1974). The Main Recent Fault strikes NW–SE parallel to the Zagros belt and can be traced as a narrow, linear series of fault segments from the Turkey–Iran border to the southeast until ~51°E for over 800 km. Several large earthquakes have been reported along the MRF, the largest one of the last century being the 1909 Ms = 7.4 Dorud event (Tchalenko and Braud, 1974; Talebian and Jackson, 2002).

The southern termination of the MRF coincides with a series of almost north trending dextral strike-slip faults (the Kazerun Fault System). Right-lateral offset along the MRF was estimated by Gidon et al. (1974a) to be ~60 km in the Dorud region. Using the offset of an Upper Cretaceous ophiolitic unit and of the major drainage, Talebian and Jackson (2002) obtain a value of 50 km. Assuming that the right-lateral slip along the MRF was initiated 3 to 5 Ma ago, they derived a strike-slip rate of about 10–17 mm/yr. This is compatible with the estimate of 10 mm/yr of Bachmanov et al. (2004) based on the offset of a river valley incised into a surface of likely postglacial age. Authemayou (2006) also propose a slip rate of 4.9-7.6 mm/yr based on offsets of geomorphological markers and the in-situ dating for the MRF. GPS measurements suggest that the present slip rate is significantly slower than the rates proposed by Talebian and Jackson (2004). Right-lateral slip on the MRF is evaluated by GPS to about 3 ± 2 mm/yr (Vernant et al., 2004).

5.1.3 The Kazerun Fault System

In the transition zone between North and Central Zagros is a series of N- to NNW-trending right-lateral strike-slip faults called the Kazerun Fault System (KFS). The longest of these faults is the Kazerun fault (e. g. Falcon, 1969). The other NNW-trending strike-slip faults to the east of the Kazerun fault are the Karehbas, Sabz Pushan and Sarvestan faults (Fig. 5-2). These are all inherited basement structures from a Neo-Proterozoic tectonic phase (Talbot and Alavi, 1996). The Kazerun fault crosses the Zagros from the southeastern end of the Main Recent Fault to the

Persian Gulf, with a total length of over 300 km (Koop and Stoneley, 1982) (Figure 5-2). The Kazerun fault comprises three segments, the Dena, Kazerun and Borazjan fault segments (Figure 5-2), each with similar lengths (~100 km), that distort and disrupt the Zagros folds (Berberian, 1995; Ricou et al., 1977; Authemayou et al., 2005). Each segment is terminated to the south by a SE-trending thrust (Authemayou et al., 2005).

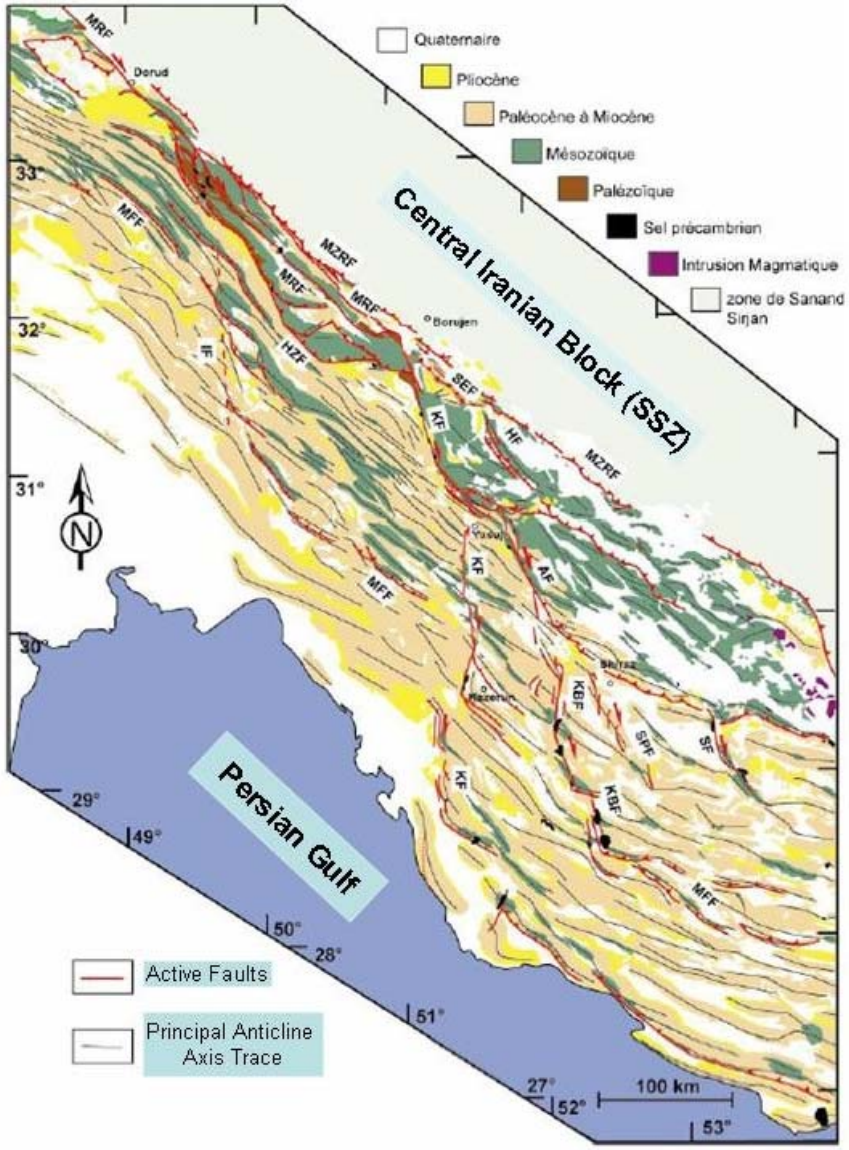

Figure 5-2. Fault map of North Zagros and the Kazerun fault system modified by Authemayou (2006). AF: Ardakan Fault, HF: Hanna Fault, HZF: High Zagros Fault, IF: Izeh Fault, KBF: Karehbas Fault, KF: Kazerun Fault, MFF: Main Frontal Fault, MRF: Main Recent Fault, MZRF(MZT) : Main Zagros Reverse Fault, SF: Sarvestan Fault, SEF: Semirom Fault, SPF: Sabz-Pushan Fault, SSZ: Sanandaj-Sirjan Zone.

The present day activity of the Kazerun fault system is emphasized by historical and instrumental earthquakes that have been recorded on different parts of the fault system. It shows a high level of seismicity along its central part and

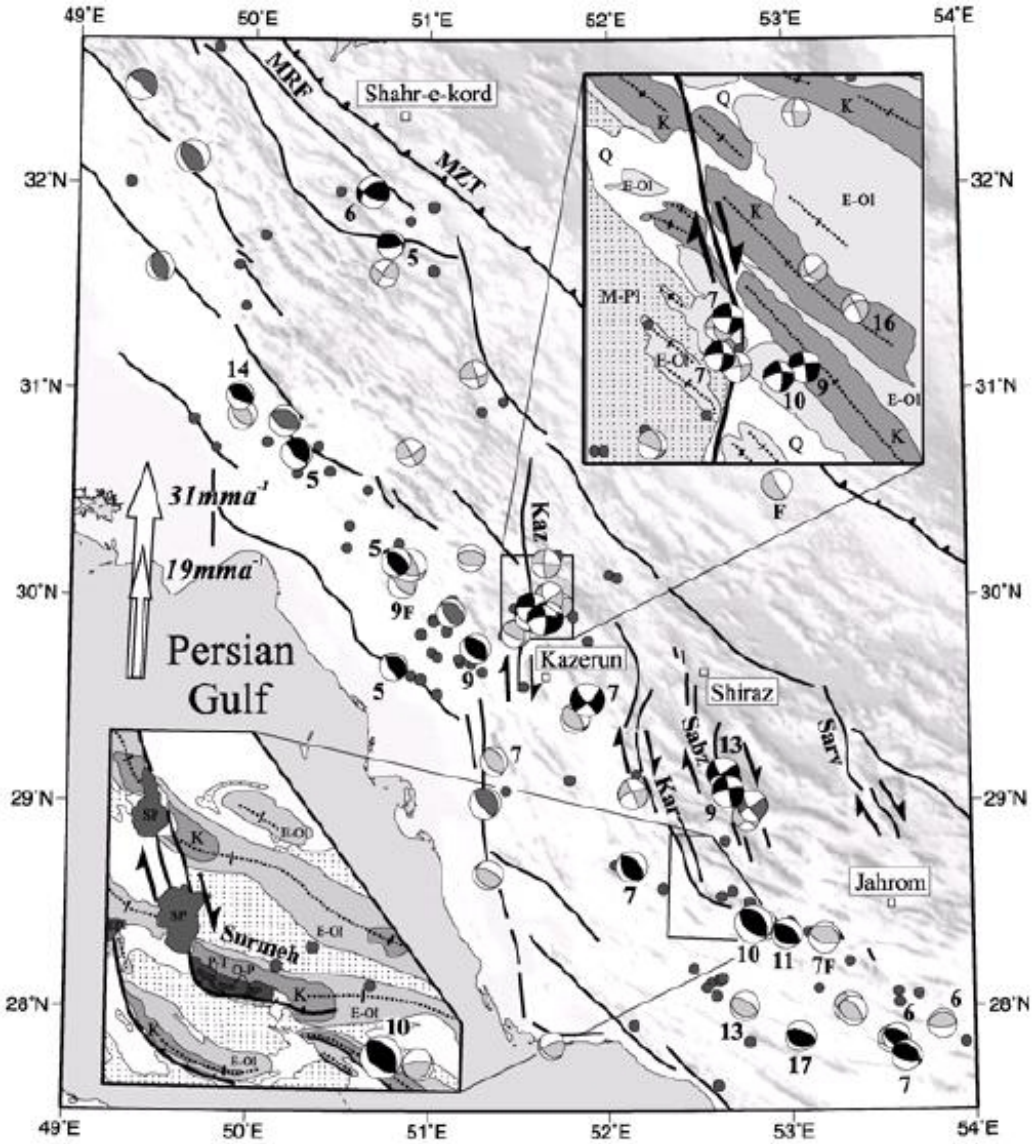

Figure 5-3. Seismotectonic map of Kazerun fault system modified by Talebian & Jackson (2004). Dark and light gray spheres are Harvard CMT above and below Mw=5.3 from Talebian & Jackson (2004) and the full spheres are other earthquakes from Engdahl et al., 1998. The white arrows are the direction and rates of the overall Arabia-Eurasia motion from DeMets et al. (1994) (big arrows) and Sella et al. (2002) (small arrows). The inset shows a summary of the geology: SP are salt plugs of Hormuz salt. Kaz: Kazerun Fault system, Kar: Karehbas Fault, MRF: Main Recent Fault, MZT: Main Zagros Thrust, Sabz: Sabz Pushan Fault, Sarv: Sarvestan Fault.

generally right-lateral focal mechanisms (Baker et al., 1993; Berberian, 1995; Talebian and Jackson, 2004) (Fig. 5-3). Estimated offsets of geological markers on the Kazerun fault are between 8-27 km (minimum values, Authemayou et al., 2005) and 140 km (maximum value, Berberian 1995). Geological horizontal slip rates along the Kazerun Fault System are of 4 mm/yr for its northern segment (Dena), 2.5 - 3 mm/yr for the central fault (Kazerun) and negligible for its southern segment (Borazjan) (Authemayou et al. 2006).

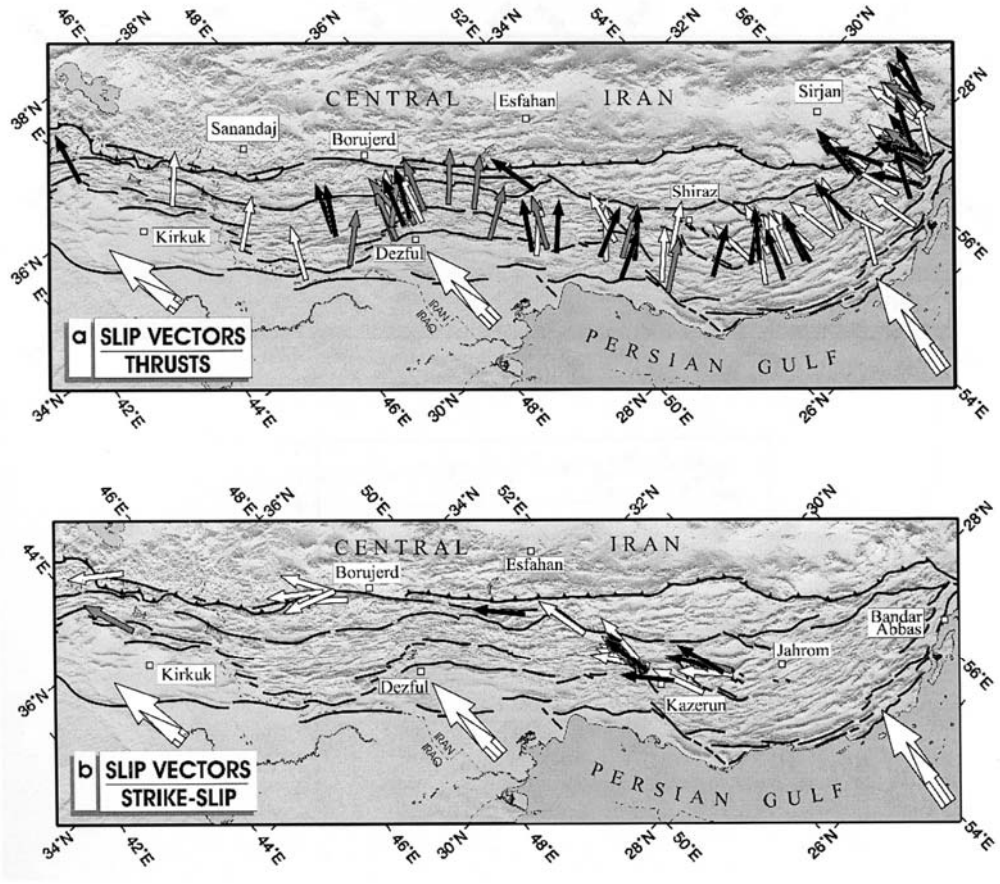

Figure. 5-4. Compilation of earthquake slip vectors in Zagros. Thrust events are shown in the upper graph, the lower graph presents strike-slip earthquakes (Talebian and Jackson, 2004). The large white arrows correspond to the Arabia-Eurasia motion from DeMets et al. (1994) and Sella et al. (2000).

5.1.4 Tectonical model

Talebian and Jackson (2004) have proposed a tectonical model constrained by earthquake slip vector directions (Fig. 5-4) to describe schematically how the Zagros accommodates presently the Arabia-Eurasia collision (Fig. 5-5). In the North Zagros (Borujerd-Dezful), oblique shortening is partitioned into right-lateral strike-slip on the Main Recent fault (MRF) and orthogonal shortening. In the Central Zagros (Bandar Abbas) no strike-slip is necessary, as the shortening is parallel to the overall convergence. The zone around the Kazerun Fault system is where the transition between these two regimes occurs, with anticlockwise rotating strike-slip faults allowing an along-strike extension between Bandar Abbas and Dezful.

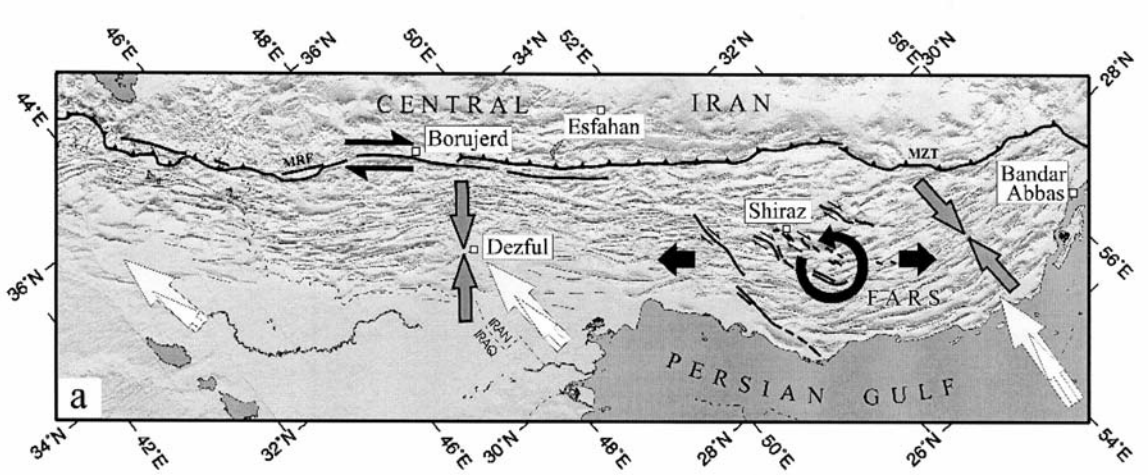

Figure 5-5. Summary sketch of the tectonic pattern in the Zagros. Overall Arabia-Eurasia motions are shown by the large white arrows (DeMets et al., 1994, and Sella et al., 2000). Grey arrow couples indicate the general orthogonal shortening, thin black arrows the strike-slip on the MRF, large black arrows along-strike extension due to the Kazerun strike-slip system.

5.2 GPS constrained velocity field

Since 1997 we have measured three GPS networks covering the Central Zagros (15 sites), the North Zagros (18 sites) and the Kazerun fault system (11 sites) (Fig. 5-6). The Central Zagros network was measured three times in 1997, 2000 and 2003. The results of the 1997 and 2000 campaigns were published by Tatar et al. (2002). The North Zagros network has been measured in 2001, 2003 and 2005. We combined the North and Central Zagros network measurements until 2003 and published the results (Walpersdorf et al., 2006) (5.2.1). The Kazerun network has been measured three times (2002, 2004 and 2006). The results of the first two campaigns are presented in this thesis as well as the article submitted by Tavakoli et al. (2007) (5.2.2). The data of the three Zagros networks have also been used in an article synthesizing the kinematics of the Zagros mountain belt as seen from geodesy, tectonics, geomorphology and seismology (Hatzfeld et al., 2007). This article is presented in 5.2.3. An update of the Zagros velocity field with the 2005 measurements in North Zagros and in the Iran Global network is presented and compared to former results (5.2.4).

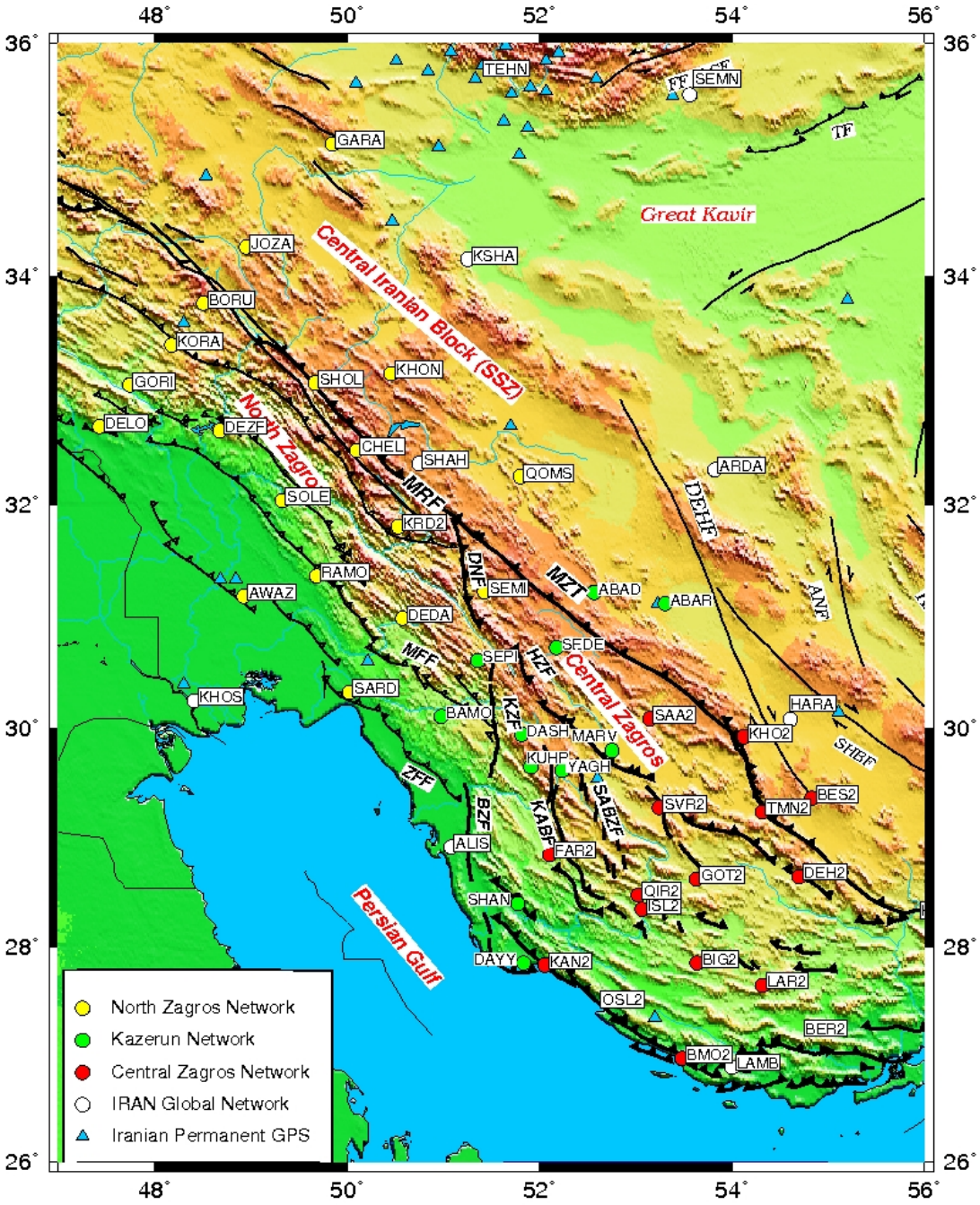

Figure 5-4. GPS networks in the Zagros mountain belt. ANF: Anar Fault, BZF: Borazjan Fault DEHF, Dehshir Fault, DNF: Dena Fault, HZF: High Zagros Fault, KABF: Karehbas Fault, KZF: Kazerun Fault, MFF: Main Frontal Fault, MRF: Main Recent Fault, MZT : Main Zagros Thrust, SABZF: Sabz-Pushan Fault, SHBF, Shahr Babak Fault, ZFF: Zagros Fore deep Fault.

5.2.1 Difference in the GPS deformation pattern of North and Central Zagros, Iran (Walpersdorf et al., 2006)

Difference in the GPS deformation pattern of North and Central Zagros (Iran)

A. Walpersdorf (1), D. Hatzfeld (1), H. Nankali (3), F. Tavakoli (3), F. Nilforoushan (3), M. Tatar (4), P. Vernant (2), J. Chéry (2) and F. Masson (2)

1) Laboratoire de Géophysique Interne et Tectonophysique, Grenoble, France
2) Laboratoire de Dynamique de la Lithosphère, Montpellier, France
3) National Cartographic Center, Research Department, Tehran, Iran
4) International Institute for Earthquake Engineering and Seismology, Tehran, Iran

Accepted *date.* Received *19/07/05*; in original form *19/07/05.*

Short title: Zagros deformation pattern.

Corresponding author: Andrea Walpersdorf, LGIT, Maison des Géosciences, BP 53, 38041 Grenoble Cedex 9, France, andrea.walpersdorf@obs.ujf-grenoble.fr, phone : +33-4-76828104, fax : +33-4-76828101

Summary.
Measurements on either side of the Kazerun Fault System in the Zagros Mountain Belt, Iran, show that the accommodation of the convergence of the Arabian and Eurasian Plates differs across the region. In northwest Zagros, the deformation is partitioned as 3-6 mm/yr of shortening perpendicular to the axis of the mountain belt, and 4-6 mm/yr of dextral strike-slip motion on northwest-southeast trending faults. No individual strike-slip fault seems to slip at a rate higher than ~2 mm/yr. In southeast Zagros, the deformation is pure shortening of 8 ± 2 mm/yr occurring perpendicular to the Simple Folded Belt and restricted to the Persian Gulf shore. The fact that most of the deformation is located in front of the Simple Folded Belt, close to the Persian Gulf, while seismicity is more widely spread across the mountain belt, confirms the decoupling of the surface sedimentary layers from the seismogenic basement. A comparison with the folding and topography corroborates a south-westward propagation of the surface deformation. The difference in deformation between the two regions suggests that right-lateral shear cumulates on the north-south trending Kazerun strike-slip fault system to 6 ± 2 mm/yr.

Keywords: Global Positioning System (GPS), Satellite geodesy, Continental deformation, Plate convergence, Fault motion, Zagros

Introduction

The aim of our GPS surveys is to study 1) the location of superficial deformation in a sedimentary cover decoupled from the basement (case of south-eastern Zagros), and 2) the different behaviour of deformation between south-eastern and north-western Zagros. This study will help to answer the following questions: Is the Zagros deformation field distributed or localized on individual faults? Is the transition between pure and oblique shortening, from south-eastern to north-western Zagros, visible in the present day deformation field? Is there any evidence for strain partitioning in north-western Zagros? How do the shallow sediments accommodate the present day deformation and how does this superficial deformation compare with the basement deformation as evidenced by the seismicity?

The tectonic settings of the Zagros are given by the Eurasia-Arabia collision, taking place entirely inside Iran's political borders. The current Eurasia-Arabia convergence rate is estimated to increase from west to east along the Iranian Persian Gulf line from 18 to 25 mm/yr oriented about 10° N (Fig. 1). This increase is due to the proximity of the Arabia-Eurasia Euler pole situated in North Africa at 27.9 ± 0.5 °N, 19.5 ± 1.4 °E with 0.41 ± 0.01 °/Myr (Vernant et al., 2004, corroborating Euler pole locations of McClusky et al., 2000, McClusky et al., 2003 and Sella et al., 2002). The shortening is concentrated on the Iranian territory mainly across two mountain ranges, the Alborz in the north, the Zagros in the south, but slip on several important strike-slip faults that bound non deforming blocks (e.g. Central Iran, Lut) also accommodate some shortening. At the south-eastern margin of the Arabia-

Eurasia collision zone, along the Makran, the shortening is absorbed by subduction of oceanic lithosphere beneath south-east Iran at 19.5 mm/yr (Vernant et al., 2004). In the Persian Gulf, no shortening is observed (Tatar et al., 2002). The first GPS results indicated that the south-eastern Zagros undergoes about 10 mm/yr of pure shortening (Tatar et al., 2002).

The Zagros mountain belt is approximately 1500 km long, 250–400 km wide, and runs from eastern Turkey, where it connects to the North- and East-Anatolian faults, to the Oman Gulf, where it dies out at the Makran subduction zone (Fig. 1). The belt lies on the former Arabian passive margin that is covered by up to 10 km of Infracambrian to Miocene sediments (e.g. Stocklin, 1974; Haynes and McQuillan, 1974; Stoneley, 1981). These sediments contain several layers of evaporite at different depths that decouple the surface deformation from the basement (Berberian, 1981, 1995; Berberian and King, 1981). During the Mesozoic, the Zagros underwent a major episode of convergence, mostly accommodated by subduction on the Main Zagros Thrust (MZT) (Stocklin, 1974; Stoneley, 1981). After the closure of the oceanic basins, a second episode of deformation during the Neogene led to the folding that affected the Simple Folded belt located between the Main Zagros Thrust and the Persian Gulf (Falcon, 1974).

The Zagros mountains are affected by the active NS trending Kazerun fault that offsets the folds and the lower Miocene terranes. Maximum and minimum displacement rates on the fault have been inferred from these offsets by Berberian (1981, 1995) and Authemayou et al. (2005) to 15 and 4 mm/yr, respectively. Present day activity of the Kazerun fault is evidenced by recent earthquakes with right-lateral mechanisms located on the fault (Baker et al., 1993). The Main Recent Fault (MRF) is an active NW-SE trending right-lateral strike-slip fault which runs along the Main Zagros Thrust (Berberian, 1995) and is observed northwest of the Kazerun fault (Tchalenko and Braud, 1974; Ricou et al., 1977). The Dorud segment of the Main Recent Fault is seismically the most active (Tchalenko and Braud, 1974; Berberian,

1981). A remarkable feature of the Zagros fold belt is that it propagates with time from the Main Zagros Thrust towards the Persian Gulf (Shearman, 1976; Falcon, 1974; Berberian, 1995; Hessami et al., 2001).

Most of the Zagros deformation seems to be aseismic (North, 1974; Jackson et al., 1995; Masson et al., 2005). The seismicity is located in the basement, probably on reactivated former normal faults, and seems to be concentrated in the west of the mountain belt, in a region with a topography lower than 1000 m (Talebian and Jackson, 2004).

Salt layers, present particularly in the south-eastern part of Zagros, are suspected to create decoupling of the superficial layers from the basement. If this is the case, the Zagros deformation, as observed by GPS in the south-eastern part, represents only the deformation of the sedimentary cover placed on top of the Arabian platform.

Talebian and Jackson (2004) proposed a kinematical description for the present day deformation of the Zagros mountain belt. The authors compiled earthquake slip vectors related to thrust and strike-slip events and compare them with respect to the overall constraints given by the NUVEL1-A (DeMets et al., 1994) or REVEL (Sella et al., 2002) plate models. According to the present day kinematics, the transition from pure shortening in south-east Zagros to oblique shortening in north-west Zagros is accommodated in the region of the Kazerun fault system.

GPS data

We have measured two GPS networks in Zagros, the Central Zagros network covering the south-eastern part, and the North Zagros network, covering the north-western part (see site locations on Fig. 3). Data were collected in campaigns during 2001 and 2003 (18 forced antenna centring sites in North Zagros) and 1997, 2000 and 2003 (15 sites with tripod antenna

setup in Central Zagros) using a mixture of Trimble SSI and Ashtech Z-12 receivers and choke ring antennae. Each site was observed for at least 48 h per campaign. During each campaign, we measured simultaneously some sites from the Iran Global network (KHOS, KSHA for North Zagros, ALIS, ARDA, LAMB for Central Zagros) (Nilforoushan et al., 2003; Vernant et al., 2004) to connect the different networks. Data from 3 Iranian permanent stations (AHVA, MASH, TEHR) were used in the campaign analyses when available. We also include the analysis of the GPS measurements (1999 and 2001) from the Iran Global network (Nilforoushan et al., 2003; Vernant et al., 2004) in the present study.

The data have been analysed with the GAMIT/GLOBK 10.1 software (King and Bock, 2002). 32 IGS stations have been included to establish the terrestrial reference frame. Final IGS orbits and corresponding Earth orientation parameters have been used. In the combination of daily solutions with the Kalman filter GLOBK, the continuous time series of daily SOPAC global solution files (IGS3 network) has been included from December 1997 to November 2003, covering all measurement epochs presented here.

The precision of the inferred site velocities has been evaluated by 1) the campaign repeatabilities, giving the short term scatter of the site coordinate estimates; 2) velocity residuals on locally inferred rigid tectonic blocks, evaluating long term uncertainties for the campaign stations (McClusky et al., 2000).

The average campaign repeatabilities are given in Table 1. They correspond to the increasing quality of the Central Zagros measurements (longer observation spans and more simultaneous observations by higher number of field teams). For the Central Zagros network, with a mean repeatability of 4 and 1 mm in 1997 and 2003 respectively on the horizontal components, we could expect velocity uncertainties of 1 mm/yr over the 6 years observation time span. Mean horizontal repeatabilities of 2 mm in the 2001 and 2003 North Zagros network yield a 2 mm/yr precision over the 2 years time span.

Table 1.

Systematic errors like tripod setup (in the Central Zagros network) or antenna phase centre offsets cannot be identified by the repeatability results only. These systematic errors do show up in the comparison of velocities for sites on the same tectonically rigid block. They contribute to the velocity residuals with respect to rigid block motion. Two rigid micro-blocks represented by several GPS sites can be used in this study to estimate velocity uncertainties (Fig. 2): The larger one is the Central Iranian block (stations MIAN, BIJA, SHAH, ARDA, HARA, KERM, the smaller one the Mesopotamian basin in the south of North Zagros (stations KHOS, AWAZ, AHVA, SARD, HAFT). We estimate horizontal residual velocities of 1.9 mm/yr on the Central Iranian block similar to Vernant et al. (2004). When we include 6 Central Zagros stations with low residual velocities with respect to Central Iran (SAA2, KHO2, BES2, SVR2, DEH2, TMN2, see Fig. 2), the average residuals with respect to a rigid motion of this block are evaluated to 1.2 mm/yr. In the Mesopotamian basin, south of North Zagros, the average residuals of the 5 site velocities KHOS, AWAZ, AHVA, SARD and HAFT are 2.2 mm/yr. These residuals with respect to a rigid block motion suggest that the uncertainty of the velocity estimates presented in this study is about 2 mm/yr with slightly smaller values for the Central Zagros measurements due to the 6 years observation span, in spite of the tripod setup in this network. Therefore, 2 mm/yr seems to be a conservative value for the uncertainties in both the Central and the Northern Zagros. This value will be used as a lower bound on deformation estimates in the tectonic interpretation (see below).

The Zagros velocity field

To focus on the Zagros deformation, we define a reference frame by minimizing the velocities of the stations located on the Central Iranian block (MIAN, BIJA, SHAH, ARDA, HARA and KERM, see Fig. 2) following Vernant et al. (2004). The velocity field we obtain on the Zagros networks with respect to the Central Iran block is shown in Table 2 and Figure 3a. A general value for the uncertainty of our velocity estimates is 2 mm/yr as indicated above.

Along the Persian Gulf (stations KHOS, SARD, ALIS, KAN2, OSL2, BMG2, LAMB), velocities of 6 to 10 mm/yr are observed representing the eastward increasing motion of the Arabian plate relative to Central Iran. While the eastern site velocities are aligned with the BAHR (Bahrain) velocity vector, the more westerly stations show a rotation to NNW. The transition between pure shortening in the east and oblique shortening in the west is located near the right-lateral Kazerun fault system (Kazerun, Sabs Pushan, Kareh Bas and Sarvestan faults, see Fig. 1 for fault locations). A large northern region of Central Zagros does not deform relative to the Central Iranian block as demonstrated by the low residual velocities of the GPS sites SAA2, KHO2, SVR2, TMN2, BES2 and DEH2. This low deformation suggests that the Main Zagros Thrust is inactive in this part of the Zagros and that the deformation in Central Zagros is concentrated further southwest, in the region close to the Persian Gulf shore. A more distributed velocity field is observed in North Zagros with velocities relative to Central Iran decreasing from 6 mm/yr at the coast to 3 mm/yr in the centre of the Zagros mountain belt and to zero on the northern side of the Main Recent Fault (MRF).

The Zagros velocity field indicates relative displacement rates of the order of 2 mm/yr (at the limit of resolution) across several individual faults. In the North Zagros, we find this magnitude of strike-slip activity for the Main Recent Fault (MRF) and for the Dena fault,

while for the Dezful Embayment fault (DEF) and for the Zagros Mountain Front Fault (MFF) the relative motion of 2 mm/yr is rather transpressive (for fault locations see Fig. 1). In the Central Zagros network, 4 to 6 mm/yr of shortening is restricted to the Zagros Mountain Front Fault (MFF). The difference in deformation between the two networks suggests 3 to 6 mm/yr of right-lateral strike-slip motion on the NS trending Kazerun fault system, distributed over the Kazerun, Borazjan, Kareh Bas (KB) and Sabz Pushan (SP) faults.

The Zagros velocity field is also represented with respect to the Arabian plate as the larger tectonical unit bordering the Zagros deformation belt (Fig. 3b). The Arabian plate reference frame has been established by applying the Arabia-Eurasia rotation pole established by Vernant et al. (2004) (27.9°N, 19.5°E, 0.41°/Myr), to the Zagros velocity field. The BAHR residual velocity is 0.4 mm/yr, and the residual velocities of the Iranian GPS sites along the Persian Gulf (AHVA, AWAZ, KHOS, SARD, ALIS, KAN2, OSL2, BMO2, LAMB) are evaluated to an average of 2.9 mm/yr mainly oriented W to WNW with larger values in the centre. The absence of velocity components parallel to the Arabia-Eurasia shortening axis and the velocity amplitudes hardly above the error limit of 2 mm/yr confirm the absence of shortening in the Persian Gulf.

The velocity field of northern Zagros has been estimated from only two measurements over a two years time span. Therefore, it is probably unreliable to analyse pairs of site velocities to quantify precisely the low (typically 2 mm/yr) displacement rates along individual faults. However, the analysis of subsets of site velocities (e.g. velocities along transects as shown in the next section) and of strain calculated over the whole velocity field or a subset of stations (as shown later) can be used to average the individual velocity observations and obtain a more significant characterization and quantification of the deformation in the Zagros networks.

The GPS site velocities are interpreted in this paper as constant, interseismic displacement rates. This supposes that no co-seismic instantaneous displacement is contained in the displacement rates of the GPS stations, due to earthquakes occurring close to the GPS stations in the time interval covered by the successive measurement campaigns. Seismic catalogues show that no significant earthquake (Ms >6) took place close to the stations in our network in the time between the surveys.

To infer fault slip velocities from GPS displacement rates, a deformation model would be necessary, taking into account the fault emplacements with respect to the GPS sites and the fault mechanisms. Both fault locations and motions are still poorly known for the Zagros, because most of the faults are blind faults (Berberian, 1995), so that in this work we restrict ourselves not to over-interpret single site velocities.

Table 2.

Comparison of the deformation between Central Zagros and North Zagros

The difference in deformation between Northern and Central Zagros can be highlighted by plotting the velocity distributions on transects (TN1, TN2, TN3 in the North Zagros, TC1 and TC2 in Central Zagros) perpendicular to the Zagros mountain belt (Fig. 4). We project the velocity of the closest stations onto directions parallel and perpendicular to the mountain axis and interpret these two directions as strike-slip and shortening components of active structures parallel to the Zagros mountain axis, with respect to Central Iran. The two velocity components are plotted with respect to the distance between the GPS site and the approximate emplacement of the Main Recent Fault (MRF) (Figure 4).

In order to illustrate (but not to compute) the deformation patterns, we superpose simple mechanical models on top of the velocity observations. For the strike-slip component,

we use a model of a locked strike-slip fault in an elastic half space (Savage and Burford, 1973) centred on the Main Recent Fault (MRF) or the Main Zagros Thrust (MZT). This model is evaluated for a locking depth at 10 km. Note that the locking depth is not significant for describing the velocity distribution on the spatial scale of the transects.

In the North Zagros, for TN1 and TN2, located north, most of the strike-slip deformation is associated with the Main Recent Fault (MRF), whereas for TN3, located further south, most of the strike-slip deformation is associated with the Zagros Mountain Front Fault (MFF). In the Central Zagros, the strike-slip component is approximately 2 mm/yr and it is located in the south-western part of the network, near the Persian Gulf. There is a marked difference between the two parts of Zagros because the total strike-slip velocities vary from 2 mm/yr in Central Zagros to 4-6 mm/yr in North Zagros.

For the compressive component we use a model with a uniformly distributed homogeneous strain over the whole Zagros, corresponding to a linear velocity distribution. This simple model is sufficient to analyse the shortening patterns related to the young continental collision taking place throughout the Zagros. In this case of shortening, we fit the model to the velocity observations. While in North Zagros the ensemble of site velocities fit a linear velocity distribution along the transects (and therefore a homogeneous strain), in Central Zagros the velocity gradients are constrained excluding the stations in the non-deformable part of Central Iran. We observe an increase of the shortening component from North Zagros to Central Zagros (from 2 mm/yr to 8 mm/yr) due to the proximity of the relative Arabia-Eurasia rotation pole (e.g. Sella et al., 2002; Vernant et al., 2004).

With an uncertainty of 2 mm/yr on our velocity estimates (not including the systematic bias that are not measurable before a third campaign), we will only provide a first order interpretation of the tectonics of the region and not try to estimate the strike-slip rates on individual faults of the Zagros folded belt (Main Recent Fault, High Zagros Fault, Zagros

Mountain Front Fault). The fault parallel component (strike-slip motion) in North Zagros increases from north to south (from transect TN1 to TN3) from 4 to 6 mm/yr. This strike-slip motion is observed along transect TN1 for the stations located on the Zagros folded belt (DELO-ILAM-GORI-DEZF-KORA-BORU) relative to Central Iran (GARA), on TN2 for the stations located south of the Dezful Embayment (AWAZ-HAFT) relative to the Zagros folded belt (SOLE-KORD-CHEL) and Central Iran (SHOL-KHON), and along transect TN3 for the stations located south of the Zagros Mountain Front Fault (ALIS-SARD) relative to the Zagros folded belt (DEDA-SEMI) and Central Iran (QOMS-ARDA).

Shortening is insignificant in the region spanned by the transect TN1 (DELO-GORI-KORA-BORU-JOZA). Further south, on transect TN2, the stations south of the Dezful Embayment fault (KHOS-AWAZ-HAFT) converge relative to the Zagros folded belt stations (SOLE-KORD-CHEL-SHOL-SHAH) with a velocity of about 3 ± 1 mm/yr. On transect TN3, the NS trending Kazerun fault marks a place of several mm/yr of shortening due to its obliqueness with respect to the profile.

For the Central Zagros, a fault parallel motion of 2 ± 1 mm/yr relative to Central Iran affects the westernmost stations (KHAN-OSL2-FAR2) suggesting that a small amount of strike-slip motion (with respect to the orientation of the MRF/MZT) is accommodated by the Kazerun fault system. On the contrary, the shortening shows a large gradient of up to 8 mm/yr between stations located on the Persian Gulf shore (KAN2-OSL2 on TC1 and BMG2-LAMB on TC2) and all other stations located further north (SAA2-TMN2-KHO2-HARA on TC1 and DEH2-KERM on TC2). Only the two stations BIG2 and LAR2 located further inland show a slow convergence (3 ± 1 mm/yr) toward Central Iran. This suggests that most of the shortening (75%) is accommodated by structures located along the Persian Gulf such as the Zagros Mountain Front Fault (MFF).

Slip rates for the Kazerun fault system

As seen in Figure 1, the Kazerun fault system separates the Zagros into two regions of contrasting deformation systems and therefore it should accommodate some differential motion. We can infer velocity estimates on different segments of the Kazerun fault system by comparing the velocity fields in the North and the Central Zagros on each side of the fault system.

The two stations located south of the Zagros Mountain Front Fault (KAN2 and ALIS) on either side of the fault system show similar motion relative to Central Iran which suggests that they both belong to the non deformable part of the Arabian plate. But going further north, we measure 3 ± 2 mm/yr of relative NS displacement between ALIS and FAR2, which characterizes the slip rate in the southern part of the Kazerun fault system. We also measure 3 ± 2 mm/yr between DEDA and SEMI which can be attributed to the Dena fault. The motion on the Karebas and on the Sabz Pushan faults can be estimated from the comparison between FAR2 and QIR2 on one hand and FAR2 and SVR2 on the other hand, suggesting a motion of about 2 ± 2 mm/yr of the Karebas fault and almost of the same order on Sabz Pushan. Therefore, the cumulated motion accommodated by the total Kazerun strike-slip fault system is of about 6 ± 2 mm/yr.

The Zagros strain distribution

The strain tensors obtained over 19 stations in the North Zagros and 15 stations in Central Zagros are shown in Figure 5a. Over the whole North Zagros network, we see a

dominating compressive component oriented perpendicular to the mountain axis. A smaller extensive component is assumed to be due to a strike-slip component present in the overall deformation pattern. In Central Zagros, we notice higher strain rates (25%) on both the compressive and the extensive component with respect to North Zagros. The decrease of the overall deformation rates from Central to North Zagros could be due to two reasons: First, the North Zagros network is larger than the Central Zagros network, so that the velocity differences are spread over larger distances; second, the relative motion between Arabia and Eurasia decreases from east to west according to the Eurasia-Arabia rotation pole (Vernant et al., 2004).

In order to compare the distribution of the deformation in both the Northern and Central Zagros, we define several subnetworks (3 in the south-east and 5 in the north-west) of similar sizes to compare strain rates (Figure 5b). The numerical values are summarized in Table 3. The formal errors of the strain estimates are 10 - 15 nanostrain/yr. We conclude that significant deformation can be shown by the present analysis in subnetworks where values of more than 10 – 15 nanostrain/yr are obtained. The values observed for two subnetworks being situated in supposedly non deforming parts of the network, NZ1 in the Mesopotamian basin in the North Zagros, and CZ1 in the northern part of Central Zagros, are of 5 - 10 nanostrain/yr. Based on significant strain observations, we note that the strain distribution is different in Central Zagros with respect to North Zagros. In Central Zagros, the compressional axes are parallel to each other and perpendicular to the fold axes and most of the deformation is concentrated in one band along the Persian Gulf coast, in CZ3. In North Zagros, the compressional axes vary in orientation, and two separate zones of significant deformation can be distinguished, NZ2, and NZ4a and NZ4b. This analysis of the strain rates in subnetworks shows that the deformation is not homogeneously distributed but concentrated in zones

located near active faults, such as the MFF (CZ3) in Central Zagros, and the DEF/MFF (NZ2) and the MRF (NZ4a/b) in North Zagros.

Table 3.

Comparison with seismicity

To compare the shallow deformation with the basement deformation, we have to compare the GPS results with seismicity. Two cross sections across the Zagros (Figure 6) have been chosen to study the distribution of seismicity with respect to the Zagros topography and the GPS measured surface displacement rates. The topography shows that the width of the belt in North Zagros is much narrower than in Central Zagros (~200 versus ~350 km). However, the average altitude of the deforming belt (the Simple Fold Belt) is lower in North Zagros (excluding Mt. Dena which is in a peculiar region) than in Central Zagros, while one expects that comparable deformation over a narrower range would lead to higher altitudes. One explanation for this difference is the additional strike-slip motion present in North Zagros while Central Zagros deformation is dominated by thrusting. This means that, contrary to the Central Zagros, the crust is not trapped in North Zagros but can escape from pure shortening (and therefore folding) by lateral translation along strike-slip faults such as the Main Recent Fault. A second reason for the lower deformation in North Zagros is the decrease of relative motion in the Arabia-Eurasia collision with respect to Central Zagros.

Talebian and Jackson (2004) showed that larger magnitude seismicity is restricted to the edge of the Zagros fold belt and therefore could be associated with only the most recent of the faults proposed by Berberian (1995) in the Zagros. This was even more apparent when considering only the earthquakes of magnitude Mb > 5 that are located in regions of low topography. However, microearthquake seismicity is spread on a wider region (Tatar et al.,

2003). We plotted both the total seismicity available in the ISC catalogue and the relocated earthquakes of magnitude mb>5 (Engdahl et al., 1998) in Fig. 6. The superficial deformation of Central Zagros inferred from GPS measurements is much more concentrated along the Persian Gulf coast than shown by the seismicity (Figure 6, TC1). Models of the Zagros folded deformation are derived from balanced cross sections of the sedimentary cover (i.e. McQuarrie, 2004; Sherkaty and Letouzey, 2004; Molinaro et al., 2005). These models assume that the sedimentary cover folds whereas the basement is affected by active faults. Some of the listed authors assume that every fold is related to an active fault. If the sedimentary cover is totally decoupled from the basement, then there is no need for the surface folds to be located at the same place as the active faults in the basement (Tatar et al., 2004). The only constraint is that both the deformation of the basement (seismicity) and of the shallow sedimentary cover (GPS) should be of comparable value. But the comparison between the brittle deformation evidenced by earthquake activity and the total deformation inferred by strain from GPS measurements shows that only 10% of the total deformation in Zagros is released by earthquakes (North, 1974; Jackson and McKenzie, 1988; Masson et al., 2005).

There are two possible explanations for the relatively aseismic deformation of the Zagros. Firstly, that the amount of deformation of the basement is smaller (by 80%) than the deformation evidenced at surface by GPS. This implies that the Zagros basement underthrusts beneath the Central Iran region to the northeast, as an active subduction. This seems unlikely because we do not observe any seismicity located north of the MZT that acted as the suture of former subduction (Talebian and Jackson, 2004; Maggi et al., 2000). Secondly, that the mechanical properties do not allow all the deformation to release seismic energy probably because of the unusually large thickness of the sedimentary cover that reduces the thickness of the brittle crust.

Conclusions

The two GPS surveys in the North Zagros give a consistent velocity field relative to Central Iran. The third survey in Central Zagros increases the precision of the velocity field and allows a comparison with North Zagros. The average velocity uncertainties are evaluated to 2 mm/yr.

Present day deformation in the North Zagros is characterized by cumulated 3-6 mm/yr of shortening and cumulated 4-6 mm/yr of right-lateral strike-slip, consistent with first estimates from the larger scale Iran Global GPS network (Vernant et al., 2004). This strike-slip motion is lower than the 10-17 mm/yr proposed on only the Main Recent Fault by Talebian and Jackson (2002). Talebian and Jackson suggested this slip rate based on the assumption that the observed offset of 50 km on the MRF was achieved in 3-5 Ma. If we assume a constant slip rate of at most 4-6 mm/yr (cumulated slip rate across the whole North Zagros mountain belt), the MRF has formed not earlier than 10 Ma ago. In our study, 2-3 mm/yr of slip rate have been localized on the Main Recent Fault, resulting in a fault age of 25 Ma. We can compare these estimates for the Main Recent Fault with those of the Kazerun fault, as their respective onsets are certainly related. On the Kazerun fault, fault offsets between 12-27 km (minimal values, Authemayou et al., 2005) and 140 km (Berberian 1995) have been suggested. The GPS inferred present day displacement rates we can take into account are 6 ±2 mm/yr (maximum value inferred across the whole Kazerun strike-slip fault system) and 2 mm/yr (restricted to the Kazerun fault sensu-stricto). Considering fault offsets of around 20 km, the latest onset time is about 3 Ma with a constant displacement rate of 6 ± 2 mm/yr, the earliest onset time is about 10 Ma with a constant slip rate of 2 mm/yr. These estimates are lower, but reaching the same order of magnitude as for the Main Recent Fault. This could evidence a simultaneous onset of both faults. The Kazerun fault offset of 140 km

as postulated by Berberian (1995) implies an earliest onset 35 Ma ago and does not seem to correspond to the same tectonical period.

In Central Zagros, 8 mm/yr of shortening and 2-3 mm/yr of strike-slip motion are observed, consistent with the first results of Tatar et al. (2002). This increase of the rate of shortening in Central Zagros compared to North Zagros is consistent with the location of the Arabia-Eurasia rotation pole which predicts an increase of 4 mm/yr for the NS component between KHOS and LAMB. We confirm Tatar et al.'s (2002) result that the MZT is currently inactive but the Central Zagros velocity field is distributed differently than proposed by Tatar et al. (2002). The northern region not deforming relatively to the Central Iranian block is spread over a larger zone, and the shortening is more concentrated along the coast of the Persian Gulf. In both studies, a small strike-slip component is observed in the western part of the network near the Kazerun strike-slip fault system, coherent to Talebian and Jackson's (2004) kinematical description.

The GPS measured deformation of Central Zagros concentrated along the coast is consistent with geomorphological observations (such as growth rates of folds evidenced by terrace uplifts, Vita-Finzi, 1987, Oveisi, personal communication, 2005) and supports a model of propagation of the folding deformation to the SW (Shearman, 1976; Hessami et al, 2001). The comparison between the superficial deformation concentrated along the coastline and the more widely spread seismicity confirms the decoupling of the sedimentary layer from the basement.

The North Zagros velocity field is more complex with the presence of shortening and strike-slip distributed across the belt. The strike-slip motion is likely associated with the MRF and shortening with the Dezful Embayment Fault but our data do not help to quantify this motion on single faults. No individual fault seems to present slip rates of more than 2 mm/yr.

Therefore, the deformation occurring in the Central Zagros (pure shortening) is different from that in North Zagros (partitioned between shortening and strike-slip), as is suggested by tectonic and seismological observations (*i.e.* Ricou et al., 1977; Berberian, 1995; Talebian and Jackson, 2004, Authemayou et al., 2006) and the morphology. The two parts of the Zagros are separated by the Kazerun fault system across which right-lateral strike-slip occurs at ~2-3 mm/yr on individual fault segments, yielding a cumulated strike-slip rate of 6 ± 2 mm/yr.

Acknowledgements

The GPS campaigns have been successful thanks to the help of many colleagues: M. Peyret, M.-N. Bouin, C. Sue, and the field teams of NCC and IIEES in Tehran. This project was financed by the CNRS-INSU « Intérieur de la Terre » programme, the NCC and the IIEES. H. Nankali, F. Nilforoushan, M. Tatar and F. Tavakoli were partially supported by the French Embassy in Tehran. The GPS receivers were provided by CNRS-INSU and NCC. We benefited from interesting discussions with M. Berberian, J. Jackson, P. Molnar, M. Talebian, C. Vita-Finzi and P. Tregoning and from a constructive review by V. Regard.

References

Authemayou, C., O. Bellier, D. Chardon, Z. Malekzade, and M. Abassi, 2005. Role of the Kazerun fault system in active deformation of the Zagros fold-and-thrust belt (Iran), Comptes Rendus Geoscience, Vol. 337, Iss. 5, 475-547.

Authemayou, C., D. Chardon, O. Bellier, Z. Malekzade, I. Shabanian and M. Abbassi, 2006. Late Cenozoic Partitioning of oblique plate convergence in the Zagros Fault-and-Thrust belt (Iran), *Tectonics*, submitted.

Baker, C., J. Jackson and K. Priestley, 1993. Earthquakes on the Kazerun Line in the Zagros mountains of Iran: Strike-slip faulting within a fold-and-thrust belt, *Geophys. J. Int.*, 115, 41-61.

Berberian, M., 1981. Active faulting and tectonics of Iran, in *Zagros-Hindu-Kush-Himalaya Geodynamic evolution*, edited by H. K. Gupta and F. M. Delany, Am. Geophys. Union, Geodyn. Ser., 3, 33-69.

Berberian, M., and King, G.C.P., 1981. Towards a paleogeography and tectonic evolution of Iran, *Can. J. Earth Sci.*, 18, 210-265.

Berberian, M., 1995. Master blind thrust faults hidden under the Zagros folds: Active basement tectonics and surface morphotectonics, *Tectonophysics*, 241, 193-224.

DeMets, C., Gordon, R.G., Argus, D.F., and Stein, S., 1994. Effects of recent revisions to the geomagnetic reversal time scale on estimates of current plate motions, *Geophys. Res. Lett.*, 21, 2191-2194.

Engdahl, E. R., Van der Hilst, R. D., and Buland, R. P., 1998. Global teleseismic earthquake relocation with improved travel times and procedures for depth determination, *Bull. Seism. Soc. Am.*, **88**, 722-743.

Falcon, N., 1974. Southern Iran: Zagros Mountains, in *Mesozoic-Cenozoic Orogenic Belts*, edited by Spencer, Spc. Publ. Geol. Soc. London, 4, 199-211.

Haynes, S. J., and H. McQuillan, 1974. Evolution of the Zagros suture zone, southern Iran, *Bull. Geol. Soc. Am.*, 85, 739-744.

Hessami, K., Koyi, H., Talbot, C. J., Tabasi, H., and Shabanian, E., 2001. Progressive unconformities within and evolving foreland fold-thrust belt, Zagros Mountains, *J. of the Geol. Soc. of London*, 158, 969-981.

Jackson, J. and D. McKenzie, 1988. The relationship between plate motions and seismic moment tensors and the rates of active deformation in the Mediterranean and Middle East, *Geophys. J. R. Astr. Soc. London,* 83, 45-73.

Jackson, J., Haines, J., and Holt, W., 1995. The accommodation of Arabia-Eurasia plate convergence in Iran, *J. Geophys. Res.*, 15,205-15,219.

King, R.W., and Bock, Y., 2002. *Documentation for the GAMIT analysis software*, release 10.1, Massachusetts Institute of Technology, Cambridge, MA.

Maggi, A., Jackson, J. A., Priestley, K., and Baker, C., 2000. A re-assessment of focal depth distributions in Southern Iran, the Tien Shan and Northern India: Do earthquakes really occur in the continental mantle? *Geophys. J. Int*., 143, 629-661.

Masson, F., J. Chéry, D. Hatzfeld, J. Martinod, P. Vernant, F. Tavakoli and M. Ghafory-Ashtiani, 2005. Seismic versus aseismic deformation in Iran inferred from earthquakes and geodetic data, *Geophys. J. Int.*, 160, 217-226.

McClusky, S., et al., 2000. Global Positioning System constraints on plate kinematics and dynamics in the eastern Mediterranean and Caucasus, *J. Geophys. Res.*, 105, 5695-5719.

McClusky, S., R. Reilinger, S. Mahmoud, D. Ben Sari and A. Tealeb, 2003. GPS constraints on Africa (Nubia) and Arabia Plate motions, *Geophys. J. Int*., 155, 126-138.

McQuarrie, N., 2004. Crustal scale geometry of the Zagros fold-thrust belt, Iran, *J. Struct. Geol.*, 26, 519-535.

Molinaro, M., Zeyen, H., and Laurencin, X., 2005. Lithospheric structure underneath the south-eastern Zagros Mountains, Iran: recent slab break-off?, *Terra Nova*, 17, 1-6.

Nilforoushan, F., F. Masson, P. Vernant, C. Vigny, J. Martinod, M. Abbassi, H. Nankali, D. Hatzfeld, R. Bayer, F. Tavakoli, A. Ashtiany, E. Doerflinger, M. Daignières, P. Collard, J. Chéry, 2003. GPS network monitors the Arabia-Eurasia collision deformation in Iran, *J. of Geodesy*, 77, 411-422.

North, R. G., 1974. Seismic slip rates in the Mediterranean and the Middle East, *Nature*, 252, 560-563.

Ricou, L. E., J. Braud, and J. H. Brunn, 1977. Le Zagros, *Mém. H. Sér. Soc. Géol. Fr.*, 8, 33-52.

Savage, J., and Burford, R., 1973. Geodetic determination of relative plate motion in Central California, *J. Geophys. Res.*, 95, 4873-4879.

Sella, G.F., Dixon, T.H. and Mao, A., 2002. REVEL: a model for recent plate velocities from space geodesy, *J. Geophys. Res.*, 107(B4), ETG 11-1, 11-32.

Sherkaty, S., and J. Letouzey, 2004. Variation of structural style and basin evolution in the central Zagros (Izeh zone and Dezful Embayment), Iran, *Marine and Petroleum Geology*, Vol. 21, No. 5, pp 535-.

Shearman, D. J., 1976. Geological evolution of Southern Iran – report of Iranian Makran Expedition, *Geographical Journal*, 142, 393-410.

Stocklin, J., 1974. Possible ancient continental margin in Iran, in *Geology of Continental Margins*, edited by C. Burke and C. Drake, Springer-Verlag, New York, 873-877.

Stoneley, R., 1981. The geology of the Kuh-e-Dalneshin area of southern Iran, and its bearings on the evolution of southern Thetys, *J. Geol. Soc. London*, 138, 509-526.

Talebian, M., and Jackson, J., 2002. Offset on the Main Recent Fault of the NW Iran and implications on the late Cenozoic tectonics of the Arabia-Eurasia collision zone, *Geophys. J. Int.*, 150, 422-439.

Talebian, M., and Jackson, J., 2004. A reappraisal of earthquake focal mechanisms and active shortening in the Zagros mountains of Iran, *Geophys. J. Int.*, 156, 506-526.

Tatar, M., Hatzfeld, D., Martinod, J., Walpersdorf, A., Ghafori-Ashtiany, M., and Chéry, J., 2002. The present-day deformation of the central Zagros from GPS measurements, *Geophys. Res. Lett.*, 29 (19), 1927.

Tatar, M., Hatzfeld, D., and Ghafory-Ashtiany, M., 2003. Tectonics of the Central Zagros (Iran) deduced from microearthquake seismicity, *Geophys. J. Int.*, **156**, 255-266.

Tchalenko, J. S., and J. Braud, 1974. Seismicity and structure of the Zagros (Iran) – the Main Recent Fault between 33 and 35°N, *Phil. Trans. Roy. Soc. London*, 277, 1-25.

Vernant, P., Nilforoushan, F., Hatzfeld, D., Abbassi, M.R., Vigny, C., Masson, F., Nankali, H., Martinod, J., Ashtiany, A., Bayer, R., Tavakoli, F., and Chéry, J., 2004. Present-day crustal deformation and plate kinematics in the Middle East constrained by GPS measurements in Iran and northern Oman, *Geophys. J. Int.*, 157, 381-398.

Vita-Finzi, C., 1987. 14C deformation chronologies in coastal Iran, Greece and Jordan, *J. Geol. Soc. of London*, 144, 553-560.

Figure legends:

Figure 1: Location of the Zagros major active faults (Berberian, 1995) and seismicity (Engdahl et al., 1998). The inset displays the global location of Zagros and Iran in the collision zone between the Arabian and Eurasian plates. The velocity vectors indicate the Arabia-Eurasia collision rate according to the rotation pole of Vernant et al., 2004. Zagros active faults are reported: MRF: Main Recent Fault; MZT: Main Zagros Thrust; HZF: High Zagros Fault; DEF: Dezful Embayment Fault; MFF: Zagros Mountain Front Fault; ZFF: Zagros Fore deep Fault; Dena fault; Kazerun fault; Borazjan fault; KB: Kareh Bas fault; SP: Sabz Pushan fault; S: Sarvestan fault; SFB: Simple Fold Belt (Berberian, 1995).

Figure 2: Identification of the two Iranian rigid blocks used for establishing the velocity precisions by evaluating the velocity residuals with respect to rigid block motion: The Central Iranian Block (stations MIAN, BIJA, SHAH, ARDA, HARA, KERM) which can be extended to the northern Central Zagros (stations SAA2, KHO2, SVR2, TMN2, DEH2, BER2), and the Mesopotamian basin (Stations AHVA, AWAZ, HAFT, KHON, SARD).

Figure 3a: North Zagros and Central Zagros velocity fields with respect to the Central Iranian block. The scale vector corresponds to 5 mm/yr. The error ellipses indicate formal errors within a 95 % confidence interval. The different networks (North Zagros, Central Zagros and Iran Global) are marked with different symbols. We observe a different velocity field on both sides of the Kazerun Fault system.

Figure 3b: North Zagros and Central Zagros velocity fields with respect to the Arabian Plate. Same captions as Fig 3a.

Figure 4: Site velocities (mm/yr) with respect to the site distance to the Main Recent Fault (MRF) / Main Zagros Thrust (MZT) (in km, on the x axis) on 5 transects (locations shown on the map), TN1, TN2 and TN3 in the North Zagros, TC1 and TC2 in the Central Zagros, from northwest to southeast. On the left, we display the fault parallel components (strike-slip component), on the right, the fault perpendicular component (shortening). A simple model is superposed on the individual velocities (dark grey lines, for details see text).

Modelled total strike-slip velocities vary from 2 to 6 mm/yr, strain rates from 8 to 39 nanostrain/yr. Light grey vertical lines indicate fault locations.

Figure 5a: Overall strain rates in the North and Central Zagros networks. Numerical values are indicated in Table 3.

Figure 5b: Strain rates in subnetworks. Black and white strain crosses distinguish relatively high and low deformation rates, respectively.

Figure 6: On the two transects TN2 and TC1 we display a) the topography, b) the seismicity (open circles: USGS, black circles: Engdahl et al., 1998), c) NW-SE strike-slip motion parallel to MRF/MZT, d) shortening perpendicular to MRF/MZT. The approximate location of different faults is indicated by vertical lines. Horizontal arrows indicate that the surface deformation evidenced by GPS measurement is concentrated in narrow areas, whereas the basement deformation evidenced by the seismicity is distributed in a larger area, suggesting a decoupling between the two.

Tables:

Repeatabilities [mm]:

Campaign	epoch	#bl	N	E	U
C. Zagros	1997.918	25	2.8	3.0	7.4
C. Zagros	2000.096	144	1.7	2.0	5.2
N. Zagros	2001.721	233	1.1	1.7	4.7
N. Zagros	2003.690	231	0.7	1.5	3.2
C. Zagros	2003.885	206	0.9	1.3	2.8

Table 1: Mean repeatabilities on the north, east and vertical baseline components in each of the 5 campaigns presented in this paper. This statistic is limited on the local North Zagros and Central Zagros network stations with maximum baseline lengths of 3000 km. # bl is the number of measured baselines entering in the statistics.

GPS station velocities [mm/yr]

	positions		velocities w.r.t. Iran Central Block		ITRF2000 velocities		velocity uncertainties (95% conf. interval)	
SITE (net)	long (°E)	lat (°N)	v east	v north	v east	v north	sig v east	sig v north
MIAN (IG)	46.162	36.908	-.06	1.34	23.87	23.55	1.59	1.46
ILAM (IG)	46.427	33.648	-.65	3.98	24.14	26.11	1.61	1.47
DELO (NZ)	47.429	32.692	.02	3.31	25.26	25.44	1.53	1.51
GORI (NZ)	47.739	33.057	-2.05	3.75	23.15	25.93	1.51	1.49
BIJA (IG)	47.930	36.232	-.46	.24	24.02	22.39	1.66	1.50
KORA (NZ)	48.175	33.406	.70	3.44	25.91	25.57	1.50	1.48
KHOS (IG)	48.409	30.246	.14	6.27	26.16	28.32	1.06	1.02
BORU (NZ)	48.506	33.772	-2.89	1.05	22.32	23.13	1.50	1.48
DEZF (NZ)	48.678	32.657	-2.45	4.58	23.06	26.66	1.50	1.48
AHVA (IP)	48.684	31.340	-.29	5.56	25.57	27.64	1.42	1.41
AWAZ (NZ)	48.925	31.188	-1.66	7.12	24.23	29.25	1.50	1.48
JOZA (NZ)	48.952	34.256	-1.84	2.71	23.36	24.77	1.50	1.48
SOLE (NZ)	49.328	32.037	-2.19	4.71	23.62	26.84	1.50	1.48

HAFT (NZ)	49.571	31.484	-1.02	7.96	24.97	29.96	1.50	1.48
SHOL (NZ)	49.668	33.073	.40	.72	26.10	22.75	1.51	1.49
GHAR (NZ)	49.851	35.140	-.26	.28	24.88	22.34	1.51	1.49
SARD (NZ)	50.026	30.325	-1.32	6.88	24.93	28.88	1.52	1.49
CHEL (NZ)	50.098	32.482	-2.80	3.75	23.12	25.81	1.51	1.49
KHON (NZ)	50.458	33.157	-1.82	-.06	23.96	21.99	1.51	1.49
KRD2 (NZ)	50.531	31.808	-3.25	1.71	22.80	23.76	1.50	1.48
DEDA (NZ)	50.578	30.990	1.05	3.85	27.31	25.63	1.51	1.48
BAHR (IGS)	50.608	26.209	4.83	6.74	31.99	28.76	0.52	0.23
SHAH (IG)	50.748	32.367	-.79	-.56	25.22	21.44	1.56	1.45
ALIS (IG)	51.082	28.919	-.87	8.17	25.92	30.13	1.04	1.00
KSHA (IG)	51.255	34.150	.21	-.60	25.94	21.34	1.05	1.02
TEHN (IP)	51.334	35.697	-.78	-3.02	24.59	18.94	1.39	1.38
TEHR (IG)	51.386	35.747	.81	-1.27	26.16	20.68	1.65	1.51
SEMI (NZ)	51.430	31.225	-2.93	.19	23.40	22.21	1.51	1.49
NOSH (IG)	51.768	36.586	-2.10	-3.09	23.17	18.79	1.71	1.50
QOMS (IG)	51.799	32.250	-1.90	.75	24.32	22.67	1.51	1.48
KAN2 (CZ)	52.056	27.834	.87	8.10	28.01	30.03	0.88	0.86
FAR2 (CZ)	52.106	28.851	-1.88	5.32	25.08	27.19	0.88	0.85
OSL2 (CZ)	52.607	27.474	.11	9.16	27.36	30.98	1.63	1.52
QIR2 (CZ)	53.029	28.477	-2.08	1.53	25.11	23.38	0.84	0.83
ISL2 (CZ)	53.066	28.347	-1.42	2.60	25.87	24.40	0.86	0.84
SAA2 (CZ)	53.146	30.087	.03	-.92	27.03	20.92	0.95	0.88
SVR2 (CZ)	53.244	29.281	-1.48	.04	25.63	21.94	0.88	0.85
BMG2 (CZ)	53.480	26.970	3.15	5.81	30.67	28.35	1.08	1.08
SEMN (IG)	53.564	35.662	.15	-5.82	26.07	15.94	1.64	1.48
GOT2 (CZ)	53.631	28.624	-.70	2.42	26.57	24.23	0.99	0.95
BIG2 (CZ)	53.637	27.852	-.56	1.52	26.81	23.37	0.92	0.90
ARDA (IG)	53.822	32.313	.10	-.75	26.78	21.02	1.02	1.00
LAMB (IG)	54.004	26.883	3.50	7.22	31.14	28.92	1.08	1.01
KHO2 (CZ)	54.126	29.923	-1.42	.24	25.70	22.02	0.86	0.85
KORD (IG)	54.199	36.860	-.78	-9.41	24.94	12.04	1.67	1.49
TMN2 (CZ)	54.316	29.239	-1.85	-.67	25.44	21.06	0.86	0.85
LAR2 (CZ)	54.320	27.644	.59	4.33	28.16	26.07	0.89	0.86
HARA (IG)	54.608	30.079	1.20	.99	28.41	22.71	1.63	1.47
DEH2 (CZ)	54.700	28.645	-2.15	-.44	25.34	21.31	0.87	0.85
BES2 (CZ)	54.832	29.363	-1.32	-.40	26.08	21.32	0.87	0.85
ROBA (IG)	56.070	33.369	1.56	-4.11	28.45	17.48	1.60	1.46
KHAS (IG)	56.233	26.208	3.32	9.79	31.43	31.31	1.83	1.50
KERM (IG)	57.119	30.277	.56	.79	28.22	22.25	2.45	1.66

Table 2: GPS velocity field with respect to the Central Iranian Block (CIB) and with respect to ITRF 2000. Networks: IG: Iran Global; NZ: North Zagros; CZ: Central Zagros; IP: Iran permanent; IGS: International GPS Service.

North and Central Zagros Strain Rates in nanostrain/yr

	North Zagros	*Major Axis*	*Sec. Axis*	Central Zagros	*Major Axis*	*Sec. Axis*
main networks:	NZ	-16.5 ± 3.0	3.9 ± 2.5	CZ	-27.3 ± 3.0	9.2 ± 2.9
subnetworks:	NZ1	-5.5 ± 10.8	2.6 ± 9.9	CZ1	-10.7 ± 6.8	-2.6 ± 5.2
	NZ2	**-16.9 ± 14.9**	**-6.8 ± 9.3**	CZ2	-23.4 ± 1.2	11.1 ± 3.8
	NZ3	-7.7 ± 15.1	5.4 ± 15.8	**CZ3**	**-57.0 ± 7.4**	**14.6 ± 3.7**
	NZ4a	**-22.5 ± 14.3**	**2.0 ± 7.8**			
	NZ4b	**-14.2 ± 13.0**	**2.6 ± 11.2**			

Table 3: Strain rate values and their uncertainties for the main networks, for the 5 North Zagros subnetworks and the 3 Central Zagros subnetworks. The most significant values in the subnetworks are highlighted. For the localisation of the subnetworks refer to Figure 5b.

Figures:

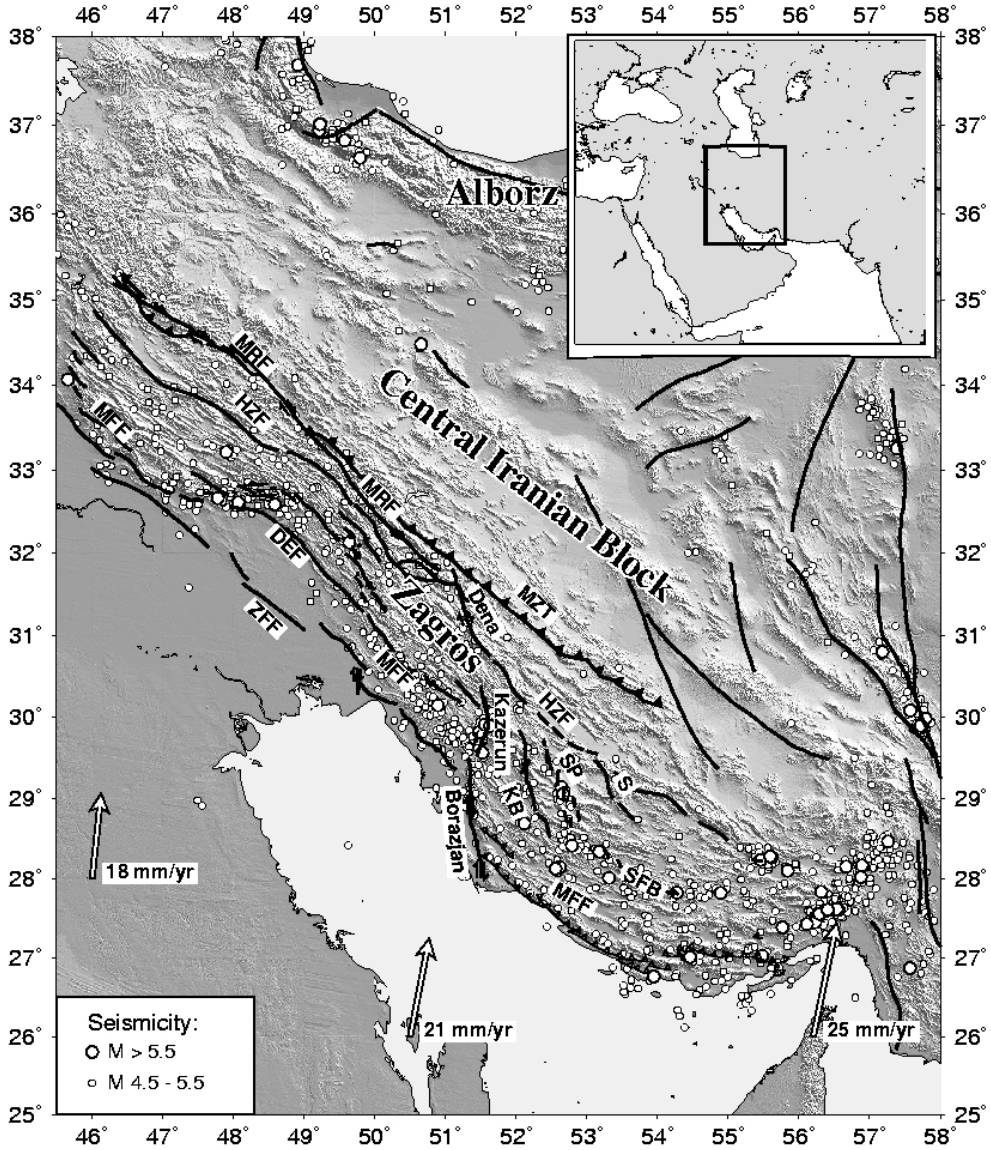

Figure 1: Location of the Zagros major active faults (Berberian, 1995) and seismicity (Engdahl et al., 1998). The inset displays the global location of Zagros and Iran in the collision zone between the Arabian and Eurasian plates. The velocity vectors indicate the Arabia-Eurasia collision rate according to the rotation pole of Vernant et al., 2004. Zagros active faults are reported: MRF: Main Recent Fault; MZT: Main Zagros Thrust; HZF: High Zagros Fault; DEF: Dezful Embayment Fault; MFF: Zagros Mountain Front Fault; ZFF: Zagros Fore deep Fault; Dena fault; Kazerun fault; Borazjan fault; KB: Kareh Bas fault; SP: Sabz Pushan fault; S: Sarvestan fault; SFB: Simple Fold Belt (Berberian, 1995).

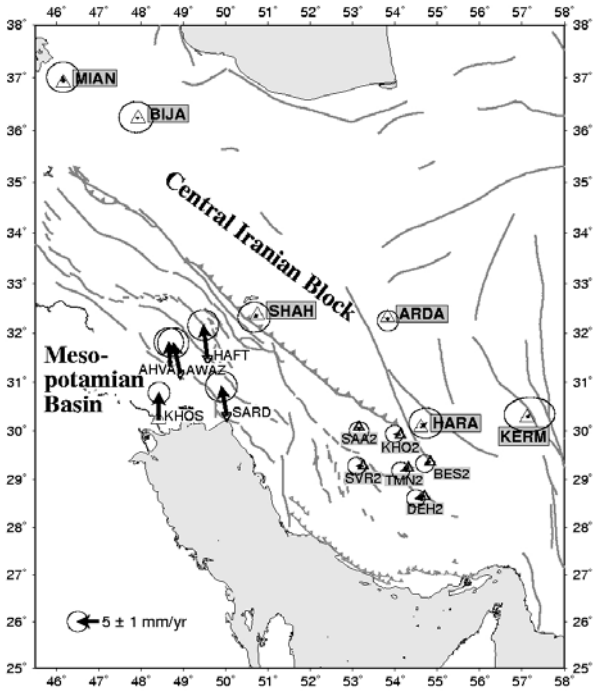

Figure 2: Identification of the two Iranian rigid blocks used for establishing the velocity precisions by evaluating the velocity residuals with respect to rigid block motion: The Central Iranian Block (stations MIAN, BIJA, SHAH, ARDA, HARA, KERM) which can be extended to the northern Central Zagros (stations SAA2, KHO2, SVR2, TMN2, DEH2, BER2), and the Mesopotamian basin (Stations AHVA, AWAZ, HAFT, KHON, SARD).

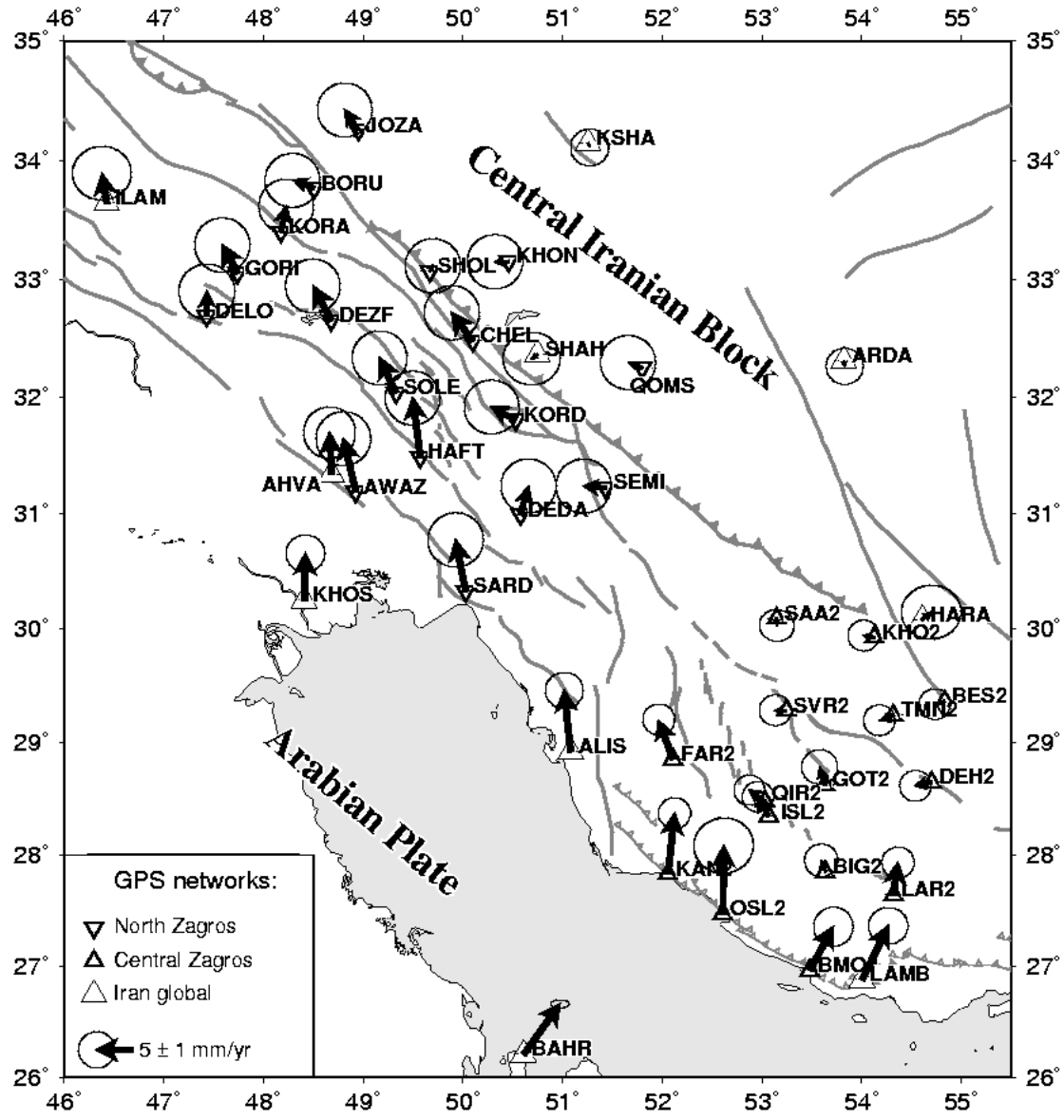

Figure 3a: North Zagros and Central Zagros velocity fields with respect to the Central Iranian block. The scale vector corresponds to 5 mm/yr. The error ellipses indicate formal errors within a 95 % confidence interval. The different networks (North Zagros, Central Zagros and Iran Global) are marked with different symbols. We observe a different velocity field on both sides of the Kazerun Fault system.

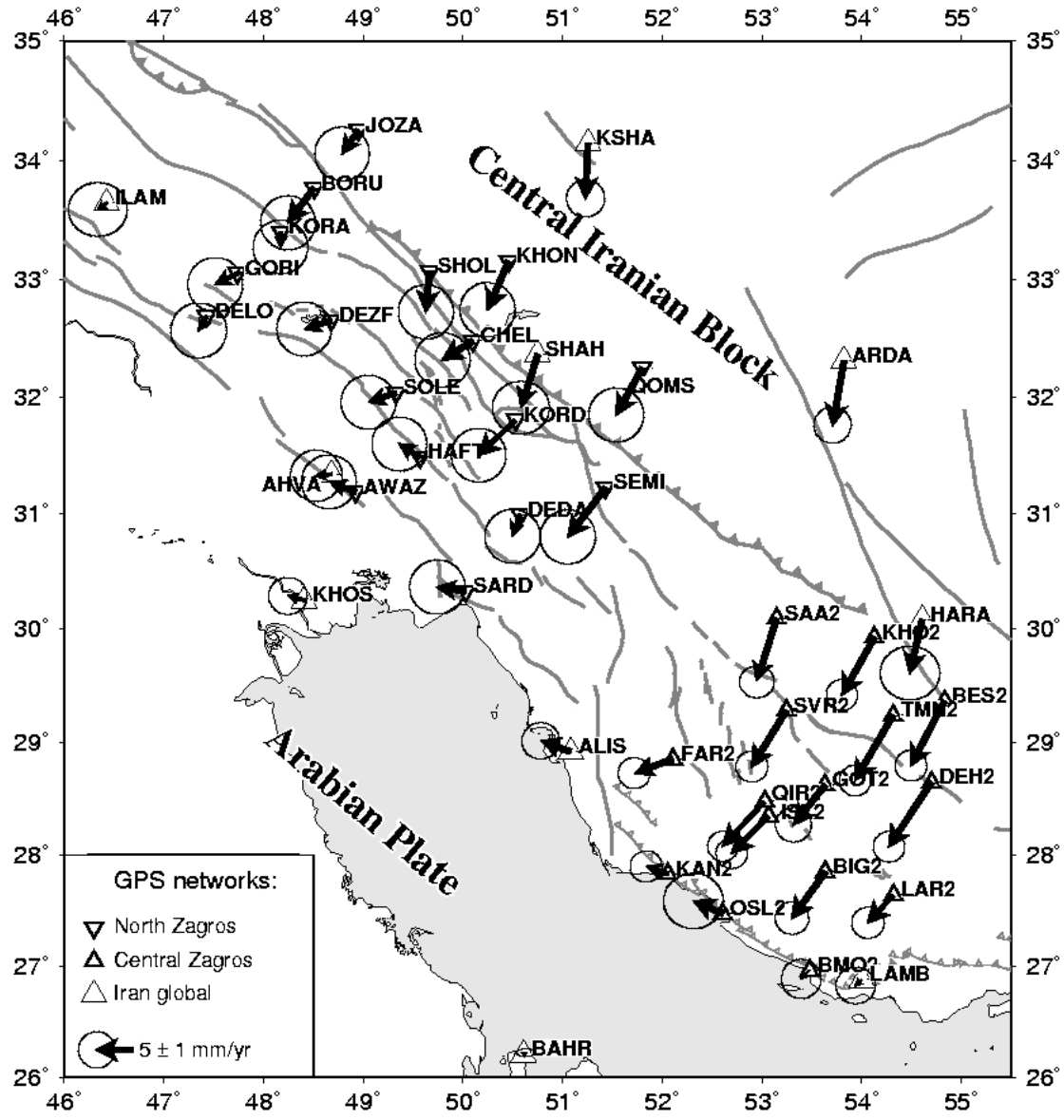

Figure 3b: North Zagros and Central Zagros velocity fields with respect to the Arabian Plate. Same captions as Fig 3a.

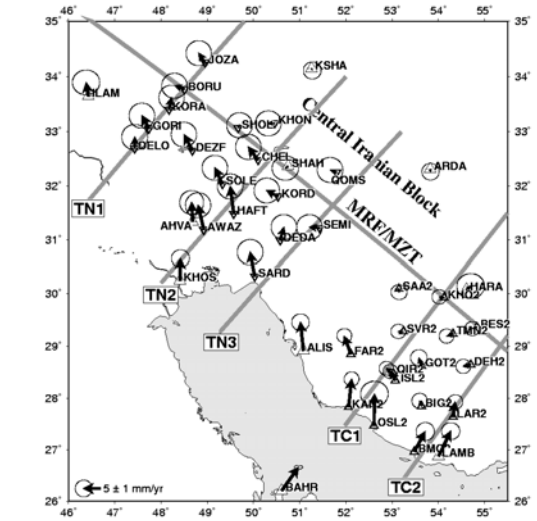
JOZA
KSHA
ILAM
BORU
KORA
GORI
SHOS
KHON
DELO
DEZF
CHEL
SHAH
ARDA
QOMS
SOLE
KORD
TN1
HAFT
AHVA
AWAZ
SEMI
DEDA
SARD
KHOS
SAA2
KHO2
HARA
TN2
SVR2
TMN2
BES2
TN3
ALIS
FAR2
GOT2
DEH2
ISL2
KAN2
BIG2
LAR2
OSL2
TC1
BMG2
LAMB
BAHR
TC2
5 ± 1 mm/yr
Central Iranian Block
MRF/MZT

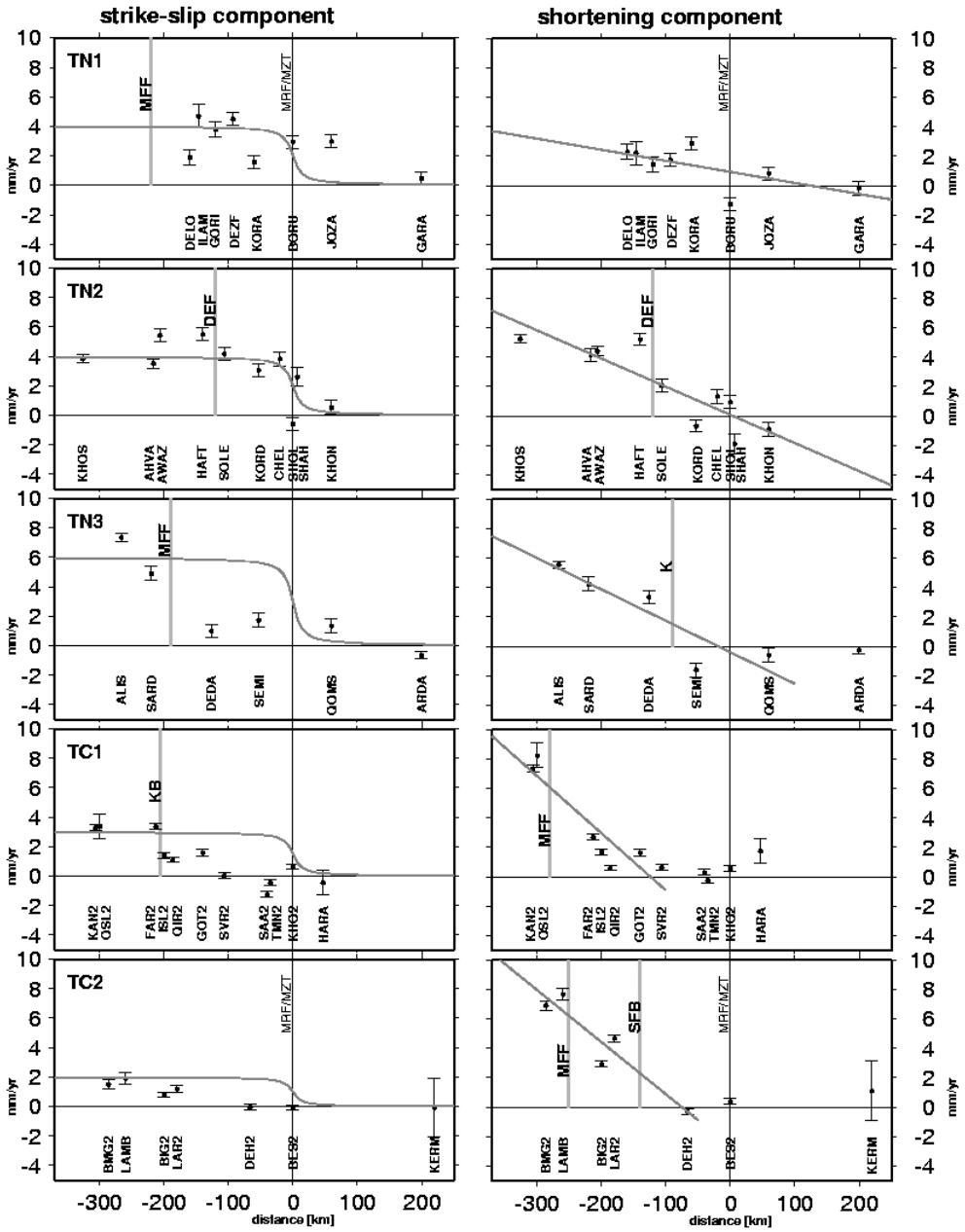
strike-slip component
shortening component
TN1
TN2
TN3
TC1
TC2
MFF
DEF
K
KB
SFB
MRF/MZT
nm/yr
distance [km]
DELO ILAM GORI DEZF KORA BORU JOZA GARA
KHOS AHVA AWAZ HAFT SOLE KORD CHEL SHAH KHON
ALIS SARD DEDA SEMI QOMS ARDA
KAN2 OSL2 FAR2 ISL2 QIR2 GOT2 SVR2 SAA2 TMN2 KHO2 HARA
BMG2 LAMB BIG2 LAR2 DEH2 BES2 KERM

Figure 4: Site velocities (mm/yr) with respect to the site distance to the Main Recent Fault (MRF) / Main Zagros Thrust (MZT) (in km, on the x axis) on 5 transects (locations shown on the map), TN1, TN2 and TN3 in the North Zagros, TC1 and TC2 in the Central Zagros, from northwest to southeast. On the left, we display the fault parallel components (strike-slip component), on the right, the fault perpendicular component (shortening). A simple model is superposed on the individual velocities (dark grey lines, for details see text). Modelled total strike-slip velocities vary from 2 to 6 mm/yr, strain rates from 8 to 39 nanostrain/yr. Light grey vertical lines indicate fault locations.

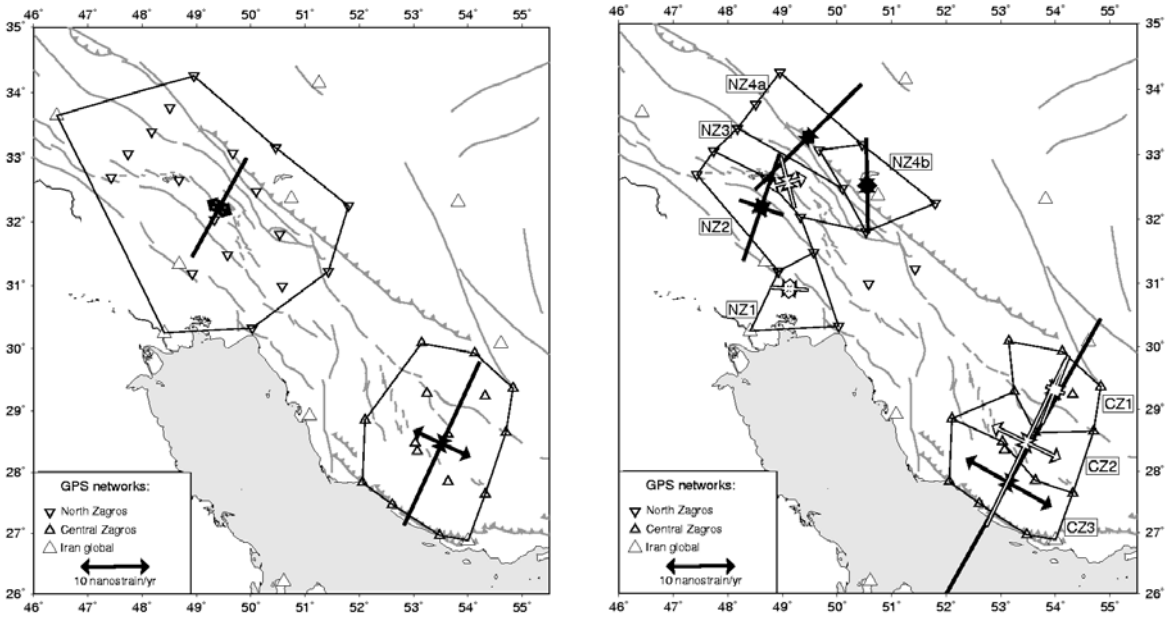

a) b)

Figure 5a: Overall strain rates in the North and Central Zagros networks. Numerical values are indicated in Table 3.

Figure 5b: Strain rates in subnetworks. Black and white strain crosses distinguish relatively high and low deformation rates, respectively.

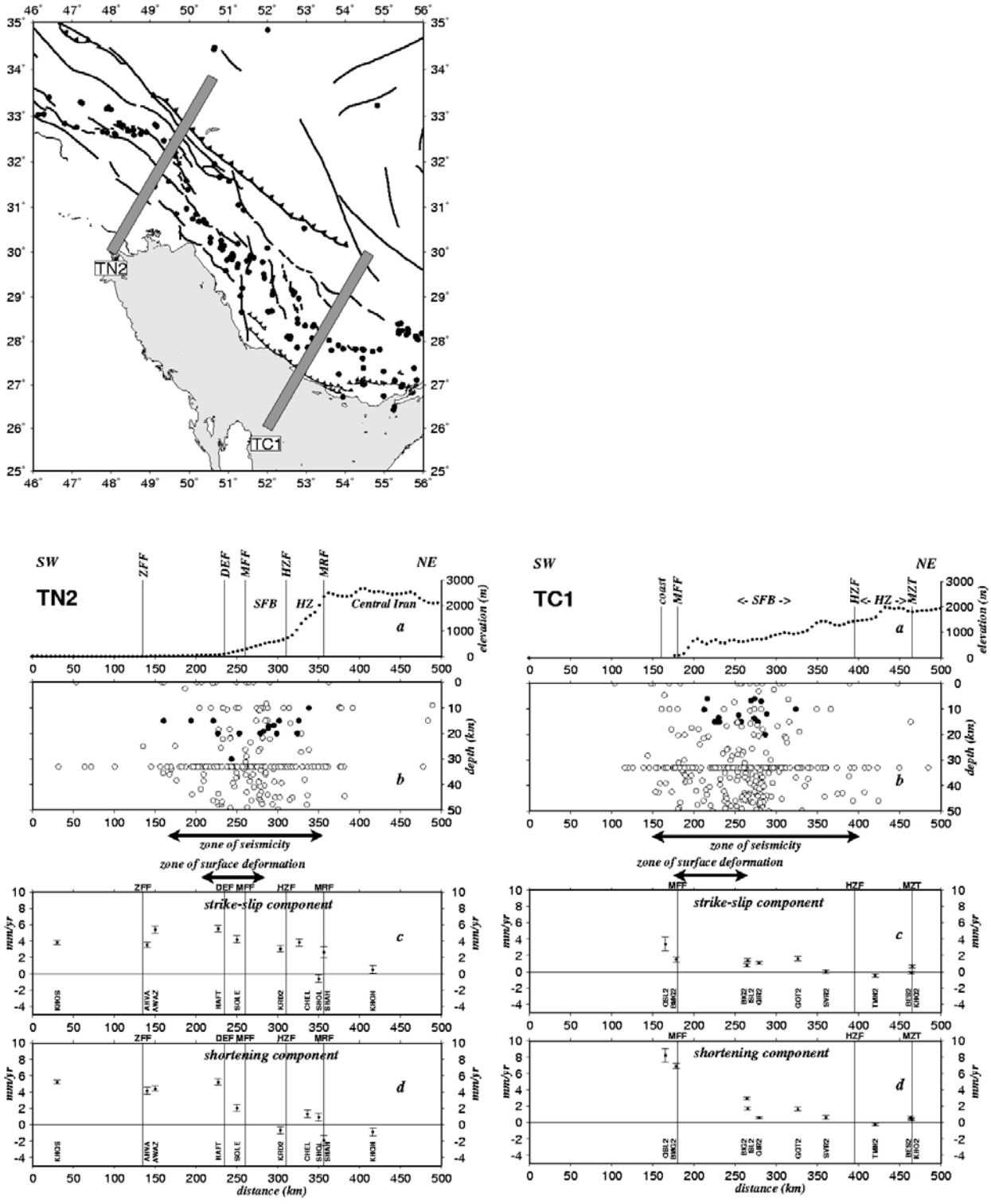

Figure 6: On the two transects TN2 and TC1 we display a) the topography, b) the seismicity (open circles: USGS, black circles: Engdahl et al., 1998), c) NW-SE strike-slip motion parallel to MRF/MZT, d) shortening perpendicular to MRF/MZT. The approximate location of different faults is indicated by vertical lines. Horizontal arrows indicate that the surface deformation evidenced by GPS measurement is concentrated in narrow areas, whereas the basement deformation evidenced by the seismicity is distributed in a larger area, suggesting a decoupling between the two.

5.2.2 Distribution of the right-lateral strike-slip motion from the Main Recent Fault to the Kazerun Fault System (Zagros, Iran): Evidence from present-day GPS velocities (Tavakoli et al., 2007, submitted)

Distribution of the right-lateral strike-slip motion from the Main Recent Fault to the Kazerun Fault System (Zagros, Iran): Evidence from present-day GPS velocities

F. Tavakoli (1,2), A. Walpersdorf (1), C. Authemayou (3, 5), H.R. Nankali (2), D. Hatzfeld (1), M. Tatar (4), Y. Djamour (2), F. Nilforoushan (2), N. Cotte (1)

(1) Laboratoire de Géophysique Interne et Tectonophysique, CNRS, Université Joseph Fourier, Maison des Géosciences, BP 53, 38041 Grenoble Cedex 9, France.

(2) National Cartographic Center, Meraj Ave. Azadi Sq., P.O.Box 13185-1684, Tehran, Iran

(3) CEREGE, CNRS, Université Aix-Marseille-3, BP 80, Europôle Méditerranéen de l'Arbois, 13 545 Aix-en-Provence Cedex 4, France

(4) International Institute for Earthquake Engineering and Seismology, P.O. Box 19395/3913, Tehran, Iran

(5) Institut de Paléontologie et Géologie, Université de Lausanne, CH-1015, Lausanne, Switzerland

Contact: Andrea.Walpersdorf@ujf-grenoble.fr

Abstract:

GPS measurements across the Kazerun fault system in the Zagros mountain belt provide first instantaneous velocities on the different segments. These results are closely consistent with the geological fault slip rates (over 150 ka), implying stable velocities over a long period. The present-day strike-slip motion is distributed from the Main Recent Fault to

the N-trending Kazerun fault system along a preferential en-echelon fault zone included in a more distributed fan-shape fault pattern. The Dena fault (3.7 mm/yr) transfers the MRF fault slip mainly to the Kazerun (3.6 mm/yr) and slightly to the High Zagros and Sabz Pushan faults (1.5 mm/yr), and the Kazerun fault further to the Kareh Bas fault (3.4 mm/yr). Total geological horizontal offsets associated with GPS slip rates imply that the right-lateral strike-slip activity of the MRF has propagated in time southeastward to the Dena and Kazerun segments, and then to the Kareh Bas fault.

INDEX TERMS: 1200 Geodesy and Gravity; 1240 Satellite Geodesy: results; 1243 Space geodetic surveys; 8100 Tectonophysics; 8107 Continental neotectonics; 8111 Continental tectonics: strike-slip and transform; Iran; Zagros.

1. Introduction

The NW-trending Zagros fold-and-thrust belt in southwest Iran is the result of the Neogene collision between the Arabian and Eurasian plates [e.g. *Falcon*, 1969]. The belt is composed of two distinct structural domains: The narrower North Zagros associated with orogen-parallel strike-slip and thrust faults, and the wider Central Zagros associated with thrust and strike-slip faults oblique to the orogen, and with the presence of the Hormuz salt detachment layer at depth [*Talebian and Jackson*, 2004].

The present day kinematics of the Zagros is characterized in North Zagros by 3-6 mm/yr of orthogonal shortening and 4-6 mm/yr of orogen-parallel right-lateral strike-slip motion (2.5 ± 2 mm/yr located on the Main Recent Fault), and in Central Zagros by 10 mm/yr of NNE shortening, mainly concentrated in the southern part of the belt close to the Persian Gulf [*Tatar et al.*, 2002; *Walpersdorf et al.*, 2006]. The Kazerun Fault System (KFS) separates North and Central Zagros (Figure 1). It is a series of N- to NNW-trending right-lateral strike-

slip faults [*Berberian*, 1995]. The longest (300 km) is the en-échelon Kazerun fault, comprising the Dena, Kazerun and Borazjan segments [e. g. *Falcon*, 1969]. KFS further includes the Kareh Bas, Sabz Pushan and Sarvestan faults located further east. These faults are all basement structures inherited from a Neo-Proterozoic tectonic phase [*Talbot and Alavi*, 1996]. The three segments Dena, Kazerun and Borazjan of the Kazerun fault have similar length (~100 km) and distort and disrupt the Zagros folds [e.g. *Berberian*, 1995; *Authemayou et al.*, 2005]. Each segment is terminated to the south by a SE-trending thrust [*Authemayou et al.*, 2005].

The present day activity of the KFS is emphasized by historical and instrumental earthquakes that have been located on different parts of the fault system (especially on the Kazerun and Kareh Bas faults), and are associated with right-lateral focal mechanisms [*Berberian*, 1995; *Talebian and Jackson*, 2004] (Figure 1). Estimated total offsets of geological markers across the Kazerun fault range between 8-27 km, [*Authemayou et al.*, 2006] and 140 km [*Berberian*, 1995]. This conducted to a poorly constrained average fault slip rate between 1 and 15 mm/yr assuming the onset of the main regional shortening phase in the late Miocene [e.g. *Hessami et al.*, 2001].

In this paper we analyze the present day kinematics of the KFS, based on the measurements of a dedicated GPS network. We quantify the slip rates along each fault and segment and examine the consistency with geological slip rates [*Authemayou et al.*, submitted].

2. GPS Measurements and Analysis

A geodetic network of 11 benchmarks (bedrock sites with forced antenna centering) was established in 2002 around the KFS. In two measurement campaigns in 2002 and 2004, each GPS site was measured during at least 48 h. The network has been completed by several measurements of adjacent temporary networks [*Nilforoushan et al.*, 2003; *Vernant et al.*,

2004; *Tatar et al.*, 2002; *Walpersdorf et al.*, 2006], up to 6 Iranian permanent GPS stations, and 32 GPS stations of the International GNSS Service (IGS) network. We analyzed the data using the GAMIT/GLOBK 10.1 software [*King and Bock*, 2002]. The daily mean repeatabilities, for north, east and vertical components in 2002 are 2 mm, 3 mm, 6mm, and in 2004 are 2 mm, 2 mm, 6 mm respectively. These repeatabilities represent the short-term errors of the GPS measurement and result in an estimate of the horizontal velocity uncertainties of 2 mm/yr. This estimate is conservative, as no network adjustments were done before comparing daily solutions. Details about the processing of the data are given by *Vernant et al.* [2004] and *Walpersdorf et al.* [2006].

3. Velocity field

We present in Fig. 2 and Table 1 the velocity field around the Kazerun fault system in the Central Iran Block (CIB) frame [*Vernant et al.*, 2004]. The average residual velocity for the 6 stations of the CIB is 0.5 mm/yr supporting that this block does not deform as suggested by *Nilforoushan et al.* [2003] and *Vernant et al.* [2004], and attested by the associated low seismic activity [*Jackson and McKenzie*, 1984]. We ensure that co-seismic displacements in the time interval do not affect the surface measurements. Assuming an elastic half space [*Okada*, 1985] and empirical relations between magnitude and slip on the fault [*Wells and Coppersmith*, 1994], the largest event of magnitude 5.7 produced a motion of less than 1 mm at the nearest GPS station.

In a first approximation, all significant (greater than 2 mm/yr) differential velocities are located southwest of the Dena – Kazerun – Kareh Bas - MFF faults. All measurements north of these faults show no motion relative to CIB suggesting that the MZRF, Sarvestan and Sabz Pushan faults are not very active. If we assume that all faults are known and delimitate rigid blocks, and that the GPS benchmarks are located far from the

elastic deformation zone at the edges of the blocks, we can increase the precision of the estimated fault velocities by averaging several measurements located on the same rigid block. We compared site velocities on three west-east transects (T1, T2, T3 from north to south) crossing the Kazerun, Kareh Bas and Sabz Pushan faults (Figure 2) to estimate the differential motion of the rigid blocks on each side of the faults. As the faults are approximately NS oriented, the north component of the velocities is assumed to represent the strike-slip component of the fault motion (Figure 3). The east component of the velocities would represent the shortening motion, but in all cases they are smaller than 2 mm/yr (and therefore within the uncertainties), indicating the absence of significant shortening perpendicular to the KFS. For each transect, we compute the total slip velocity on a fault as the difference between the average velocities of the stations on each site of the fault (Figure 3).

For the northernmost transect T1 across the Dena segment we measure a well resolved right-lateral strike-slip rate of 3.7 ± 2 mm/yr. The middle transect T2 across the Kazerun segment yields a similar significant rate of 3.6 ± 2 mm/yr, but the 1.5 mm/yr velocity cumulated over the Sabz Pushan (SBZF) and High Zagros (HZF) faults is within the uncertainties.

The southernmost transect T3 crosses the Borazjan segment, the Kareh Bas and the Sabz Pushan faults. There is no significant horizontal motion neither on the Borazjan fault (constrained only by ALIS) nor on the Sabz-Pushan fault. Only the Kareh Bas fault shows a significant dextral strike-slip motion of 3.4 ± 2 mm/yr.

4. Comparison with geological displacement rates

The identification of total horizontal fault displacements and dating of offset alluvial fans by *Authemayou et al.* [2006; submitted] enable us to compare the GPS inferred instantaneous

velocities with long term average slip rates over several thousands of years (Table 2). Figure 4 presents a map with the main information on present day slip rates and fault ages.

For the Dena and the Kazerun fault segments, geological displacement rates are available and evaluated to 3.1 - 4.7 mm/yr and 1.5 - 3.2 mm/yr, respectively. The comparison of these long term slip rates with the instantaneous slip rate of 1.7 - 5.7 and 1.6 – 5.6 mm/yr respectively shows that the geological and the instantaneous displacement rates are coherent (within the uncertainties) and less than the 15 mm/yr suggested by *Berberian* [1995]. The coherent observations also suggest that the faults might have slipped at constant rates for a long time period. Assuming a constant slip rate since the onset of the faults and considering the total fault offsets of 13 and 8 km on the Dena and the Kazerun fault segments, respectively, the coherent short and long term slip rates yield comparable onset ages for Dena (2.3 – 7.6 Ma by GPS with respect to 2.8 – 4.2 Ma by geology) and Kazerun (1.5 - 5.1 Ma by GPS with respect to 2.6 – 5.5 Ma by geology).

We do not have a geological onset time for the Kareh Bas fault. Supposing a constant slip rate of 1.4 – 5.4 mm/yr as measured by GPS, the 7.2 km fault offset [*Authemayou et al.*, 2006] observed on the Kareh Bas fault could be achieved in 1.3 – 5.1 Ma.

5. Discussion and Conclusions

Our GPS measurements provide a reliable estimate of the present-day dextral strike-slip motion on the Dena (3.7 ± 2 mm/yr) and Kazerun (3.6 ± 2 mm/yr) segments, and on the Kareh Bas fault (3.4 ± 2 mm/yr). The comparison with the Kazerun geological slip rates [*Authemayou et al.*, submitted] indicates stable rates over ~150 ka (Table 2). These three segments accommodate the main part of the differential motion between North and Central Zagros.

The MRF GPS velocity of 2.5 ± 2 mm/yr is slower than the Kazerun fault slip rate contrary to the geological slip rates (Table 2). However, the GPS orogen-parallel strike-slip motion across the total North Zagros mountain belt is 4-6 mm/yr [*Walpersdorf et al.*, 2006] and corresponds to the MRF geological slip rate. Therefore, the MRF GPS velocity could be under-estimated or a transpressional regime across the Zagros has developed after 150 ka.

Total geological horizontal offsets and GPS slip rates for the Dena and Kazerun segments permit to determine fault ages of 2.3 – 7.6 and 1.5 - 5.1 Ma, respectively. The Kareh Bas fault age was determined supposing constant GPS slip rates to 1.3-5.1 Ma, comparable to but slightly younger than the Kazerun segment.The comparison of strike-slip onset times with respect to the MRF (6-10 Ma) [*Authemayou et al.*, 2006] could imply that the right-lateral strike-slip activity of the MRF has propagated in time southeastward to the Dena and the Kazerun segments, and then to the Kareh Bas fault.

The SBZF and HZF show a cumulative slip rate at the limit of resolution (1.5 ± 2 mm/yr). This slip rate from NS velocity components could be underestimated due to the departure of the HZF from the general NS fault trend in the KFS. No significant strike-slip motion has been revealed on the southernmost Borazjan segment of the Kazerun fault, as well as on the easternmost fault of the KFS, the Sarvestan fault.

The general pattern of slip rate suggests that the present-day deformation is distributed from the MRF to the Dena fault, from the Dena fault mainly to the Kazerun and slightly to the HZF and the Sabz Pushan fault, and from the Kazerun to the Kareh Bas fault. The coherent slip in this complex en-echelon system shows that location of deformation is different from the more distributed fan-shape fault pattern evidenced by tectonics. This implies that the slip pattern evolves in time. We may infer that the distribution of strike-slip motion from the MRF to the KFS is related to the presence of the very ductile Hormuz salt layer restricted to the Central Zagros, east of the KFS. However, the shallow activity on the Dena, Kazerun and

Kareh Bas faults is associated with large strike-slip earthquakes attesting that the basement is also involved in the distributed deformation.

Acknowledgements.

We are grateful to all the French and Iranian observers without whom these results would not exist. We had fruitful discussions with J. Jackson, O. Bellier and M. Vergnolle. This work has been supported by NCC, IIEES, and CNRS/INSU via the program Dyeti. F. Tavakoli benefited of a scholarship from Total.

References.

Altamimi, Z., P. Sillard and C. Boucher (2002), ITRF2000: A new release of the International Terrestrial Reference Frame for earth Science applications, *J. Geophys. Res., 107*, B10, 2214.

Authemayou, C., O. Bellier, D. Chardon, Z. Malekzade and M. Abassi (2005), Role of Kazerun fault system in active deformation of the Zagros fold-and-thrust belt (Iran), *C. R. Geoscience, 337*, 539-545.

Authemayou, C., D. Chardon, O. Bellier, Z. Malekzadeh, E. Shabanian, and M. R. Abbassi (2006), Late Cenozoic partitioning of oblique plate convergence in the Zagros fold-and-thrust belt (Iran), *Tectonics, 25*, TC3002, doi:10.1029/2005TC001860.

Authemayou, C., O. Bellier, D. Chardon, L. Benedetti, Z. Malekzadeh, C. Claude, B, Angeletti, E. Shabanian, and M. R. Abbassi (submitted), Quaternary Kazerun and Main Recent Faults' slip-rates: Evidence for strike-slip partitioning in the Zagros fold-and-thrust belt, *J. Geophys. Res.*

Berberian, M. (1995), Master blind thrust faults hidden under the Zagros folds: Active basement tectonics and surface morphotectonics, *Tectonophysics 241*,193-224.

Engdahl, E. R., R. D. Van der Hilst and R. P. Buland (1998), Global teleseismic earthquake relocation with improved travel times and procedure for depth determination, *Bull. Seism. Soc. Am., 88*, 722-743.

Falcon, N. L. (1969), Problem of the relationship between surface structures and deep displacement illustrated by the Zagros range, in *Time and Place in Orogeny*, edited by P. E. Kent, G. E. Satterwaite, and A. M. Spencer, *Geol. Soc. Spec. Publ., 3*, 9-22.

Hessami, K., H. A. Koyi, C. J. Talbot, H. Tabasi, and E. Shabanian (2001), Progressive unconformities within an evolving foreland fold-thrust belt, Zagros mountains, *J. Geol. Soc. London, 158,* 969-981.

Jackson, J. and D. McKenzie (1984), Active tectonics of the Alpine-Himalayan belt between Western Turkey and Pakistan, *Geophys. J. R. Astr. Soc. London, 77*, 185-264.

King, R. W. and Y. Bock (2002), Documentation for the GAMIT analysis software, Release 10.1, Massachusetts Institute of Technology. Cambridge, MA.

Nilforoushan, F., F. Masson, P. Vernant, C. Vigny, J. Martinod, M. Abbasi, H.R. Nankali, D. Hatzfeld, R. Bayer, F. Tavakoli, M. Ashtiany, E. Doerflinger, M. Daignieres, P. Collard and J. Chéry (2003), GPS network monitors the Arabia-Eurasia collision deformation in Iran, *J. of Geodesy, 77*, 411-422.

Okada, Y. (1985), Surface deformation due to shear and tensile faults in a half-space, *Bull. Seism. Soc. Am., 75* (4), 1135-54.

Talbot, C. J., and M. Alavi (1996), The past of a future syntaxis across the Zagros, in *Salt Tectonics*, edited by G. I. Alsop, D. J. Blundell and I. Davison, Geol. Soc. Spec. Publ., London, 100, 89-110.

Talebian, M. and J. Jackson (2004), A reappraisal of earthquake focal mechanisms and active shortening in the Zagros mountains of Iran, *Geophys. J. Int., 156*, 506-526.

Tatar, M., D. Hatzfeld, J. Martinod, A. Walpersdorf, M. Ghafory-Ashtiany, and J. Chéry (2002), The present-day deformation of the central Zagros from GPS measurements, *Geophys. Res. Lett., 29*(19), doi: 10.1029/2002GL015159.

Vernant, P., F. Nilforoushan, D. Hatzfeld, M.R. Abbassi, C. Vigny, F. Masson, H.R. Nankali, J. Martinod, A. Ashtiany, R. Bayer, F. Tavakoli and J. Chéry (2004), Present-day deformation and plate kinematics in the Middle East constrained by GPS measurements in Iran and northern Oman, *Geophys. J. Int.*, 157, 381-398.

Walpersdorf, A., D. Hatzfeld, H. Nankali, F. Tavakoli, F. Nilforoushan, M. Tatar, P. Vernant, J. Chéry and F. Masson (2006), Difference in the GPS deformation pattern of North and Central Zagros (Iran), *Geophys. J. Int.*, *167*, (3), 1077-, doi:10.1111/j.1365-246X.2006.03147.x.

Wells, D.L., and K.J. Coppersmith (1994), New empirical relationships among magnitude, rupture length, rupture width, rupture area and surface displacement, *Bull. Seismol. Soc. Am., 84*, pp. 1940–1959.

Tables.

			CIB		ITRF2000			
site	lon °E	lat °N	Ve	Vn	Ve	Vn	σ Ve	σ Vn
ABAD	52.568	31.228	1.58	-1.32	21.94	9.60	1.41	1.40
ABAR	53.308	31.123	1.42	-2.03	21.84	8.91	1.43	1.41
ALIS	51.082	28.919	.45	5.13	21.06	16.10	0.95	0.92
BAMO	50.980	30.109	1.44	3.38	21.82	14.40	1.43	1.41
BIG2	53.637	27.852	.04	1.19	21.05	12.18	0.94	0.92
DASH	51.814	29.945	.26	.39	20.79	11.34	1.45	1.43

DAYY	51.836	27.850	6.18	4.93	27.01	15.96	1.47	1.43
DEDA	50.578	30.990	2.10	1.86	22.29	12.80	1.19	1.18
FAR2	52.106	28.851	-1.13	4.90	19.59	15.89	0.90	0.87
GOT2	53.631	28.624	-.14	1.96	20.79	12.94	1.01	0.97
HARA	54.608	30.079	.75	1.45	21.46	12.38	1.65	1.49
ISL2	53.066	28.347	-.66	2.24	20.25	13.22	0.88	0.86
KAN2	52.056	27.834	1.70	7.79	22.55	18.82	0.90	0.88
KHO2	54.126	29.923	-.86	-.16	19.89	10.83	0.89	0.87
KRD2	50.531	31.808	-1.72	.15	18.37	11.14	1.51	1.50
LAR2	54.320	27.644	1.25	4.03	22.33	15.00	0.91	0.88
MARV	52.752	29.798	2.11	-.92	22.70	10.09	1.45	1.42
OSL2	52.607	27.474	1.11	9.49	22.08	20.41	1.65	1.54
QIR2	53.029	28.477	-1.30	1.32	19.52	12.23	0.86	0.85
SAA2	53.146	30.087	.77	-1.33	21.38	9.64	0.97	0.90
SARD	50.026	30.325	1.73	4.49	21.94	15.51	1.20	1.18
SEDE	52.179	30.726	1.97	-3.09	22.36	7.85	1.41	1.39
SEMI	51.430	31.225	.28	-2.41	20.48	8.59	1.20	1.18
SEPI	51.358	30.610	.02	1.05	20.37	12.09	1.43	1.42
SHAN	51.775	28.400	1.47	3.51	22.20	14.54	1.44	1.42
SVR2	53.244	29.281	-.74	-.23	19.98	10.75	0.90	0.87
TMN2	54.316	29.239	-1.24	-1.06	19.64	9.93	0.88	0.86
YAGH	52.235	29.617	.56	.36	21.15	11.33	1.42	1.40

Table 1: Kazerun site velocities in mm/yr with respect to Central Iran Block (CIB) and ITRF2000 [*Altamimi et al.*, 2002].

fault	total horizontal slip [km]	age of fault onset [Ma]	average geological slip rate [mm/yr]	GPS velocity [mm/yr]	GPS inferred fault onset [Ma]
Dena	13	2.8 – 4.2	3.1 – 4.7	1.7 – 5.7	2.3 – 7.6
Kazerun	8.2	2.6 – 5.5	1.5 – 3.5	1.6 – 5.6	1.5 – 5.1
Borazjan	0	-	-	0 – 1	-
Kareh Bas	7.2	still undetermined	still undetermined	1.4 – 5.4	1.3 – 5.1
MRF	50	6.6 – 10.2	4.9 – 7.6	0.5 – 4.5	11 – 100

Table 2. Total horizontal fault slips and age of strike-slip onsets from *Authemayou et al.* [2006], and *Authemayou* [submitted]. GPS velocities from this study except for MRF from *Walpersdorf et al.* [2006].

Figures.

Figure 1. Map indicating the major tectonic features [*Authemayou et al.*, 2006], grey circles represent the seismicity [*Engdahl et al.*, 1998] and CMT focal mechanisms for the Kazerun region. MZRF: Main Zagros Reverse Fault, MRF: Main Recent Fault, DF: Dena Fault, KF: Kazerun Fault, BF: Borazjan Fault, KB: Kareh Bas Fault, SBZF: Sabz Pushan Fault, SF: Sarvestan Fault, HZF: High Zagros Fault, MFF: Main Front Fault, ZFF: Zagros Front Fault. The inset shows the location of the study area (black frame) in the global tectonic context of the Arabia-Eurasia collision. The white vectors indicate GPS velocities according to the Arabia-Eurasia Euler pole of *Vernant et al.* [2004].

Figure 2. Velocity field in the Kazerun region with respect to the Central Iran Block. Transects T1 – T3 of Figure 3 are highlighted.

Figure 3. Modeling of the Dena (T1), Kazerun (T2) and Kareh Bas (T3) fault kinematics as faults separating rigid blocks. Total strike-slip velocities are indicated for each fault by differences between average NS velocities per block, corresponding to the strike-slip motion on the roughly NS oriented faults. T2 also evaluates 1.5 mm/yr of cumulated strike-slip rate over HZF and SBZF.

Figure 4. Compilation of GPS inferred strike-slip onset ages and present day slip rates (uncertainties ± 2 mm/yr) for the major faults in the Kazerun region.

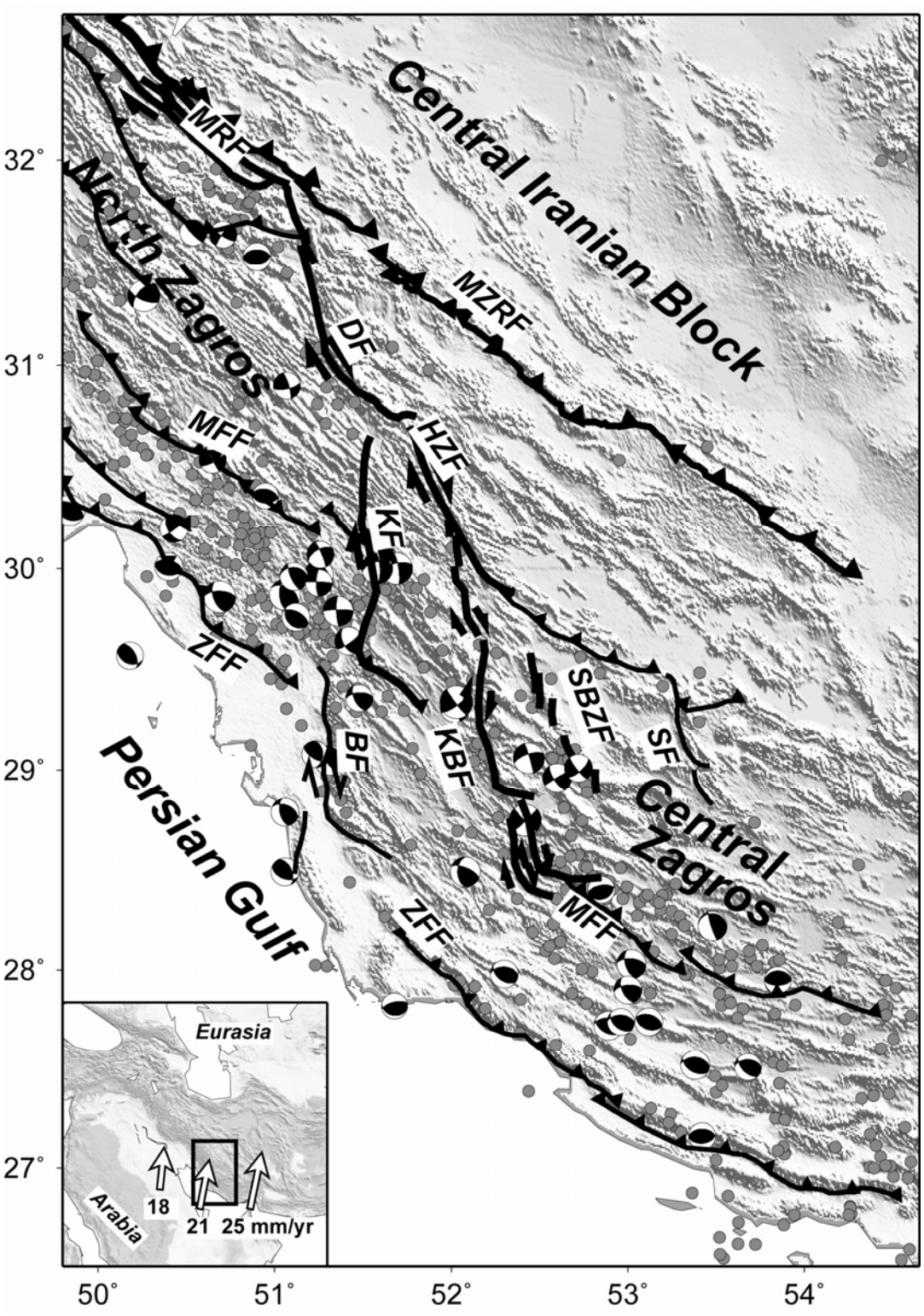
Central Iranian Block
North Zagros
Central Zagros
Persian Gulf
MRF
MZRF
DF
HZF
MFF
KF
ZFF
SBZF
SF
BF
KBF
MFF
ZFF
32°
31°
30°
29°
28°
27°
50°
51°
52°
53°
54°
Eurasia
Arabia
18
21
25 mm/yr

Figure 1.

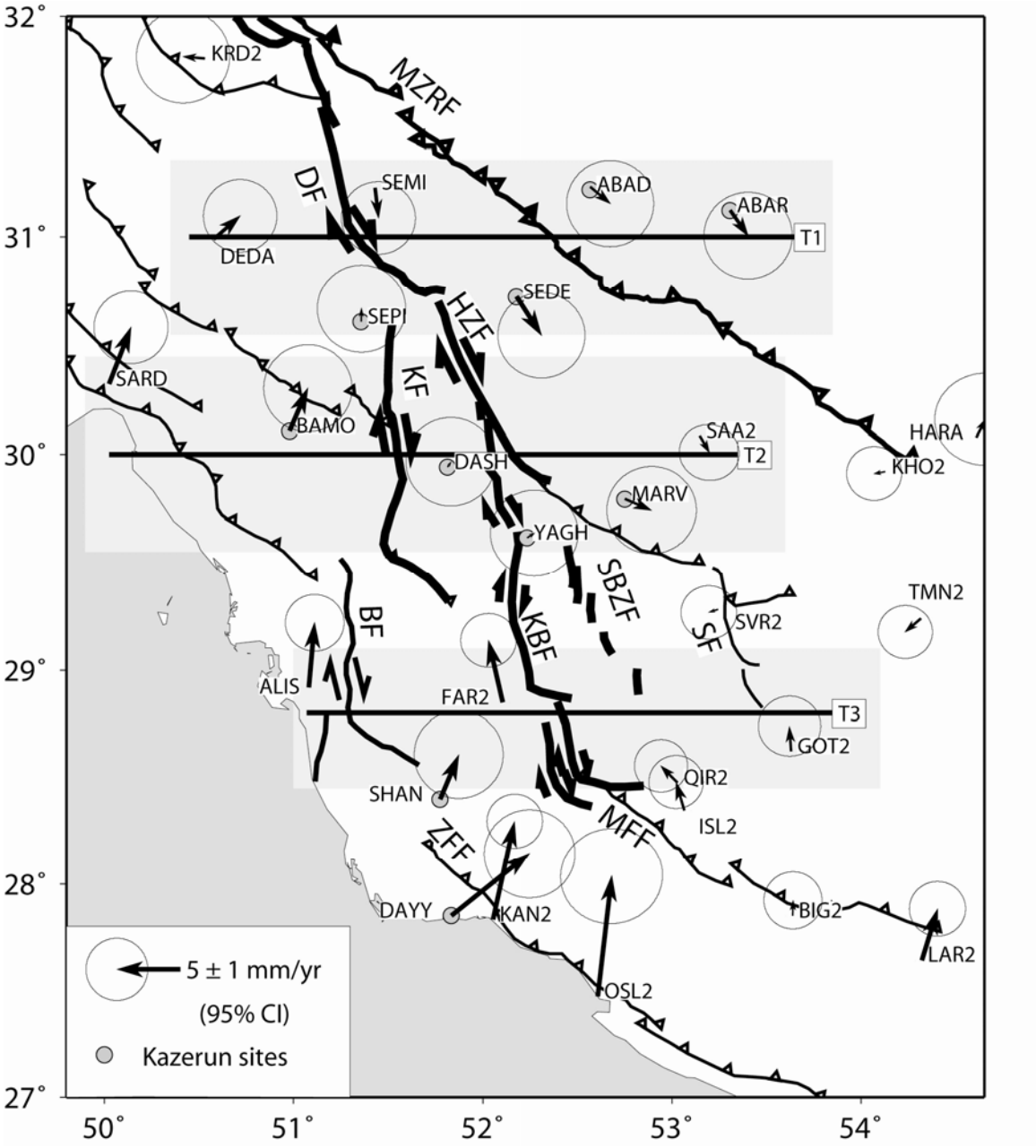
32°
31°
30°
29°
28°
27°
50°
51°
52°
53°
54°
KRD2
MZRF
DF
SEMI
ABAD
ABAR
T1
DEDA
SEDE
SEPI
HZF
KF
SARD
BAMO
SAA2
HARA
T2
DASH
KHO2
MARV
YAGH
SBZF
TMN2
BF
KBF
SF
SVR2
ALIS
FAR2
T3
GOT2
QIR2
SHAN
MFF
ISL2
ZFF
DAYY
KAN2
BIG2
LAR2
OSL2
5 ± 1 mm/yr
(95% CI)
Kazerun sites

Figure 2.

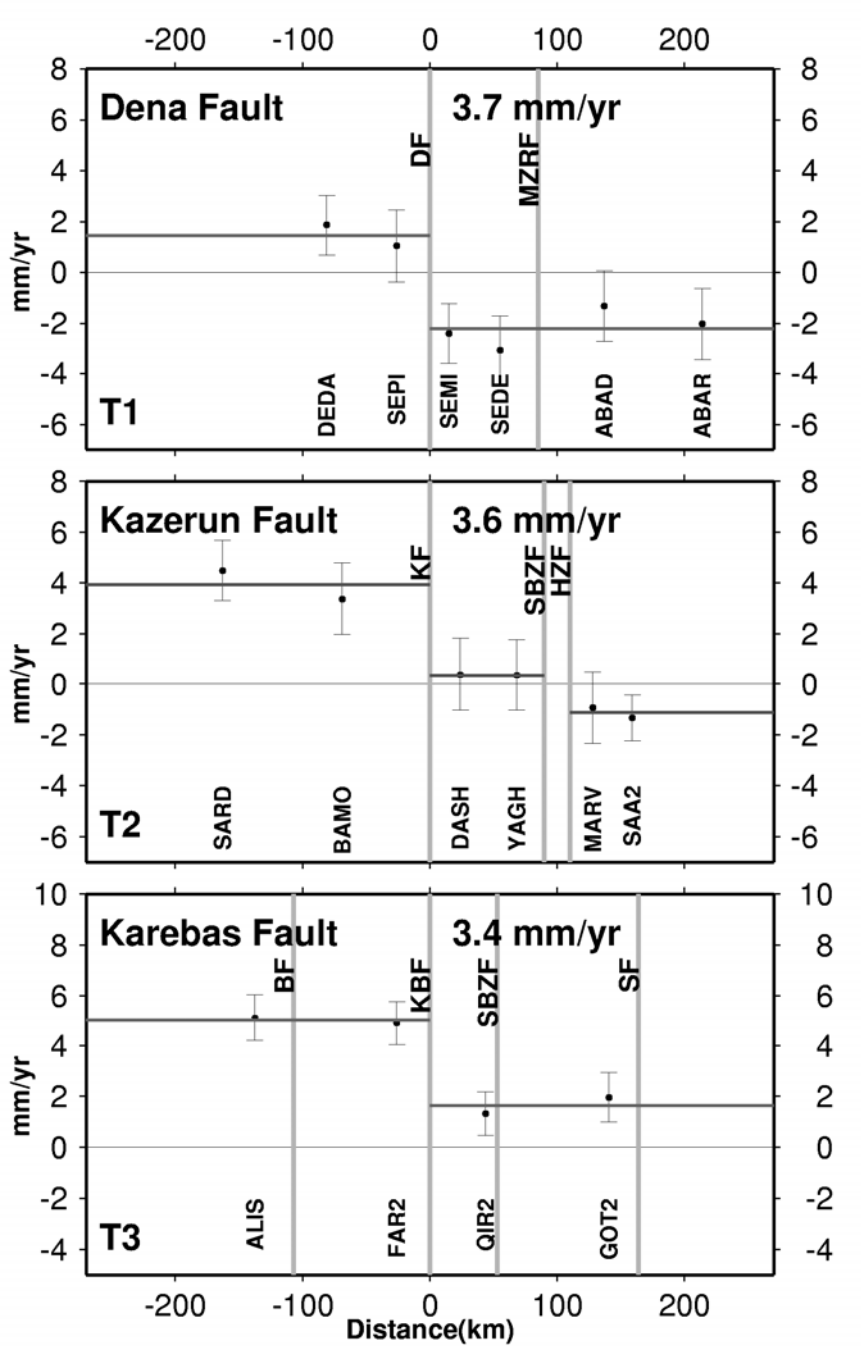
Dena Fault
3.7 mm/yr
DF
MZRF
T1
DEDA
SEPI
SEMI
SEDE
ABAD
ABAR
Kazerun Fault
3.6 mm/yr
KF
SBZF
HZF
T2
SARD
BAMO
DASH
YAGH
MARV
SAA2
Karebas Fault
3.4 mm/yr
BF
KBF
SBZF
SF
T3
ALIS
FAR2
QIR2
GOT2
mm/yr
Distance(km)

Figure 3.

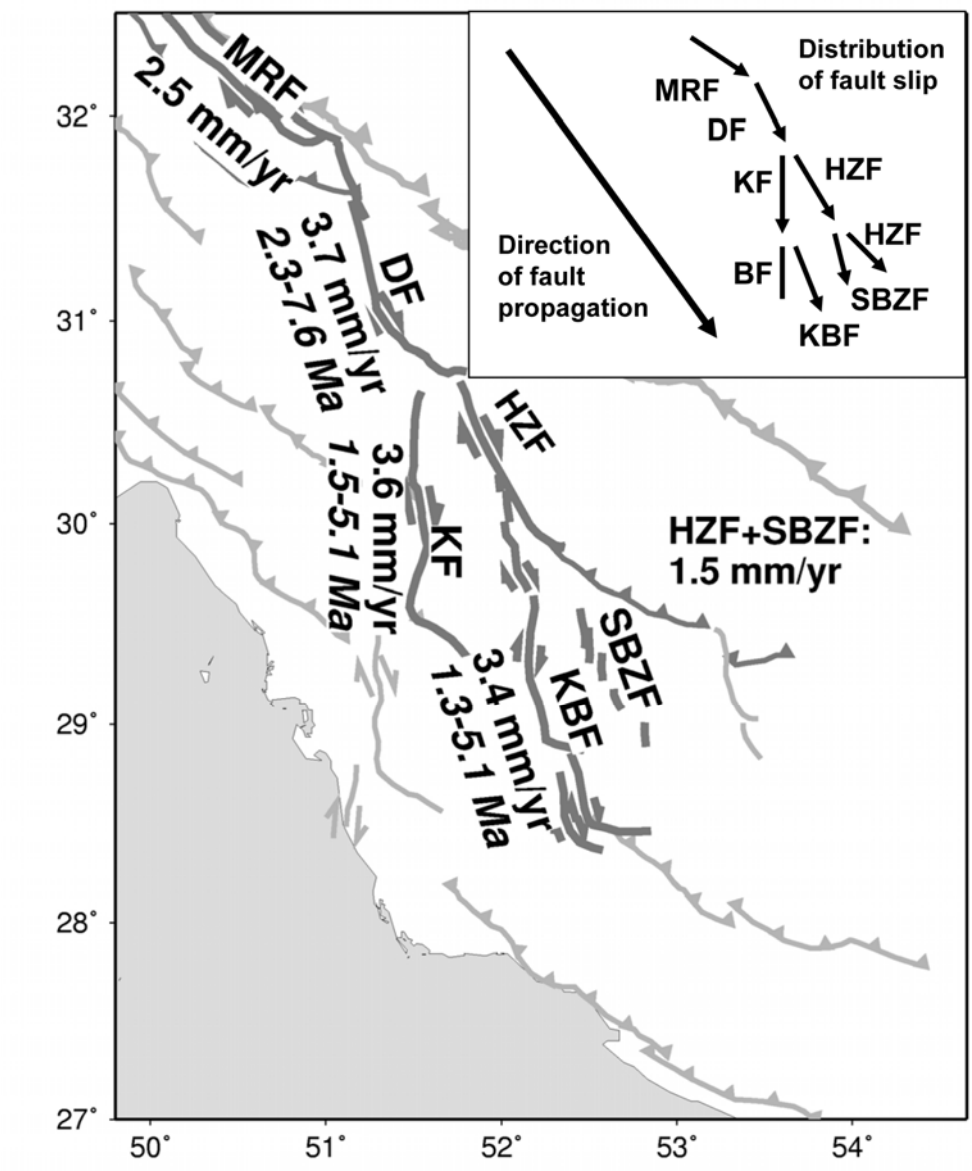
MRF
2.5 mm/yr
DF
3.7 mm/yr
2.3-7.6 Ma
KF
3.6 mm/yr
1.5-5.1 Ma
HZF
SBZF
KBF
3.4 mm/yr
1.3-5.1 Ma
HZF+SBZF:
1.5 mm/yr
Distribution
of fault slip
MRF
DF
KF
HZF
HZF
BF
SBZF
KBF
Direction
of fault
propagation
32°
31°
30°
29°
28°
27°
50°
51°
52°
53°
54°

Figure 4.

5.2.3 The Kinematics of the Zagros Mountains (Iran). (Hatzfeld et al., 2007, submitted)

The kinematics of the Zagros Mountains (Iran)

D. Hatzfeld [1], C. Authemayou [2, 3], P. van der Beek [4], O. Bellier [2], J. Lavé [4], B. Oveisi [4, 5], M. Tatar[1, 6], F. Tavakoli [1, 7], A. Walpersdorf [1], F. Yamini-Fard[1, 6]

1) Laboratoire de Géophysique Interne et Tectonophysique, CNRS, Université J. Fourier, Maison des Géosciences, BP 53, 38041 Grenoble cedex 9, France, denis.hatzfeld@ujf-grenoble.fr

2) Cerege-UMR CNRS 6635-Aix-Marseille Université, BP80, Europôle. Méditerranéen de l'Arbois, 13545 Aix-en-Provence cedex 4, France

3) Institut de Géologie et Paléontologie, Faculté des géosciences et de l'environnement, Université de Lausanne, Quartier UNIL-Dorigny, Bâtiment Anthropole 3183, CH-1015, Lausanne, Suisse.

4) Laboratoire de Géologie des Chaînes Alpines, CNRS, Université J. Fourier, Maison des Géosciences, BP 53, 38041 Grenoble cedex 9, France

5) Geological Survey of Iran, PO Box 13185-1494, Tehran, Iran

6) International Institute of Earthquake Engineering and Seismology, PO Box 19395/3913, Tehran, Iran

7) National Cartographic Center, PO Box 13185/1684, Tehran, Iran

10130 words, 59 references, 0 table, 12 figures

Abbreviated title : Zagros kinematics

Abstract

We present a synthesis of recently conducted tectonic, GPS, geomorphologic and seismic studies to describe the kinematics of the Zagros mountain belt, with a special focus on the transverse right-lateral strike-slip Kazerun fault system. Both the seismicity and present-day deformation (as observed from tectonics, geomorphology and GPS) appear to concentrate near the 1000-m elevation contour, suggesting that basement and shallow deformation are related. This observation supports a thick-skinned model of south-westward propagation of deformation, starting from the Main Zagros Reverse Fault. The Kazerun Fault System (KFS)

distributes right-lateral strike-slip motion of the Main Recent Fault onto several segments located in an en-échelon system to the east. We observe a marked difference in the kinematics of the Zagros across the Kazerun fault system. To the NW, in the North Zagros, present-day deformation is partitioned between localized strike-slip motion on the Main Recent Fault and shortening located on the deformation front. To the SE, in the Central Zagros, strike-slip motion is distributed on several branches of the KFS. The decoupling of the Hormuz salt layer, restricted to the east of the KFS, and favouring the spreading of the sedimentary cover cannot be the only cause of this distributed mechanism because seismicity (and therefore basement deformation) is associated with all active strike-slip faults, including those to the East of the Kazerun Fault System.

Mountain building is the surface expression of crustal thickening due to plate convergence. Mountains are located on continental lithosphere which, because of its mechanical properties, generally accommodates plate convergence in a more distributed and diffuse way than oceanic lithosphere. Because thickening stores gravitational potential energy, it reaches a limit imposed by the mechanical strength of the crust and lithosphere, after which further storage of gravitational energy is only possible by increasing the lateral size of the mountain belt rather than its height (e.g. Molnar and Lyon-Caen, 1988). Therefore, mountain building is a dynamic process, which requires a detailed description of both the surface kinematics and their relation with crustal deformation in order to be quantified. In this paper, we show that shallow deformation, as evidenced by GPS measurements and geomorphology correlates well, both spatially and temporally, with basement deformation as evidenced by seismicity and topography, suggesting that they image the same mountain building process.

The Zagros fold-and-thrust belt is located within Iran at the edge of the Arabian plate (Fig. 1). It is ~1200 km long, trends NW-SE between eastern Turkey, where it connects to the Anatolian mountain belt, and the Strait of Hormuz, where it connects to the Makran subduction zone. Its width varies from ~200 km in the west to ~350 km in the east. The Zagros mountain belt results from convergence between Arabia and Eurasia, which has been continuous since Late Cretaceous times, with a late episode of accentuated shortening during the Pliocene-Quaternary. The Zagros is classically described in terms of longitudinal units separated by lateral discontinuities (Fig. 1). The High Zagros comprises highly deformed metamorphic rocks of Mesozoic age; it is bounded to the NE by the Main Zagros Thrust (MZT), which is the boundary with Central Iran, and to the SW by the High Zagros Fault (HZF). This is the highest part of the Zagros, with maximum elevations reaching more than

4.500 m. The High Zagros overthrusts to the south the Zagros Fold Belt, which comprises a 10 km thick Palaeozoic-Cainozoic sequence of sediments. The Zagros Fold Belt is characterized by large anticlines several tens of km long. Longitudinally, the Zagros is divided into two geological domains, the North Zagros (and the Dezful embayment) to the west and the Central Zagros (or Fars) to the east, separated by the N-trending strike-slip Kazerun Fault System that cross-cuts the entire belt. Significant differences in mechanical stratigraphy exist between the North and the central Zagros; the sedimentary cover of the latter has been deposited on top of the infra-Cambrian Hormuz salt layer, whereas this layer is absent in the North Zagros.

The amount of shortening between Arabia and Iran since Jurassic times, resulting from subduction of the Neotethys, is about 2000 km (McQuarrie et al., 2003). Ocean closure and cessation of subduction probably occurred during the Oligocene (Agard et al., 2005). This event is recorded by a slight decrease in the convergence velocity from 30 to 20 mm/y (McQuarrie et al., 2003). The total amount of shortening since the onset of continental collision is debated, depending on which marker is used to measure it. Estimates have been based on reconstructions of Upper Cretaceous (Haynes and McQuillian, 1974; Stöcklin, 1974) to late Miocene (Stoneley, 1981) strata. Shortening is accommodated differently in the North and Central Zagros because of the differing boundary conditions and pre-existing tectonics. In the North Zagros, the Main Recent Fault accommodates the lateral component of oblique convergence and may transfer some of the motion to the North Anatolian system, whereas deformation partitioning does not appear to exist in the Central Zagros.

Basement deformation

Morphotectonics and balanced cross-sections

Because the basement is decoupled from the shallow sediments by several ductile layers (e.g. the infra-Cambrian Hormuz and Miocene Gahsaran interfaces), surface deformation may not be representative of the total crustal deformation. Furthermore, deformation mechanisms may differ between the basement and the sedimentary cover because of their different mechanical properties. This view is partially supported by the fact that less than 10% of the total deformation of the Zagros (as measured at the surface) is released by seismic deformation (supposed to be related to the crustal deformation) whereas most of the deformation is seismic in other areas of Iran (Jackson & McKenzie, 1988; Masson et al., 2005). There is no direct access to basement deformation in the Zagros because there are no basement outcrops at the

surface, seismic reflection profiles do not clearly image the basement and earthquake ruptures on the reverse faults generally do not reach the surface.

An approach that implies a model assumption is to indirectly infer basement deformation from surface observations. Berberian (1995) mapped first-order changes in the stratigraphy and identified five morphotectonic units with different characteristics of folding, uplift, erosion and sedimentation. He suggested that these morphotectonic units are separated by major reverse faults affecting the basement and striking parallel to the main structures (Fig. 1). These faults are partially associated with seismicity, consistent mostly with reverse mechanisms, but the accuracy of earthquake locations (~20 km, Engdahl et al., 1998) does not permit mapping of active faults in detail. Moreover, some large earthquakes are not related to any of the inferred faults.

Another approach to indirectly infer crustal deformation is to compute the amount of shortening from balanced cross-sections (Molinaro et al., 2004; Sherkati and Letouzey, 2004; Blanc et al., 2003; McQuarrie 2004). In this method, the different layers that constitute the sedimentary cover are supposed to only fold or fault, without internal deformation. However, the location at depth of the decoupling layers, the amount of decoupling due to these layers, and the relationship between folding and faulting are all complex, and solutions are generally non-unique. Usually, basement faults are assumed where unfolding creates a space problem in the core of folds. The link between surface and basement deformation is strongly debated. Some authors do not require faults in the basement (McQuarrie, 2004), whereas others propose that deformation started in a thin-skinned mode and continued as thick-skinned deformation (Blanc et al., 2003; Molinaro et al., 2004; Sherkati et al., 2005). Some authors suggest that faulting post-dates folding (Blanc et al., 2003; Molinaro et al., 2005), whereas others propose that basement faulting predated folding (Mouthereau et al., 2006). It is therefore problematic to infer basement faulting, and moreover to estimate the amount of shortening, from balanced cross sections alone, without complete control of the geometry of the different interfaces.

Seismicity

The other way to access basement deformation is to study seismicity (Fig. 2). Two sets of data provide complementary information: earthquakes located teleseismically and earthquakes located by local networks. Teleseismically located earthquakes have been recorded since the early 1960s; the duration of the available time window is thus comparable to the usual return period of continental earthquakes. However, because of the lack of regional stations, catalogs

(ISC, USGS) of teleseismically located earthquakes in Zagros suffer from large mislocations (Ambraseys, 1978; Berberian, 1979; Jackson, 1980; Engdahl et al., 1998; 2006). Errors in epicentre location reach up to ~20 km and depths are generally unreliable.

Jackson and McKenzie (1984), Ni and Barazangi (1986) and Engdahl et al. (2006), amongst others, filtered catalogs or relocated seismicity in order to improve the accuracy of epicentres and depths. The Zagros seismicity is totally confined between the Persian Gulf coast and the Main Zagros Thrust (MZT), which both limit the active (or deforming) area and exclude seismic accommodation of shortening by the MZT (Fig. 2). Moreover, although seismicity is spread over the entire width of the Zagros, the larger magnitude (mb>5) earthquakes appear to concentrate in the Zagros Fold Belt, which is an area of low (z<1500-2000m) topography (Jackson and McKenzie, 1984; Ni and Barazangi, 1986, Talebian and Jackson, 2004). This larger seismic energy release at low elevations has been explained by differential stress due to the gradient in topography (Jackson and McKenzie, 1984; Talebian and Jackson, 2004). Epicentres are not obviously correlated with geological structures or surface tectonics (Fig. 2). Moreover, no instrumental earthquake has a magnitude Mw greater than 6.7 and, as a consequence, no co-seismic ruptures have been observed, except for one earthquake in 1990 (Mw~6.4) located at the eastern termination of the High Zagros fault (Walker et al., 2005).

The only reliable depths for teleseismically located earthquakes are those computed by body-waves modelling with uncertainties in depth +/- 4km (Talebian & Jackson, 2004). In Zagros these depth of large earthquakes is 5-19 km with a mean ~11 km, suggesting that earthquakes occur in the basement below the sedimentary cover.

Most focal mechanisms computed from first-motion polarities (McKenzie, 1978; Jackson and McKenzie, 1984) or by body-wave modeling (Talebian and Jackson, 2004) are reverse faulting with NW-SE strikes, parallel to the folding (Fig. 3). Some of these mechanisms are associated with the major faults proposed by Berberian (1995) but others are not. Most of the mechanisms are high-angle reverse faulting likely occurring in the basement at depth between ~5-15 km; they are thus unrelated to a low-angle detachment at the base of the sedimentary layer (Fig. 3). Jackson (1980) proposed that they reactivate normal faults inherited from a stretching episode affecting the Arabian platform during opening of the Tethys Ocean in the Early Mesozoic.

Strike-slip mechanisms are related to two faults systems: the NS trending Kazerun Fault System (KFS; comprising the Kazerun, Kareh-Bas, Sabz-Pushan and Sarvestan faults), which crosses the Zagros between 51.5° E and 54.0° E, and the Main Recent Fault (MRF),

which runs parallel to the MZT and connects at its SE termination to the Kazerun Fault System. The MRF helps to accommodate the oblique shortening experienced by the North Zagros by partitioning the slip motion into pure reverse faulting and strike-slip faulting.

Early studies based on unfiltered earthquake catalogs (Nowroozi, 1971; Haynes and McQuillan, 1974; Bird et al., 1975; Snyder and Barazangi, 1986) postulated that some intermediate seismicity could be related to continental subduction located northeast of the MZT. However, no reliably located earthquake is located northeast of the MZT (Engdahl et al, 1998) and no earthquakes have been located at a depth greater than 20 km in this area (Jackson and Fitch, 1981; Jackson and McKenzie, 1984; Maggi et al., 2000; Engdahl et al., 2006), implying that continental subduction is either aseismic or active.

Microearthquake studies complement the teleseismic information because they locate epicenters with an accuracy of a few km; an order of magnitude better than teleseismic locations. On the other hand, they span a relatively short time window which may not record the tectonic processes in a representative manner. Several temporary networks have been installed in the Zagros, at Qir (Savage et al., 1977; Tatar et al., 2003), Kermansha (Niazi et al., 1978), Bandar-Abbas (Niazi, 1980, Yamini-Fard et al., 2007) and near the Kazerun fault system (Yamini-Fard et al., 2006). Whereas earlier studies are of limited use because the small number of stations does not allow sufficient accuracy in earthquake location, more recent studies have helped to determine some aspects of the crustal structure by inverting travel time delays of local earthquakes recorded in stations located directly above the seismicity. Tatar et al. (2003) confirmed that seismicity in Central Zagros is confined between ~10 and ~15 km depth, beneath the sedimentary cover and in the upper part of the basement (Fig. 4). As for the teleseismic events, no micro-earthquake is located north of the MZT and no earthquake is deeper than 20 km. The seismicity is not confined to the main faults, as observed at the surface, but is spread over a wider area. More interestingly, the micro-seismicity defines elongated NW-SE trending lineaments parallel to the fold axes but with a different spacing, suggesting that folds and faults are not directly related. The seismicity clusters appear to dip NE (Fig. 4), supporting the model of normal-fault reactivation (Jackson, 1980). Focal mechanisms are consistent with NW-SE striking reverse faults connected by NNW-SSE right-lateral strike-slip faults. The main direction of the P-axes fits well the direction of GPS shortening, suggesting that micro-earthquakes are the response of the crust to NS shortening.

Two other surveys, at the intersection between the Kazerun Fault and the MRF in Borujen (Yamini-Fard et al., 2006) and at the transition between the Zagros collision zone and

the Makran subduction zone near Bandar-Abbas (Yamini-Fard et al., 2007), show an intriguing result. Reverse-slip focal mechanisms are confined to depths greater than 12 km along NE-dipping décollement striking perpendicular to the motion, whereas dextral strike-slip focal mechanisms are recorded at shallower depths under the trace of the MRF. This difference in mechanism with depth suggests that the upper brittle crust deforms mostly by slip (either strike-slip or reverse, depending on the orientation) on weak pre-existing faults, but that the lower crust is more pervasively weakened and accommodates the shortening by reverse faulting perpendicular to regional motion.

Surface deformation

GPS deformation

GPS measurements provide instantaneous velocities between benchmarks. Depending on the surveying procedure and on the duration of the measurements for each survey, the accuracy of the position can reach ~2 mm. If the time span between 2 measurements is of several years, and moreover if 3 or more measurements are available allowing some redundancy, we estimate the velocity uncertainties to be less than 2 mm/y.

Several campaigns have been conducted in Zagros. One was part of a regional-scale survey conducted throughout Iran, with a spacing between stations larger than ~150 km (Nilforoushan et al., 2003; Vernant et al., 2004; Masson et al., 2007), which does not provide sufficient resolution to study the deformation in great detail. However, a dozen benchmarks from this network record 6-7.5 mm/y of NNE-SSW shortening for the Zagros, which corresponds to ~30% of the total convergence between Arabia and Eurasia at this longitude. The transition between the Makran subduction and the Zagros collision is clearly evidenced by the contrast in the velocities relative to Central Iran across the area..

Hessami et al. (2006) installed a network of 35 benchmarks covering the entire Zagros. These stations were measured during 3 campaigns over 3 years in 1998, 1999 and 2001. Each station was measured several times and sessions lasted 8 hours. The observations of 4-6 IGS stations were included for reference. The authors claim their accuracy to be 3 mm/y. The main results are that west of the Kazerun fault shortening is accommodated by the Mountain Front Fault whereas east of it, it seems to be accommodated 100 km north of the Mountain Front Fault and by the Main Zagros reverse Fault.

Since 1997, we installed several regional GPS networks in the Zagros (Fig. 5). These networks covered the Central Zagros (15 benchmarks), the Kazerun fault system (11 benchmarks) and the Northern Zagros (18 benchmarks) and were measured simultaneously

with several stations of the Iran Global network as well as with Iranian permanent stations. Each site was continuously observed for at least 48 hours per campaign. All networks were measured a minimum of 3 times over a time period lasting usually 2-5 years. The data have been analysed with the GAMIT/GLOBK 10.1 software (King and Bock, 2002). As many as 32 IGS stations (depending on the survey) have been included to establish the terrestrial reference frame. Final IGS orbits and corresponding Earth orientation parameters have been used. In the combination of daily solutions with the Kalman filter GLOBK, the continuous time series of daily SOPAC global solution files (IGS3 network) has been included, covering all measurement epoch presented here. Mean repeatability is estimated to be less than 2 mm, which yields a precision better than 2 mm/y. All details about processing procedures can be found in previous papers (Tatar et al., 2002; Walpersdorf et al., 2006; Tavakoli et al., 2008).

The main results (Fig. 5) show some differences with those of Hessami et al. (2006). As observed by these authors, the shortening component increases from NW to SE, consistent with a Arabia-Central-Iran pole of rotation located 29.8 N, 35.1 E, inferred by Vernant et al. (2004). But the deformation on each side of the Kazerun fault system is different from that proposed by Hessami et al. (2006). West of the Kazerun fault system, most of the deformation is located north of the MFF, far from the Zagros Frontal Fault (ZFF). It is clearly partitioned between 4-6 mm/y of dextral strike-slip motion concentrated in the north, with probably 2-4 mm/y on the MRF alone, and 3-6 mm/y of shortening probably on the MFF. East of the Kazerun Fault, the deformation is pure shortening of 8 mm/y located along the Persian Gulf shore and associated with the ZFF. In contrast to Hessami et al. (2006), we do not observe significant along-strike extension (i.e., larger than 2 mm/y) between the two extremities of the Zagros. The KFS strike-slip system induces some extension oblique to the faults, but we do not observe significant along-strike extension of the Zagros associated with perpendicular shortening or thickening of the belt. This view is also evidenced by the strain rate between the benchmarks.

We computed the strain rate and rigid rotation in all triangles defined by 3 adjacent benchmarks, and report here the amount and direction of shortening, as well as the rotation experienced by each triangle assumed to be a rigid block (Fig 6). GPS measurements show that most of the shortening is neither uniformly located across the belt, nor located on one of the major basement faults (i.e. MFF, ZFF) proposed by Berberian (1995). In contrast, shortening appears to be associated again with the topography and more specifically between the1000-m elevation contour and sea level (Fig. 6a). The correlation between the gradient in topography, basement seismicity (Talebian and Jackson, 2004) and instantaneous shortening

rate supports the hypothesis that basement and surface deformation are related and that both propagate south-westtward. Therefore, a total decoupling by the Hormuz salt of the shallow sediments from the basement is not needed..

Finally, we observe a consistent pattern of clockwise rotation throughout the Zagros (Fig. 6b). As expected, the largest rotations are associated with the largest strain rates and follow the 1000 m elevation contour. This general rotation is probably induced by the general right-lateral transcurrent motion between Central Iran and Arabia. We do not observe larger rotation associated with the strike-slip Kazerun Fault System, nor any anti-clockwise rotation as proposed by Talebian and Jackson (2004).

Tectonics

The Zagros deformation is characterized by constant-wavelength folding, thrusting and strike-slip faulting. Models suggest that detachment folding is the main folding style (Sherkati et al., 2006, Mouthereau et al., 2006). Fold geometries vary significantly with the presence of intermediate décollements (Sherkati et al., 2006). Some thrusts branched on décollement levels are formed by progressive fault propagation within the core of the folds. Other thrusts, associated with topographic steps, appear to be linked to basement faults. These reverse faults are generally blind. The difference in elevation of some stratigraphic marker horizons on both sides of the thrusts indicates 5-6 km finite vertical offset on both the MFF and the HZF (Berberian, 1995, Sherkati and Letouzey, 2004). The south-westward migration of sedimentary depocentres from Late Cretaceous times to Miocene collision, as well as the existence of several stages of folding suggests that the shortening rates have varied through time (Sherkati and Letouzey, 2004, Mouthereau et al, 2006).

In contrast to the blind reverse faults, the active traces of strike-slip faults are observable. Finite displacements on strike-slip faults are constrained by piercing points, major river offsets and fold offsets. Talebian and Jackson (2002) suggest 50 km of strike-slip offset on the MRF which, assuming an onset 3-5 My ago (by analogy with the North Anatolian Fault), would require a slip rate of 10-17 mm/y; much larger than the GPS velocity estimate. Lateral offsets of geomorphic markers and in-situ cosmogenic dating yield an estimated slip rate of 4.9-7.6 mm/yr on the MRF (Authemayou et al., in review). The other strike-slip fault is the Kazerun system, which we will discuss separately.

Geomorphological record of deformation

Numerous geomorphic markers such as fluvial and marine terraces occur throughout the central Zagros and can be used to constrain fold kinematics at timescales of 10^4-10^5 y, intermediate between the instantaneous deformation recorded by GPS and seismic studies and the long-term deformation inferred from section balancing. Such markers record incremental deformation and may therefore aid in discriminating between fold models. If they can be dated sufficiently precisely they also constrain deformation rates, which can be transformed into shortening rates using an appropriate fold model.

Oveisi et al. (2007 and in review) studied surface deformation as recorded by marine terraces along the coastal Mand anticline, located south of the Borazjan fault, as well as by fluvial terraces along the Dalaki and Mand rivers, which cross the north-western Fars east of the Kazerun Fault System. Their results indicate that shortening on Late Pleistocene timescales is concentrated in the frontal part of the belt, consistent with the GPS results discussed above (Fig. 7). Three or four frontal structures appear to absorb practically all of the shortening across the Central Zagros on intermediate timescales. Immediately east of the Kazerun Fault System, the coastal Mand anticline accommodates 3-4 mm y^{-1} shortening in a NE-SW direction. The Gisakan fold, located at the intersection of the Borazjan Fault and the MFF, also accommodates 2-4 mm y^{-1} of shortening in the same direction. These two structures together thus account for at least 70% and possibly all of the shortening between the stable Arabian and Iranian platforms. Further to the southeast, the situation is slightly more complex; with thin-skinned deformation concentrated on the Halikan fold located inboard of the MFF and only ~10 % ($\leq$ 1 mm y^{-1}) of the shortening taken up on the most frontal structures, such as the coastal Madar anticline.

For the active coastal anticlines, structural data as well as seismic sections preclude significant basement involvement. Instead, they evolve as open detachment or fault-propagation folds above basal (Hormuz Salt) or intermediate (Gachsaran evaporites) décollement levels. Crustal-scale shortening is fed into these structures either from the MFF of from the most internal parts of the Zagros. Active folds associated with the MFF, in contrast, do suggest basement involvement and occasional fault rupture up to the surface, as observed at the Gisakan fold. Inboard of the MFF, minor (< 1 mm y^{-1} along small-scale structures east of the Kazerun Fault) to significant (up to 5 mm y^{-1} for the Halikan anticline) amounts of shortening are absorbed by thin-skinned structures, whereas the surface expressions of major basement faults (e.g., the Surmeh Fault) provide no geomorphic evidence for recent activity.

The total amount of shortening on 10^4 – 10^5 y timescales, as recorded by geomorphologic markers of deformation is consistent, within error, to the GPS-derived present-day deformation rates of 8-10 mm y^{-1} across the Zagros. The geomorphic data also show that deformation has been concentrated in the outboard regions of the belt, associated with the MFF and other frontal structures, during Late Quaternary times, and that both thick- and thin-skinned structures are active simultaneously.

The Kazerun Fault System

The Kazerun Fault System (KFS) separates the North Zagros from the Central Zagros (Fig. 1). It comprises several ~NS trending right-lateral strike-slip faults. The Kazerun Fault itself is composed of 3 NS-trending segments (Fig. 8): the Dena, Kazerun and Borazjan segments which all terminate to the south with a north dipping reverse fault (Authemayou et al., 2005, 2006). The Kazerun Fault is associated with exhumation of Hormuz salt (Talbot and Alavi, 1996) and modifies the trend of folds adjacent to it. The KFS, as well as the other NS trending faults, is probably inherited from a Cambrian tectonic event that affected the Arabian platform because it controls the distribution of Hormuz salt, which is present to the east of the fault system but not to the west (Talbot and Alavi, 1996; Sepehr and Cosgrove, 2005). It was reactivated as early as in the Middle Cretaceous (Koop and Stoneley, 1982). The total offset along the Kazerun fault is a matter of debate, varying from 5 (Pattinson and Takin, 1971) or 8.2 km (Authemayou et al., 2006) to 140 km (Berberian, 1995) depending on the markers used to quantify strike-slip motion. This large difference in displacement results in inferred slip rates of 1 to 15 mm/y. Careful mapping of the active faults and of the lateral offsets along the different segments of the fault (Fig. 9) together with precise dating of fans yields a slip rate of ~3.1-4.7 mm/y on the Dena fault and 1.5-3.2 mm/y on the Kazerun fault (Authemayou et al., in review). The southernmost segment, the Borazjan fault, seems to have a dominant dip-slip motion (e.g., Oveisi et al., in review). East of the Kazerun fault, the Kareh-Bas fault is very active and accommodates ~5.5 mm/y of right-lateral strike slip; the Sabz-Pushan fault in contrast looks inactive, and the Sarvestan fault accommodates only little motion.

The onset of strike-slip motion on the Main Recent fault is probably of Upper Miocene age and therefore synchronous to the increase in shortening rate within the Zagros and the general tectonic re-adjustment observed throughout Iran (Allen et al., 2004). The onset of motion on both the Dena and Kazerun segments is more recent, probably ~3 my, and it is much younger (~0.8-2.8 my) for the Kareh-Bas Fault (Authemayou, 2006; Authemayou et al., in review).

GPS measurements of 11 benchmarks across the Kazerun fault system (Fig. 10) allow us to infer slip rates on the different faults with uncertainties of ~2 mm/y (Tavakoli et al., 2008). The Dena and Kazerun faults accommodate ~3.5 mm/y of right-lateral strike-slip motion. The Borazjan fault is almost inactive, but the Kareh-Bas Fault also accommodates ~3.5 mm/y of right-lateral strike-slip motion. A cumulated motion of ~1.5 mm/y (within the uncertainties) affects the High Zagros Fault and the Sabz-Pushan Fault. It seems, therefore, that the motion distributes from the Main Recent Fault to the Dena and Kazerun faults, jumps to the Kareh-Bas fault and distributes slightly on the High Zagros and Sabz-Pushan faults.

The Kazerun Fault System is seismically active (Berberian, 1995; Baker et al., 1993; Talebian and Jackson, 2004). Clearly, most of the seismicity and especially the largest magnitude earthquakes are located on the central segment of the Kazerun Fault (Fig. 8). The 3 largest (Ms>6) instrumental earthquakes were located on the Kazerun segment and the Kareh-Bas and Sabz-Pushan faults. Very little activity is observed on both the Dena and Borazjan faults and no activity is associated with either the High Zagros Fault or the Sarvestan Fault. The depth of the reliably located earthquakes associated with the KFS is 9+/-4 km which associate them likely to the basement. Most mechanisms are strike-slip on the Kazerun, Kareh-Bas and Sabz-Pushan faults. Reverse mechanisms are associated with the Mountain Front Fault, on both sides of the Kazerun Fault system. A few reverse mechanisms are also associated with the Borazjan segment, which suggests that it is not an active strike-slip fault but more probably a transpressive lateral ramp (e.g., Oveisi et al., in review).

Discussion

The separation of the Zagros mountain belt into 3 longitudinal structural domains (sedimentary, ophiolitic and metamorphic, Ricou et al., 1977) is valid only as a first-order approximation. In a second approximation the Zagros can be divided into two main units along strike, the North Zagros and the Central Zagros (the Fars) separated by the Kazerun Fault System (Berberian, 1995, Talebian and Jackson, 2004). These two domains present differences in width, in the activity of bounding faults, and in the direction of folding. To further investigate the present-day kinematics of the Zagros, one needs to know the relative roles of the basement (and ultimately of the lithosphere) and the surface cover. The present-day kinematics is certainly influenced by both the structure and the tectonic evolution of the fold-belt, and therefore should be studied in this perspective. We thus concentrate in this discussion on the comparison of shallow and crustal deformation patterns, both spatially and in time.

Surface deformation

The coupling between surface and basement varies across the Kazerun fault system. This variation in coupling may induce variations in the response of the surface layer to the deformation. To estimate the shortening of the North Zagros, we use the balanced cross-sections of Blanc et al. (2003) and McQuarrie (2004), because those of Sherkati and Letouzey (2004) cross the Kazerun fault and may not be representative of the shortening of the whole Zagros. For the Fars region, we use the cross-section of McQarrie (2004) which is the only section which really crosses Fars; the section of Molinaro et al. (2004) being located at the Zagros-Makran transition. Paradoxically, the total amount of shortening is larger in North Zagros than in Fars, both for the whole Zagros (from 57 to 85 km) and for the Zagros Fold Belt (from 35 to 50 km), even though the Fars is located further from the long-term Arabia-Central Iran pole of rotation located at 29.8N 35.1E. This variation in finite shortening could be explained by an underestimate of the displacement along the suture zone in the Central Zagros by McQuarrie (2004), or by an earlier onset of deformation in the North Zagros compared to the Central Zagros due to the progressive south-eastward closure of the Neotethys associated with the anti-clockwise rotation of the Arabian plate.

The GPS measurements also show a difference in present-day deformation across the Kazerun Fault System (Walpersdorf et al., 2006). In contrast to the total shortening, the present-day shortening rates increase slightly from the North Zagros (4-6 mm/y) to the Fars (8 mm/y), consistent with the increasing distance to the pole of rotation. The strike-slip component is mostly localized on the Main Recent Fault in the North Zagros but seems to be smaller and distributed in Fars. Both in the North Zagros and in the Fars, shortening seems to be concentrated between the 1000 m elevation topography and sea level.

Geomorphological observations suggest that the folds located at the shore of the Persian Gulf are the most active structures of the Zagros. This is consistent with the GPS measurements showing that most of the present-day shortening in Fars is also accommodated at the shore. This present-day activity located at the edge of the Zagros fold belt, along the Persian Gulf shore, is consistent with the south-westward propagation of the front of the Simply Folded Belt from the Eocene (and therefore earlier than the onset of collision) to the present time (Shearman, 1977; Hessami et al., 2001).

Basement deformation

The discussion between thick-skinned and thin-skinned models for Zagros fold belt deformation may never find a satisfactory answer because of the lack of seismic profiles reaching the basement. The only reliably (on the base of balanced cross sections) inferred basement reverse faults are the HZF and the MFF (Sherkati and Letouzey, 2004; Bosold et al., 2005; Blanc et al., 2003) because they clearly offset the sedimentary sequence and are controlled by seismic reflection profiles. The Zagros Frontal Fault itself generally does not propagate to the surface through the sedimentary cover, although a few surface breaks have been described (Bachmanov et al., 2004; Oveisi et al., in review).

The seismicity associated with shortening and reverse mechanisms is mostly located in the Zagros Fold belt (Fig. 11). Therefore neither the MZT nor the HZF are active or both are lubricated and slip aseismically. This seems true both for the North Zagros, where the only large earthquakes located north of the HZF belong to the strike-slip MRF, and for the Fars, where the seismic inactivity of these two faults is consistent with the absence of surface motion from GPS measurements across them. More precisely, the seismicity associated with reverse mechanisms is restricted to topography less than 1000 m as pointed out by Talebian and Jackson (2004). This could be due to the gradient in topography (Talebian and Jackson, 2004) but we suspect it is related to the propagation of the deformation front to the SW as evidenced both from structural studies (Sherkati and Letouzey, 2004), geomorphology and GPS. The two could be linked, however, if we consider a critical-wedge model for the evolution of the Zagros Fold Belt (e.g., Mouthereau et al., 2006). This propagation of deformation, and therefore of the construction of topography explains why seismicity is bounded by the Persian Gulf shore (Fig. 12), even though this shoreline has no tectonic significance and the water-depth in the Persian Gulf is less than 70 m.

The relation between seismicity and surface faults differs between the North Zagros and the Fars arc (Fig. 11). In the North Zagros, seismicity is restricted to a narrow band limited by the 1000-m elevation contour, which is also the trace of the MFF. Because the topography is relatively steep, the relation between the 1000-m contour and the MFF is clear. The seismicity does not fit totally with the distribution of GPS shortening, which also affects the low topography north of the Persian Gulf. However, because GPS deformation there is controlled only by the station KHOS (Fig. 5a) and no folding or topography generation is observed in the lowland, this frontal shortening remains to be confirmed.

In Fars, seismicity is spread throughout the area between 1000 m elevation and the shore (which might be related to the MFF and the ZFF, respectively); the zone of seismicity is

wider than in north Zagros but does not encompass the entire width of the fold belt. The gradient in topography is also smoother in Fars than in the North Zagros. GPS shortening is restricted to the shore and unrelated to the high elevation.

Thus, both the seismicity and the gradient in topography (which record basement deformation) are correlated with the pattern of cumulative (~ My) deformation. On the other hand, GPS and geomorphology (which record shallow deformation) are concentrated at the front of the deformation.

Less than 10% of the total deformation is released by earthquakes. However, there is a remarkable good fit in the directions of the tensor of deformation computed from both the GPS measurements and the seismological catalogs (Masson et al., 2005). This deficit could mean that some faults slip aseismically. An alternative and complementary explanation is that seismicity is restricted between 10 and 15 km because of the thick sedimentary cover, which limits the thickness of the brittle part of the crust to 5 km only (rather than 15-18 km as usua)l. The stress accumulated from boundary conditions is released by seismic energy for the brittle part but also by ductile deformation for both the sedimentary cover (by folding) and by lower crustal flow. If the brittle part of the crust is 30% of the usual thickness, we expect only 30% of seismic energy release.

Significance of the Kazerun fault system

The tectonics of the Kazerun Fault System is more complex than it looks first. The KFS is generally interpreted as an inherited fracture of an old tectonic event affecting the Arabian platform. Such inherited fractures are observed in several places in both the Zagros and the Arabian platform across the Persian Gulf, whereas we observe motion and seismicity only on part of the fractures located within the Zagros and only around the Kazerun zone. This focusing of seismicity could be due either to a non homogeneous state of stress within the Zagros or because the Zagros part of the Arabian platform is more brittle (it is thinner) than the remaining part.

These inherited fractures were activated during Permian and Mesozoic sedimentation, resulting in a change of the mechanical behaviour of the lithostratigraphic horizons. During collision, because the Kazerun fault system marks the boundary of the Hormuz salt layer in the Central Zagros, the fault plays the role of a lateral ramp for the Fars arc. A lateral ramp generally implies transpressional motion as observed along the Borazjan segment, which can be interpreted as the active part of the Kazerun fault lateral ramp. The southward propagation of this segment can be detected by a structural study of the Mand anticline. The bending of

this large coastal anticline suggests the presence of a hidden segment of the Kazerun fault system bounding the Mand fold to the west. As the Mand anticline is a Plio-Quaternary fold, the propagation of the Kazerun fault lateral ramp must be very recent.

If the Kazerun Fault is a lateral ramp of the Fars arc, the fault motion must be restricted to the cover. However, the seismic activity localized along the Kazerun segment implies basement faulting because earthquakes are likely located in the basement and thus an important role for the Kazerun Fault System in the Zagros deformation.

We observe an important contrast in the style of deformation west and east of the KFS. To the west, the belt is narrow and the deformation is partitioned between the strike-slip MRF and the shortening. To the east, the belt is wider, the deformation is more localized than in the west, and the MRF spreads into several strike-slip faults that look like a large distributed en-echelon system (Dena, Kazerun-HZF, HZF-Kareh-bas-Sabz-Pushan). In fact, the Kazerun Fault System is connected to the MRF (Authemayou et al., 2005). Consequently, since the Pliocene, the right-lateral strike-slip motion from the MRF is distributed onto several N- to NNE-trending strike-slip faults which are part of the Kazerun Fault System. The Dena Fault connects to both the Kazerun and the High Zagros faults, the High Zagros Fault connects to both the Sabz-Pushan and the Sarvestan faults, and the Kazerun Fault connects to both the Kareh-Bas and Borazjan faults. The connection between the MRF and the KFS has been attributed to the existence of inherited fractures (which were ultimately reactivated as the KFS) disturbing and stopping eastward propagation of slip on the MRF. The presence of Hormuz salt limited to the east of the Kazerun fault may facilitate the diffusion of deformation above a ductile layer and thus the slip motion. But the existence of the Hormuz salt cannot explain on its own the distribution of motion because some of these faults (Kareh-Bas, Sabz-Pushan) are also seismically very active. Furthermore, our GPS results do not support a “spreading” pattern of deformation for the Kazerun Fault System similar to gravity spreading as claimed by Nilforoushan and Koyi (2007) on the basis of analog experiments. They predict a divergent motion of the GPS vectors relative to Arabia, as reported by Hessami et al. (2006) but which does not correspond to our observations. We think that the distribution of deformation from the MRF to the Kazerun Fault System affects both the shallow sediments and the basement beneath the ductile layer.

Partitioning

Partitioning is one of the mechanisms which accommodate oblique motion (e.g. Fitch, 1972). Usually, strike-slip and reverse motion occur on two parallel faults which are a few tens of km

apart. In continental areas, it is likely that pre-existing faults localize the deformation because they are weak (e.g. Zoback et al., 1987). It also been proposed that a ductile layer decouples the oblique motion; (Richard and Cobbold, 1989) and helps partitioning. However, we observe partitioning of oblique convergence between shortening perpendicular to the belt and strike-slip motion on the MRF to the west of the Kazerun Fault System only, where the coupling between sediments and basement is strongest. Therefore, a ductile layer is probably not responsible for deformation partitioning in the North Zagros. We rather suspect that the MRF introduces a weak discontinuity which localizes strike-slip motion and, as a consequence, favours partitioning.

Vernant and Chéry (2006) designed a numerical mechanical model to explain the oblique convergence in Zagros. They suggest low partitioning along the MRF (1 to 2 mm/yr) associated with transpressionnal deformation throughout the belt. In contrast to their model predictions, GPS strike-slip motion is slightly higher (2-4 mm/y) and geomorphologic slip rate estimates on the MRF appear to match nearly completely the strike-slip component of convergence between Arabia and Central Iran. Fault kinematic measurements along the HZF, south of the MRF, indicate a transpressional regime on this fault (Malekzadeh, 2007). If partitioning exists, the shortening that complements the minimum Quaternary slip rate on the MRF of 4.9-7.6 mm/yr (Authemayou et al., in review) must be accommodated somewhere else. However, the fast slip rate along the MRF probably suggests a very weak MRF fault with a lower friction coefficient than adopted by Vernant and Chéry (2006), or possibly strong decoupling of the surface from the basement, rendering a model without mechanical layering somewhat irrelevant.

Conclusion

Our first conclusion is that we find, on both sides of the KFS, a good correlation between present-day surface deformation, as measured by GPS and geomorphology on one hand, and seismicity (affecting only the upper basement) and topography on the other hand (Fig. 11), suggesting that both the sedimentary cover and the basement deform together (i.e. a thick-skinned system). Because we know that deformation of the sedimentary cover propagates south-westward, we suspect basement deformation, which is required to explain the average topography, to do the same (Fig. 12). In contrast to Hessami et al. (2006), we do not observe any active shortening across the southern segment of the MZT. Thus, the reason for such propagation is probably the recent locking of the continental collision, propagating the stress away from the MZT onto inherited normal faults of the Arabian platform (Jackson, 1980).

Because the strike of the belt is perpendicular to the motion of Arabia relative to Central Iran, no partitioning is required in the Central Zagros (Talebian & Jackson, 2004).

The second conclusion is that the Kazerun Fault system separates the North Zagros (experiencing slip partitioning), from the Central Zagros (experiencing distributed deformation), as proposed previously. There is a good agreement between present-day deformation observed by GPS and tectonic observations, suggesting that this deformation has been stable for some time. The Kazerun Fault System distributes the strike-slip motion from the MRF onto different branches in an en-echelon arrangement, from the Dena segment to the Sabz-Pushan and High Zagros faults. The presence of the decoupling Hormuz salt layer cannot be the only reason for such distribution because seismicity is associated with the active faults, attesting that the basement deforms in the same way. Consequently, the Kazerun Fault System affects both the sedimentary cover and the basement, playing the role of a lateral ramp of the deformation front for its southern Borazjan segment and of a "horse-tail" termination of the MRF for its northern and central segments.

Acknowledgments

This work is part of a Franco-Iranian collaborative program between French and Iranian scientific institutions conducted between 1997 and 2007. It has been funded by CNRS-INSU, the French Embassy in Tehran, the International Institute of Earthquake Engineering and Seismology of Iran, the Geological Survey of Iran, the National Cartographic Center of Iran. We warmly thank all the people who enthusiastically participated in the field work. We are considerably indebted to all drivers of Iranian institutions who countlessly spent time to help in all aspects of the field work. The thank M. Goraishi, M. Ghafory-Ashtiany, M. Madad and P. Vidal for encouragement and support. We benefited of numerous scientific discussions with several colleagues and especially P. Agard, J. Jackson, L. Jolivet, J. Letouzey, L.-E. Ricou, M. Talebian. The paper greatly benefited from careful reviews of R. Bendick and J. Jackson.

References

Agard, P., J. Omrani, L. Jolivet, and F. Mouthereau, F., 2005. Convergence history across Zagros (Iran): constraints from collisional and earlier deformation. *International Journal of Earth Sciences*, DOI 10.1007/s00531-005-0481-4.

Allen, M., Jackson, J., Walker, R., Late Cenozoic re-organisation of the Arabia-Eurasia collision and the comparison of short-term and long-term deformation rates, *Tectonics*, 23, doi:10.1029/2003TC001530, 2004.

Ambraseys, N. N., 1978. The relocation of epicenters in Iran, *Geophysical Journal of the Royal astronomical Soceity*, 53, 117-121.

Authemayou, C., 2006. *Partitionnement de la convergence oblique en zone de collision : Exemple de la chaîne du Zagros (Iran),* Ph.D. thesis, 334p, Univ. Paul Cézanne, Aix-Marseille, France.

Authemayou C., O. Bellier, D. Chardon, Z. Malekzadeh, M. Abbassi, 2005. Active partitionning between strike-slip and thrust faulting in the Zagros fold-and-thrust belt (Southern Iran). *Compte Rendu Géoscience, Académie des Sciences de Paris*, 337, 539-545.

Authemayou C, D. Chardon, O. Bellier, Z. Malekzadeh, E. Shabanian, M.R. Abbassi, 2006. Late Cenozoic partitioning of oblique plate convergence in the Zagros fold-and-thrust belt (Iran). *Tectonics*, 25, Art. No. TC3002.

Authemayou, C., Bellier, O., Chardon, D., Benedetti, L., Malekzadeh, Z., Claude, C., Angeletti, B., 2007. Quarternary Kazerun and the Main Recent Faults slip rates: evidence for strike-slip partitioning in the Zagros fold-and-thrust belt, *Journal of Geophysical Research*, submitted.

Bachmanov, D.M., Trifonov, V.G., Hessami, K.T., Kozhurin, A.I., Ivanova, T.P., Rogozhin, E.A., Hademi, M.C. & Jamali, F.H., 2004. Active faults in the Zagros and central Iran, *Tectonophysics*, 380, 221-241.

Baker, C., Jackson, J., & Priestley, K., 1993. Earthquakes on the Kazerun Line in the Zagros Mountains of Iran: strike-slip faulting within a fold-and-thrust belt, *Geophysical Journal International*, 115, 41-61.

Berberian, M., 1979. Evaluation of the instrumental and relocated epicenters of Iranian earthquakes, *Geophysical Journal of the astronomical Society*, 58, 625-630.

Berberian, M., 1995. Master blind thrust faults hidden under the Zagros folds: active basement tectonics and surface morphotectonics, *Tectonophysics*, 241, 193-224.

Blanc, E. J.-P., Allen, M. B., Inger, S., and Hassani, H., 2003. Structural styles in the Zagros Simple Folded Zone, Iran, *Journal of the Geological Society of London*, 160, 401-412.

Bosold, A., Schwarzhans, W., Julapour A., Ashrazadeh, A. R., and Ehsani, S. M., 2005. The structural geology of the High Central Zagros revisisted (Iran), *Petroleum Geosciences*, 11, 225-238.

Engdahl, E. R., Van der Hilst, R. D., and Buland, R. P., 1998. Global teleseismic earthquake relocation with improved travel times and procedures for depth determination, *Bulletin Seismological Society of America*, 88, 722-743.

Engdahl, E. R., Jackson, J. A., Myers, S. C., Bergman, E. A., and Priestley, K., 2006. Relocation and assessment of seismicity in the Iran region, *Geophysical Journal International*, 167, 761-778.

Haynes, S. J., & McQuillan, H., 1974. Evolution of the Zagros suture zone, southern Iran, *Bulletin of the geological Society of America*, 85, 739-744.

Hessami, K., Koyi, H., Talbot, C. J.,, Tabasi, H., and Shabanian, E., 2001. Progressive unconformities within and evolving foreland fold-thrust belt, Zagros Mountains, *Journal of the Geological Society of London*, 158, 969-981.

Hessami, K., Nilforoushan, F., and Talbot, C., 2006. Active deformation within the Zagros Mountains deduced from GPS measurements, *Journal of the Geological Society of London*, 163, 143-148.

Jackson, J. A., 1980. Reactivation of basement faults and crustal shortening in orogenic belts, *Nature*, 283, 343,-346.

Jackson, J., 1980, Errors in focal depth determination and depth of seismicity in Iran and Turkey, *Geophysical Journal of the astronomical Society*, 61, 285-301.

Jackson, J. and T. Fitch, 1981. Basement faulting and the focal depths of the larger earthquakes in the Zagros mountains (Iran), *Geophysical Journal of the astronomical Society,* 64, 561-586.

Jackson, J. A., & McKenzie, D., 1984. Active tectonics of the Alpine-Himalayan Belt between western Turkey and Pakistan, *Geophysical Journal of the astronomical Society*, 77, 185-264.

Jackson, J. and D. McKenzie, 1988. The relationship between plate motions and seismic moment tensors and the rates of active deformation in the Mediterranean and Middle East, *Geophysical Journal of the astronomical Society,* 83, 45-73.

King, R.W., and Bock, Y., 2002. *Documentation for the GAMIT analysis software*, release 10.1, Massachusetts Institute of Technology, Cambridge, MA.

Koop, W. J., and Stoneley, R.,1982. Subsidence history of the Middle East Zagros Basin, Permian to Recent, *Philosophical Transactions of the Royal Society of London*, 305, 149-168.

Maggi, A., Jackson, J. A., Priestley, K., and Baker, C., 2000. A re-assessement of focal depth distributions in Southern Iran, the Tien Shan and Northern India,; Do earthquakes really occur in the continental mantle? *Geophysical Journal International*, 143, 629-661.

Malekzadeh, Z., 2007, The accommodation of the deformation from Main Recent Fault to Kazerun, Ph.D. thesis, 371p, Institute of Earthquake Engineering and Seismology, Tehran, Iran.

Masson, F., J. Chéry, D. Hatzfeld, J. Martinod, P. Vernant, F. Tavakoli, M. Ghafory-Asthiani, 2005. Seismic versus aseismic deformation in Iran inferred from earthquakes and geodetic data, *Geophysical Journal International*, 160, 217-226.

Masson, F., Anvari, M., Djamour, Y., Walpersdorf, A., Tavakoli, F., Daignières, M., Nankali, H. and Van Gorp, S., 2007. Large-scale velocity field and strain tensor in Iran inferred form GPS measurements: new insight for the present-day deformation pattern within NE Iran, *Geophysical Journal International.*, 170, 436-440.

McKenzie, D.P., 1978. Active tectonics of the Alpine-Himalayan belt: the Aegean Sea and surrounding regions, *Geophysical Journal of the astronomical Society*, 55, 217-254.

McQuarrie, N., 2004. Crustal scale geometry of the Zagros fold-thrust belt, Iran, *Journal of Structural Geology*, 26, 519-535.

McQuarrie, N., Stock, J. M., Verdel, C., and Wernicke, B. P., 2003. Cenozoic evolution of Neothethys and implications for the causes of plate motion, *Geophysical Research Letters*, 30, doi:10.1029/2003GL017992.

Molinaro, M., Guezou, J. C., Leturmy, P., Eshraghi, S. A., Frizon de Lamotte, D., 2004. The origin of changes in structural style across the Bandar Abbas syntaxis, SE Zagros (Iran), *Marine and Petroleum Geology*, 21, 735-752.

Molinaro, M., Leturmy, P., Guezou, J.-C., Frizon de Lamotte, 2005. The structure and kinematics of the south-eastern Zagros fold-thrust belt, Iran: from thin-skinned to thick-skinned tectonics, *Tectonics*, 24, NIL42-NIL60.

Molnar, P., and H. Lyon-Caen, 1988. Some simple physical aspects of the support, structure, and evolution of mountain belts, in Processes in Continental Lithospheric Deformation, *Geological Society America Special Paper*. 218, 179-207.

Mouthereau, F., Lacombe, O., and Meyer, B., 2006. The Zagros folded belt (Fars, Iran): constraints form topography and critical wedge modeling, *Geophysical Journal International*, 165, 336-356.

Ni., J., & Barazangi, M., 1986. Seismotectonics of the Zagros Continental Collision Zone and a Comparison with the Himalayas, *Journal of Geophysical Research*, 91, 8205-8218.

Niazi, M., Asudeh, G., Ballard, G., Jackson, J. A., King, G., & McKenzie, D. P., 1978. The depth of seismicity in the Kermansha region of the Zagros mountains (Iran), *Earth and Planetary Science Letters*, 40, 270-274.

Niazi, M., 1980. Microearthquakes and crustal structure off the Makran coast of Iran, *Geophysical Research Letters*, 7, 297-300.

Nilforoushan, F., Vernant, P., Masson, F., Vigny, C., Martinod, J., Abbassi, M., Nankali, H.,, Hatzfeld, D., Tavakoli, F., Ashtiany, M.,, Doerflinger, E.,, Daignieres, M.,, Collard, P., Chéry, J., (2003), GPS network monitors the Arabia-Eurasia collision deformation in Iran, *Journal of Geodesy*, 77 (7-8): 411-422.

Nilforoushan, F., and Koyi, H. A., 2007, Displacement fields and finite strains in a sandbox model simulating a fold-thrust-belt, *Geophysical Journal International*, 169, 1341-1355.

Oveisi, B., Lavé, J., and van de Beek, P, 2007, Rates and processes of active folding evidenced by Pelistocene terraces at the central Zagros front (Iran), in *Thrust Belt and Foreland Basin*, ed. Lacombe, O et al., Frontiers in Earth Sciences, Springer, in press.

Oveisi, B., Lavé, J., ven der Beek, P., Carcaillet, J., Benedetti, L., Braucher, R., and Aubourg, C., 2007. Thick- and thin-skinned deformation rates in the Zagros Simple Folded Zone (Iran) indictaed by displacement of geomorphic surfaces, *Geophysical Journal International*, in review.

Richard, P., & Cobbold, P., 1989. Structures en fleur positives et décrochements crustaux : modélisation analogique et interprétation mécanique, *C. R. Acad. Sci. Paris*, **308**, 553-560.

Ricou, L.E., Braud, J., and Brunn, J.H., 1977. Le Zagros, Mém h. sér. Soc. Géol. Fr., 8, 33-52.

Shearman, D. J., 1977. The geological evolution of Southern Iran, *Geographical Journal*, 142, 393-410.

Sherkati, S., Letouzey, J., 2004. Variation of structural and basin evolution in the cebtral Zagros (Izeh zone and Dezful Embayment), Iran, *Marine and Petroleum Geology*, 21, 535-554.

Sherkati, S., Molinaro, M., Frizon de Lamotte, D., Letouzey, J., 2005, Detachment folding in the Central and Eastern Zagros fold-belt (Iran): salt mobility, multiple detachments and late basement control, *Journal of Structural Geology*, 27, 1680-1696.

Snyder, D. B., & Barazangi, M., 1986. Deep crustal structure and flexure of the Arabian plate beneath the Zagros collisional mountain belt as inferred from gravity observations, *Tectonics*, 5, 361-373.

Talebian, M., and Jackson, J., 2004, A reappraisal of earthquake focal mechanisms and active shortening in the Zagros mountains of Iran, *Geophysical Journal International*, 156, 506-526.

Talebian, M., and Jackson, J., 2002. Offset on the Main Recent Fault of NW Iran and implications for the late Cenozoic tectonics of the Arabia-Eurasia collision zone, *Geophysical Journal International*, 150, 422-439.

Tatar, M., D. Hatzfeld, J. Martinod, A. Walpersdorf, M. Ghafori-Ashtiany and J. Chéry, 2002. The present-day deformation of the central Zagros (Iran) from GPS measurements, *Geoph. Res. Lett.*, Vol. 29, No. 19, pp. 1927-1930.

Tatar, M., Hatzfeld, D., Ghafory-Ashtiany, M., 2003. Tectonics of the Central Zagros (Iran) deduced from microearthquake seismicity, *Geophysical Journal International*, 156, 255-266.

Tavakoli, F., Walpersdorf, A., Authemayou, C., Nankali, H. R., Hatzfeld, D., Tatar, M., Djamour, Y., Nilforoushan, F., and Cotte, N., 2008. Distribution of the right-lateral strike-slip motion from the Main Recent Fault to the Kazerun Fault System (Zagros, Iran): Evidence from present-day GPS velocities, Earth Planet Lett., submitted.

Vernant, P., Nilforoushan, F., Hatzfeld, D., Abbassi, M., Vigny, C., Masson, F., Nankali, H., Martinod, J., Ashtiany, M., Bayer, R., Tavakoli, F., Chéry, J., 2004. Contemporary crustal deformation and plate kinematics in the Middle East Constrained by GPS measurements in Iran and Northern Oman, *Geophysical Journal International* , 157, 381-398 .

Vernant P, Chery J, 2006. Mechanical modelling of oblique convergence in the Zagros, Iran, *Geophysical Journal International*, 165, 991-1002.

Walpersdorf, A., Hatzfeld, D., Nankali, H., Tavakoli, F., Nilforoushan, F., Tatar, M., Vernant, P., Chery, J., and Masson, F., 2006. Difference in the GPS deformation pattern of North and Central Zagros (Iran), *Geophysical Journal International*, 167, 1077-1088.

Yamini-Fard, F., Hatzfeld, D., Tatar, M., and Mokhtari, M., 2006. Microseismicity at the intersection between the Kazerun fault and the Main Recent Fault (Zagros-Iran), *Geophysical Journal International*, 166, 186-196.

Yamini-Fard, F., Hatzfeld, D., Farahbod, A., Paul, A., Mokhtari, M., 2007. The diffuse transition between the Zagros continental collision and the Makran oceanic subduction (Iran): microearthquake seismicity and crustal structure , *Geophysical Journal International*, 170, 182-194.

Figure captions

Figure 1 : Location map showing the main geographic and tectonic features of the Zagros (Iran) modified after Berberian (1995), Talebian and Jackson (2004), Authemayou et al., (2006). For the faults, we use the terminology of Berberian (1995). MZRF is the Main Zagros Reverse Fault, MRF is the Main Recent Fault, HZF is the High Zagros Fault, MFF is the Main Frontal Fault, ZFF is the Zagros Frontal Fault, KFS is the Kazerun Fault system that separates the North Zagros from the Central Zagros. We represent the color topography with changes at 1000, 2000 and 3000 m levels.

Figure 2 : Seismicity map of Zagros based on the USGS catalogue, confirming Talebian and Jackson's (2004) observation that seismicity, and especially large magnitude earthquakes, is restricted to the southwest of the Zagros topography.

Figure 3 : Fault plane solutions in Zagros. Blue focal spheres are body waves solutions modelled by Talebian and Jackson (2004) and red focal spheres are CMT solutions (http://www.seismology.harvard.edu/CMTsearch.hml). As pointed out by Talebian and Jackson (2004), most of the Zagros experiences reverse faulting, except near the MZRF and the KFS.

Figure 4 : SW-NE cross-section across the Central Zagros (after Tatar et al., 2003). a) Topography, b) Well-located (better than 2 km) microseismicity recorded during a 7-week period. Microseismicity is restricted to the upper basement beneath the sedimentary layer and dips slightly NE c) Fault plane solutions (in cross section), showing mostly reverse mechanisms d) Our interpretation of clustering possibly associated with active faults (red lines). Black arrows at the surface represent fold axes, the spacing of which is unrelated to any clustering in seismicity.

Figure 5:GPS motion of Zagros (Tatar et al., 2002; Walpersdorf et al., 2006; Tavakoli et al., 2007) with 95% confidence ellipses. a) Motion relative to Arabia and b) motion relative to Central Iran. Deformation appears localized near the MFF. We do not observe a fan shape pattern in Central Zagros, as expected from spreading of the motion due to the Hormuz salt layer.

Figure 6:a) Strain rate deduced form GPS observations. Triangles are coloured as a function of the intensity of the deformation. The arrows are the principal strain rates. The triangles with significant deformation (exceeding the uncertainties) are surrounded with a bold line. The direction of shortening consistently trends NNE-SSW with a slight NS rotation near the Kazerun Fault System. East of the KFS, the deformation is localized at the MFF near

the Persian Gulf. West of the KFS, the deformation is localized further north, also at the MFF. In both case it can be associated with the 1000 m topography elevation.

b) Rotations of triangles defined by 3 benchmarks. Although uncertainties are large, we observe a consistent clockwise rotation. Only 2 triangles located at the easternmost location show significant anticlockwise rotation. Triangles with rotations larger than 1^0/My are associated with large strain and located along the MFF as the strain does.

Figure 7: Summary of the geomorphological observations of Oveisi et al. (2007 and in review) (a) Map of the central Zagros showing the inferred shortening rates across individual structures (Gis: Gisakan fold; Hal: Halikhan fold; Mand: Mand fold; Mar: Madar fold) as deduced from Late Pleistocene terrace uplift rates (dark shaded arrows, annotated with inferred rate in mm/yr). Compare this pattern to the pattern of present-day strain rates in Fig. 6. Fault abbreviations on map: BF: Borazjan Fault; HZF: High Zagros Fault; KF: Kazerun Fault; MFF: Main Frontal Fault; SF: Surmeh Fault Light and dark shaded dashed lines indicate locations of transects shown in b. (b) Synthetic profiles of convergence rates (relative to stable Arabia) across the central Zagros according to GPS and geomorphic data, compared to topographic profiles along a northwestern (light shading) and southeastern (dark shading) transect. Modified from Oveisi et al. (in review).

Figure 8: Detailed seismotectonic map of the Kazerun Fault system. The active faults (Authemayou et al., 2006) with significant present-day motion (Tavakoli et al., 2007) are bold. Symbols for seismicity and focal mechanisms are the same as in Fig. 2 and Fig. 3. The MZRF fault looks totally inactive. Most seismicity is restricted to the SW of the MFF. Seismicity is associated with the Dena, Kazerun, Kareh-Bas and Sabz-Pushan strike-slip faults.

Figure 9: Quaternary slip rate and finite horizontal displacement showing the motion distribution from the Main Recent Fault to the Kazerun fault system (after Authemayou et al., 2006)

Figure 10: GPS velocity for benchmarks located near the Kazerun fault system (after Tavakoli et al., 2007). a) motion relative to Arabia, b) motion relative to Central Iran

Figure 11: Cross sections through the North and Central Zagros (see location in Fig. 2) displaying a) topography, b) seismicity, c) present-day GPS motion parallel to the mountain belt, d) present-day shortening perpendicular to the mountain belt. Symbols for seismicity are as in Fig. 2. The present-day motion is from GPS velocities relative to Central Iran. We plot the location of the main faults (Berberian, 1995). There is a strong correlation between the gradient in topography, the seismicity (relative to the basement

deformation), and the shallow deformation. In North Zagros, the strike-slip motion is concentrated near the MRF, whereas it is more distributed in Central Zagros.

Fig 12; Sketch summarizing our results and interpretation. C.I is Central Iran and MZT is Main Zagros Thrust. Both the shallow deformation of the sedimentary cover and the brittle deformation of the basement are associated with the gradient in topography, suggesting that they are related. Faulting in the basement is unrelated to faulting and folding in the sedimentary cover. Because we know the shallow deformation propagated southwestward with time, we suspect the basement deformation to do the same.

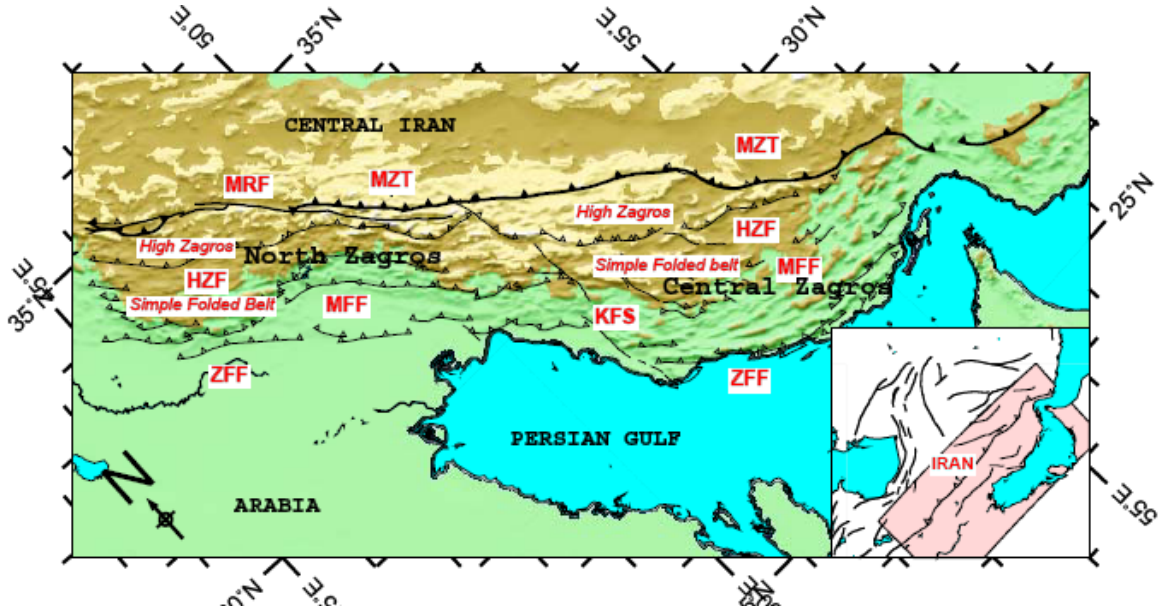

Figure 1

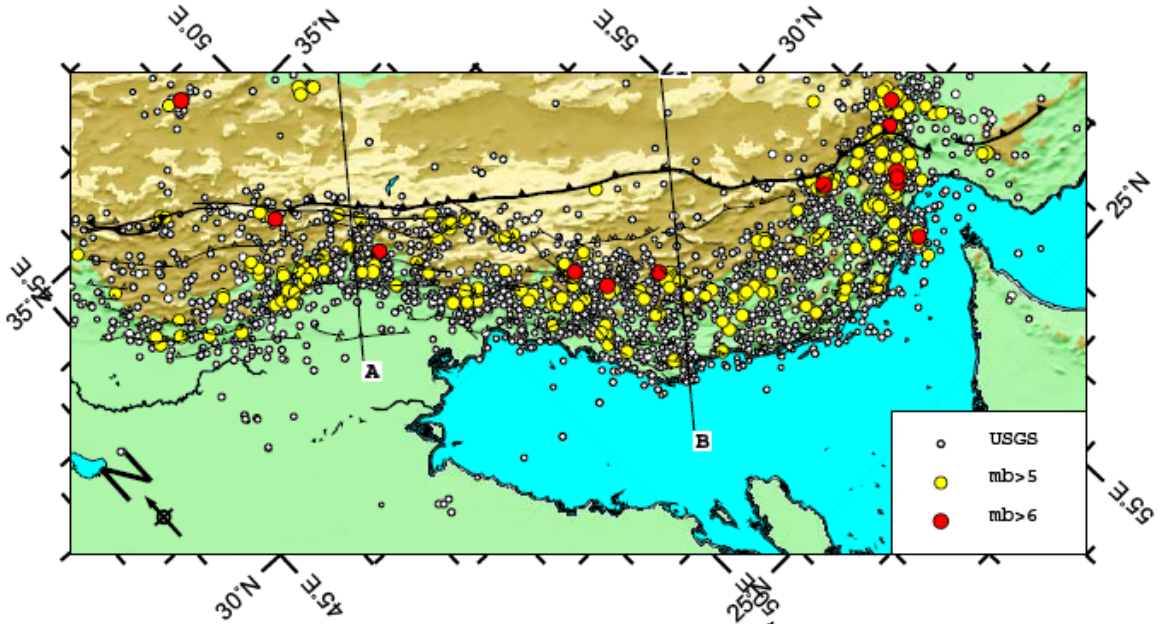

Figure 2

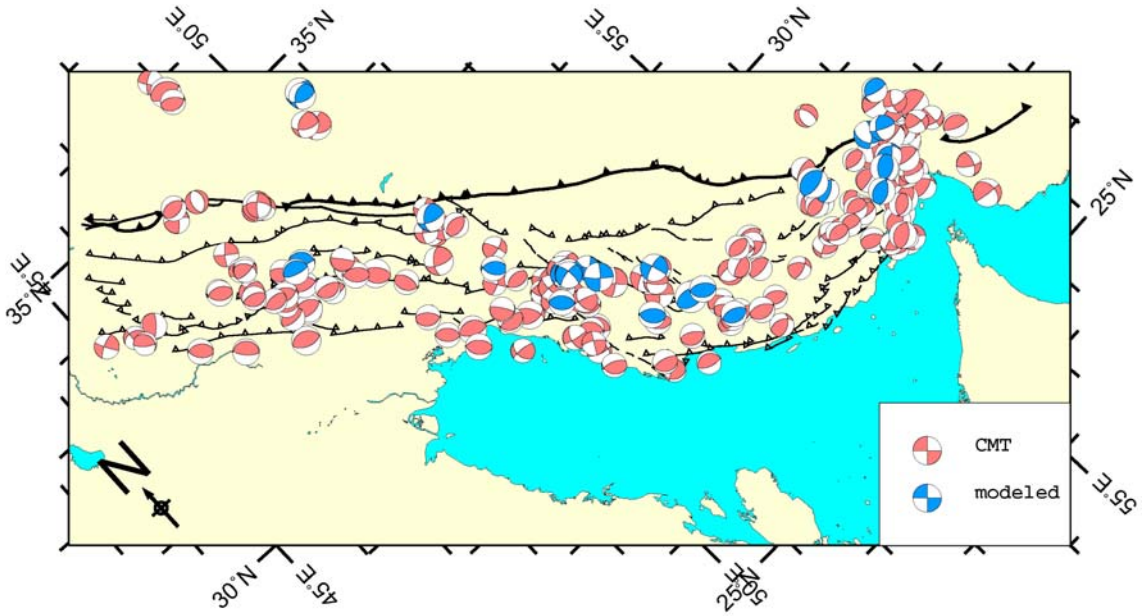

Figure 3

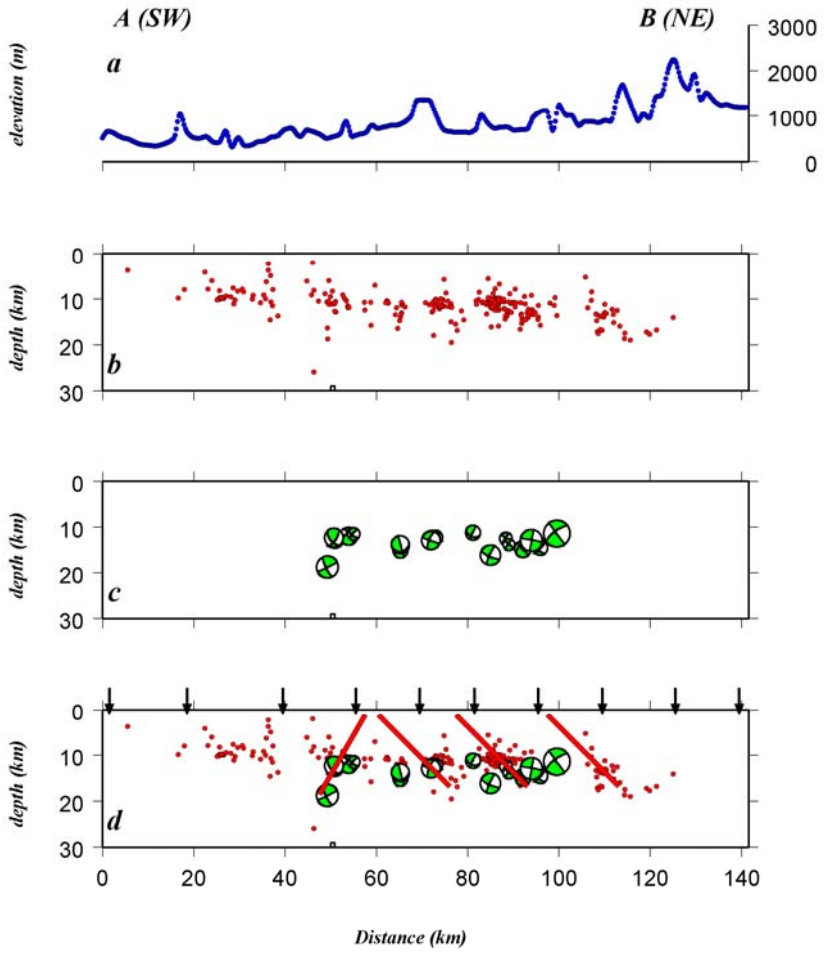
A (SW)
B (NE)
a
elevation (m)
3000
2000
1000
0
depth (km)
b
c
d
0
10
20
30
0
20
40
60
80
100
120
140
Distance (km)

Figure 4

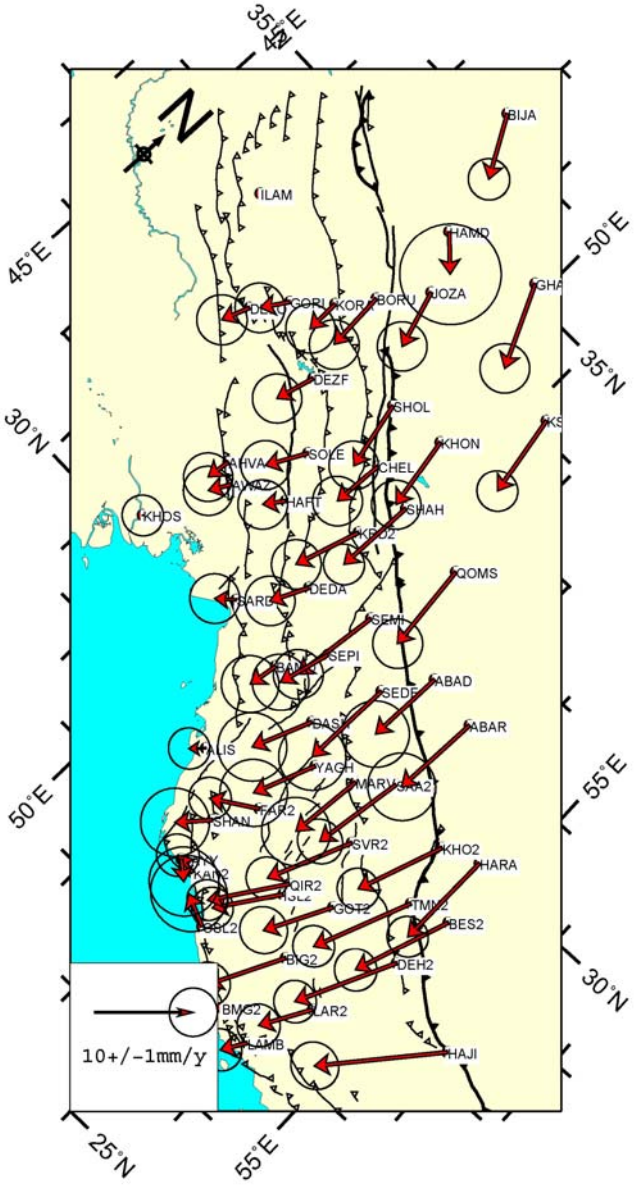
35°E
40°E
45°E
50°E
55°E
60°E
25°N
30°N
35°N
40°N
N
BIJA
ILAM
HAMD
GHA
BORU
JOZA
DEZF
SHOL
KHON
SOLE
CHEL
AHVA
HAFT
SHAH
KHDS
DEDA
QOMS
SEPI
SEDE
ABAD
ABAR
YAGH
SVR2
KHO2
HARA
TMB2
BES2
DEH2
BMG2
LAR2
LAMB
HAJI
10+/-1mm/y

Figure 5a

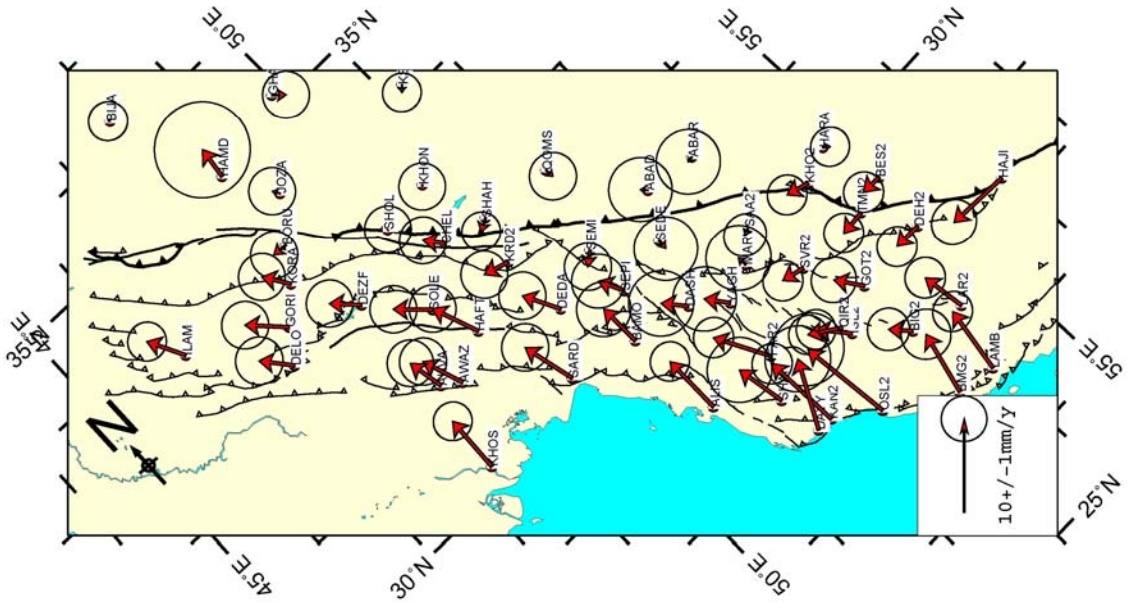

Figure 5b

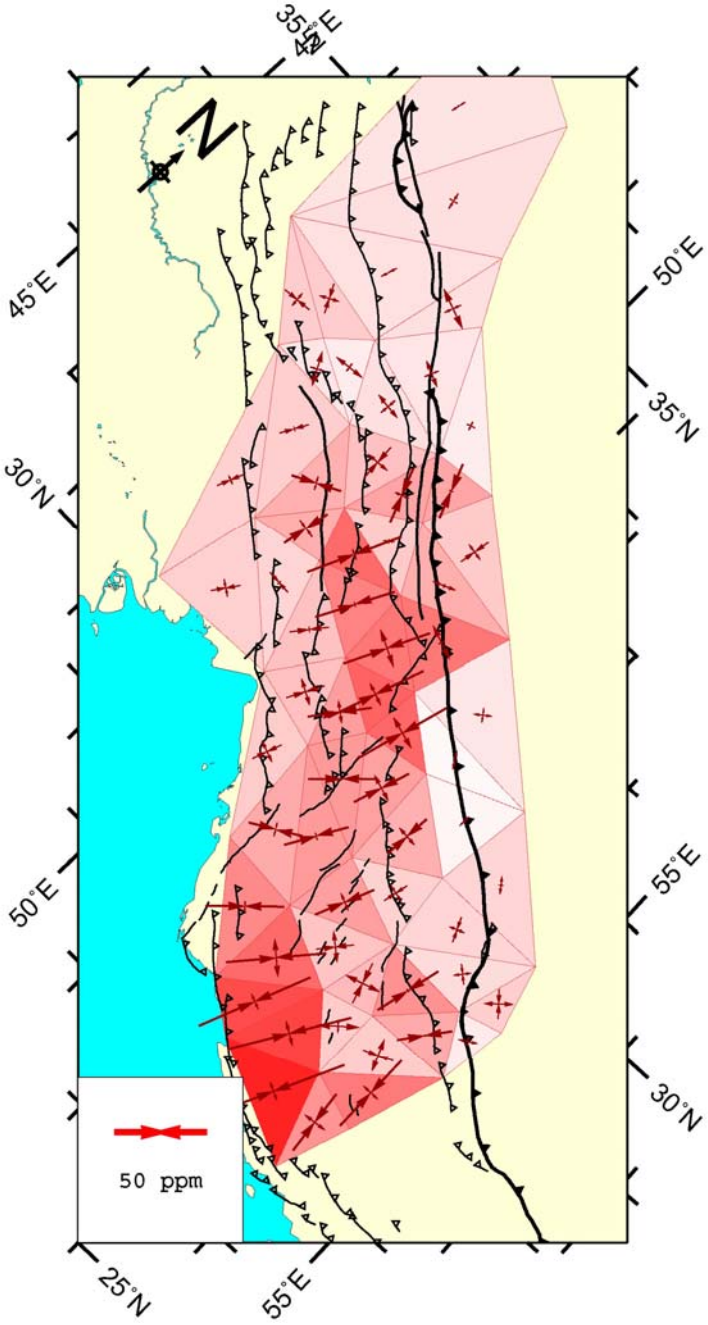

Figure 6a

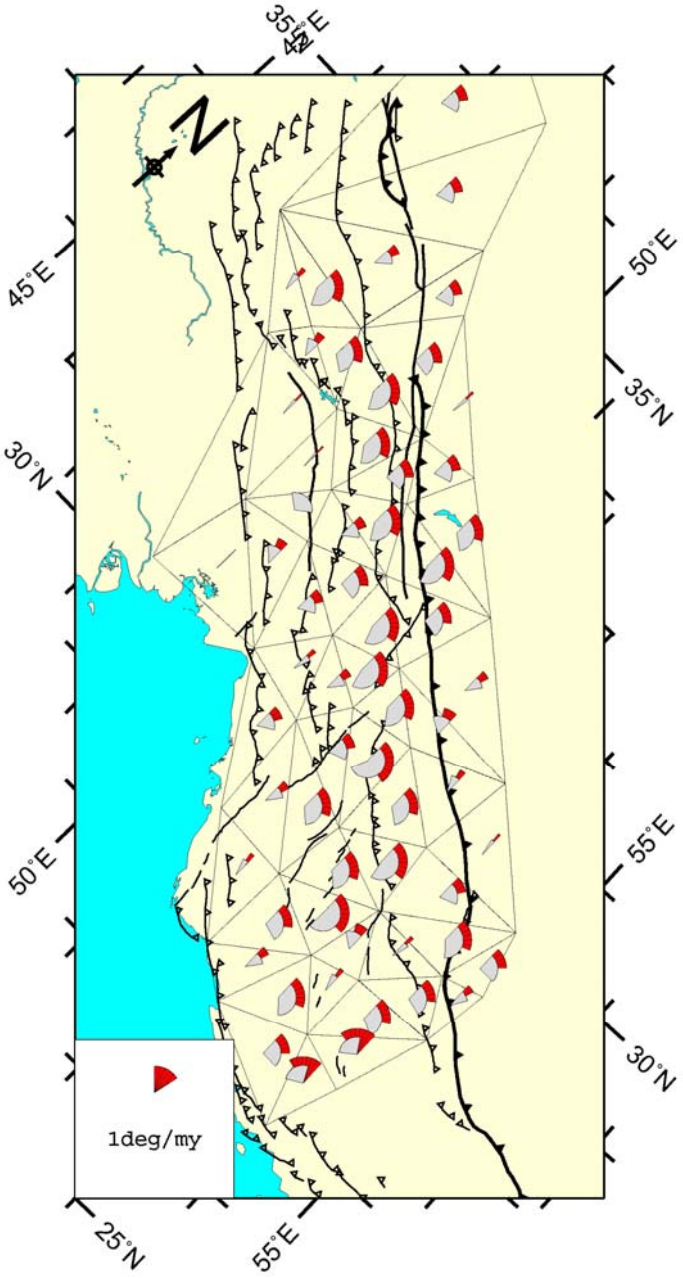

Figure 6b

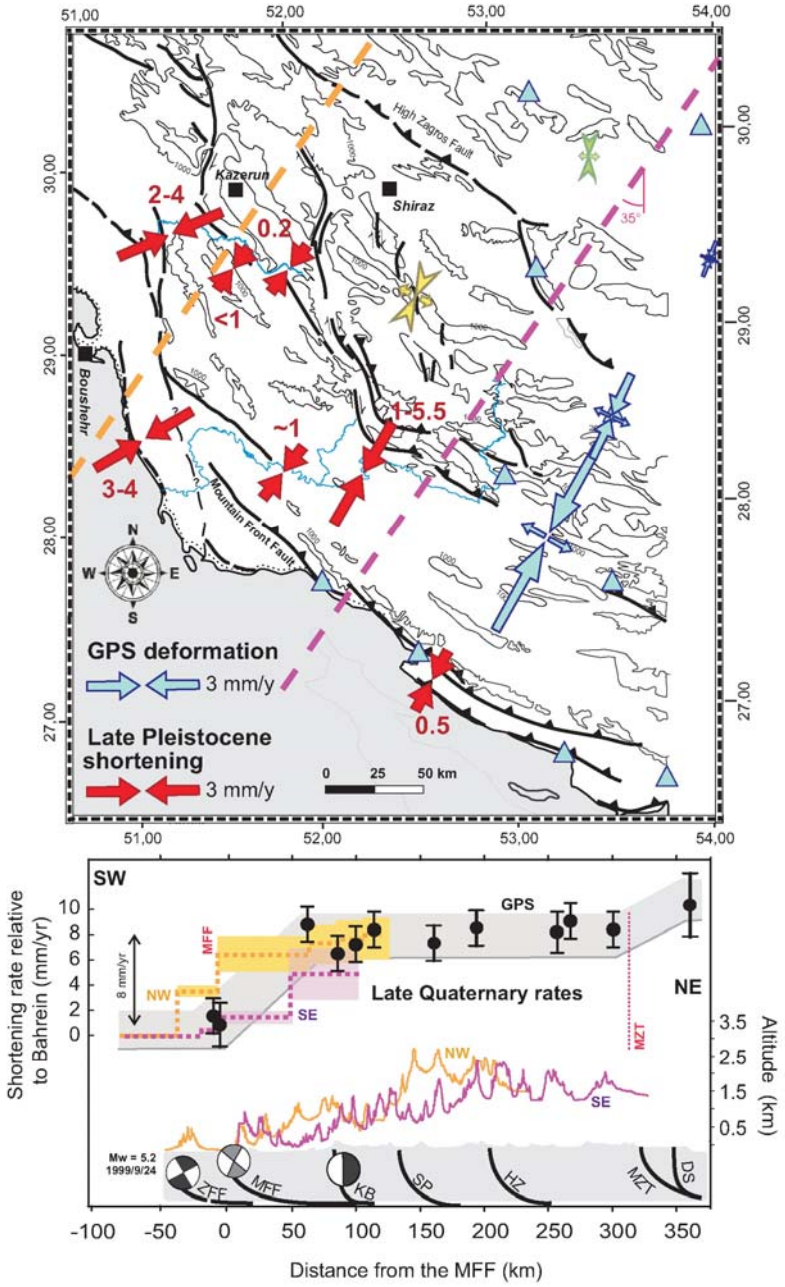
51,00
52,00
53,00
54,00
30,00
29,00
28,00
27,00
High Zagros Fault
Kazerun
Shiraz
Boushehr
Mountain Front Fault
2-4
0.2
<1
~1
1-5.5
3-4
0.5
35°
N
W
E
S
GPS deformation
3 mm/y
Late Pleistocene shortening
3 mm/y
0 25 50 km
SW
NE
GPS
Late Quaternary rates
MFF
MZT
NW
SE
8 mm/yr
Shortening rate relative to Bahrein (mm/yr)
Altitude (km)
Mw = 5.2
1999/9/24
ZFF
KB
SP
HZ
DS
Distance from the MFF (km)

Figure 7

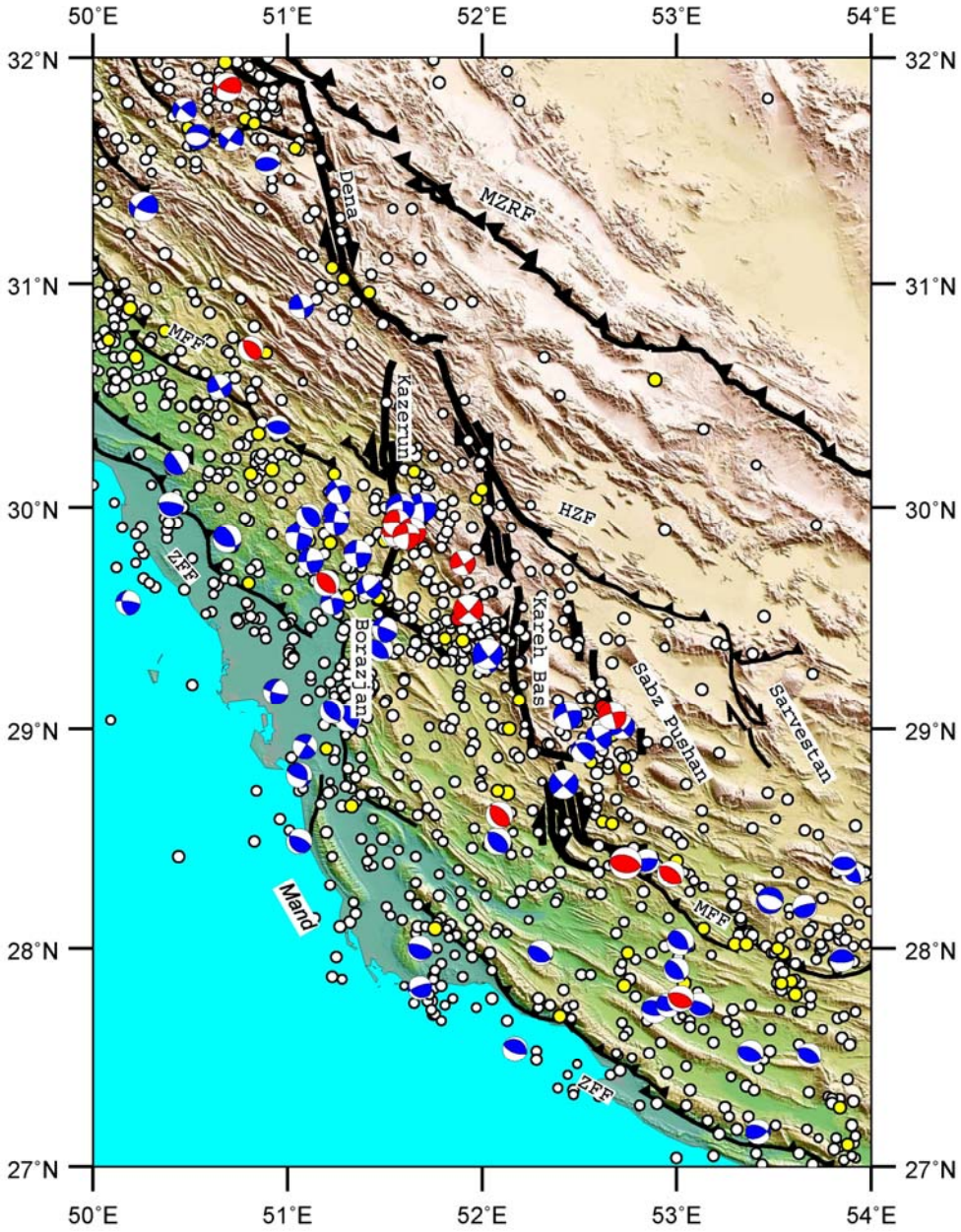
50°E
51°E
52°E
53°E
54°E
32°N
31°N
30°N
29°N
28°N
27°N
Dena
MZRF
MFF
Kazerun
HZF
ZFF
Borazjan
Karen Bas
Sabz Pushan
Sarvestan
Mand
MFF
ZFF

Figure 8

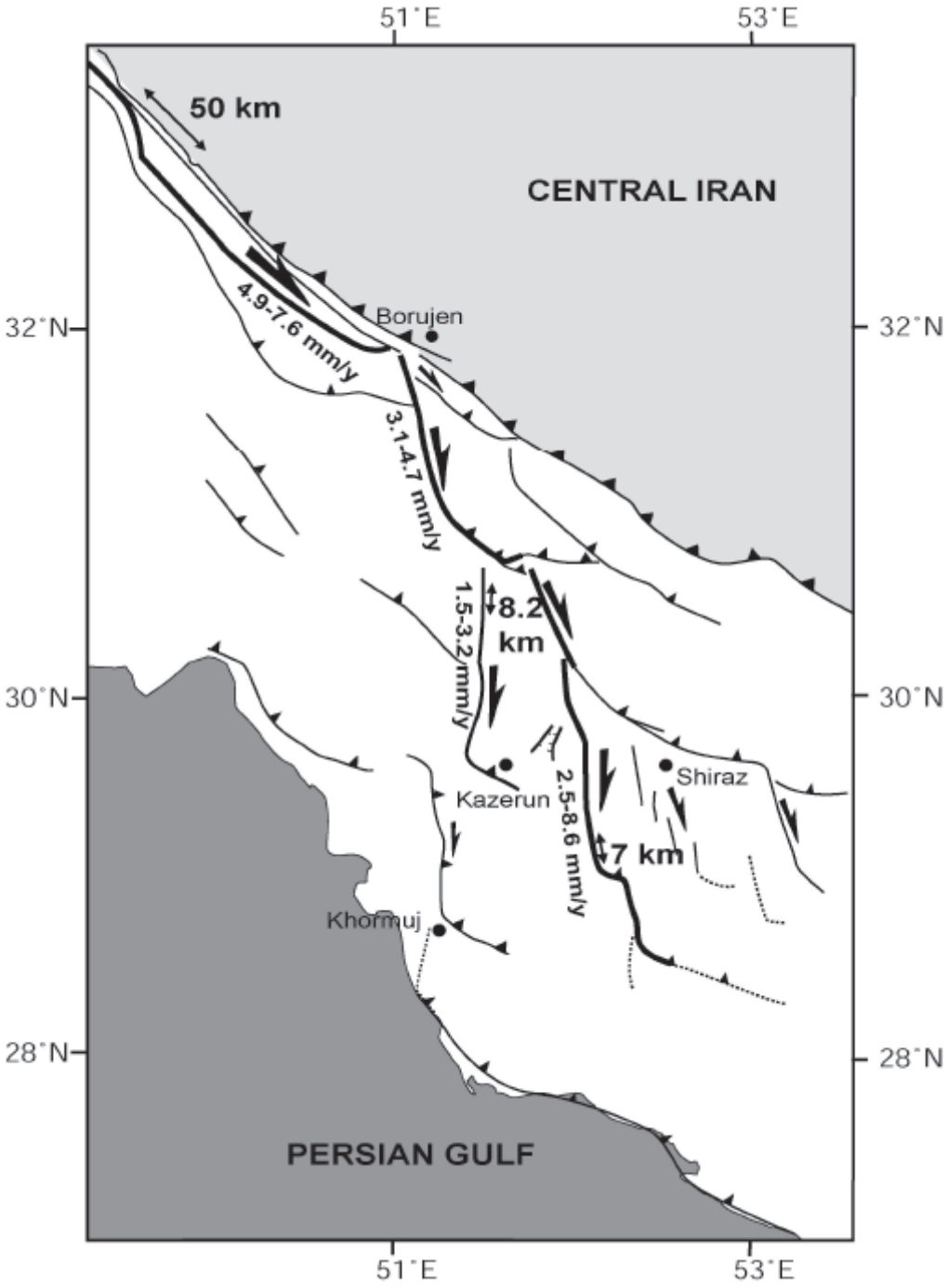
51˚E
53˚E
50 km
CENTRAL IRAN
4.9-7.6 mm/y
Borujen
32˚N
3.1-4.7 mm/y
1.5-3.2 mm/y
8.2
km
30˚N
Kazerun
Shiraz
2.5-8.6 mm/y
7 km
Khormuj
28˚N
PERSIAN GULF

Figure 9

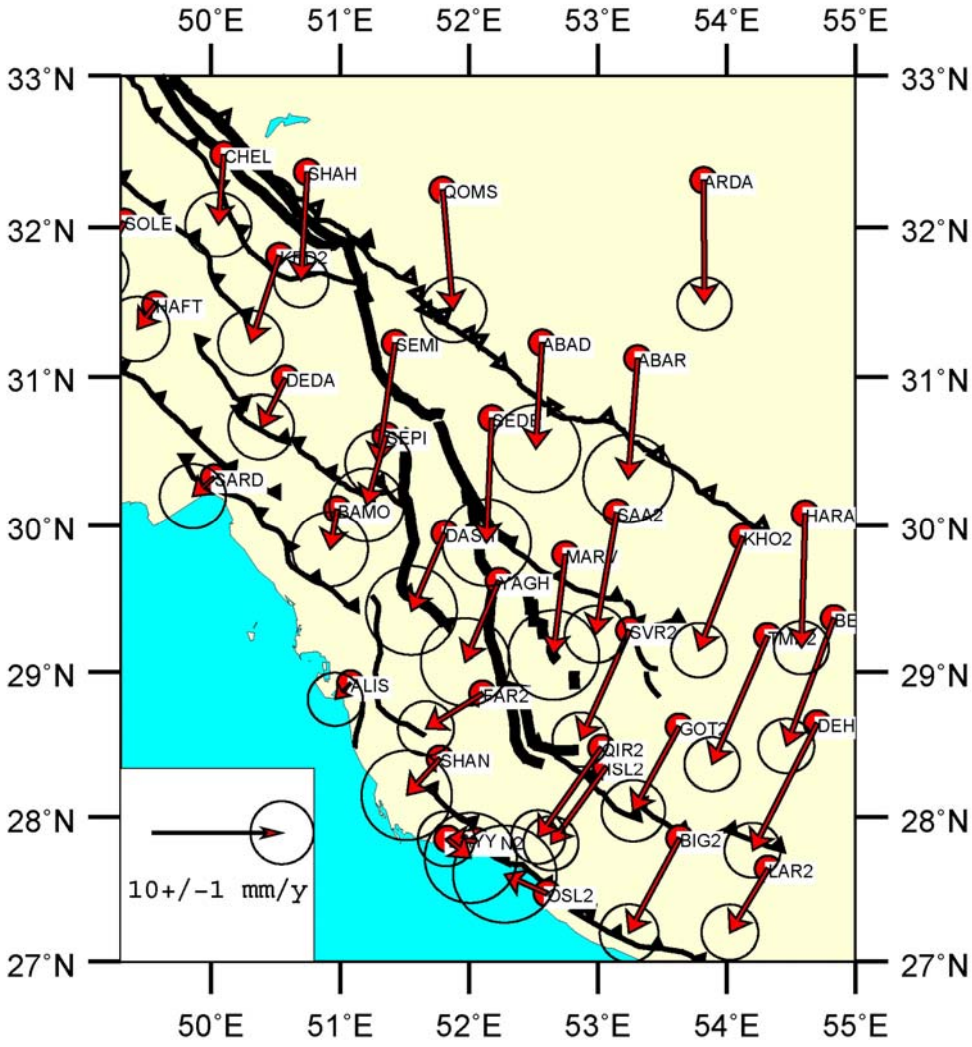
50°E
51°E
52°E
53°E
54°E
55°E
33°N
32°N
31°N
30°N
29°N
28°N
27°N
CHEL
SHAH
QOMS
ARDA
SOLE
KHO2
KHAFT
SEMI
ABAD
ABAR
DEDA
SEPI
SARD
BAMO
DASH
SAA2
KHO2
HARA
MARV
YAGH
SVR2
ALIS
FAR2
GOT2
DEH
QIR2
SHAN
ISL2
BIG2
LAR2
OSL2
10+/-1 mm/y

Figure 10a

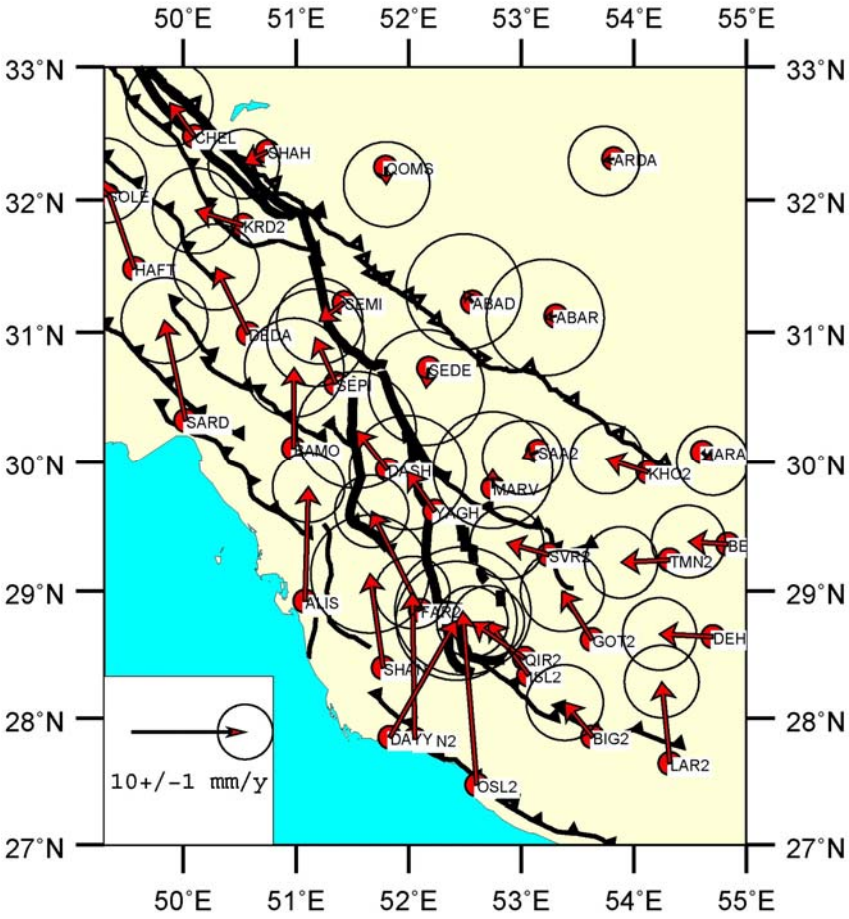
50°E
51°E
52°E
53°E
54°E
55°E
33°N
32°N
31°N
30°N
29°N
28°N
27°N
CHEL
SHAH
QOMS
FARDA
SOLE
KRD2
HAFT
SEMI
ABAD
ABAR
DEDA
SEDE
SEPI
SARD
BAMO
DASH
SAA2
KHO2
MARA
MARV
YAGH
SVRS
TMN2
BE
ALIS
FARS
GOT2
DEH
QIR2
ISL2
SHAH
DAYY N2
BIG2
LAR2
OSL2
10+/-1 mm/y

Figure 10b

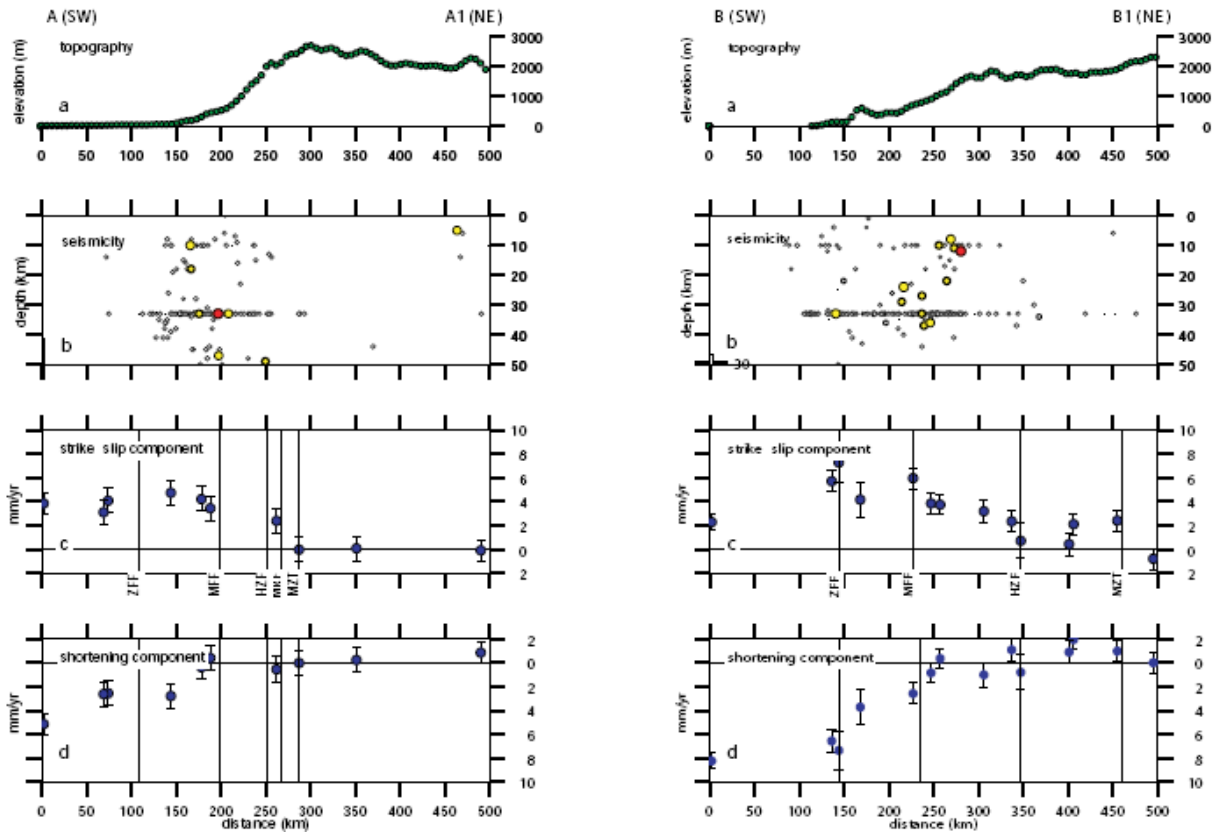

Figure 11a and 11b

5.2.4 Update of the Zagros velocity field with the 2005 North Zagros and Iran Global measurements

The velocity field of North Zagros and Central Zagros measured up to 2003 was published by Walpersdorf et al. (2006). After that, we re-measured the North Zagros network and we combined the data with the Kazerun 2002 and 2004 measurements, and with the re-measurement of the Iran Global network in 2005. Now we release the new velocity field including these data and compare with the published results.

The new velocity field (Fig. 5-6) does not differ significantly from Walpersdorf et al. (2007). The average differences on the east and north components are about 1.1 mm/yr and 1.0 mm/yr, respectively. Exceptions are two sites, DEDA and HAFT, where we use a tripod for the antenna set up since the original screw marker got damaged. The velocities of these two sites differ by ~2 mm/yr. For all other sites the differences are inside the limit of uncertainty. Moreover, the formal uncertainty of the re-measured sites is reduced from ~2 mm/yr to ~1.5 mm/yr.

The new velocity field is more consistent than the previous solution. Velocities vary more smoothly from one station to the next one. Some noise due to the short time span covered by the first two measurements has been removed. In a reference frame with respect to the Central Iran block, the velocity vectors in the North Zagros network present now a continuous rotation from northward velocities in the southern part of the network to trend parallel (northwestward) velocities in the northern part of the network.

We have used the Iran Global stations MIAN, BIJA, ARDA, SHAH and HARA for computation of the Central Iran Block. In contrast to Vernant et al. (2004),

Walpersdorf et al. (2006) and Tavakoli et al. (2007) we have not used the KERM (Kerman) site because this station shows ~2 mm/yr of residual velocity with respect to the Central Iran block. This residual was inside the uncertainties after the 2 first Iran Global measurements but becomes significant after the third measurement of this network, increasing the observation span to 5 years. We see now that KERM is located in a place moving differently from the Central Iran block, in particular as it is located east of the Dehshir, Anar and Rafsanjan faults which accommodate 1 mm/yr (Dehshir) and 2 mm/yr (Anar and Rafsanjan in its southern continuation) of right-lateral strike-slip, respectively. Applying the new Central Iran Euler pole (calculated without KERM and based on 3 measurements of the Central Iran sites) to establish the Central Iran reference frame causes a change of 1-3 mm/yr in some site velocities in the Central Zagros with respect to the CIB. Some part of the former residual velocities of ABAD, ABAR, SEDE, MARV and SAA2 with respect to CIB has been transferred to KHO2, TMN2, SVR2, BES2 and DEH2. While in the 2004 solution ABAD, ABAR, SEDE, MARV and SAA2 had a slight motion to the SE and the Central Zagros sites KHO2, TMN2, SVR2, BES2 and DEH2 were stable with respect to CIB, now the first group of stations is stable but a westward motion of the Central Zagros sites is observed. The velocity residuals of the stations used to define the Central Iran Block (Sanandaj-Sirjan zone) have decreased by 1-2 mm/yr with respect to the last realization of the Central Iranian block reference after only two measurements of the Iran Global network, remaining residuals 0-1 mm/yr.

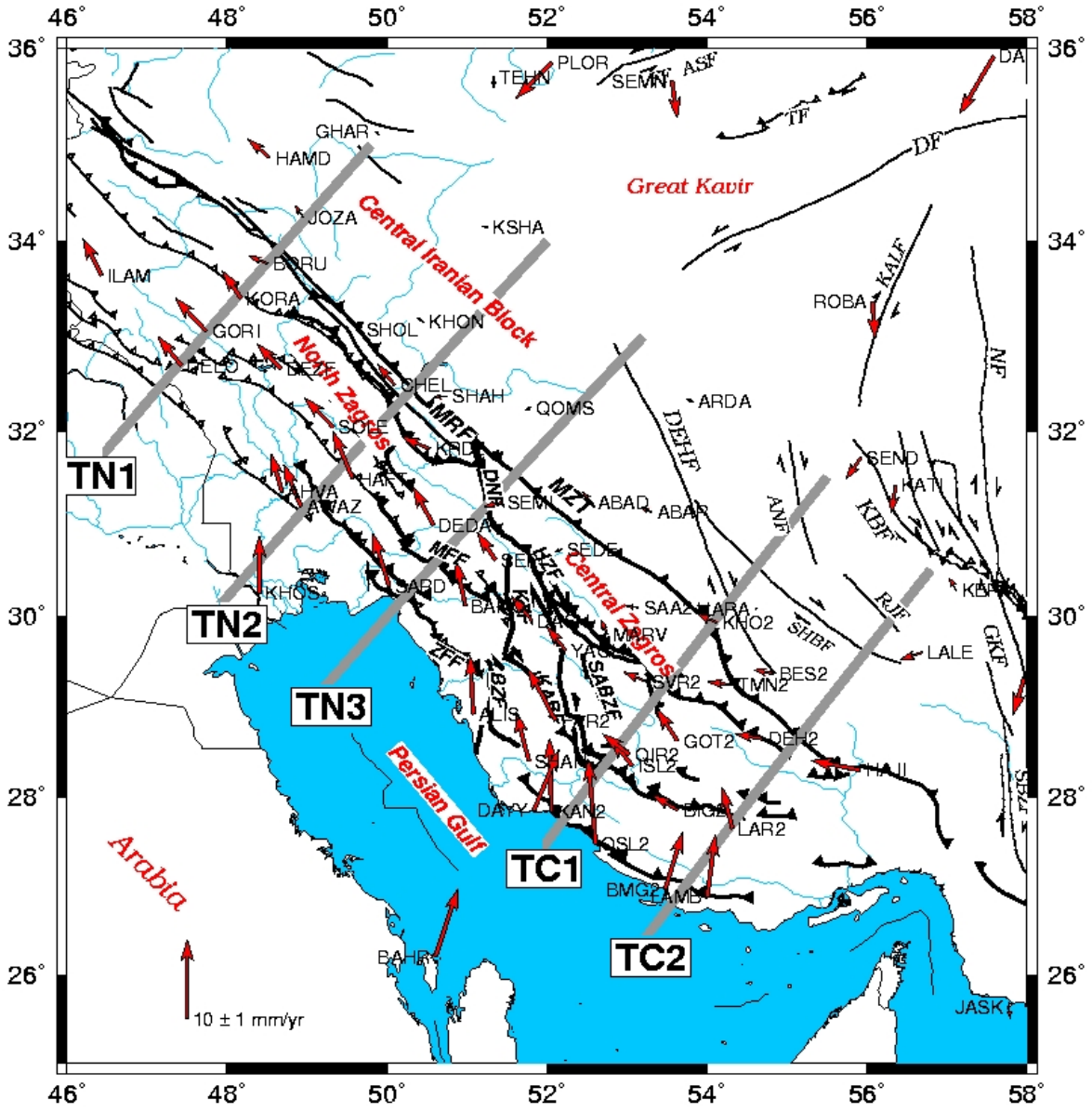

Figure 5-6. Velocity vectors of the Zagros measured since 1997 up to 2005 with their 95% confidence interval. The velocities are with respect to the Central Iran block. TN1, TN2, TN3, TC1 and TC2 (grey lines) are transects which are perpendicular to the mountain belt. In Fig. 5-7 and 5-8, the station velocities are projected on these transects. ANF: Anar Fault, BZF: Borazjan Fault DEHF, Dehshir Fault, DNF: Dena Fault, HZF: High Zagros Fault, KABF: Karehbas Fault, KZF: Kazerun Fault, MFF: Main Frontal Fault, MRF: Main Recent Fault, MZT : Main Zagros Thrust, , SABZF: Sabz-Pushan Fault, SHBF, Shahr Babak Fault, ZFF: Zagros Fore deep Fault.

For better interpretation we have projected the velocity components on transects perpendicular to the mountain belt (Fig. 5-7 and 5-8), following Walpersdorf et al. (2006). Along the westernmost transect TN1 we do not find any significant shortening (trend perpendicular component) within the Zagros Fold Belt. The main

deformation is centered on the MRF with 4.1 mm/yr of strike-slip motion (trend parallel component). This is slightly larger than our former results, with a more precise localization of the deformation on the MRF and more consistency with the motion on the Kazerun Fault system which has been evaluated to 3.4-3.7 $\pm$ 2 mm/yr on the different segments and faults.

Along the transect TN2 we can see about 3.7 mm/yr of strike-slip motion on the belt which is localized in proximity of the MFF (1.4 mm/yr) and the MRF (2.3 mm/yr), while our former results pointed rather to the Dezful Embayment fault as second fault accommodating the strike-slip motion besides the MRF. Along this transect the belt accommodates 3.7 mm/yr of strike-slip motion and 5.5 mm/yr of shortening. This shortening of 5.5 mm/yr is distributed in the southern part of the transect on the MFF, the Dezful Embayment fault and the ZFF. These observations are consistent but more precise than in Walpersdorf et al. (2006).

Along the transect TN3 we found a total of 4.2 mm/yr of right-lateral motion, localized on the Dena segment of the Kazerun fault system. This is a different result than in Walpersdorf et al. (2006) where a total amount of 6 mm/yr was observed and related mainly to the MFF further south. The new result (lower total strike-slip rate and more precise localization of the strike-slip component on the Dena fault) was obtained by the refined site velocities in particular of stations ALIS, DEDA and ARDA on this transect. A shortening rate of 6.6 mm/yr is observed on ZFF (1.7 mm/yr), MFF (2.0 mm/yr) and Dena fault (2.9 mm/yr) which still consistent with the previous study (Walpersdorf et al. (2007).

In the Central Zagros, along transect TC1, we observed cumulative strike-slip motion of 4 mm/yr on the ZFF, MFF (2.8 mm/yr) and Sarvestan faults (1.2 mm/yr), and 2.6 mm/yr of lateral motion cumulated on the Dehshir fault and the Main Zagros

Thrust (the latter being probably inactive). On this transect, Walpersdorf et al. (2007) have determined 3 mm/yr of right-lateral motion. This difference may be due to additional measurements of the HARA site during the Iran Global 2005 campaign. In particular, the new EW velocity component of HARA (which yields the major part of the strike parallel component presented here) is suspected to show some inconsistencies in the regional velocity field (see chapter 4). The increased strike-slip rate on this transect is therefore not necessarily significant. The shortening rate is as before (Walpersdorf et al., 2006) (8.2 mm/yr) localized close to the Persian Gulf south of the MFF.

Along the transect of TC2 in Central Zagros again we observe a total of 8.2 mm/yr of shortening distributed on the MFF (4.9 mm/yr) and the HZF (3.3 mm/yr). We also observed 1.6 mm/yr of strike-slip motion distributed over the transect and which is lower than our velocity uncertainty. In this part of Zagros, the shortening starts south of the HZF. This is coherent with Walpersdorf et al. (2006) where this zone between DEH2 and LAR2 was identified as the Simple Folded Belt.

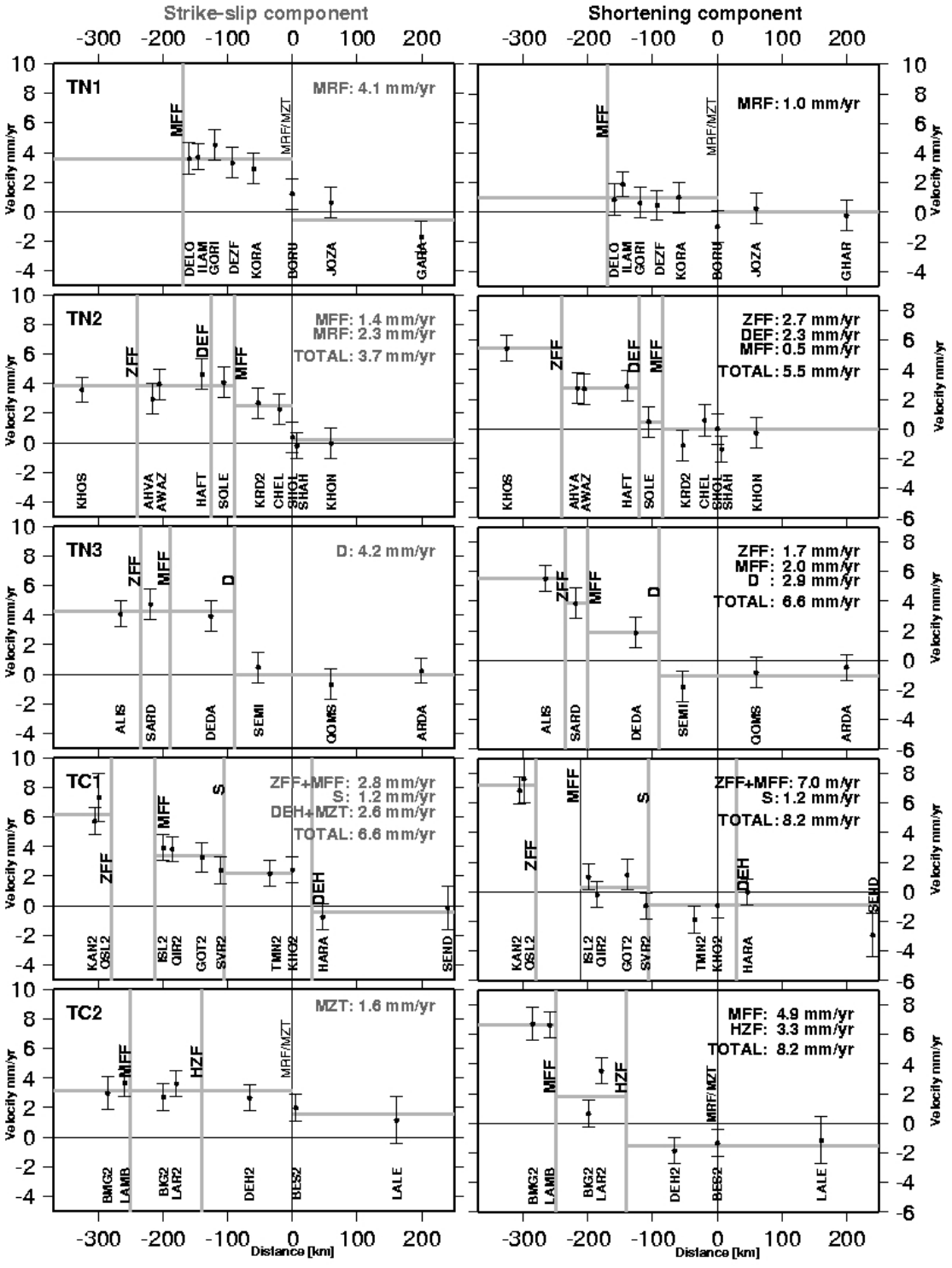

Figure 5-7. Site velocities (mm/yr) with respect to the site distance to the Main Recent Fault (MRF)/Main Zagros thrust (MZT) (in km, on the *x*-axis) on 5 transects (locations shown on the map Figure 5-6). On the left, we display the fault parallel components (strike-slip component), on the right, the fault perpendicular component (shortening). A simple model is superposed on the individual velocities. Light grey vertical lines indicate fault locations. D: Dena fault, DEF: Dezful Ebayment fault, DEH: Dehshir fault, HZF: High Zagros Fault, , MFF: Main Frontal Fault, MRF: Main Recent Fault, MZT : Main Zagros Thrust, S: Sarvestan Fault, ZFF: Zagros fore deep fault.

5.3 Global conclusion on Zagros present-day kinematics

The Zagros can be divided into three segments according to different tectonical regimes, the North Zagros, the Kazerun Fault System (KFS) and the Central Zagros. This right-lateral strike-slip fault system with other associated NNW trending strike-slip faults has the role of transferring the deformation from the Main Recent fault (MRF) in the North Zagros to the Central Zagros. The seismicity in the North Zagros shows reverse faulting mechanism on different thrust faults and strike-slip motion localized on the MRF. It is mainly concentrated on the Simple Folded belt and limited to the topography with altitudes of more than 1000 m. South of MFF there is only little seismicity in North Zagros. The Kazerun fault system experiences strike-slip earthquakes. The earthquakes of the Central Zagros are pure reverse faulting mechanisms distributed between elevations of 0 - 1000 m and limited to the south by the ZFF running along the Persian Gulf coast. In the Zagros, the presence of the Hormuz salt layer is limited to the east of the Kazerun fault system. This salt layer has no role in the deformation in the Central Zagros to the east of the Kazerun fault system.

In the northwest Zagros (North Zagros network) the deformation is partitioned between1-6 mm/yr of shortening perpendicular to the axis of the mountain belt, and 4 mm/yr of dextral strike-slip motion with 2-4 mm/yr localized on the Main Recent fault. Authemayou et al. (2007 submitted) have estimated 4.9-7.6 mm/yr of slip rate on the MRF based on geomorphological marker offsets and in-situ cosmogenic dating over time spans of some ka. They infer the onset of MRF fault activity to 6.6 – 10.2 Ma. Talebian and Jackson (2004) have proposed a 10-17 mm/yr slip rate based on a total 50 km offset which is thought to be initiated 3-5 Ma ago. If we assume a constant rate of the 2-4 mm/yr of slip rate on MRF, the MRF initiated between 13 and 25 Ma ago.

As the estimation of the total offset of 50 km seems to be reliable, a part of this offset must have been created before 5 Ma or the slip rate of the MRF must have slowed down since the initialization of the slip 3-5 Ma ago. The other active faults of North Zagros are the MFF, the Dezful Embayment fault (DEF) and the ZFF. The observed shortening across the ZFF (i.e. 2.7 mm/yr of shortening between KHOS and AHVA on TN2, and ~1.7 mm/yr of shortening between ALIS and SARD on TN3) is in contrast to the lack of seismicity in the low elevation area in the Persian Gulf

plane, south of MFF and DEF. Unfortunately, there is no station south of ZFF in the northwestern part of North Zagros (transect TN1) to confirm the ZFF activity at this longitude.

In the southeast Zagros (Central Zagros) the deformation is a pure shortening of 8±2 mm/yr occurring perpendicular to the mountain belt trend. The shortening rate increases throughout Zagros from west to east consistent with the regional shortening imposed by the Arabia-Eurasian Euler pole located in the north of Africa. Most of the shortening in Central Zagros is restricted to a zone located in front of the Simple Folded Belt and south of MFF, close to the Persian Gulf, while seismicity is more widely spread across the mountain belt. This confirms the role of the Hormuz salt layer which decouples the surface sedimentary layers from the seismogenic basement and lubricates the deformation propagation from NE to SW. The MZT is not active and the northern part of the Central Zagros moves with the same velocity as the Central Iran block.

Vernant et al. (2004) have estimated 7±2 mm/yr of N-S shortening for the Central Zagros and 3±2 mm/yr of strike-slip motion on the MRF with their large scale GPS network. Considering the 2 mm/yr of uncertainty, these large scale results are consistent with our more detailed observations.

The updated results including the 2005 measurements on the North Zagros and the Iran Global network did not change the results of Walpersdorf et al. (2007) significantly but increased the precision. A more precise realization of the Central Iran reference frame localizes now some residual westward velocities south of the MZT in the northeast of the Central Zagros network, while these sites have been coherent with the Central Iran block motion in the former solution. If this residual motion is significant (recall that the Central Zagros network has not been re-measured since 2003) it indicates a zone of EW shortening parallel to and south of MZT (between KHO2, TMN2 and GOT2 in the east and SAA2, MARV, SEDE in the west). No tectonical feature is known that corresponds to this deformation pattern. However, this region of EW shortening is situated directly south of the intersection of the Dehshir fault with the Zagros mountains. Walker and Jackson (2004) postulate that a region with a strain gradient between the parts of the Zagros to the east and the west of this intersection must exist if the Dehshir fault accommodates right-lateral shear between east and central Iran. The zone of EW shortening is therefore eventually related with the Dehshir fault kinematics.

The Kazerun fault is seismically active with earthquakes mainly concentrated on the Kazerun segment. Very few earthquakes have been recorded for the southernmost Borazjan segment. Most of the mechanisms are right-lateral strike-slip on the Kazerun, Karehbas, and Sabz Pushan faults. A few reverse faulting mechanisms have been recorded, probably on the south terminations of these faults ending in EW trending thrust faults (Baker et al., 1993; Authemayou et al., 2005).

The GPS measurements around the Kazerun Fault system (Tavakoli et al., 2007) show significant present-day dextral strike-slip motions on the Dena (3.7 ± 2 mm/yr) and Kazerun (3.6 ± 2 mm/yr) segments, and on the Karehbas fault (3.4 ± 2 mm/yr). The Sabz Pushan and High Zagros faults seem to show active slip at the limit of resolution (cumulated 1.5 ± 2 mm/yr). No motion has been observed on the Sarvestan fault further east and on the MZT in the north. No significant strike-slip activity has been revealed as well on the Borazjan segment in the south of the Kazerun fault system.

The comparison to geological slip rates determined for the Dena and the Kazerun segment (Authemayou et al., 2006) indicates stable rates over ~150 ka. Also fault ages are evaluated coherently to 2-8 Ma for the Dena and Kazerun segments, using dating of geomorphological offsets and extrapolation to the total geological horizontal slip on one hand, and suggesting the total offset was achieved with constant present-day slip rates on the other hand. Supposing the slip rate of the Karehbas fault is stable as for the Kazerun and the Dena faults, the GPS inferred present-day velocity compared to the total fault offset indicates that this fault's age is comparable to the Dena and the Kazerun segment (or maybe a little younger).

Compared to the MRF activity (long term strike-slip velocities of 4.9 to 7.6 mm/yr and onset time inferred to 6.6 – 10.2 Ma ago) it seems that the deformation of the Kazerun fault system and related strike-slip faults (Kareh Bas and Sabz Pushan faults) is younger and might have been initiated by progressive transfer of the MRF motion to the southeast along a preferential en-echelon fault zone included in a more distributed fan-shape fault pattern. The Dena fault transfers the MRF fault slip mainly to the Kazerun and slightly to the High Zagros and Sabz Pushan faults, and the Kazerun fault further to the Kareh Bas fault. The Hormuz salt layer could have facilitated the propagation of deformation from NW to the SE, but the Dena, Kazerun and Kareh Bas fault slip is related to seismicity, indicating that the basement is also involved in the distributed fault activities in the KFS.

Chapter 6 General Conclusion

On the Iranian territory, the present orography, the active faults and deformations result from the north–south convergence between the plates of Arabia to the south and Eurasia to the north (Jackson & McKenzie, 1984) at a rate of about 22 mm/yr (Sella et al., 2002; Vernant et al., 2004). The type of plate convergence in Iran is a continental collision except for the Makran in southeast Iran where the Arabian oceanic margin subducts northward under southeast Iran (Byrne *et al.* 1992). Most of the deformation is accommodated in the major mountain belts of Zagros, Alborz and Kopeh Dagh and along large strike-slip faults which surround blocks (Central Iran, Lut and the South Caspian basin) with mountain building and seismicity (Jackson & McKenzie 1984; Berberian & Yeats 1999).

Onset of this deformation is a topic of discussion of the geologists, seismologists and recently the geodesists. It seems that the initial collision of the Arabia-Eurasia plates occurred 16-23 million years ago. Now the question is whether the faulting of Iran started at that time or before the Arabia-Eurasia collision, and in the latter case, which were the pre-collision active faults and what was their movement? Comparison of present-day GPS constrained slip rates of the faults with geologic short term and long term slip rates can give us information on the onset and evolution of the deformation. To extrapolate our GPS measurements spanning less than 20 years and constraining a linear present-day velocity to geological short term and long term rates we have to consider that the GPS slip rate is constant in time. We identify some cases where the present-day and geologic slip rates are comparable and could therefore have been constant since slip onset, but also some cases where the present-day velocities are too slow to be compatible with a fault onset after the initiation of the Arabia-Eurasia collision.

GPS is an excellent tool for the measurement of regional deformation and individual fault slip rates with millimeter precision. Before the 1990s, the geodetic tools for measuring deformation precisely were limited to the very sparse VLBI, SLR and LLR techniques. But now in almost all countries GPS is used in campaign mode or by continuous measurements to quantify the present-day deformation. The use of GPS for measuring fault slip rates and kinematics of Iran returns to 1996, but after the start of the French-Iranian cooperation on crustal deformation and seismic hazard

in 1997, this task is accelerated. For example, the present-day deformation over the total Iranian territory has been evaluated by GPS by Nilforoushan et al. (2003), Vernant et al. (2004a) and Masson et al. (2007). After acquiring the expertise of GPS applications for crustal deformation studies, the National Cartographic Center has installed more than 100 permanent GPS stations around the populated cities which are situated close to active faults and face seismic hazard. In the framework of this thesis, we have densified the GPS network in the Zagros, the Kopeh Dagh and the Lut region. Our objectives are to:

1- measure the precise present-day slip rates of the faults
2- determine the deformation distributed inside the different regions
3- establish and interpret the eventual differences between geologic and geodetic slip rates
4- constrain the kinematics model of the faults and the regional deformation
5- recognize the high seismic risk areas of the studied regions
6- understand the deformation mechanism in the studied area

Here we present the results of several GPS campaigns in the Zagros and the east of Iran, covering the last 10 years (1997-2006) and conducted in the framework of the French-Iranian scientific cooperation. This data set provides up-to-date direct measurement of the present-day kinematics of the faults inside Zagros, Kopeh Dagh and around the Lut region on the NS trending strike-slip faults. It allows the determination of an accurate strain rate tensor. We present comparisons of our results with other seismologic and geologic results and complement and improve the precision of previous studies (Nilforoushan et al. 2003; Vernant et al. 2004a; Masson et al. 2005, 2007; Talebian et al., 2002, 2004, Authemayou et al., 2005, 2006, 2007; Walker and Jackson, 2002, 2004; Hollingsworth et al., 2006; and Meyer et al., 2006, 2007). Our GPS measurements show that with 3 measurement campaigns at 2 years intervals a precision of 1 mm/yr for the velocity vectors is achievable. Each site has been observed at least during 48 h per campaign. The self centering antenna set up plays an important role for achieving optimal precisions.

It is difficult to infer global conclusions from the comparison between GPS present-day and geologic short-term and long term slip rates of the different Iranian faults studied in this thesis, because in some places the slip rates are coherent over long time spans and in some places not. Most of the geologic slip rate estimates

have high uncertainties (Allen et al., 2004). Generally the long term slip rates for the Iranian faults are higher than geodetic rates (Talebian & Jackson, 2002, and Bachmanov et al., 2004, for MRF, Lyberis and Manby, 1999, for the Ashkabad fault, Walker and Jackson, 2004, for the Sistan suture zone). This apparent discrepancy between geodetic and geological slip rate estimates suggests that a) the GPS sites are too close to the fault (to avoid recording the slip rate of the next fault) and do not register the total fault velocity in the inter-seismic state; b) fault slip rates have decreased since the activation of the fault; c) the total offset of the faults were overestimated and overlapped with other unidentified faults; d) the age of the fault onset is underestimated. We think that in spite of Iran being a region of young continental collision, many major faults seem to have reactivated inherited fault zones from previous tectonic regimes so that the observed total offset is not only related to the present-day regime and deformation onsets younger than the Arabia-Eurasia collision. Moreover, in many cases a general age of deformation onset in Iran of 5-7 Ma is proposed, corresponding to the epoch of global, major tectonic reorganization in presently active fault zones. This age seems to be too young for many deformation mechanisms we observe today in Iran.

We have estimated the 2D horizontal velocity field and we have not examined the vertical velocity because of the high uncertainties of the vertical positions due to differences in the antenna set ups and measurement equipments between the individual campaigns. The uncertainty of our vertical velocity estimates varies from 1 – 6 mm/yr depending on the number and time interval of the measurements. In the Mashhad network with 2 measurements over 2 years the uncertainty is about 5.5 mm/yr.

In the Zagros the deformation is partitioned in its north-western part, into 2-4 mm/yr of strike-slip on the MRF and 1-6 mm/yr of shortening on the MFF, ZFF and Dezful Embayment fault. The lack of the seismicity south of the ZFF confirms that the deformation is confined to the north of the ZFF above elevations of 1000 meter.

Deformation of the Kazerun fault system and related strike-slip faults (Kareh Bas and Sabz Pushan faults) might have been initiated by progressive transfer of the MRF motion to the southeast along a preferential en-echelon fault zone included in a more distributed fan-shape fault pattern. The Dena fault transfers the MRF fault slip mainly to the Kazerun and slightly to the High Zagros and Sabz Pushan faults, and the Kazerun fault further to the Kareh Bas fault. The Hormuz salt layer could have

facilitated the propagation of deformation from NW to the SE, but persistent seismicity in the SE indicates that the basement is also involved in the deformation.

In order to facilitate the northward motion of the Central Iran block with respect to Eurasia, the faults around the rigid Lut block should slip to accommodate the shear between the Central Iran block and the Hellmand block. This accommodation decreases from east to west, with the Sistan Suture zone absorbing a major part (7.5 mm/yr) which is however still lower than geologic estimations. The Central Iran faults (Dehshir and Anar faults) have little contribution in the accommodation of the shear. A part of the northward motion of the Lut block is absorbed by thrust faults in the north of the Lut block, but 6-8 mm/yr of NS shortening remain to be accommodated in the Binalud and Kopeh Dagh ranges to the north. The motions along and across the Binalud are about 2 mm/yr of strike-slip and 3.5 mm/yr of shortening, respectively. The eastern Kopeh Dagh absorbs the remaining shortening of about 2 mm/yr. In the central part of Kopeh Dagh the incoming N-S shortening rate of 7 mm/yr is accommodated by the Quchan fault zone. The micro blocks limited by the faults are supposed to rotate counter clockwise which should produce an EW elongation along the range. Effectively, 5 mm/yr of EW elongation have been observed, accommodated to the west by the Ashkabad fault, as well as 5 mm/yr of cumulated right-lateral motion across the Quchan fault system. In the western part of Kopeh Dagh, the total incoming NS shortening rate of 8 mm/yr is absorbed by both the Ashkabad fault (shortening and strike-slip) and the Shahrud fault system (strike-slip motion and maybe thrusting on the parallel Khazar fault). We estimated 7 mm/yr of westward expulsion of the South Caspian basin.

We provided precise present-day rates and orientations of the active tectonic mechanism. These rates help characterize the role of the different faults involved in the present-day deformation. If we extrapolate these present-day rates over geological time spans, they give some constraints on the age of different parts of the tectonically active structures and on the long–term stability of the deformation rates. Generally, our estimated ages for faulting are older than the ages of deformation onset proposed in the literature (3-9 Ma, Talebian and Jackson, 2004; Walker and Jackson, 2004; Lyberis and Manby, 1999). With our estimates, the faulting in our research areas started 2 Ma (Zagros) to 24 Ma ago (eastern Kopeh Dagh). However, over the geological short-term (Holocene age), Meyer et al. (2007) have provided slip

rates of ~2 mm/yr, 0.5-0.75 mm/yr and ~2.0–7.5 mm/yr across the Dehshir fault, the Anar fault and the Sistan suture zone, respectively, which are consistent with our present-day results considering the uncertainties.

The overall tectonical features of the Kopeh Dagh present some similarities with the Zagros: NS shortening is absorbed by trend parallel right-lateral strike-slip motion in the west, on the MRF in Zagros like on the Ashkabad fault in Kopeh Dagh. In the central part we find a series of ~NS oriented strike-slip faults, the Kazerun fault system in Zagros and the Quchan fault zone in Kopeh Dagh. In the eastern part of both ranges (Central Zagros and Eastern Kopeh Dagh) thrusting prevails. The differences are 1) that in Kopeh Dagh the NS shortening is increasing from east to west (0-8 mm/yr) while in Zagros it decreases from east to west (8-3 mm/yr). The maximum shortening is absorbed by expulsion of the South Caspian Basin to the west in Kopeh Dagh, and by thrusting and crustal thickening in Central Zagros, without any eastward expulsion. In the Zagros the deformation, seismicity and topography are related to each other. The onset time of deformation varies along each of the mountain belts, with the oldest deformation in the part of smallest deformation: In the Zagros, the deformation seems to have propagated from the MRF (10-16 Ma) to the southeast into the Kazerun Fault System (1-5 Ma), while in the Kopeh Dagh we find some evidence for the shortening in the eastern part being the oldest (24 Ma), block rotation in the central part having an intermediate age (5-8 Ma) and expulsion of the South Caspian Basin being the most recent stage of deformation (5 Ma). In general, the eastern Kopeh Dagh deformation seems to be more ancient than the onset of deformation in the other Iranian mountain belts like Zagros and Alborz, but it is still consistent with geological constraints (<30 Ma, Berberian and King, 1981).

References

.

Agard, P., J. Omrani, L. Jolivet, and F. Mouthereau (2005), Convergence history across Zagros (Iran): constraints from collisional and earlier deformation. *International Journal of Earth Sciences*, DOI 10.1007/s00531-005-0481-4.

Alavi, M. (1992), Thrust tectonics of the Binalood region, NE Iran, *Tectonics,* 11(2), pp 360–370.

Alavi, M. (1996), Tectonostratigraphic synthesis and structural style of the Alborz mountain system in northern Iran, *J. Geodyn.,* 21(1), 1–33.

Alavi, M. (1980), Tectonostratigraphic evolution of the Zagros sides of Iran, Geology, 8, 144– 14.

Alavi, M., and M. A. Mahdavi (1994), Stratigraphy and structures of the Nahavand region in western Iran, and their implications for the Zagros tectonics, Geol. Mag., 131, 43– 47.

Alavi, M.,(1994), Tectonics of the Zagros orogenic belt of Iran; new data and interpretations. Tectonophysics 229, 211–238.

Allen, M., J. Jackson, R., Walker (2004), Late Cenozoic re-organisation of the Arabia-Eurasia collision and the comparison of short-term and long-term deformation rates, *Tectonics*, 23, doi:10.1029/2003TC001530.

Allen, M., M.R. Ghassemi, M. Sharabi, and M. Qorashi (2003a.), Accommodation of late Cenozoic oblique shortening in the Alborz range, Iran, *J. Struct. Geol.*, *25*, 659-672.

Allen, M.B, E. J-P. Blanc, E, R., Walker, J., Jackson, M., Talebian, M.R. Ghassemi (2006), Contrasting styles of convergence in the Arabia-Eurasia collision: why escape tectonics does not occur in Iran. *Geol. Soc. Am. Spec. Publ.* , 409, 579-589.

Allen, M.B., S.J. Vincent, I. Alsop, A. Ismail-zadeh, and R. Flecker (2003b), Late Cenozoic deformation in the South Caspian region: effects of a rigid basement block within a collision zone, *Tectonophysics*, *366*, 223-239.

Allen, M. B., S. Jones, A. Ismail-Zadeh, M. Simmons, and L. Anderson (2002), Onset of subduction as the cause of rapid Pliocene-Quaternary subsidence in the South Caspian Basin, Geology, 30, 775– 778.

Altamimi, Z., P. Sillard and C. Boucher (2002), ITRF2000: A new release of the International Terrestrial Reference Frame for earth Science applications, J. Geophys. Res., 107, B10, 2214.

Altamimi, Z., X. Collilieux, J. Legrand, B. Garayt, and C. Boucher (2007), ITRF2005: A new release of the International Terrestrial Reference Frame based on time series of station positions and Earth Orientation Parameters , J. Geophys. Res., 112, B09401, doi:10.1029/2007JB004949.

Amidi, S. M. (1975), Contribution al etude biostratigraphique, petrologique et petrographique des roches magmatiques de la region Natanz-Nain-Surk (Iran Centrl). Unpubl. Ph.D thesis, University of Grenoble, France, 250 p.

Ambraseys, N. N., and C. P. Melville (1982), A History of Persian Earthquakes, Cambridge Univ. Press,New York.

Ambraseys, N. N., and J. S. Tchalenko (1969), TheDasht-e-Bayas (Iran) earthquake of August 31,1968: A field report, Bull. Seismol. Soc. Am., 59, 1751 – 1792.

Authemayou, C. (2006), *Partitionnement de la convergence oblique en zone de collision : Exemple de la chaîne du Zagros (Iran),* Ph.D. thesis, 334p, Univ. Paul Cézanne, Aix-Marseille, France.

Authemayou C., O. Bellier, D. Chardon, Z. Malekzadeh and M. Abbassi (2005), Active partitionning between strike-slip and thrust faulting in the Zagros fold-and-thrust belt (Southern Iran). *Compte Rendu Géoscience, Académie des Sciences de Paris*, 337, 539-545.

Authemayou C, D. Chardon, O. Bellier, Z. Malekzadeh, E. Shabanian and M.R. Abbassi (2006), Late Cenozoic partitioning of oblique plate convergence in the Zagros fold-and-thrust belt (Iran). *Tectonics*, 25, Art. No. TC3002.

Authemayou, C., O. Bellier, D. Chardon, D., Benedetti, Z., Malekzadeh, C., Claude, and B., Angeletti (2007), Quarternary Kazerun and the Main Recent Faults slip rates: evidence for strike-slip partitioning in the Zagros fold-and-thrust belt, *Journal of Geophysical Research*, submitted.

Authemayou, C., O. Bellier, D. Chardon, Z. Malekzade and M. Abassi (2005), Role of Kazerun fault system in active deformation of the Zagros fold-and-thrust belt (Iran), C. R.Geoscience 337, 539-545.

Axen, G. J., P. S. Lam, M. Grove, D. F. Stockli, and J. Hassanzadeh (2001), Exhumation of the westcentral Alborz Mountains, Iran, Caspian subsidence, and collision-related tectonics, Geology, 29, 559 – 562.

Baker, C., J. Jackson and K. Priestley (1993), Earthquakes on the Kazerun Line in the Zagros Mountains of Iran: strike-slip faulting within a fold-and-thrust belt, *Geophysical Journal International*, 115, 41-61.

Bayer, R., J. Chery, M. Tatar, Ph. Vernant, M. Abbassi, F. Masson, F. Nilforoushan, E. Doerflinger, V. Regard and O. Bellier (2006), Active deformation in Zagros–Makran transition zone inferred from GPS measurements , *Geophys. J. Int.*, 165, 373–381.

Bachmanov, D.M., V.G. Trifonov, Kh.T. Hessami, A.I. Kozhurin, T.P. Ivanova, E.A. Rogozhin, M.C. Hademi and F.H. Jamali (2004), Active faults in the Zagros and central Iran, Tectonophysics 380 , 221– 241.

Berberian, M. (1981), Active faulting and tectonics of Iran, in Zagros-Hindu Kush-Himalaya Geodynamic Evolution, pp. 33-69, AGU, Geodyn. Ser.

Berberian, M., and G.C.P. King (1981), Towards a paleogeography and tectonic evolution of Iran, *Can. J. Earth Sci.*, *18(2)*, 210-285.

Berberian, M. (1995), Master "blind" thrust faults hidden under the Zagros folds: active basement tectonics and surface morphotectonics, *Tectonophysics*, *241*, 193-224.

Berberian, M., J.A. Jackson, M. Qorashi, M.M. Khatib, K. Priestley, M. Talebian and M. Ghafory-Ashtiany (1999)**,** The 1997 may 10 Zirkuh (Qa'enat) earthquake (Mw 7.1): faulting along the Sistan suture zone of eastern Iran, *Geophys. J. Int.*, *136*, 671-694.

Berberian, M., and R. Yeats (1999), Patterns of historical earthquake rupture in the Iranian Plateau, *Bull. Seismol. Soc. Am.*, *89*, 120-139.

Berberian, M., and R. Yeats (2001), Contribution of archaeological data to studies of earthquakes history in the Iranian plateau, *J. Struct. Geol.*, *23*, 563-584.

Berberian, M. (1979), Evaluation of the instrumental and relocated epicenters of Iranian earthquakes, *Geophysical Journal of the astronomical Society*, 58, 625-630.

Berberian, M. (1995), Master blind thrust faults hidden under the Zagros folds: active basement tectonics and surface morphotectonics, *Tectonophysics*, 241, 193-224.

Berberian, M., J. Jackson, C. Baker, E. Fielding, B.E. Parsons, K. Priestley, M. Qorashi, M., Talebian, R. Walker and T.J. Wright (2001), The 14 March 1998 Fandoqa earthquake (Mw 6.6) in Kerman province, S.E. Iran: re-rupture of the 1981 Sirch earthquake fault, triggering of slip on adjacent thrusts, and the active tectonics of the Gowk fault zone. *Geophysical Journal International* , 146, 371-398.

Berberian, M., J. Jackson, M. Qorashi, M. Talebian, M. Khatib and K. Priestley (2000), The 1994 Sefidabeh earthquakes in eastern Iran: blind thrusting and bedding-plane slip on a growing anticline, and active tectonics of the Sistan suture zone. *Geophysical Journal International* , 142, 283-299.

Berberian, M (2005), The 2003 Bam Urban Earthquake: Predictable Seismotectonic Pattern Along the Western Margin of the Rigid Lut Block, Southeast Iran, *Earthquake Spectra,* Volume 21, No. S1, pages S35–S99.

Berberian, M. (1976), *Contribution to the seismotectonics of Iran (Part II),*

Vol.,39, Geological Survey of Iran.

Blanc, E.J.-P., M.B. Allen, S. Inger, and H. Hassani (2003), Structural styles in the Zagros Simple Folded Zone, Iran, *J. Geol. Soc. London*, *160*, 401-412.

Blewitt, G. (1989), Carrier phase ambiguity resolution for the Global Positioning System applied to geodetic baselines up to 2000 km, *J. Geophys. Res.*, *94*, 10187-10203.

Blewitt, G. (1990), An automatic editing algorithm for GPS data, *Geophys. Res. Lett.*, *17* (3), 199- 202.

Blewitt, G., D. Lavallée, P. Clarke, and K. Nurutdinov (2001), A new global model of Earth deformation: seasonal cycle detected, *Science*, *294*, 2342-2345.

Blewitt, G., and D. Lavallée (2002), Effect of annual signals on geodetic velocity, *J. Geophys. Res.*, *107* (B7), ETG_9-1-ETG_9-11.

Bock, Y., S.A. Gourevitch, C.C. Counselman, R.W. King, and R.I. Abbot (1986), Interferometric analysis of GPS phase observations, *Manuscripta Geodaetica*, *11*, 282-288.

Bock, Y., J. Behr, P. Fang, J. Dean, and R. Leigh (1997), Scripps Orbit and Permanent Array Center (SOPAC) and Southern Californian Permanent GPS Geodetic Array (PGGA), in *The Global Positioning System for the Geosciences*, pp. 55-61, Nat. Acad. Press,Washington, D.C.

Bock, Y. (1991), Continuous monitoring of crustal Deformation, GPS World, Innovation Column, June 1991, 40-47.

Bouchon, M., D. Hatzfeld, J. Jackson, E. Haghshenas (2006), Some insight on why Bam (Iran) was destroyed by an earthquake of relatively moderate size, *Geophysical Research Letters* , 33**,** L09309.

Bosold, A., W. Schwarzhans, A. Julapour A.R. Ashrazadeh, S.M. Ehsani (2005), The structural geology of the High Central Zagros revisisted (Iran), *Petroleum Geosciences*, 11, 225-238.

Bowie, W. (1924), Earth movements in California, Spec. Publ. No. 106, U.S. Coast and Geodetic Survey, 1924. (Reprinted in Reports on Geodetic Measurements of Crustal Movement, 1906-71 U.S. National Geodetic Survey, Rockville.

Bowie, W. (1928), Comparison of old and new triangulation data in California, U.S. Coast , Spec. Publ. No. 151, . (Reprinted in Reports on Geodetic Measurements of Crustal Movement, 1906-71 U.S. National Geodetic Survey, Rockville.

Byrne, D.E., L.R. Sykes, and D.M. Davis (1992), Great thrust earthquakes and aseismic slip along the plate boundary of the Makran subduction zone, *J. Geophys. Res. 97*, 449-478.

Calais, E. (1999), Continoous GPS measurements across the Western Alps, 1996-1998, *Geophys. J. Int.*, *138* (1), 221-230.

Calais, E., L. Galisson, J.-F. St´ephan, J. Delteil, J. Deverch`ere, C. Larroque, B. Mercier de L´epinay, M. Popoff, and M. Sosson (2000), Crustal strain in the Southern Alps, 1948-1998, Tectonophysics, 319, 1-17.

Camp, V.E., and R.J. Griffis (1982), Character, genesis and tectonic setting of igneous rocks in the Sistan suture zone, eastern Iran, *Lithos*, *15*, 221-239.

Copley, A. and J. Jackson (2006), Active tectonics of the Turkish-Iranian plateau. *Tectonics.,* 25, TC6006.

DeMets, C., R.G. Gordon, D.F. Argus, and S. Stein (1990), Current plate motions, *Geophys. J. Int.*, *101*, 425-478.

DeMets, C., R.G. Gordon, D.F. Argus, and S. Stein (1994), Effects of recent revisions to the geomagnetic reversal time scale on estimates of current plate motions, *Geophys. Res. Lett.*, *21*, 2191-2194.

Dewey, J. F., W. C. Pitman III, W. B. F. Ryan, and J. Bonnin (1973), Plate Tectonics and the Evolution of the Alpine System, Geol. Soc. Am. Bull., 84, 3137– 3180.

Dewey, J. F., M. R. Hempton, W. S. F. Kidd, F. Saroglu, and A. M. C. Sengor (1986), Shortening of continental lithosphere: The neotectonics of eastern Anatolia, a young collision zone, in Collision Tectonics, edited by M. P. Coward and A. C. Ries, Geol. Soc. Spec. Publ., 19, 3 – 36.

Dewey, J. F., M. L. Helman, E. Turco, D. H. W. Hutton and S. D. Knott (1989), Kinematics of the western Mediterranean, in Alpine Tectonics, edited by M. P. Coward, D. Dietrich, and R. G. Park, Geol. Soc. Spec. Publ., 45, 265 – 283.

Dixon, T. (1991), An introduction to the Global Positioning System and some geological applications, *Rev, Geophys.*, *29*, 249-276.

Djamour, Y., R. Bayer, Y. Hatam, J. Ritz, J. Hinderer, P. Vernant, B. Luck, H. Nankali, N. Moigne, M. Sedighi, J. Boy (2007), Analysing the present-day deformation in central Alborz and Tehran region with GPS and gravity (Iran) , Submitted.

Djamour, H.R. Nankali, Z. Rahimi (2006), Iranian Permanent GPS network , GIM international Vol. 20, Issue 9.

Djamour, Y. (2004), Contribution de la Géodésie (GPS et nivellement) à l'étude de la déformation tectonique et de l'aléa sismique sur la région de Téhéran (montagnes de l'Alborz, Iran), Phd Thesis, University of Montpellier II, France.

Dong, D., T.A. Herring, and R.W. King (1998), Estimating regional deformation from a combination of space and terrestrial geodetic data, *J. Geod.*, *72*, 200-211.

Dong, D., P. Fang, Y. Bock, M.K. Cheng, and S. Miyazaki (2002), Anatomy of apparent seasonal variation from GPS-derived site position time series, *J. Geophys. Res.*, *107* (B4), ETG9-1/18.

England, P.C., and D.P. McKenzie (1982), A thin viscous sheet model for continental deformation, *Geophys. J. R. Astron. Soc.*, *73*, 523-532.

Engdahl, E. R., R.D. Van der Hilst, R.P. Buland (1998), Global teleseismic earthquake relocation with improved travel times and procedures for depth determination, Bulletin Seismological Society of America, 88, 722-743.

Engdahl, E. R., J. Jackson, S.C. Myers, E.A. Bergman, K. Priestley (2006), Relocation and assessment of seismicity in the Iran region, *Geophysical Journal International*, 167, 761-778.

Falcon, N. L. (1969), Problem of the relationship between surface structures and deep displacement illustrated by the Zagros range, in Time and Place in Orogeny, edited by P. E. Kent, G. E. Satterwaite, and A. M. Spencer, Geol. Soc. Spec. Publ., 3, 9-22.

Falcon, N.L., Southern Iran: Zagros Mountains. In: A. M. Spencer (Editor) (1974), Mesozoic-Cenozoic Orogenic Belts, Data for Orogenic Studies, *Geol. Soc. London, Spec. Publ.*,*4*, 199-211.

Falcon, N.L. (1976), The Minab Anticline, in *The Geological Evolution of Southern Iran: the report of the Iranian Makran expedition*, pp. 409-410, Geogrl J.

Fattahi, M., R. T. Walker, M. Khatib, A. Dolati and A. Bahroudi (2006), Slip-rate estimate and past earthquakes on the Doruneh fault, eastern Iran, *Geophys. J. Int.* doi: 10.1111/j.1365-246X.2006.03248.x.

Fattahi, M., R. Walker, J. Hollingsworth , A. Bahroudi, H. Nazari, M. Talebian , S. Armitage, S. Stokes (2006), Holocene slip-rate on the Sabzevar thrust fault, NE Iran, determined using optically stimulated luminescence (OSL) Earth and Planetary Science Letters 245 (2006) 673–684.

Feigl, K.L., R.W. King, and T.H. Jordan (1990), Geodetic measurement of tectonic deformation in Santa Maria fold and thrust belt, California, *J. Geophys. Res.*, *95*, 2679-2699.

Feigl, K.L. (1991), Geodetic Measurements of Tectonic Deformation in Central California, 223 p., thesis.

Feigl K.L, D.C. Agnew, Y. Bock, D. Dong, A. Donnellan (1993), Space geodetic measurement of crustal deformation in central and southern California, 1984–1992. *J. Geophys. Res.* 98(B12):1677–712.

Fielding, E., M. Talebian, P., Rosen, H., Nazari, J., Jackson, M., Ghorashi and R. Walker (2005), Surface ruptures and building damage of the 2003 Bam, Iran,

earthquake mapped by satellite synthetic aperture radar interferometric correlation. *Journal of Geophysical Research*, 110**,** B03302, doi:10.1029/2004JB003299.

Fitch, T.J. (1972), Plate convergence, transcurrent faults, and internal deformation adjacent to Southeast Asia and the western Pacific, J. Geophys. Res., 77, 4432-4460.

Freund, R. (1970), Rotation of strike-slip faults in Sistan, southeast Iran, *J. Geol.*, *78*, 188-200.

Funning, G.J., B. Parsons, T.J. Wright, J.A. Jackson and E. Fielding (2005), Surface displacements and source parameters of the 2003 Bam (Iran) earthquake from Envisat advanced synthetic aperture radar imagery *Journal of Geophysical Research* , 110, B09406.

Gidon, M., F. Berthier, J.P. Billiault, B. Halbronn and P. Maurizot (1974), Sur le carateres et l'ampleur du coulissement de la 'Main Fault' dans la region de Borujerd Dorud, Zagros oriental, Iran, *C.R. Acad. Sci., Paris, Ser. D.,* 278, 701–704.

Giese, P., J. Makris, B. Akashe, P. Rower, H. Letz, and M. Mostaanpour (1983), Seismic crustal studies in southern Iran between the central Iran and the Zagros belt, Geodynamic Project in Iran (Geotraverse), in *Rep. Geol. Surv. Iran*, edited by V. Madelat, pp. 71-89.

Haghipour, A. and M. Amidi (1980), The November 14 to December 25, 1979 Ghaen Earthquakes of northeast Iran and their Tectonic implication, Bulletin of the Seismological Society of America, Vol. 70, No. 5, pp 1751-1757.

Hatzfeld, D., M. Tatar, K. Priestley and M. Ghafory-Ashtiany (2003), Seismological constraints on the crustal structure beneath the Zagros mountain belt (Iran), *Geophys. J. Int.,* 155, 403–410.

Hatzfeld D., C. Authemayou, P. van der Beek , O. Bellier , J. Lavé, B. Oveisi , M. Tatar, F. Tavakoli, F. Yamini-Fard and A. Walpersdorf (2007), The kinematics of the Zagros Mountains (Iran), Submitted.

Haynes, S. J. and H. McQuillan (1974), Evolution of the Zagros suture zone, southern Iran, *Bulletin of the geological Society of America*, 85, 739-744.

Herring, T.A. (2002), *GLOBK: Global Kalman filter VLBI and GPS analysis program, version 10.0*, Mass. Inst. of Technol., Cambridge.

Hempton, M. R. (1987), Constraints on Arabian plate motion and extensional history of the Red Sea, Tectonics, 6, 687 – 705.

Hessami, K., F. Nilforoushan and C. Talbot (2006), Active deformation within the Zagros Mountains deduced from GPS measurements, *Journal of the Geological Society of London*, 163, 143-148.

Hessami, K., H.A. Koyi, and C.J. Talbot (2001a), The significance of strike-slip faulting in the basement of the Zagros fold and thrust belt, *J. Petroleum Geol.*, *24* (1), 5-28.

Hessami, K., H. A. Koyi, C. J. Talbot, H. Tabassi, and E. Shabanian (2001b), Progressive unconformities within an evolving foreland fold-thrust belt, Zagros mountains, J. Geol. Soc. London, 158, 969-981.

Hessami, K., D. Pantosti, H. Tabassi, E. Shabanian, M. Abbassi, K. Feghhi, and S. Soleymani (2003), Paleoearthquakes and slip rates of the North Tabriz fault, NW Iran: preliminary results, Ann. Geophys. 46 (2003) 903–915.

Hoffman-Wellenhof, B., H. Lichtenegger, and J. Collins (1992), *GPS theory and practice*,S. Verlag.

Hollingsworth, J., J. Jackson, J.E. Alarcon, J.J. Bommer and M.J. Bolourchi (2007), The 4th February 1997 Bojnurd (Garmkhan) earthquake in NE Iran: field, teleseismic, and strong-motion evidence for rupture directivity effects on a strike-slip fault. *J. Earthquake Engineering,* 11, 193-214.

Hollingsworth, J., Jackson, J., Walker, R., Gheitanchi, M. and Bolourchi, M. (2006), Strike-slip faulting, rotation, and along-strike elongation in the Kopeh Dagh mountains, NE Iran. *Geophys. J. Int.* , 166, 1161-1177.

Jackson, J. (2001), Living with earthquakes: know your faults. *Journal of Earthquake Engineering* , 5, Special Issue 1, 5-123.

Jackson, T.H. Jordan, R.W. King, S. Larsen, K.M. Larson, M.H. Murray, Z. Shen, and F.H. Webb (1993), Space geodetic measurement of crustal deformation in central and southern California, *J. Geophys. Res.*, *98*, 21677-21712.

Jackson, J.A. (1992), Partitioning of strike-slip and convergent motion between Eurasia and Arabia in eastern Turkey and Caucasus, *J. Geophys. Res.*, *97*, 12471-12479.

Jackson, J. (1980), Errors in focal depth determination and depth of seismicity in Iran and Turkey, *Geophysical Journal of the astronomical Society*, 61, 285-301.

Jackson, J. and T. Fitch (1981), Basement faulting and the focal depths of the larger earthquakes in the Zagros mountains (Iran), *Geophysical Journal of the astronomical Society,* 64, 561-586.

Jackson, J. A., and D. McKenzie (1984), Active tectonics of the Alpine-Himalayan Belt between western Turkey and Pakistan, *Geophysical Journal of the astronomical Society*, 77, 185-264.

Jackson, J. and D. McKenzie (1988), The relationship between plate motions and seismic moment tensors and the rates of active deformation in the

Mediterranean and Middle East, *Geophysical Journal of the astronomical Society,* 83, 45-73.

Jackson, J.A., J. Haines and W. Holt (1995), The accommodation of the Arabia-Eurasia plate convergence in Iran, *J. Geophys. Res.*, *100*, 15205-15219.

Jackson, J.A., K. Priestley, M. Allen and M. Berberian (2002), Active tectonics of the South Caspian Basin, *Geophys. J. Int.*, *148*, 214-245.

Jestin, F., P. Huchon, and J.M. Gaulier (1994), The Somalia plate and the East African Rift System, present-day kinematics, *Geophys. J. Int.*, *116*, 637-654.

Johnson, J., J. Braun, C. Rocken, and T. Van Hove (1995), The role of multipath in antenna height tests at Table Mountain, pp. 19, UNAVCO.

Johansson, J.M., J.L. Davis, H.-G. Scherneck, G.A. Milne, M. Vermeer, J.X. Mitrovica, R.A. Bennett, G. Elgered, P. El´osegui, H. Koivula, M. Poutanen, B.O. Ronn¨ang, and I.I. Shapiro (2002), Continuous GPS measurements of postglacial adjustments in Fennoscandia–1. Geodetic results. *J. Geophys Res.* 107(B8):2157.

Kadinsky-Cade, K. and M. Barazangi (1982), Seismotectonics of southern Iran : the Oman Line, *Tectonics*, *1*, 389-412.

Karakhanian, A.S., R.T. Djrbashian, V.G. Trifonov, H. Philip, and J.F. Ritz (1997), Active faults and strong earthquakes of the Armenian upland, in *Historical and Prehistorical Earthquakes in the Caucasus*, edited by Giardini, D., Balassanian, and S., pp. 181-187, Kluwer Academic Publishers, Dordrecht.

King, R. W. and Y. Bock (2002), Documentation for the GAMIT analysis software, Release 10.1, Massachusetts Institute of Technology. Cambridge, MA.

Koop, W. J., and R. Stoneley (1982), Subsidence history of the Middle East Zagros Basin, Permian to Recent, *Philosophical Transactions of the Royal Society of London*, 305, 149-168.

Kopp, C., J. Fruehn, E. R. Flueh, C. Reichert, N. Kukowski, J. Bialas and D. Klaeschen (2000), Structure of the Makran subduction zone from wide-angle and reflection seismic data, Tectonophysics, Volume 329, Issues 1-4, 31 December 2000, Pages 171-191.

Larson, K.M., and D.C. Agnew (1991), Application of the Global Positioning to crustal deformation measurement: 1. Precision and Accuracy, *J. Geophys. Res.*, *96*, 16547 16565.

Larson, K.M., R. Bürgmann, R. Bilham, and J.T. Freymueller (1999), Kinematics of the India-Eurasia collision zone from GPS measurements, *J. Geophys. Res.*, *104*, 1077-1093.

Leick A. (1995), *GPS Satellite Surveying.* New York: Wiley & Sons.

Lyberis, N., and G. Manby (1999), Oblique to orthogonal convergence across the Turan block in the post-Miocene, *Am. Assoc. Petroleum Geologists Bull.*, *83*, 1135-1160.

Maggi, A., J.A. Jackson, K. Priestley, and C. Baker (2000b), A re-assessment of focal depth distribution in southern Iran, the Tien Shan and northern India: Do earthquakes really occur in the continental mantle?, *Geophys. J. Int.*, *143*, 629-661.

Malekzadeh, Z. (2007), The accommodation of the deformation from Main Recent Fault to Kazerun, Ph.D. thesis, 371p, Institute of Earthquake Engineering and Seismology, Tehran, Iran.

Masson, F., J. Chéry, D. Hatzfeld, J. Martinod, P. Vernant, F. Tavakoli and M. Ghafory Asthiani (2005), Seismic versus aseismic deformation in Iran inferred fromearthquakes and geodetic data, *Geophysical Journal International*, 160, 217 226.

Masson, F., M. Anvari, Y. Djamour, A. Walpersdorf, F. Tavakoli, M. Daignières, H. Nankali and S. Van Gorp (2007), Large-scale velocity field and strain tensor in Iran inferred form GPS measurements: new insight for the present-day deformation pattern within NE Iran, *Geophysical Journal International.*, 170, 436-440.

Masson, F., Y. Djamour , S. Van Gorp, J. Chéry, M. Tatar , F. Tavakoli, H. Nankali and P. Vernant (2006), Extension in NW Iran driven by the motion of the South Caspian Basin" Earth and Planetary Science Letters, 252 (2006) 180–188.

Massonnet, D., and K.L. Feigl (1995), Discrimination of geophysical phenomena in satellite radar interferograms. *Geophysical Research Letters*, 22(12), 1537-154.

McCall, G. J. H. (1997), The geotectonic history of the Makran and adjacent areas of southern Iran, J. Asian Sci., 15, 517 – 531.

McClusky, S., S. Balassanian, A. Barka, C. Demir, S. Ergintav, I. Georgiev, O. Gurkan, M. Hamburger, K. Hurst, H. Kahle, K. Kasten, G. Kekelidze, R.W. King, V. Kotzev, O. Lenk, S. Mahmoud, A. Mishin, M. Nadariya, A. Ouzoumis, D. Paradissis, Y. Peter, M. Prilepin, R. Reilinger, I. Sanli, H. Seeger, A. Tealeb, M.N. Toksöz, and G. Veis (2000), GPS constraints on plate motions and deformations in eastern Mediterranean and Caucasus, *J. Geophys. Res.*, *105*, 5695-5719.

McClusky, S., R. Reilinger, S. Mahmoud, D. Ben Sari, and A. Tealeb (1978), GPS constraints on Africa (Nubia) and Arabia plate motions, *Geophys. J. Int.*, *in press*.McKenzie, D.P., Active tectonics of the Mediterranean region, *Geophys. J. R. Astron. Soc.*, *55*, 217-254.

McKenzie, D.P. (1978), Active tectonics of the Alpine-Himalayan belt: the Aegean sea and surrounding regions, *Geophysical Journal of the astronomical Society*, 55, 217-254.

McQuarrie, N. (2004), Crustal scale geometry of the Zagros fold-thrust belt, Iran, *Journal of Structural Geology*, 26, 519-535.

McQuarrie, N., J.M. Stock, C. Verdel, and B.P. Wernicke (2003), Cenozoic evolution of Neotethys and implications for the causes of plate motion, *Geophysical Research Letters*, 30, doi:10.1029/2003GL017992.

McQuarrie, N. (2004), Crustal scale geometry of the Zagros fold-thrust belt, Iran, Journal of Structural Geology 26 (2004) 519–535.

Meade, B.J., B.H. Hager, S. McClusky, R. Reilinger, S. Ergintav, O. Lenk, A. Barka, and H. Özener (2002), Estimates of seismic potential in the Marmara Sea regions from block models of secular deformation constrained by Global Positioning System Measurements, *Bull. Seismol. Soc. Am.*, *92* (1), 208-215.

Meade, B.J. and B.H. Hager (2005), Block models of crustal motion in thesouthern California constrained by GPS measurements, *J. Geophys. Res.,* 110, B03403, doi:10.1029/2004JB003209.

Meade, B.J., B.H. Hager, S.C. McClusky, R.E. Reilinger, S. Ergintav, O. Lenk, A. Barka, and H. Ozener (2002), Estimates of seismic potential in the Marmara Sea region from block models of secular deformation constrained by Global Positioning System measurements, *Bull. seism. Soc. Am.,* 92**,** 208–215.

Meyer, B., F. Mouthereau, O. Lacombe and P. Agard (2006), Evidence of Quaternary activity along the Deshir Fault: implication for the Tertiary tectonics of Central Iran" *Geophys. J. Int.* (2006) 164**,** 192–201.

Meyer, B. and K. Le Dortz (2007), Strike-slip kinematics in Central and Eastern Iran: Estimating fault slip-rates averaged over the Holocene, TECTONICS, VOL. 26, TC5009, doi:10.1029/2006TC002073.

Minster, J. and T. Jordan, (1978), Present-day plate motions. J. Geophys. Res. 83, pp. 5331-5354.

Mohajer-Ashjai, A., H. Behzadi and M. Berberian (1975), Reflections on the rigidity of the Lut block and recent crustal deformation in eastern Iran, *Tectonophysics*, *28*, 281-301.

Molinaro, M. Leturmy, P. Guezou and J.-C. Frizon de Lamotte (2005), The structure and kinematics of the south-eastern Zagros fold-thrust belt, Iran: from thin-skinned to thick-skinned tectonics, *Tectonics*, 24, NIL42-NIL60.

Molnar, P., and H. Lyon-Caen (1988), Some simple physical aspects of the support, structure, and evolution of mountain belts, in Processes in Continental

Lithospheric Deformation, Geological Society America Special Paper. 218, 179-207.

Muller, J. (1895), Nota Betreffende de verplaatsing van eenige triangulatie pilaren in de residentie Tapanuli tgv. de aardbeving van 17 Mei 1892. *Natuurk. Tidschrift van Nederlandsche Oost IndiO, 54,* 299-307.

Motagh, M., J. Klotz, F. Tavakoli, Y. Djamour, S. Arabi, H. Wetzel, J. Zschau (2006), Combination of Precise Leveling and InSAR Data to Constrain Source Parameters of the M_w =6.5, 26 December 2003 Bam Earthquake, Pure appl. Geophys. 163 1–18.

Motagh, M.,Y. Djamour, T. Walter, H. Wetzel, J. Zschau, S. Arabi (2007), Land Subsidence in Mashhad Valley, northeast Iran: Results from InSAR, Leveling and GPS'. *Geophysical Journal International* 168:518–526.

Mouthereau, F., O. Lacombe, and B. Meyer (2006), The Zagros folded belt (Fars, Iran): constraints form topography and critical wedge modelling, *Geophysical Journal International*, 165, 336-356.

Nabavi, M. H. (1970), Geological Map of Yazd sheet (H9), scale 1:250,000, Geol. Survey of Iran, Teheran.

Ni, J., and M. Barazangi (1986), Seismotectonics of the Zagros Continental Collision Zone and a Comparison with the Himalayas, *Journal of Geophysical Research*, 91, 8205-8218.

Niazi, M. (1980), Microearthquakes and crustal structure off the Makran coast of Iran, *Geophysical Research Letters*, 7, 297-300.

Nilforoushan, F., P. Vernant, F. Masson, C. Vigny, J. Martinod, M. Abbassi, H. Nankali, D. Hatzfeld, F. Tavakoli, M. Ashtiany, E. Doerflinger, M. Daignieres, P. Collard, J. Chéry (2003), GPS network monitors the Arabia-Eurasia collision deformation in Iran, *Journal of Geodesy*, 77 (7-8): 411-422.

Nilforoushan, F., and H.A. Koyi (2007), Displacement fields and finite strains in a sandbox model simulating a fold-thrust-belt, *Geophysical Journal International*, 169, 1341-1355.

Nocquet, J.-M., E. Calais, Z. Altamimi, P. Sillard, and C. Boucher (2001), Intraplate deformation in western Europe deduced from an analysis of the ITRF-97 velocity field, *J. Geophys. Res.*, *106*, 11239-11258.

Nocquet, J.-M. (2002), Mesure de la déformation crustal en Europe occidentale par géodésie spatiale, Nice-Sophia Antipolis, Nice, pp 311 p.,thesis, France.

Nocquet, J.-M., and E. Calais (2003), Crustal velocity field of the western Europe from permanent GPS array solutions, 1996-2001, *Geophys. J. Int.*, *154*, 72-88.

Nowroozi, A. A., and A. Mohajer-Ashjai (1985), Fault movements and tectonics of eastern Iran: Boundaries of the Lut plate, Geophys. J. R. Astron. Soc., 83, 215 – 237.

Okada, Y. (1985), Surface deformation due to shear and tensile faults in a half space, *Bull. seism. Soc. Am.,* 75**,** 1135–1154.

Oral M.B., R.E. Reilinger, M.N. Toksoz, R.W.King and A.A.Barka (1995), Global Positioning System offers evidence of plate motions in the eastern Mediterranean. *Eos, Trans. Am. Geophys. Union* 76(2):9–11.

Okada, Y. (1985), Surface deformation due to shear and tensile faults in a half-space, Bulletin of the Seismological Society of America, 75 (4), 1135-54.

Oveisi, B., J. Lavé, and P. Van der Beek (2007), Rates and processes of active folding evidenced by Pelistocene terraces at the central Zagros front (Iran), in *Thrust Belt and Foreland Basin*, ed. Lacombe, O et al., Frontiers in Earth Sciences, Springer, in press.

Oveisi, B., J. Lavé, P. Van der Beek, J. Carcaillet, L. Benedetti, R. Braucher and C. Aubourg (2007), Thick- and thin-skinned deformation rates in the Zagros Simple Folded Zone (Iran) indictaed by displacement of geomorphic surfaces, *Geophysical Journal International*, submitted.

Owen, S., and P. Segall (2000), Rapid deformation of Kilauea Volcano: global positioning system measurements between 1990 and 1996'. *J. Geophys Res.* 105(B8):18983–18998.

Parsons, B., T. Wright, P. Rowe, J. Andrews, J. Jackson, R. Walker, M. Khatib and M. Talebian (2006), The 1994 Sefidabeh (eastern Iran) earthquakes revisited: new evidence from satellite radar interferometry and carbonate dating about the growth of an active fold above a blind thrust fault, *Geophysical Journal International* , 164, 202-217.

Paul, A., A. Kaviani, D. Hatzfeld and M. Mokhtari (2003), Lithospheric Structure of Central Zagros from Seismological Tomography, Fourth International Conference of Earthquake Engineering and Seismology Proceeding.

Philip, H., A. Cisternas, A. Gvishiani and A. Gorshkov (1989), The Caucasus: An actual example of the initial stages of a continental collision, Tectonophysics, 161, 1– 21.

Philip, H., A. Avagyan, A.S. Karakhanian, J.F. Ritz and S. Rebai (2001), Estimating slip rates and recurrence intervals for strong earthquakes along an intercontinental fault: example of the Pambak-Sevan-Sunik fault (Armenia), *Tectonophysics*, *343*, 205-232.

Priestley, K., C. Baker, and J. Jackson (1994), Implications of earthquake focal mechanism data for the active tectonics of the south Caspian Basin and surrounding regions, Geophys. J. Int., 118, 111 – 141.

Quennell, A. M. (1984), The Western Arabia rift system, in The Geological Evolution of the Eastern Mediterranean, edited by J. E. Dixon and A. H. F. Robertson, Geol. Soc. Spec. Publ., 17, 775 – 788.

Ravaut, P., R. Bayer, R. Hassani, D. Rousset and A. Al Yahya'ey (1997), Structure and evolution of the Northern Oman margin: gravity and seismic contstaints over the Zagros-Makran-Oman collision zone, *Tectonophysics,* 279**,** 253–280.

Regard, V., O.Bellier, J.C. Thomas, M. Abbassi, J.L. Mercier, E. Shabanian, KH. Feghhi, and Sh Soleymaani (2004), The accommodation of the Arabia-Asia convergence in the Zagros-Makran transfer zone, SE Iran: a transition between collision and subduction through a young deforming system, *Tectonics,* 23, TC4007, doi:10.1029/2003TC00599.

Regard, V., O. Bellier, J.-C. Thomas, D. Bourl`es, S. Bonnet, M. R. Abbassi, R. Braucher, J. Mercier, E. Shabanian, Sh. Soleymani and Kh. Feghhi *(*2005), Cumulative right-lateral fault slip rate across the Zagros-Makran transfer zone: role of the Minab-Zendan fault system in accommodating Arabia-Eurasia convergence in southeast Iran, *Geophys. J. Int.,* 162**,** 177–203.

Reilinger, R., S. McClusky, B. Oral, R.W. King, M.N. Toksöz, A. Barka, I. Kinik, O. Lenk, and I. Sanli (1997), Global Positioning System measurements of present-day crustal movements in the Arabia-Eurasia plate collision zone, *J. Geophys. Res.*, *102* (B5),9983-9999.

Reilinger, R. S. McClusky, P. Vernant, S. Lawrence,S. Ergintav, R. Cakmak, H. Ozener, F. Kadirov, I. Guliev, R. Stepanyan, M. Nadariya, G. Hahubia, S. Mahmoud, K. Sakr, A. ArRajehi, D. Paradissis, A. Al-Aydrus, M. Prilepin, T. Guseva, E. Evren, A. Dmitrotsa, S. V. Filikov, F. Gomez, R. Al-Ghazzi, and G. Karam (2006), GPS constraints on continental deformation in the Africa-Arabia-Eurasia continental collision zone and implications for the dynamics of plate interactions, J. Geophys. Res., 111, B05411, doi:10.1029/2005JB004051.

Richard, P., and P. Cobbold (1990), Experimental insights into partitioning of fault motions in continental convergent wrench zones, Ann. Tectonicae, 4, 35 – 44.

Ricou, L.E., J. Braud, and J.H. Brunn, (1977), Le Zagros, Mém h. sér. Soc. Géol. Fr., 8, 33-52.

Robertson, A. H. F. (2000), Mesozoic-Tertiary tectonic sedimentary evolution of a south Tethyan oceanic basin and its margins in southern Turkey, in Tectonics and Magmatism in Turkey and the Surrounding Area, edited by E. Bozkurt, J. A. Winchester, and J. D. A. Piper, Geol. Soc. Spec. Publ., 173, 97–138.

Rothacher, M., and G. Mader (1996), *Combination of antenna phase center offsets and variations, Antenna Calibration set IGS_01*,U.o. Berne, IGS Central Bureau, Berne, Switzerland.

Segall, P., J. L. Davis (1997), GPS application for geodynamics and earthquake studies, (1997) *Annu. Rev. Earth Planet. Sci. ,. 25:301–36.*

Savage, J., and R. Burford (1973). Geodetic determination of relative plate motion in Central California, *J. Geophys. Res.*, *95*, 4873-4879.

Seeber, G. (1993), *Satellite Geodesy*, W.d. Gruyter, Berlin, New York.

Sella, G.F., T.H. Dixon, and A. Mao (2002), REVEL: A model for recent plate velocities from space geodesy, *J. Geophys. Res.*, *107* (B4), ETG 11-1,11-32.

Shabanian, E, L. Siame, O. Bellier, L. Benedetti, M. R. Abbassi (2007), Quaternary slip-rates in the Kopet Dagh Mountains NE Iran, European geosciences Union general assembly 2007.

Shearman, D. J. (1977), The geological evolution of Southern Iran, *Geographical Journal*, 142, 393-410.

Sherkati, S., J. Letouzey (2004), Variation of structural and basin evolution in the cebtral Zagros (Izeh zone and Dezful Embayment), Iran, *Marine and Petroleum Geology*, 21, 535-554.

Sherkati, S., Molinaro, M., Frizon de Lamotte, D., J. Letouzey (2005), Detachment folding in the Central and Eastern Zagros fold-belt (Iran): salt mobility, multiple detachments and late basement control, *Journal of Structural Geology*, 27, 1680-1696.

Sjöberg, L., M. Pan, E. Asenjo and S. Erlingsson (2000), Glacial rebound near Vatnajokull, Iceland, studied by GPS campaigns in 92 and 96.'. *Journal of Geodynamics* 29:63–70.

Snyder, D. B., and M. Barazangi (1986), Deep crustal structure and flexure of the Arabian plate beneath the Zagros collisional mountain belt as inferred from gravity observations, *Tectonics*, 5, 361-373.

Stöcklin, J. (1968), Structural history and tectonics of Iran : A review, *Am. Ass. Petrol. Geol. Bull.*, *52*, 1229-1258.

Stöcklin, J., (1974), Possible ancient continental margins in Iran, in *The Geology of Continental Margins,* pp. 873–887, eds Burke, C.A. & Drake, C.L., Springer-Verlag, New York.

Stoneley, R. (1981), The geology of the Kuh-e Dalneshin area of southern Iran and its bearing on the evolution of southern Tethys, J. Geol. Soc. London,138, 509-526.

Talbot, C. J., and M. Alavi (1996), The past of a future syntaxis across the Zagros, in Salt Tectonics, edited by G. I. Alsop, D. J. Blundell and I. Davison, Geol. Soc. Spec. Publ., London, 100, 89-110.

Talebian, M., E.J. Fielding, G.J. Funning, M. Ghorashi, J. Jackson, H. Nazari, B. Parsons, K. Priestley, P.A. Rosen, R. Walker and T. Wright (2004), The 2003 Bam (Iran) earthquake: rupture of a blind strike-slip fault. *Geophysical Research Letters*, 31, L11611, doi: 10.1029/2004GL020058.

Talebian, M., J., Biggs, M., Bolourchi, A., Copley, A., Ghassemi, M., Ghorashi, J., Hollingsworth, J., Jackson, E., Nissen, B., Oveisi, B., Parsons, K., Priestley and A. Saiidi (2006), The Dahuiyeh (Zarand) earthquake of 2005 February 22 in central Iran: reactivation of an intra-mountain thrust, *Geophysical Journal International* , 164, 137-148.

Talebian, M., and J. Jackson (2004), A reappraisal of earthquake focal mechanisms and active shortening in the Zagros mountains of Iran, *Geophysical Journal International*, 156, 506-526.

Talebian, M., and J. Jackson (2002), Offset on the Main Recent Fault of NW Iran and implications for the late Cenozoic tectonics of the Arabia-Eurasia collision zone, *Geophysical Journal International*, 150, 422-439.

Tatar, M., D. Hatzfeld, J. Martinod, A. Walpersdorf, M. Ghafory-Ashtiany, and J. Chéry (2002), The present-day deformation of the central Zagros from GPS measurements, Geophys. Res. Lett., 29(19), doi: 10.1029/2002GL015159.

Tatar, M. (2001), Etude sismotectonique de deux zones de collision continentale: le Zagros central et l'Alborz (Iran), univ. J. Fourier, Grenoble, 258 pp. p.,thesis, France.

Tchalenko, J.S., and J. Braud (1974), Seismicity and structure of the Zagros (Iran): the Main Recent Fault between 33° and 35° N, *Philosophical transactions of the Royal Society of London*, *277* (1262), 1-25.

Tchalenko, J.S. (1975), Seismicity and structure of the Kopet Dagh (Iran, USSR), *Phil. Trans. R. Soc. Lond.,* Series A., 278(1275), 1–28.

Tirrul, R., I.R. Bell, R.J. Griffis, and V.E. Camp (1983), The Sistan suture zone of eastern Iran, *Geol. Soc. Am. Bull.*, *94*, 134-150.

Trifonov, V.G. (1971), The pulse-like character of tectonic movements in regions of most recent mountain-building (Kopet Dagh and southeast Caucasus), Geotectonics 4, 234-235. (ENGL. Transl.).

Trifonov, V.G. (1978), Late Quaternary tectonic movements of the western and central Asia, *Geol. Soc. Am. Bull.*, *89*, 1059-1072.

Tavakoli, F., A. Walpersdorf, C. Authemayou, H. R. Nankali, D. Hatzfeld, M. Tatar, Y. Djamour, F. Nilforoushan. and N. Cotte (2007), Transition form thick skinned to thin skinned tectonics across the Kazerun fault system (Zagros, Iran): evidence form present-day GPS velocities, Submitted.

Teunissen, P., A. Kleusberg (1998), GPS for Geodesy, Publisher: Springer.

Vanicek, P. and E. Krakiwsky (1986), Geodesy the concept, Elesevier Science Publication.

Vanicek, P., P. Cross, J. Hannah, H. Heradilek, R. Kelm, J. Makinen, C. Merry, L., Sjoberg, R. Steeves and D. Ziloski (1987), Four dimentional geodetic Positioning, Manuscripta Geodetica, 12: 147-222.

Vernant, P., F. Nilforoushan, D. Hatzfeld, M. Abbassi, C. Vigny, F. Masson, H. Nankali, J. Martinod, M. Ashtiany, R. Bayer, F. Tavakoli and J. Chéry (2004), Contemporary crustal deformation and plate kinematics in the Middle East Constrained by GPS measurements in Iran and Northern Oman, *Geophysical Journal International ,* 157, 381-398 .

Vernant, P. (2004), Cinématique actuelle et dynamique de l'Iran: GPS et modélisation numérique, Thesis, University of Montpellier II, France.

Vernant P and J. Chery (2006), Mechanical modelling of oblique convergence in the Zagros, Iran, *Geophysical Journal International*, 165, 991-1002.

Vigny, C., J. Chéry, T. Duquesnoy, F. Jouanne, J. Ammann, M. Anzidei, J.-P. Avouac, F. Barlier, R. Bayer, P. Briole, E. Calais, F. Cotton, F. Duquenne, K.L. Feigl, G. Ferhat, M. Flouzat, J.-F. Gamond, A. Geiger, A. Harmel, M. Kasser, M. Laplanche, M. Le Pape, J. Martinod, G. Ménard, B. Meyer, J.-C. Ruegg, J.-M. Scheubel, O. Scotti, and G. Vidal (2002), GPS network monitors the Western Alps deformation over a five-year period: 1993-1998, *J. Geod.*, *76*, 63-76.

Vita-Finzi, C. (1979), Rates of Holocene folding in the coastal Zagros near Bandar Abbas, Iran, *Nature*, 278, 632–634.

Walker, R. and J. Jackson (2004), Active tectonics and late Cenozoic strain distribution in central and eastern Iran. *Tectonics*, 23, TC5010, doi:10.1029/2003TC001529.

Walker R., J. Jackson and C. Baker (2004), Active faulting and seismicity of the Dasht-e-Bayaz region, eastern Iran, *Geophysical Journal International,* 157, 265-282.

Walker, R., J. Jackson, and C. Baker (2003), Surface expression of thrust faulting in eastern Iran: Source parameters and surface deformation of the 1978 Tabas and 1968 Ferdows earthquake sequences, Geophys. J. Int., 152, 749 – 765.

Walker, R., and J.A. Jackson, (2002), Offset and evolution of the Gowk fault, S.E.

Iran: a major intracontinental strike-slip system, *J. Struct. Geol.*, *24*, 1677-1698.

Walpersdorf, A. (1997), L'observation de la tectonique active en Asie du Sud-Est par géodésie spatiale : un projet GPS, ENS, Paris, 295 p.,thesis.

Walpersdorf, A., and C. Vigny (1998), Determining the sula block kinematics in the triple junction area in Indonesia by GPS, *Geophys. J. Int.*, *135*, 351-361.

Walpersdorf, A., D. Hatzfeld, H. Nankali, F. Tavakoli, F. Nilforoushan, M. Tatar, P. Vernant, J. Chéry and F. Masson (2007), Difference in the GPS deformation pattern of North and Central Zagros (Iran), Geophys. J. Int., doi:10.1111/j.1365-246X.2006.03147.x, Vol. 167, Issue 3, 1077-1088.

Wang, Q., P.Z. Zhang, J.T. Freymueller, R. Bilham, K.M. Larson, X. Lai, X. You, Z. Niu, J. Wu, Y. Li, J. Liu, Z. Yang, and Q. Chen(2001), Present-day crustal deformation in China by Global Positioning System measurements, *Science*, *294*, 574-577.

Wellman, H. W. (1966), Active wrench faults of Iran, Afghanistan and Pakistan, Geol. Rundsch., 18, 217 – 234.

Wells, A. J. (1969), The Crush Zone of the Iranian Zagros Mountains, and its implications, Geol. Mag., 106, 385 – 394.

Wells, D.E., D. Berck, A. Delikaraoglou, G. Krakiwsky, R.B. Lachapelle, M. Langley, K.P. Nakiboglou, K.P. Scharz, J.M. Tranquilla, and P. Vanicek,(1986), *Guide to GPS positioning*, C.G.a., University of New Brunswick.

Wells, D.L., and K.J. Coppersmith (1994), New empirical relationships among magnitude, rupture length, rupture width, rupture area, and surface displacement, *Bull. Seismol. Soc. Am.*, *84* (4), 974-1002.

Wessel, P. & Smith, W.H.F. (1998), New, improved version of Generic Mapping Tools (GMT) released, *EOS, Trans. Am. Geophys. Un.,* 79(47), 579.

Westaway, R. (1994), Present-day kinematics of the Middle East and eastern Mediterranean, J. Geophys. Res., 99, 12,071– 12,090.

Yamini-Fard, F., D. Hatzfeld, M., Tatar and M. Mokhtari (2006), Microseismicity at the intersection between the Kazerun fault and the Main Recent Fault (Zagros Iran), *Geophysical Journal International*, 166, 186-196.

Yamini-Fard, F., D. Hatzfeld, A., Farahbod, A., Paul, M., Mokhtari (2007), The diffuse transition between the Zagros continental collision and the Makran oceanic subduction (Iran): microearthquake seismicity and crustal structure , *Geophysical Journal International*, 170, 182-194.

Yilmaz, Y. (1993), New evidence and model on the evolution of the southeast Anatolian orogen, Geol. Soc. Am. Bull., 105, 251 – 271

Appendix A

Session Table (SESTABLE) for regional + global analysis

```
Processing Agency = LGIT
Station Number = *
Station Constraint = Y
Satellite Number =  *
Satellite Constraint = Y         ; Y/N
 all    a     e     i     node   arg per    M    rad1   rad2  rad3  rad4
rad5  rad6  rad7  rad8  rad9
      0.01  0.01   0.01   0.01    0.01    0.01   0.01   0.01  0.01  0.01
0.01  0.01  0.01  0.01  0.01
Type of Analysis = 0-ITER       ; 0-ITER/1-ITER/2-ITER/1-CLEAN/2-CLEAN/3-
CLEAN
Data Status = RAW               ; CLN/RAW
Choice of Observable = LC_HELP  ; L1_SINGLE/L1&L2/L1_ONLY/L2_ONLY/LC_ONLY/
                                ; L1,L2_INDEPEND./LC_HELP
Choice of Experiment = RELAX.   ; BASELINE/RELAX./ORBIT

Ionospheric Constraints =  0.0 mm + 8.00 ppm ; Set for mid-solar max
Zenith Delay Estimation = YES   ; YES/NO
Number Zen = 9                 ; number of zenith-delay parameters
Zenith Constraints = 0.50       ; zenith-delay a priori constraint in
meters (default 0.5)
Zenith Model = PWL              ; PWL (piecewise linear)/CON (step)
Zenith Variation = 0.02 100.    ; zenith-delay variation, tau in
meters/sqrt(hr), hrs
Elevation cutoff = 10.          ; Elevation angle cutoff for postfit
solution
Atmospheric gradients = YES     ; YES/NO  (default no)
Num Grad = 1                    ; number of gradient (E/W or N/S)
parameters)  (default 1)
Gradient Constraints = 0.01     ; gradient at 10 deg elevation in meters
Gradient Variation = 0.01 100.  ; gradient variation, tau in
meters/sqrt(hr), hrs (defaults .01 100)
Station Constraint = Y          ; Y/N

Ambiguity resolution WL = 0.15 0.15 1000. 99. 1000.  ; Increased chi-square
ratio to stop searched
Ambiguity resolution NL = 0.15 0.15 1000. 99. 1000.  ; values from being
used.
Geodetic Datum = GEOCENTRIC     ; GEOCENTRIC/WGS84/NAD82/WGS72
Reference System for ARC = IGS92 ; WGS84/WGS72/MERIT/IGS92(default)
Initial ARC = YES               ; YES/NO  default = NO for
BASELINE/KIINEMATIC, YES for RELAX/ORBIT
Update T/L files = L_ONLY       ; T_AND_L (default), T_ONLY, L_ONLY, NONE
Final ARC = NO
Yaw Model = YES                   ; YES/NO  default = YES
Delete eclipse data = NO          ; ALL/NO/POST (Default = NO); 30 mins
post shadow removal is
                                  ; hardwired for ALL/POST
AUTCLN Command File = autcln.cmd  ; Filename; default none (use default
options)
AUTCLN Postfit = Y                ; Run autcln for postfit run; R causes
repeat run.
Use N-file = Y                    ; Y/N (default no): automatic procedure
to reweight by station
Delete AUTCLN input C-files = YES ; YES/NO  default = NO ; I --
Intermediate keep (stops) second model
Earth Rotation = 7                ; Diurnal/Semidirunal terms: Binary
coded: 1=pole 2=UT1 4=Ray model  default=7
Estimate EOP = 15                 ; Binary coded: 1 wob   2 ut1   4 wob
rate   8 ut1 rate
Wobble Con = 0.01 0.01            ; default = 3. 0.3  arcsec arcsec/day
UT1 Con = 0.00001 0.01            ; default = .2 0.02 sec sec/day
Tide Model = 15                   ; Binary coded: 1 earth  2 freq-dep  4
pole  8 ocean   default=15
Antenna Model = ELI1              ; NONE/ELEV/AZEL  default = NONE
```

```
Radiation Model for ARC = BERNE   ; SPHRC/BERNE/SRDYB/SVBDY  default =
BERNE
Inertial frame = J2000            ; J2000/B1950
SCANDD control = NONE             ; When to run SCANDD:
NONE/IFBAD(default)/FIRST/FULL/BOTH
Decimation Factor = 1             ; Decimation factor in solve
Quick-pre observable = LC_ONLY    ; For 1st iter or autcln pre, default
same as Choice of observable
Quick-pre decimation factor = 10  ; 1st iter or autcln pre, default same as
Decimation Factor
Station Error = ELEVATION 10. 0.0001 ; 1-way L1 , a**2 + b**2/sin(elev)**2
in mm, default = 4.3 7.0


Full list of controls:

  Required:
  ----------
  Type of Analysis    PREFIT      : Prefit manipulations including cleaning
(no solution)
                      QUICK       : Quick solution
                      0-ITERATION : Full solution with good prior station
coordinates and orbits
                      1-ITERATION : Full solution with approximate prior
station coordinates
                      2-ITERATION : Full solution with approximate prior
station coordinates and orbits
                      SOLVE-only  : Do a solution from C-files (rarely
used, better to run SOLVE batch file)

  Data Status : RAW for automatic editing with AUTCLN; CLN (CLEAN) for no
editing

  Choice of Observable    LC_HELP: Ambiguity-free and ambiguity-fixed
solutoins with LC
                          LC_RANGE: Same as LC_HELP but with pseudo-range
priorty
                          LC_ONLY: Ambiguity-free solution with LC
                          L1_ONLY: Ambiguity-free and ambiguity-fixed
solutions with L1
                          L2_ONLY: Ambiguity-free and ambiguity fixed
solutions with L2
                          L1,L2_INDEPEND: Ambiguity-free and -fixed
solutions with L1 and L2
                          L1&L2: (see notes in manual)

  Choice of Experiment = RELAX.   ; BASELINE/RELAX./ORBIT

  Optional:
  ---------
  Inertial frame                  ; B1950/J2000 (default = J20000)

  Initial ARC                     ; YES/NO  default = NO for
BASELINE/KIINEMATIC, YES for RELAX/ORBIT
  Final ARC                       ; YES/NO  default = YES
  Radiation Model for ARC         ; SPHRC/BERNE/SRDYB/SVBDY  default =
SPHRC
  Reference System for ARC        ; WGS72/WGS84/MERIT/IGS92 (default =
IGS92)
  Tabular interval for ARC        ; 900. seconds (new default), 1350.
seconds (old default)
  Stepsize for ARC                ; 75. seconds (new default), 168.75
seconds (old default)

  Earth Rotation                  ; Diurnal/Semidirunal terms: Binary
coded: 1=pole 2=UT1 4=Ray model; default=7
  Earth Rotation                  ; Diurnal/Semidirunal terms: Binary
coded: 1=pole 2=UT1 default=3
  Estimate EOP                    ; Binary coded: 1 wob  2 ut1  4 wob rate
8 ut1 rate; default=0 (BL) or 15 (orbits)
```

```
  Wobble Constraint = 3. 0.3      ; Default 3. (arcsec) 0.3 (arcsec/day)
  UT1 Constraint = 0.00002 0.02   ; Default .00002 (sec) 0.02 (sec/day)

  Antenna Model                   ; NONE/ELEV/AZEL  default = NONE
  Tide Model                      ; Binary coded: 1 earth  2 freq-dep  4
pole  8 ocean   default = 1
  Yaw Model                       ; YES/NO  default = YES
  I-file = N                      ; Use I-file (Y/N)  (default Y)

  Number Zen = 4                  ; number of zenith-delay parameters
(default 1)
  Zenith Constraints = 0.50       ; zenith-delay a priori constraint in
meters (default 0.5)
  Zenith Model = PWL              ; PWL (piecewise linear)/CON (step)
  Zenith Variation = 0.02 100.    ; zenith-delay variation, tau in
meters/sqrt(hr), hrs (default .02 100.)
  Gradient Constraints = 0.03     ; gradient at 10 deg elevation in meters
  Tropospheric Constraints = NO   ; YES/NO   (spatial constraint)

  Choice of Observable = LC_HELP  ;
L1_SINGLE/L1&L2/L1_ONLY/L2_ONLY/LC_ONLY/
                              ; L1,L2_INDEPEND./LC_HELP
  Choice of Experiment = RELAX.   ; BASELINE/RELAX./ORBIT
  Quick-pre observable = LC       ; For 1st iter or autcln pre, default
same as Choice of observable
  Ambiguity resolution WL         ; default = 0.15 0.15 1000.  10.
  Ambiguity resolution NL         ; default = 0.15 0.15 1000.  10.
  Type of Biases                  : IMPLICIT (default for quick), EXPLICIT
(default for full)
  H-file solutions                ; ALL ; LOOSE-ONLY
  Station Error = BASELINE 10. 0.   ; 1-way L1, a**2 + (b**2)(L**2) in mm,
ppm, default = 10. 0.
  Station Error = UNIFORM 10.       ; 1-way L1 in mm, default = 10.
  Station Error = ELEVATION 4.3 7.0 ; 1-way L1 , a**2 + b**2/sin(elev)**2
in mm, default = 4.3 7.0
  Satellite Error = UNIFORM 0.      ; 1-way L1 in mm (added quadratically
to station error) default = 0.
  Select Epochs                   ; Enter start and stop epoch number
(applies only to SOLVE)
  Decimation Factor               ; FOR SOLVE, default = 1
  Elevation Cutoff = 10.          ; For SOLVE, overrides the MODEL or
AUTCLN values if they are lower
  Quick-pre decimation factor = 10
  Correlation print               ; Threshhold for printing correlations
(default 0.9999)

  Clean Option                    ; AUTCLN(default)/SINCLN/DBLCLN
  AUTCLN Command File             ; Filename; default none (use default
options)
  Edit AUTCLN Command File        ; YES/NO; Add delete commands for bad
clocks;  default = NO
  Clean Option = AUTCLN           ; SINCLN/AUTCLN(default)/DBLCLN
  AUTCLN Postfit                  ; NO/YES/R:  Yes=repeat AUTCLN and SOLVE
R=repeat AUTCLN and SOLVE again if bad nrms
  Use N-file = Y                  ; Y/N (default no): automatic procedure
to reweight by station
  Delete AUTCLN input C-files = YES ; YES/NO  default = NO ; I --
Intermediate keep (stops) second model
  Delete eclipse data = POST      ; ALL/NO/POST (Default = NO)
  SCANDD control                  ; BOTH (default) /NONE/FIRST/FULL/IFBAD
see manual sec. 5.2
  Iteration                       ; CFILES / XFILES (default)

  Export Orbits                   ; YES/NO  default = NO
  Orbit id                        ; 4-char code read only if Export Orbits
= YES
  Orbit Format                    ; SP1/SP3 (NGS Standard Products)
  Orbit organization              ; 3-char code read only if Export Orbits
= YES
```

```
  Reference System for Orbit = ITR93 ; ITR92/ITR91/ITR90/WGS84/MERIT (for
SP3 header)

  Delete all input C-files        ; YES/NO  default = NO
  Delete MODEL input C-files      ; YES/NO  default = NO
  Delete SINCLN input C-files     ; YES/NO  default = NO
  Delete DBLCLN input C-files     ; YES/NO  default = NO
  Delete AUTCLN input C-files     ; YES/NO  default = NO
  Update T/L files                ; T_AND_L (default), T_ONLY, L_ONLY, NONE
                                    (Applies only to update for full
solution after quick)
  Update tolerance                ; minimum adjustment for updating L-file
coordinates, default .3 m
  X-compress = YES                ; Uncompress/compress X-files  default =
NO
  SCANDD control                  ; FULL (default), FIRST, BOTH, IFBAD,
NONE
  Run CTOX = YES                  ; Make clean X-files from C-files
default = NO
```

Appendix B

```
* Globk file for combination of daily h-files
*
  eq_file ../tables/renames
  make_svs ../tables/sat1.apr
  com_file globk_comb.com
  srt_file glb.srt
  sol_file globk_comb.sol
#  earth-rotation values
x   (not needed if pmu free in final combination; pmu.bull_b begins only at 1 Jan 1992)
 in_pmu  ../tables/pmu.usno
# apr site file(s)
#  apr_file postfit_prt.apr
  apr_file ../tables/itrf_local.sort
  apr_file ../tables/itrf00.apr
#  apr_file ../tables/itrf00_local.apr
# Optionally use separate file for sites to be used and random or Markov noise
x source ../tables/globk.uselist
#     (1) Max chi**2, (2) Max prefit diff, (3) Max rotation; defaults are 100 10000 10000
  max_chi 30 50 2000.0
* Apply the pole tide whenever not applied in GAMIT
  app_ptid ALL
# Allow the network to be loose since using glorg for stabilization
* original solution:
  apr_neu  all  0.1 0.1 0.1  0.1 0.1 0.1
* apr_neu  all  1 1 1 1 1 1
* solution with random walk:
* apr_neu  all  10 10 10  1 1 1
#  apr_neu  all  100 100 1000  0 0 0
* Add random walk noise as McClusky et al. [2000] selon Vernant
* only horizontal coordinates
  mar_neu all 4.e-6 4.e-6 0 0 0 0
#mar_neu all 8.e-6 8.e-6 8.e-6 0 0 0
# Satellites are loose if combining with global SOPAC H-files
#              X      Y      Z    XDOT  YDOT  ZDOT  DRAD YRAD ZRAD BRAD XRAD
DCOS DSIN YCOS YSIN BCOS BSIN
  apr_svs all   100    100    100   10    10    10    1    1  .02  .02  .02 . 02  .02 . 02 . 02  .02 . 02
#  tight if not combining with global data
x  apr_svs all .05 .05 .05 .005 .005 .005 .01 .01 F F F F F F F F F F F F F F
# Keep EOP loose
# apr_wob  100.  100.  10. 10.0  0.0  0.0  0.0  0.0
#  apr_ut1  100.  10.  0.0  0.0  0.0  0.0
#  mar_wob  36500 36500 365 365 0 0 0 0
#  mar_ut1  36500 365 0 0 0 0
#  unless not using global data
  apr_wob  .25 .25  .001 .001 0 0 0 0
  apr_ut1  .25 .25 .001 .001 0 0
  mar_wob    1 1  .001 .001
  mar_ut1    1 .001
```

```
* Estimate translation   -   .0005 m**2/yr = 15 mm/half-yr
* selon Vernant:
  apr_tran .005 .005 .005 0 0 0
  mar_tran .0025 .0025 .0025 0 0 0
# Set minimal globk print options since using glorg output
   prt_opt cdms
# Invoke glorg for stabilization
  org_cmd glorg_comb.cmd
x  org_opt cmds psum gdlf
  org_opt cmds vsum gdlf brat
x omit this for naming with sh_glred:
  org_out  name1.org
# Write out an h-file if needed for future combinations
 out_glb  NAME1.GLX
```

Appendix C

*** Glorg file for repeatabilities**

```
*
# apr site file(s)
# ITRF00 for global stabilization
#    NNR frame
 apr_file ../tables/itrf00.apr
#    Eurasian frame
x  apr_file ../tables/itrf00_eura.apr

#  Define the stabilization frame
 use_site clear ALGO ARTU BAHR FORT GRAZ GOLD GUAM HRAO IISC
 use_site IRKT KERG KIT3 KOKB KOUR LHAS MAS1 POL2 POTS TIDB TSKB WSRT
 use_site WUHN ZECK ZWEN

# Set parameters to estimate in stabilization
  pos_org  xrot yrot zrot xtran ytran ztran scale
  rate_org xrot yrot zrot xtran ytran ztran scale
x no rotation if regional stabilzation
x  pos_org  xtran ytran ztran

# Set height ratios
x  cnd_hgtv 1000 1000 2.0 2.0
x loosen height tolerance
  cnd_hgtv 1000 1000 2.0 10.0
# Tectonic Plates( Euler pole Determination )
 plate irancent  mian_gps shah_gps bija_gps arda_gps hara_gps
 plate eurasia1  bor1_gps graz_gps hers_gps joze_gps kit3_gps vill_gps
 plate eurasia1  kosg_gps nyal_gps onsa_gps pol2_gps pots_gps artu_gps
 plate eurasia1  trom_gps wtzr_gps zimm_gps zwen_gps sele_gps irkt_gps
 plate arabian1  bahr_gps khos_gps musc_gps khas_gps
# Iterations and editing
  stab_ite 4 0.8 4.

# equate SAA2_GPS xpos SAAN_GPS xpos
# equate SAA2_GPS ypos SAAN_GPS ypos
# equate SAA2_GPS zpos SAAN_GPS zpos
# equate SAA2_GPS xdot SAAN_GPS xdot
# equate SAA2_GPS ydot SAAN_GPS ydot
# equate SAA2_GPS zdot SAAN_GPS zdot
```

Déformation actuelle et cinématique des failles actives observées par GPS dans le Zagros et l'Est iranien

Résumé

La convergence entre l'Arabie et l'Eurasie est accommodée à l'intérieur du territoire iranien. Nous présentons des champs de vitesse GPS denses couvrant une grande partie de l'Iran (Zagros, block de Lut et Kopeh Dagh) avec des précisions meilleures que 2 mm/an.

Dans le Zagros, la convergence est accommodée par du partitionnement dans la partie nord. 2-4 mm/an de décrochement dextre sur la MRF sont transférés sur les failles de Dena, Kazerun et Kareh Bas dans le système de failles de Kazerun, se déplaçant à 3-4 mm/an chacune. Dans le Zagros Central, 8 mm/an de raccourcissement sont concentrés près du Golf Persique, contrastant avec une sismicité plus distribuée et indiquant un découplage de la déformation superficielle du socle.

A l'est de l'Iran, entre le block central Iranien et le block de Hellmand, 14 mm/an de cisaillement dextre orienté NS sont observés au travers du block de Lut, avec 6.5 mm/an absorbés à l'ouest (failles de Bam, Gowk et Sabzevaran) et 7.5 mm/an à l'est (zone de suture de Sistan). Des failles majeures senestres orientées EW au nord du block de Lut accommodent une partie du cisaillement (Dasht-e-Bayaz 1.5 mm/an, Doruneh 2.5 mm/an). Au sud de la chaîne du Kopeh Dagh 8 mm/an de cisaillement persistent, dont 3.5 et 2.5 mm/an sont absorbés par du raccourcissement NS dans le Binalud et l'est Kopeh Dagh, 5 mm/an par du décrochement dextre au travers le système de failles de Quchan, et 5-8 mm/an par l'expulsion du basin Sud Caspien vers l'ouest.

La comparaison des taux de glissement actuels avec des taux géologiques court et long terme montre une évolution complexe des activités des failles même dans le contexte de collision continental récente de l'Iran.

Mots clé : Geodesy, GPS, Tectonic Deformation, Crustal Deformation, continental collision, Iran, Zagros, Kazerun fault system, Lut, Kopeh Dagh, South Caspian Basin, Central Iranian Block

Present-day deformation and kinematics of the active faults observed by GPS in the Zagros and east of Iran

Summary

The convergence between the Arabian and the Eurasian plates is accommodated inside the Iranian territory. We have measured dense GPS networks covering wide parts of Iran (Zagros, Lut block and Kopeh Dagh) and present velocity fields with precisions better than 2 mm/yr.

In Zagros, convergence is accommodated by partitioning in the northern part with 2-4 mm/yr of right lateral strike-slip on the MRF. This motion is transferred to the Dena, Kazerun and Kareh Bas faults of the Kazerun fault system slipping each at 3-4 mm/yr. In Central Zagros, 8 mm/yr of NS shortening is concentrated mainly along the Persian Gulf shore while seismicity is more widely spread, evidencing decoupling of the surface deformation from the basement probably facilitated by the presence of Hormuz salt.

In eastern Iran, 14 mm/yr of right lateral NS shear between the Central Iranian Block and the Hellmand block is observed across the Lut block, with 6.5 mm/yr across its western limit (Bam, Gowk and Sabzevaran faults) and 7.5 mm/yr across its eastern limit (Sistan Suture zone). Major EW trending left lateral strike-slip faults absorb part of this shear at the northern limit of the Lut block (Dasht-e-Bayaz 1.5 mm/yr, Doruneh 2.5 mm/yr). 8 mm/yr remaining shear south of the Kopeh Dagh range is accommodated mainly by NS shortening across the Binalud and eastern Kopeh Dagh range (3.5 and 2.5 mm/yr), by right lateral strike-slip on the Quchan fault system (5 mm/yr) and westward expulsion of the South Caspian Basin (5-8 mm/yr).

Comparison of GPS present-day slip rates with short and long term geological estimates show complex slip evolution even in the context of young continental collision present in Iran.